School of Pharmacy and Biomedical Sciences

Mediation of triple-negative breast cancer cell fate via cellular redox and Wnt signalling

Sebastian Öther-Gee Pohl

This thesis is presented for the Degree of
Doctor of Philosophy
of
Curtin University

June 2018

DECLARATION

To the best of my knowledge and belief this thesis contains no material previously published by any other person except where due acknowledgment has been made.

This thesis contains no material which has been accepted for the award of any other degree or diploma in any university.

Signature: …….

Date: 21st June, 2018…..

DEDICATION

I dedicate this thesis to my family; Deborah, Mum, Dad, Paul, Anna, Rowan, Tom and Ben …..and Izzy

ACKNOWLEDGEMENTS

Firstly, I would like to acknowledge my supervisor Professor Arun Dharmarajan (Dharma) who's continuous support from the beginning of my PhD to the end has meant so much to me. He believed in me from the start and gave me the freedom to explore ideas and develop as a scientist. I would like to thank him for his guidance, friendship and of course, the morning coffees.

To my partner Deborah, there was no way I could have done this without you. Your constant love and support over the past few very stressful years has meant more to me than you will ever know. I love you very much.

To my parents, who have done everything to support me without a second thought. I could never do enough to repay you for everything you have done, but I want you to know how much it means to me. To my twin sister Anna and her partner Rowan, thank you for always being there when I needed someone to talk to and for the unconditional support. You are the best family I could have ever asked for and I hope I have made you proud.

To my friend and co-supervisor, Dr. Mark Agostino, your guidance, advice but most importantly friendship through my PhD has meant so much to me. Thank you for the countless tinnies over the past couple of years, I have no doubt they may be responsible for some of our greatest hypotheses!

To Professor Shazib Pervaiz and my co-supervisor Dr. Alan Prem Kumar. Thank you for the opportunity to come to Singapore and learn in a new environment. I truly believe that it was some of the most valuable months I have had in the past few years. I would like to thank you, and your labs both so much for welcoming me in and the friendship while I was there.

To the members past and present of Stem Cell and Cancer Biology laboratory, Frank, Abhi and Malini. Thank you for the support.

I would like to thank Dr. Kevin Keane, who has given me technical support, encouragement and friendship throughout my time at Curtin.

I would like to thank my friends Ben, Dista, Matt and Emily who have given me all the support I could ever ask for and drag me out of the lab whenever I have needed a break.

To the technical facility staff at CHIRI, especially Jeanne, thank you for the continuing support with everything flow related, I have learned so much!

Lastly, I would like to thank the Rotary Club of Belmont and the Australian Rotary Health Research fund for the opportunity to pursue my PhD with the scholarship they provided. The Rotary Club of Belmont in particular have always been extremely welcoming and supportive of me, so I would like to express my deepest thank you to them all again.

FINANCIAL SUPPORT

Sebastian Öther-Gee Pohl is supported by a “Researching Cancer” partner scholarship from the Australian Rotary Health Research Fund (ARHF), The Rotary Club of Belmont and Curtin University School of Biomedical Sciences. Additional funds from the Australian Government Research Training Program Scholarship were made available for the duration of the Doctor of Philosophy (PhD).

TABLE OF CONTENTS

TABLE OF FIGURES

CHAPTER 1

CHAPTER 3

CHAPTER 4

CHAPTER 5

LIST OF TABLES

CHAPTER 1

CHAPTER 2

LIST OF ABBREVIATIONS

7AAD - 7-aminoactinomycin D

7TM - Seven-transmembrane

ANOVA - analysis of variance

ANT - Adenine nucleotide translocase

APCDD1 - Adenomatosis polyposis coli down-regulated 1

AR - Androgen receptors

ATP - Adenosine triphosphate

ATP5γ1 - ATP synthase subunit 5γ1

Bcl-2 - B-cell lymphoma-2

bFGF - Basic fibroblast growth factor

BL2 - Basal-like 2

BL1 - Basal-like 1

BLIA - Basal-like immune-activated

BLIS - Basal-like immune-suppressed

CaMKII - Calcium/calmodulin-dependent protein kinase II

CDH1 - Cadherin-1

ChIP - Chromatin immunoprecipitation

CM-H_2DCFDA - Chloromethyl-2',7'-dichlorodihydrofluorescein

CRD - Cysteine-rich domain

ctDDX20 - Control siRNA

DAAM1 - Dishevelled-associated activator of morphogenesis 1

DDXs - DEAD-Box helicases

DISC - Death initiating signalling complex

DKK2 - Dickkopf Wnt signalling pathway inhibitor 1-3

DMEM - Dulbecco's modified eagle medium

Dmnt1 - DNA methyltransferase 1

DMSO - Dimethyl sulphoxide

dnTCF4 - Dominant-negative TCF4

DRP1 - Dynamin-1-like protein

dsRNA - Double-stranded RNA

DTT - Dithiothreitol

EBNA3C - Epstein-Barr virus encoded nuclear antigen 3C

ECAR - Extracellular acidification rate

ECL - Electrogenerated chemiluminescence

EDTA - Ethylenediaminetetraacetic acid

EGF - Epidermal growth factor

EGFR - Epidermal growth factor receptor

Egr2 - Early growth response protein 2

EMT - Epithelial-mesenchymal transition

ER - Oestrogen receptor

ERBB2/HER2 - Human epidermal growth receptor 2

ESC - Embryonic stem cells

ETC - Electron transport chain

FACS - Fluorescence activated cell sorting

FBS - Foetal bovine serum

FOXL2 - Forkhead box protein L2

FOXO – Forkhead box proteins

FZD1-10 – Frizzled receptors 1-10

GAPDH – Glyceraldehyde 3-phosphate dehydrogenase

GFP - Green fluorescence protein

GPCR - G protein-coupled receptors

GSH - Reduced glutathione

GSSG - Oxidised glutathione

GTPase - Guanosine trisphosphatase

H_2O_2 - Hydrogen peroxide

HDACi - Histone deacetylase inhibitors

HO• - Hydroxyl radical

HSCs - Haematopoietic stem cells

IGFBP4 - Insulin-like growth factor binding protein 4

IKK2 - NF-κB-activating IκB kinase 2

IM – Immunomodulatory

JACoP - Just Another Colocalization Plugin

LiCl - Lithium chloride

MAPK - Mitogen activated protein kinase

MES - Mesenchymal

MET - Mesenchymal-to-epithelial-like transition

mitoROS - Mitochondrial ROS

MMP2 - Metalloproteinase-2

mtDNA – Mitochondrial DNA

MuSK - Skeletal muscle receptor tyrosine-protein kinase

NAFLD - Non-alcoholic fatty liver disease

NF-κB - Nuclear factor kappa-light-chain-enhancer of activated B cells

NLD - Netrin-like domain

NLK - Nemo-like kinase

NOX - NADPH oxidase

NS - Neural stem cells

O_2^- - Superoxide anion

OCR - Oxygen consumption rate

$ONOO^-$ - Peroxynitrite

OXPHOS - Oxidative phosphorylation

PARP - Poly (ADP-ribose) polymerase

PARPi - PARP inhibitors

PBS - Phosphate buffered saline

PCP pathway – Planar cell polarity pathway

PEDF - Pigment Epithelial-derived Factor

PI - Propidium iodide

PIK3CA – Phosphatidylinositol 4,5-bisphosphate 2-kinase catalytic subunit alpha

PIPES - Piperazine-N, N'-bis

PKC - Protein kinase C

PP2A - Protein phosphatase 2

PR - Progesterone receptor

PTEN - Phosphotase and tensin homolog

RecA - Recombinase A

RIPA - Radioimmunoprecipitation assay

RISC - RNA induced silencing complex

RNA - Ribonucleic acid

RNAi - RNA interference

RNF43 - Ring finger protein 43

RO• - Alkoxyl radical

ROCK - Rho-associated kinase

ROO• - Peroxyl radical

ROS - Reactive oxygen species

rRNAs - Ribosomal RNA

RTKs - Receptor tyrosine kinases

SD - Standard deviation

SF-1 - Steroidogenic factor 1

SFRP1-5 - Secreted-frizzled related protein 1-5

shRNA - Short hairpin RNA

siRNA - Small interfering ribonucleic acid

Smo - Smoothened receptor

SNAI2 - Zinc finger protein SNAI2

snRNPs - Small ribonucleoprotein

SOD2 - Superoxide dismutase 2

STAT - Signal transducer and activator of transcription

SUMO - Small ubiquitin-like modifier

TAK1 - TGF-β-activated kinase 1

TBS - Tris-buffered saline

TCF4 - Transcription factor 7-like 2

TNBC - Triple-negative breast cancer

TNKS1/2 - Tankyrase-1/2

tRNAs - Transfer ribonucleic acids

TWIST - Twist-related protein 1

UCPs - Uncoupling proteins

UQCRC2 - Ubiquinol-Cytochrome C reductase Core protein 2

VTCN1 - T-cell activation inhibitor

Wg - Wingless

WIF - Wnt inhibitory factors

ABSTRACT

Breast cancer is the most common cause of malignancy affecting women worldwide. The complexity of breast cancer is reflected in the different classification of molecular subtypes. Included in these subtypes is triple-negative breast cancer (TNBC), or basal-like breast cancer. Occurring in approximately 15-20% of all breast cancer cases, TNBC is characterised by the lack of expression of oestrogen receptor (ER) and progesterone (PR), and the low expression of the human epidermal growth factor receptor (HER2). This phenotype precludes the use of therapies such as tamoxifen and trastuzumab that target these receptors. Due to the lack of specific treatment options, TNBC has a poorer patient prognosis and is associated with increased metastasis and recurrence.

The Wnt/β-catenin signalling pathway is an evolutionarily conserved pathway that regulates many aspects of cell fate and is a hallmark of many cancers. The canonical Wnt signalling pathway involves binding of Wnt ligands to Frizzled receptors and LRP5/6 co-receptors to initiate destabilisation of the β-catenin destruction complex. This results in nuclear translocation of β-catenin where it binds to TCF/LEF transcription factors which regulate the transcription of Wnt target genes. TNBC features increased Wnt signalling activity compared to other subtypes of breast cancer. Similar to the increased Wnt signalling observed in TNBC, the RNA helicase DDX20 (Gemin3, DP103) has also been identified to be critical in the progression and aggressive nature of the disease. Importantly, DDX20 has been found to be overexpressed in the same subset of basal-like breast cancers that also display the most active Wnt signalling, suggesting a potential role for DDX20 in modulating Wnt signalling.

This thesis focusses on the role of DDX20 in regulating Wnt/β-catenin signalling and its impact on cell fate in TNBC.

A novel mechanism of DDX20 regulation of Wnt/β-catenin signalling was identified, as well as a previously unknown role for Wnt/β-catenin signalling in

the regulation of cellular redox and mitochondrial function. The loss of DDX20 in TNBC results in increased ROS production and oxidative stress through differential regulation of two major redox regulators, catalase and MnSOD. The loss of DDX20 also causes mitochondrial dysfunction and impaired cellular respiration, via downregulation of mitochondrial complex III in a Wnt3a/β-catenin/TCF4-dependent signalling cascade.

The role of DDX20 in cancer stem cells (CSCs) isolated from the MDA-MB-231and BT549 cell lines was elucidated. Consistent with the parental cell lines, DDX20 was shown to be an essential regulator of Wnt/β-catenin signalling. The results indicated that DDX20 is overexpressed in CSCs when compared to the parental cell lines and the loss of DDX20 results in cell death and loss of spheroid formation. Stemness and drug resistance associated with CSCs were abolished when DDX20 is silenced. DDX20 drives a positive feedback loop wherein it promotes its increased transcriptional regulation by TCF4 to drive the aggressiveness displayed in TNBC through Wnt/β-catenin signalling.

Overall, this study has demonstrated a novel regulatory mechanism of DDX20-dependent Wnt/β-catenin signalling in TNBC through cellular redox. This study implicates that canonical Wnt signalling has a novel role in maintaining cellular redox and mitochondrial homeostasis. The implications for Wnt regulation of mitochondrial function and reactive oxygen species may be applicable to other cancer cell types. This non-canonical function of DDX20 may represent a valuable therapeutic target and biomarker in TNBC.

DECLARATION FOR CONTRIBUTIONS FOR CHAPTER 1

Declaration by candidate

In the case of Chapter 1 there are contributions from previously published works where I was the first author and are included as part of the literature review. The articles from which some of this chapter is partly made up include:

- Pohl *et al*, Wnt signaling in triple-negative breast cancer, *Oncogenesis*
- Pohl *et al*, Crosstalk between cellular redox state and the anti-apoptotic protein Bcl-2, *Antioxidants and Redox Signalling.*

The nature and extent of my contribution to the work was the following:

NATURE OF CONTRIBUTION	CONTRIBUTION (%)
LITERATURE REVIEW, MANUSCRIPT PREPARATION	70

The following co-authors contributed to the work:

NAME	NATURE OF CONTRIBUTION	CONTRIBUTION (%)
NAOMI BROOK	Literature review, input manuscript preparation	5
FRANK ARFUSO	Literature review, input manuscript preparation	5
ALAN PREM KUMAR	Literature review, input manuscript preparation	5
MARK AGOSTINO	Literature review, input manuscript preparation	5
SHAZIB PERVAIZ	Literature review, input manuscript preparation	5
ARUN DHARMARAJAN	Literature review, input manuscript preparation	5

Signed: …….

Date:

21.06.2018

Declaration by co-authors

The undersigned hereby certify that:

1. The above declaration correctly reflects the nature and extent of the candidate's contribution to this work, and the nature of each of the co-authors.
2. They meet the criteria for authorship in that they have participated in the conception, execution, or interpretation, of at least that part of the publication in their field of expertise;
3. They take public responsibility for their part of the publication, except for the responsible author who accepts overall responsibility for the publication;

4. There are no other authors of the publication according to these criteria;
5. Potential conflicts of interest have been disclosed to (a) granting bodies (b) the editor or publisher of journals or other publications and (c) the head of the responsible academic unit; and
6. The original data are stored at the following locations(s) and will be held for at least five years from the date indicated below:

Location of data storage: Stem Cell and Cancer Biology, Curtin Health and Innovation Research Institute, B305, Kent St, Bentley, W.A, 6102, Australia.

Signed:  **Date:** 20.06.2018

Naomi Brook

Signed: 

Date: 19.06.2018

Frank Arfuso

Signed:  **Date:** 19.06.2018

Alan Prem Kumar

Signed:  **Date:** 19.06.2018

Mark Agostino

Signed: 

Date: 19.06.2018

Shazib Pervaiz

Signed: 

Date: 19.06.2018

Arun Dharmarajan

CHAPTER 1: LITERATURE REVIEW

1.1 INTRODUCTION

Breast cancer represents one of the most significant disease burdens of any cancer worldwide. Today, women have a one in eight chance of developing breast cancer over their lifetime, a risk that is significantly increased if they have inherited harmful mutations in *BRCA1* or *BRCA2.*[1] However, breast cancer is a complex, heterogeneous disease characterized by a great multitude of aberrations at the genomic and molecular level, which can manifest in dysregulated signalling pathways.

Triple-negative breast cancer (TNBC), an aggressive subtype of breast cancer with a poor prognosis,[2] is characterized by tumours that do not express oestrogen receptors (ERs) or progesterone receptors (PRs), nor display an overexpression of human epidermal growth factor receptor 2 (HER2).[3] Therapies targeted against HER2-positive breast cancers, such as trastuzumab (Herceptin)[4], and those targeted against ER-positive breast cancers, such as tamoxifen,[5] have no therapeutic benefit to individuals with the TNBC subtype. Surgical intervention and chemotherapy have been the major treatment avenues for TNBC; however, recently developed small molecules and immunotherapeutics[6] are showing promise.[7] A hallmark of many cancers is aberrant regulation of the Wnt signalling pathway and oxidative stress, and breast cancer is no exception.[8]

1.2 TNBC SUBTYPES

Breast cancer is a diverse and complex disease, broadly characterized by four molecularly distinct subtypes including luminal A, luminal B, HER2-overexpressed, and TNBC.[9] The luminal A subtype is characterized as ER/PR positive and HER2 negative, expressing Bcl-2, cytokeratin 8/18, and low Ki67.[10] Luminal B subtypes are more aggressive ER^+ breast tumours, characterized as $HER2^-$ with high Ki67, or $HER2^+$, PR^-, and ER^+,[11] with cyclin B1 overexpression.[12] The HER2 subtype is characterized by amplification of the ERBB2/HER2 gene.[13]

TNBC, including basal-like and claudin-low subtypes, accounts for 10-20% of breast cancers and is characterized by a lack of PR, ER, and HER2 overexpression.[14] TNBC patients present with higher incidence of distant disease recurrence within 3 years of diagnosis, with a high frequency of visceral metastases.[15] The prognosis for patients diagnosed with TNBC is poor, with patients who respond poorly to adjuvant treatment exhibiting worse outcomes.[3]

TNBC has been categorized into a number of distinct molecular subtypes; however, there remains much intertumoural mutational and transcriptional heterogeneity within these subtypes. The molecular heterogeneity of TNBC confounds the clinical approach to TNBC treatment.[16] TNBCs are characterized by high clonal frequencies of single gene mutations in key tumorigenesis driver genes, including *p53*, *PIK3CA*, and *PTEN*, indicating that clonal evolution of these mutated genes is an early event in TNBC development.[16] However, mutation frequencies within these genes are not uniform amongst TNBC cases.[16,17]

Lehmann *et al*.[18] determined the gene expression signatures in 587 TNBC cases from 21 breast cancer datasets, and identified six molecularly distinct TNBC subtypes. These include basal-like 1 (BL1), basal-like 2 (BL2), immunomodulatory (IM), mesenchymal (M), mesenchymal stem-like (MSL), and luminal androgen receptor (LAR). These subtypes, various gene ontology pathways, and associated Wnt genes are described in Table 1. Recent RNA profiling performed by Burstein *et a*l.[19] showed overlap of LAR and MES subtypes based on Lehmann's gene expression profiling, but was unable to reproduce all observations.[19] The findings of both these studies indicate the presence of at least four molecularly distinct and stable TNBC subtypes, defined as luminal androgen receptor (LAR), mesenchymal (MES), basal-like immune-suppressed (BLIS), and basal-like immune-activated (BLIA).[19] Furthermore, these studies suggest molecular targets for the development of therapeutics specific to the treatment of TNBC.

1.2.1 LAR subtype

The LAR subtype accounts for approximately 10% of TNBCs, whereby tumour cells exhibit positive staining of androgen receptors (ARs) and are driven by AR signalling.[14,18] There is some discordance within the literature in regards to the prognostic utility of AR status, with studies indicating no significant effect on survival rates associated with AR expression[20], although AR^+ TNBC individuals have been shown to have a positive clinical response to the nonsteroidal antiandrogen, bilcautamide.[21,22] In a study designed to test the benefit of tamoxifen on ER^- and TNBC patients, it was found that expression of AR^+ versus AR^- individuals predicted a decreased recurrence rate and treatment benefit with AR^+ patients;[23] this is a result of tamoxifen exhibiting agonist activity on AR expressing cells.[24]

1.2.2 MES subtype

The MES subtype, encompassing Lehmann's mesenchymal (M) and mesenchymal stem-like (MSL) and claudin-low subtypes, is characterized by the overexpression of genes associated with cellular motility, proliferation, and growth signalling pathways.[18,19] MES subtypes have high expression of platelet derived growth factor, insulin-like growth factor 1, and c-kit.[19] MES tumours express mesenchymal stem cell markers, including the breast stem cell marker ALDH1A1, and are enriched in genes associated with epithelial-mesenchymal transition (EMT) and other stem-like properties.[18,25] Within Lehmann's M and MSL subtype, there are a number of enriched genes associated with EMT that are also modulated by Wnt signalling, including metalloproteinase-2 (*MMP2*), *Twist-related protein 1* (*TWIST*), *Zinc finger protein SNAI2* (*SNAI2*), and Transcription factor 7-like 2 (*TCF4*).[26] A gene set involved in Wnt/β-catenin signalling in the M and MSL subtypes, including β-catenin (*CTNNB1*), *Dickkopf-related protein 2* (*DKK2*), *Dickkopf-related protein 3* (*DKK3*), Secreted-frizzled related protein 4 (*SFRP4*), *TCF7L2*, and Frizzled-4 (*FZD4*), was also found to be enriched.[18] MES tumours are associated with a poorer distant metastasis-free survival at five years compared to other subtypes, likely associated with increased expression of cellular motility genes leading to increased metastasis.[18]

1.2.3 BLIS subtype

BLIS is characterized as an immune-suppressed TNBC subtype with downregulated immune signalling pathways and reduced expression of immune function genes.[19,27] BLIS tumours exhibit enhanced expression of mitotic and cell cycle pathway genes, with overexpression of proliferative genes, including *CENPF*, *BUB1*, and *PRC1,*[27] Sry-related HMG box (SOX) transcription factors, and the immune-regulatory molecule V-domain-containing T-cell activation inhibitor (VTCN1).[19] Survival analysis shows that patients with the BLIS subtype TNBC experience lower rates of recurrence-free survival compared to other TNBC subtypes.[27]

1.2.4 BLIA subtype

The BLIA subtype is characterized by upregulation of immune activating pathways, with overexpression of signal transducer and activator of transcription (STAT) transcription factors and cytotoxic T-lymphocyte-associated protein 4.[19] BLIA tumours have increased levels of lymphocytic infiltration and are thus associated with improved disease-free survival rates and patient outcomes compared to other TNBC subtypes, although still associated with a relatively high risk of recurrence (~20%).[19,28]

1.3 WNT SIGNALLING

1.3.1 Wnt signalling pathways

1.3.1.1 WNT/β-catenin pathway (Canonical pathway)

There are currently two models of canonical Wnt/β-catenin signalling. In the classical model, the destruction complex remains intact in the absence of Wnt stimulation (Figure 1A). Casein kinase 1 (CK1) primes β-catenin for destruction by phosphorylating Ser45, which then allows activated Glycogen synthase kinase 3 (GSK3) to phosphorylate β-catenin at Ser33, Ser37, and Thr41.[29] The phosphorylated residues of β-catenin interact with the β-propeller domain of the E3 ubiquitin ligase β-TrCP, which then ubiquitinates β-catenin, thus targeting it for proteosomal degradation.[30] Wnt/β-catenin signalling is initiated by Wnt ligands binding to a Frizzled receptor (FZD), as

well as the co-receptors low density lipoproteins 5/6 (LRP5/6). This results in activation of FZD, permitting binding of Dishevelled (Dvl)[31] and phosphorylation of one or more cytoplasmic motifs of LRP5/6. A single phosphorylated motif is sufficient to activate Wnt signalling.[32] Phosphorylated LRP5/6 can then interact with Axin. This interaction destabilizes the β-catenin destruction complex, which requires Axin as a scaffold and contains Dvl, the serine-threonine kinases casein kinase 1α/β (CK1), glycogen synthase kinase 3α/β (GSK3), and adenomatous polyposis coli (APC).[33] Destabilizing the destruction complex prevents phosphorylation of β-catenin, which then accumulates in the cytosol before translocating to the nucleus. Once there, it binds to Transcription factor/lymphoid enhancer-binding factor (TCF/LEF) transcription factors and displaces transcriptional repressor Groucho to initiate the transcription of Wnt target genes (Figure 1B).[34]
In the new model,[35-37] the destruction complex is stabilized by Axin in both the presence and absence (Figure 1C) of Wnt activation, and β-catenin is degraded through phosphorylation-mediated recognition by β-TrCP in the intact complex. This allows newly synthesized β-catenin to accumulate in the cytosol before nuclear translocation (Figure 1D). This was demonstrated through co-immunoprecipitation, whereby β-catenin phosphorylated at Ser33/Ser37/Thr41 was shown to interact with the destruction complex upon Wnt activation, which also disrupted the interaction of β-TrCP with the Axin1-β-catenin complex.[36] It has also been proposed that GSK3 inhibition, and thus β-catenin translocation after Wnt activation, is mediated through the sequestration of GSK3 inside multivesicular endosomes.[38] This further demonstrates the complexity of Wnt signalling.

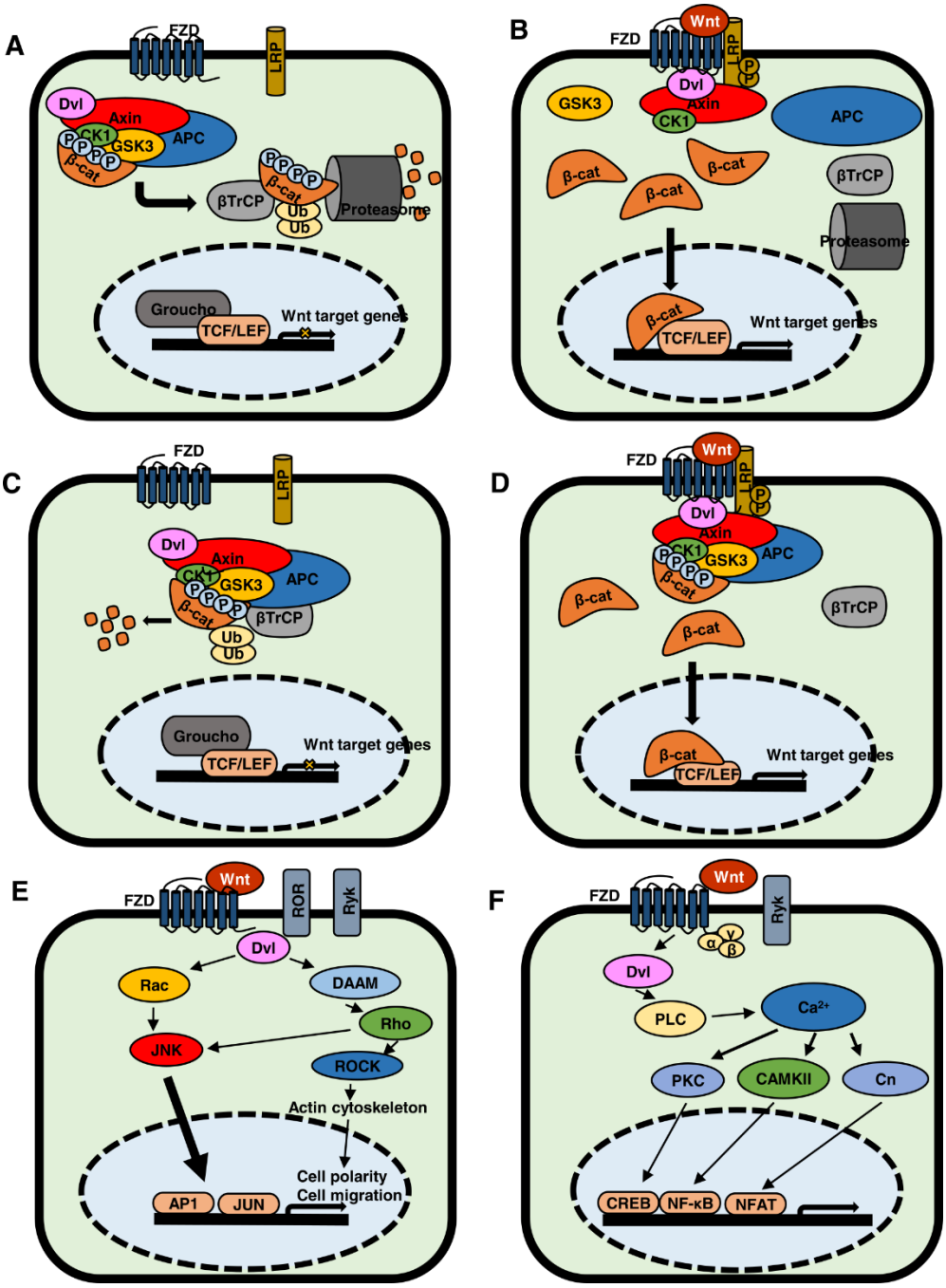

Figure 1.1. Classical and new Wnt/β-catenin canonical and non-canonical pathways. A. Overview of the 'classical' model of Wnt/β-catenin signalling in OFF state with no ligand bound to FZD receptor B. Overview of the 'classical' model of Wnt/β-catenin signalling pathway in the ON state where Wnt ligand is bound to FZD receptor. C. Overview of the 'new' model of Wnt/β-catenin signalling in ON state with Wnt ligand bound to FZD receptor. D. Overview of 'new' model of Wnt/β-catenin signalling in OFF state with no ligand bound to FZD receptor. E. Overview of Wnt planar cell polarity pathway (PCP) in ON state. Wnt binds multiple receptors including FZD and co-receptors ROR and Ryk. This activates Rho and Rac, which activate ROCK and JNK respectively, leading to actin polymerization and regulation of cytoskeletal arrangements. F. Overview of Wnt/Ca^{2+} pathway in the ON state. Wnt is able to bind FZD, Ryk to initiate signal transduction which is effected through Dvl and G-proteins (α, β, γ). Gene transcription is induced through proteins PKC, CaMKII, and Cn (Calcineurin) activating transcription factors.

1.3.1.2 Planar cell polarity (PCP) pathway

The PCP pathway (Figure 1E) is a non-canonical, β-catenin independent pathway that regulates cellular organisation and polarity, partly through cytoskeletal organisation.[39] Wnt ligands, such as Wnt5a, bind to FZD receptors and co-receptors, including ROR, [40] Ryk,[41] and PTK.[42] Dvl interacts with Rac1[43] and Dishevelled-associated activator of morphogenesis 1 (DAAM1). Rac1 activates c-Jun N-terminal kinase (JNK), leading to actin polymerization,[43] while DAAM1 activates Rho, which in turn activates Rho-associated kinase (ROCK) to regulate cellular cytoskeletal arrangements.[44]

1.3.1.3 WNT/Ca^{2+} pathway

The Wnt/Ca^{2+} pathway (Figure 1F) is activated through Wnt binding to FZD, which interacts with G proteins and Dvl.[45] These interactions can activate cGMP-specific phosphodiesterase or phospholipase C, resulting in a release of intracellular calcium. This results in the activation of downstream signalling proteins, Protein kinase C (PKC), calcineurin, and Calcium/calmodulin-dependent protein kinase II (CaMKII).[46] CaMKII activates nuclear factor of activated T-cells (NFAT), which can regulate cell adhesion and migration.[47] Wnt5a induces activation of CaMKII-dependent Wnt/Ca^{2+} signalling. CaMKII phosphorylates transforming growth factor β-activated kinase (TAK1), which activates Nemo-like kinase (NLK).[48] This cascade antagonizes canonical Wnt/β-catenin signalling by NLK phosphorylation of TCF4 and prevents the β-catenin-TCF4 complex from binding to DNA.[49]

1.3.2 WNT SIGNALLING COMPONENTS

1.3.2.1 WNT ligands

To date, 19 members of the Wnt family have been identified in mammals, all ranging between 350-400 amino acids in length and characterized by a conserved fold containing a conserved motif of 24 cysteine residues (Figure 2A).[50] Wnt ligands are modified by lipidation, specifically, the addition of a palmitoleyl group to a conserved serine by the membrane bound *O*-acyltransferase Porcupine (PORCN).[51] Wnt lipidation is crucial for secretion from the endoplasmic reticulum [52] and essential for Wnt function. Wnt

lipidation was initially suggested to occur at Cys77 of Wnt3a (cysteine 3 of the Wnt fold);[53] however, lipidation at this cysteine has been conclusively disproven by crystallographic,[54] mutational, [52] and imaging studies.[51]

1.3.2.2 Frizzled (FZD) receptors

FZD receptors are a group of ten membrane proteins featuring an extracellular cysteine-rich domain (CRD) and a seven-transmembrane (7TM) domain.[55] Along with the Smoothened receptor (Smo), the FZDs comprise the family of Class F G protein-coupled receptors (GPCRs). The crystal structure of XWnt8 in complex with the mouse FZD8 CRD[54] revealed an unusual interaction involving the direct binding of the Wnt lipid to a binding site on one side of the CRD (the "thumb" region), as well as the binding of the region from cysteines 19-22 of XWnt8 to the other side of the CRD (the "index finger" region) (Figure 2A).[56] Although no complete structures are available for any FZD, several structures of Smo are known,[57-59] most recently including both the CRD and 7TM regions (Figure 2B),[60] which are suggestive of the likely structure of FZD.

1.3.2.3 Disheveled (DVL)

Three Dvl homologues are known (Dvl1/2/3), sharing high overall sequence similarity.[61] Dvl consists of three structurally-defined domains: the DIX, PDZ, and DEP domains. These three domains are separated by large insertions of unknown structure (Figure 2C); however, some functional significance has been ascribed to conserved sequences within the unstructured regions.[62]

Dvl polymerizes via the head-to-tail interaction of its DIX domain (Figure 2D). The DIX domain also mediates interaction with Axin.[63] Mutations (V67A, K68A, Y27D) in the polymerization interface of the DIX domain strongly suppress Wnt signalling.[64] The PDZ domain of Dvl (Figure 2E) interacts with a conserved motif in the FZD C-terminal (KTxxxW).[45] The PDZ-FZD interaction is relatively weak, and is likely supplanted by interactions of the DEP domain with FZD. Greater insight in the role of the DEP domain in Wnt signalling was recently revealed, with this domain shown to bind as a monomer to FZD, then undergo subsequent domain swapping to assemble

Wnt signalosomes. Furthermore, upon Wnt stimulation, DEP domain swapping initiates DIX-dependent Dvl and Axin polymerization, leading to the inhibition of GSK3 and Wnt signal transduction. Mutants (E499G, D460K, G436P, K438M, D449I, and D452I) in the DEP domain strongly diminish Wnt signalling upon Wnt stimulation (Figure 2F)[65,66]. Dvl has also been shown to promote ubiquitination-mediated FZD degradation by RNF43.[67] This finding suggests a dual agonist/antagonist role for Dvl in Wnt signalling.

1.3.2.4 Low density lipoprotein receptor 5/6 (LRP5/6)

The extracellular domain of LRPs consists of 4 β-propeller repeats interspersed with epidermal growth factor (EGF) repeats, followed by three LRP type A repeats (Figure 2G).[31] The majority of Wnts bind to the first β-propeller/EGF repeat (P1E1-P2E2), although Wnt3 and 3a preferentially bind to the second repeat (P3E3-P3E4).[68] Wnt3 and Wnt3a binding to LRPs is competitively inhibited by Dickkopf (Dkk) binding to LRP (Figure 2H).[69-71] The intracellular action of LRP5/6 is less clearly understood, although it is known that Wnt activation initiates phosphorylation of the intracellular PPPSPxP motifs of LRP5/6 by GSK3 and CK1, allowing the recruitment of Axin.[72] Importantly, it has also been shown that without the FZD-Dvl interaction, Wnt is unable to induce phosphorylation of LRP6, reinforcing the complex interplay of proteins involved in Wnt signalling.[45,72]

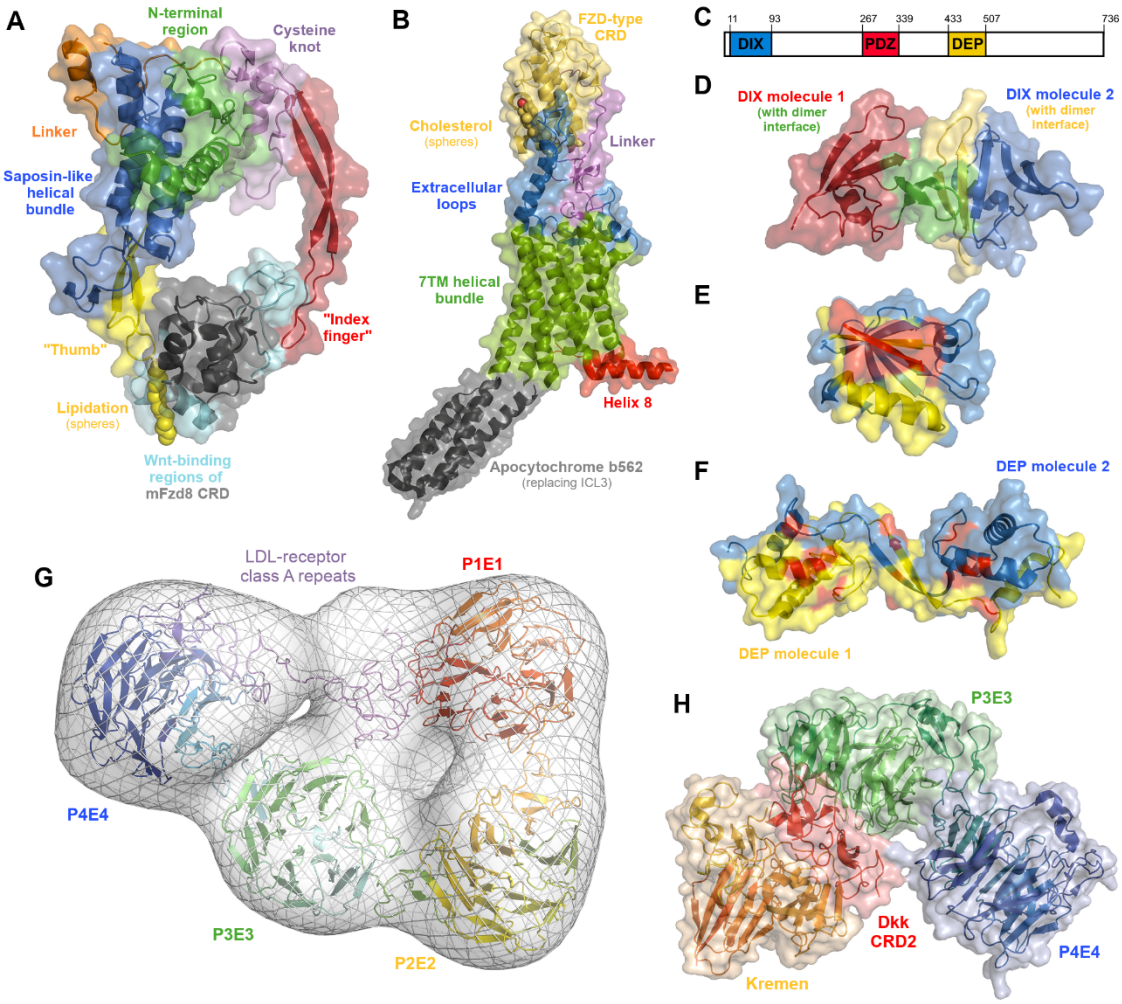

Figure 1.2. Molecular structures of key Wnt signalling proteins and interactions. A. X-ray crystal structure of the *Xenopus* Wnt8 complex with the mouse FZD8 cysteine-rich domain (PDB 4F0A). Key structural regions of the Wnt fold are highlighted, as are the major Wnt-interacting regions of the CRD. B. X-ray crystal structure the Smoothened receptor (PDB 5L7D), a Class F G protein-coupled receptor, related to FZD. Key structural regions of Smo are highlighted, as well as helix 8, which is of relevance for Dishevelled binding by FZD. C. Schematic representation of the location of the DIX, PDZ, and DEP domains within Dvl. D. X-ray crystal structure of the DIX homodimer (PDB 4WIP). E. X-ray crystal structure of the PDZ domain bound to a peptide (red) (PDB 3CBX). The peptide-binding site is shown in yellow. F. X-ray crystal structure of a DEP homodimer (PDB 5LNP), highlighting residues known to affect Wnt signalling (shown in red). G. Model of the LRP6 ectodomain generated by molecular dynamics flexible fitting of the crystal structures of the P1E1-P2E2 domains (PDB 3S94) and P3E3-P4E4 domains (PDB 4A0P), and a homology model of the LDL-R type A domains (generated in Prime, based on the crystal structure of the LDL receptor ectodomain (PDB 1N7D)) to the electron microscopy structure (EMDatabank accession 1964). Gaps in the crystal structures and between the various components modelled using Prime. H. X-ray crystal structure complex of the cysteine-rich domain 2 of Dickkopf with Kremen and the LRP6 P3E4-P4E4 domains (PDB 5FWW) Figures from Pohl *et al*, 2017.[7]

1.3.2.5 ROR-Family receptor tyrosine kinases (RTKs)

The ROR-family of receptor tyrosine kinases (RTKs) consists of two evolutionarily conserved members, ROR1 and ROR2.[73] The ROR

ectodomains feature a FZD-type CRD most closely related to that of the skeletal muscle receptor tyrosine-protein kinase (MuSK)[74]. ROR2 is involved in Wnt5a-mediated signalling; Wnt5a binding to ROR2 initiates ROR2 homodimerization, stimulating autophosphorylation at Tyr646. [75] It has been demonstrated that Wnt5a and Wnt3a both bind to ROR2; however, only Wnt5a is able to initiate the activation of the ROR2 signalling cascade.[76] Recently, high expression of ROR1 has been demonstrated in TNBC cell lines, where it interacts with CK1ε to promote tumour survival and growth after stimulation with Wnt5a to activate phosphoinositide 3-kinase (PI3K)/AKT signalling.[77]

1.3.3 WNT ANTAGONISM AND SECRETED FRIZZLED-RELATED PROTEINS

There are two classes of antagonists that inhibit canonical and/or non-canonical Wnt signalling. The first class are secreted factors that can bind to either the Wnt ligands or FZD receptors. Included in this class are the secreted frizzled-related proteins (SFRPs), Wnt inhibitory factors (WIFs), Cerberus, and soluble Adenomatosis polyposis coli down-regulated 1 (APCDD1) [78]. The second class of Wnt antagonists can bind to LRP5/6 co-receptors, such as Dkk, Wise/SOST, and Insulin-like growth factor binding protein 4 (IGFBP4).[78] A subclass of Wnt signalling negative regulators includes the membrane bound proteins RNF43/ZNRF3 and Tiki. RNF43/ZNF3 are E3 ubiquitin ligases that downregulate FZD receptors through ubiquitin-mediated endocytosis in a Dvl-dependent manner.[67,79] Furthermore, RNF43/ZNRF3 have been demonstrated to be direct targets of TCF4 transcription, suggesting an evolutionarily conserved mechanism to regulate turnover of FZD receptors and thereby mediate Wnt signalling.[80] Tiki, a recently discovered Wnt signalling antagonist, proteolytically cleaves Wnt ligands, resulting in reduced receptor binding.[81]

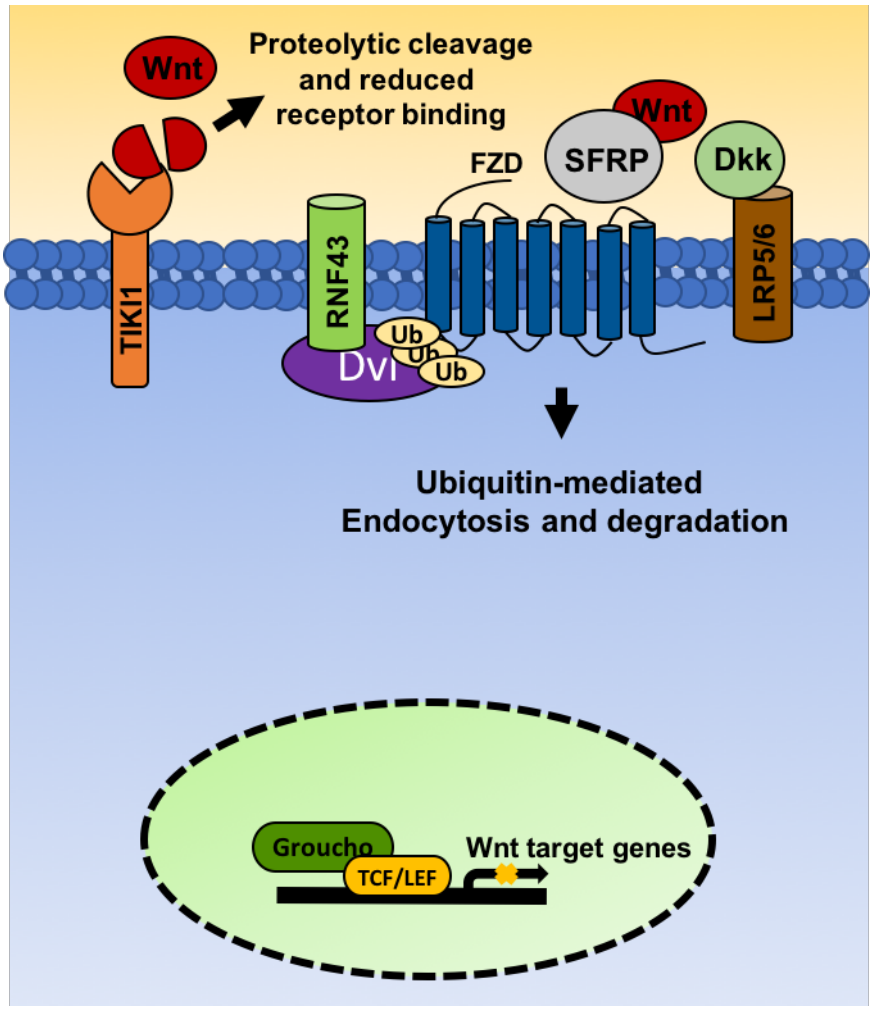

Figure 1.3. Model of Wnt signalling antagonism. Wnt signalling antagonism can occur through proteolytic cleavage of Wnt ligands mediated by TIKI1, RNF43 dependent ubiquitin-mediated Frizzled receptor endocytosis and degradation, and Wnt ligand antagonism through SFRPs inhibiting Wnt binding to Fzd, and Dkk inhibiting Wnt binding to LRPs. This can result in a decrease in signal transduction in both canonical and non-canonical Wnt signalling.

1.3.3.1 Secreted Frizzled Related Proteins (SFRPs)

Secreted frizzled-related proteins (SFRP1–5) are a family of secreted glycoproteins that classically act as antagonists of Wnt ligands.[82] Structurally, SFRPs consist of two ordered domains, an N-terminal cysteine-rich domain (CRD) and a C-terminal netrin-like domain (NLD); the structure of a *Xenopus* analogue, Sizzled, was recently revealed (Figure 4). Wnt antagonism has been reported to be mediated through the CRD[78], although SFRP1 has been

demonstrated to bind to the Wnt Drosophila orthologue Wingless (Wg) in a CRD-independent manner[83]. SFRPs have also been demonstrated to bind to numerous proteins involved in other signalling pathways, including integrins [84,85] and epidermal growth factor (EGF).[86]

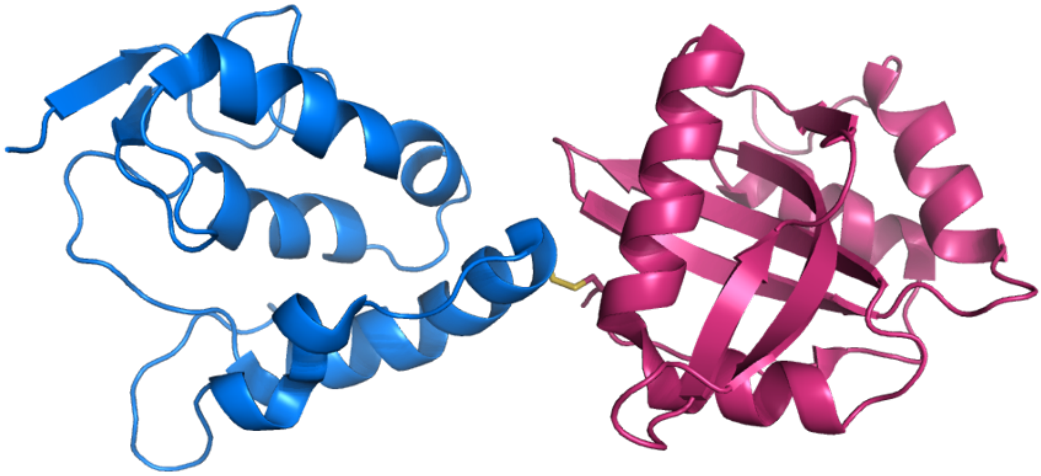

Figure 1.4. Structure of *Xenopus* Sizzled. Ribbon model of *Xenopus* Sizzled including the cysteine-rich domain (blue) and netrin-like domain (pink) with inter-domain linker (residues 143-154). (PDB 5XGP)

1.3.3.2 Secreted Frizzled-Related Protein 4 (SFRP4)

The SFRP4 gene is located on the short arm of chromosome 7 (7p14.1) and codes for a 346 amino acid protein with a molecular weight of 39.9kDa.[78] SFRP4 (formerly DDC-4) was originally discovered through differential display in the mammary gland and corpus luteum undergoing apoptosis and has been implicated in various diseases, including cancer and diabetes.[87,88] Hypermethylation of the promoter region of the SFRP4 gene in cancerous tissue has been linked to its downregulation and the subsequent progression of carcinogenesis, presumably through increased Wnt signalling.[89] The exogenous addition of SFRP4 to cancer cells with demonstrated SFRP4 gene downregulation has shown its pro-apoptotic and anti-angiogenic role.[90] Recently, in studies of glioblastoma multiforme (GBM), ovarian, head and neck, prostate, and breast cancer stem cells, the addition of SFRP4 has

been shown to induce mitochondrial outer membrane permeability (MOMP)-mediated apoptosis.[91-93] Furthermore, the addition of SFRP4 in the same cells has a demonstrated additive effect on their response to first-line chemotherapeutics.[91] The role of SFRP4 in inducing apoptosis and antagonising the canonical and non-canonical Wnt signalling pathways has led to its interest as a potential therapeutic option and a lead molecule for pharmaceutical development.

1.3.4 WNT DYSREGULATION IN TNBC AND TNBC STEM CELLS

Aberrant Wnt signalling is a characteristic of TNBC, with both canonical and non-canonical pathways implicated in TNBC tumorigenesis[94,95] and metastasis.[96] Enrichment of Wnt/β-catenin signalling is evident in TNBC and is associated with poor clinical outcomes within this subtype.[97,98] TNBC patients displaying dysregulated Wnt/β-catenin signalling are more likely to develop lung and brain secondary metastases.[96] Studies have shown that nuclear accumulation of β-catenin promotes cell migration, colony formation, stem-like features, and chemoresistance of TNBC cells *in vitro*, and TNBC tumorigenesis in mouse cancer models; thus suggesting that canonical Wnt signalling is a major driving force of TNBC tumorigenesis.[94] Although the Wnt/β-catenin pathway is associated with the clinicopathological features of TNBC, this is not due to *CTNBB1* mutations.[98] Studies have also implicated dysregulation of non-canonical Wnt signalling pathways in the highly metastatic behaviour of TNBC cells and cancer stem cells, specifically through aberrant JNK activation.[99]

Cancer stem cells (CSCs), or cancer stem-like cells, are a small subset of cells within the heterogeneous tumour bulk that are thought to be responsible for tumour initiation.[100] These cells also have intrinsic mechanisms for chemoresistance, such as upregulation of drug transporters, including the breast cancer resistance protein (also known as ABCG2).[101] By evading the standard chemotherapeutic treatments, it is thought the CSCs are also responsible for the relapse experienced in many cancers, especially TNBCs.[102] Studies have also shown that these cells are a main contributor to metastasis, and are able to initiate solid tumour formation when xenotransplanted at low cell densities.[103] TNBC stem cells are isolated from

tumours as $CD44^+$ (homing cell adhesion molecule), $CD24^-$ (heat stable antigen), $CD49f^+$ cells.[104] CSCs also differ metabolically to other cancer cells. They are more reliant on mitochondrial respiration, which is supported by their higher mitochondrial reactive oxygen species, enhanced oxygen consumption, and higher mitochondrial mass, allowing for features such as resistance to DNA damage.[105]

Wnt signalling is essential for normal breast stem cell function and mammary gland development during embryogenesis, postnatal development, and pregnancy,[106] with adult mammary glands containing Wnt-responsive stem cell populations.[107] Studies have shown that aberrant Wnt signalling in breast cancer stem cells (BCSCs) is a key event in breast tumorigenesis.[108] Wnt/β-catenin signalling has been linked to TNBC tumorigenesis by regulating key tumour-associated characteristics, including migration, stemness, proliferation, and chemoresistance in TNBC cells and CSCs.[94] A recent study has also demonstrated that Wnt/β-catenin signalling activity is higher in breast CSCs than the bulk tumour population, based on β-catenin, TCF4, and LEF1 expression in Aldefluor positive cells versus Aldefluor negative cells.[109] Treatment with Wnt3a increased the number of $ALDH^+$ breast CSCs, and knockdown of Wnt1 reduced the tumour forming efficiency of breast CSCs *in vitro*.[109]

Studies have shown that Wnt-derived breast tumours are maintained by clones capable of re-activating Wnt overexpression post Wnt inhibition, indicating that aberrant Wnt activation is a key driver of breast cancer recurrence and progression.[110] A recent review highlighted the potential importance of Wnt/β-catenin signalling, along with other developmental signalling pathways, including Cripto-1 and Notch/CSL, in the regulation of TNBC stem cells and therapy resistance in TNBC.[111]

The TNBC subtypes also display characteristics associated with increased Wnt signalling. The LAR subtype of TNBC displays genomic amplification of *CCND1*, a gene regulated by the Wnt/β-catenin pathway. [19] This BLIS subtype contains increased SOX transcription factor expression, which share a closely related consensus binding sequence to TCF/LEF transcription factors [112] and are known modulators of Wnt/β-catenin signalling. [113] Furthermore, the BLIA subtype demonstrates amplification of

CDK1, which was recently found to phosphorylate the Wnt regulator TAZ. [19,114]. A table summarising the genes found with Wnt association in the Lehmann subtypes can be found in Table 1.

Table 1.1. Molecular subtypes of TNBC and their association with Wnt signalling

TNBC Lehmann *et al* Subtype	Gene Ontology Pathways (GOP)	Genes found in GOPs with Wnt association
Luminal Androgen Receptor (LAR)	Steroid pathway	*FKBP5*[115]
	Androgen metabolism	*SPDEF*[116]
	Fatty acid synthesis	*FASN*[117]
Mesenchymal (M)/Mesenchymal stem-like (MSL)	EMT	*MMP2*[26], *SNAI2*[26], *TCF4*[26], *TWIST1*[26], *ZEB1*[118]
	Wnt/β-catenin signalling	*CTNNB1*[18], *DKK2/3*[18], *TCF4*[18], *TCF7L2*[18], *CCND2*[18], *FZD4*[18], *CAV1*[18], *CAV2*[18]
Basal 1 (BL1)/ Basal 2 (BL2)	DNA Damage	*CHEK1*[119], *FANCA*[120], *FANCG*[120], *MSH2*[121], *RAD21*[122]
	Proliferation/Cell Cycle	*AURKB*[123], *PLK1*[124], *CENPA*[124], *BUB1*[124], *CCNA2*[125], *PRC1*[126], *MYC*[127], *NRAS*[128]
Immunomodulatory (IM)	JAK/STAT Cytokine Pathway	*CCR2*[129], *CCR5*[130]
	IL7 Pathway	*IL7*[131]

Table 1. Summary of the six molecular subtypes of TNBC characterized by Lehmann *et al*[18]. Various gene ontology pathways were found to be enriched in the LAR, MSL, BL1, BL2, and IM subtypes. Analysis of the genes enriched in these pathways identified genes associated with Wnt signalling.

1.3.4.1 FZDs in TNBC

1.3.4.1.1 FZD6

FZD6 exhibits increased gene copy number variations and overexpression in breast cancers. This is more frequent in TNBC than ER^+ tumours. A study by Corda *et al*. [132] determined that FZD6 was involved in the regulation of cell motility, invasion, and 3-D growth, although it did not regulate proliferation in TNBC. This was confirmed by a significant reduction in distant metastases detected in various organs *in vivo* after the injection of MDA-MB-231 TNBC cells depleted of FZD6. shRNA directed at FZD6 *in vitro* was found to reduce cell invasion through a reduction in active Rho and the subsequent reduction in fibronectin fibres. This indicated that FZD6 regulates cell motility and invasion through non-canonical Wnt signalling. This study also suggests that FZD6 overexpression in TNBC has a high prognostic value in determining the risk of metastasis.[132]

1.3.4.1.2 FZD7

Microarray analysis determined that FZD7 expression is upregulated in TNBC tissue and cell lines, and promotes tumorigenesis via canonical Wnt signalling pathways.[133] shRNA-mediated silencing of FZD7 reduced invasiveness and colony formation in TNBC cell lines.[133] A recent study found that ΔNp63, an isoform of Transformation-related protein 63 (p63), enhanced FZD7 expression and increased Wnt signalling in TNBC tumour tissue and cell lines.[134]

Aberrant FZD7 expression is implicated in TNBC stem cell-mediated tumorigenesis. A study recently found that knockdown of ΔNp63 in TNBC cell lines decreased FZD7 expression and tumoursphere formation, indicating that ΔNp63/FZD7 upregulation induced TNBC stem cells and promoted tumour formation in TNBC.[134] The findings of this study highlight the potential clinical importance of ΔNp63/FZD7-Wnt signalling in TNBC stem cells as a key driver of tumorigenesis and progression of TNBC.[134,135]

1.3.4.1.3 FZD8

Gene expression studies have recently linked FZD8-driven Wnt signalling to chemoresistance in TNBC cell lines and TNBC stem cells. Treatment with

cisplatin and tumour necrosis factor-related apoptosis-inducing ligand (TRAIL) in TNBC cell lines resulted in increased FZD8 expression in residual tumours of xenograft models.[136] Furthermore, FZD8 silencing led to increased Wnt pathway-driven TNBC cell apoptosis *in vitro* and *in vivo.*[136] The study showed that treatment with TRAIL/cisplatin increased expression of LEF-1 and TCF-7 in residual TNBC stem cells, thus implicating upregulation of Wnt signalling components in the development of chemoresistance.[136] An inverse correlation between FZD8 and miR-100 was shown, where decreased miR-100 expression was linked to increased FZD8 expression and Wnt signalling, resulting in increased loco-regional breast cancer metastasis.[136,137] The role of microRNAs in Wnt signalling and TNBC is discussed in further detail below. c-Myc overexpression has been linked to FZD8 overexpression in TNBC cell lines, associating c-Myc driven transcription to chemoresistance and TNBC cancer stem cell survival.[138]

1.3.4.2 LRP5/6 in TNBC

LRP5/6 are essential for normal mammary development by regulating breast stem cell activity and are linked to basal-derived breast tumorigenesis.[139-141] Studies in transgenic mice indicated that LRP5 knockdown led to resistance to Wnt1-induced tumour formation.[140]

Gene expression analyses found that LRP6 is overexpressed in human TNBC.[133,141] *In vivo* studies have shown that LRP6 silencing inhibited tumour growth in TNBC cell line-derived xenograft models.[142] LRP6 and Wnt target gene *SOX9* have been shown to influence regulation of one another in TNBC cell lines. LRP6 overexpression lead to *SOX9* upregulation, while knockdown of *SOX9* reduced LRP6 transcription, and decreased cell invasion and proliferation.[143]

LRP6 overexpression led to the upregulation of Wnt signalling and was associated with increased stemness in TNBC cells.[144] CD138 (Syndecan-1) is an EMT marker associated with both development and breast tumorigenesis,[145] and has been shown to modulate TNBC stem cell properties by targeting Wnt signalling.[144] Ibrahim *et al*.[144] showed that CD138

modulates Wnt signalling in TNBC stem cells through LRP6, whereby CD138 silencing resulted in downregulated LRP6 expression and Wnt signalling.[144]

1.3.4.3 RORs in TNBC

Primary breast cancer cDNA microarray dataset analysis has shown that ROR1 is expressed in breast cancer cells and absent in normal breast cells, with high ROR1 expression associated with poorer survival.[146] Furthermore, the study showed that ROR1 silencing in TNBC cell lines increased apoptosis and reduced cell growth. High ROR1 expression in breast cancer cells is associated with high expression of EMT gene profiles and high incidences of disease recurrence and progression.[147] ROR1 knockdown in TNBC cell lines resulted in reduced EMT-associated protein expression, reduced cell migration and invasion *in vitro*, and inhibited metastasis in xenograft models.[147] ROR2 expression is present in both TNBC and non-TNBC, with $ROR2^{+}$ TNBC patients exhibiting poorer survival outcomes compared to other subtypes.[148] The study found that ROR2 knockdown in TNBC cell lines inhibited Wnt signalling and reduced TCF/LEF transcription.[148] These findings indicate the potential prognostic and therapeutic significance of high ROR1/2 expression in TNBC.

1.3.5 CURRENT AND EMERGING THERAPIES FOR TNBC AND TNBC STEM CELLS

Systemic cytotoxic chemotherapy is clinically indicated in early TNBC and is associated with a greater treatment benefit and reduced reoccurrence rate than hormone receptor positive tumours.[149] Numerous early phase clinical trials are currently underway, investigating various targeted molecules and combination therapies for the treatment of TNBC. In this section, we review current and emerging small molecule therapeutics for the treatment of TNBC (Figure 1.5); immunotherapeutics are reviewed elsewhere.[6]

1.3.5.1 Chemotherapy

Anthracycline/taxane-based regimens are currently the standard of care in the treatment of adjuvant and neoadjuvant TNBC. However, a recent *in vitro*

study has shown that treatment with docetaxel or doxorubicin had transient and negligible impact on cell growth in two TNBC cell lines respectively, which may be due to the molecular subtype of the cell lines. Furthermore, the study found that docetaxel and doxorubicin treatment resulted in deregulation of genes associated with stemness in TNBC cells.[150] Molecular analysis found that doxorubicin treatment deregulated stem cell signalling pathways associated with cell growth, renewal, and differentiation, with altered gene expression demonstrated in components of the Wnt signalling pathway, including FZD2, FZD4, FZD5, FZD6, FZD7, FZD9, Axin1, Wnt11, Wnt10a, and Wnt5a. As such, the study concluded that docetaxel and doxorubicin induce stemness in differentiated TNBC cells, which likely accounts for acquired chemoresistance seen in refractory TNBC tumours.[150]

1.3.5.2 Platinum Agents

Platinum-based chemotherapeutics are a class of DNA-damaging agents, including cisplatin, carboplatin, and oxaliplatin; these have established efficacy in breast cancer treatment.[151] *In vitro* studies have indicated that combining TRAIL and cisplatin significantly increased BCSC death compared to other standard of care treatments in TNBC cell lines.[152] The study showed that treatment with TRAIL and cisplatin inhibited Wnt1-mediated signalling and expression of cyclin D1, as well as the phosphorylation of β-catenin. Combination treatment with cisplatin and TRAIL also enhanced apoptosis, and inhibited proliferation and tumoursphere formation.[152]

1.3.5.3 Wnt signalling inhibitors

Treatment with the small molecule β-catenin/TCF inhibitor CWP232228, inhibited β-catenin-mediated transcription, leading to inhibition of stem cell proliferation and reduction in tumour bulk in TNBC cell lines and TNBC patient-derived xenograft models respectively.[153] PRI-724, a CREB-binding protein inhibitor, and LGK-974, a Porcupine inhibitor, are two small molecules currently undergoing clinical development. Both molecules are currently under investigation for single agent use in ongoing phase I clinical trials in TNBC patients,[154] with interim results yet to be released. Recent *in*

vitro studies have shown that LGK-974 in combination with the PI3K/AKT/mTOR inhibitor BKM120, worked synergistically to decrease cell viability and enhance anti-tumour efficacy in TNBC cell lines.[155]

1.3.5.4 PARP inhibitors

Poly (ADP-ribose) polymerase (PARP) is an enzyme involved in DNA repair mechanisms necessary for maintaining BRCA-mutated cell viability.[156,157] Included in the PARP enzyme family are tankyrase-1 (TNKS1) and tankyrase-2 (TNKS2). TNKS1 and TNKS2 are regulators of Wnt signalling through their interaction with Axin.[158,159] Many TNBCs share phenotypic characteristics with BRCA-mutated cancers, thus providing support for the use of PARP inhibitors (PARPi).[160] The small molecule TNKS1/2 inhibitor XAV939 showed effectiveness in the destabilization of Axin and reduction of Wnt activity, although data suggest a combination approach may be more beneficial.[159] Clinical trials evaluating the oral PARP inhibitor (PARPi) olaparib in BRCA1/2 positive metastatic breast cancer are currently underway, with interim results showing efficacy.[161] Veliparib is another PARPi currently being evaluated in combination with paclitaxel and carboplatin for metastatic TNBC.[162] Data from Phase I clinical trials of veliparib show acceptable safety, tolerance, and good anti-neoplastic activity.[162]

1.3.5.5 HDAC inhibitors

Histone deacetylase inhibitors (HDACis) are emerging as promising anti-TNBC agents due to their multifunctional capacity to regulate gene expression, cell growth, and survival, as well as their ability to restore cellular aberrations due to epigenetic effects.[163] Entinostat is an HDACi recently shown to have anti-CSC effects in TNBC stem cells. An *in vivo* study found that entinostat treatment reduced TNBC stem cell populations, tumoursphere formation, and miR-181a expression in TNBC cell lines.[164] Furthermore, the study found that entinostat treatment in TNBC patient-derived xenografts reduced tumour growth and inhibited the development of lung metastases.[164] Further *in vivo* studies have shown that triple therapy, combining entinostat,

all-*trans* retinoic acid, and doxorubicin, induced apoptosis of TNBC stem cells in culture and induced differentiation of TNBC CSCs both *in vitro* and *in vivo.*[165] Panobinostat (LBH589) decreased cell survival and cell cycle progression at the G2/M stage in TNBC cell lines and *in vivo*. It also increased acetylation of the histones H3 (Lys3) and H4 (Lys8).[163] Treatment with panobinostat upregulated cadherin-1 (CDH1) and reversed the mesenchymal phenotype; CDH1 has been identified as a Wnt signalling component in invasive breast carcinoma.[166] An *in vivo* study found that salinomycin, a compound that selectively inhibits CSCs,[167] in combination with panobinostat, significantly inhibited the growth of TNBC stem cells in TNBC patient-derived xenografts. The study found salinomycin and panobinostat worked synergistically to inhibit cell cycle progression, enhance apoptosis, and regulate EMT in TNBC stem cells.[167]

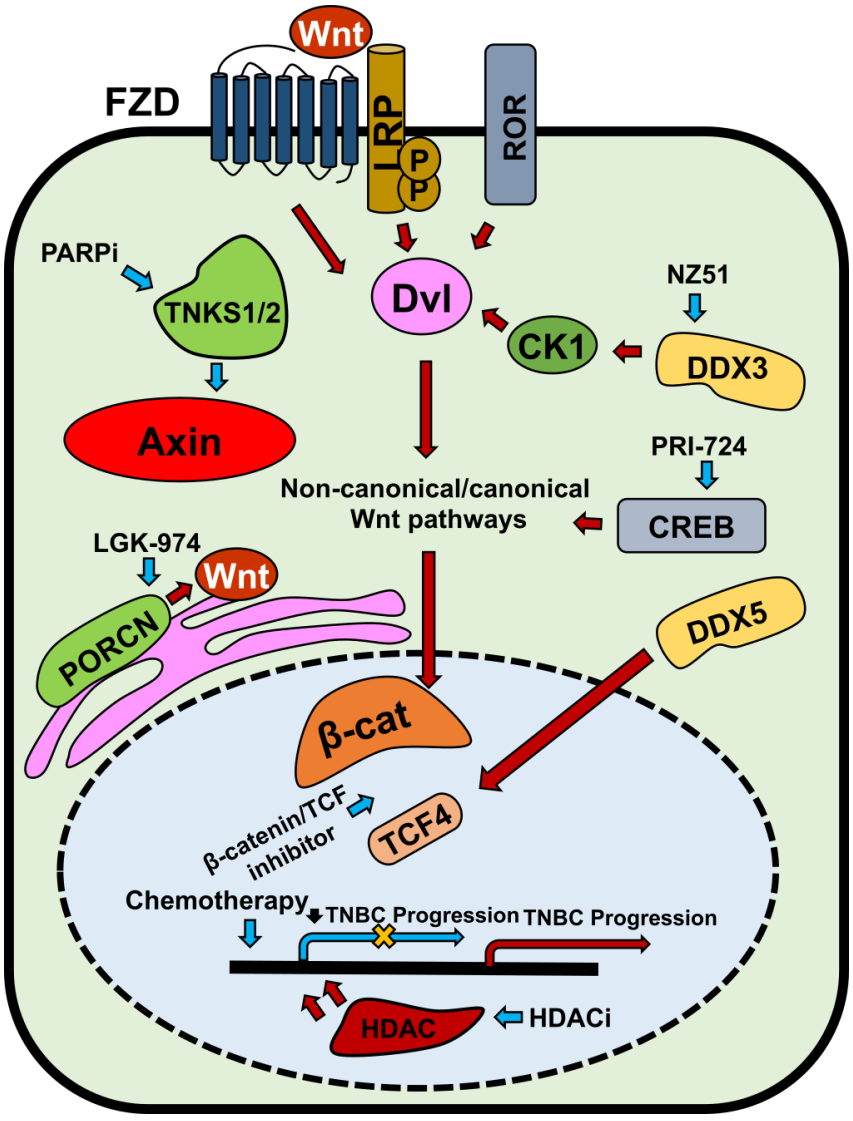

Figure 1.5. Overview of Wnt signalling regulators contributing to TNBC progression and their targeted therapies. Canonical and non-canonical Wnt pathways are activated through Fzd, LRP, and ROR receptors. Blue arrows indicate suppression or inhibition of Wnt regulators and pathways (with a net result of downregulation of Wnt target gene transcription, indicated by yellow cross), red arrows indicate activation of Wnt regulators and pathways.

1.4 DEAD-BOX RNA HELICASE FAMILY

1.4.1 Structure of DEAD-Box family proteins

DEAD-Box helicases (DDXs) are characterised by an evolutionarily conserved motif of D-E-A-D (Asp-Glu-Ala-Asp) in the Walker B (II) motif of the helicase core. There are currently 44 DEAD-box proteins identified within the *H.sapiens* genome, with many of these being assigned yeast orthologues.[168] The N-terminus of DEAD-box proteins contains the helicase core, made up of two separate domains; domains 1 and 2, which resemble the recombinase A (RecA) protein found in bacteria. Domain 1 contains the Q, I, Ia, Ib, Ic, II and III motifs. Domain 2 contains the IV, Iva, V, Va, and VI motifs. Domains 1 and 2 are separated by an amino acid linker, allowing flexibility for ATP binding and ATP hydrolysis.[169] Within Domain 1 and 2, motifs Q, I, II, and VI have been shown to mediate ATP binding, while the Ia, Ib, Ic, IV, Iva, and V are mediators of interactions with RNA (Figure 6). The DEAD-box proteins belong to a larger family of helicase proteins known as the superfamily 2, or SF2. The SF2 superfamily contains proteins that feature the Walker B motif, although the D-E-A-D is conserved as D-E-x-D/H (Asp-Glu-x-Asp/His).[170] While the primary role of DEAD-box helicases is unwinding, eIF4aIII can act as an RNA clamp during RNA splicing[171] through its interaction with serine/arginine-rich splicing factor 2 (SRSF2).[172]

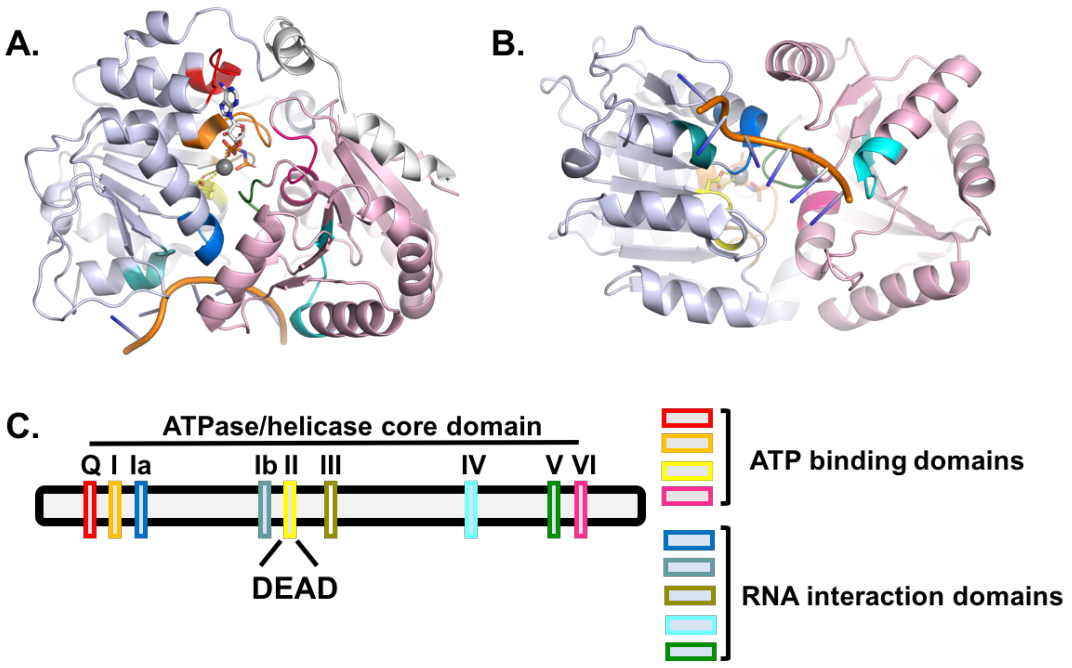

Figure 1.6 ***(previous page)*****. Structure of DEAD-Box helicases**. A. Ribbon model of DDX19B in view of ATP-binding domain. Light pink = c-terminal domain of helicase core, light blue = n-terminal helicase core. ATP analogue ANP-PNP is depicted as ball and stick model. Colours of segments correspond to domains within ATP or RNA binding domain. Red (Q), Orange (I), Blue (Ia), Teal (Ib), Yellow (II), Olive (III), Sky blue (IV), Green (V), Pink (VI). B. Ribbon model of DDX19B rotated 90 degrees to show RNA binding site. C. Schematic representation of ribbon models, with domain colours corresponding to the model. Models developed from crystal structure of DDX19B (PDB 3G0H).[173]

1.4.2 Functional roles of DEAD-Box helicase proteins

DEAD-box helicases have functional roles in many aspects of RNA metabolism, including transcriptional regulation, ribosome biogenesis, and non-sense mediated decay. It has been found that many DDX proteins are preferentially expressed in specific tissue and cell types, and have key functional roles in the homeostatic or carcinogenic behaviours of these cells. DDX protein involvement in RNA metabolism is summarised in Table 2, while their associations with cancer are listed in Table 3.

1.4.2.1 DEAD-Box helicases in RNA splicing

The role of DDX proteins in pre-mRNA splicing has been widely studied in a multitude of organisms, including *Saccharomyces cerevisiae* (yeast), *Homo sapiens* (human), and *Drosophila melanogaster* (fruit fly). The yeast DDX protein, Prp5p, has been demonstrated to activate the U2 small ribonucleoprotein (snRNP), a protein that specifically binds to the polypyrimidine tract adenine nucleotide, which initiates lariat formation.[174]

It was identified that seven different genes all encoding for yeast DDX proteins, when mutated, all regulated different steps of spliceosome assembly and pre-mRNA splicing. For example, Brr2 regulated ATP-dependent dissociation of U4/6 snRNPs, while Prp16 initiated the second transesterification step.[175] The role of DEAD-box proteins in the regulation of pre-mRNA splicing and spliceosome assembly is frequently comprehensively reviewed. [168-170,176]

1.4.2.2 DEAD-Box helicases in stem cells

DDX proteins are highly involved in the regulation of embryonic (ESC), neural stem cells (NS), and haematopoietic stem cells (HSCs). In a comprehensive transcriptional profiling analysis of ESCs, NS, and HSCs,

DDX1 and DDX4 were found to be enriched in all three cell types.[177] DDX4 (or Vasa) is a cytoplasmic protein expressed in primordial germ cells in both males and females. It was found to bind to uracil-rich (U) motifs in the 3' UTR of mRNAs to inhibit miRNA activity and regulate germline stem cell fate.[178] Controversially, it was reported that oogonial stem cells were able to be FACS-isolated using DDX4 as a marker; it has subsequently been shown that these cells are neither DDX4-positive or germ cells.[179,180]

In HSCs, DDX46 was implicated in the regulation of erythropoiesis and lymphopoiesis in zebrafish caudal haematopoietic tissue.[181] The same phenotypic haematopoietic changes were observed in zebrafish with the homozygous DDX18 mutation, although the embryos exhibited increased cell death in a p53-dependent manner. The same study revealed that non-synonymous variants of DDX18 are found in human acute myeloid leukaemia. [182]

Recently, Li *et al.*[183] determined DDX5 to be a key regulator of pluripotency in induced pluripotent stem cells. DDX5 negatively regulated somatic reprogramming through downregulation of development-specific genes by directly targeting the non-canonical polycomb complex 1 (PRC1) subunit RYBP. DDX5 simultaneously increased the transcription of pluripotency-associated genes, such as *Kdm2b*, through RYBP-mediated recruitment of OCT4 to their respective promoter regions.

1.4.2.3 DEAD-Box helicases in organelle-specific RNA metabolism

The mitochondrial genome contains 37 genes, 13 of which are components of the electron transport chain (ETC) and are fundamental for oxidative phosphorylation (OXPHOS); the others are rRNAs and tRNAs.[184] Within the mitochondrial matrix exists the RNA granule-contained mitoribosomal proteins, assembly factors, and RNA metabolism factors, which translate mitochondrial mRNA into nascent polypeptides. It was reported that DDX28 is a key RNA metabolism factor located within the RNA granule.[185] DDX28 was localised to the mitochondria where depletion of DDX28 resulted in decreased OXPHOS assembly and respiration through downregulation of Complex I, III, IV, and V. DDX28 interacted with 16s RNA and mt-LSU

proteins to regulate mitoribosome biogenesis. Furthermore, it was found that this was dependent on its helicase C-terminal domain.[185]

Table 1.2. Cellular functions of DEAD-Box family members and cellular localisations in RNA metabolism.

FUNCTION	DDX FAMILY MEMBER	CELLULAR LOCALISATION
Ribosome biogenesis	DDX3X, DDX3Y, DDX5, DDX10,DDX18, DDX21, DDX24, DDX27, DDX31, DDX47, DDX48, DDX49, DDX50, DDX51, DDX52, DDX54, DDX55, DDX56	Nucleus
Transcription	DDX5, DDX17, DDX20, DDX21	Nucleus
Pre-mRNA splicing	DDX3X, DDX3Y, DDX23, UAP56, DDX42, DDX46	Nucleus
RNA export	DDX3X, DDX3Y, DDX19, DDX25, DDX39, UAP56	Nuclear pore complex
snRNP biogenesis	DDX20	Cytoplasm
Nonsense mediated decay	DDX48	Cytoplasm
miRNA processing (RISC assembly)	DDX5, DDX20	Cytoplasm
Translation	DDX2A, DDX2B, DDX3X, DDX3Y, DDX4, DDX19	Ribosome
RNA storage	DDX3X, DDX3Y, DDX6	Cytoplasm
RNA decay	DDX5, DDX6	Cytoplasm
Organelle-specific RNA metabolism	DDX28	Mitochondrion

1.4.3 DEAD-Box proteins in cancers

DDXs are frequently mutated and overexpressed in many cancers. Many of the mutations have yet to be determined as possessing oncogenic or loss-of-function properties, and may be silent mutations.[186]

In hormone receptor-positive breast cancer, DDX5 and DDX17 have been implicated in the activation of oestrogen receptor α (ERα) in a co-dependent manner. They were determined to be critical in the transcription of

ERα target genes and oestrogen-dependent growth. [187] Furthermore, it was demonstrated that DDX5/DDX17 regulated alternative splicing of GSK3β, controlling the stability of the ER and AR in breast and prostate cancers respectively.[188]

DDX proteins have been implicated in the progression and development of colorectal cancer. DDX3 was shown to drive Wnt-dependent tumorigenesis through CK1ε and Dvl2, which ultimately lead to inhibition of β-catenin degradation by PP2A.[189] Mechanistically, it was earlier shown that DDX3 binds to CK1ε, directly activating it to phosphorylate Dvl to promote Wnt signalling.[190] In colorectal cancer, it was also reported that DDX5 directly promoted cell survival by through inhibition of FOXO3a and subsequent activation of Akt.[191]

A role for DDX proteins in CSCs has also been demonstrated. Prominin-1 (CD133) is a common cell surface marker for the sorting of cancer stem cells from gliomas and ovarian carcinomas. In ovarian CD133positive stem cells, it was found that expression of DDX4 was positively correlated with the expression of CD133 and co-localised in immunofluorescence evaluation. This was not observed in CD133 negative cells.[192]

1.4.3.1 DDXs in Wnt and TNBC

1.4.3.1.1 DDX3

DDX3 is known to play an oncogenic role in breast cancer, where non-tumorigenic MCF10A cell lines overexpressing DDX3 showed increased EMT, motility, and invasiveness.[193] The same study demonstrated that DDX3 expression was positively correlated with a more aggressive phenotype, and was highly expressed in TNBC cell lines. DDX3 overexpression resulted in E-cadherin downregulation and subsequent nuclear β-catenin translocation.[193] Similarly, DDX3 inhibition by NZ51, a ring-expanded nucleoside analogue that is predicted to bind to the ATP-binding site of DDX3, led to decreased proliferation, motility, and invasiveness in TNBC cell lines and reduced tumour load and metastatic burden in preclinical *in vivo* models.[194]

1.4.3.1.2 DDX5 (p68)

DDX5 acts as a co-activator of Wnt/β-catenin signalling through regulation of TCF4 expression. In turn, β-catenin/TCF4 regulates DDX5 expression, forming a positive feedback loop associated with increased EMT marker expression in TNBC cells.[195] DDX5 is thought to regulate p53-mediated repair of DNA damage, and DDX5 overexpression contributes to tumorigenesis and progression in breast cancers.[196] DDX5 is highly expressed in basal-like breast cancers compared to luminal-like, and correlates with high epidermal growth factor receptor (EGFR) and Ki67 expression in TNBC tissue.[197] Furthermore, the study found that DDX5 regulates the expression of miR-21 and miR-182 in basal breast cancers, and is associated with malignant disease.

Table 1.3. Associations of DEAD-Box family members in cancers.[186]

TUMOUR TYPE	CANCER	DEAD-BOX PROTEIN
SOLID	Prostate	DDX5, DHX9
	Hepatocellular carcinoma	DDX3, DDX20, DDX27
	Testicular	DHX9
	Colorectal	DDX3, DDX6, DDX5, DDX17, DHX32
	Breast	DDX2, DDX3, DDX5, DDX17, DDX10, DDX18, DDX20, DDX21, DDX24, DDX43, DHX9
	Lung	DDX2, DDX3, DDX5, DHX9
BLOOD	Chronic myeloid leukaemia	DDX10, DDX43
	Chronic lymphocytic leukaemia	DDX10, DDX3X
	Acute lymphoblastic leukaemia	DDX3, DDX5, DDX53
	Acute myeloid leukaemia	DDX6, DDX10, DDX43

1.4.4 DEAD-Box Helicase DDX20 (Gemin3, DP103)

DDX20 (Gemin3, DP103) is an evolutionarily conserved protein that can be found in the genome of multicellular, eukaryotic, phagotrophic bacterivores.[198] While there is significant sequence variation in DDX20 between species, the nine conserved motifs remain present. Structurally, DDX20 has the characteristic conserved N-terminal helicase core, and an approximately 368 amino acid long, potentially highly phosphorylated (and presumably, structurally disordered) C-terminal region that is thought to modulate its RNA helicase activity and co-factor interactions.[199](Figure 7) The C-terminal of DDX20 has been shown to interact with a variety of proteins in both Human and *Drosophila*, and in doing so, regulating a variety of cellular functions. These include RNP assembly,[200] RNA silencing,[201] and transcriptional regulation[201] in both homeostatic and carcinogenic conditions.

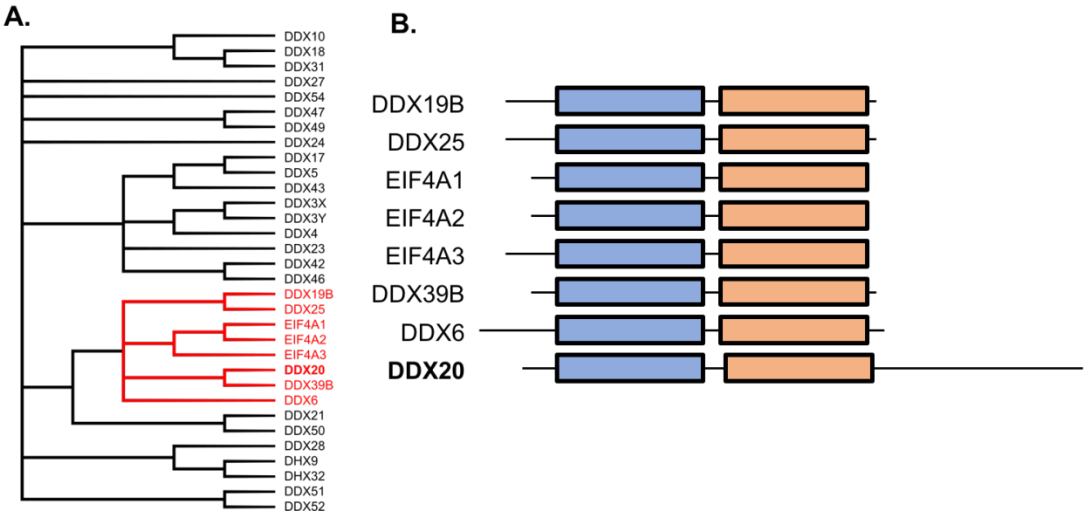

Figure 1.7. Sequence comparison of DDXs to DDX20. A. The evolutionary history was inferred by using the Maximum Likelihood method based on the Poisson correction model[202]. The bootstrap consensus tree inferred from 50 replicates[53] is taken to represent the evolutionary history of the taxa analyzed[53]. Branches corresponding to partitions reproduced in less than 50% bootstrap replicates are collapsed. The percentage of replicate trees in which the associated taxa clustered together in the bootstrap test(50 replicates) are shown next to the branches[53]. Initial tree(s) for the heuristic search were obtained automatically by applying Neighbor-Join and BioNJ algorithms to a matrix of pairwise distances estimated using a JTT model, and then selecting the topology with superior log likelihood value. The analysis involved 32 amino acid sequences. All positions containing gaps and missing data were eliminated. There were a total of 211 positions in the final dataset. Evolutionary analyses were conducted in MEGA X B. Schematic of DDX20 in comparison to other DDXs. The N-terminal (light blue) and C-terminal (light orange) are separated by an amino acid linker (black line) – extended in DDX20. The elongated C-terminal contains the primary regions known for DDX20 protein-protein interaction.

1.4.4.1 DDX20 regulation of snRNP biogenesis

DDX20 is a member of the large, multiprotein survival motor neuron (SMN) complex. Gemins 2, 3 (DDX20), 4, 5, 6, 7, and 8, named for their subcellular localisation in Gemini of Cajal bodies (gems), primarily function in maintaining the SMN complex to assemble snRNPs. snRNPs are indispensable for spliceosome assembly and pre-mRNA splicing.[203] Within this complex, DDX20 (Gemin3) has been shown to interact with Gemin 4, 5[204] and SMN1.[205] DDX20 has been shown to localise to subcellular organelles rich in snRNPs, named U bodies.[206] Knockdown of DDX20 gene expression in these systems has been demonstrated to disrupt snRNP assembly and other processes of RNA metabolism, including proofreading of snRNAs.[207,208] These roles in snRNP biogenesis and ultimately spliceosome assembly have implicit consequences for development. Homozygous deletion of Gemin3 (Mouse) and mel-46 (*C. elegans*) is embryonically lethal.[209,210] The role of DDX20 in RNA splicing mechanisms may be of interest in a disease such as cancer, in which aberrant RNA splicing is frequently found.[211]

1.4.4.2 DDX20 regulation of gene expression

DDX20 has also been shown to influence gene expression, both through gene silencing pathways[212] and as a cofactor for transcriptional activation and repression.[213] RNA interference (RNAi) is the process of gene silencing where double-stranded RNA (dsRNA) is cleaved by Dicer into small interfering RNAs (siRNAs). These siRNAs are then introduced into the RNA induced silencing complex (RISC), which then base pairs with mRNA containing the antisense sequence to the siRNA, initiating cleavage of the mRNA and reducing gene expression.[214] Argonaute (Ago) proteins are an essential component of the RISC complex and are required for translation inhibition. There has been a demonstrated physical interaction between Ago2 and DDX20, which regulates miRNA metabolism.[201] In hepatocellular carcinoma, miRNA-140 is associated with DDX20 expression and directly targets DNA methyltransferase 1 (Dmnt1) mRNA expression[215]. Interestingly, in this tissue context, DDX20 acts as a tumour suppressor, which is contrary to findings in other cancerous tissues.[216]

DDX20 can influence gene expression through directly interacting with and subsequently modulating the activity of transcription factors such as Steroidogenic factor 1 (SF-1) and Forkhead box protein L2 (FOXL2).[217] DDX20 interacts with the PRD domain of SF-1 to act as a transcriptional repressor for genes essential in early development, including early growth response protein 2 (Egr2).[218] It was later found that DDX20 could only interact after a small ubiquitin-like modifier (SUMO) was added to SF-1 by protein inhibitor of activator STAT (PIASγ); this mechanism is independent of the ATPase/RNA helicase activity of DDX20.[219] In granulosa cells, DDX20 has been shown to directly interact with FOXL2 in the region necessary for SF-1 interaction.[220] The co-expression of DDX20 and FOXL2 increases apoptosis, potentially through a redox-dependent mechanism, as SOD2 has been shown to be a direct target of FOXL2 transcription.[217,221]

1.4.4.3 DDX20 in carcinogenesis

DDX20 is frequently mutated or exhibits copy number variations in a variety of cancers. Analysis of large data cohorts from the TCGA PanCancer Atlas demonstrates that DDX20 is mutated in uterine, colorectal, lung, head & neck, cervical, stomach, breast, pancreas, and liver cancers (Figure 1.8). While the role of DDX20 in these cancers has not yet been identified, it is already known that the tumour suppressor or oncogene activity of DDX20 is tissue-specific.[199]

The role of DDX20 in regulating carcinogenesis is not yet fully understood, although in lymphomas and TNBC, mechanistic data suggest that DDX20 is a key regulator of cell fate. In B cell lymphoma cell lines, DDX20 was shown to physically interact with Epstein-Barr virus encoded nuclear antigen 3C (EBNA3C), which mediates its subsequent interaction with p53. In EBNA3C$^+$ cells, this interaction negatively regulated p53-mediated apoptosis. Short hairpin RNA (shRNA) knockdown of DDX20 increased gene expression of p53, Bax, and p21, and significantly increased cell death.[222]

Recently, it was discovered through a comprehensive bioinformatics and laboratory based study that DDX20 was overexpressed in the basal or TNBC subtype of breast cancer.[216] The protein expression of

DDX20 also positively correlated with the metastatic potential of isogenic cell lines and correlated with an increased breast metastatic gene signature.[216] Mechanistically, DDX20 interacted with TGF-β-activated kinase 1 (TAK1), which lead to increased NF-κB activity through increased phosphorylation of NF-κB-activating IκB kinase 2 (IKK2). Furthermore, depletion of DDX20 resulted in decreased NF-κB-mediated matrix metalloproteinase-9 (MMP9) expression and increased invasion, both *in vitro* and *in vivo.*[216]

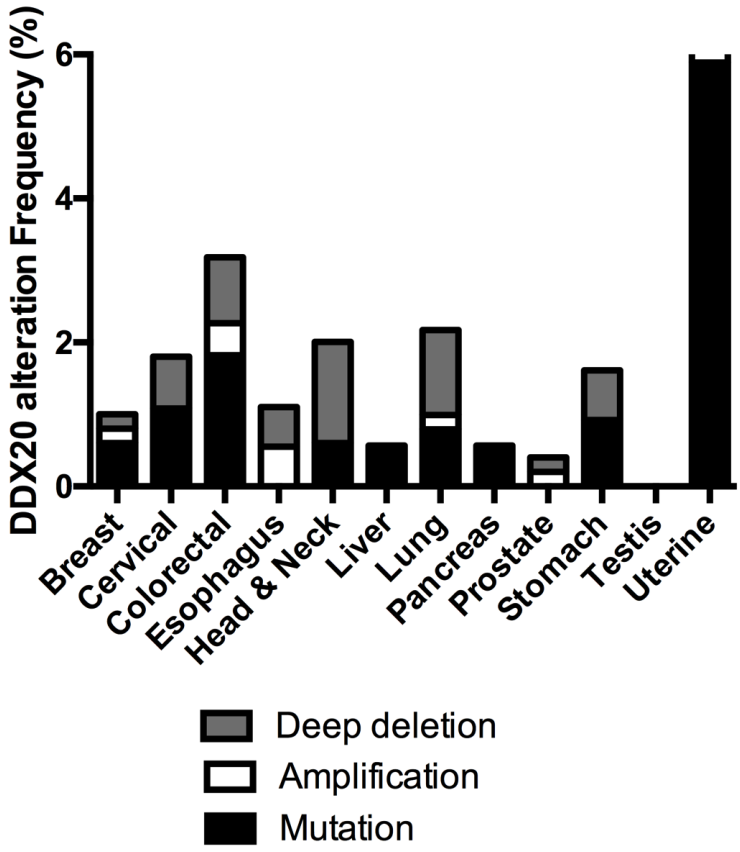

Figure 1.8. Alteration frequency of DDX20 across TCGA cancer types. Data accessed through cBioPortal.

1.5 REACTIVE OXYGEN SPECIES AND THEIR ROLE IN CELL SIGNALLING

Reactive oxygen species (ROS) collectively refers to oxygen-derived (O_2) free radical and non-radical species.[223] Radical ROS species include the superoxide anion (O_2^-), hydroxyl radical (HO•), peroxyl radical (ROO•), and alkoxyl radical (RO•).[224] Non-radical ROS species include hydrogen peroxide (H_2O_2) and peroxynitrite ($ONOO^-$)[225,226]. A tight balance between intracellular

ROS and ROS regulating systems is critical for maintaining cellular homeostasis.[227] Therefore, excessive generation of ROS or deficient anti-oxidant capacity alters the cellular redox state, with profound effects on cell growth, proliferation, and survival. Homeostatic levels of ROS are maintained by both enzymatic and non-enzymatic antioxidants. A depletion or overexpression of these antioxidants can alter cell fate. For example, overexpression of antioxidant enzyme superoxide dismutase 2 (SOD2) can protect cells from TNF-induced apoptosis.[228] This protected the cell from H_2O_2 cell death and promoted cell survival. On the other hand, SOD1 has been shown to be a potential therapeutic target in some cancers.[229] These contrasting roles for similar antioxidant enzymes demonstrates that the tight balance of ROS levels can determine whether cells will survive or undergo apoptosis. The dogmatic view that any increase in intracellular ROS is linked to cell injury and death has been challenged by substantial experimental evidence attributing a secondary messenger function to a mild increase in ROS or a 'pro-oxidant' milieu. Alterations in the cellular redox metabolism is linked to ageing [230] as well as a host of pathological states, such as cancer,[231] Alzheimer's disease,[232] Parkinson's disease,[233] diabetes,[234] atherosclerosis,[235] non-alcoholic fatty liver disease (NAFLD),[236] and asthma.[237]

1.5.1 Intracellular sources of ROS

The mitochondrion serves as an important source of intracellular ROS [elegantly reviewed in [238]], mainly generating O_2^- from Complex I (NADH dehydrogenase)[239] and Complex III (cytochrome *c* reductase)[240], when electrons derived from NADH or flavin adenine dinucleotide$_2$ leak out onto and reduce molecular oxygen.[241] The mitochondrial O_2^- levels are regulated by the action of manganese superoxide dismutase (MnSOD) in the inner matrix that generates H_2O_2 in the process.[242] H_2O_2 in turn can be scavenged by catalase, glutathione peroxidases, and peroxiredoxins.[243] A second important site of O_2^- generation, best exemplified in phagocytic cells, is the NADPH oxidase (NOX) family of enzymes. NOX enzymes are made up of six subunits: a Rho guanosine trisphosphatase (GTPase) and five phagocytic oxidase subunits (gp91, p22phox, p40phox, p47phox and p67phox)(Figure

9).[244] Additional sources of ROS include O_2^- from xanthine oxidases,[245] cyclooxygenases or prostaglandin-endoperoxide synthase (PTGS),[246] the cytochrome P450 enzyme family,[247] and non-heme lipoxygenases.[248]

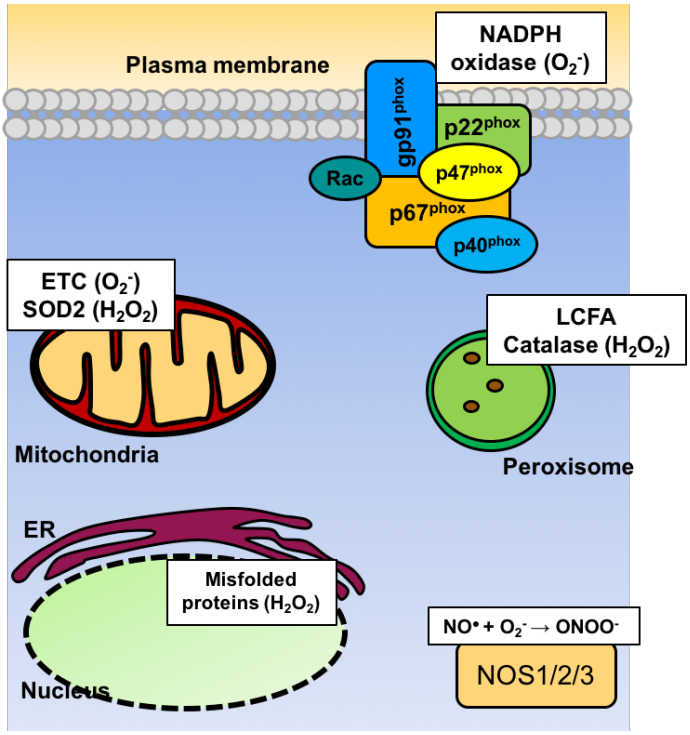

Figure 1.9. Sources of ROS. Intracellular sources of ROS are primarily through superoxide generation from the electron transport chain (ETC). Superoxide (O_2^-) generated from the ETC can undergo dismutation to H_2O_2 by SOD2 in the inner mitochondrial membrane. O_2^- is also produced by the NADPH oxidase complex in the plasma membrane. Misfolding of proteins can undergo redox reactions and generate H_2O_2 in the endoplasmic reticulum. While nitric oxide (NO) can react with O_2^- to form peroxynitrite ($ONOO^-$). Long chain fatty acids (LCFA) can produce H_2O_2 following β-oxidation, which is scavenged in the peroxisome by catalase.

1.5.2 Reactive oxygen species as signalling molecules

It is now widely accepted that ROS function as important signalling molecules, implicated in nuclear factor kappa-light-chain-enhancer of activated B cells (NF-κB), mitogen activated protein kinase (MAPK), Keap1-Nrf2-ARE, PI3K-Akt, Notch and Wnt signalling pathways.[249,250] The various functional consequences of an altered redox milieu have been associated with a critical balance between the two major ROS molecules, O_2^- and H_2O_2.[251-253] Whereas, an overwhelming increase in either of these species results in cell injury and death; a tilt in the ratio in favour of O_2^- confers a survival advantage while a significant shift towards H_2O_2 creates a permissive environment for death execution.[254,255] For example, H_2O_2 is

known to suppress Wnt/β-catenin signalling, an important survival and growth pathway, through a variety of mechanisms, including targeting the interaction between nucleoredoxin and dishevelled (Dvl)[256] and via oxidative modification of the zinc-coordinating cysteines of tankyrase, resulting in its inactivation.[257] ROS-mediated Wnt signalling regulation of Bcl-2 involving GSK3β/β-catenin has been reported upon chronic exposure to Cr(VI) compounds.[258] Furthermore DEAD-Box family members have been implicated in the regulation of mitochondrial stress responses and the detoxification of ROS, namely H_2O_2.[259]

1.5.3 Reactive oxygen species mediation of cell fate

Upon apoptotic stimulation, either death receptor- or drug-induced, a cascade of caspase activation results in the induction of mitochondrial outer membrane permeabilization (MOMP). In the case of death receptor signalling, direct executioner caspase activation is induced in certain cell types where the death initiating signalling complex (DISC) is efficiently formed (Type 1 or extrinsic pathway); however, in other cell types, the initiator caspase activation is relatively weak to autonomously engage the executioner caspase(s), and therefore the signal is routed through the mitochondria for efficient death execution (Type 2 or intrinsic signalling). The latter is also the preferred mode of execution triggered upon exposure of cells to DNA damaging agents, γ-irradiation, as well as other forms of chemotherapy. Importantly, the recruitment of the mitochondria is a function of the pro-apoptotic members of the Bcl-2 family that, upon apoptotic stimulation, translocate to the mitochondria, forming oligomeric complexes[260] that compromise the permeability of the outer membrane[261], thereby facilitating the egress of death amplification factors such as cytochrome *c*[262], Smac/DIABLO,[263] and apoptosis inducing factor (AIF).[264] The anti-apoptotic members of the Bcl-2 family, in particular Bcl-2 and Bcl-xL, prevent MOMP by competing with and inhibiting the oligomerization of the pro-apoptotic members, such as Bax and Bak.[265-267] As such, the apoptosis inhibitory function of Bcl-2 is strongly associated with the Type 2 death signalling pathway (Figure 10).

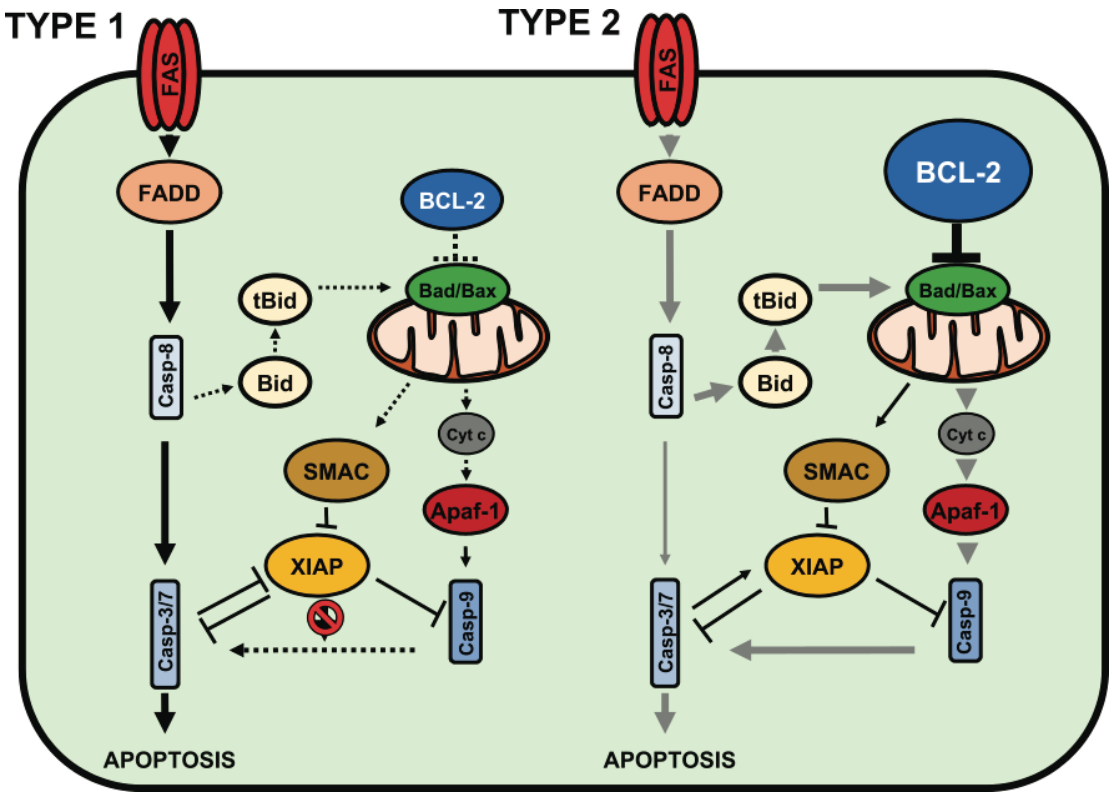

Figure 1.10. Schematic of type 1 and type 2 death receptor pathways. Type 1 (bold black line) FAS (CD95) death signalling pathway signals independent of the intrinsic pathway. Following FAS ligand binding, signals are transduced through FADD mediated caspase-8 activation and caspase-3/7 activation for cells to undergo apoptosis. Type 2 (bold grey line) death signalling through FAS is directed through caspase-8 mediated Bid activation. Bcl-2 is the primary inhibitor of anti-apoptosis in type 2 signalling. Bad/Bax can direct apoptosis by the release of cytochrome *c*, and the activation of Apaf-1 and caspase-9. Dotted lines indicate no pathway involvement.

1.5.4 Reactive oxygen species in triple-negative breast cancer

The role of ROS in the progression of breast cancer is not yet fully understood. Changes to the intracellular and extracellular redox environment favouring a pro-oxidant state have been shown to be a crucial factor in the initiation of cancer growth and metastasis.[268] The generation of electrons by oxidative phosphorylation can result in the production of O_2^-, primarily by complex I and complex III.[241] In TNBC stem cells, it has been demonstrated that increased oxidative phosphorylation and increased ROS, regulated through MYC transcriptional regulation of mtDNA genes and MCL-1 regulation of OXPHOS, was a key feature of drug-resistant TNBC cells.[269] Conversely, in MDA-MB-231 cells, the overexpression of a rotenone-insensitive yeast NADH Dehydrogenase gene, Ndi1, subsequently increased

complex I activity and resulted in a shift of the NAD^+/NADH redox balance and acted to suppress metastasis and tumour growth.[270]

The role of several antioxidant scavenging enzymes in tumour progression and metastasis is currently far from clear, with numerous conflicting results reported. Catalase has been reported to be overexpressed in TNBC and to be associated with lower tumour occurrence and increased overall survival rates in one South Korean cohort.[271] SOD2 is overexpressed in TNBC and was demonstrated to promote a strong EMT phenotype driven by H_2O_2, while knockdown of SOD2 promoted a mesenchymal-to-epithelial-like (MET) phenotype, primarily driven by O_2^{-}.[272] Furthermore, SOD2 was also demonstrated to restrict transformation from a $CD44^{low}/CD24^{high}$ epithelial phenotype to a $CD44^{high}/CD24^{low}$ mesenchymal-like type in head and neck cancers.[273] In MDA-MB-436 cells, oxidative stress from increased H_2O_2 was able to promote expression of N-cadherin and induce phosphorylation of EGFR; this could be ameliorated in the presence of *N*-acetylcysteine (NAC). NAC was also able to reduce the migratory capacity of the same cells.[274] The knockdown or downregulation of other antioxidant enzyme systems has also been demonstrated to influence TNBC cell fate. Thioredoxin reductase inhibition was associated with an increase in ROS, increase in radio-sensitivity, as well as increased DNA damage in TNBC cell lines.[275]

This shows a clear role for ROS and ROS scavenging enzymes systems in the initiation, progression, and metastasis of TNBC. The exact role of the various ROS species in cell fate is not yet entirely known. It is clear that a tight balance exists, whereby high levels of various ROS species can promote tumour progression or cause cell death. This is tissue-specific and relies on feedback mechanisms from the other ROS generating and regulatory systems when there is dysfunction or an unbalance in one.[276-278]

1.5.5 WNT/β-Catenin signalling in the regulation of mitochondrial ROS and mitochondrial function

The role of Wnt/β-catenin signalling in regulating mitochondrial function and ultimately mitochondrial ROS (mitoROS) has yet to be fully elucidated.

Conflicting evidence as to whether activation of Wnt/β-catenin signalling positively or negatively regulates mitochondrial function has been presented. This may be dependent on the cell type and mutational status of these cells.

In a model of haematopoetic stem cells (HPSC) derived from mouse bone marrow, it was demonstrated that the activation of canonical Wnt signalling induced apoptosis mediated through a loss in mitochondrial function. Mice with a floxed exon3 of β-catenin (*CTNNB1*$^{(ex3)fl/-}$), leaving it constitutively active, had a higher level of HSP cell death, significant downregulation of Bcl-2 and a loss of mitochondrial membrane potential. This was able to be restored with the ectopic expression of Bcl-2.[279] This study, although implicating Wnt/β-catenin signalling in mitochondrial function and depolarisation, did not demonstrate any substantial mechanistic data.

Conversely, inhibition of canonical Wnt signalling in colorectal cancer through the depletion of LGR5 resulted in decreased mitochondrial membrane potential and increased apoptosis.[280] Similar findings in a model of lung cancer were found, when the addition of a soluble form of the LRP6 E1-E2 domains (sLRP6E1E2) was introduced to lung cancer cells. When overexpressed, sLRP6E1E2 acted as a decoy receptor, leading to antagonism of Wnt/β-catenin signalling and, ultimately, to cell death. This mitochondrial-mediated cell death was evident by the transition from mitochondrial-embedded cytochrome *c* to its localisation in the cytoplasm. The signalling mechanisms in this study were demonstrated to be due to a loss of PI3K-Akt signalling.[281]

A study by Chen *et al.*[282] in Rat-1 fibroblast cells expressing Wnt1 demonstrated that Wnt1 activation of TCF4/β-catenin-mediated transcription inhibited cytochrome *c* release and supressed apoptosis. The overexpression of a dominant-negative TCF4 (dnTCF4; missing the β-catenin binding domain) blocked Wnt1-mediated survival. While luciferase assays were used to demonstrate that this suppressed canonical Wnt signalling transcriptional activity, there were no specific genes implicated in the induction of mitochondrial-mediated apoptosis.

In a study that provided strong mechanistic data for a role in mitochondrial ROS generation, function, and biogenesis by canonical Wnt signalling, Yoon

et al.[283] developed an siRNA screen implicating Wnt/β-catenin signalling in mitochondrial dynamics. The addition of Wnt3a increased mitochondrial DNA, volume, and O_2^- production. Furthermore, Wnt3a increased the expression of numerous genes involved in oxidative phosphorylation. To implicate canonical Wnt signalling further, a dnTCF4 was overexpressed in the presence of Wnt3a and could supress the increase in mtDNA. Chromatin immunoprecipitation (ChIP) of TCF4 was then performed on the insulin receptor substrate-1 (IRS-1) promoter and of IRS-1 on the MYC promoter, to demonstrate that the changes in mitochondrial function were directed through a Wnt3a-IRS-1-MYC transcriptional axis.

Finally, in melanoma cell lines, the addition of Wnt3a was able to regulate mitochondrial bioenergetics and mitochondrial morphology. Interestingly, this was dependent on the presence of a phosphatase and tensin homologue (PTEN) allelic deletion. In $PTEN^{WT}$ cells, the addition of Wnt3a was shown to negatively regulate mitochondrial function and cause a remodelling of cellular mitochondrial networks. Furthermore, in $PTEN^{Mut}$ cell lines, Wnt3a increased overall mitochondrial bioenergetics, which were decreased in the $PTEN^{WT}$ melanoma cells.[284]

These studies illustrate a clear role for canonical Wnt signalling in mitochondrial function, although this is tissue specific and as yet no direct evidence for TCF4 transcription of genes involved in mitochondrial regulation has been provided.

The multitude of studies which have yet to identify a conclusive role for TCF4 and DDX20-mediated Wnt/β-catenin signalling in the regulation of mitochondrial function and cellular redox demonstrates the importance for studies which may elucidate these mechanisms. In doing so, a better understanding of the role of mitochondrial metabolism and ROS is the determination of cell fate decisions in TNBC may be identified.

1.6 THESIS AIMS AND SCOPE

This thesis will contain a “Materials and Methods” as Chapter 2, followed by three experimental chapters, each with its own Introduction, Results, and Conclusions. The thesis will be concluded with a chapter consisting of an overall discussion, conclusions, and future directions.

Experimental Chapter 1 (Chapter 3) is titled “DDX20 regulates TNBC intracellular redox in a Wnt/β-catenin dependent manner”. Overall, I addressed several key experimental questions. The aim was to determine the role of DDX20 in regulating intracellular redox conditions through modulation of Wnt/β-catenin signalling. Therefore, I addressed several hypotheses including;

- DDX20 depletion results in oxidative stress-induced cell death in triple negative breast cancer.
- DDX20, through mediation of canonical Wnt signalling, regulates the intracellular redox status of TNBC cells through transcriptional control.

Overall, this was an important study to fill gaps in the knowledge of DDX20 regulation of Wnt and Wnt-mediated regulation of ROS. There is no direct evidence for canonical Wnt signalling through TCF/LEF transcription factors in the regulation of ROS scavengers. Currently, there is no published evidence of DDX20 mediating canonical Wnt signalling. The present evidence of ROS regulating Wnt/β-catenin signalling is currently through upstream activation or inhibition of important Wnt signalling molecules including Dvl and Axin stabilisation.[256,257] There is currently no evidence for transcriptional regulation of ROS scavengers. Previous studies have demonstrated that β-catenin-mediated transcription of ROS is through FOXO transcription factors, which are widely known to regulate the gene expression of ROS scavenger enzymes, such as Catalase.[285,286] In this study it is shown that depletion of DDX20 causes increased oxidative stress through TCF4-mediated transcription of Catalase.

Experimental Chapter 2 (Chapter 4) is titled “DDX20 regulates TNBC mitochondrial homeostasis in a Wnt/β-catenin manner”. In this chapter, the aim was to determine whether diminished DDX20 would negatively regulate mitochondrial bioenergetics and function. Furthermore, I wanted to determine whether this was mediated in a Wnt dependent manner. Therefore, our hypotheses were;

- DDX20 depletion results in mitochondrial dysregulation in triple negative breast cancer.
- Mitochondrial dynamics and bioenergetics are regulated through TCF4-mediated transcription of mitochondrial redox regulators dependent on DDX20.

There are currently no experimental data that demonstrate that DDX20 can regulate mitochondrial function. Furthermore, there is no direct evidence that canonical Wnt transcriptional regulation can regulate genes involved in mitochondrial respiration or mitochondrial ROS scavenging. In this study it was found that DDX20, through TCF4-transcription, can differentially regulate mitochondrial electron transport component, UQCRC2, and ROS scavenger, SOD2, to cause mitochondrial dysfunction, which inevitably impacts mitochondrial dynamics.

The final experimental chapter (Chapter 5) is titled “DDX20 is an essential regulator of Wnt/β-catenin signalling in triple-negative breast cancer stem cells”. The aims were to determine if, in enriched CSCs from TNBC cell lines, DDX20 played a functional role in regulating Wnt signalling. It is known that CSCs exhibit features such as a quiescent cell cycle, multi-drug resistance, and properties characteristic of stem cells. Therefore, the hypotheses were;

- DDX20 in an essential regulator of Wnt/β-catenin signalling in triple-negative breast cancer stem cells
- Depletion of DDX20 will diminish the characteristic CSC features of drug resistance, altered cell cycle, and increased stem cell transcription factors.
- Antagonism of the Wnt signalling pathway will downregulate DDX20 expression.

In this chapter, it was explored whether depletion of DDX20 will result in the same functional cellular changes regardless of PTEN mutational status of the cell. This was an important question as unpublished data demonstrate that DDX20 directly associates with GSK3β, which is known to interact with PTEN and be a downstream target of PI3K-Akt signalling.

It was found that depletion of DDX20 resulted in diminished Wnt signalling, chemosensitisation to doxorubicin, altered cell cycle progression, and downregulation of transcription factors that classically regulate stem cell pluripotency. Interestingly, there were some effects from DDX20 knockdown that were differentially observed between cell lines, suggesting that future studies on DDX20 will needed to be considered within an entire cell signalling context.

Overall this study has found a novel protein, DDX20, that regulates Wnt/β-catenin signalling in triple-negative breast cancer, and a new regulator of cellular redox and mitochondrial function. Furthermore, a new role for Wnt signalling in the regulation of mitochondrial function and redox homeostasis was determined, which, through an *in vivo* drosophila model, suggests may be partially evolutionarily conserved.

CHAPTER 2: MATERIALS AND METHODS

CHAPTER 2: MATERIALS AND METHODS

2.1. CELL CULTURE

Monolayer culture - MDA-MB-231 and MDA-MB-436 TNBC cell lines were purchased from ATCC and cultured in Dulbecco's Modified Eagle Medium/High glucose with L-glutamine and sodium pyruvate (SH3002201 - Hyclone, GE Healthcare), 10% foetal bovine serum (FBS) (SFBS-AU, Bovogen, Australia), and 1X penicillin-streptomycin (15070063 – Thermo Fisher Scientific). BT549 cells were a kind gift from Peter Leedman (Harry Perkins Institute of Medical Research) and MCF-7 cells were purchased from ATCC; both cell lines were maintained in RPMI-1640 (SH30096.01, Hyclone, GE Healthcare), 10% FBS (SFBS-AU, Bovogen, Australia), and 1X penicillin-streptomycin (15070063 – Thermo Fisher Scientific). MCF10A cells were a kind gift from Peter Hartman (University of Western Australia) and were cultured in DMEM/F12 (Gibco, GE Healthcare), 20ng/mL epidermal growth factor (EGF, Prospec), 0.5mg/ml hydrocortisone (H0888 – Sigma Alrdrich, Missouri, USA), 10μg/mL insulin (I-1882 – Sigma Alrdrich, Missouri, USA), 10% FBS (SFBS-AU, Bovogen, Australia), and 1X penicillin-streptomycin (15070063 – Thermo Fisher Scientific). Cells were maintained at 37°C and 5% CO_2.

3-D Spheroid Culture - Monolayer cells were dissociated from the flask using TrypLE™Express (12604013 - ThermoFisher Scientific). Cancer stem cells (CSCs) were then isolated by plating them at a density of $1x10^4$ cells/cm^2 on low attachment plates (Corning) in a medium consisting of a 1:1 ratio of basal medium DMEM (MDA-MB-231) or DMEM/F12 (BT549) with DMEM High Glucose (Hyclone) and supplemented with 20ng/mL epidermal growth factor (EGF, CYT-217, Prospec, Israel), 20ng/mL basic fibroblast growth factor (bFGF, CYT-218, Prospec, Israel), B-27 (Life Technologies), and 1X Penicillin-Streptomycin (CSC medium). Cells were cultured for at 37°C and 5% CO_2 until the presence of mammospheres were visible (5-7 days). The breast cancer stem-like cells were then assessed for the surface markers,

$CD44^{high}/CD24^{-/low}$, by flow cytometry using an LSRFortessa flow cytometer (BD Biosciences).[91]

2.2. REAGENTS, CHEMICALS, AND RECOMBINANT PROTEINS

Recombinant human Wnt3a (5036-WN-010), human Dickkoff1 (Dkk1) (5439-DK-010), and human secreted frizzled related protein 4 (SFRP4) (1827-SF-025) were all acquired from R&D Systems. Wnt3a, Dkk1 and SFRP4 were all used at concentrations of 200ng/mL, 100ng/mL and 250pg/mL respectively.

The purified recombinant cysteine-rich domain (CRD) and netrin-like domain (NLD) were a kind gift from Prof. E. Y. Jones (STRUBI, University of Oxford).

β-catenin/TCF inhibitor III (iCRT3) was made by Calbiochem (#219332) and purchased from Merck Millipore. It was dissolved to a stock concentration of 12.1625μM in dimethyl sulphoxide (DMSO) (D8414 - Sigma Aldrich). Doxorubicin hydrochloride (D1515 – Sigma Aldrich) was dissolved in MilliQ H_2O. Staurosporine (S5921 – Sigma Aldrich) was dissolved in DMSO.

Hydrogen peroxide (30% v/w) was purchased from Merck Millipore (#107209). Stock solutions were made to 100μM, protected from light, and frozen at -20°C. Riboflavin (R1706 - Sigma Aldrich) was prepared as a 30mM stock solution in MIlliQ H_2O, protected from light, and stored at 4°C. Glutathione stock (5mM) was purchased from Promega (#V6611) and catalase (1000U/μL) was purchased from Abcam (ab83464).

Oligomycin A (75351-5MG), carbonyl cyanide 4-trifluoromethoxyphenylhydrazone (FCCP) (C2920), rotenone (R8855), and antimycin A (A8674-50MG) were all purchased from Sigma Aldrich, and prepared as 100X stock solutions in DMSO. Ac-DEVD-AFC (#14459) was purchased from Cayman Chemical and resuspended in DMSO. MitoSox Red (M36008, chloromethyl-2,7- dichlorodihydrofluorescein diacetate acetyl ester (CM-H_2DCFDA) (C6827), and dihydroethidium (DHE) (D11347) were purchased from Thermo Fisher Scientific and used at concentrations of 5μM,

5μM, and 10μM respectively. Mitotracker™ DeepRed (M22426) and Mitotracker™ Green (M7514) were purchased from ThermoFisher Scientific. All ROS probes and Mitotracker reagents were prepared in DMEM High Glucose basal medium.

2.3. siRNA AND PLASMID DNA TRANSFECTIONS

A combination of three unique siRNA duplex oligonucleotides (27mer) targeting DDX20 and universal scrambled control (SR323381 - Origene Technologies, Rockville, MD) were each transfected at 20nM using RNAiMAX transfection reagent (13778030 - Thermo Fisher Scientific) in complete medium minus antibiotic. The culture medium was changed to complete medium with antibiotic six hours post-transfection and protein knockdown was assessed 72 hours later. DNA plasmids, pCMV-HA-vector, pCMV-DDX20-HA (purchased from Sinobiologicals, Beijing, China), pcDNA3.1-dnTCF4, and pcDNA3.1-vector (a kind gift by Prof. David Virshup, Duke-NUS) were transfected with Lipofectamine 2000 (11668027 – Thermo Fisher Scientific) in OPTI-MEM reduced serum medium (31985062 – Thermo Fisher Scientific). The culture medium was changed 4 hours post-transfection and over-expression was validated 48 hours post-transfection. Prior to transfection, all siRNAs and plasmid DNA was prepared in OPTI-MEM medium.

2.4. TCF/LEF REPORTER ASSAY

The Cignal™ TCF/LEF reporter assay was purchased from Qiagen (#CCS-018L) and performed following the manufacturer's instructions for the luciferase-based system. Briefly, after optimisation with a constitutively-expressing green fluorescence protein-containing (GFP) plasmid, cells were seeded at 3,500 cells/well before transfection with the TCF/LEF-responsive *Firefly* luciferase construct and constitutively-expressing *Renilla* luciferase construct in Lipofectamine®2000 in OPTI-MEM medium. The medium was changed 4 hours after transfection and incubated for an additional 48 hours. Luciferase *Firefly* and *Renilla* were detected using Dual-Glo® Luciferase

Assay system (E2920 – Promega, Australia) following the manufacturer's instructions.

2.5. MEASURE OF MITOCHONDRIAL MEMBRANE POTENTIAL

Mitochondrial behaviour was measured using the JC-1 mitochondrial membrane potential assay kit (701560 - Cayman Chemical, MI, USA). Cells were cultured in ultra low-adherent 24 well plates, at a density of 15,000 cells/cm^2. After 24 hours of treatment with 1μM doxorubicin, 50μl of JC-1 staining solution was added to the medium and incubated for 15 mins at 37°C and 5% CO_2. Cells were then analysed using an LSRFortessa flow cytometer (BD Biosciences). Emissions at approximately 529nm and 590nm for the green monomers and red dimers respectively were monitored using two separate instrument channels. FloJo (version 10) software was then used for post experimental data processing.

2.6. CASPASE 3/7 ACTIVITY ASSAY

Equal amounts of protein lysate (20μg) were loaded into a black 96-well plate. The Ac-DEVD-AFC substrate was diluted to a final concentration of 1:20 in protease assay buffer (20mM PIPES, 100mM NaCl, 10mM DTT, 1mM EDTA, 0.1% (w/v) CHAPS, 10% sucrose, pH 7.2). Following the addition of the substrate to lysates, cells were incubated for two hours at 37°C in the dark. Excitation of 400nm and measurement of emission at 505nm was performed using a Perkin Elmar Enspire plate reader.

2.7. CELL CYCLE ANALYSIS

MDA-MB-231 cells were transfected with scrambled siRNA or siRNA against DDX20, then fixed in 70% ethanol (459844 – Sigma Aldrich) overnight at 4°C, washed twice in PBS (P5493 – Sigma Aldrich), and stained for ten minutes at room temperature with propidium iodide (PI)/RNase staining solution (4087 - Cell Signaling Technologies). Samples were analysed using a BD FACS CantoII cell sorter and FloJo v10 software.

2.8. FLOW CYTOMETRY FOR CANCER STEM CELL CHARACTERISATION

MDA-MB-231- and BT549-enriched cancer stem cells were grown in culture for seven days. Cells were collected, washed twice with PBS, and stained with CD44 conjugated to allophycocyanin (CD44-APC) at 0.25μg in 100μl of medium and CD24 conjugated to phycoerythrin/Cy7 (CD24-PE/Cy7) at 0.25μg in 100μl of medium. Cells were incubated for 30 minutes in the dark before being analysed using a BD FACS CantoII flow cytometer and FloJo v10 software.

2.9. FLOW CYTOMETRY FOR ROS PROBES

Cells were stained with MitoSox Red, CM-H_2DCFDA, and DHE for 15 minutes in DMEM medium at 37°C in 5% CO_2, followed by two washes with PBS. Cells were then collected in PBS and detected by flow cytometry (BD LSRFortessa™). Emission/excitation for probes were 510/580nm for MitoSox Red, 492/530nm for CM-H_2DCFDA, and 518/605nm for DHE.

2.10. FLOW CYTOMETRY FOR MITOTRACKER PROBES

Mitotracker stains were used at 10nM for flow cytometry. Cells were stained in 12 well plates with Mitotracker™ dyes in serum-free DMEM high glucose medium for 15 minutes in the dark at 37°C in 5% CO_2. Plates were then washed twice in PBS, before being scraped into 400µl of PBS and detected by flow cytometry (BD LSRFortessa™). Emission/excitation for probes were 644nm/665nm for Mitotracker™ DeepRed and 490nm/516nm for Mitotracker™Green.

2.11. IMMUNOFLUORESCENCE FOR MITOTRACKER PROBES

Cells were stained in 96 and 12 well plates with Mitotracker™ dyes in serum-free DMEM high glucose medium for 15 minutes in the dark at 37°C in 5% CO_2. Plates were then washed twice in PBS, and phenol red-free RPMI-medium (SH3060501 – Hyclone, GE Healthcare) with 5% FBS was added. Images were photographed using a Nikon A1 confocal microscope and data were visualised on NIS Elements Viewer software (V4.11.0).Co-localisation

analysis was performed on Fiji Software plugin JACoP (Just Another Colocalization Plugin).[287]

2.12. WESTERN BLOTTING

Whole cell lysates were collected using radioimmunoprecipitation assay (RIPA) buffer (150mM NaCl, 1.0% IGEPAL-630, 0.5% sodium deoxycholate, 0.1% SDS, 50mM Tris, pH 8.0) (R0278-500ML, Sigma Aldrich) with protease and phosphatase inhibitor (5872S - Cell Signaling Technologies). Protein was separated using 10-12% SDS-PAGE gels and transferred onto 0.45μm nitrocellulose membranes (10600002 – Amersham Protran, GE Healthcare). Membranes were blocked in 5% skim milk powder in Tris-buffered saline (1706435 – Bio-Rad, CA, USA) with 0.1% Tween®20 (P9416 – Sigma Aldrich) (TBST) for 1 hour at room temperature. Primary antibodies were incubated overnight at 4°C. Following three washes in TBST, secondary antibodies were incubated at room temperature for 1 hour. Proteins were visualised by electrogenerated chemiluminescence (ECL) detection (RPN-2106 - Amersham, GE Healthcare) using ChemiDoc (Bio-Rad). Primary and secondary antibody details are in Table 2.1.

Table 2.1. Primary and secondary antibody details

ANTIBODY	COMPANY	CATALOGUE NUMBER	DILUTION
DDX20	BD Biosciences	612152	1:1000
β-CATENIN	Cell Signaling Technologies	D10A8	1:1000
ACTIVE β-CATENIN	Cell Signaling Technologies	8814S	1:1000
GSK3β	Cell Signaling Technologies	27C10	1:1000
^{PSER9}GSK3β	Cell Signaling Technologies	9336S	1:1000
DVL3	Cell Signaling Technologies	3218S	1:1000

DVL2	Cell Signaling Technologies	30D2	1:1000
CYCLIN D1	Abcam	ab134174	1:10,000
C-MYC	Cell Signaling Technologies	D84C12	1:1000
TCF4	Cell Signaling Technologies	2569S	1:1000
PARP	Cell Signaling Technologies	9542S	1:1000
BCL-XL	Cell Signaling Technologies	54H6	1:1000
SFRP4	Abcam	ab154167	1:1000
SOD2	Cell Signaling Technologies	D3X8F	1:1000
SOD1	Cell Signaling Technologies	71G8	1:1000
CATALASE	Cell Signaling Technologies	D4P7B	1:1000
β-TUBULIN	Cell Signaling Technologies	D2N5G	1:1000
β-ACTIN	Cell Signaling Technologies	13E5	1:1000
α-RABBIT IgG, HRP	Cell Signaling Technologies	7074S	1:10,000
α-MOUSE IgG, HRP	Cell Signaling Technologies	7076S	1:10,000

2.13. GENE EXPRESSION ANALYSIS

Total intracellular RNA was extracted using ISOLATE II RNA Mini Kit (BIO-52072 - Bioline, London, UK) following the manufacturer's protocol. The ratio between absorbance at 260nm and 280nm was assessed using Nanodrop spectrophotometers (Thermo Scientific). RNAs with a 260/280 ratio greater than 1.8 were used for downstream experiments. RNA was subjected to reverse transcription using High-capacity cDNA Reverse Transcription Kit

(4368813 - Applied Biosystems, California, USA). Samples were subject to thermal cycling. The thermal cycler protocol was as follows: (25°C for 10 mins, 37°C for 120 mins, 85°C for 5 mins, and 4°C for ∞). KAPA SYBR FAST qPCR Universal Kit (#KK460) was used following the manufacturer's instructions. The thermal cycler protocol was as follows: (95°C for 3mins, (97°C for 1min, Tm°C for 1mins) x 40 cycles). Housekeeping genes, *18S* and *GAPDH* were validated against each other to ensure experimental treatments did not alter *18S* or *GAPDH* mRNA levels. The ΔΔCT method was used to calculate fold change ($2^{-\Delta\Delta Ct}$). Primer sequences for genes of interest are as follows in Table 2.2:

Table 2.2. Human primer sequences, melting temperature, and size of amplicon for QPCR (quantitative PCR)

GENE NAME	PRIMER (5' - 3')	Tm (°C)	SIZE (BP)
DDX20 Fwd	GCACAGCAGAGCACAACATT	59	171
DDX20 Rev	GCATCAATCCCACGAGAAGT	58	171
TCF7L2 Fwd	GGGAGCCTCCAGAGTAGACA	60	286
TCF7L2 Rev	ATCCTAGCGGATGGGGGATT	60	286
LEF1 Fwd	TTCTTGGCAGAAGGTGGCAT	60	198
LEF1 Rev	AGGCAGCTGTCATTCTTGGA	59	198
AXIN2 Fwd	TAACCCCTCAGAGCGATGGA	60	80
AXIN2 Rev	CCTCCTCTCTTTTACAGCAGGG	60	80
FZD7 Fwd	CGACGCTCTTTACCGTTCTC	59	247
FZD7 Rev	GCCATGCCGAAGAAGTAGAG	58	247
SOX2 Fwd	CCATCCACACTCACGCAAAA	59	139
SOX2 Rev	TATACAAGGTCCATTCCCCCG	59	139
POU5F1 Fwd	TCCCATGCATTCAAACTGAGG	59	103
POU5F1 Rev	CCAAAAACCCTGGCACAAACT	60	103
NANOG Fwd	TGGACACTGGCTGAATCCTTC	60	142
NANOG Rev	CGTTGATTAGGCTCCAACCAT	59	142
KLF4 Fwd	CTGCGGCAAAACCTACACAA	59	182
KLF4 Rev	GGTCGCATTTTTGGCACTG	59	182

SOD2 Fwd	TGCTCCCCGCGCTTTCTTA	62	124
SOD2 Rev	AACATGCTGCTAGTGCTGGT	60	124
CAT Fwd	ACTGTTGCTGGAGAATCGGGT	62	228
CAT Rev	AGGACGTAGGCTCCAGAAGT	60	228
UQCRC2 Fwd	GGGAAAGTGTTAGCGGGGAA	60	80
UQCRC2 Rev	ACGGTCACTGCCGGATTAAA	60	80
ATP5F1A Fwd	TCGGCCATTTTGTCCCAGTC	61	145
ATP5F1A Rev	AGCATTTCTGGAGACCAGTCC	60	145
GAPDH Fwd	CAGAACATCATCCCTGCCTCTACT	62	258
GAPDH Rev	GTCGCTGTTGAAGTCAGAGGAGAC	62	258
18S Fwd	GCAATTATTCCCCATGAACG	60	68
18S Rev	GGGACTTAATCAACGCAAGC	60	68

2.14. ROS-Glo™H_2O_2 ASSAY

A luciferase-based H_2O_2 assay was obtained from Promega Corporation (#G8820) and used following the manufacturer's instructions. Briefly, 72 hours after control siRNA and siRNA targeting DDX20 were transfected, the H_2O_2 substrate was added to the complete medium and incubated at 37°C for 30 minutes. Following this, the ROS-Glo detection solution was added and incubated at room temperature for 20 minutes before luminescence was read on a Perkin Elmar Enspire plate reader.

2.15. GSH/GSSG-Glo™ ASSAY

A luciferase based GSH/GSSG-Glo™ assay was obtained from Promega Corporation (V6611) and used following the manufacturer's instructions. Briefly, 72 hours after control siRNA and siRNA targeting DDX20 were transfected, a reagent for total glutathione content and cell lysis, or oxidised glutathione content and cell lysis, was added to the cells. The plate was shaken for five minutes before the luciferin generation reagent was added and incubated for 30 minutes. The luciferase detection reagent was then added and allowed to equilibrate at room temperature for 15 minutes before detection of luminescence on the Perkin Elmar Enspire plate reader.

2.16. IMMUNOFLUORESCENCE

Immunofluorescent staining was performed by fixation in 100% methanol for 20 minutes at -20°C. Samples were washed three times with cold PBS, and blocked for 1 hour at room temperature in PBS with 5% BSA. They were then incubated overnight at 4°C with the following primary antibodies: 1:100 DDX20/Gemin3 (sc-57007 Santa Cruz Biotechnology, USA), 1:400 active (non-phospho$^{s33/s37/t41}$) β-catenin (8814S - Cell Signaling, USA), 1:200 cytochrome C (sc-13561 - Santa Cruz Biotechnology, USA), 1:400 CD44 (3570S - Cell Signaling, USA), 1:100 Bcl-2 (sc-509, Santa Cruz Biotechnology), 1:50 8-deoxyguanosine (OHdG) (ab10802 – Abcam), 1:400 catalase (sc-271803 - Santa Cruz Biotechnology), 1:400 c-MYC (5605S - Cell Signaling, USA), and 1:400 GSK3β (27C10 - Cell Signaling, USA). Anti-rabbit Alexafluor488 (ab150077), anti-mouse Alexafluor488 (ab150113), anti-rabbit Alexafluor555 (ab150074), anti-mouse Alexafluor555 (ab150106), and anti-rabbit Alexafluor647 (ab150079) were all purchased from Abcam and were incubated for 1 hour at room temperature at a dilution of 1:500. ProlongGold with DAPI (P36935 – Molecular Probes, Life Technologies, USA) was then added for counterstaining and preservation. Images were photographed using a Nikon A1 confocal microscope and data were visualised on NIS Elements Viewer software (V4.11.0).

2.17. CELL SORTING FOR ROS^{BRIGHT} AND ROS^{DIM} POPULATIONS

Cells were grown in 15cm plates until 90% confluent. Cells were then washed twice in PBS before being scraped into 5mL of PBS. The cells were then centrifuged at 350*g* for five minutes and resuspended in 2ml of basal DMEM medium containing a 1:1000 dilution of CM-H_2DCFDA for 15 minutes at 37°C. Cells to run as the unstained control were incubated for 15 minutes at 37°C in basal DMEM medium without CM-H_2DCFDA. Cells were then stained with 5μL 7-aminoactinomycin D (7-AAD) (420404 - Biolegend) before being run on a BD FACSJazz™ cell sorter and collected in PBS contained 10% FBS. Cells were then immediately centrifuged at 350*g* for five minutes before being washed once in PBS and then lysed in 1X RIPA buffer for downstream protein expression analysis.

2.18. CELL VIABILITY ASSAYS

Cell viability was assessed by seeding 2,500 cells/well and allowing the cells to attach overnight. The following day, siRNA transfections were performed following the previously described protocol ("siRNA and plasmid DNA transfections"), with a medium change performed 4-6 hours post-transfection. After the indicated treatments, cells were measured for viability using the Cell Counting Kit-8 (96992 CCK8 – Sigma Aldrich), WST-8, and colorimetric probe following the manufacturer's protocol. Briefly, 10μL was added to 100μL complete medium and incubated in the dark for 4 hours. Absorbance was then measured at 450nm using a Perkin Elmar Enspire plate reader.

2.19. MAMMOSPHERE FORMING ASSAYS

CSCs were isolated as previously described ("3-D spheroid culture) and seeded at 1,000 cells/well in low-adherent 24-well plates. The following day, siRNA transfection before the cells were left to incubate at 37°C in 5% CO_2 for seven days. After the culture period, mammospheres greater than 40μm were counted at 20X magnification from four random fields. Mammosphere-forming efficiency (MFE) was calculated with the following equation:

$$MFE\ (\%) = 100 \times \frac{number\ of\ mammospheres\ per\ well}{number\ of\ cells\ seeded\ per\ well}$$

2.20. CHROMATIN IMMUNOPRECIPTATION

Bioinformatics analysis to determine TCF4-binding sites on DNA was conducted using using the USCD ENCODE ChiP-seq matrix (https://www.encodeproject.org/chip-seq/). If ChIP-seq peaks were found, primers were designed using Primer-Blast (NCBI) around the consenus TCF4 binding motif (T-C/G-A-A-A-G/A). Cells were cultured in 15cm dishes. After their respective treatments, they were crosslinked with 1% formaldehyde at room temperature for ten minutes, and quenched for five minutes with 125mM glycine. Cells were washed with ice-cold PBS and lysed in ChIP cell lysis buffer (20mM TrisHCl, pH 8.0, 85mM KCl, 0.5% IGEPAL-630) containing protease inhibitor cocktail, and then kept on ice for ten minutes. Cells were centrifuged at 5,000rpm for five minutes at 4°C. Nuclei

were resuspended in nuclear lysis buffer (50mM TrisHCl, pH 8.0, 10mM EDTA, 1% SDS with protease inhibitors) and kept on ice for 30 minutes. Sheared chromatin of 500-1000 base pairs in length was generated by sonication for 15 cycles (ten seconds on, ten seconds off) at 4°C. Samples were then centrifuged at 13,000rpm for 20 minutes at 4°C. Samples were precleared with Protein A Dynabeads (10001D – Invitrogen, Thermo Fisher Scientific) for 1 hour at 4°C, before 1:50 dilution of TCF4 antibody (2569S - Cell Signaling Technologies) and 2µg of normal rabbit IgG (NI01 – Merck Millipore) with Protein A Dynabeads were added overnight on rotation at 4°C. Beads were washed twice with low salt wash (0.1% SDS, 1% Triton X-100, 2mM EDTA, 20mM TrisHCl, pH 8.0, 150mM NaCl), twice with high salt wash (0.1% SDS, 1% Triton X-100, 2mM EDTA, 20mM TrisHCl, pH 8.0, 500mM NaCl), once with LiCl wash (250mM LiCl, 1% Igepal-630, 1% sodium deoxycholate, 1mM EDTA, 20mM TrisHCl, pH 8.0), and twice with TE buffer (10MM Tris-Cl, 1mM EDTA, pH 8.0). All washes were performed for five minutes at 4°C. Elution was performed with 120µl of elution buffer for 15 minutes at room temperature, twice, and reverse crosslinked with added RNase A (EN0531 - Thermo Fisher Scientific) overnight at 65°C, followed by heating with Proteinase K (71049 – Merck Millipore) for 45°C for 1 hour. DNA was purified using GeneJET PCR purification Kit (K0701 - Thermo Fisher Scientific), and eluted into 30µl of buffer. PCR and Q-PCR were performed as described previously. Primer sequences are described in Table 2.3.

Table 2.3. Human primer sequences, melting temperature, and size of amplicon for ChIP-QPCR (quantitative PCR)

GENE NAME	PRIMER (5' - 3')	Tm (°C)	SIZE (BP)
CAT –Fwd^{binding}	CAGTATTTCAAGAAGGGCACCA	59	245
CAT –Rev^{binding}	TTTTACATTCGCCGAAGCAGG	60	245
CAT –Fwd$^{non\text{-}binding}$	CGCTTTCTAAACGGACCTTC	57	231
CAT –Rev$^{non\text{-}binding}$	TGATTGGCTGAGCCTGAAGT	59	231
SOD2 –Fwd^{binding}	TAGTGAGGAAGGTGGGAACT	57	187
SOD2 –Rev^{binding}	CCTAAGAACAGTTCTTGGACA	55	187

SOD2 –Fwd$^{non\text{-}binding}$	AACCAAAACTCAGGGGCAGG	60	162
SOD2 –Rev$^{non\text{-}binding}$	CCTGTCTGCCGTACTTGAGT	59	162
UQCRC2 Fwd^{binding}	AACTACGCCGGGCTTCGATA	61	74
UQCRC2 Rev^{binding}	CGTTGGAGGCTTCAGGAGAT	59	74
ATP5F1A Fwd^{binding}	ACGGACAGCATCTTTGCAGT	60	181
ATP5F1A Rev^{binding}	AAAAATGCAGAGTGGCGG	57	181
NDUFB8 Fwd^{binding}	CTTTGCAGCCACTGGACT	58	161
NDUFB8 Rev^{binding}	GTTGAACCCTTCGGCTTTTC	58	161

Fold enrichment was calculated relative to IgG control using the $2^{-\Delta\Delta CT}$ method.

2.21. MITOCHONDRIAL MASS QUANTIFICATION

Cells were seeded in a 6-well plate. Following transfection with either control siRNA or siDDX20 for 72 hours cells cells was collected and washed once with PBS before the cell pellet was re-suspended in 300μl lysis buffer (10mM Tris-HCl, 400mM NaCl, 2mM EDTA, 1% SDS, 0.5% Proteinase K, pH 8.0). Samples were then cooled on ice before 100μl 6M NaCl was added and vortexed for 30secs. Sample was then centrifuged at maximum speed for 2 minutes before supernatant was transferred to a new tube and centrifuged again for 2 minutes at maximum speed. DNA was precipitated by adding 350μl isopropanol on ice and inverting before centrifugation at maximum speed for 2 minutes. The supernatant was discarded before 1mL of cold 70% ethanol was added, vortex and centrifuged again at maximum speed, twice. The ethanol is discarded before the DNA pellet is air-dried and resuspended in 100μl MIlliQ H_2O. The DNA is rehydrates at 65°C for 1 hour. DNA is quantified on NanoDrop before Q-PCR is performed using primers in Table 2.3.

Table 2.4. Human primer sequences for mitochondrial and nuclear DNA

GENE NAME	PRIMER (5' - 3')	TM (°C)	SIZE (BP)
nucDNA Fwd	AACTACGCCGGGCTTCGATA	55	74

nucDNA Rev	CGTTGGAGGCTTCAGGAGAT	55	74
mtDNA Fwd	TTCCTAATGCTTACCGAACG	55	98
mtDNA Rev	TCAGCGAAGGGTTGTAGTA	55	98

2.22. SEAHORSE XF96 EXTRACELLULAR FLUX ASSAY

Seahorse XF96 flux analyser (Agilent) was used to perform mitochondrial stress tests according to the manufacturer's instructions. Cells were seeded at 2,500 cells/well and allowed to attach overnight. The following day, siRNA targeting DDX20 or control siRNA was transfected for 72 hours. For plasmid DNA of pCDNA-dnTCF4 and pCMV-DDX20 and empty vector controls, cells were seeded at 3,500 cells/well and allowed to attach overnight before transfection, which was assessed 48 hours later. Prior to performing Seahorse analysis, cell culture medium was removed and changed to serum-free DMEM with phenol red (pH 7.4) containing 1mM sodium pyruvate (P2256-25G – Sigma Aldrich), 2mM glucose (G7021-1KG – Sigma Aldrich), and 2mM sodium bicarbonate (S5761-1KG – Sigma Aldrich), and incubated for at least 60 mins at 37°C in 5% CO_2. The injection strategy was oligomycin (2 µM), carbonyl cyanide-p-trifluoromethoxyphenylhydrazone (FCCP, 0.3 µM), and finally, rotenone/antimycin A in combination (1 µM). Normalisation of data was determined using BCA assay. Basal respiration, proton leak, spare respiratory capacity, and maximal respiration were all determined following normalisation and performed using Wave software (version 2.3.0).

2.23. BIOINFORMATICS ANALYSIS OF COHORT DATASETS

Data Analysis and Collection - Breast carcinoma datasets were obtained from the TCGA and METABRIC studies via cBioPortal [288] in November 2017; specifically, the Breast Invasive Carcinoma (TCGA, Provisional)[289] Breast Cancer (METABRIC)[290] data sets. Examination of various Wnt, redox, and mitochondrial regulatory genes for correlations, survival, and enrichment of gene families was facilitated via Perl scripts developed in-house.

Survival Analysis - Survival analysis was performed for selected patient groups meeting specific criteria. Patients were categorized as "high" or "low" expressers of genes, using an absolute mRNA expression *z*-score cut-off of

0.75; such groups required a minimum of 10 patients before further analysis was performed. The log-rank test was used to assess whether differences in survival were statistically significant; comparisons yielding *p*-values less than 0.05 were selected as statistically significant. Patient groups with single gene high/low phenotypes were assessed, as well as groups with two gene high/low phenotypes.

Gene set enrichment analysis – Gene set enrichment analysis (GSEA) was performed using the GSEA software.[291,292] TNBC subtypes were selected on the criteria of being $ER^-/PR^-/HER2^-$ by immunohistochemistry (IHC). The list of patients corresponding to each patient group for comparison were manually provided to GSEA to create phenotypes for analysis. GO gene sets [293] were used in the analysis. Gene sets affording *p*-values less than 0.05 and *q*-values (false discovery rates) of less than 0.25 were selected as being significantly altered between the patient groups.

2.24. *DROSOPHILA* STOCKS, GENE EXPRESSION, AND MITOCHONDRIAL MASS

Drosophila *fly stocks* – The loss of function Gem3B and the overexpressing UAS-Flag-Gemin3 fly stocks were gifted from Prof. A Gregory Matera, University of North Carolina, Chapel Hill. Two ubiquitous drivers were used in combination for overexpression of UAS-Gemin3, armadillo-GAL4, and daughterless-GAL4.[294] The double GAL4 driver line and Oregon R flies were used as wild-type controls.

Drosophila *RNA extraction and qPCR* – Total RNA was extracted from 50µl *Drosophila* embryos selected for fertilisation and development stage for each genotype using a Qiagen RNA extraction kit following the manufacturer's protocol. RNA preparations were incubated with RNAse-free DNase1 (NEB) at 37°C for ten minutes to remove any potential DNA contamination. After the treatment, DNase1 was inactivated by incubating the RNA samples at 75°C before quantification using Nanodrop 2000. 1µg RNA was used as template for the first strand cDNA synthesis. cDNA was synthesised using oligonucleotide dT, random primers, and reverse transcriptase from

QuantiTect Reverse Transcription Kit (Qiagen - #205314). Primer sequences to amplify the target gene regions were designed using NCBI primer design tool for all target genes and reference gene (RpL32). Real time PCR was carried out using a PikoReal 96 real time PCR system (Thermo Scientific) following the manufacturer's instructions. Expression levels were determined in a 10µl reaction volume in triplicate using QuantiFast SYBR Green. qPCR was conducted at 95°C for seven mins, followed by 40 cycles of 95°C for five seconds and 60°C for one minute. The specificity of the reaction was verified by melt curve analysis. Raw data has been analysed by the $2^{-\Delta\Delta CT}$ method.[295] Results were generated from three technical repeats and three biological repeats for each mRNA. The average relative expression ± standard deviation (SD) was determined and two-way ANOVA was carried out to determine statistical significance. Primer sequences are given in Table 2.5.

Table 2.5. Drosophila primer sequences, melting temperature, and size of amplicon for QPCR (quantitative PCR)

GENE NAME	PRIMER (5' - 3')	Tm (°C)	SIZE (BP)
Sod1 Fwd	GGACCGCACTTCAATCCGTA	60	127
Sod1 Rev	TGGAGTCGGTGATGTTGACC	60	127
Sod2 Fwd	TTTCGCAAACTGCAAGCCTG	60	99
Sod2 Rev	TGATCTCCCGGCAGATGATAG	59	99
Sod3 Fwd	GTGCTCACTATAACCCCGATAAG	58	112
Sod3 Rev	GTAACGTCGATAATGCCCGTG	60	112
Cat Fwd	GATGCGGCTTCCAATCAGTTG	60	139
Cat Rev	GCAGCAGGATAGGTCCTCG	60	139
Trx2 Fwd	GACGATAAAGTTTCTGCGATCCT	59	98
Trx2 Rev	GGTCGTAATCATAGCGTGGTCT	60	98
Prx3 Fwd	ATGTCTTTCGTAGCACGCTCA	60	83
Prx3 Rev	GCGGCAATCTGTTTCTGCTG	60	83
Dhd Fwd	TGGATCTGCGCGACAAGAAAG	61	116
Dhd Rev	GAAGGTCTGGGCGGTGATTG	61	116

Rpl32	GCCCAAGGGTATCGACAACA	60	85
Rpl32	GCGCTTGTTCGATCCGTAAC	60	85

Drosophila *mtDNA copy number quantification* - Developmental stage-synchronized *Drosophila* embryos were collected from three different crosses (wildtype, Gemin3B KO, and Gem3B OE). Experiments were performed using 10ng of DNA in a 20µL reaction mix to determine the mtDNA copy number. Real-time PCR (qRT-PCR) method with SYBR Green was used. Data were analyzed using the $2^{-\Delta\Delta CT}$ method.[296] Primer sequences are given in Table 2.6.

Table 2.6. Drosophila primer sequences for mitochondrial and nuclear DNA

GENE NAME	PRIMER (5' - 3')	TM (°C)	SIZE (BP)
nucDNA Fwd	CGAGGGATACCTGTGAGCAGCTT	65	152
nucDNA Rev	GTCACTTCTTGTGCTGCCATCGT	65	152
mtDNA Fwd	GCTCCTGATATAGCATTCCCACGA	61	151
mtDNA Rev	CATGAGCAATTCCAGCGGATAAA	61	151

2.25. STATISTICAL ANALYSIS

Statistical analysis was performed using one-way analysis of variance (ANOVA) for groups with one variable or two-way ANOVA for groups with two variables. For single comparisons an unpaired Student's *t*-test was performed, where $p < 0.05$ was considered significant. For multiple *t*-test comparisons, a Bonferroni post hoc test was utilised with an α of 0.05. All calculations were performed using Prism GraphPad v6.0e.

CHAPTER 3: DDX20 REGULATES INTRACELLULAR REDOX IN A WNT/β-CATENIN DEPENDENT MANNER

CHAPTER 3: DDX20 REGULATES INTRACELLULAR REDOX IN A WNT/β-CATENIN DEPENDENT MANNER

3.1. INTRODUCTION

DDX20 is an ATP-dependent RNA helicase that has been implicated as a regulator of apoptosis in cancer cells through a variety of mechanisms, including Wnt and reactive oxygen species (ROS). This chapter focuses on elucidating the mechanisms of DDX20-dependent regulation of canonical Wnt signalling and intracellular ROS in TNBC. For this study, two TNBC cell lines were utilised, MDA-MB-231 and MDA-MB-436. These were chosen due to their high DDX20 expression, highly invasive phenotype[297] and lack of PI3K pathway mutations;[298] PI3K regulation of the Akt-FOXO pathway is important in ROS detoxification, especially the transcriptional regulation of catalase.[299] Previous reports have implicated β-catenin regulation of both FOXO and TCF/LEF transcription factors, which is dependent on intracellular redox conditions.[286,300] These cell lines allow the study of Wnt-mediated transcriptional regulation of ROS scavengers without variations in FOXO and TCF/LEF transcriptional activity. The results demonstrate that depletion of DDX20 results in an increase in intracellular ROS, predominately in the form of H_2O_2; high intracellular H_2O_2 can adversely affect canonical Wnt signalling. They also demonstrate that high intracellular ROS levels are partially due to a decrease in catalase expression, which is transcriptionally regulated by TCF4 transcription factors through Wnt/β-catenin signalling dependent on DDX20 (Figure 3.1).

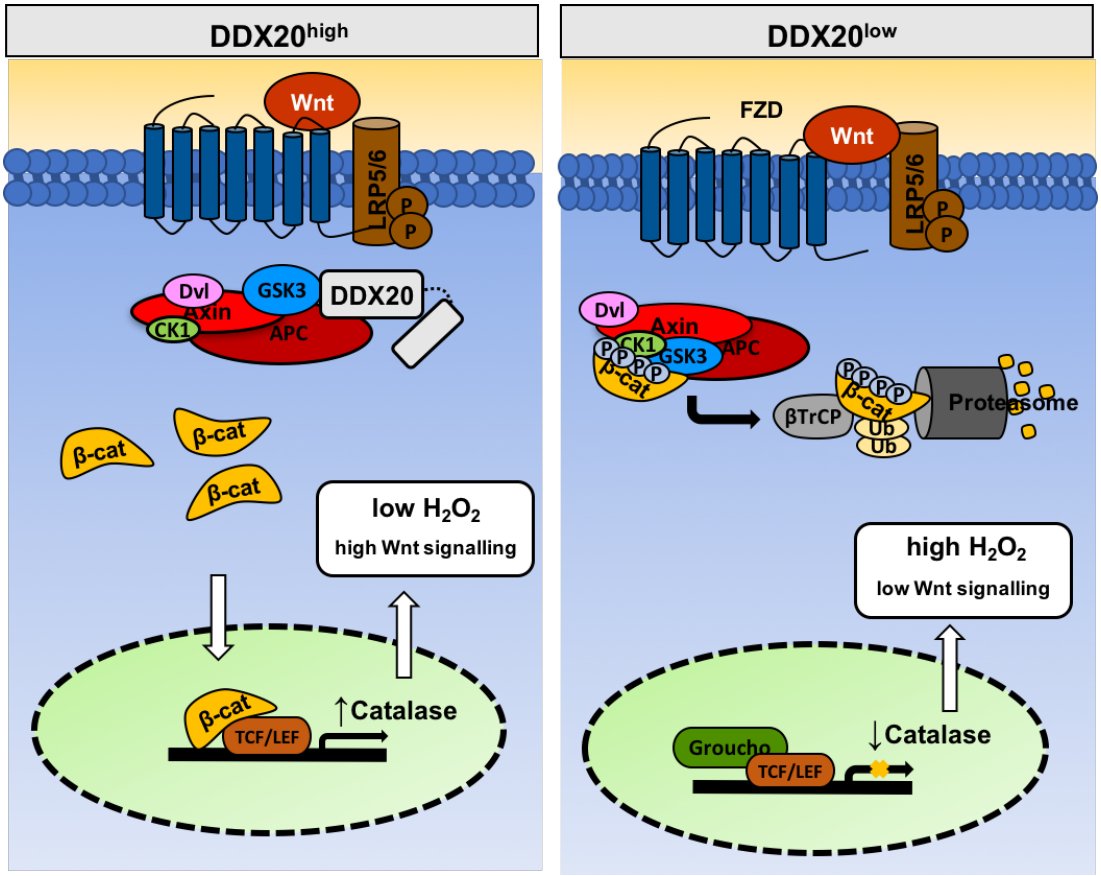

Figure 3.1. Schematic of Wnt-mediated ROS regulation in TNBC. DDX20^{high} cells stimulated by Wnt3a demonstrate lower levels of ROS and proper conductance of Wnt signalling. This is mediated through increased expression of catalase-mediated by TCF4. DDX20^{low} cells have higher levels of ROS and impaired Wnt signalling. There is a loss of catalase expression and an increase in intracellular ROS.

3.2. RESULTS

3.2.1. DDX20 is associated with oxidative stress regulation and catalase is associated with Wnt signalling in TNBC

Data from the METABRIC TNBC (n=270) were used to perform gene-set enrichment analysis (GSEA).[291,292] GSEA on individuals with a DDX20^{high} (n=73) phenotype compared to a DDX20^{low} (n=73) phenotype revealed an enrichment of genes associated with regulation of oxidative stress-induced cell death (GO:1903201) in the DDX20^{high} phenotype. This gene set included regulators of ROS such as thioredoxin (*TXN*) and NRF2 (*NFE2L2*) (Fig 3.2A).

A bioinformatics approach was used to determine if there was an association of redox regulators with Wnt signalling. Using data accessed from cBioPortal,[288,301] it was determined that catalase was commonly amplified in three large cohort data sets: METABRIC,[290] TCGA,[289] and the

newly created TCGA PanCancer Atlas.[302] Furthermore, DDX20 and AXIN2 exhibited amplification among the patient data sets (Fig 3.8B). Analysis of the different molecular subtypes revealed that catalase is significantly overexpressed in the claudin-low TNBC subtype, compared to both luminal B and $HER2^{+}$ breast tumours (Fig 3.8C). To determine if there was an association with canonical Wnt signalling, gene expression correlation studies between mRNA expression of catalase (*CAT*) and β-catenin (*CTNNB1*) were performed. Data from 1898 patients from the METABRIC cohort revealed a strong positive correlation between *CAT* and *CTNNB1* gene expression. When the subtypes were analysed individually, both TNBC subtypes - Basal and claudin-low - also demonstrated a strong positive correlation (Fig 3.8D,E,F). When survival analysis was performed on the METABRIC basal subtype cohort of individuals exhibiting either a $DDX20^{hi}/CAT^{hi}$ individuals versus $DDX20^{low}/CAT^{low}$ phenotype or a $CTNNB1^{hi}/CAT^{hi}$ individuals versus $CTNNB1^{low}/CAT^{low}$ phenotype, no significant differences in survival were observed. Median survival rates increased in individuals with a low DDX20 and CAT expression (7.58 to 9.9 years) and low CTNNB1 and CAT expression (5.42 to 8.75 years) when compared to individuals exhibiting high gene combinations of the respective gene combinations (Fig S3.1).

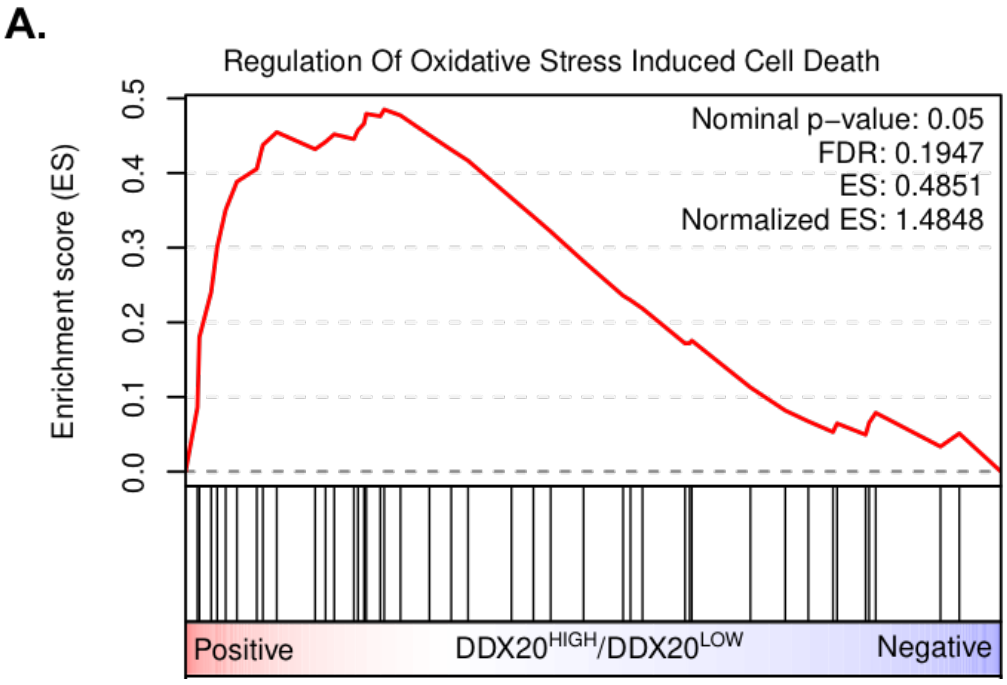

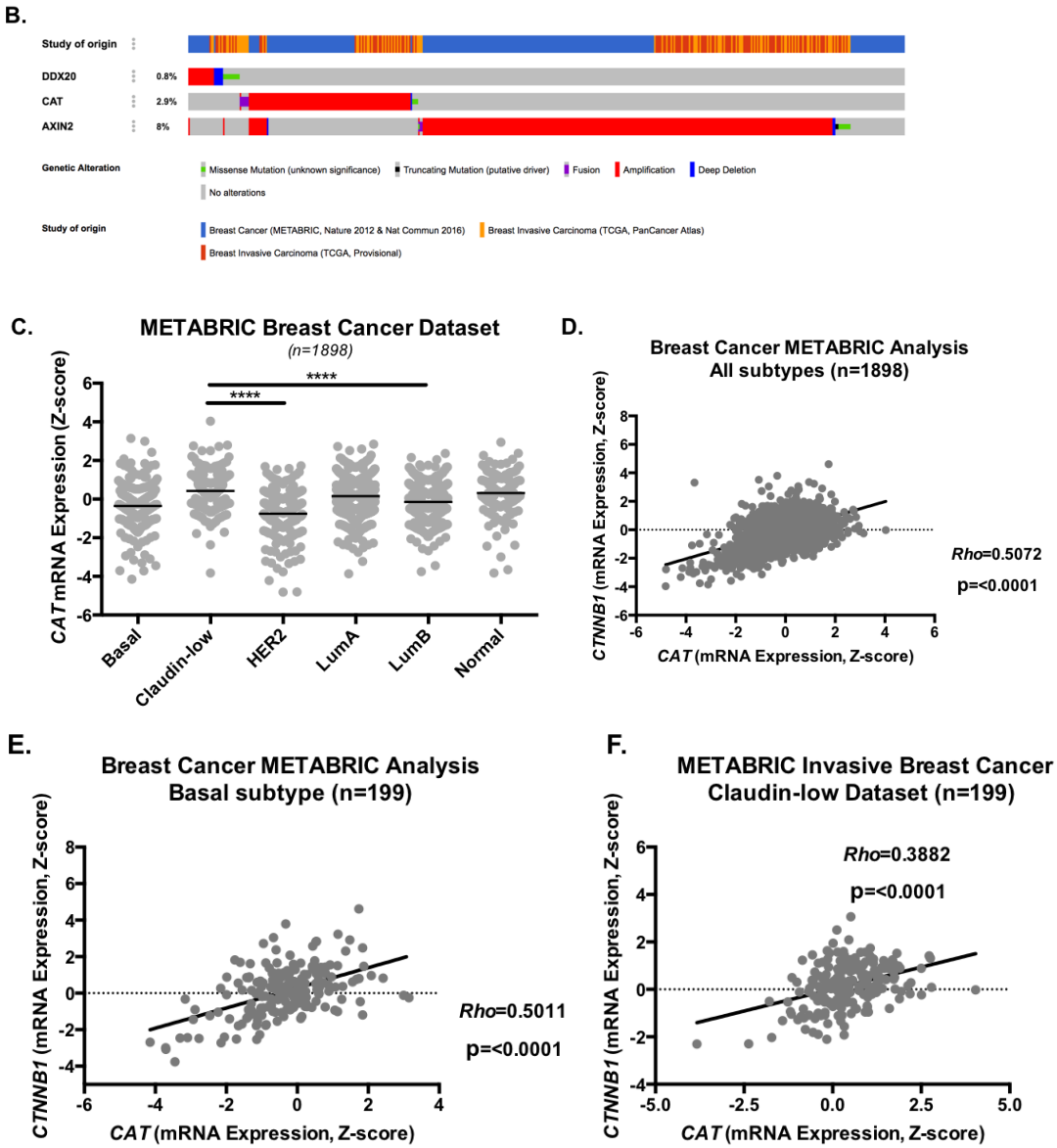

Figure 3.2. Gene set enrichment analysis of DDX20 and bioinformatics analysis on DDX20 and catalase A) GSEA enrichment plot of GO gene set Regulation of Oxidative Stress induced Cell Death in DDX20^{high} vs DDX20^{low} patient phenotypes. Nominal p-value, FDR (False discovery rate), enrichment score (ES), normalised ES were calculated using GSEA software from Broad Institute. B) Oncoprint of mutations, amplifications, and deletions accessed from cBioPortal for *CAT, DDX20*, and *AXIN2*. C) Catalase mRNA expression based on PAM50 molecular subtypes of breast cancer. D) Spearman's correlation (ρ or Rho) of *CAT* and *CTNNB1* in TCGA cohorts for all breast cancer subtypes and PAM50 E) claudin-low and F) basal subtypes. Data are represented as mean±SEM of at least 3 biological replicates. Statistical analysis was performed using unpaired students *t*-test, *p<0.05, **p<0.01, ***p<0.001.

3.2.2. DDX20 and Wnt signalling regulate intracellular redox conditions

To validate whether DDX20 regulated intracellular redox conditions *in vitro*, we first utilised two ROS probes, DHE, to measure superoxide production, and CM-H_2DCFDA, to measure oxidative stress induced by multiple ROS

species, by flow cytometry. Knockdown of DDX20 was assessed 72 hours after transfection and resulted in a significant increase in ROS, as indicated by a significant increase in the mean fluorescence intensity (MFI) of CM-H_2DCFDA in both cell lines. This was only partially rescued by the addition of exogenous catalase in both cases (Fig 3.3A & 3.3B).

To test the effect of Wnt activation on intracellular redox conditions, a GSK3β inhibitor, lithium chloride (LiCl) (20mM), was added to the medium for three and six hours. There was a significant decrease in the MFI of CM-H_2DCFDA at the six hour time point in both MDA-MB-436 and MDA-MB-231 cell lines (Fig 3.3C & 3.3D). Conversely, there was a significant increase in intracellular superoxide levels, as indicated by a significant increase in the MFI of DHE at the six hour time point in both cell lines (Fig 3.3E & 3.3F).

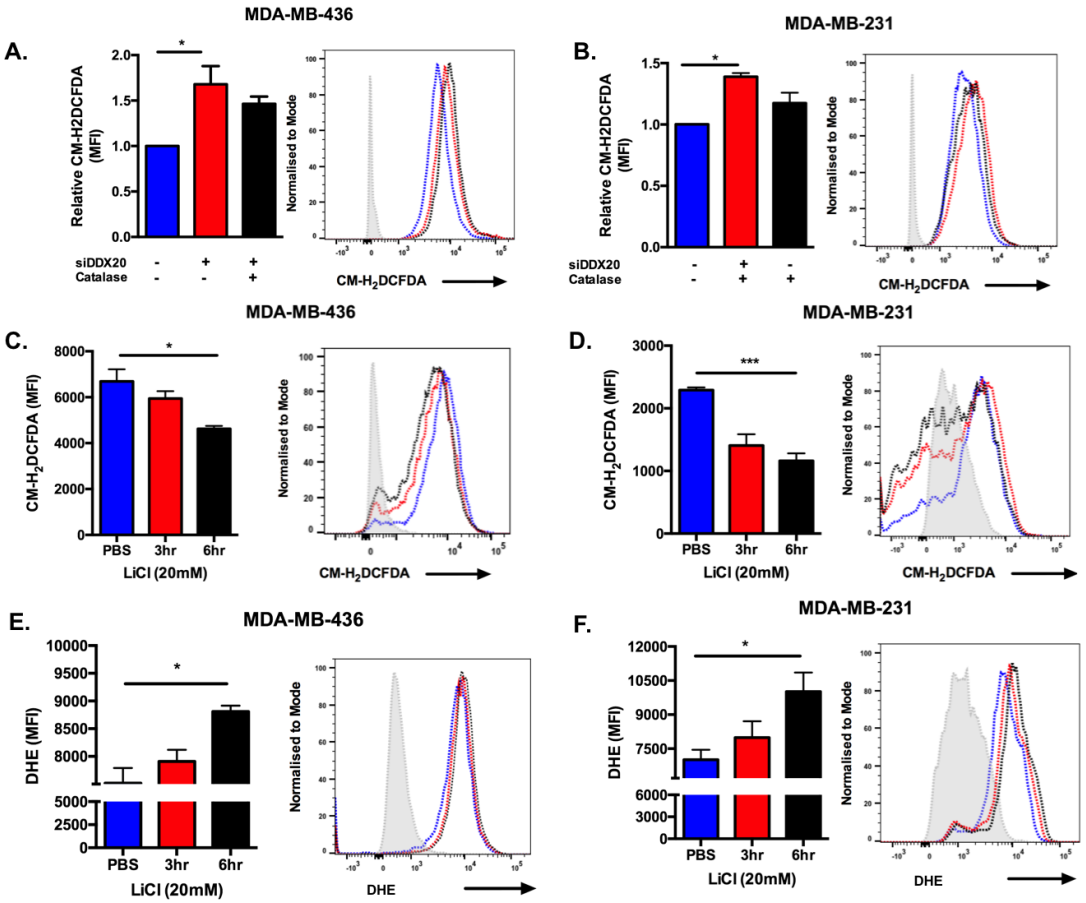

Figure 3.3. Evaluation of intracellular redox after modulation of DDX20 and Wnt signalling. A. Bar graph and representative histogram of CM-H_2DCFDA of MDA-MB-436 and B. MDA-MB-231 cell lines 72 hours post-transfection with ctDDX20, siDDX20 and siDDX20 with the addition of catalase (1000U/mL) for 1 hour. Grey = negative control, Blue = ctDDX20, Red = siDDX20 and Black = siDDX20+catalase. C. Bar graph and representative

histogram of CM-H_2DCFDA of MDA-MB-436 and D. MDA-MB-231 cell lines with LiCl for three and six hours. Grey = negative control, Blue = PBS control, Red = 3hr and Black = 6hr. E. Bar graph and representative histogram of DHE of MDA-MB-436 and F. MDA-MB-231 with LiCl for three and six hours.. Grey = negative control, Blue = PBS control, Red = 3hr and Black = 6hr. All data are represented as mean±SEM of at least three biological replicates. Statistical analysis was performed using unpaired students *t*-test, *p<0.05, **p<0.01, ***p<0.001.

To determine the primary species of ROS that is upregulated on depletion of DDX20, a H_2O_2-specific luciferase assay was utilised. Upon depletion of DDX20, a >3-fold and >2.5-fold increase in H_2O_2 production in MDA-MB-436 and MDA-MB-231 cell lines respectively was observed (Fig 3.4A & 3.4B). The increase in overall oxidative stress mediated by H_2O_2 was confirmed by measuring the ratio of reduced glutathione (GSH) to oxidised glutathione (GSSG). In both cell lines, a significant reduction in the ratio between GSH/GSSG was observed in cells with diminished DDX20 (Fig 3.4C & 3.4D).

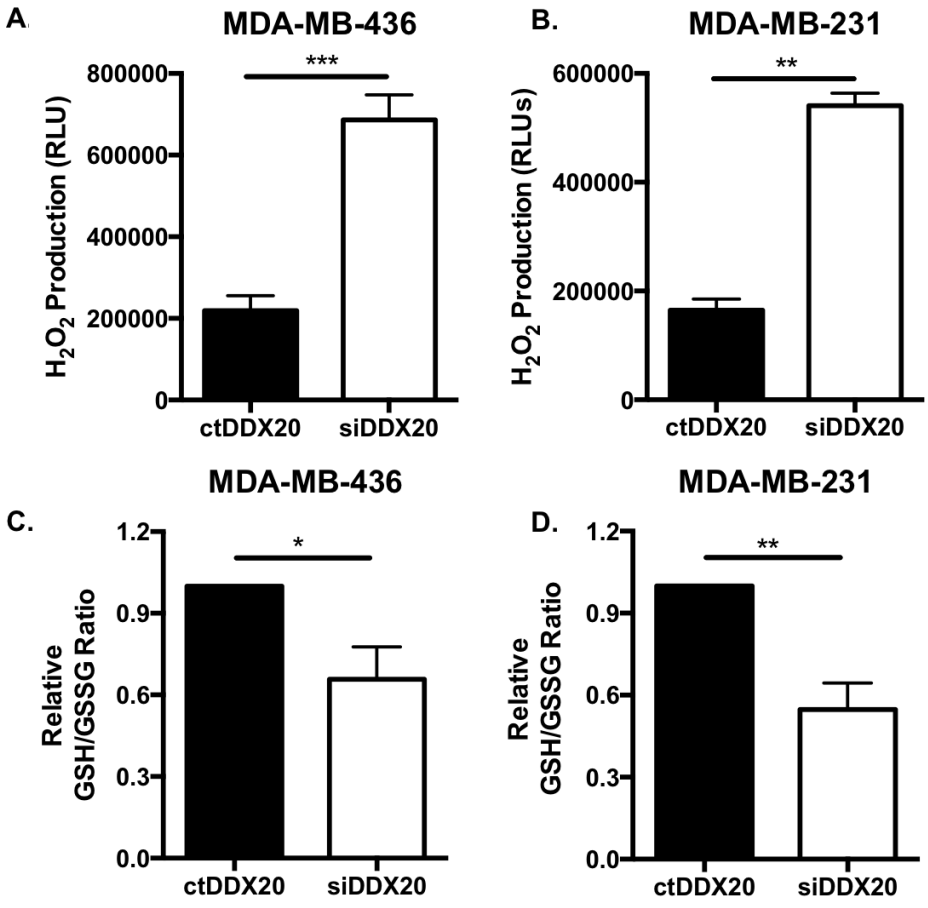

Figure 3.4. Hydrogen peroxide induced oxidative stress in TNBC cells. A&B) ROS-Glo H_2O_2 assay of MDA-MB-231 and MDA-MB-436 cells after transfection with siDDX20. H_2O_2 production is measured as relative luciferase units (RLUs). C&D) GSH/GSSG-Glo assay of MDA-MB-231 and MDA-MB-436 cells after transfection with siDDX20. Data are relative to cells transfected with control siRNA. All data are represented as mean±SEM of three

biological replicates. Statistical analysis was performed using unpaired students *t*-test, *p<0.05, **p<0.01, ***p<0.001.

3.2.3. TCF4 transcription mediated by DDX20 is responsible for Wnt signalling-mediated oxidative stress

To further validate that Wnt signalling can cause changes to intracellular redox conditions, immunofluorescence was used to co-stain for CM-H_2DCFDA and Mitotracker Deep Red. To confirm that the Wnt-mediated regulation of intracellular redox was due to DDX20 activating TCF4 transcription, a dnTCF4, which has a deleted N-terminal β-catenin-binding domain (Δ1-67), and DDX20 (pCMV-DDX20) were overexpressed. The ratio of Mitotracker Deep Red fluorescence intensity to CM-H_2DCFDA staining was measured to determine if the resultant increase in ROS was associated with changes to the mitochondrial membrane potential ($\Delta\varphi$m).

In both cell lines, cells transfected with either control siRNA or empty vectors exhibited a Mitotracker Deep Red to CM-H_2DCFDA ratio that was close to or greater than one, indicating Mitotracker fluorescence was greater than CM-H_2DCFDA fluorescence. In cells with a loss of DDX20 ROS fluorescence exceeded that of the Mitotracker Deep Red fluorescence. This was mirrored in cells transfected with dnTCF4. Furthermore, cells that overexpressed DDX20 and the dnTCF4 exhibited significantly increased ROS intensity relative to Mitotracker Deep Red intensity (Fig 3.5 A-L).

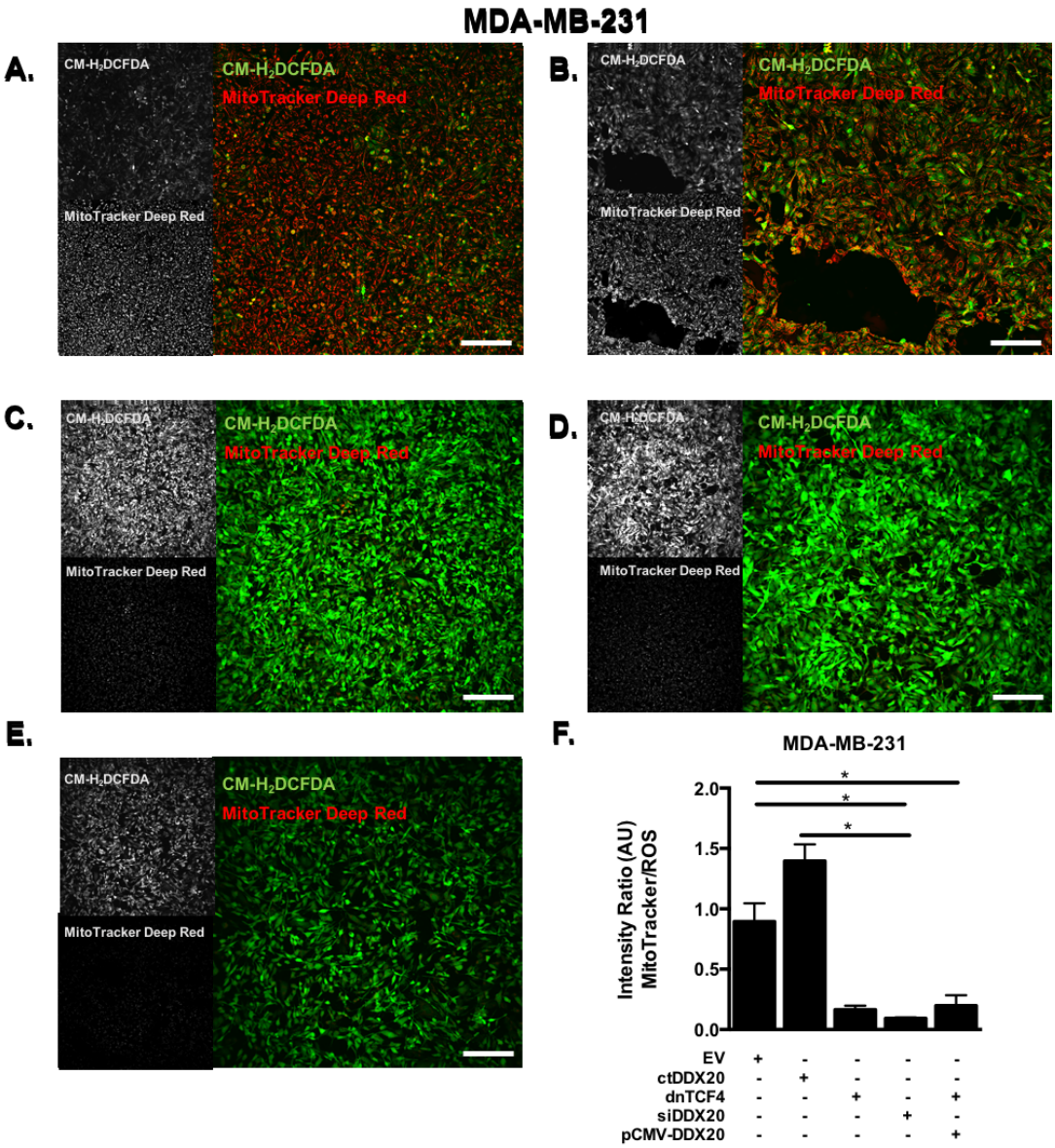
MDA-MB-231
A.
B.
C.
D.
E.
F.
CM-H2DCFDA
MitoTracker Deep Red
MDA-MB-231
Intensity Ratio (AU)
MitoTracker/ROS
2.0
1.5
1.0
0.5
0.0
*
*
*
EV + - - - -
ctDDX20 - + - - -
dnTCF4 - - + - +
siDDX20 - - - + -
pCMV-DDX20 - - - - +

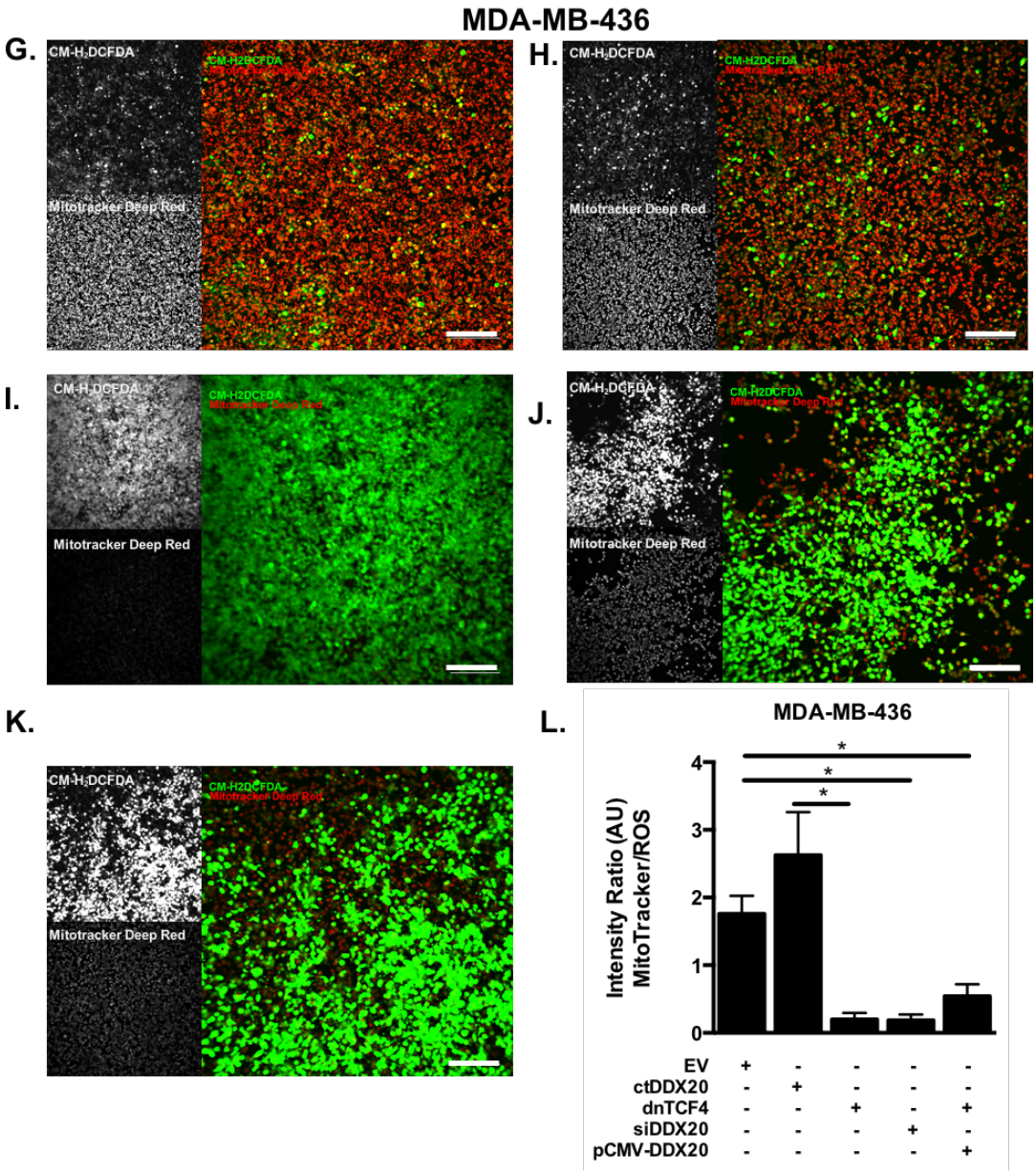

Figure 3.5. Wnt signalling mediation of intracellular redox and mitochondrial membrane potential. Immunofluorescence images of cells co-stained with CM-H_2DCFDA (Green) and Mitotracker Deep Red (Red). MDA-MB-231 cells were transfected with A) control siRNA B) empty vector C) siRNA targeting DDX20 D) dominant-negative TCF4 (dnTCF4) and E) dnTCF4 and pCMV-DDX20. F) Quantification of Mitotracker Deep Red to CM-H_2DCFDA ratio. MDA-MB-436 cells were transfected with G) control siRNA H) empty vector I) siRNA targeting DDx20 J) dominant-negative TCF4 (dnTCF4) and K) dnTCF4 and pCMV-DDX20. L) Quantification of Mitotracker Deep Red to CM-H_2DCFDA ratio. All data are represented as mean±SEM of three biological replicates. Statistical analysis was performed using students *t*-test, determined using the Sidak-Bonferroni method, α=0.005. *p<0.05, **p<0.01, ***p<0.001. Scale bar = 100μm.

3.2.4. Intracellular redox conditions modulate Wnt/β-catenin signalling in TNBC

To test what effect the overall cellular ROS levels would have on Wnt/β-catenin signalling in TNBC cells, fluorescent-activated cell sorting (FACS) was performed on both MDA-MB-231 and MDA-MB-436 cells using the CM-H_2DCFDA general ROS probe. We sorted cells based on a ROS^{dim} and ROS^{bright} phenotype that were also 7-AAD negative (as cells positive for 7-AAD are dead and exhibit higher levels of ROS) (Fig 3.6A). Following cell sorting, we performed Western blot analysis for the Wnt proteins active β-catenin (unphosphorylated S33/S37/T41) and Dvl3, as well as DDX20. The ROS^{bright} population in MDA-MB-231 cells demonstrated a significant decrease in the levels of both Dvl3 and active β-catenin proteins compared to the ROS^{dim} population. DDX20 protein levels were decreased, although not significantly. In the MDA-MD-436 cells, the same trends were observed in ROS^{bright} cells (Fig 3.6B & 3.6C).

Both cell lines were then subject to general Wnt signalling stimulation with LiCl (20mM) coupled with increasing doses of exogenous H_2O_2. We performed Western blotting and probed for proteins involved in canonical Wnt signalling. A dose-dependent decrease in the expression of both Dvl3 and active β-catenin proteins was observed, with the most effective doses being 100 and 150μM of H_2O_2 (Fig 3.6D). To further validate this, we used the same concentrations of H_2O_2 and performed a luciferase based TCF/LEF reporter assay to test for Wnt signalling activity. In both cell lines, doses of 150μM of H_2O_2 led to significant decreases in the levels of TCF/LEF transcriptional activity (Fig 3.6E). A H_2O_2 dose reponse was carried out on both cell lines, which revealed that MDA-MB-436 cells were more sensitive to lower doses of H_2O_2 than MDA-MB-231 cells (Fig S3.2).

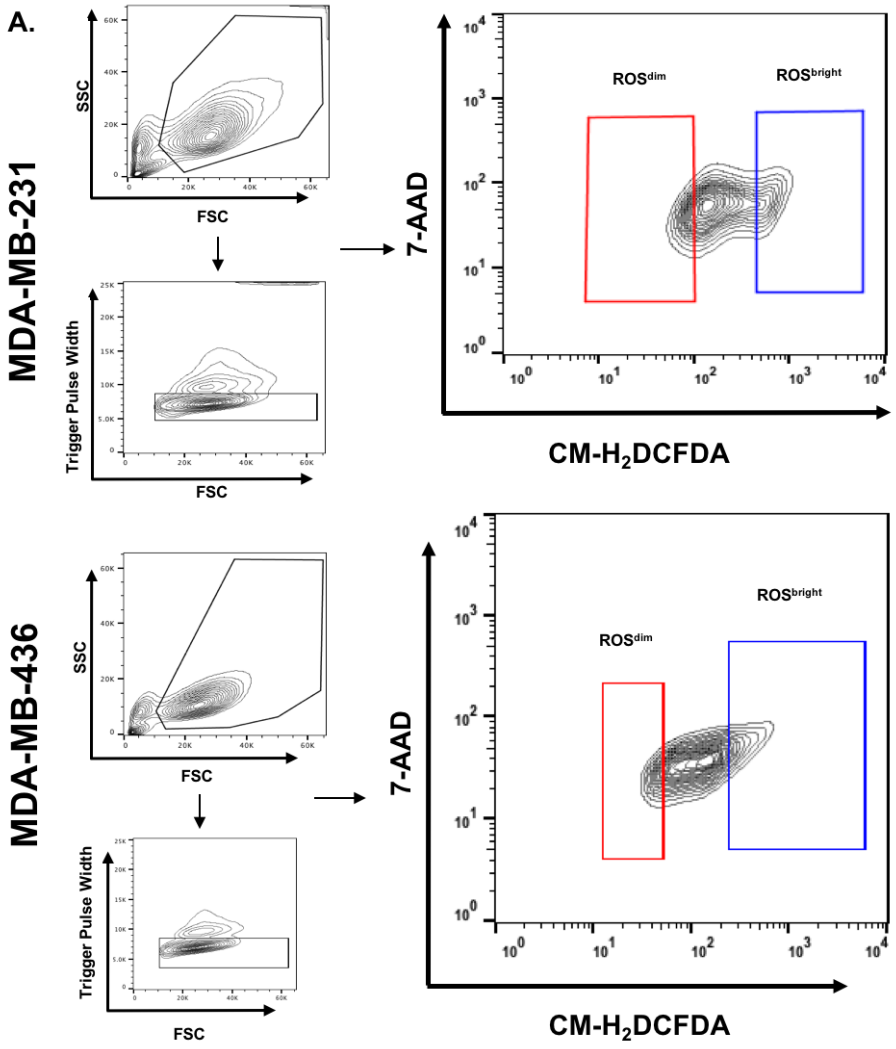
A.
MDA-MB-231
SSC
FSC
Trigger Pulse Width
FSC
7-AAD
ROSdim
ROSbright
CM-H2DCFDA
MDA-MB-436
SSC
FSC
Trigger Pulse Width
FSC
7-AAD
ROSbright
ROSdim
CM-H2DCFDA

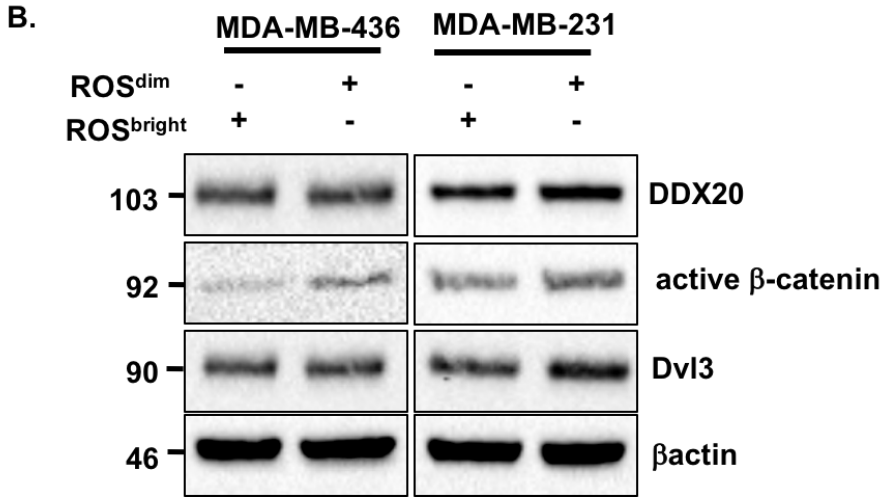
B.
MDA-MB-436
MDA-MB-231
ROSdim - + - +
ROSbright + - + -
103
DDX20
92
active β-catenin
90
Dvl3
46
βactin

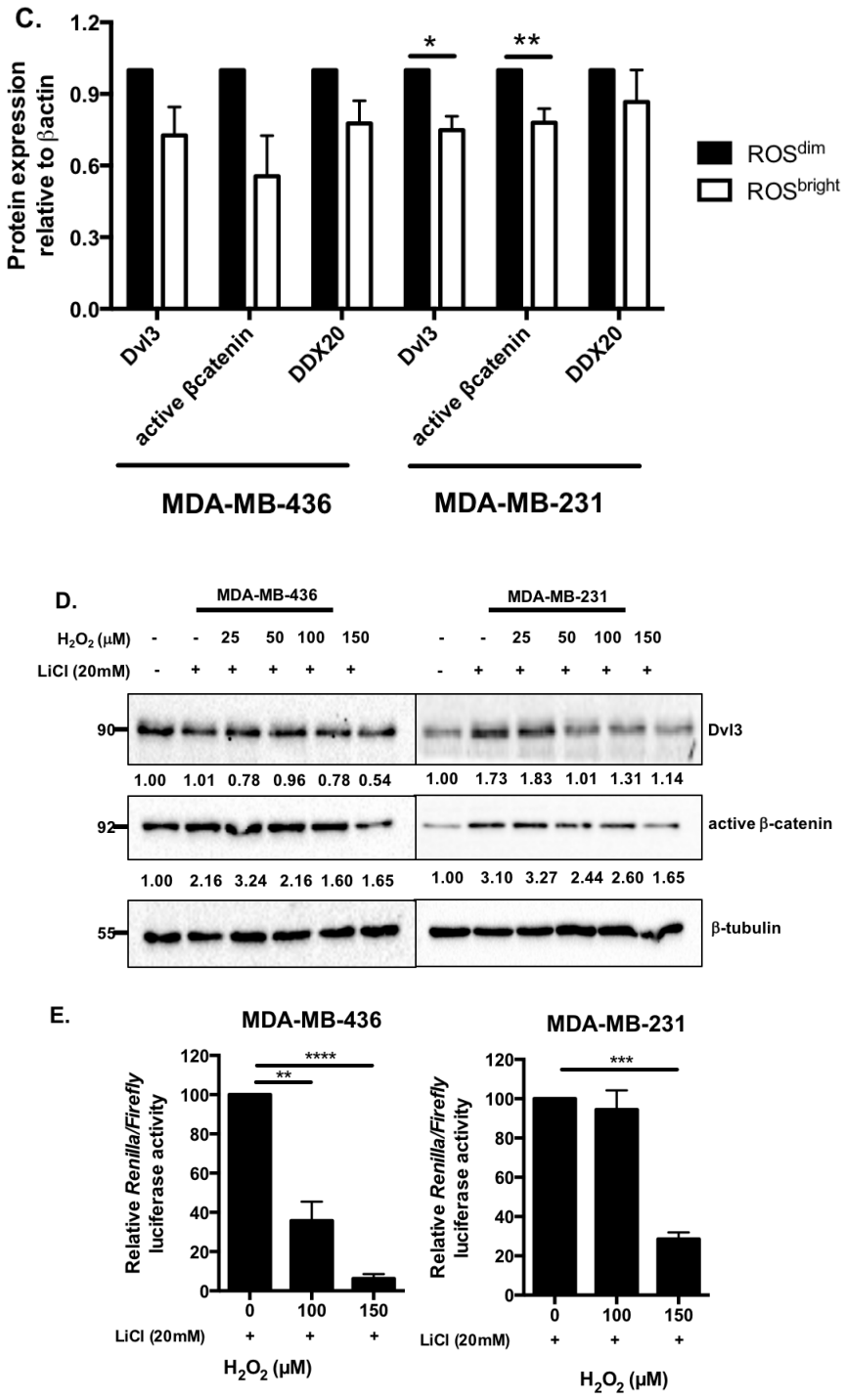

Figure 3.6. Effect of oxidative stress on Wnt/β-catenin signalling. A) Flow cytometry contour plots of gating strategy and sort populations for MDA-MB-231 and MDA-MB-436 ROS^{bright} and ROS^{dim} populations. Cell sorting populations are represented by red and blue gates for ROS^{dim} and ROS^{bright} populations respectively. X-axis is log scale CM-H_2DCFDA fluorescence and Y-axis is log scale 7-AAD fluorescence. B) Western blots of MDA-MB-231 and MDA-MB-436 ROS^{dim} and ROS^{bright} cell populations for DDX20, Dvl3, and active-β-catenin. C) Quantification of Western blots for MDA-MB-231 and MDA-MB-436 ROS^{dim} and ROS^{bright} cell populations for DDX20, Dvl3, and active-β-catenin. D) Western blot of MDA-MB-231 and MDA-MB-436 cells after stimulation with 20mM LiCl for 1 hour and increasing doses of H_2O_2 for 4 hours. Blots represent the results of one experiment, repeated three times with the same trend. E. TCF/LEF reporter assay of MDA-MB-436 and MDA-MB-231

cells after stimulation with 20mM LiCl for 1 hour and increasing doses of H_2O_2 for 8 hours. Data are represented as mean±SEM of at least three biological replicates. Statistical analysis was performed using unpaired students *t*-test, *p<0.05, **p<0.01, ***p<0.001.

3.2.5. Antioxidants partially rescue DDX20-mediated cell death

To validate whether the previously observed cell death upon loss of DDX20 (Cai & Pohl et al, unpublished) was due to oxidative stress, we performed cell viability rescue experiments with two antioxidants, glutathione and riboflavin ($vitB_2$). The loss of DDX20 resulted in significant cell death in both cell lines. The addition of glutathione at regular 24-hour timepoints was able to completely restore the cell viability lost by DDX20 depletion (Fig 3.7A & 3.7B). To further test whether the oxidative stress-mediated cell death was due to lipid peroxidation, riboflavin was added every 24 hours to one group of cells transfected with both control siRNA and siDDX20. In both cell lines, a partial restoration of cell viability 96 hours post-transfection was observed (Fig 3.7C & 3.7D).

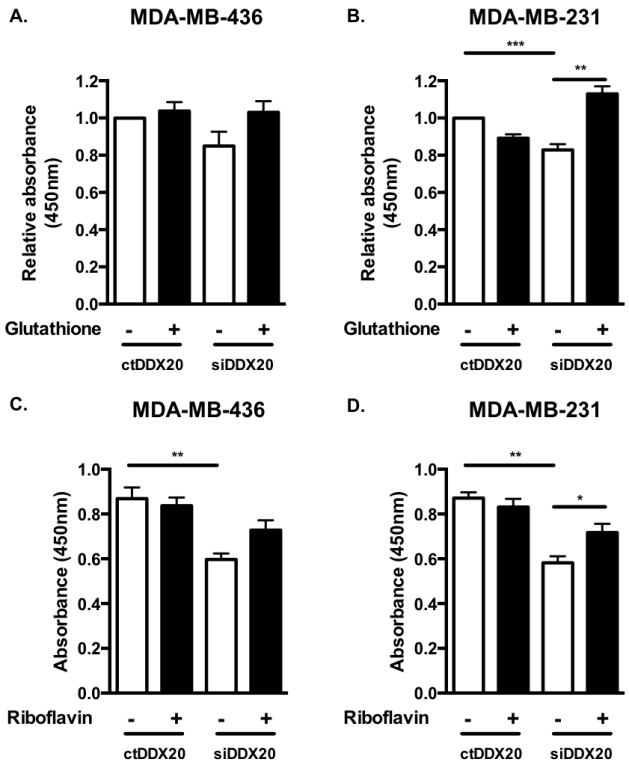

Figure 3.7. Effect of antioxidants on DDX20 depleted cells. A & B) MDA-MB-436 and MDA-MB-231 cells treated with 500nM glutathione every 24 hours for 96 hours in one group of cells transfected with control of siRNA targeting DDX20. C & D) MDA-MB-436 and MDA-MB-231 cells treated with 600nM riboflavin every 24 hours for 96 hours in one group of cells transfected with control of siRNA targeting DDX20. Data are represented as mean±SEM of at least 3 biological replicates. Statistical analysis was performed using unpaired students *t*-test, *p<0.05, **p<0.01, ***p<0.001.

3.2.6. Catalase expression is mediated through a Wnt-DDX20-TCF4 axis

To validate the *in silico* finding that catalase was associated with DDX20 and canonical Wnt signalling, DDX20 was knocked down and Western blotting for catalase expression performed. In both cell lines, catalase expression was significantly reduced (Fig 3.8A & 3.8B). Furthermore, when a dnTCF4 plasmid was overexpressed, a significant reduction in catalase expression was observed. This was unable to be rescued with the ectopic overexpression of DDX20 (Fig 3.8C & 3.8D).

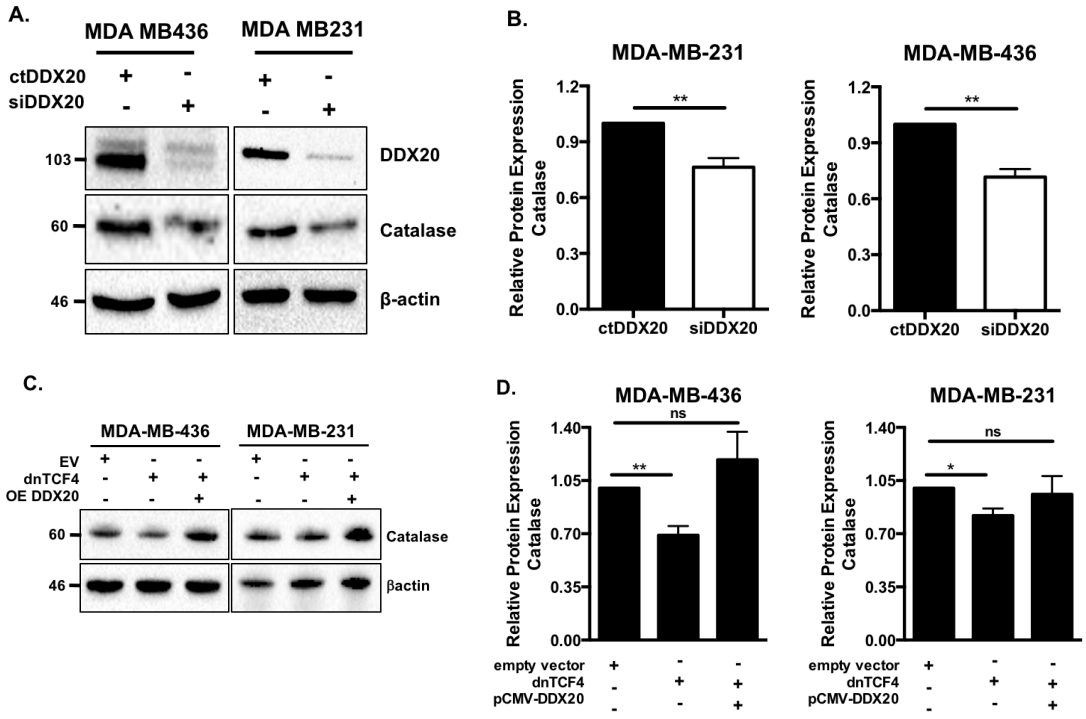

Figure 3.8. Catalase expression regulation by DDX20 and Wnt signalling. A) Western blots of Catalase expression in MDA-MB-231 and MDA-MB-436 cells transfected with control siRNA or siRNA targeting DDX20. B) Quantification of catalase expression from Western blots. C) Western blots of catalase in MDA-MB-436 and MDA-MB-231 cells transfected with empty vector, dnTCF4 or pCMV-DDX20 in combination with dnTCF4. D) Quantification of Western blots for catalase protein expression in MDA-MB-436 and MDA-MB-231 cells. Data are represented as mean±SEM of at least three biological replicates. Statistical analysis was performed using unpaired students *t*-test, *p<0.05, **p<0.01, ***p<0.001.

3.2.7. Catalase is transcriptionally regulated by TCF4 mediated by Wnt3a and DDX20

Using the ENCODE ChIP-seq portal (http://genome.ucsc.edu/encode), it was found that there were TCF4 (TCF7L2) ChIP-seq peaks situated distal to the

core promoter region in the DNA of catalase (Fig 3.9A). To validate whether this occurred MDA-MB-231 and MDA-MB-436 cells, chromatin immunoprecipitation (ChIP) was performed using primers designed around the TCF4 binding site, and a binding site proximal to the core promoter to which TCF4 was not predicted to bind. After immunoprecipitation of TCF4, it was found that TCF4 was bound to catalase DNA at the predicted binding site (Fig 3.9C). Furthermore, we witnessed an increase in the recruitment of TCF4 to the catalase gene in cells stimulated with Wnt3a for two hours (Fig 3.9D). Conversely, in cells depleted of DDX20, there was a decrease in the recruitment of TCF4 to the catalase gene, albeit in the presence of Wnt stimulation (Fig 3.9E). These changes in TCF4 recruitment were mirrored by changes in gene expression. We witness significant decreased catalase gene expression following knockdown of DDX20 (Fig 3.9F) and increased expression of catalase following Wnt3a stimulation (Fig 3.9G).

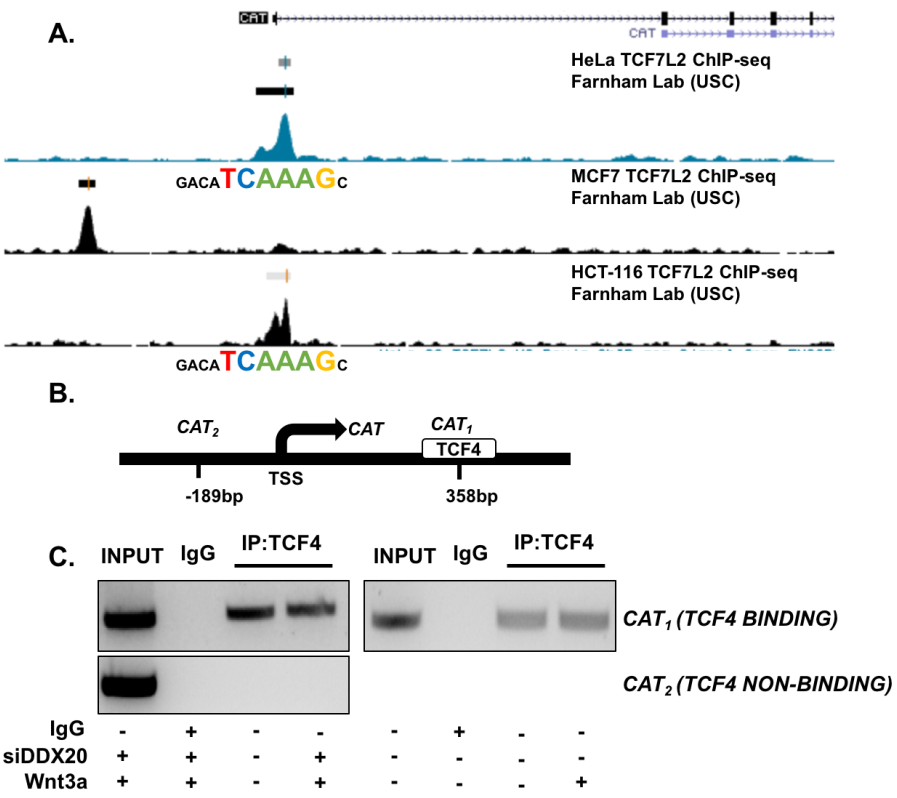

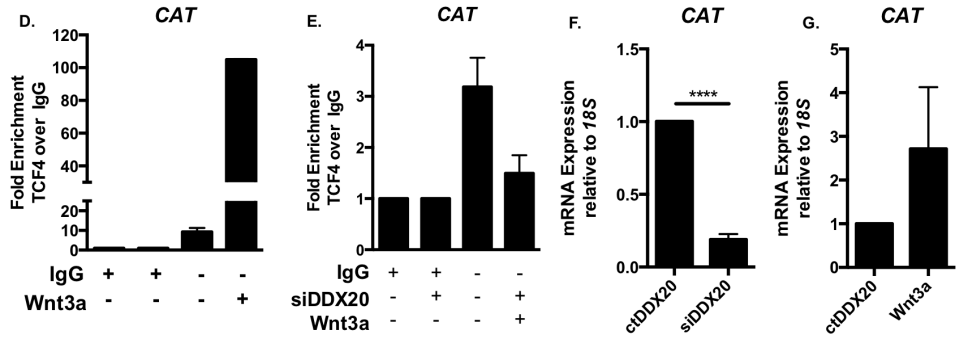

Figure 3.9. Transcription regulation of Catalase by TCF4. A) ChIP-seq tracks and peaks from MCF-7, HCT-116, and HeLa cells from ENCODE ChIP-seq data viewer centred around catalase gene TSS. Coloured bases indicate TCF4 binding sequence on *CAT* DNA. B) Schematic of primer design and binding sites of TCF4 on Catalase DNA. CAT_1 is TCF4 binding site, CAT_2 is non-TCF4 binding site. C) Semi-quantitative PCR of TCF4 ChIP in cells stimulated with Wnt3a (200ng/mL) for two hours and cells stimulated with Wnt3a and silenced DDX20. D) ChIP-qPCR of fold recruitment relative to IgG control after Wnt3a simulation. E) ChIP-qPCR of fold recruitment relative to IgG control after transfection with siDDX20 and Wnt3a stimulation. ChIP-qPCR for siDDX20 treated cells is a representative result of three biological repeats with a similar trend. ChIP-qPCR for Wnt3a represents a representative result of two biological repeats with a similar trend. F) Q-PCR of catalase expression following knockdown of DDX20. G) Q-PCR of catalase expression following stimulation with 200ng/mL for 4 hours. Q-PCR data are represented as mean±SEM of at least three biological replicates. Statistical analysis was performed using unpaired students *t*-test, *p<0.05, **p<0.01, ***p<0.001.

3.2.8. DDX20 regulates intracellular redox *in vivo*

A Gemin3 (DDX20) knockout and Gemin3 over-expressing *Drosophila* model was generated (Tolwinski Lab, Yale-NUS College, Singapore). Gemin3 knockout is embryonically lethal, therefore, the assessment of ROS scavenger gene expression was performed on embryos. A GAL4/UAS system was utilised to develop the Gemin3-overexpressing model driven by an ubiquitously-expressed double driver of Armadillo and Daughterless ($Gemin3^{arm/da}$), the *Drosophila* orthologues for β-catenin and TCF4 respectively (Fig 3.10A).

When gene expression in the Gemin3 KO and $Gemin3^{arm/da}$ was performed, the results clearly demonstrated that Gemin3 regulates the gene expression of a variety of ROS scavengers. In the Gemin3 knockout, expression of Sod1, Sod3, and dhd (*Drosophila* orthologue of thioredoxin-1) were all significantly increased, while all were significantly decreased when Gemin3 was overexpressed (Fig 3.10B). Catalase expression was decreased in the Gemin3 knockout, although the overexpression of Gemin3 had a similar effect.

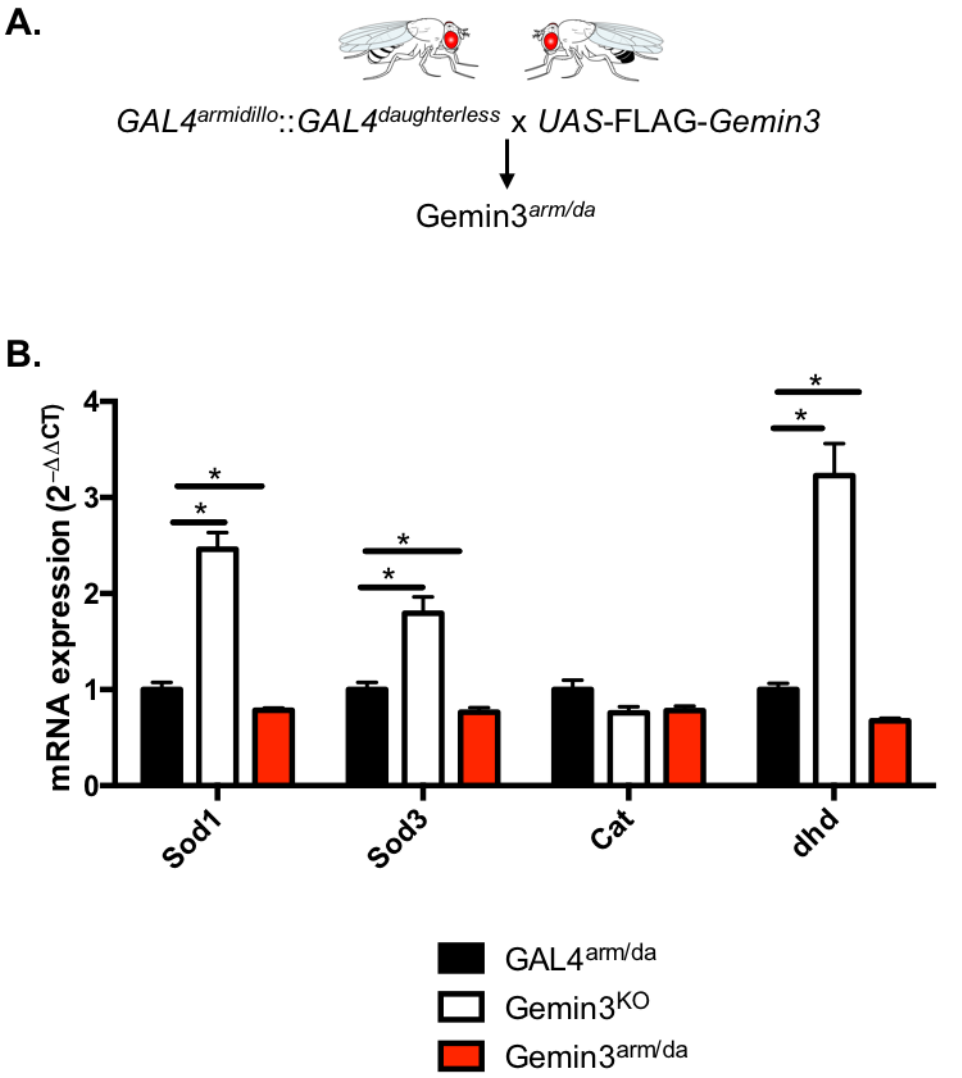

Figure 3.10. *In vivo* validation of DDX20 regulation of ROS. A) Schematic of generation of Gemin3 overexpressing Drosophila fly embryos. B) Q-PCR of Drosophila mRNA expression for Sod1, Sod3, Cat, and dhd in control ($GAL4^{arm/da}$), Gemin3 knockout ($Gemin3^{KO}$) and Gemin3 overexpressing ($Gemin^{arm/da}$) flies. Data are represented as mean±SEM of at least three biological replicates. Statistical analysis was performed using unpaired students *t*-test, *p<0.05, **p<0.01, ***p<0.001.

3.3 DISCUSSION

This is the first study to implicate DDX20 in the regulation of cellular redox. Furthermore, this is also the first time that canonical Wnt signalling – directly through TCF4-mediated gene transcription – has been directly associated with the regulation of genes involved in ROS detoxification, namely catalase. We have provided evidence to demonstrate that DDX20 is essential for canonical Wnt signalling and the loss of DDX20 can cause an increase in oxidative stress, mediated through decreased catalase expression, resulting in cell death.

Using a combination of ROS probes, it was demonstrated that a loss of DDX20 resulted in increased oxidative stress, primarily through increased H_2O_2 production; conversely, the activation of the Wnt pathway decreased overall oxidative stress while increasing superoxide (O_2^-) production. While GSK3β inhibition with LiCl is known to activate other targets, it is widely known for increasing active β-catenin and promoting its nuclear translocation.[303,304] Superoxide is a known activator of oncogenic signalling. A recent study by Ogrunc *et al.*[305] demonstrated that superoxide generated from Rac1 and NADPH4 initiates hyperproliferation of cancer cells. Conversely, lower concentrations of H_2O_2 have been shown to be pro-proliferative in mammalian cells.[306] Furthermore, favouring O_2^- over H_2O_2 has been clearly shown to promote oncogenic signalling.[251] This is consistent with results in this study, wherein the activation of Wnt signalling coincides with intracellular redox conditions favouring a pro-oxidant environment.

H_2O_2 and oxidative stress have been shown to both positively and negatively regulate Wnt/β-catenin signalling. Previous studies suggest that apoptotic doses (>200μM) activate Wnt signalling initially (<60 minutes),[256] although longer term treatment results in the suppression of β-catenin-mediated signalling.[307] Exogenous treatment with H_2O_2 was found to suppress Wnt signalling at the level of Dvl, which affects downstream active β-catenin expression. This is consistent with a study by Shin *et al.*[307], which demonstrated that overexpression of Dvl-1 rescued H_2O_2-mediated suppression of Wnt signalling. By using cell sorting to separate cells based on their overall levels of oxidative stress, it was determined that even in clonal cell populations, there are differences in the variations in ROS levels. These levels were shown to impact Wnt signal transduction through regulation of protein expression of Dvl3 and active β-catenin. A significant decrease in DDX20 was not observed, which suggests that DDX20 is either upstream or parallel to Dvl in Wnt signalling transduction and may not be affected by H_2O_2 suppression of Dvl3.

High levels of basal ROS have been shown to be pivotal in carcinogenesis, specifically by activating oncogenic signalling pathways.[308] When levels of ROS become too high, this can initiate cell death through a

variety of mechanisms, including DNA damage,[309] caspase activation,[310] and iron-dependent cell death, or ferroptosis.[311] The loss of DDX20 increases intracellular ROS to a point that results in cell fate decisions favouring cell death. This was completely rescued after the cells were treated with glutathione. Glutathione is able to reduce oxidative stress through its redox cycle[312] and has been demonstrated to be required for cancer initiation.[313] Riboflavin was evaluated for its ability to rescue DDX20-mediated cell death, which would provide evidence that DDX20 loss results in high levels of lipid peroxidation and is suggestive of death by ferroptosis.[314,315] Cell death was incompletely rescued after the loss of DDX20, suggesting that although increased lipid peroxidation may be partially responsible, it is not the major contributor to the observed cell death.

Catalase is an ROS scavenging enzyme responsible for catalysing the breakdown of H_2O_2 to oxygen and water. This study suggests that the downregulation of catalase mediated by the loss of DDX20 may be partially responsible for the increased H_2O_2-induced oxidative stress and cell death demonstrated. The exogenous addition of catalase did not completely abrogate the increase in ROS levels after DDX20 depletion, although catalase will not directly endocytose into the cell within a short period of time and therefore will not scavenge intracellular H_2O_2. Furthermore, this study provides direct evidence that Wnt/β-catenin signalling through TCF4 transcription regulates catalase expression. Higher levels of catalase through Wnt activation keep H_2O_2 levels low, and confer a pro-oxidant environment permissive for oncogenic signalling. Low levels of catalase following the loss of DDX20 create high levels of H_2O_2 and oxidative stress-induced cell death. A previous report has demonstrated that the loss of β-catenin in haematopoietic stem cells resulted in increased oxidative stress, which was concurrent with decreased catalase expression, although there was no mechanistic data provided.[316] All previous reports of β-catenin-mediated transcription of catalase were through the association of β-catenin with FoxO transcription factors,[285,300] which have a primary role in the regulation of ROS-scavenging enzymes.[317] This occurs during oxidative stress, where β-catenin is diverted from TCF transcription factors to FoxO transcription

factors.[318] A possible explanation why catalase expression is not kept at homeostatic levels by β-catenin diverting to FoxO transcription factors under oxidative stress in this study, is that the loss of DDX20 also results in the loss of transcriptionally active β-catenin (Cai & Pohl, unpublished, also see Chapter 5). This results in the loss of available β-catenin, which would otherwise be diverted to FoxO, and instead could lead to the suppression of FoxO-mediated transcription of catalase, resulting in high intracellular concentrations of H_2O_2.

DDX20 has been confirmed in this study to influence the transcription of redox regulator genes *in vivo* using a *Drosophila* embryo model in which Gemin3 (DDX20) is knocked out and in a Gemin3-overexpressing model driven by the orthologues of human β-catenin and TCF transcription factors. This is also the first report of Gemin3 influencing cellular redox in an *in vivo* model. Catalase gene expression was reduced in Gemin3^{KO} embryos, although Gemin3^{KO} embryos had increased expression of Sod1, Sod3, and dhd (thioredoxin 1). Conversely, the overexpression of Gemin3 decreased the expression of Sod1, Sod3, and dhd. A genetically encoded ROS probe was attempted to be used in the Gemin3^{KO} and Gemin3^{OE} models, although the ROS sensor was not able to be expressed at high enough levels at the embryonic stage in which embryos were still viable. The changes in gene expression of these redox regulators are suggestive of changes in overall cellular redox. It has been previously demonstrated that differences in the intracellular redox mileu can directly lead to changes in the expression of specific gene targets to counter a rise or fall in ROS concentrations.[319] A recent study by Wang *et al*,[320] has implicated Wnt signalling in redox regulation of germ cell differentiation in *Drosophila* larvae through glutathione-S-transferase (GST) expression. Upon knockdown of dishevelled (Dsh) in *Drosophila* larvae, intracellular ROS was increased, which also coincided with a decrease in germ cell differentiation. This was rescued in dsh^{KD} larvae that overexpressed catalase, Sod1, and GST2. This study demonstrates that Wnt signalling is a determinant of cell fate in a redox-mediated mechanism.

Overall, this report has demonstrated that DDX20/Gemin3 is a regulator of cellular redox *in vitro* and *in vivo* in a Wnt-dependent manner. This is the first study to directly implicate TCF4 is the regulation of cellular redox through catalase expression. An increase in oxidative stress, predominately in the form of increased H_2O_2, was observed, which resulted in cell death. The addition of catalase was unable to completely rescue the increased ROS, which suggests that there is another source of ROS within these cells that is contributing to the increased oxidative stress. A major source of ROS within the cells is from the mitochondria. These findings demonstrated that mitochondrial polarisation is dependent on DDX20 and Wnt signalling through TCF4. Mitochondrial ROS and redox regulators involved in ROS detoxification located within the mitochondria may provide a further source contributing to the increased oxidative stress witnessed with depletion of DDX20 and suppression of Wnt signalling.

3.4 ACKNOWLEDGMENTS

This study would like to acknowledge members of the Tolwinski Lab (Yale-NUS College, Singapore), Nicholoas S Tolwinski and Jahnavi Suresh for the generation of the Drosophila data.

3.5 SUPPLEMENTARY MATERIALS CHAPTER 3

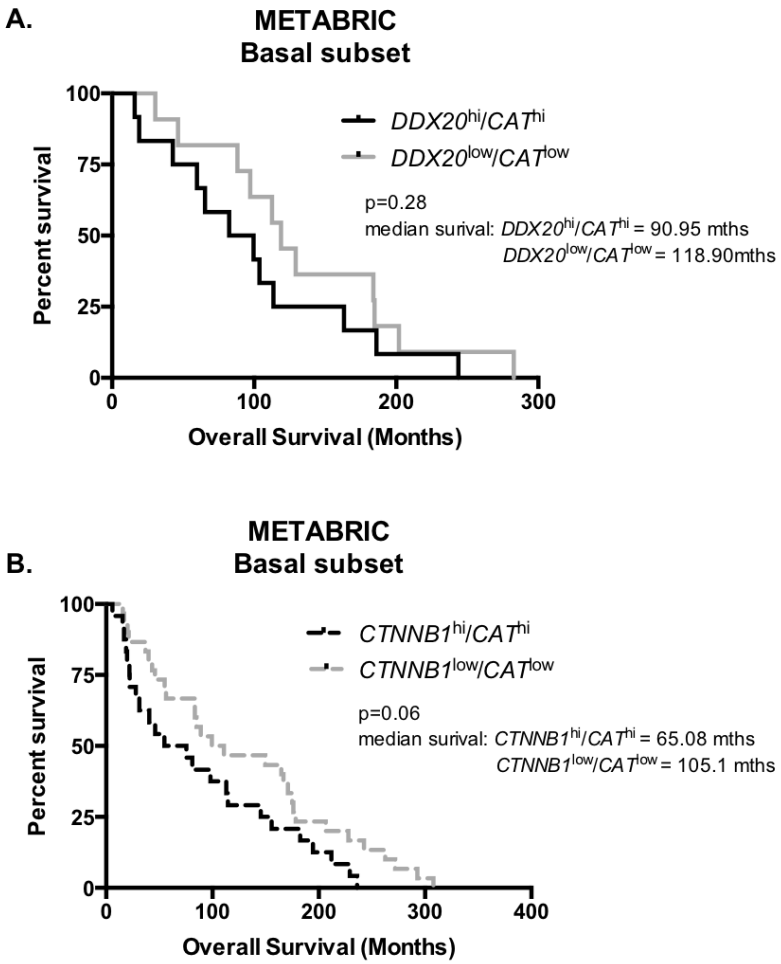

Fig S3.1. Survival analysis from TNBC METABRIC cohorts. A) Overall survival analysis of *DDX20^{hi}/CAT^{hi}* individuals versus *DDX20^{low}/CAT^{low}* from PAM50 basal subtype of METABRIC cohort. B) Overall survival analysis of *CTNNB1^{hi}/CAT^{hi}* individuals versus *CTNNB1^{low}/CAT^{low}* from PAM50 basal subtype of METABRIC cohort. Survival statistics were performed using Mantel-Cox (logrank) test and calculated on Prism GraphPad.

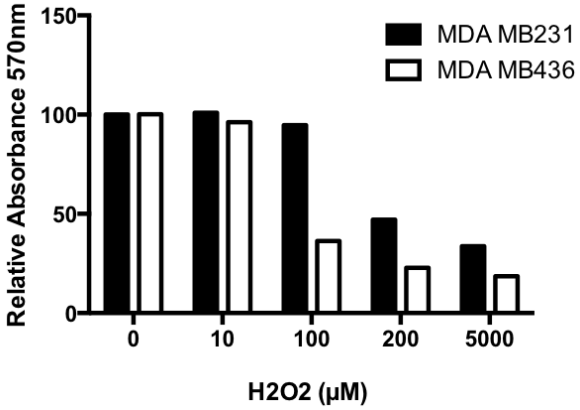

Fig S3.2. Dose response to H_2O_2 treatment. CCK8 viability assay of MDA-MB-231 and MDA-MB-436 cells after increasing doses of H_2O_2 for 24 hours. Data is representative of two biological repeats with four technical replicates.

CHAPTER 4: DDX20 REGULATES MITOCHONDRIAL FUNCTION IN A WNT/β-CATENIN DEPENDENT MANNER

CHAPTER 4: DDX20 REGULATES MITOCHONDRIAL FUNCTION IN A WNT/β-CATENIN DEPENDENT MANNER

4.1 INTRODUCTION

Mitochondrial dynamics and metabolism play a crucial role in the progression of cancer.[321] TNBC is characterised by having many mitochondrial functional and genetic defects that contribute to the mitochondrial heterogeneity among TNBC patients.[322] This chapter will focus on the role of DDX20 mediation of mitochondrial function through Wnt/β-catenin signalling in two TNBC cell lines, MDA-MB-231 and MDA-MB-436. In a study investigating mitochondrial dysfunction in TNBC, MDA-MB-231 and MDA-MB-436 cells both exhibited a similar mitochondrial metabolic profile in terms of oxygen consumption rate (OCR) and extracellular acidification rate (ECAR).[323] The results demonstrate that the loss of DDX20 results in differential regulation of Ubiquinol cytochrome c Reductase subunit 2 (UQCRC2) – a component of the mitochondrial electron transport chain Complex III – and SOD2, a membrane-bound mitochondrial ROS scavenger. This leads to increased mitochondrial oxidative stress, respiratory dysfunction, loss of membrane potential, and changes to mitochondrial DNA (mtDNA) copy numbers. Activation of Wnt signalling results in increased expression of *UQCRC2* and decreased expression of *SOD2* (Fig 4.1). This is the first report of TCF4-mediated regulation of SOD2 and UQCRC2, clearly implicating canonical DDX20-medated Wnt signalling in the regulation of mitochondrial ROS (mitoROS) and mitochondrial respiration.

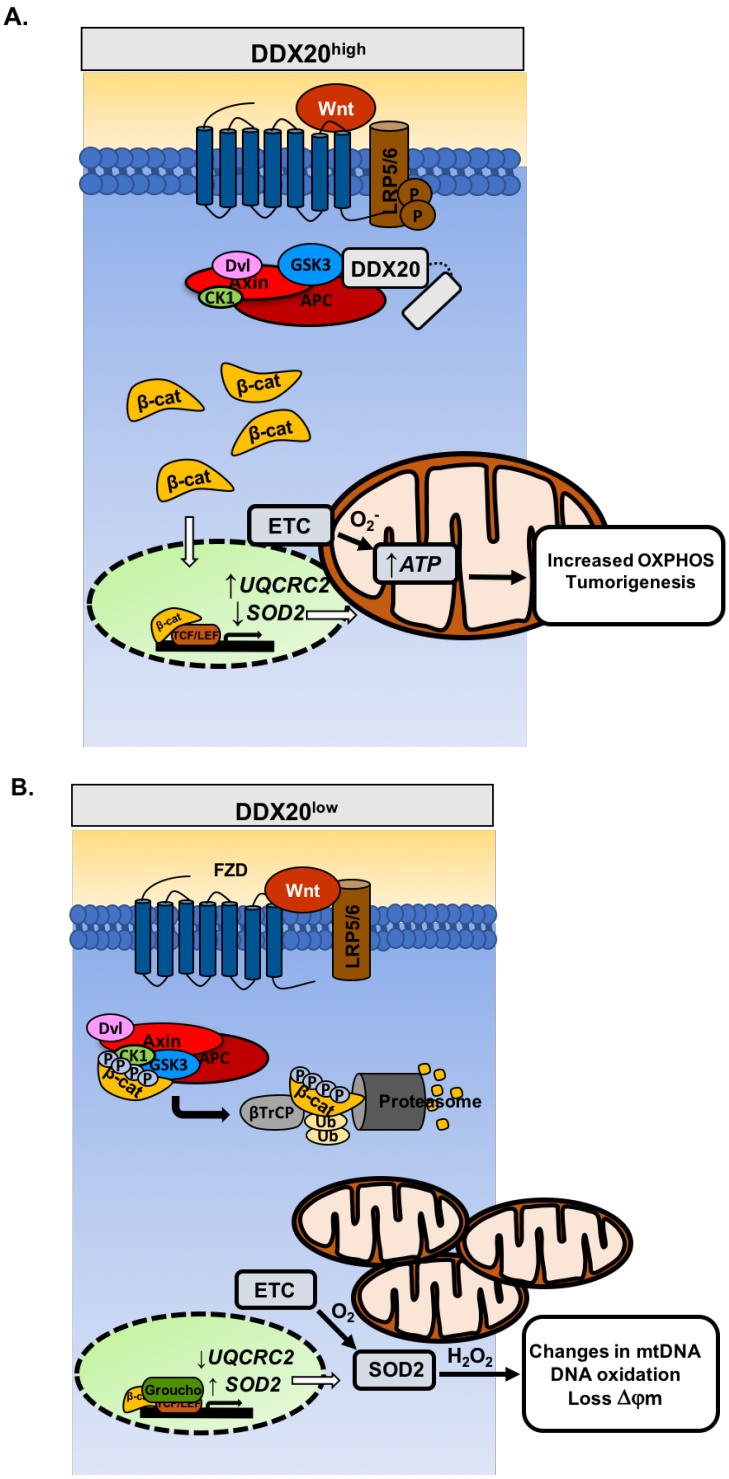

Figure 4.1. DDX20 mediation of mitochondrial function. A) DDX20^{high} cells demonstrate increased canonical Wnt signalling, which increases UQCRC2 expression while decreasing SOD2 expression mediated through TCF4. This results in higher OXPHOS and increased energy production for tumorigenesis. B) The loss of DDX20 results in increased SOD2 expression and decreased UQCRC2 expression. This results in decreased mitochondrial respiration and increased oxidative stress, ultimately leading to loss of mitochondrial membrane potential, mitochondrial dysfunction, and changes in mtDNA copy number.

4.2 RESULTS

4.2.1 DDX20^{HIGH} phenotypes are enriched in gene sets relating to mitochondrial processes and mitochondrial apoptosis regulation

To determine whether DDX20 was associated with mitochondrial function and regulation, GSEA was performed on the DDX20^{high} and DDX20^{low} phenotypes from the METABRIC TNBC cohort. The results indicated numerous gene sets enriched in the DDX20^{high} population involved with mitochondrial processes, including apoptotic mitochondrial changes (GO:0008637), protein localization to mitochondrion (GO:0070585), mitochondrial RNA metabolic process (GO:0000959), and regulation of release of cytochrome C from mitochondria (GO:0090199) (Fig 4.2A,B,C&D).

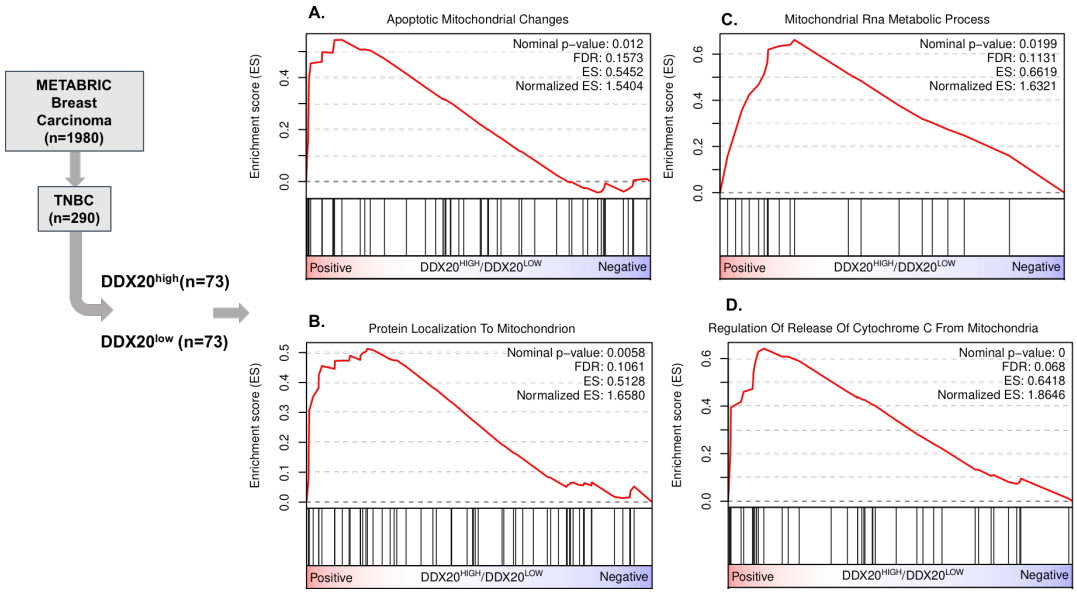

Figure 4.2. Gene set enrichment analysis of DDX20 in TNBC. GSEA enrichment plot of GO gene set A) Apoptotic mitochondrial changes; B) Protein localization to mitochondrion; C) Mitochondrial RNA metabolic process; and D) Regulation of release of cytochrome C from mitochondria in DDX20^{high} vs DDX20^{low} patient phenotypes. Nominal *p*-value, FDR (false discovery rate), enrichment score (ES), and normalised ES were calculated using GSEA software from Broad Institute.[291]

To determine whether there was an association between DDX20, canonical Wnt signalling, and mitochondrial gene expression, publicly-available datasets from cBioPortal were accessed. To confirm an association between DDX20 and UQCRC2, co-expression analysis was performed on DDX20 and nine nuclear-encoded complex III subunits. The only positive correlation in gene expression between DDX20 and the complex III subunits was with

UQCRC2 (Fig 4.3A). When this analysis was performed for multiple cancer types, it was demonstrated that the highest frequency of *UQCRC2* was in the METABRIC and TCGA breast cancer cohorts (Fig 4.3B). It was previously demonstrated (Chapter 3) that the loss of DDX20 results in increased H_2O_2. This observation led to the examination of the major producer of H_2O_2 in the mitochondria, *SOD2*. It was revealed that *SOD2* is overexpressed in the basal and claudin-low TNBC subtypes (Fig 4.3C) and in TNBC cell lines when compared to luminal subtypes (Fig 4.3D). When co-expression analysis was performed on SOD2 and the Wnt target gene AXIN2, there was a significant negative correlation between the two (Fig 4.3E). Survival analysis on individuals with combinatorial patterns of *DDX20* and *SOD2* expression failed to reveal any phenotype with a significantly better or poorer survival outcome; when median survival was calculated, it was identified that individuals with a $DDX20^{hi}/SOD2^{hi}$, $DDX20^{low}/SOD2^{low}$, $DDX2^{low}/SOD2^{hi}$, and $DDX20^{hi}/SOD2^{low}$ phenotype had median overall survivals of 7.3, 8.7, 7.1, and 5.2 years respectively (Fig S4.1A).

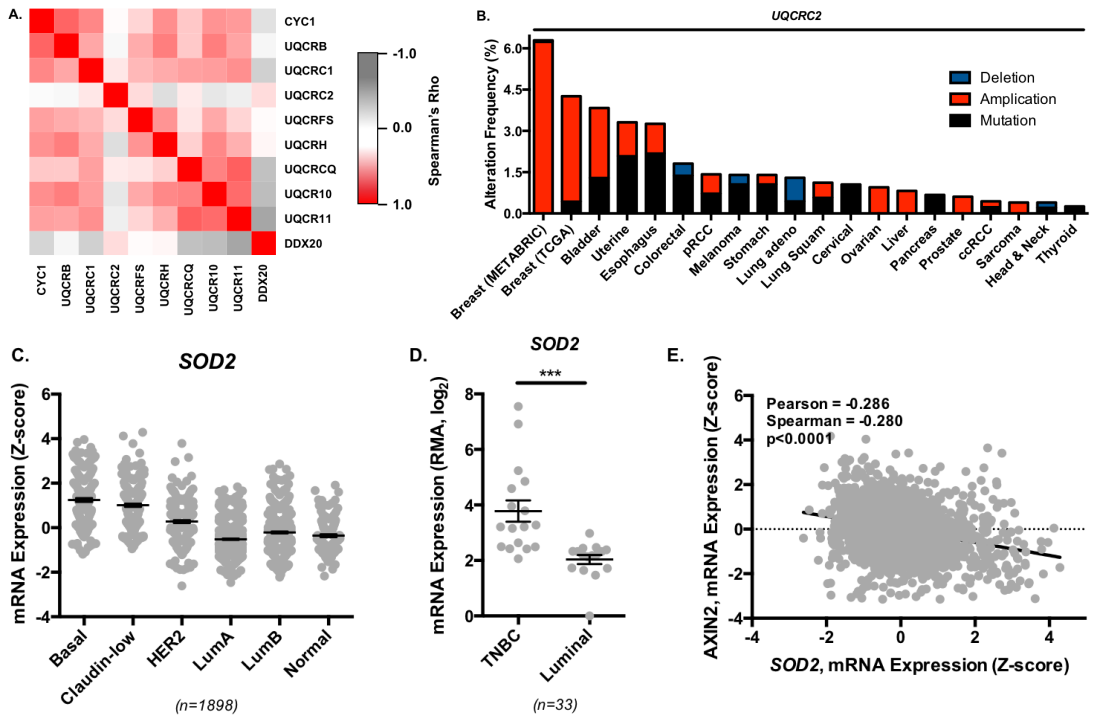

Figure 4.3. Bioinformatics analysis on DDX20, SOD2, and UQCRC2 in breast cancer cohorts. A) Spearman's correlation (ρ or Rho) of DDX20, UQCRC2 and all mitochondrial complex III subunits in TCGA cohorts for all breast cancer. B) Alteration frequency of *UQCRC2* in various cancer cohorts. C) PAM50 subtypes for *SOD2* expression in METABRIC breast cancer cohort. D) *SOD2* expression in a selection of TNBC and luminal

subtype cell lines. Accessed from CCLE data through cBioPortal. E) Spearman's correlation (ρ or Rho) of *SOD2* and *AXIN2* in TCGA cohorts for all breast cancer subtypes. Statistical analysis was performed using unpaired Student's *t*-test, *p<0.05, **p<0.01, ***p<0.001.

4.2.2 DDX20 regulates mitochondrial ROS and mitochondrial membrane potential

To confirm the previous observations (Chapter 3) that depletion of DDX20 results in changes to mitochondrial membrane potential and mitochondrial morphology, higher magnification immunofluorescence was used to stain for Mitotracker Deep Red. The results revealed that polarised mitochondrial membranes in the control cells (ctDDX20) were much more tubular and dispersed throughout the cytoplasm, whereas cells diminished of DDX20 (siDDX20) presented a more fragmented appearance and were situated around the perinuclear regions of the cell (Fig 4.3A&B). Next, mitochondrial superoxide levels were assessed. These results indicated that the loss of DDX20 in both cell lines corresponded to a significant decrease in mitochondrial superoxide, as measured by the MitoSox Red probe (Fig 4.3C&D). Furthermore, 3D immunofluorescence stacking of MDA-MB-231 cells after DDX20 knockdown demonstrates a clear decrease in the distribution and amount of Mitotracker Deep Red in siDDX20 transfected cells (Fig S4.2).

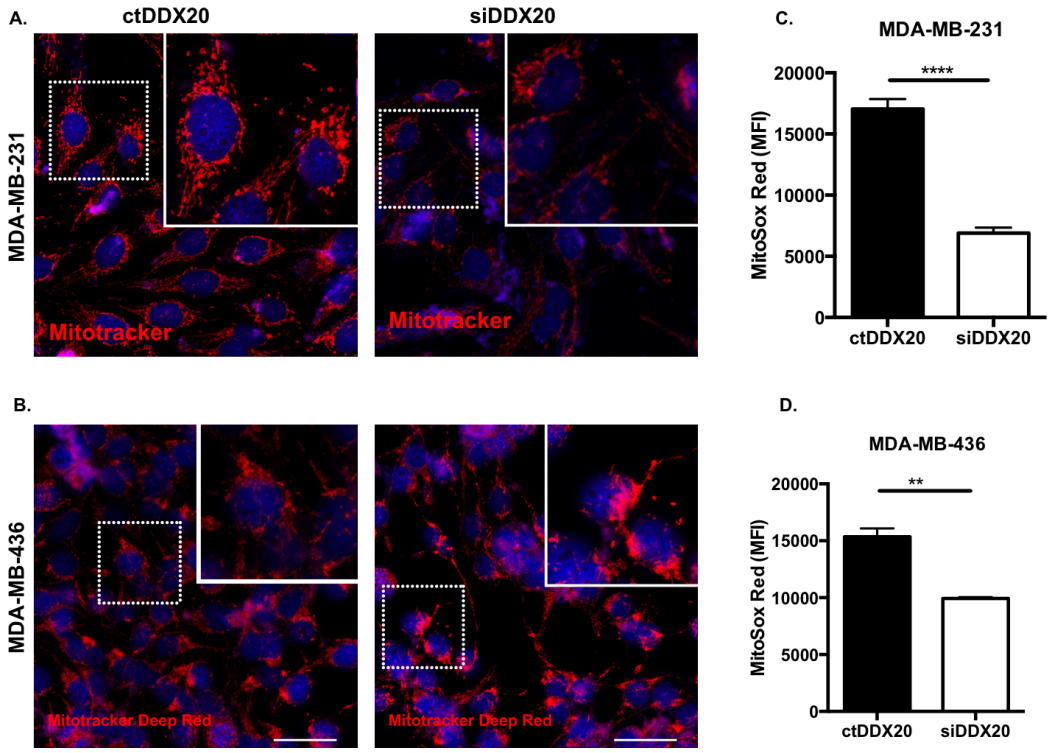

Figure 4.4 Measurement of mitoROS and membrane potential. A) MDA-MB-231 cells transfected with control siRNA (ctDDX20) or siDDX20 stained for Mitotracker Deep Red (Red) and DAPI (Blue). B) MDA-MB-436 cells transfected with control siRNA (ctDDX20) or siDDX20 stained for Mitotracker Deep Red (Red) and DAPI (Blue). Images were taken at 60X, scale bar = 75μm. C) Flow cytometric measurement of MitoSox Red in MDA-MB-231 cells, and D) Flow cytometric measurement of MitoSox Red in MDA-MB-436 cells. Data are represented as mean fluorescence intensity (MFI). Statistical analysis was performed using unpaired Student's *t*-test, *$p < 0.05$, **$p < 0.01$, ***$p < 0.001$.

4.2.3 Mitochondrial membrane potential and mass is regulated by DDX20 in a TCF4-dependent manner

To determine whether the changes in mitochondrial membrane potential were associated with a change in mitochondrial mass, co-staining of MDA-MB-231 and MDA-MB-436 cells was performed using Mitotracker Green and Mitotracker Deep Red; Mitotracker Green stains mitochondria irrespective of membrane potential, while Mitotracker Deep Red will only stain mitochondrial membranes that are not depolarised. To assess the proportion of mitochondria with polarised membranes relative to overall mitochondrial number, Pearson's correlation coefficient was calculated to quantify the amount of colocalisation of Mitotracker Green with Mitotracker Deep Red. In MDA-MB-231 cells, both controls (ctDDX20 and empty vector) demonstrated a higher Pearson's correlation coefficient compared to the siDDX20 transfected cells. There was a significant decrease in the correlation coefficient in cells transfected with the dnTCF4 plasmid (Fig 4.4A-F). When

the same analysis was performed on MDA-MB-436 cells, the results indicated that transfection with either siDDX20 or dnTCF4 significantly reduced the correlation coefficient, which was unable to be rescued after overexpressing DDX20 in cells transfected with a dnTCF4. MDA-MB-436 cells treated with either siDDX20, dnTCF4 or pCMV-DDX20 and dnTCF4 in combination all exhibited an increase in Mitotracker Green fluorescence relative to the control cells (Fig 4.4G-L).

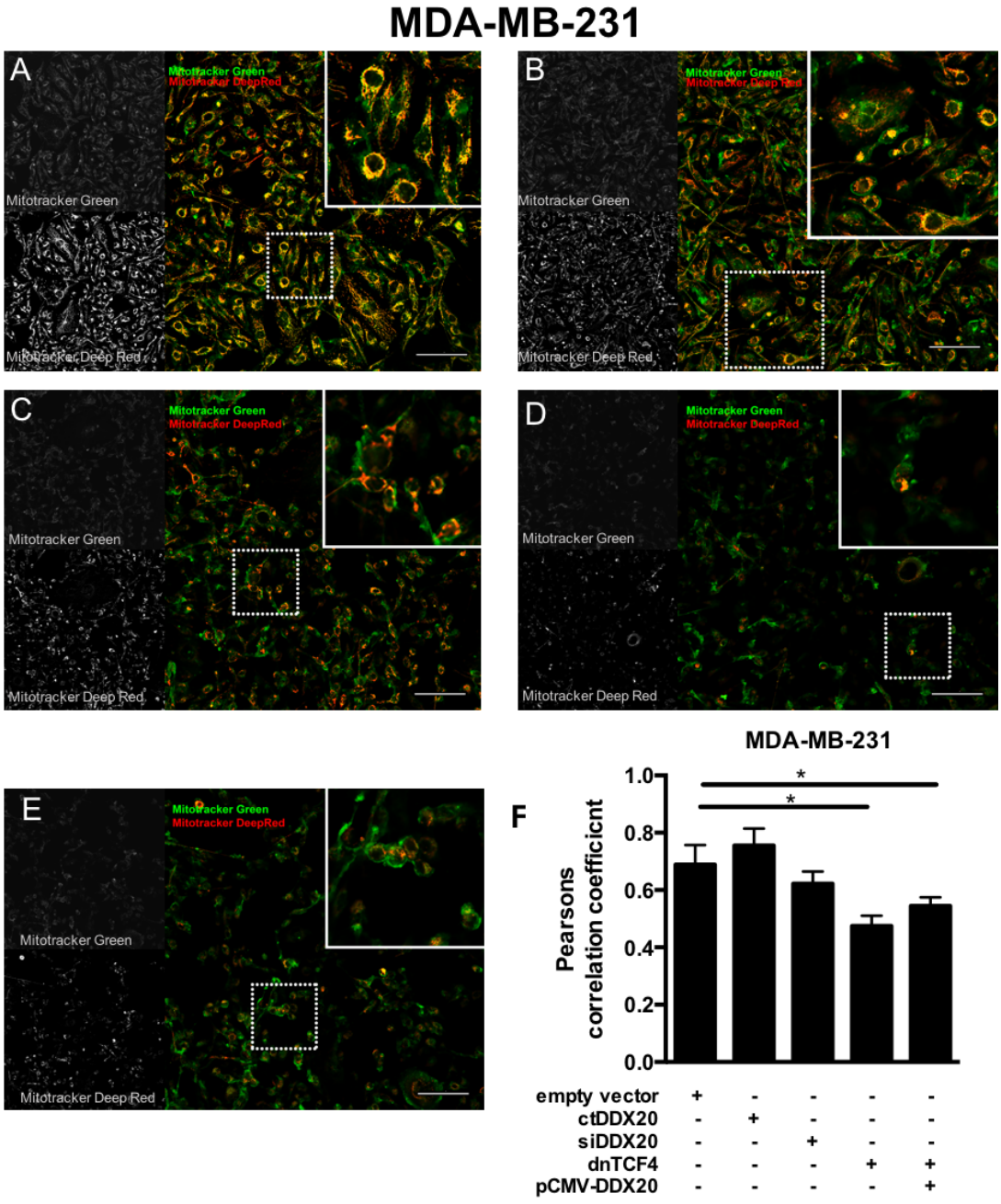

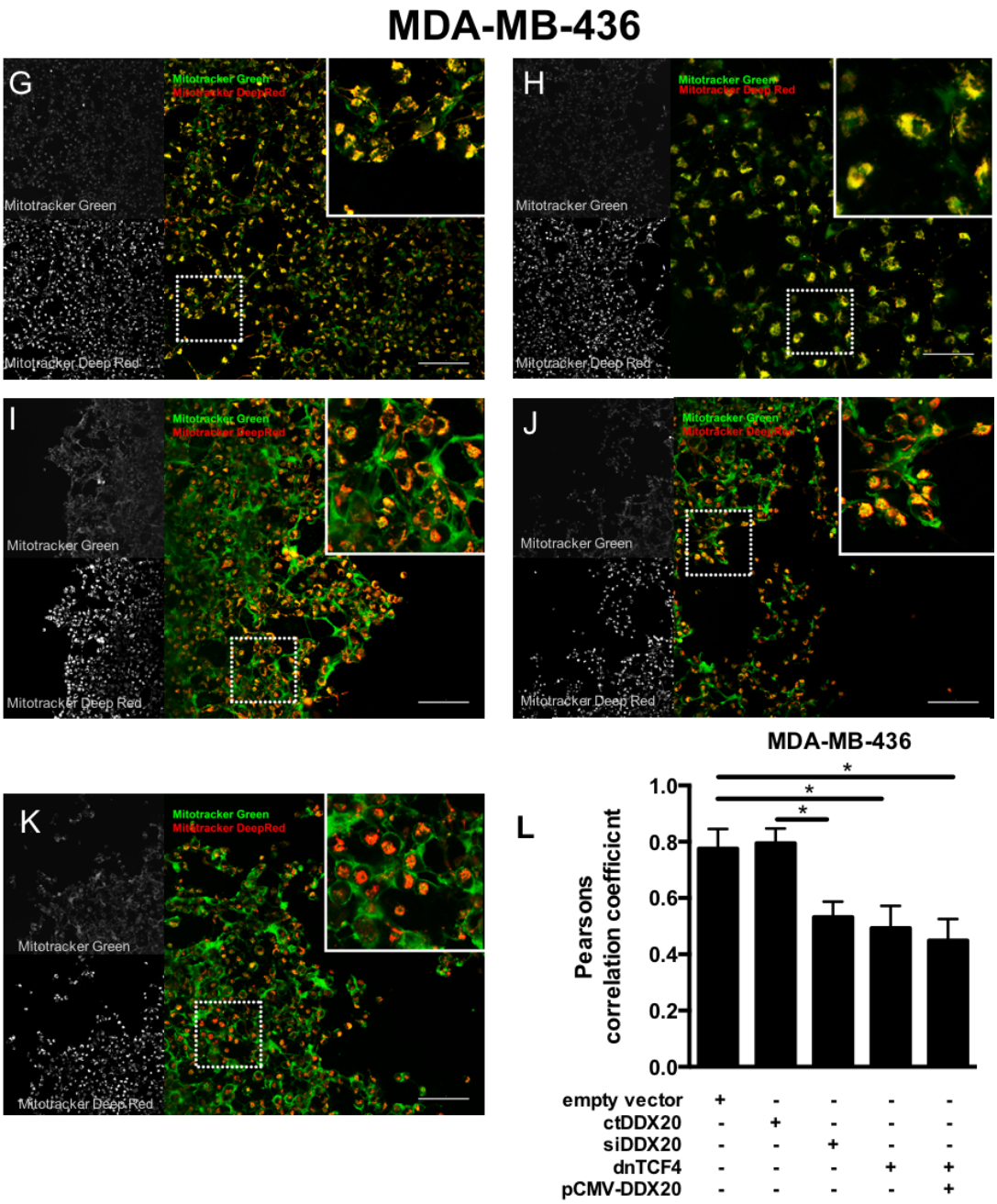

Figure 4.5. Colocalisation of Mitotracker Green and Mitotracker Deep Red. Immunofluorescence images of MDA-MB-231 cells stained with Mitotracker Green (Green) and Mitotracker Deep Red (Red). Colocalisation analysis was carried out for cells treated with: A) ctDDX20; B) empty vector; C) siDDX20; D) dnTCF4; and E) pCMV-DDX20+dnTCF4. F) Quantification of Pearson's correlation coefficient for colocalisation of Mitotracker Green and Mitotracker Deep Red. Immunofluorescence images of MDA-MB-436 cells. Colocalisation analysis was carried out for cells treated with: G) ctDDX20; H) empty vector; I) siDDX20; J) dnTCF4; and K) pCMV-DDX20+dnTCF4. L) Quantification of Pearson's correlation coefficient of colocalisation of Mitotracker Green and Mitotracker Deep Red. Correlation coefficients were calculated using Fiji software plugin JACoP (Just Another Colocalization Plugin).[287] Data represented as mean±SEM of at least three biological replicates. Statistical analysis was performed using unpaired Student's *t*-test, **p* < 0.05, ***p* < 0.01, ****p* < 0.001. Scale bar = 50μm.

4.2.4 Pharmacological inhibition of TCF4-β-catenin complex determines mitochondrial fate

To assess the single cell populations stained with Mitotracker Deep Red and Mitotracker Green, flow cytometry was performed 16 and 24 hours after the addition of a small molecule inhibitor of the TCF4-β-catenin complex, iCRT3. The results in MDA-MB-436 cells revealed that after the addition of iCRT3 there was a shift in a cell population, predominately Mitotracker Green^{high}/Mitotracker Deep Red^{high} to a small subset of cells that now exhibited a Mitotracker Green^{low}/Mitotracker Deep Red^{low} profile in a time-dependent manner (Fig 4.5A&B). Similarly, in the MDA-MB-231 cells, the addition of iCRT3 initiated the formation of a subset of cells exhibiting a Mitotracker Green^{low}/Mitotracker Deep Red^{low} profile (Fig 4.5C&D)

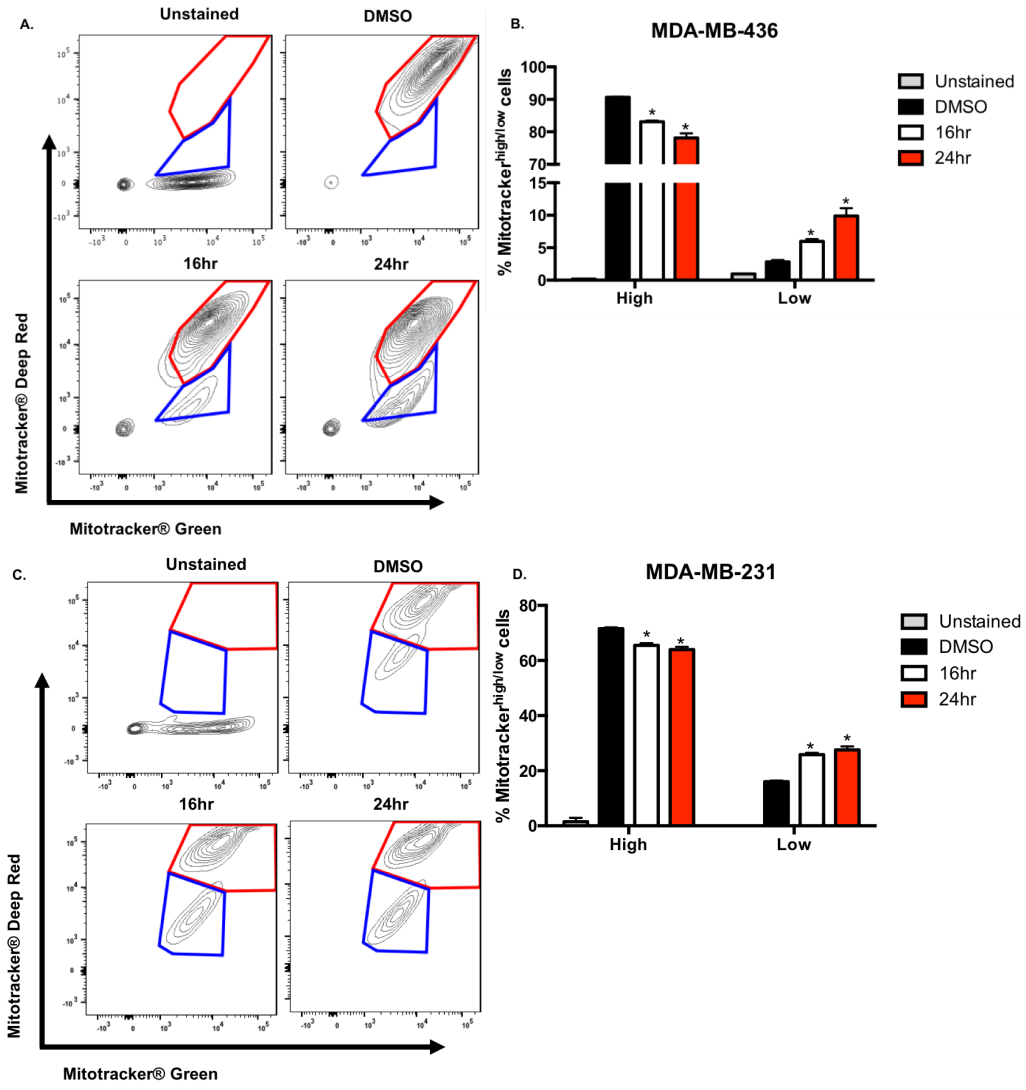

Figure 4.6. Pharmacological inhibition of β-catenin-mediated TCF4 transcription determines mitochondrial fate. A) Representative dot plots of MDA-MB-436 cells co-

stained with Mitotracker Green and Mitracker Deep Red. B) Quantification of percentage of Mitotracker$^{high/low}$ populations after each treatment for MDA-MB-436 cells. C) Representative dot plots of MDA-MB-436 cells co-stained with Mitotracker Green and Mitracker Deep Red. D) Quantification of percentage of Mitotracker$^{high/low}$ populations after each treatment for MDA-MB-436 cells. Gates included represent a Mitotracker Green^{high}/Mitotracker Deep Red^{high} profile (red) and a Mitotracker Green^{low}/Mitotracker Deep Red^{low} profile (blue). iCRT3 was given at 50μM for 16 and 24 hours, with controls cells treated with DMSO. Data are represented as mean±SEM of at least 3 biological replicates. Statistical analysis was performed using unpaired Student's *t*-test, *p<0.05, **p<0.01, ***p<0.001.

4.2.5 Mitochondrial morphology is regulated by DDX20 in a Wnt-dependent manner.

To better assess the changes in mitochondrial morphology and mitochondrial dynamics, Mitotracker Green images were assessed. In the MDA-MB-436 cells, the control cells exhibited mitochondria that were small and rod-shaped, with a condensed network appearance (Fig 4.6A&B). After knockdown of DDX20, the mitochondria appeared as larger rods with larger networks. After ectopic expression of a dnTCF4 and overexpression of DDX20, the mitochondrial morphology mirrored that of the cells where DDX20 was knocked down (Fig 4.6E). Quantification of the mean network size and length revealed an increase in both parameters in the cells diminished of DDX20 and the cells transfected with the dnTCF4 and DDX20 compared to their respective controls (Fig 4.6F&G). The MDA-MB-231 control cells exhibited a large network size, with a corresponding increase in rod size (Fig 4.6H&I). Similarly to the MDA-MB-436 cells, the average network length of the mitochondria of the MDA-MB-231 cells increased after knockdown of DDX20, the introduction of dnTCF4 or overexpression of both DDX20 and dnTCF4 (Fig 4.6M). Conversely, the mean network size decreased after the respective treatments (Fig 4.6N).

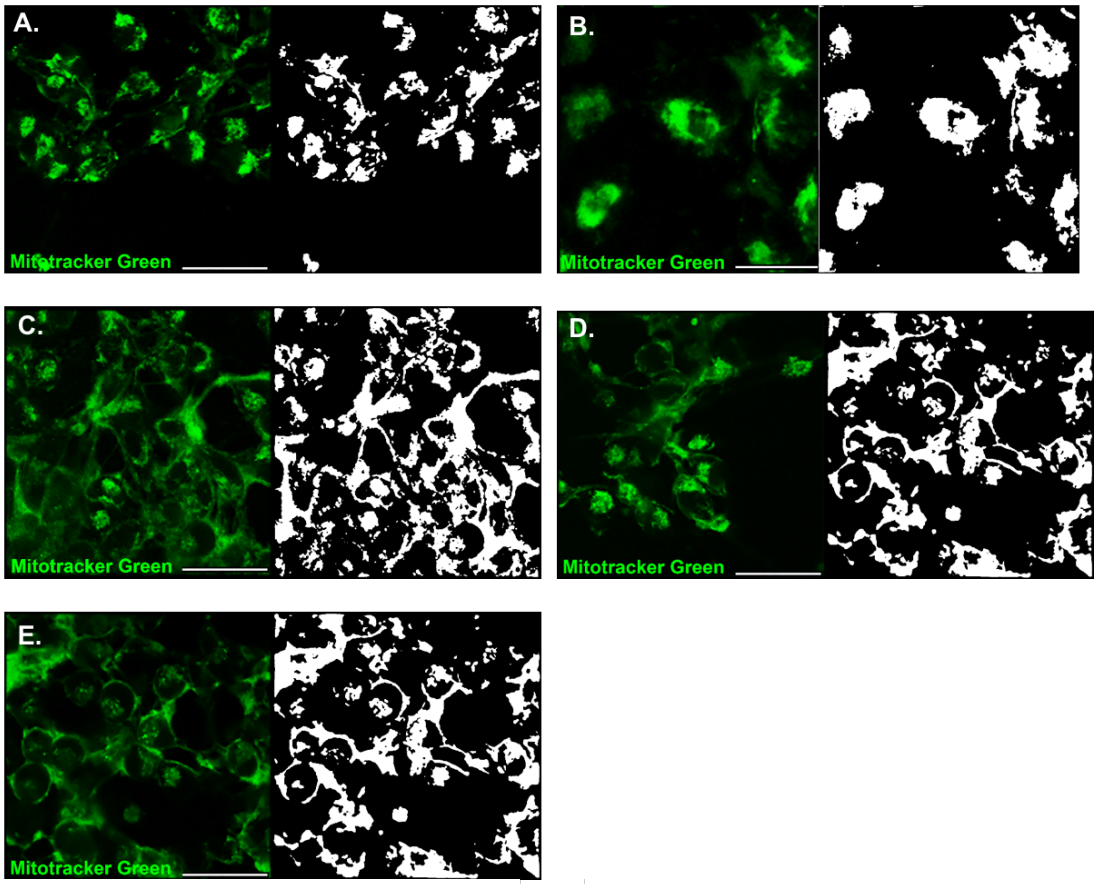
A.
Mitotracker Green
B.
Mitotracker Green
C.
Mitotracker Green
D.
Mitotracker Green
E.
Mitotracker Green

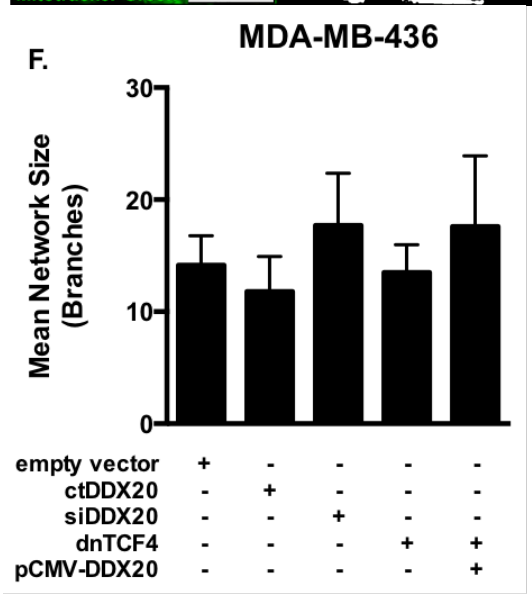
F.
MDA-MB-436
Mean Network Size (Branches)
30
20
10
0
empty vector + - - - -
ctDDX20 - + - - -
siDDX20 - - + - -
dnTCF4 - - - + +
pCMV-DDX20 - - - - +

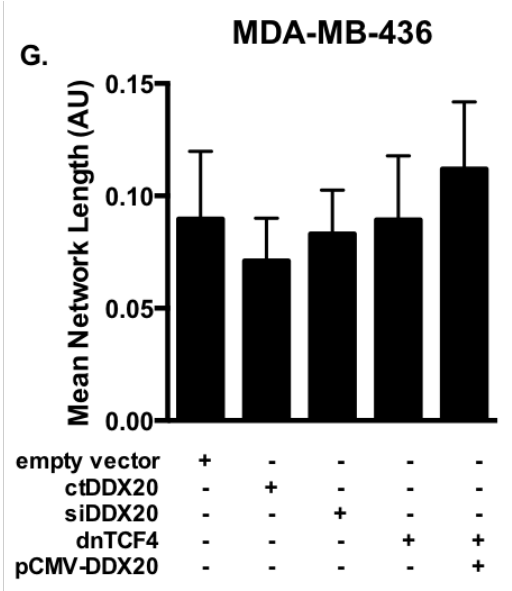
G.
MDA-MB-436
Mean Network Length (AU)
0.15
0.10
0.05
0.00
empty vector + - - - -
ctDDX20 - + - - -
siDDX20 - - + - -
dnTCF4 - - - + +
pCMV-DDX20 - - - - +

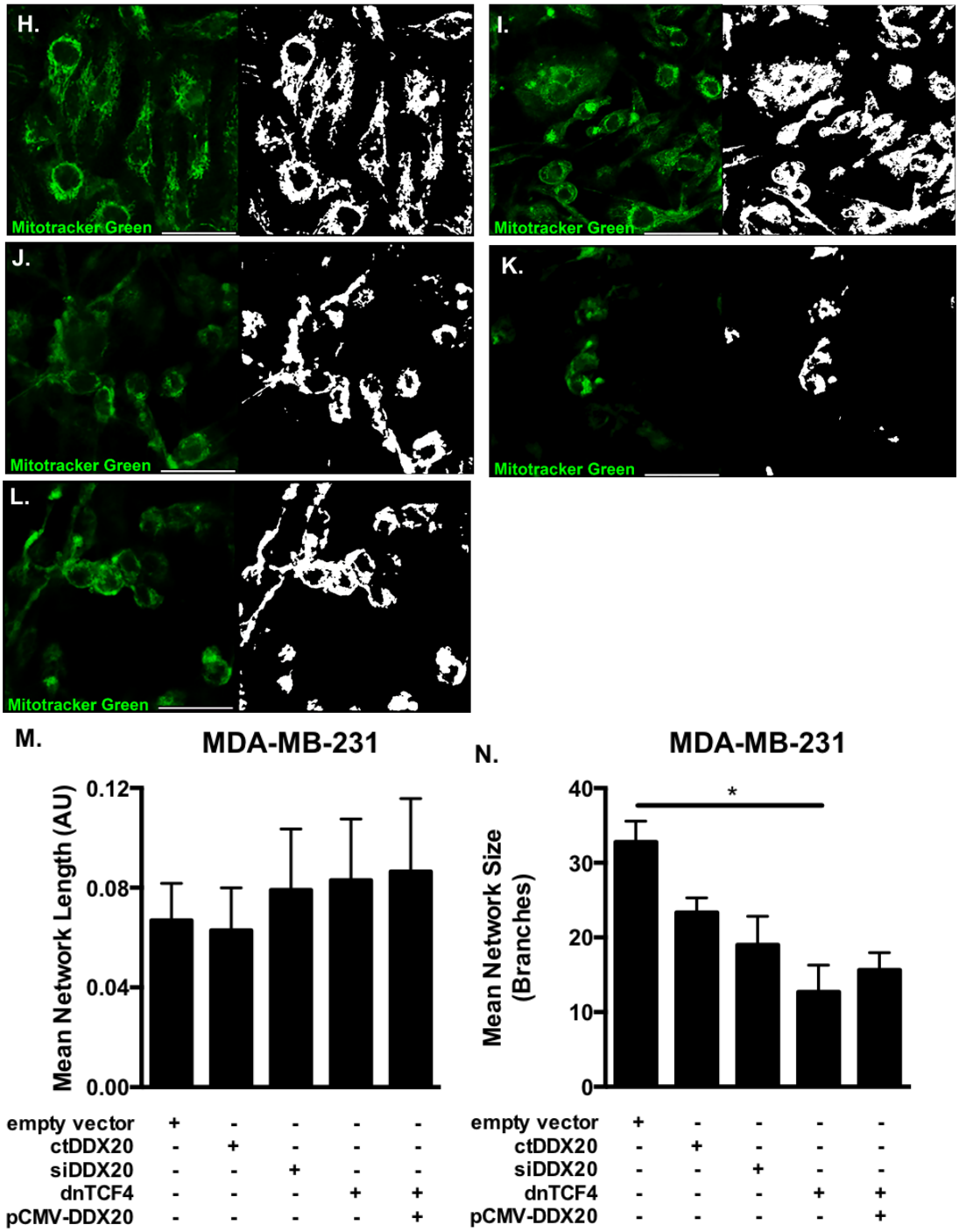

Fig 4.7. Morphological assessment of mitochondria. Mitotracker Green staining and corresponding binary images for MDA-MB-436 cells treated with: A) control siRNA; B) empty vector; C) siDDX20; D) dnTCF4; and E) pCMV-DDX20+dnTCF4. Quantification of MDA-MB-436 cells :F) Mean network size (branches), and G) Mean network length. Mitotracker Green staining and corresponding binary images for MDA-MB-231 cells treated with: H) control siRNA; I) empty vector; J) siDDX20; K) dnTCF4; and L) pCMV-DDX20+dnTCF4. Quantification of MDA-MB-231 cells: M) Mean network size (branches) and N) Mean network length. Mitochondrial morphological parameters were calculated on MiNA (Mitochondrial Network Analysis) plugin for Fiji software. Data are represented as mean±SEM of at least three biological replicates. Statistical analysis was performed using unpaired Student's *t*-test, **p* < 0.05, ***p* < 0.01, ****p* < 0.001. Scale bar = 50μm.

To further quantify the changes in mitochondrial mass, flow cytometric analysis of Mitotracker Green was performed. Confirming the immunofluorescence analysis, MDA-MD-231 cells that were transfected with the dnTCF4 or the combination of DDX20 and the dnTCF4 demonstrated a decrease in Mitotracker Green fluorescence (Fig 4.7A-D). The results from the flow cytometric analysis of the MDA-MB-436 cells were also consistent with the immunofluorescent images. Cells transfected with either siDDX20, dnTCF4 or a combination of dnTCF4 and DDX20 all exhibited significantly higher Mitotracker Green fluorescence than the respective control cells (Fig 4.7E-H).

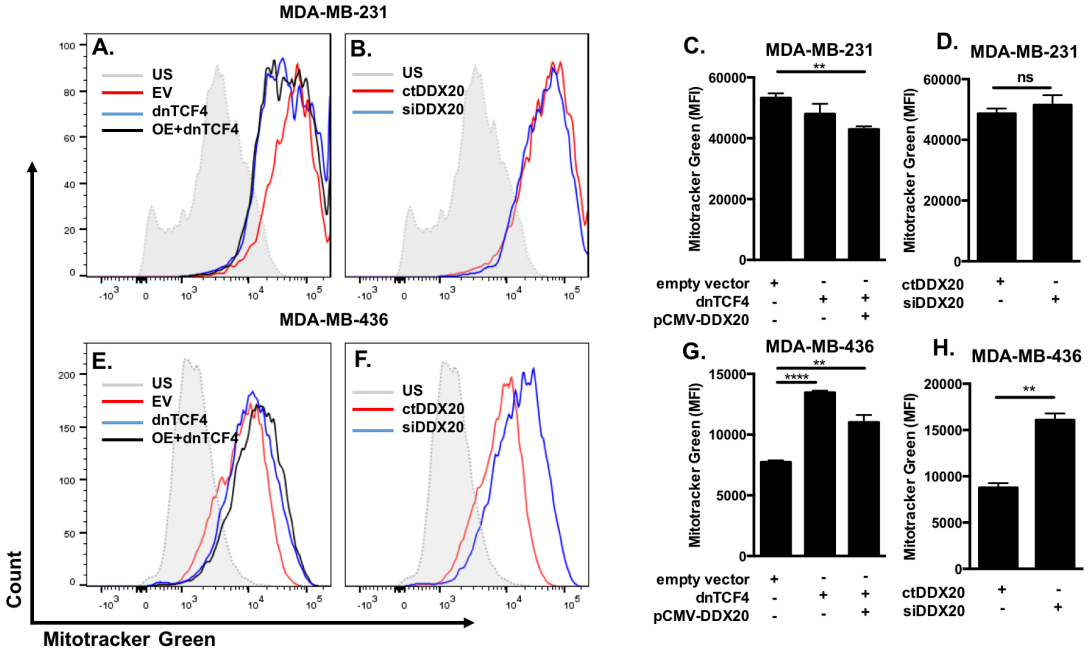

Figure 4.8. Flow cytometric analysis of Mitotracker Green after suppression of Wnt signalling. Flow cytometry assessment of Mitotracker Green for MDA-MB-231 cells treated with A) empty vector, dnTCF4, pCMV-DDX20(OE)+dnTCF4, and B) ctDDX20 and siDDX20. Quantification of Mitotracker Green median fluorescence intensity (MFI) in cells treated with C) empty vector, dnTCF4, pCMV-DDX20(OE)+dnTCF4, and D) ctDDX20 and siDDX20. Mitotracker Green assessment for MDA-MB-436 cells treated with E) empty vector, dnTCF4, pCMV-DDX2O(OE)+dnTCF4, and F) ctDDX20 and siDDX20. Quantification of Mitotracker Green median fluorescence intensity (MFI) in cells treated with G) empty vector, dnTCF4, pCMV-DDX20(OE)+dnTCF4, and H) ctDDX20 and siDDX20. Data are represented as mean±SEM of at least three biological replicates. Statistical analysis was performed using unpaired Student's *t*-test, **p* < 0.05, ***p* < 0.01, ****p* < 0.001.

4.2.6 DDX20-TCF4 axis is an essential regulator of mitochondrial respiration and bioenergetics.

To determine if the differences in mitochondrial mass quantification witnessed between MDA-MB-231 and MDA-MB-436 cells resulted in

differential functional outcomes, a mitochondrial stress test to measure changes in oxygen consumption rate (OCR) was performed using a Seahorse Flux Analyser. It was confirmed the overexpression of DDX20 and the combination of dnTCF4 and pCMV-DDX20 both resulted in overexpression of DDX20 by Western blotting analysis (Fig 4.8A). MDA-MB-231 and MDA-MB-436 cell lines both exhibited severe mitochondrial respiration dysfunction after treatment with siDDX20 and dnTCF4 with DDX20 (Fig 4.8B&C). Analysis of key mitochondrial respiration and bioenergetics parameters revealed that knockdown of DDX20 resulted in increased proton leak and decreased maximal respiration in both cell lines. ATP production was only affected in the MDA-MB-436 cells following the loss of DDX20. Strikingly, both cell lines completely lost their spare respiratory capacity following knockdown of DDX20 (Fig 4.8D&E). The results following the overexpression of the dnTCF4 and DDX20 mirrored those seen after the knockdown of DDX20, with the addition that ATP production was decreased in MDA-MB-231 cells. Consistent with the knocked down cells, the spare respiratory capacity of both cell lines was completely abolished following the expression of a dnTCF4 and DDX20 (Fig 4.8D&E).

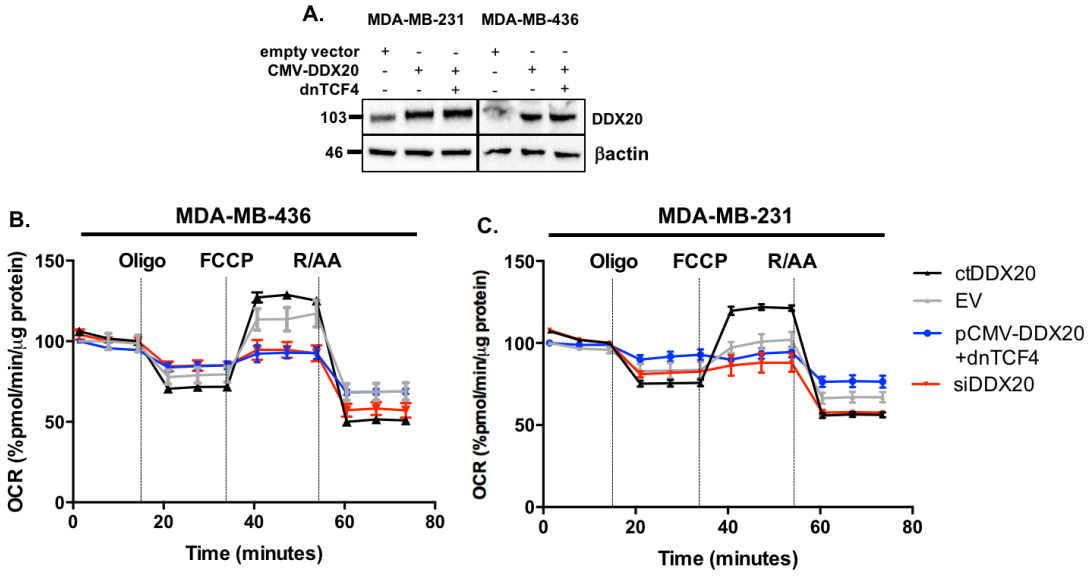

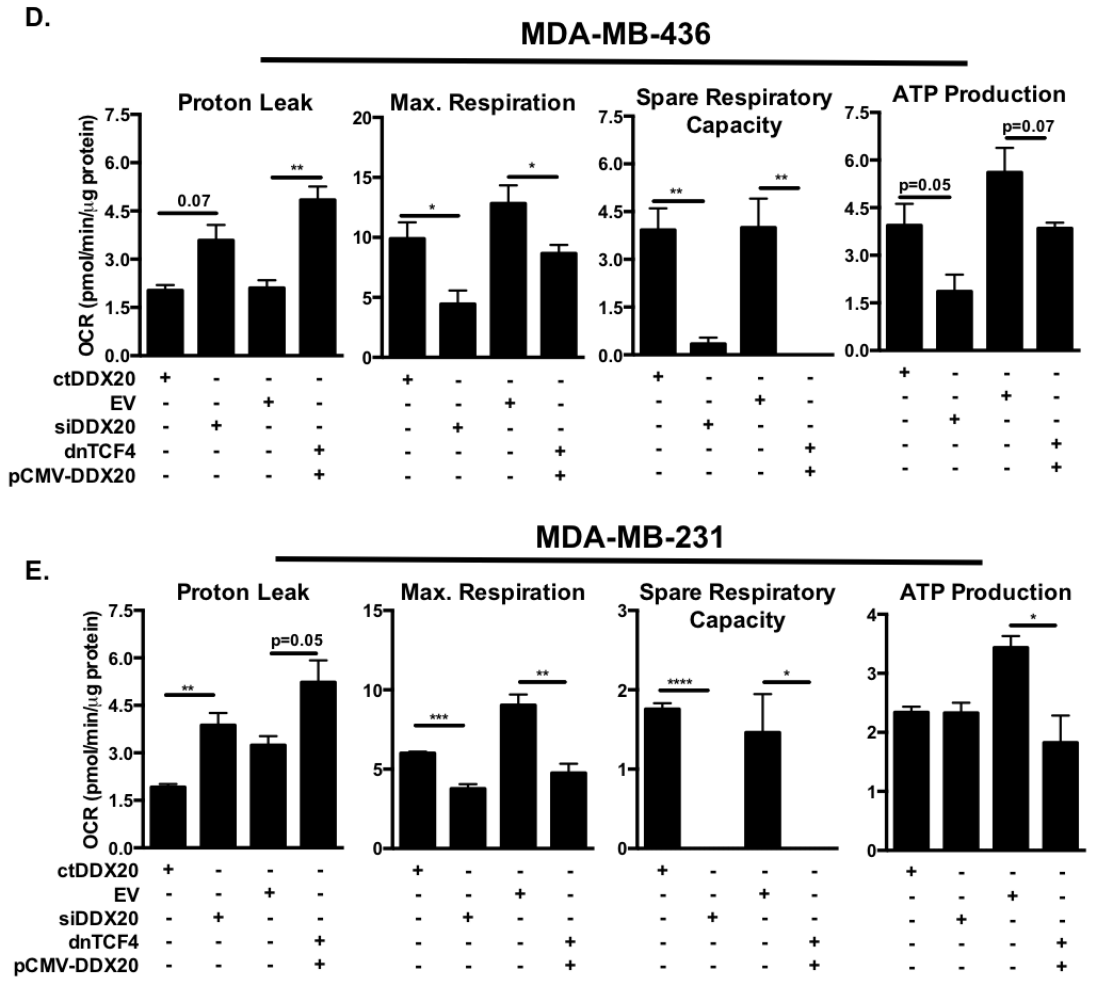

Fig 4.9. Mitochondrial bioenergetics analysis of DDX20 depleted and TCF4 suppressed cells. A) Western blot of DDX20 following overexpression of empty vector, pCMV-DDX20, and pCMV-DDX20 and dnTCF4. Representative Seahorse analysis trace of oxygen consumption rate following treatment with ctDDX20, siDDX20, empty vector, and dnTCF4 with pCMV-DDX20 in B) MDA-MB-436 and C) MDA-MB-231 cells. D) Quantification of mitochondrial respiratory parameters protein leak, maximal respiration, spare respiratory capacity, and ATP production measured in MDA-MB-436 cells following transfection with ctDDX20, siDDX20, empty vector, and dnTCF4 with pCMV-DDX20. E) Quantification of mitochondrial respiratory parameters protein leak, maximal respiration, spare respiratory capacity, and ATP production measured in MDA-MB-231 cells following transfection with ctDDX20, siDDX20, empty vector, and dnTCF4 with pCMV-DDX20. Data are represented as mean±SEM of at least 3 biological replicates for ctDDX20 and siDDX20 treated cells. Data are represented as mean±SEM of at least 5 technical repeats of one experiment performed three times with the same trend. Statistical analysis was performed using unpaired Student's *t*-test, $*p < 0.05$, $**p < 0.01$, $***p < 0.001$.

4.2.7 *SOD2* and *UQCRC2* are regulated through Wnt-mediated TCF4 transcription dependent on DDX20.

The resultant mitochondrial dysfunction and increased H_2O_2 that was previously witnessed suggested dysregulation in mitochondrial ROS scavengers and components of the ETC mediated by Wnt signalling. Using the ENCODE ChIP-seq database, it was identified that *SOD2* and *UQCRC2* have TCF4 binding sites and TCF4 ChIP-seq peaks at their 5'-UTR promoter

regions in MCF-7, HCT-116, and HeLa cell lines (Fig S4.3A&C). These binding sites are located 744 and 449 base pairs upstream of the transcription start sites for *SOD2* and *UQCRC2* respectively (Fig S4.3B&D). To confirm if this was also the case in MDA-MB-231 cells, ChIP-QPCR for TCF4 on the predicted binding sites on both *SOD2* and *UQCRC2* was performed. ChIP-QPCR revealed that TCF4 bound to the promoter of both genes. The depletion of DDX20 yielded differential results for TCF4 binding; after DDX20 knockdown, there was increased recruitment of TCF4 to the *SOD2* promoter region and decreased recruitment of TCF4 to the *UQCRC2* promoter (Fig 4.9A&B). The loss of DDX20 increased *SOD2* mRNA expression while decreasing the expression of *UQCRC2* (Fig 4.9C,D,G,H). Conversely, the addition of Wnt3a increased *UQCRC2* expression while decreasing the expression of *SOD2* (Fig 4.9E,F,I,J). These results were corroborated with Western blotting, revealing that pharmacological inhibition of the β-catenin-TCF4 complex resulted in an increase in the protein level of SOD2 (Fig 4.9K&L). Similarly, overexpression of a dnTCF4 and DDX20 resulted in an increase in SOD2 expression.

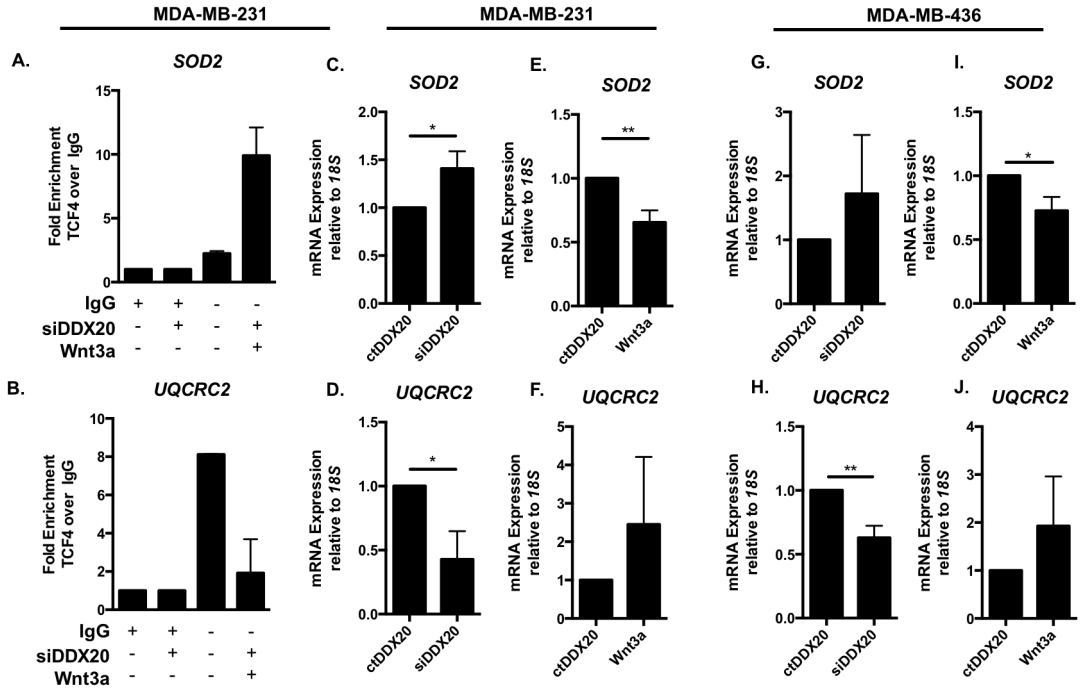

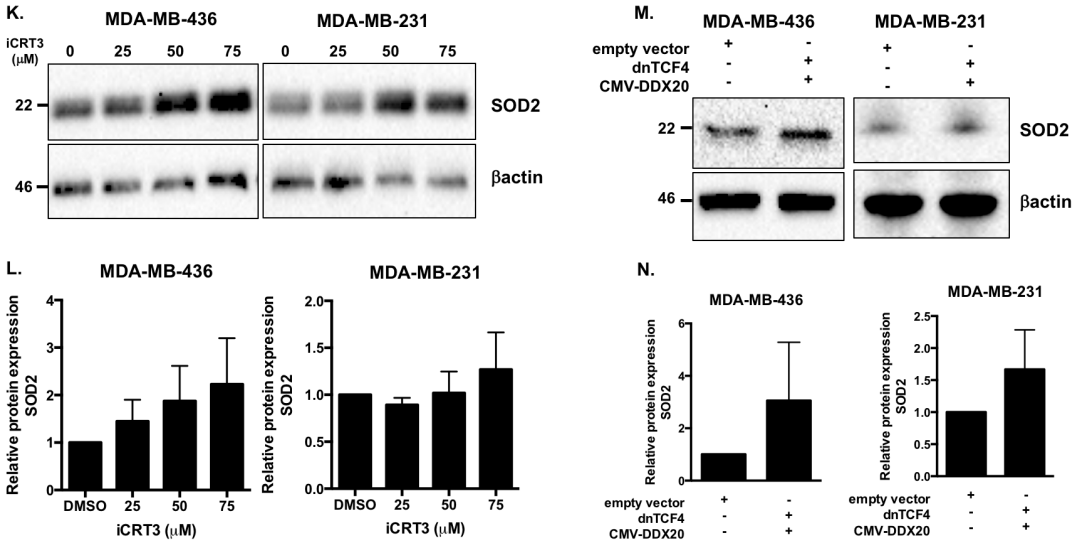

Fig 4.10. Transcriptional regulation of SOD2 and UQCRC2 mediated by TCF4. ChIP-QPCR of TCF4 on the promoters of A) SOD2 and B) UQCRC2 in MDA-MB-231 cells transfected with ctDDX20 or siDDX20 with the addition of 200ng/mL Wnt3a for two hours. Gene expression of MDA-MB-231 cells after transfection with siDDX20 for C) *SOD2* and D) *UQCRC2*. Gene expression of MDA-MB-231 cells after the addition of 200ng/mL Wnt3a for 4 hours for E) *SOD2* and F) *UQCRC2*. Gene expression of MDA-MB-436 cells after transfection with siDDX20 for G) *SOD2* and H) *UQCRC2*. Gene expression of MDA-MB-436 cells after the addition of 200ng/mL Wnt3a for 4 hours for I) *SOD2* and J) *UQCRC2*. K) Western blot of MDA-MB-436 and MDA-MB-231 cells after the addition of increasing doses of iCRT3 for 24 hours. L) Quantification of iCRT3 treated of MDA-MB-436 and MDA-MB-231 cells. M) Western blot of MDA-MB-436 and MDA-MB-231 cells after transfection of empty vector control or dnTCF4 with pCMV-DDX20. N) Quantification of transfected MDA-MB-436 and MDA-MB-231 cells. ChIP-PCR data are representative of one experiment repeated three times with similar results. All other data are represented as mean±SEM of at least 3 biological replicates. Statistical analysis was performed using unpaired Student's *t*-test, *$p < 0.05$, **$p < 0.01$, ***$p < 0.001$.

4.2.8 DDX20 regulates mitoROS genes and mtDNA copy number *in vitro* and *in vivo*

To test whether these results were replicated *in vivo*, gene expression from Gemin3^{KO} and overexpressing Gemin3$^{arm/da}$ *Drosophila* embryos were analysed. Confirming the *in vitro* results, Sod2 gene expression was significantly increased in Gemin3^{KO} embryos, while being significantly decreased in Gemin3$^{arm/da}$ embryos. When the mRNA expression of mitochondrial ROS regulators – thioredoxin-2 (Trx2) and peroxiredoxin-3 (Prx3) – were analysed, a similar result was observed (Fig 4.10A). To quantify the changes of mitochondrial mass after DDX20/Gemin3 depletion, mtDNA copy number was quantified by QPCR. Contrasting results were witnessed between the *in vivo* model and the TNBC cell lines. Gemin3^{KO} embryos had a significant decrease in mtDNA copy numbers, while a significant increase was observed in the MDA-MB-436 cells after loss of

DDX20 (Fig 4.10B&C). There was no significant change in the amount of mtDNA in MDA-MB-231 cells depleted of DDX20 (Fig 4.10D).

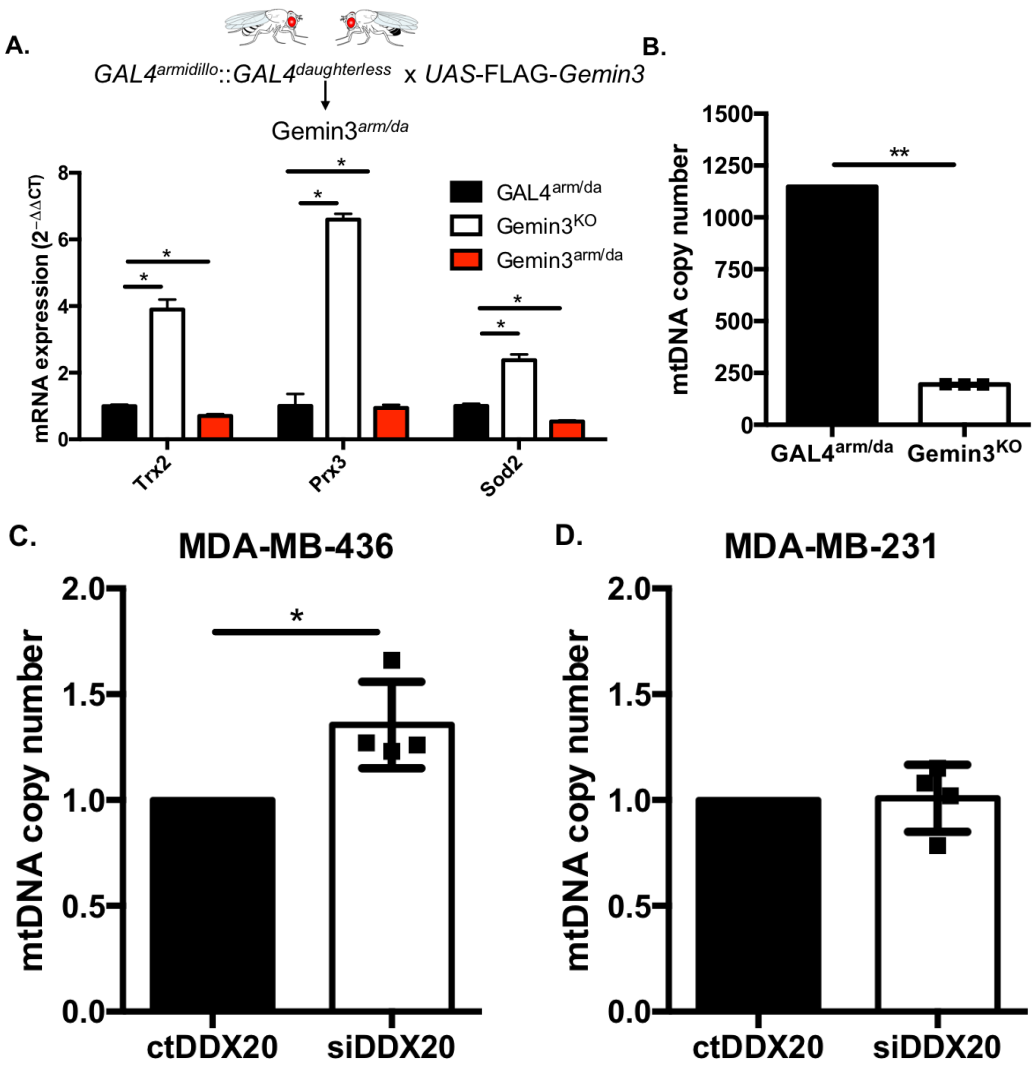

Figure 4.11. *In vivo* validation of DDX20 regulation of Mitochondrial ROS regulators and dynamics. A) Schematic of generation of Gemin3-overexpressing *Drosophila* fly embryos and Q-PCR of *Drosophila* mRNA expression for Trx2, Prx3, and Sod2 in control ($GAL4^{arm/da}$), Gemin3 knockout ($Gemin3^{KO}$), and Gemin3 overexpressing ($Gemin^{arm/da}$) flies. B) Mitochondrial DNA (mtDNA) copy number assessment by QPCR in $GAL4^{arm/da}$ and $Gemin3^{KO}$ flies. C) mtDNA copy number assessment by QPCR of MDA-MB-436 cells after transfection with control siRNA or siDDX20. D) mtDNA copy number assessment by QPCR of MDA-MB-4231 cells after transfection with control siRNA or siDDX20. Data are represented as mean±SEM of at least three biological replicates. Statistical analysis was performed using unpaired Student's *t*-test, **p* < 0.05, ***p* < 0.01, ****p* < 0.001.

4.3 DISCUSSION

This study implicates DDX20 in the regulation of mitochondrial redox and function. This regulation occurs in a Wnt-mediated manner that is dependent on TCF4 transcription. This is the first report of direct regulation of SOD2 and UQCRC2 by canonical Wnt signalling and DDX20.

Previous reports have demonstrated that increased ROS-mediated oxidative stress is associated with an increase in mitochondrial mass.[324,325] This observation was mirrored in MDA-MB-436 cells, which upon depletion of DDX20 resulted in an increased mitochondrial mass, measured by Mitotracker Green fluorescence through confocal microscopy, flow cytometry, and mtDNA copy number. Contrarily, MDA-MB-231 cells had no significant alteration in mitochondrial mass when mtDNA was measured, although the immunofluorescence images demonstrated that overexpression of a dominant-negative TCF4 and DDX20 resulted in an overall reduction in Mitotracker Green fluorescence, indicative of a reduction in mitochondrial mass. These results could be explained by the mutational differences between the cell lines, which lead MDA-MB-231 to be more sensitive to mitophagy; MDA-MB-231 harbours an oncogenic Kras mutation (G13D) and oncogenic BRAF mutations, while MDA-MB-436 is Kras wild-type.[326] It has previously been demonstrated that oncogenic Kras is a mediator of mitophagy and is associated with increased levels of the autophagy-associated proteins Beclin-1, Atg5, and LC3-II.[327] Furthermore, the decrease in mitochondrial mass and increased fragmentation in MDA-MB-231 cells can be associated with increased oncogenic RAS and MAPK pathways through the regulation of Ser592 phosphorylation of dynamin-1-like protein (DRP1), which regulates mitochondrial fission and fragmentation events.[328] Previously, it was demonstrated that mitochondrial fission and fusion events were modulated by Wnt5a/Ca^{2+} signalling, where Wnt5a increased intracellular calcium, leading to increased phosphorylation of Drp1 at Ser616 and decreased phosphorylation of Drp1 at Ser637. The addition of Wnt5a led to a dynamic change in mitochondrial fusion and fission events. The regulation of TCF4 transcription through canonical Wnt signalling mediated by DDX20 demonstrates that canonical Wnt signalling is a regulator of mitochondrial fusion and fission.[329]

Despite the differences in mitochondrial dynamics between the cell lines upon DDX20 depletion and the suppression of TCF4 transcription, overall mitochondrial bioenergetics and respiration were both equally affected. Proton leak was increased while maximum respiration and spare respiratory capacity were severely depleted. Increased proton leak can be induced through uncoupling proteins and adenine nucleotide translocase, which can be activated due to increased ROS and byproducts of peroxidation. A large increase in proton leak is also generally seen in damaged mitochondria.[330] Furthermore, increased proton leak can be due to dysregulation of both Complex I and Complex III of the ETC.[331] The addition of FCCP acts as a protonophore, uncoupling the mitochondrial ETC. In both cell lines, mitochondria were unable to respond to stress and were unable to conduct proper respiration after knocking down DDX20. The same result was observed when dnTCF4 and DDX20 were simultaneously overexpressed, which indicated that this was due to suppression of Wnt signalling mediated by DDX20. A previous study implicated Wnt signalling in mitochondrial function, where the addition of Wnt3a increased both the basal and maximum respiration of muscle cells, while the overexpression of dnTCF4 reduced the OCR. Furthermore, it was demonstrated that Wnt3a increased the gene expression of ATP synthase subunit 5γ1 and Cytochrome c oxidase subunit II (Cox2) while increasing mtDNA. This study then implicated MYC-mediated transcription in the mitochondrial biogenesis observed with Wnt3a stimulation.[283]

The loss of mitochondrial spare respiratory capacity in MDA-MB-231 and MDA-MB-436 cells suggests that there is dysregulation in a component critical for the regulation of oxidative phosphorylation. Ubiquinol cytochrome c Reductase subunit 2 (UQCRC2) is a component of Complex III and has been demonstrated to be essential for the assembly and stabilisation of the Ubiquinol cytochrome c Reductase supercomplex. Structural analysis revealed that a point mutation (A183W) of UQCRC2 resulted in impaired Complex III assembly.[332] DDX20 knockdown resulted in decreased *UQCRC2* expression, regulated through canonical Wnt signalling, which was mediated by TCF4 transcription. The reduction of *UQCRC2* would destabilise Complex III and impair mitochondrial respiration, leading to

increased electron slippage. UQCRC2 has also been demonstrated to be upregulated, along with other components of the ETC, in breast cancer. This leads to hyperactivation of oxidative metabolism and may partly explain the differences in energy requirements between normal and cancer cells.[333] These data clearly demonstrate a DDX20-dependent mechanism of Wnt signalling, whereby TCF4 transcription is responsible for expression of UQCRC2 and mitochondrial function.

Mitochondrial superoxide can be released to both sides of the inner mitochondrial membrane from Complex III.[240] Inhibition or dysfunction of Complex III increases mitochondrial superoxide production through the increased slippage of electrons.[334] The loss of DDX20 and the dysregulation of mitochondrial respiration resulted in a decrease in mitochondrial superoxide. This decrease in superoxide can be attributed to the increase in SOD2 expression that occurred after DDX20 knockdown. SOD2 is a mitochondrial membrane-bound protein that primarily acts as an antioxidant through the dismutation of superoxide to hydrogen peroxide.[335] Increased superoxide production and increased SOD2 expression would result in increased mitochondrial H_2O_2, leading to oxidative stress, mitochondrial DNA damage,[336] and mitochondrial membrane peroxidation.[337] Interestingly, lipid peroxidation of the mitochondrial membrane has been shown to decrease the activity of Complex III.[338] H_2O_2 has also been demonstrated to induce depolarisation of mitochondrial membranes.[339,340] This suggests that the loss of mitochondrial membrane potential following the loss of DDX20 and suppression of TCF4 transcription may be the result of increased H_2O_2 formed due to increased SOD2 expression.

SOD2 is overexpressed in TNBC, and has been demonstrated to negatively impact survival outcomes in individuals with high SOD2 expression.[341] The overexpression of SOD2 has also been implicated in the induction of an EMT phenotype in basal breast cancer. Forced expression of SOD2 reduced E-cadherin expression while increasing N-cadherin, vimentin, and β-catenin expression.[272] These reports are contrary to the findings of this study, which demonstrates that SOD2 overexpression may be pivotal in inducing oxidative stress-mediated mitochondrial dysfunction through increased H_2O_2. These findings are consistent with a study by Gong *et al*.[342]

that demonstrated that Pigment Epithelial-derived Factor (PEDF) antagonised Wnt signalling mediated by Wnt3a and induced autophagy in pancreatic neoplasms; antagonism by PEDF lead to an increase in SOD2 expression. This is consistent with the observations of this study, whereby antagonising Wnt signalling through the loss of DDX20 or suppression of TCF4-mediated transcription leads to an increase in SOD2 expression. Gong *et al*. demonstrated that the addition of PEDF resulted in increased recruitment of the p65 subunit of NFκB to the SOD2 promoter, resulting in increased transcription; while these data demonstrate that canonical Wnt signalling mediated through TCF4 is responsible for the changes in the expression of SOD2. Interestingly, this study also demonstrated that the overexpression of a dnTCF4 resulted in an increase in SOD2 expression. This suggests that β-catenin may act as a repressor when TCF4 is bound to SOD2 DNA, or prevent the transcriptional activation of TCF4, which is completely at odds with its canonical function.

The Gemin3 (DDX20)-mediated regulation of Sod2 was confirmed in this study *in vivo* in a *Drosophila* model. The depletion of Gemin3 triggered an elevation in the expression levels of the antioxidant genes Trx2 and Prx3, which may be explained as a rescue mechanism following increased ROS levels. Furthermore, it has been demonstrated that Prx3 and Prx5 play a critical role in thiol homeostasis, survival, and lifespan in *Drosophila*.[343] As Gemin3 knockouts are embryonically lethal in *Drosophila*, it is therefore feasible that increased Prx3 in Gemin3^{KO} embryos is a mechanism to attempt to prolong lifespan. The *in vivo* data demonstrated that Gemin3 knockout embryos were depleted of mtDNA, a result which is contrary to mtDNA copy numbers increasing with oxidative stress.[344] The increase in mtDNA is thought to be a feedback mechanism to compensate for dysfunctional mitochondria or mutated mtDNA.[345] While these results were all witnessed after short term (24-72 hours) exposure to oxidative stress, it is possible that while increasing mtDNA copy number is the initial mechanism, longer term treatment and exposures to oxidative stress result in decreased mitochondrial number. This may be the effect seen in the later stage Gemin3^{KO} embryos.

This study has demonstrated that the depletion of DDX20-mediated Wnt signalling results in an increase in *SOD2* expression and a decrease in *UQCRC2* expression. The result of UQCRC2-mediated changes in mitochondrial respiration lead to increased superoxide production. The increased superoxide is dismutased by the increased SOD2 expression, leading to increased H_2O_2-induced mitochondrial oxidative stress and loss of mitochondrial membrane potential. These results elucidate a novel role for canonical Wnt signalling in the regulation of mitochondrial dynamics and function through transcription of mitochondrial ROS scavengers and ETC components.

4.4 ACKNOWLEDGMENTS

This study would like to acknowledge members of the Tolwinski Lab (Yale-NUS College, Singapore), Nicholoas S Tolwinski and Jahnavi Suresh for the generation of the Drosophila data.

4.5 SUPPLEMENTARY MATERIALS CHAPTER 4

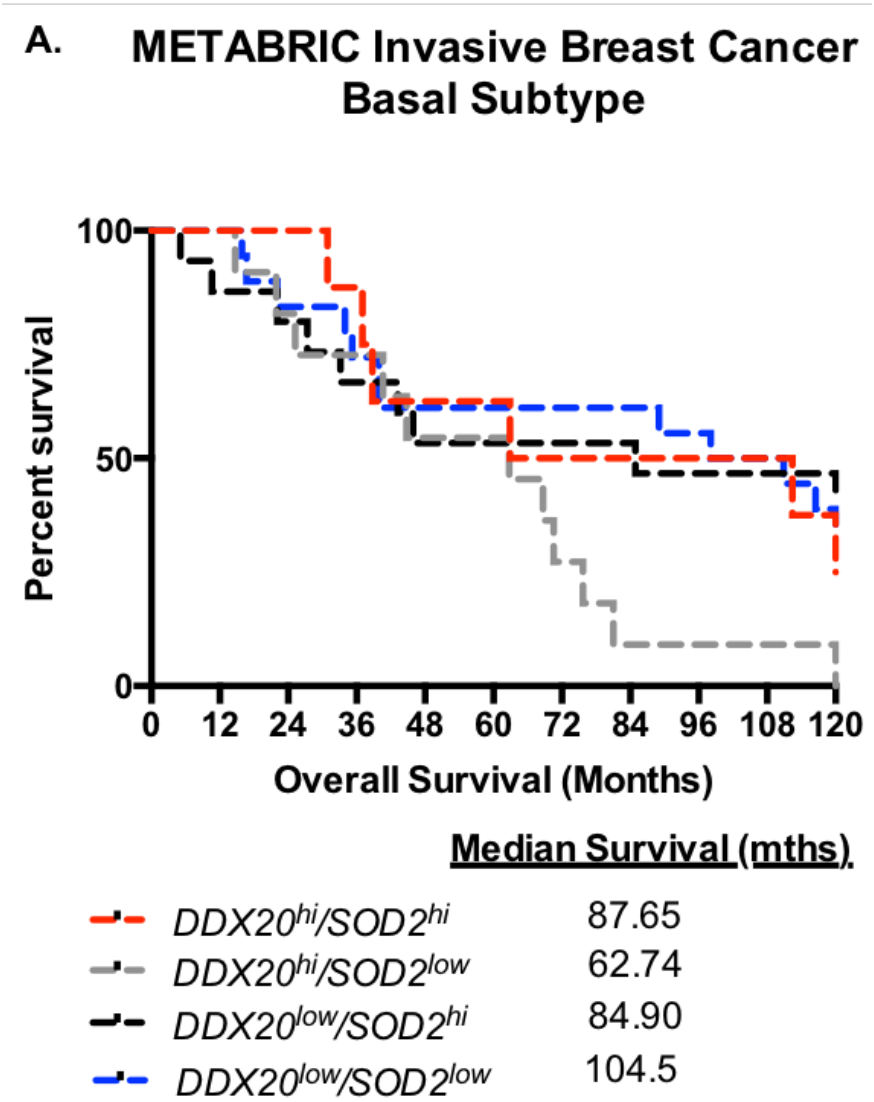

Fig S4.1 Survival analysis of SOD2 and DDX20. A) Kaplan-Meier survival analysis of METBRIC PAM50 basal cohort of individuals with *DDX20^{hi}/SOD2^{hi}*, *DDX20^{low}/SOD2^{low}*, *DDX2^{low}/SOD2^{hi}*, and *DDX20^{hi}/SOD2^{low}* phenotype. Statistics were performed using Log-rank (Mantel-Cox) test calculated median survival in Prism GraphPad.

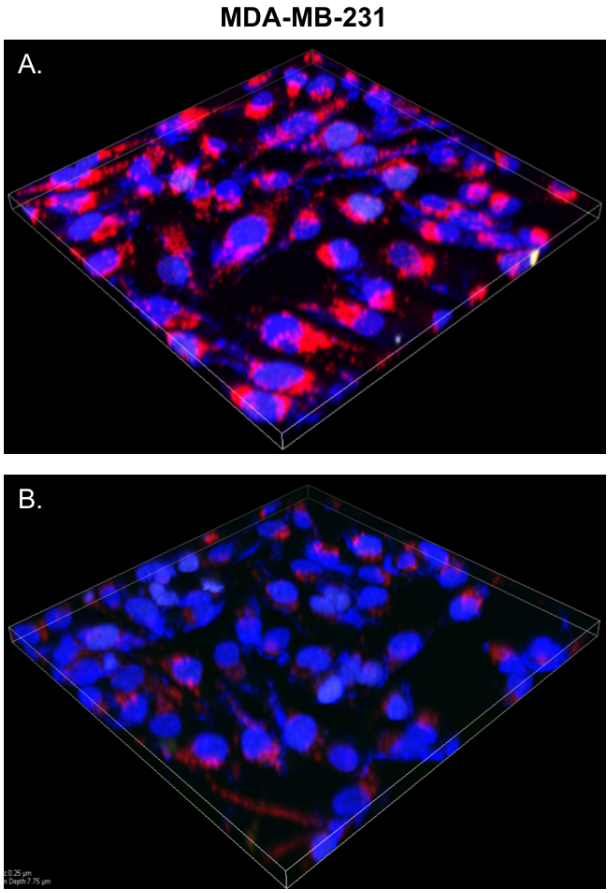

Fig S4.2. 3D Mitotracker Deep Red staining. MDA-MB-231 cells stained for Mitotracker Deep Red (Red) and DAPI (blue) were transfected with either A) control siRNA or B) siDDX20. 3D images were taken using a Nikon A1 confocal microscope using Z-stacks. Z-stack parameters used were; width: 210.91μm, height: 210.91μm: and depth: 9.25μm. Each image was taken at a depth of 0.25μm.

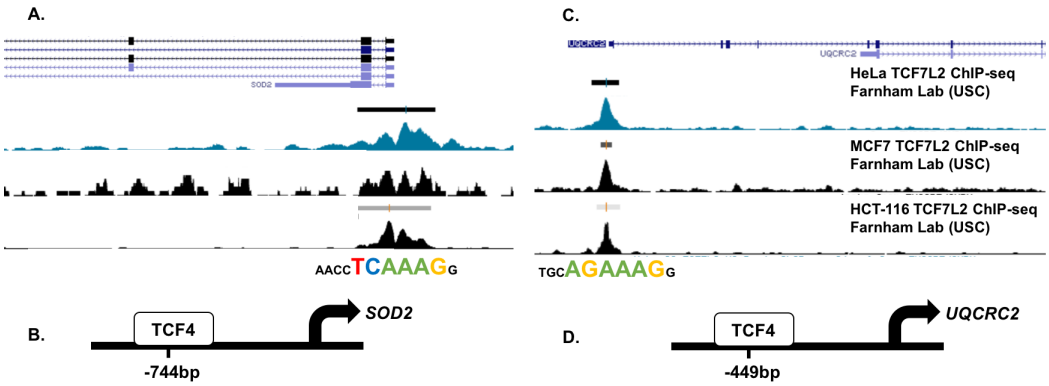

Fig S4.3. TCF4 binding sites on *SOD2* and *UQCRC2*. A) ChIP-seq tracks and peaks from MCF-7, HCT-116, and HeLa cells from ENCODE ChIP-seq data viewer centred around the *SOD2* gene TSS. Coloured bases indicate the TCF4 binding sequence on *SOD2* DNA. B) Schematic of primer design and binding sites of TCF4 on SOD2 DNA. C) ChIP-seq tracks and peaks from MCF-7, HCT-116, and HeLa cells from ENCODE ChIP-seq data viewer centred around the *UQCRC2* gene TSS. Coloured bases indicate the TCF4 binding sequence on UQCRC2 DNA. B) Schematic of primer design and binding sites of TCF4 on UQCRC2 DNA.

CHAPTER 5: DDX20 IS AN ESSENTIAL REGULATOR OF WNT/β-CATENIN SIGNALLING IN TRIPLE-NEGATIVE BREAST CANCER STEM CELLS

CHAPTER 5: DDX20 IS AN ESSENTIAL REGULATOR OF WNT/β-CATENIN SIGNALLING IN TRIPLE-NEGATIVE BREAST CANCER STEM CELLS

5.1 INTRODUCTION

Wnt/β-catenin signalling is a fundamental driver of TNBC progression and has been demonstrated to enhance many of the characteristic traits of CSCs.[7] CSCs display a quiescent cell cycle, multi-drug resistance, and the ability to self-renew and to differentiate into a heterogeneous population.[346] The common cell surface markers for the characterisation of TNBC stem cells are $CD44^{high}/CD24low^{/-}$.[347] The basal-like molecular subtype of TNBC displays increased Wnt signalling and also a higher proportion of cells displaying the phenotypic characteristics and functions of CSCs (Figure 5.1). Transcription factors, such as Homeobox protein NANOG (Nanog), sex-determining region-box 2 (Sox2), and octamer-binding transcription factor 4 (Oct4) regulate the expression of genes involved in embryonic stem cell pluripotency and differentiation, and are overexpressed in CSCs.[348,349].

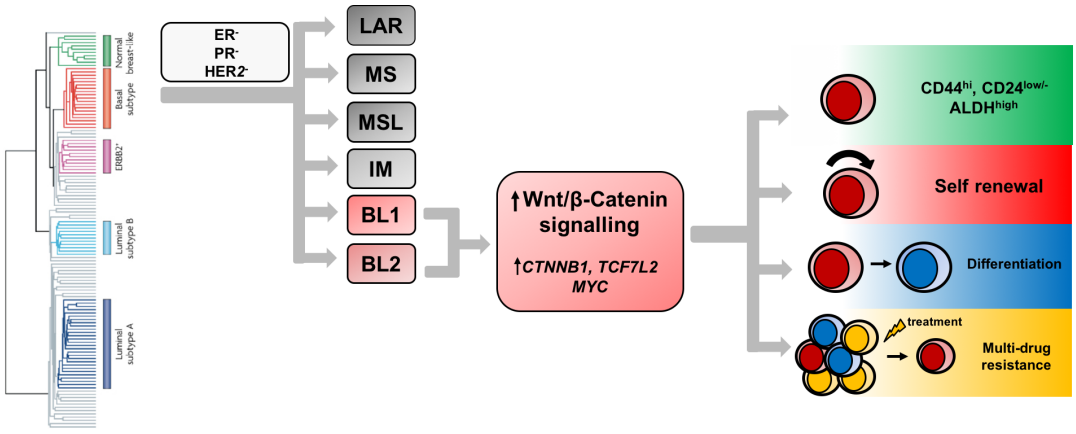

Figure 5.1. Association between the molecular subtypes of TNBC, Wnt signalling and CSCs. (Adapted from [7,9,18])

This chapter explores the role of DDX20 in the regulation of Wnt/β-catenin in TNBC stem cells. DDX20 directly associates with GSK3β, leading to increased canonical Wnt signalling (Cai & Pohl et al., unpublished). As Wnt signalling is increased in CSCs, it is important to evaluate whether there

were any differences in DDX20 expression in TNBC stem cells, and if depletion of DDX20 through RNAi would negatively alter the characteristic traits exhibited by these cells. Two TNBC cells lines were selected, MDA-MB-231 and BT549, and compared with the non-tumorigenic MCF-10A and oestrogen receptor-positive MCF-7 cell lines. MDA-MB-231 is a poorly differentiated invasive TNBC cell line that also exhibits downregulation of claudin-3 and claudin-4.[298] Originally established from the pleural effusion of a 51-year-old Caucasian female,[350] this cell line carries $BRAF^{G464V}$, $CDKN2A^{1\_471del471}$, RAS^{G13D}, and $p53^{R280K}$ mutations, and is mutationally BRCA1 and PTEN wild-type, although it exhibits an allelic loss of BRCA1. MDA-MB-231 has been reported to express the highest levels of DDX20 expression in a large panel of breast cancer cell lines.[216] BT549 was derived from a 74-year old Caucasian female and is an epithelial-like TNBC cancer cell line exhibiting giant multinucleated cells.[298] It carries $PTEN^{V275fs*1}$, $RB1^{265\_607del343}$, and $p53^{R249S}$ mutations. BT549 has an allelic loss of BRCA1, although is mutation status wild-type. This chapter explores whether the PTEN mutational status of the cell lines would impact the effect of DDX20 knockdown. Cell lines with PTEN mutations exhibit constitutively active PI3K-Akt signalling.[351] It has been previously reported that GSK3β can regulate the stability of PTEN, and PTEN can regulate GSK3β through activation of Akt.[352,353] Furthermore Protein phosphatase 2A (PP2A), which is responsible for the dephosphorylation of β-catenin, has been shown to interact with PTEN.[354] Therefore PTEN deficiency and mutations can lead to dysregulation and β-catenin and Wnt signalling.[355] The use of these cell lines allowed us to determine whether DDX20 could regulate GSK3β and Wnt signalling independent or dependent of PTEN mutational status.

5.2. RESULTS

5.2.1. Enrichment of cancer stem cells from immortalised cell lines

The evaluation of the ability of MCF-10A, MCF-7, BT549, MDA-MB-436, and MDA-MB-231 cells to form mammospheres in culture was followed using a previously published method.[91] After seven days in culture, all tumorigenic cell lines were able to form mammospheres, while the non-tumorigenic cell

line MCF-10A failed to form mammopsheres that exceeded 40μm in size (Figure 5.2).

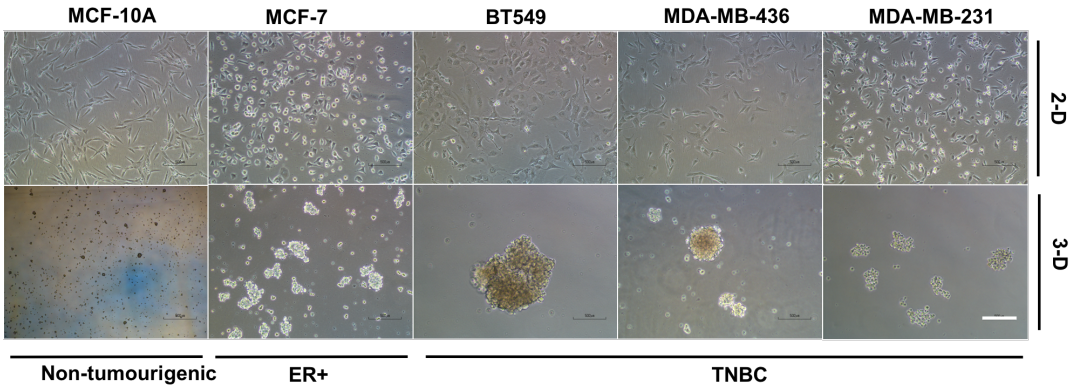

Figure 5.2. Evaluation of CSCs enriched from immortalised cell lines. A variety of cell lines were cultured under conditions for the enrichment of CSCs. MCF-10A failed to form mammospheres, oestrogen receptor positive and TNBC cell lines formed mammospheres after 7 days in 3-D culture. Scale bar = 40μm.

5.2.2. Characterisation of TNBC stem cells

After seven days in culture, MDA-MB-231 and BT549 cells were assessed for CD44 and CD24 expression using flow cytometry. 93.% of MDA-MB-231 enriched CSCs exhibited a $CD44^+/CD24^-$ phenotype, and 4.23% exhibited a $CD44^+/CD24^+$ phenotype. BT549-enriched CSCs had cell populations of 80.1% $CD44^+/CD24^-$ and 11.1% $CD44^+/CD24^+$ (Figure 5.3A).

To assess if these enriched CSCs also displayed overexpression of classical stem cell transcription factors, Q-PCR was utilised for mRNA expression of *KLF4, POU5F1* (Oct4)*, NANOG*, and *SOX2*, and the canonical Wnt target gene *AXIN2* as an indicator of Wnt activity. In both cell lines, *KLF4, POU5F1, NANOG*, and *SOX2* were overexpressed. *NANOG* was 6-fold and 4-fold higher in MDA-MB-231 and BT549 enriched CSCs respectively when compared to the parental cells. MDA-MB-231 and BT549 CSCs both overexpressed *AXIN2*, indicating higher Wnt activity, although this was much more pronounced in the MDA-MB-231 CSCs (Fig 5.3B&C).

CSCs from TNBC cell lines characteristically overexpress CD44. To validate this, Western blotting was performed on cells from the parental cell lines and enriched CSCs. It was found that both cell lines significantly ($p > 0.05$) overexpressed CD44 protein in the CSC-enriched population (Fig 5D).

Finally, to determine *DDX20* expression in the CSC-enriched population, Q-PCR was performed. It was found that only in MDA-MB-231 cells were *DDX20* mRNA levels significantly overexpressed in CSCs compared to the parental cell line (Fig 5E&F).

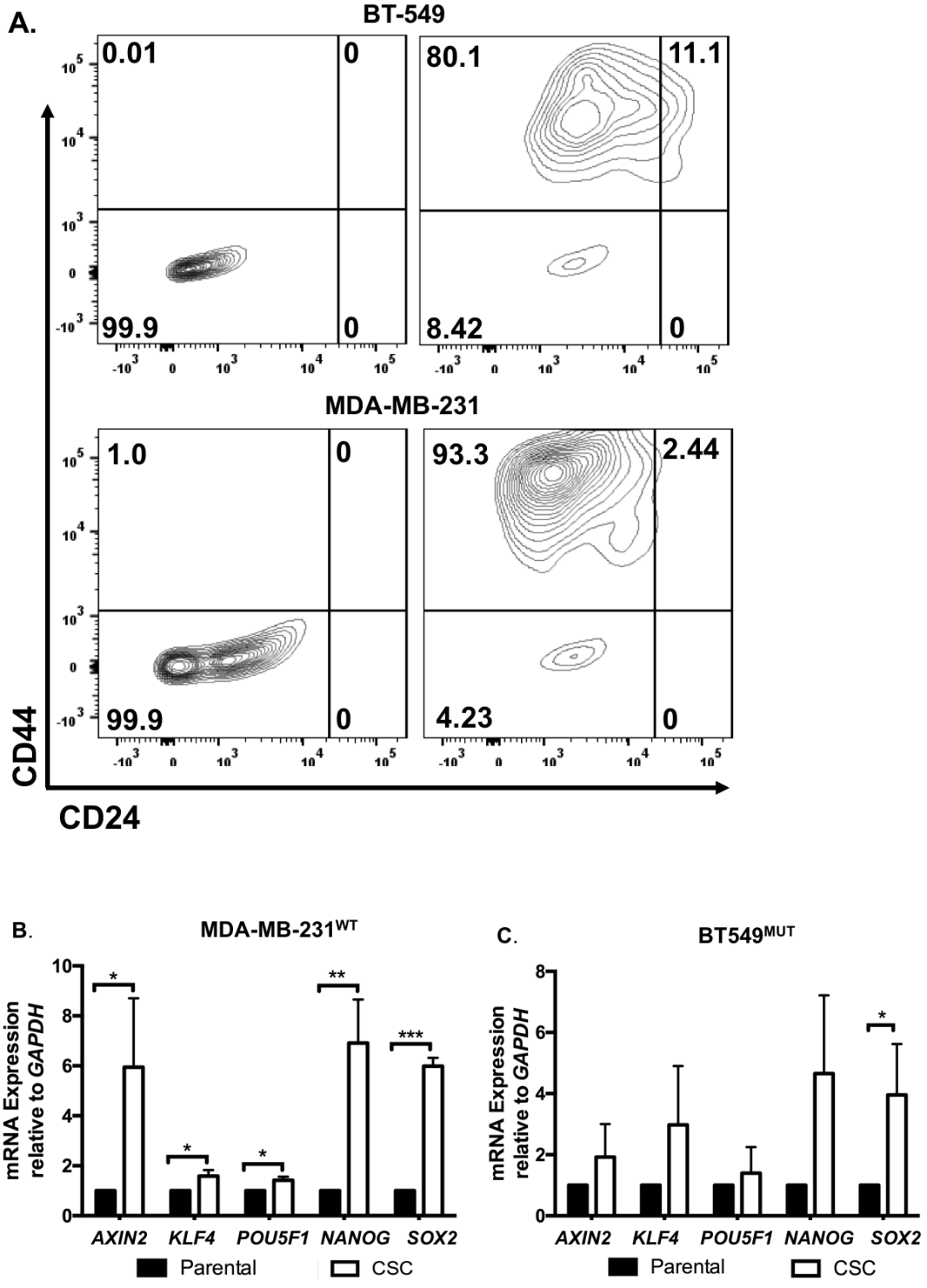

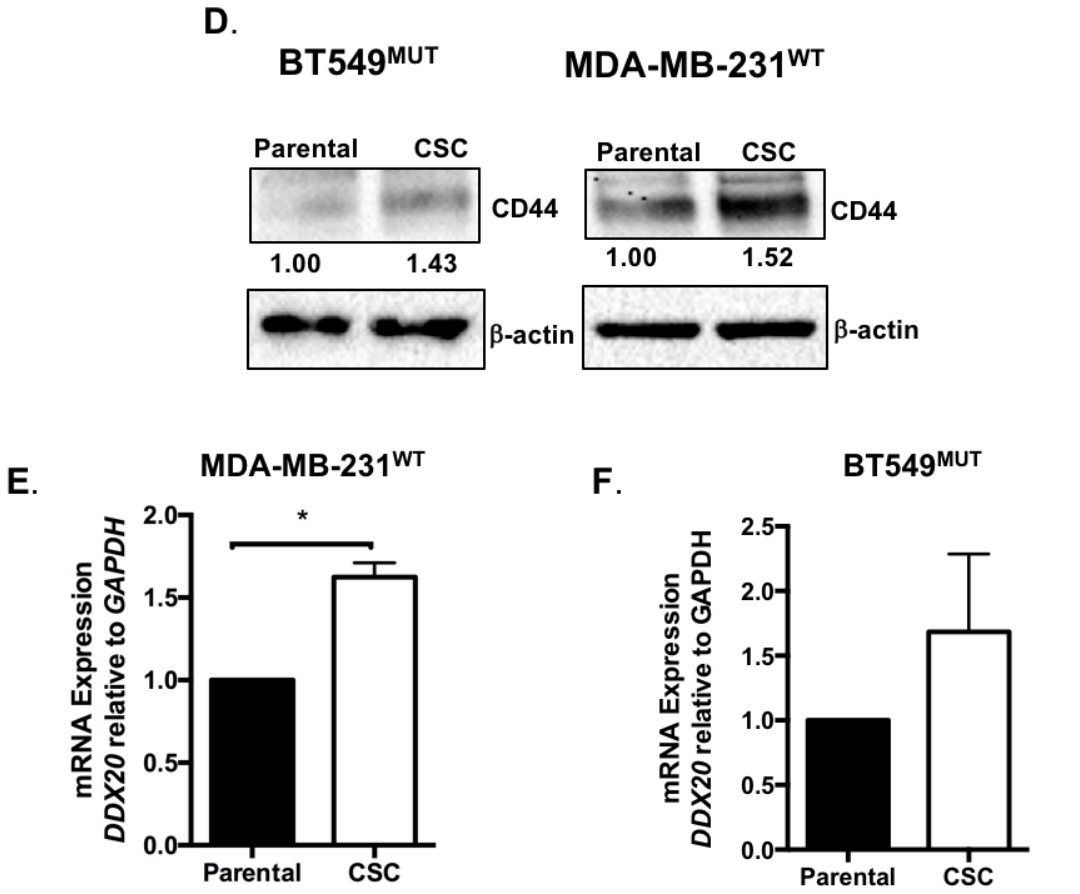

Figure 5.3. Characterisation of TNBC stem cells. A) Flow cytometry assessment of MDA-MB-231 and BT549 enriched CSCs using CD44-APC and CD24-PE/Cy7 antibodies. B & C) mRNA expression of *AXIN2, KLF4, POU5F1, NANOG*, and *SOX2* in MDA-MB-231 and BT549 CSCs. D. Protein expression of CD44 in CSC and parental cells from MDA-MB-231 and BT549 cells. E&F) mRNA expression of *DDX20* from MDA-MB-231 and BT549 cells. All data represented as mean±SEM, of at least three biological replicates. Statistical analysis was performed using unpaired students *t*-test, **p* < 0.05, ***p* < 0.01, ****p* < 0.001.

5.2.3. DDX20 is an essential regulator of Wnt/β-catenin signalling in TNBC stem cells

To evaluate whether DDX20 was a regulator of Wnt/β-catenin signalling in TNBC stem cells, a knockdown strategy using three separately-targeting siRNAs against DDX20 was used. 72 hours post-transfection, we examined protein expression of total levels of cellular β-catenin, as well as the transcriptionally active β-catenin (Ser33/Ser37/Thr41). Successful knockdown of the DDX20 protein was concomitant with a significant decrease in the levels of active β-catenin in both cell lines, while total β-catenin remained unchanged (Fig 5.4A,B,C).

To further evaluate the role of DDX20 in the regulation of Wnt signalling, cells were subjected to a “Wnt ON” environment, whereby we stimulated both cell lines with recombinant Wnt3a ligand for three hours with and without depletion of DDX20. While stimulation with Wnt3a in MDA-MB-231 and BT549 cells with DDX20 led to an increase in the levels of active β-catenin, cells without DDX20 were unable to properly conduct Wnt signalling upon Wnt3a stimulation (Fig 5.4D).

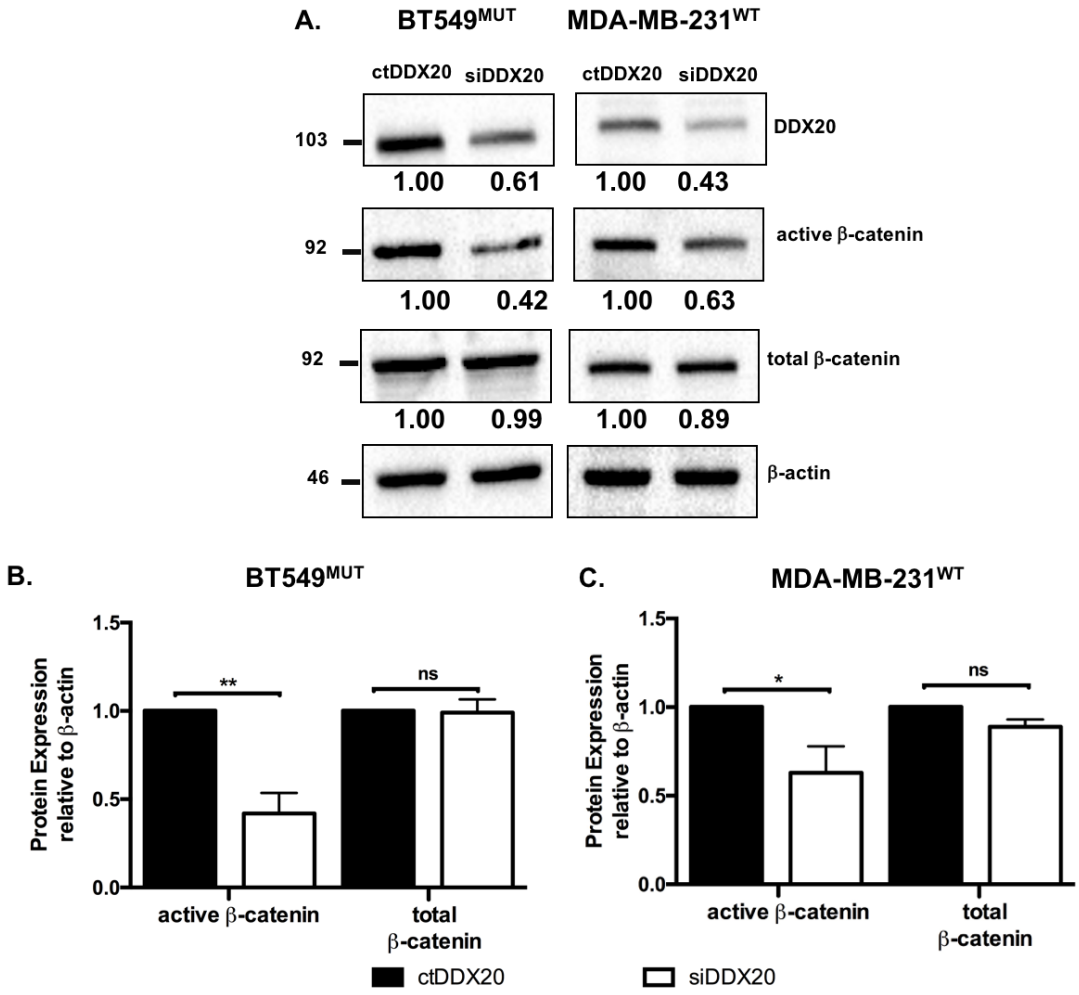

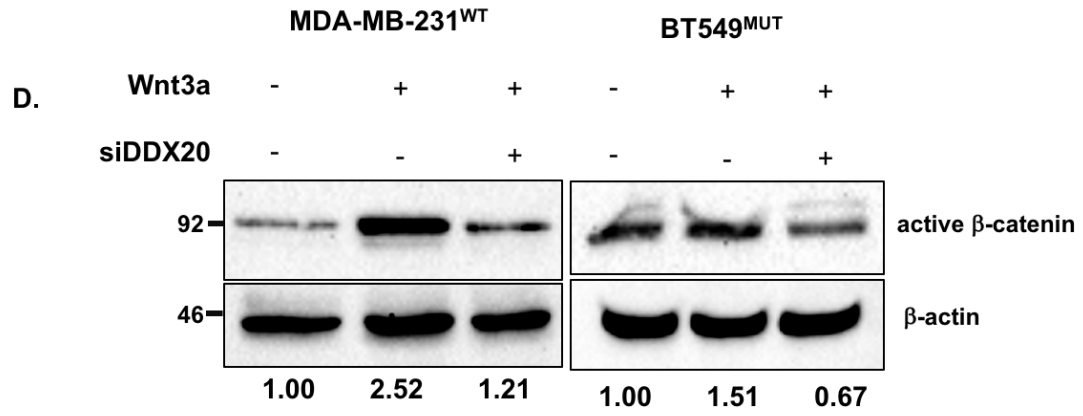

Fig 5.4. DDX20 is an essential regulator of Wnt/β-catenin signalling. A) Western blots of siRNA knockdown of DDX20 in BT549 and MDA-MB-231 cells for active β-catenin levels. B&C) Quantification of protein levels of total and active β-catenin protein following DDX20 knockdown 72 hours post-transfection. D) Western blots for active β-catenin in cells stimulated with 200ng/ml recombinant Wnt3a for three hours. All data are represented as mean±SEM of at least three biological replicates. Statistical analysis was performed using unpaired Student's *t*-test, **p* < 0.05, ***p* < 0.01, ****p* < 0.001.

5.2.4. Depletion of DDX20 results in destabilisation of the β-catenin destruction complex

Destabilisation of the β-catenin destruction complex is responsible for increased levels of transcriptionally active β-catenin in cells. To evaluate the effect DDX20 has on expression of destruction complex proteins, protein expression for Dishevelled 2 (Dvl2), levels of GSK3β phosphorylated at Ser9 (^{pSer9}GSK3β), as well as total cellular levels of GSK3β, after knockdown of DDX20 was assessed (Fig 5.5A).

While the levels of Dvl2 were significantly decreased in both cell lines, there was a differential regulation in the levels of phosphorylation of GSK3β. In BT549 cells, knockdown of DDX20 resulted in an increased level of GSK3β phosphorylation, while it was decreased in the MDA-MB-231 cells (Fig 5.5B&C).

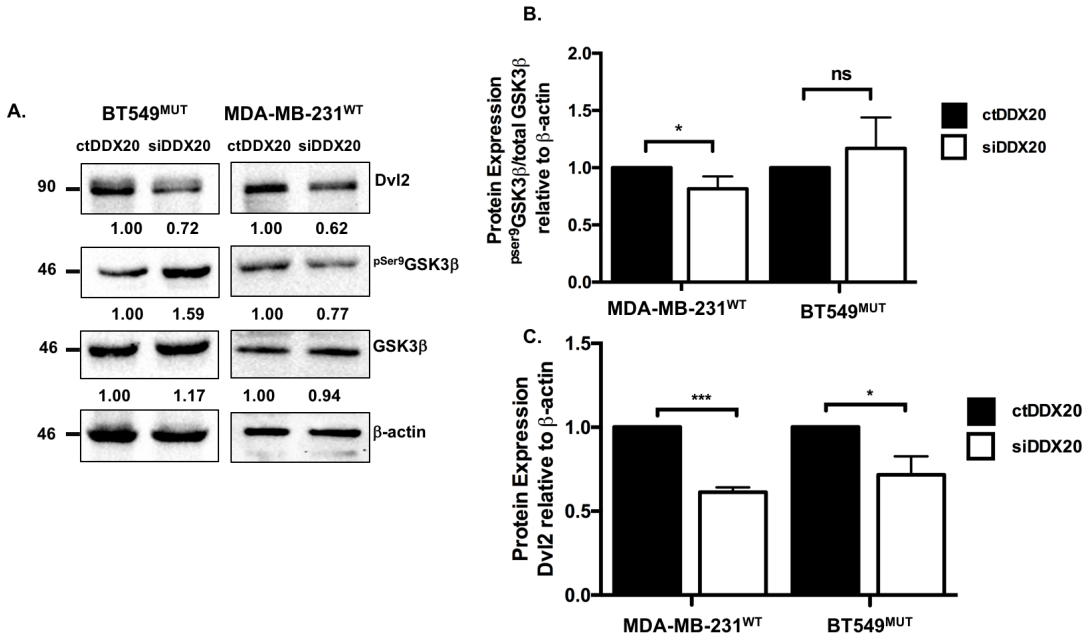

Figure 5.5. DDX20 causes destabilisation of the β-catenin destruction complex. A) Western blots of Dvl2, ^{pSer9}GSK3β, and GSK3β in BT549 and MDA-MB-231 cell lines following knockdown of DDX20. B) Quantification of ^{pSer9}GSK3β relative to total GSK3β protein expression. C) Quantification of Dvl2 protein expression in BT549 and MDA-MB-231 cell lines. All data are represented as mean±SEM, of at least three biological replicates. Statistical analysis was performed using unpaired Student's *t*-test, **p* < 0.05, ***p* < 0.01, ****p* < 0.001.

5.2.5. DDX20 co-localises with CD44 and regulates transcription factors involved in pluripotency

It has also been reported that CD44 promotes Wnt signalling through its direct association with LRP6.[356] Due to these previous findings, we decided to determine whether DDX20 and CD44 could associate with one another.

Co-staining for DDX20 and CD44 in MDA-MB-231 CSCs revealed extensive co-localisation of CD44 and DDX20 at the membrane in basal conditions. Furthermore, when assessing protein levels by immunofluorescence, there was a noticeable decrease in CD44 membranous expression on DDX20 knockdown (Fig 5.6A). Western blotting demonstrated that DDX20 depletion in MDA-MB-231 cells - but not BT549 – resulted in markedly reduced protein expression of CD44 (Fig 5.6B).

To test whether DDX20 could regulate 'stemness' characteristics of TNBC stem cells, mRNA expression of *NANOG, POU5F1*, and *SOX2* were determined in both cell lines. All genes displayed a significant reduction

in expression upon depletion of DDX20 (Fig 5.6C). Furthermore, *AXIN2* was also significantly reduced in both cell lines after siRNA-mediated knockdown of DDX20 (Fig 5.6D).

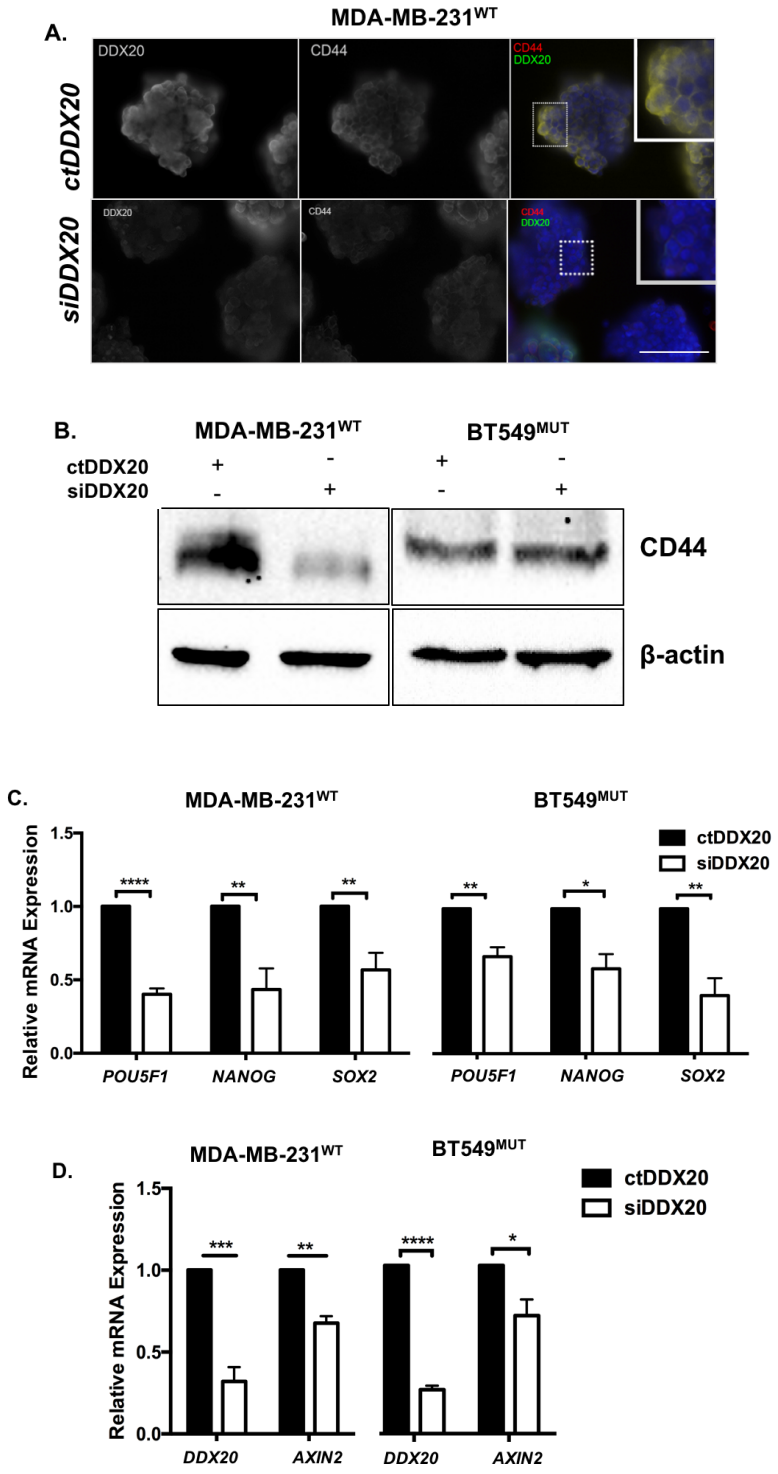

Figure 5.6. DDX20 co-localises with CD44 and regulates mRNA expression of transcription factors involved in stemness. A) Immunofluorescence co-staining of DDX20 (Alexafluor488) and CD44 (Alexafluor555) in cells with and without DDX20. B) Western blots showing protein expression of CD44 in MDA-MB-231 and BT549 cell lines. C) mRNA

expression of *NANOG*, *POU5F1*, and *SOX2* in MDA-MB-231 and BT549 cells after transfection with siRNA against DDX20. D) mRNA expression of *AXIN2* in MDA-MB-231 and BT549 cells after transfection with siRNA against DDX20. All data are represented as mean±SEM of at least three biological replicates. Statistical analysis was performed using unpaired Student's *t*-test, **p* < 0.05, ***p* < 0.01, ****p* < 0.001. Scale bar = 50μm.

5.2.6. DDX20 is a regulator of cell cycle progression

CSCs are quiescent cells, and this property is one of the reasons they are able to evade forms of chemotherapy targeting highly proliferative cells.[357]

Western blotting was used to assess the protein levels of cyclin D1 and c-MYC after DDX20 depletion. Cyclin D1 was significantly decreased in both cell lines after DDX20 knockdown. Interestingly, cMYC protein expression was unaltered in BT549 cells but was significantly decreased in MDA-MB-231 cells (Fig 5.7A&B). Flow cytometric analysis of cell cycle progression in MDA-MB-231 CSCs, demonstrated that knockdown of DDX20 was able to significantly alter cells in various stages of the cell cycle. In DDX20-depleted cells there was a significant increase in cells in the sub G0 phase, and a decrease in cells in the G0-G1 and G2 phases (Fig 5.7C&D). Furthermore, GSEA on DDX20^{high} versus DDX20^{low} phenotypes from METABRIC cohort revealed significantly upregulated gene sets involved in cell cycle regulation, including cell division (GO:0051301), mitotic cell cycle checkpoint (GO:0007093), cell cycle checkpoint (GO:0000075), cell cycle phase transition (GO:1901989), and cell cycle G1-S phase transition (GO:0044843) (Fig 5.7E).

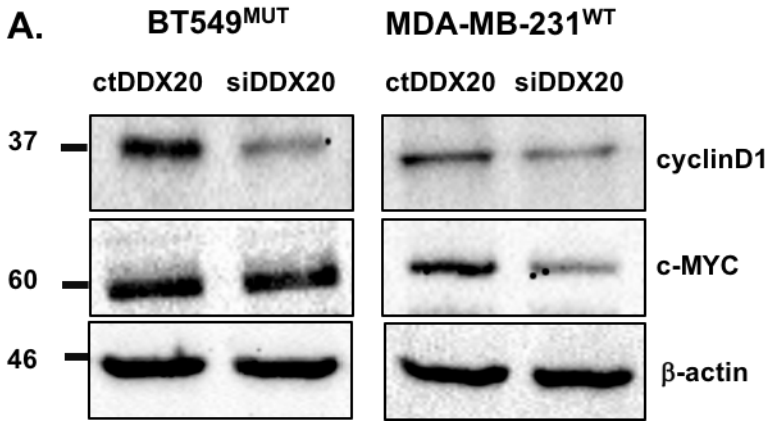

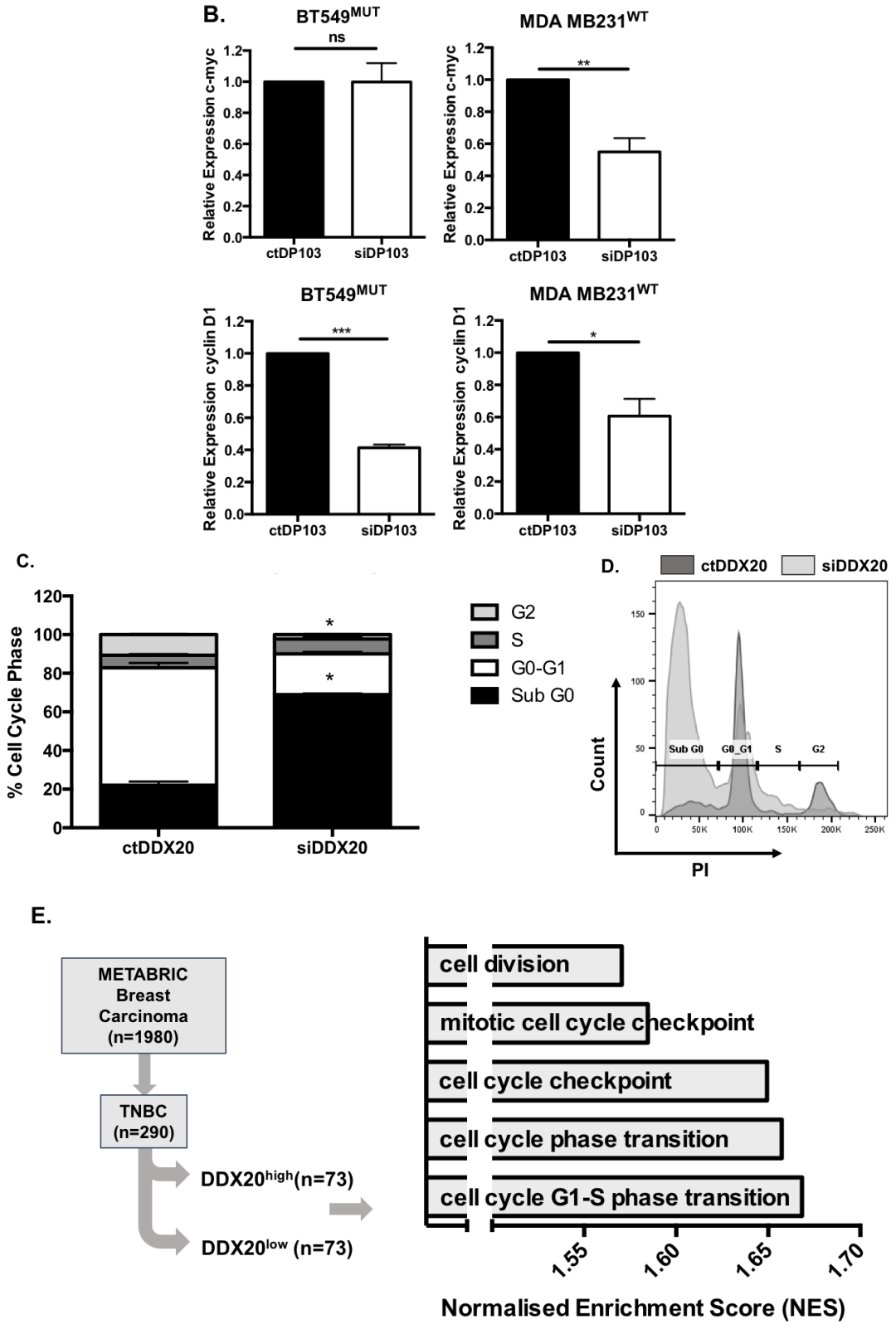

Figure 5.7. DDX20 regulates cell cycle progression. A) Western blots of cyclin D1 and c-MYC in BT549 and MDA-MB-231 cells after treatment with siRNA targeting DDX20 (siDDX20) or control siRNA (ctDDX20). B) Quantification of Western blots of cyclin D1 and c-MYC. C) Quantification of the percentage of cells in cell cycle phase (Sub G0, G0-G1, S, and G2) in MDA-MB-231 cells after DDX20 depletion. D) Representative histogram of cell

counts after cell cycle analysis of MDA-MB-231 cells after transfection with siDDX20. E) Schematic and bar graph of enriched gene sets involved in cell cycle regulation in $DDX20^{high}$ vs $DDX20^{low}$ phenotype of the METABRIC TNBC cohort. All data are represented as mean±SEM of at least three biological replicates. Statistical analysis was performed using unpaired Student's *t*-test, $*p < 0.05$, $**p < 0.01$, $***p < 0.001$.

5.2.7. Knockdown of DDX20 induces apoptosis and increases sensitivity to doxorubicin

The ability of MDA-MB-231 and BT549 cells to form mammospheres after transfection with siRNA was assessed using a mammosphere forming assay. BT549 cells were able to form more spheroids than MDA-MB-231 cells, although this ability was significantly diminished in both cell lines following siDDX20 knockdown (Fig 5.8A). It was found that knockdown of DDX20 only caused a significant decrease in viability in the MDA-MB-231 cells, not in the BT549 CSCs (Fig 5.8B).

As there was no significant difference in viability in the BT549 cell line, MDA-MB-231 was used for the subsequent cell death assays. The ability of MDA-MB-231 cells to be sensitised to 1μM doxorubicin following DDX20 knockdown was assessed using the JC-1 probe, which accumulates in live mitochondria. Increased JC-1 monomers are an indicator of a loss of mitochondrial membrane potential. Transfection with siDDX20 increased JC-1 monomers compared to cells transfected with control siRNA. There was an additive effect when siDDX20 and doxorubicin were added in combination, when compared to doxorubicin alone (Fig 5.8C).

To further confirm the increase in cell death, Western blotting was performed for the anti-apoptotic mitochondrial proteins Bcl-xL and PARP (Fig 5.8D&E). Depletion of DDX20 results in a significant decrease in levels of PARP, as well as the presence of the cleaved PARP protein fragment. A caspase-3/7 assay was performed, which indicated increased caspase activity in cells transfected with siDDX20 (Fig5.8F). To validate the previous findings in the parental cells, we used the H_2O_2 assay to test whether ROS - specifically H_2O_2 – were increased in the CSCs after knockdown of DDX20. Consistent with the previous reports, silencing of DDX20 produced a significant increase in H_2O_2 production (Fig 5.8G).

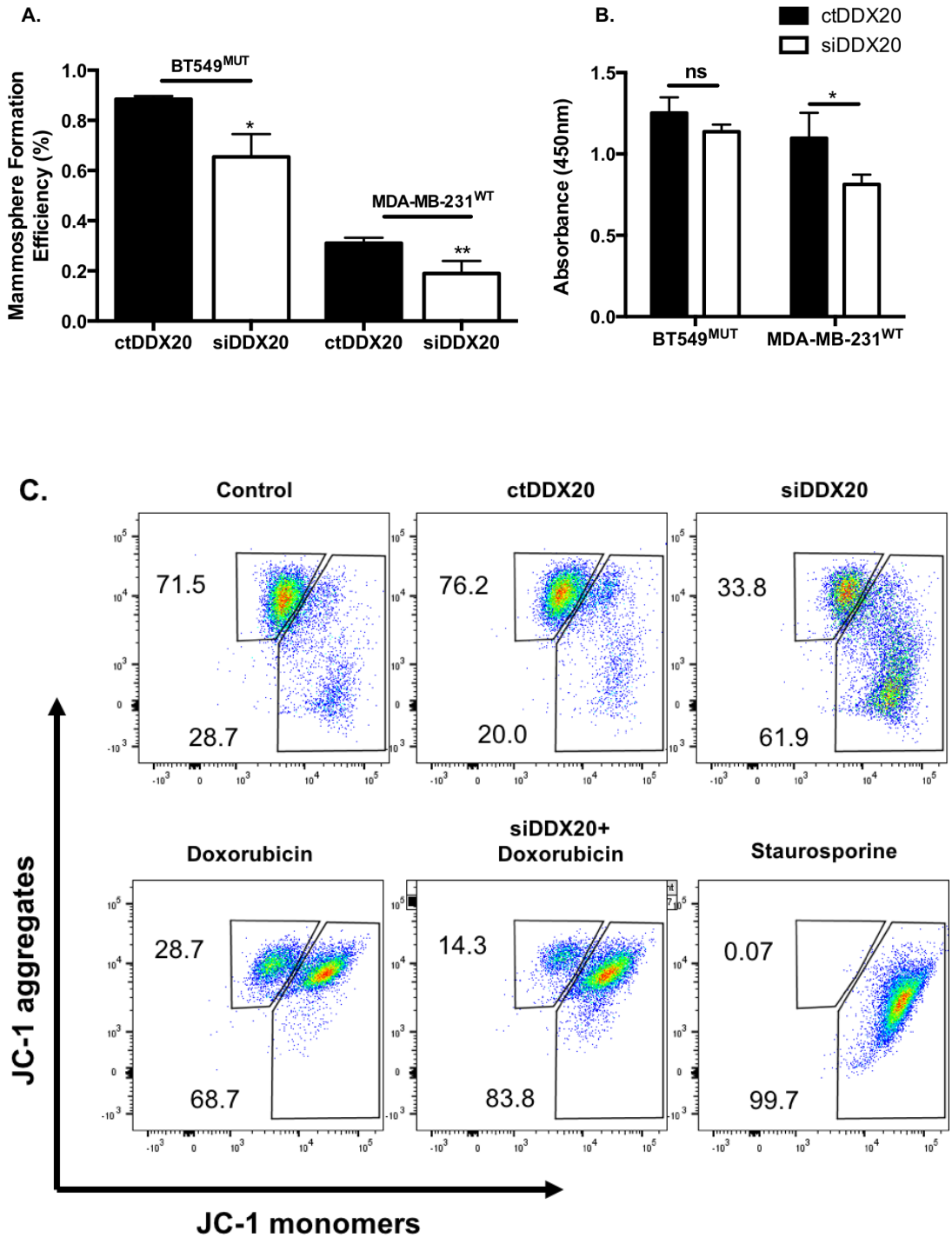
A.
Mammosphere Formation Efficiency (%)
1.0
0.8
0.6
0.4
0.2
0.0
BT549MUT
*
MDA-MB-231WT
**
ctDDX20
siDDX20
ctDDX20
siDDX20
B.
ctDDX20
siDDX20
Absorbance (450nm)
1.5
1.0
0.5
0.0
ns
*
BT549MUT
MDA-MB-231WT
C.
Control
ctDDX20
siDDX20
71.5
28.7
76.2
20.0
33.8
61.9
Doxorubicin
siDDX20+ Doxorubicin
Staurosporine
28.7
68.7
14.3
83.8
0.07
99.7
JC-1 aggregates
JC-1 monomers

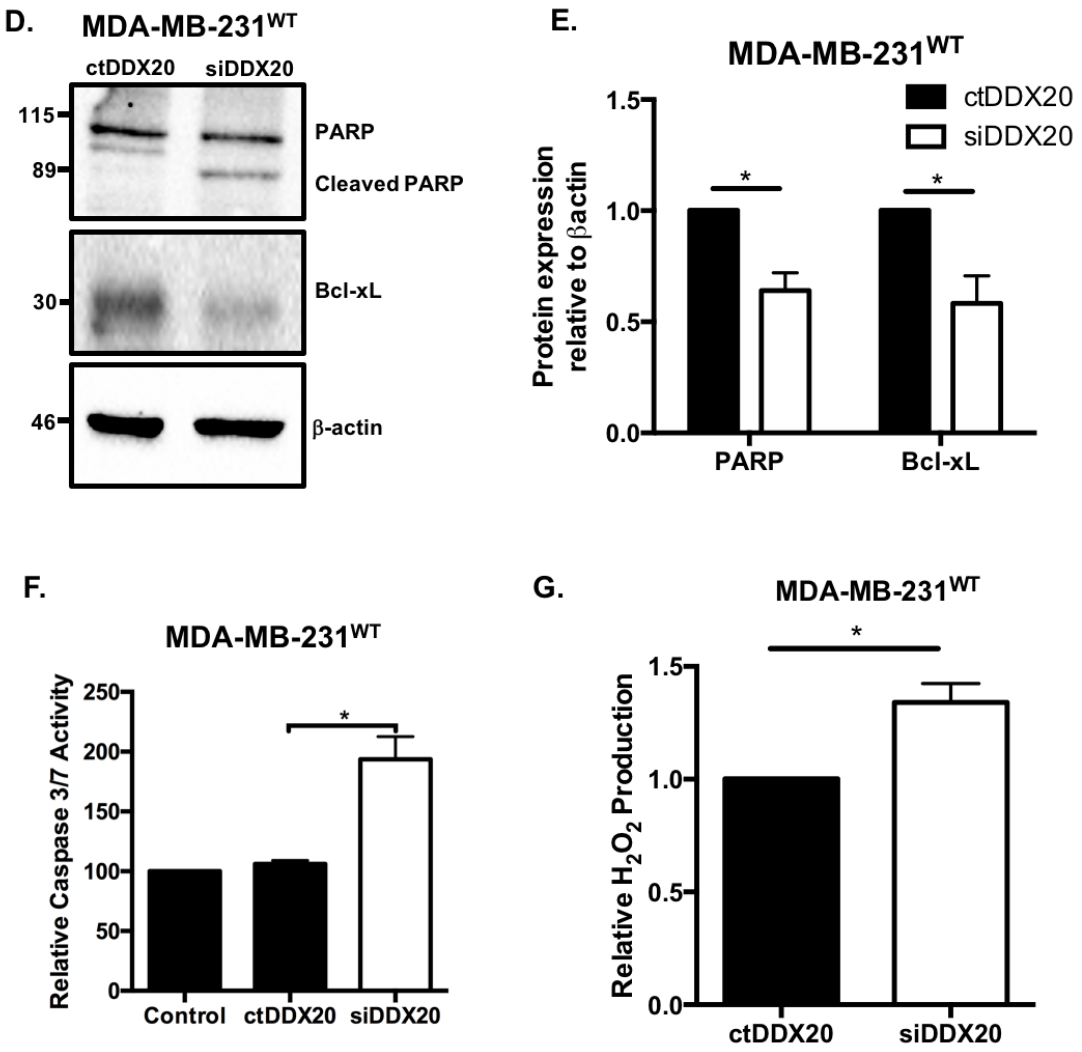

Figure 5.8. Loss of DDX20 induces apoptosis and increases chemosensitisation. A) Mammosphere-forming efficiency in BT549 and MDA-MB-231 cells transfected with siRNA targeting DDX20. B) Cell viability measured by CCK8 assay in cells transfected with siRNA targeting DDX20. C) JC-1 assayed measured by flow cytometry in control cells, cells transfected with control siRNA, cells transfected with siRNA targeting DDX20, 1μM doxorubicin, or a combination of the two. 1μM staurosporine was used as a positive control. Cells were treated with doxorubicin and staurosporine for 24 hours. D) Western blots of PARP and Bcl-xL in MDA-MB-231 cells after DDX20 knockdown. E) Quantification of Western blots. F) Fluorogenic Caspase-3/7 assay in MDA-MB-231 cells after siDDX20. G) ROS-Glo H_2O_2 assay of MDA-MB-231 cells after transfection with siDDX20. JC-1 data are a representative dot plot of three individual experiments with similar results. All other data are represented as mean±SEM of at least three biological replicates. Statistical analysis was performed using unpaired Student's *t*-test, **p* < 0.05, ***p* < 0.01, ****p* < 0.001.

5.2.8. Wnt antagonist, SFRP4, downregulates DDX20 through its cysteine-rich domain (CRD)

Previous data suggest that DDX20 is upstream of the β-catenin destruction complex (Cai & Pohl et al., unpublished). To test whether antagonism of the Wnt pathway could decrease the expression of DDX20, recombinant SFRP4

was exogenously added to the cell medium for 48 hours. In MDA-MB-231 cells there was a significant decrease in DDX20 protein expression, while in BT549 cells, there was no significant difference (Fig 5.9A&B). In MCF-10A cells, SFRP4 could not significantly decrease DDX20 expression, and conversely, Wnt3a could not significantly increase DDX20 expression (Fig 5.9C&D).

The CRD of SFRP4 has been previously shown to bind Wnt ligands to antagonise Wnt signalling, while the exact mechanisms of action of the netrin-like domain (NLD) of SFRP4 have yet to be fully elucidated. To determine which domain is responsible for the decrease in DDX20, we added purified CRD and NLD protein to both cell lines. The addition of $SFRP4_{\Delta NLD}$ (consisting of just the CRD) resulted in a significant decrease in DDX20 expression in MDA-MB-231 cells. This was not observed in BT549 cells. The addition of $SFRP4_{\Delta CRD}$ (consisting of just the NLD) had no significant effect on either cell line (Fig 5.9E&D).

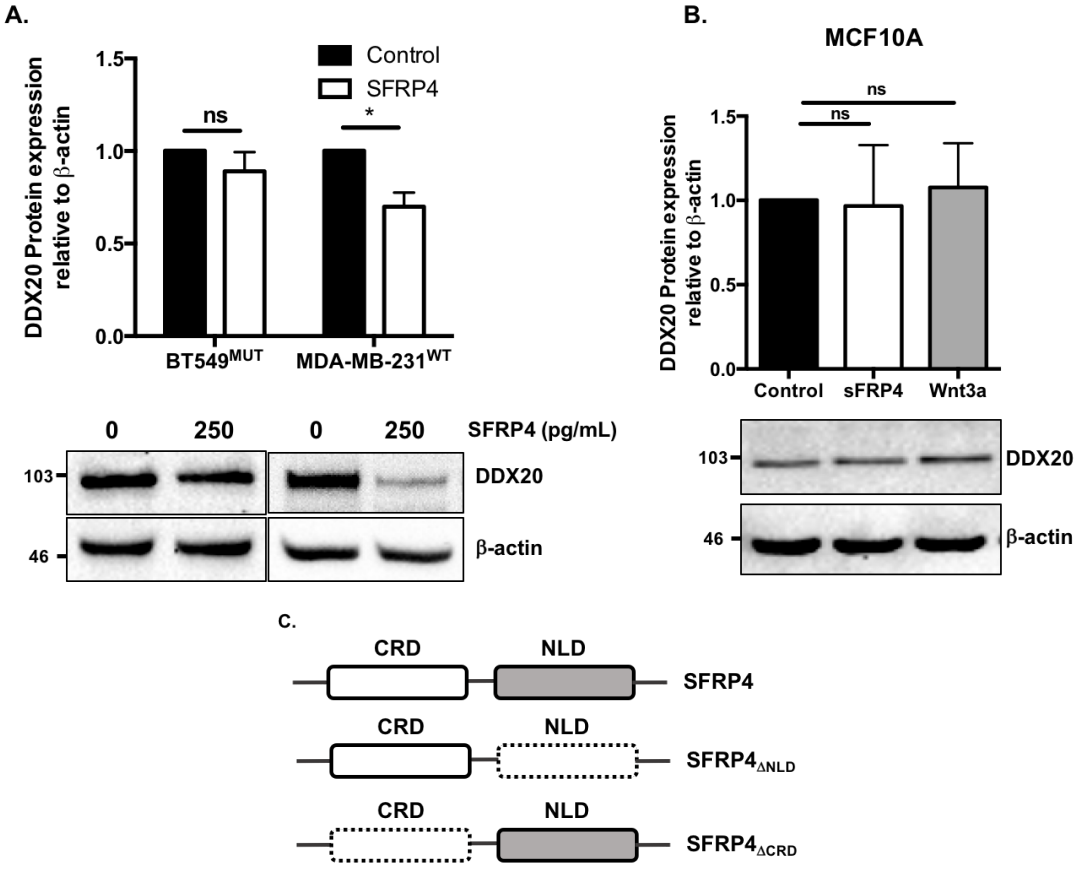

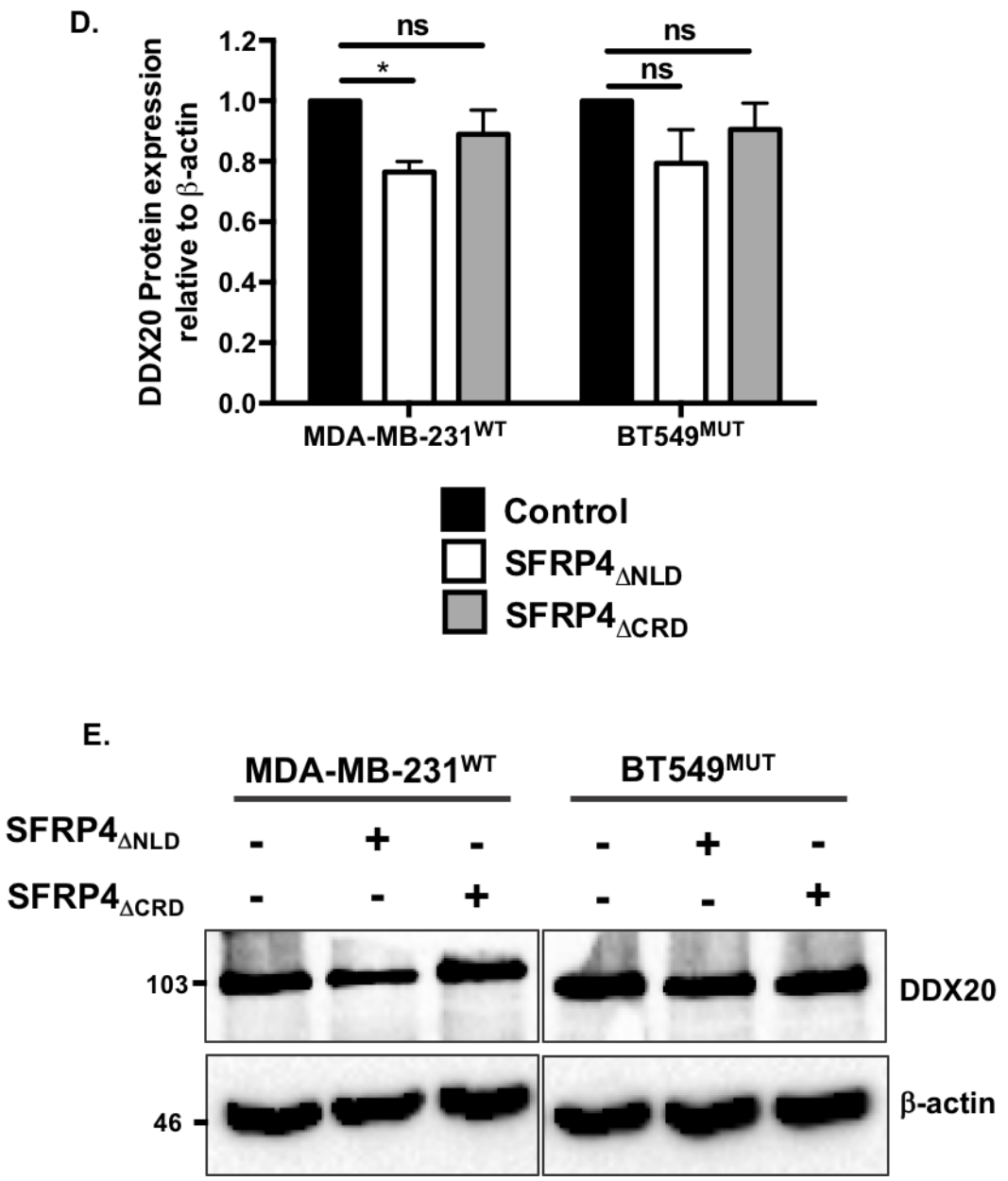

Figure 5.9. DDX20 is downregulated by the CRD of SFRP4. A) Western blots and quantification of SFRP4 (250pg/mL) treated MDA-MB-231 and BT549 cells. B) Western blots and quantification of SFRP4 (250pg/mL) and Wnt3a (200ng/mL) treated MCF-10A cells. C) Schematic of purified proteins of SFRP4 domains. D&E) Western blots and quantification of $SFRP4_{\Delta CRD}$ and $SFRP4_{\Delta NLD}$ (250pg/mL) treated MDA-MB-231 and BT549 cells. All data are represented as mean±SEM of at least three biological replicates. Statistical analysis was performed using unpaired Student's *t*-test, $*p < 0.05$, $**p < 0.01$, $***p < 0.001$.

5.2.9. DDX20 regulates Wnt signalling through a positive feedback loop

Wnt3a causes increased nuclear localisation of β-catenin, where it binds to TCF/LEF transcription factors. This is diminished in the absence of DDX20 (Fig 5.10A). To determine the effect of Wnt3a stimulation on DDX20 mRNA expression, a time course experiment was conducted after the addition of Wnt3a (200ng/mL) from two to 16 hours. Significant increases in *DDX20*

expression were found at 4, 8, and 12 hours, with maximum gene expression at 12 hours. *AXIN2* was used as a positive control and exhibited similar results, although maximal gene expression was reached at eight hours (Figure 5.10B).

To determine if DDX20 is a direct target of TCF/LEF transcription, an inhibitor of β-catenin/TCF4 transcription, iCRT3, was added to MDA-MB-231 cells. Cells treated with iCRT3 exhibited a significant dose-dependent decrease in DDX20 expression (Fig 5.10C&D).

To further validate that DDX20 was a target of TCF4 transcription, USCD ChIP-seq data across three different cell lines - HeLa, MCF7, and HCT-116 – were examined. All three cell lines demonstrated peak signals of TCF4 (TCF7L2) on the 5'-UTR region of the DDX20 promoter (Fig 5.10E).

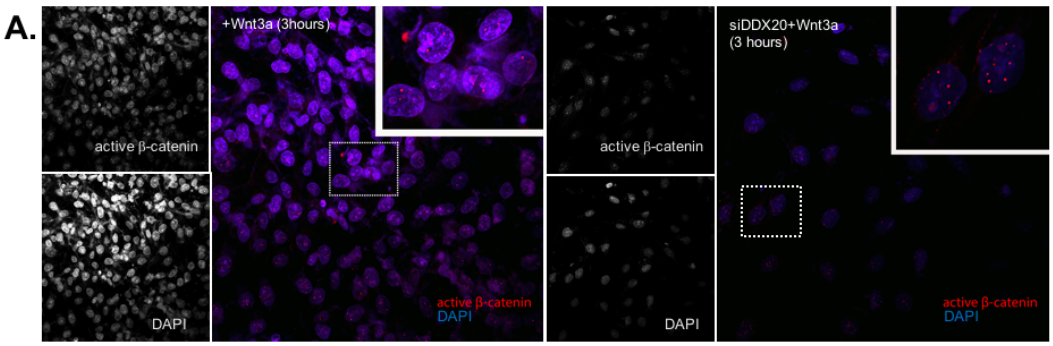

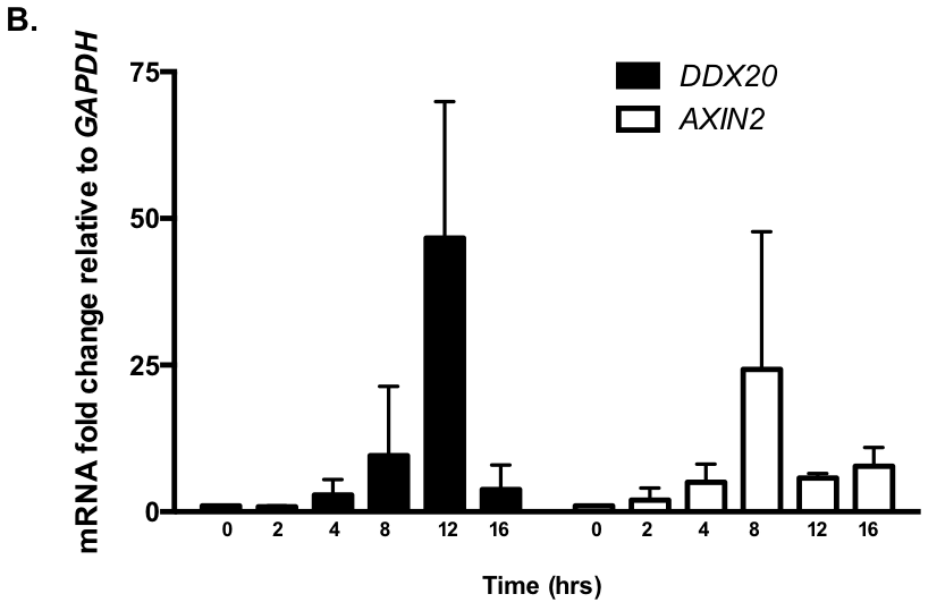

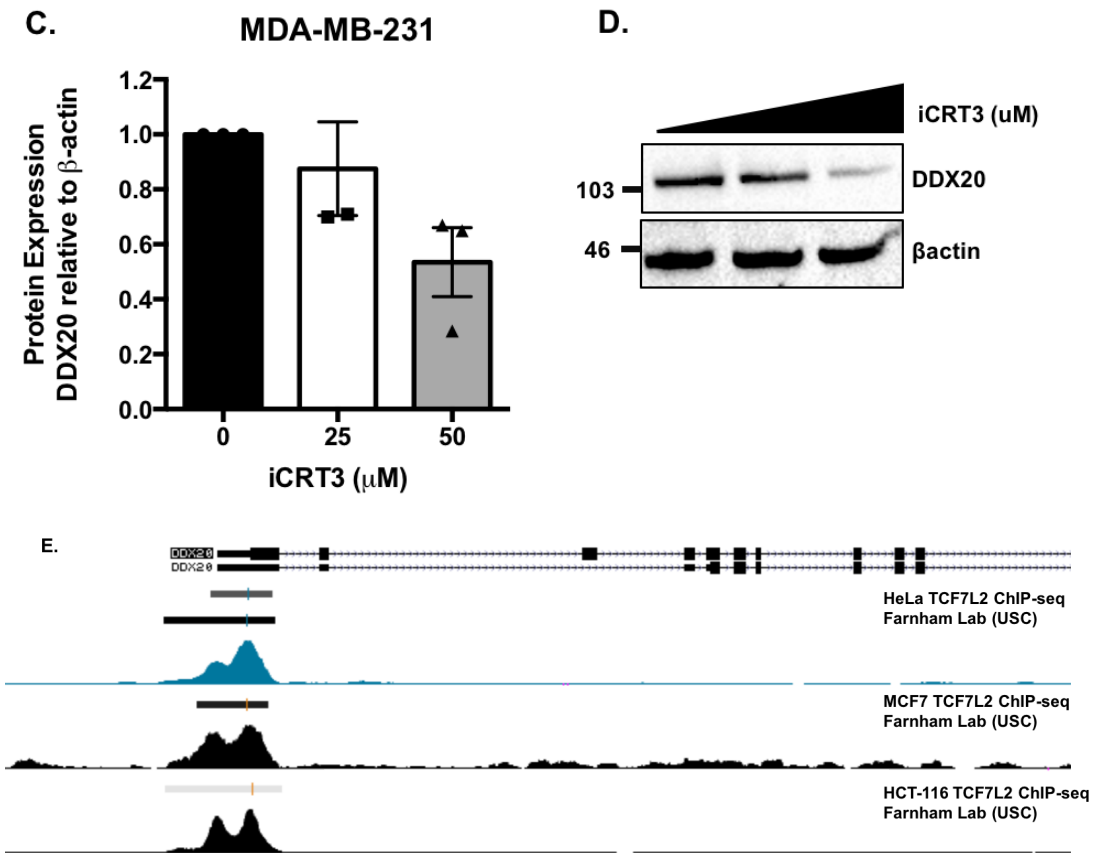

Figure 5.10. DDX20 regulates a Wnt/β-catenin positive feedback loop. A) Immunofluorescence of active β-catenin (Alexafluor555) and DAPI after Wnt3a (200ng/mL) stimulation for three hours with and without DDX20 in MDA-MB-231 cells. B) mRNA expression of *DDX20* and *AXIN2* at indicated time points after the addition of Wnt3a. C) Quantification of DDX20 protein expression after treatment with iCRT3 for 24 hours. D) Western blot of DDX20 protein expression after treatment with iCRT3 for 24 hours. E) ENCODE ChIP-seq data view of TCF4 (TCF7L2) ChIP-seq in HeLa, MCF7, and HCT116 cells visualised over DDX20 DNA. Statistical analysis was performed using unpaired Student's *t*-test, **p* < 0.05, ***p* < 0.01, ****p* < 0.001. Scale bar = 50μm.

5.3. DISCUSSION

This is the first report of DDX20 regulating Wnt signalling in any cell type. These data convincingly show that depletion of DDX20 results in a decrease in the transcriptionally-active form of β-catenin, albeit with Wnt3a stimulation, as well as destabilisation of the destruction complex through Dvl downregulation. Other DDX family members have been implicated in the regulation of Wnt signalling in TNBC.[7] DDX5 has been demonstrated to directly interact with β-catenin and promote Wnt signalling,[358] while DDX3 has also been reported to directly interact with CK1ε to influence Dvl phosphorylation and positively regulate Wnt signalling.[189] Interestingly, depletion of DDX20 exhibited the same effect on both active β-catenin and

Dvl2 expression, although there was a differential regulation in the phosphorylation of Ser9 of GSK3β. Inhibition of GSK3β is a known event for the activation of Wnt signalling.[359] Recent reports suggest that phosphorylation of GSK3β Tyr216 may have a greater influence.[360] A recent study has demonstrated that phosphorylated C-terminal motifs of the Wnt receptor LRP6 are responsible for the inhibition of GSK3β by binding to the residues surrounding Tyr216 of GSK3β.[361] It is possible that loss of DDX20 can influence the Akt-mediated-phosphorylation of GSK3β without affecting Wnt signalling.

The B56 subunit of PP2A regulates the dephosphorylation of β-catenin, leading to its ubiquitin-mediated degradation.[362] It has been shown that PP2A interacts with PTEN, and therefore PTEN deficiency can in fact lead to an increase in β-catenin stabilisation and tumour progression through increased Wnt signalling.[354,363] The increased basal active β-catenin levels in BT549 cells compared to MDA-MB-231 was confirmed in this study.

CD44 is a transmembrane glycoprotein that binds extracellular ligands to regulate extracellular matrix adhesion. CD44 has also been implicated as an important mediator of intracellular signalling, in which it can elicit signal transduction through heterodimerisation with receptor tyrosine kinases and other plasma-membrane bound receptors. These separate functions explain its role in tumour progress and metastasis.[364]

These data demonstrated that CD44 is overexpressed in CSCs when compared to parental cell lines. When both cell lines were depleted of DDX20, a significant decrease in CD44 expression was observed in the MDA-MB-231 cell line. BT549 expresses a constitutively active Akt, which has been reported to inhibit hyaluronan synthase (HAS2) repression of CD44 expression; this was found to be mediated by FOXO1 and worked through a positive feedback loop.[365] Therefore, CD44 expression may be kept high in BT549 cells through Akt signalling, independent of DDX20 expression. We used co-staining immunofluorescence to determine whether DDX20 would co-localise with CD44. We saw extensive co-localisation of DDX20 and CD44 at the membrane of MDA-MB-231 CSCs. It may be possible that

DDX20 and CD44 are involved in Wnt signalosome assembly and signal transduction with other Wnt signalosome components.

This study demonstrated that depletion of DDX20 results in a reduction in gene expression of transcription factors regulating pluripotency, including *NANOG*, *SOX2*, and *POU5F1*, and the Wnt target gene *AXIN2*. This is consistent with the decrease in transcriptionally active β-catenin seen with knockdown of DDX20. β-catenin has been demonstrated to upregulate Nanog expression through its interaction with Oct3/4.[366] Furthermore, it has been shown that TCF4 downregulation coincides with decreased expression of *SOX2*[367] and *POU5F1*.[368]

The regulation of cell cycle progression by DDX20 in CSCs was also examined. We focussed on two master regulators of cell cycle progression – c-MYC, which is essential for the entry of quiescent cells into the cell cycle,[369] and cyclin D1, which progresses the cells from G1 to S phase.[370] Unexpectedly, while levels of cyclin D1 protein were reduced after DDX20 knockdown in both cell lines, c-MYC levels were altered in BT549 cells. A previous report implicated active GSK3β in the phosphorylation (Thr58) and degradation of cMYC.[371] BT549 has higher levels of inhibited GSK3β after DDX20 depletion, which, in turn, could suggest less c-MYC degradation. After flow cytometric cell cycle analysis of MDA-MB-231 cells, the majority of cells were in the sub G0 phase, indicative of cells undergoing apoptosis.[372]

To evaluate the impact of DDX20 depletion on apoptosis, the ability of these cells to form mammospheres was examined and their cellular viability assessed through CCK8 assay. Both cell lines had significantly reduced mammosphere formation after DDX20 depletion, although cell viability was only significantly reduced in the MDA-MB-231 cells. It is quite possible that BT549 cells are dependent on PI3K/Akt/mTOR signalling, and depletion of Wnt signalling itself is not enough to initiate apoptosis. A study in BT549 cells demonstrated that dual targeting of both the PI3K/Akt/mTOR and MEK/ERK pathways was critical to induce high levels of apoptosis.[373]

As CSCs are known to exhibit drug resistance,[374] we used a measure of mitochondrial membrane potential, the JC-1 assay, to determine

the response of MDA-MB-231 cells to combinatorial treatment. We found that the knockdown of DDX20 increased the response of the cells to doxorubicin, compared to doxorubicin alone. Previous studies have demonstrated the effect of antagonising the Wnt pathway on the sensitivity of cells to chemotherapeutics.[375] The addition of the Wnt antagonist SFRP4 has been reported to increase the response of ovarian cancer,[376] glioma stem cells,[93] and head and neck CSCs[92] to a variety of chemotherapeutics.

Next, whether antagonising Wnt signalling was able to decrease DDX20 protein expression was examined. The addition of SFRP4 to MDA-MB-231 cells resulted in a significant decrease in the expression of DDX20 at 48 hours, although this was not seen in the BT549 cells. It was shown that basal breast CSCs with high levels of Wnt signalling also expressed higher levels of SFRP1.[377] SFRP1 and SFRP4 can bind Wnt3a,[378,379] therefore, the exogenous addition of SFRP4 in the presence of endogenous SFRP1 may no longer be able to exert its normal function on Wnt antagonism. DDX20 is under expressed in non-tumorigenic MCF-10A cells, and MCF-10A cells have been shown to be minimally responsive to both Wnt3a stimulation and Dkk1 antagonism.[216,377] We tested the addition of Wnt3a and SFRP4 on MCF-10A cells but saw no response in regards to changes in DDX20 expression.

To confirm that the decrease of DDX20 expression was due to canonical Wnt signalling, exogenous CRD and NLD proteins from SFRP4 were added to the cell medium. A significant decrease in CRD-mediated DDX20 expression in MDA-MB-231 cells, although not in BT549 cells, was witnessed. This confirmed that the decrease was due to canonical Wnt signalling, as the CRD has been widely studied and confirmed to be the SFRP domain responsible for binding and antagonising Wnt ligands.[380-382] This is thought to be due to homology between the CRD of SFRPs and Fzd receptors, allowing SFRPs to act as soluble decoy receptors for Wnt ligands.

Finally, as SFRP4 was able to downregulate DDX20 protein expression, it was conceivable that DDX20 gene expression was regulated by canonical Wnt signalling. A time course experiment was conducted with Wnt3a stimulation, which resulted in a maximal peak of DDX20 gene expression at 12 hours. This indicated that DDX20 was a downstream target

of Wnt signalling. It has been previously reported that DDX5 is a target of β-catenin-dependent TCF4 transcription in breast cancer.[358] To validate if the same regulatory mechanism was governing DDX20 expression, pharmacological inhibition of the β-catenin/TCF4 complex was utilised. This demonstrated that DDX20 expression was downregulated by directly targeting TCF4 transcription. To further validate this, previously published ChIP-seq data from three different cell lines were examined. In all cell lines, the data indicated that TCF4 was bound to the promoter region of the DDX20 gene. This indicates that DDX20 is regulated by a positive feedback loop through a Wnt3a-β-catenin-TCF4 axis, all of which is dependent on DDX20 being able to facilitate Wnt signalling. This is the first report of Wnt regulation by DDX20 in TNBC stem cells.

Overall, this study provides evidence for the role of DDX20 in the regulation of Wnt/β-catenin signalling in TNBC stem cells. Depletion of DDX20 led to a reduction in the classical characteristics exhibited by CSCs, including overexpression of stem cell transcription factors and drug resistance. While many of the results were consistent between cell lines, particular cell functions were not diminished in PTEN mutant cells upon depletion of DDX20. This may be due to cellular signalling mechanisms that are reliant on PI3K/Akt signalling to function.

These data propose a model for the progression of TNBC, whereby increased Wnt signalling, through increased stromal Wnt ligands, leads to increased DDX20. DDX20, in turn, increases Wnt signalling, which drives tumorigenesis.

CHAPTER 6: DISCUSSION AND FUTURE DIRECTIONS

CHAPTER 6: DISCUSSION AND FUTURE DIRECTIONS

This thesis has determined that DDX20 is an essential regulator of Wnt/β-catenin signalling in triple-negative breast cancer. In regulating Wnt signalling, it has been found that DDX20 regulates the TCF4-mediated expression of key genes involved in ROS scavenging and mitochondrial function - catalase, SOD2 and UQCRC2.

The depletion of DDX20 results in increased H_2O_2-mediated oxidative stress and cell death. Mechanistically, it was found that excessive ROS may be generated from two sources: the mitochondria and from downregulation of catalase. Mitochondrial ROS was generated from ETC dysfunction, where UQCRC2 downregulation may result in the destabilisation of mitochondrial Complex III, leading to increased superoxide production. The superoxide produced is dismutated by SOD2 within the mitochondrial membrane to give increased H_2O_2, which can lead to loss of mitochondrial membrane potential and induce DNA damage.[383] Catalase may be partially localised to the mitochondria to protect against exogenous and endogenous H_2O_2 production.[384] Thus, mitochondrial oxidative stress due to increased H_2O_2 may be exacerbated by the downregulation of catalase. Furthermore, it has been demonstrated that peroxisomal catalase inhibition results in increased MitoROS and a decrease in the membrane potential of the inner mitochondrial membrane.[385]

The differential changes in the expression of catalase and SOD2 following Wnt antagonism were previously demonstrated by Gong *et al*.[342] In pancreatic neoplasms, the addition of PEDF antagonised Wnt3a-mediated Wnt/β-catenin signalling activation and reduced catalase expression, while increasing SOD2 expression. The details of the transcriptional regulation of catalase were not determined, although the increase of SOD2 expression was due to nuclear translocation of NF-κB. The data presented in this thesis clearly demonstrates that the changes in catalase and SOD2 mRNA expression can be both directly associated with TCF4 transcription.

After the enrichment of CSCs from both MDA-MB-231 and BT549 cell lines, it was determined that DDX20 was overexpressed in TNBC stem cells compared to the parental cell lines. There have been many reports

implicating the essential role of Wnt/β-catenin signalling in stem cell maintenance and fate.[386,387] This study implicates DDX20 in the regulation of CSC fate through a Wnt-mediated mechanism. The loss of DDX20 resulted in an altered cell cycle, increased chemotherapeutic sensitivity and a loss of stemness characteristics. Furthermore, following the knockdown of DDX20, there was cell death and increased H_2O_2 production, suggesting that the mechanism of cell death is consistent with that of the parental cell lines. Tumours have high levels of ROS compared to normal tissue, while low levels of ROS in CSCs are required for stem cell maintenance.[388] The low levels of ROS may be partly a result of increased Wnt signalling activity in CSCs.[7] This study demonstrated increased expression of ROS scavenging enzymes following Wnt stimulation. This may be a mechanism by which ROS levels are kept low in stem cell populations.

Through the use of a *Drosophila* model, this study has confirmed the regulation of cellular redox genes by Gemin3/DDX20 *in vivo*. Several signalling pathways critical in responding to changes in the oxidative stress tolerance have been identified in *Drosophila* [389,390]. This is the first report of Gemin3 driven by an armadillo and daughterless expression system regulating cellular redox in a *Drosophila* model. The embryonic lethality of the Gemin3 knockout flies, together with the evidence of redox changes after the loss of Gemin3, suggests that the mechanism of cell death in *Drosophila* is due to oxidative stress and mitochondrial dysfunction.

Future directions include confirming the mechanism of cell death following DDX20 depletion in an *in vivo* mouse model. DDX20 knockout is embryonically lethal in mice embryos,[199] which precludes the development of a DDX20$^{-/-}$ mouse. An appropriate mouse model to gain mechanistic insight could be using a Cre-loxP approach, with a DDX20 conditional allele crossed with a MMTV-*Cre* transgene. This would allow for the conditional knockout of DDX20 in cells primarily in mammary epithelium.[391]

Small molecule inhibitors of DDX proteins are currently under development. A small molecule inhibitor of phosphorylated DDX5 is in Phase I clinical trials for various solid tumours.[392] Previous data (Cai & Pohl, unpublished) has demonstrated that DDX20 may also require phosphorylation to interact with

GSK3β. Preliminary studies demonstrate that the inhibitor of phospho-DDX5 may be efficacious in targeting DDX20. Optimising this small molecule to directly target DDX20 may prove to be a new therapeutic option in TNBC. Furthermore, identification of the kinase responsible for phosphorylation of DDX20 may also provide a potential target for drug development.

The canonical role of DDX20 was reported to be in spliceosome assembly, where its primary subcellular localisation has been in subnuclear structures known as Cajal bodies.[219] The localisation of DDX20 in the cytoplasmic-plasma membrane region in TNBC could provide evidence of how DDX20 dysregulation may lead to aberrant Wnt signalling. One possible explanation is the disruption of the nuclear localisation sequence (NLS) of DDX20. The C-terminal of DDX20 contains many residues that have been demonstrated to be phosphorylated.[199] The C-terminal contains the NLS, with a number of residues that may be substrates for phosphorylation. Mutagenesis of these residues, followed by the examination of DDX20 localisation, may provide mechanistic insight into the mislocalisation of DDX20 in TNBC.

This study has presented a novel role for Wnt/β-catenin signalling in the regulation of intracellular redox and mitochondrial function. Future studies may extend this finding to both human-derived and murine-derived organoid models. These have proven invaluable in providing models that recapitulate the whole organ system and mimic the tumour microenvironment[393] and may confirm the role of Wnt/β-catenin-driven ROS production in tumour progression. The evaluation of changing ROS levels through organoid development in cancer models may provide new insight into the role of ROS in carcinogenesis. This has been made easier with genetically encoded ROS probes, such as HyPer, that are able to be stably transfected into cells for the evaluation of specific ROS species in a live-cell system.[394]

This report has clearly demonstrated a role for DDX20 and Wnt/β-catenin signalling in the regulation of mitochondrial function and dynamics. An interesting observation was the differences in mitochondrial morphology between the MDA-MB-231 and MDA-MB-436 cell lines after the loss of

DDX20 and the suppression of TCF4 mediated signalling. Future studies may focus of difference between the fission and fusion machinery after these respective treatments. Identifying changes in key fission proteins, such as Drp1 and Mff, or fusion proteins Opa1, Mfn1 and Mfn2 may provide insight to the differences in mitochondrial morphology that were seen in these two cell lines.[395]

Overall, this study has clearly demonstrated a DDX20-dependent mechanism of Wnt signalling, whereby TCF4 transcription is responsible for expression of catalase, SOD2 and UQCRC2, which regulates the intracellular redox environment and mitochondrial function. While catalase, SOD2 and UQCRC2 were identified as targets of canonical Wnt signalling in TNBC it would be valuable to explore TCF4-regulated redox genes in a variety of cancers, and determine their impact on tumour progression, metastasis and overall patient survival.

7. REFERENCES

1 Chen, S. & Parmigiani, G. Meta-analysis of BRCA1 and BRCA2 penetrance. *J Clin Oncol* **25**, 1329-1333, (2007).

2 Ovcaricek, T., Frkovic, S. G., Matos, E., Mozina, B. & Borstnar, S. Triple negative breast cancer - prognostic factors and survival. *Radiol Oncol* **45**, 46-52, (2011).

3 Foulkes, W. D., Smith, I. E. & Reis-Filho, J. S. Triple-negative breast cancer. *The New England journal of medicine* **363**, 1938-1948, (2010).

4 Hudis, C. A. Trastuzumab--mechanism of action and use in clinical practice. *The New England journal of medicine* **357**, 39-51, (2007).

5 Jordan, V. C. Tamoxifen (ICI46,474) as a targeted therapy to treat and prevent breast cancer. *British journal of pharmacology* **147 Suppl 1**, S269-276, (2006).

6 Pusztai, L., Karn, T., Safonov, A., Abu-Khalaf, M. M. & Bianchini, G. New Strategies in Breast Cancer: Immunotherapy. *Clin Cancer Res* **22**, 2105-2110, (2016).

7 Pohl, S. G. *et al.* Wnt signaling in triple-negative breast cancer. *Oncogenesis* **6**, e310, (2017).

8 Polakis, P. Wnt signaling in cancer. *Cold Spring Harb Perspect Biol* **4**, (2012).

9 Perou, C. M. *et al.* Molecular portraits of human breast tumours. *Nature* **406**, 747-752, (2000).

10 Eroles, P., Bosch, A., Perez-Fidalgo, J. A. & Lluch, A. Molecular biology in breast cancer: intrinsic subtypes and signaling pathways. *Cancer Treat Rev* **38**, 698-707, (2012).

11 Creighton, C. J. The molecular profile of luminal B breast cancer. *Biologics: targets & therapy* **6**, 289, (2012).

12 Eroles, P., Bosch, A., Pérez-Fidalgo, J. A. & Lluch, A. Molecular biology in breast cancer: intrinsic subtypes and signaling pathways. *Cancer treatment reviews* **38**, 698-707, (2012).

13 Prat, A. *et al.* Molecular features and survival outcomes of the intrinsic subtypes within HER2-positive breast cancer. *Journal of the National Cancer Institute* **106**, dju152, (2014).

14 Abramson, V. G., Lehmann, B. D., Ballinger, T. J. & Pietenpol, J. A. Subtyping of triple-negative breast cancer: Implications for therapy. *Cancer* **121**, 8-16, (2015).

15 Kast, K. *et al.* Impact of breast cancer subtypes and patterns of metastasis on outcome. *Breast cancer research and treatment* **150**, 621-629, (2015).

16 Shah, S. P. *et al.* The clonal and mutational evolution spectrum of primary triple-negative breast cancers. *Nature* **486**, 395-399, (2012).

17 Weisman, P. S. *et al.* Genetic alterations of triple negative breast cancer by targeted next-generation sequencing and correlation with tumor morphology. *Modern Pathology*, (2016).

18 Lehmann, B. D. *et al.* Identification of human triple-negative breast cancer subtypes and preclinical models for selection of targeted therapies. *The Journal of clinical investigation* **121**, 2750-2767, (2011).

19 Burstein, M. D. *et al.* Comprehensive genomic analysis identifies novel subtypes and targets of triple-negative breast cancer. *Clinical Cancer Research* **21**, 1688-1698, (2015).
20 Pistelli, M. *et al.* Androgen receptor expression in early triple-negative breast cancer: clinical significance and prognostic associations. *Cancers* **6**, 1351-1362, (2014).
21 Arce-Salinas, C., Riesco-Martinez, M. C., Hanna, W., Bedard, P. & Warner, E. Complete Response of Metastatic Androgen Receptor-Positive Breast Cancer to Bicalutamide: Case Report and Review of the Literature. *J Clin Oncol* **34**, e21-24, (2016).
22 Gucalp, A. *et al.* Phase II trial of bicalutamide in patients with androgen receptor-positive, estrogen receptor-negative metastatic Breast Cancer. *Clin Cancer Res* **19**, 5505-5512, (2013).
23 Hilborn, E. *et al.* Androgen receptor expression predicts beneficial tamoxifen response in oestrogen receptor-alpha-negative breast cancer. *Br J Cancer* **114**, 248-255, (2016).
24 Ciupek, A. *et al.* Androgen receptor promotes tamoxifen agonist activity by activation of EGFR in ERalpha-positive breast cancer. *Breast Cancer Res Treat* **154**, 225-237, (2015).
25 Prat, A. *et al.* Phenotypic and molecular characterization of the claudin-low intrinsic subtype of breast cancer. *Breast cancer research* **12**, 1, (2010).
26 Laezza, C. *et al.* Anandamide inhibits the Wnt/beta-catenin signalling pathway in human breast cancer MDA MB 231 cells. *Eur J Cancer* **48**, 3112-3122, (2012).
27 Liu, Y.-R. *et al.* Comprehensive transcriptome analysis identifies novel molecular subtypes and subtype-specific RNAs of triple-negative breast cancer. *Breast Cancer Research* **18**, 1, (2016).
28 Prat, A. *et al.* Clinical implications of the intrinsic molecular subtypes of breast cancer. *The Breast* **24**, S26-S35, (2015).
29 Wu, G., Huang, H., Garcia Abreu, J. & He, X. Inhibition of GSK3 phosphorylation of beta-catenin via phosphorylated PPPSPXS motifs of Wnt coreceptor LRP6. *PLoS One* **4**, e4926, (2009).
30 Liu, C. *et al.* beta-Trcp couples beta-catenin phosphorylation-degradation and regulates Xenopus axis formation. *Proc Natl Acad Sci U S A* **96**, 6273-6278, (1999).
31 MacDonald, B. T. & He, X. Frizzled and LRP5/6 receptors for Wnt/beta-catenin signaling. *Cold Spring Harb Perspect Biol* **4**, (2012).
32 Tamai, K. *et al.* A mechanism for Wnt coreceptor activation. *Mol Cell* **13**, 149-156, (2004).
33 Clevers, H. Wnt/beta-catenin signaling in development and disease. *Cell* **127**, 469-480, (2006).
34 Roose, J. *et al.* The Xenopus Wnt effector XTcf-3 interacts with Groucho-related transcriptional repressors. *Nature* **395**, 608-612, (1998).
35 Azzolin, L. *et al.* YAP/TAZ incorporation in the beta-catenin destruction complex orchestrates the Wnt response. *Cell* **158**, 157-170, (2014).
36 Li, V. S. *et al.* Wnt signaling through inhibition of beta-catenin degradation in an intact Axin1 complex. *Cell* **149**, 1245-1256, (2012).

37 Azzolin, L. *et al.* Role of TAZ as mediator of Wnt signaling. *Cell* **151**, 1443-1456, (2012).
38 Taelman, V. F. *et al.* Wnt signaling requires sequestration of glycogen synthase kinase 3 inside multivesicular endosomes. *Cell* **143**, 1136-1148, (2010).
39 Gomez-Orte, E., Saenz-Narciso, B., Moreno, S. & Cabello, J. Multiple functions of the noncanonical Wnt pathway. *Trends Genet* **29**, 545-553, (2013).
40 Nishita, M. *et al.* Ror2/Frizzled complex mediates Wnt5a-induced AP-1 activation by regulating Dishevelled polymerization. *Mol Cell Biol* **30**, 3610-3619, (2010).
41 Habu, M. *et al.* Ryk is essential for Wnt-5a-dependent invasiveness in human glioma. *J Biochem* **156**, 29-38, (2014).
42 Golubkov, V. S. *et al.* The Wnt/planar cell polarity protein-tyrosine kinase-7 (PTK7) is a highly efficient proteolytic target of membrane type-1 matrix metalloproteinase: implications in cancer and embryogenesis. *J Biol Chem* **285**, 35740-35749, (2010).
43 Li, L. *et al.* Dishevelled proteins lead to two signaling pathways. Regulation of LEF-1 and c-Jun N-terminal kinase in mammalian cells. *J Biol Chem* **274**, 129-134, (1999).
44 Habas, R., Kato, Y. & He, X. Wnt/Frizzled activation of Rho regulates vertebrate gastrulation and requires a novel Formin homology protein Daam1. *Cell* **107**, 843-854, (2001).
45 Wong, H. C. *et al.* Direct binding of the PDZ domain of Dishevelled to a conserved internal sequence in the C-terminal region of Frizzled. *Mol Cell* **12**, 1251-1260, (2003).
46 De, A. Wnt/Ca2+ signaling pathway: a brief overview. *Acta Biochim Biophys Sin (Shanghai)* **43**, 745-756, (2011).
47 Dejmek, J., Safholm, A., Kamp Nielsen, C., Andersson, T. & Leandersson, K. Wnt-5a/Ca2+-induced NFAT activity is counteracted by Wnt-5a/Yes-Cdc42-casein kinase 1alpha signaling in human mammary epithelial cells. *Mol Cell Biol* **26**, 6024-6036, (2006).
48 Ishitani, T. *et al.* The TAK1-NLK mitogen-activated protein kinase cascade functions in the Wnt-5a/Ca(2+) pathway to antagonize Wnt/beta-catenin signaling. *Mol Cell Biol* **23**, 131-139, (2003).
49 Ishitani, T., Ninomiya-Tsuji, J. & Matsumoto, K. Regulation of lymphoid enhancer factor 1/T-cell factor by mitogen-activated protein kinase-related Nemo-like kinase-dependent phosphorylation in Wnt/beta-catenin signaling. *Mol Cell Biol* **23**, 1379-1389, (2003).
50 Cadigan, K. M. & Nusse, R. Wnt signaling: a common theme in animal development. *Genes & development* **11**, 3286-3305, (1997).
51 Gao, X. & Hannoush, R. N. Single-cell imaging of Wnt palmitoylation by the acyltransferase porcupine. *Nat Chem Biol* **10**, 61-68, (2014).
52 MacDonald, B. T. *et al.* Disulfide bond requirements for active Wnt ligands. *J Biol Chem* **289**, 18122-18136, (2014).
53 Willert, K. *et al.* Wnt proteins are lipid-modified and can act as stem cell growth factors. *Nature* **423**, 448-452, (2003).
54 Janda, C. Y., Waghray, D., Levin, A. M., Thomas, C. & Garcia, K. C. Structural basis of Wnt recognition by Frizzled. *Science* **337**, 59-64, (2012).

55 Dijksterhuis, J. P., Petersen, J. & Schulte, G. WNT/Frizzled signalling: receptor-ligand selectivity with focus on FZD-G protein signalling and its physiological relevance: IUPHAR Review 3. *British journal of pharmacology* **171**, 1195-1209, (2014).
56 Takada, R. *et al.* Monounsaturated fatty acid modification of Wnt protein: its role in Wnt secretion. *Dev Cell* **11**, 791-801, (2006).
57 Wang, C. *et al.* Structure of the human smoothened receptor bound to an antitumour agent. *Nature* **497**, 338-343, (2013).
58 Wang, C. *et al.* Structural basis for Smoothened receptor modulation and chemoresistance to anticancer drugs. *Nat Commun* **5**, 4355, (2014).
59 Weierstall, U. *et al.* Lipidic cubic phase injector facilitates membrane protein serial femtosecond crystallography. *Nat Commun* **5**, 3309, (2014).
60 Byrne, E. F. *et al.* Structural basis of Smoothened regulation by its extracellular domains. *Nature* **535**, 517-522, (2016).
61 Sussman, D. J. *et al.* Isolation and characterization of a mouse homolog of the Drosophila segment polarity gene dishevelled. *Dev Biol* **166**, 73-86, (1994).
62 Gao, C. & Chen, Y. G. Dishevelled: The hub of Wnt signaling. *Cell Signal* **22**, 717-727, (2010).
63 Fiedler, M., Mendoza-Topaz, C., Rutherford, T. J., Mieszczanek, J. & Bienz, M. Dishevelled interacts with the DIX domain polymerization interface of Axin to interfere with its function in down-regulating beta-catenin. *Proc Natl Acad Sci U S A* **108**, 1937-1942, (2011).
64 Schwarz-Romond, T. *et al.* The DIX domain of Dishevelled confers Wnt signaling by dynamic polymerization. *Nat Struct Mol Biol* **14**, 484-492, (2007).
65 Gammons, M. V., Renko, M., Johnson, C. M., Rutherford, T. J. & Bienz, M. Wnt Signalosome Assembly by DEP Domain Swapping of Dishevelled. *Mol Cell* **64**, 92-104, (2016).
66 Tauriello, D. V. *et al.* Wnt/beta-catenin signaling requires interaction of the Dishevelled DEP domain and C terminus with a discontinuous motif in Frizzled. *Proc Natl Acad Sci U S A* **109**, E812-820, (2012).
67 Jiang, X., Charlat, O., Zamponi, R., Yang, Y. & Cong, F. Dishevelled promotes Wnt receptor degradation through recruitment of ZNRF3/RNF43 E3 ubiquitin ligases. *Mol Cell* **58**, 522-533, (2015).
68 Gong, Y. *et al.* Wnt isoform-specific interactions with coreceptor specify inhibition or potentiation of signaling by LRP6 antibodies. *PLoS One* **5**, e12682, (2010).
69 Cheng, Z. *et al.* Crystal structures of the extracellular domain of LRP6 and its complex with DKK1. *Nat Struct Mol Biol* **18**, 1204-1210, (2011).
70 Ahn, V. E. *et al.* Structural basis of Wnt signaling inhibition by Dickkopf binding to LRP5/6. *Dev Cell* **21**, 862-873, (2011).
71 Bourhis, E. *et al.* Wnt antagonists bind through a short peptide to the first beta-propeller domain of LRP5/6. *Structure* **19**, 1433-1442, (2011).
72 Zeng, X. *et al.* Initiation of Wnt signaling: control of Wnt coreceptor Lrp6 phosphorylation/activation via frizzled, dishevelled and axin functions. *Development* **135**, 367-375, (2008).

73 Minami, Y., Oishi, I., Endo, M. & Nishita, M. Ror-family receptor tyrosine kinases in noncanonical Wnt signaling: their implications in developmental morphogenesis and human diseases. *Dev Dyn* **239**, 1-15, (2010).
74 Stiegler, A. L., Burden, S. J. & Hubbard, S. R. Crystal structure of the frizzled-like cysteine-rich domain of the receptor tyrosine kinase MuSK. *J Mol Biol* **393**, 1-9, (2009).
75 Schlessinger, J. Cell signaling by receptor tyrosine kinases. *Cell* **103**, 211-225, (2000).
76 Liu, Y., Rubin, B., Bodine, P. V. & Billiard, J. Wnt5a induces homodimerization and activation of Ror2 receptor tyrosine kinase. *J Cell Biochem* **105**, 497-502, (2008).
77 Zhang, S. *et al.* ROR1 is expressed in human breast cancer and associated with enhanced tumor-cell growth. *PLoS One* **7**, e31127, (2012).
78 Pohl, S., Scott, R., Arfuso, F., Perumal, V. & Dharmarajan, A. Secreted frizzled-related protein 4 and its implications in cancer and apoptosis. *Tumour Biol* **36**, 143-152, (2015).
79 Koo, B. K. *et al.* Tumour suppressor RNF43 is a stem-cell E3 ligase that induces endocytosis of Wnt receptors. *Nature* **488**, 665-669, (2012).
80 de Lau, W., Peng, W. C., Gros, P. & Clevers, H. The R-spondin/Lgr5/Rnf43 module: regulator of Wnt signal strength. *Genes & development* **28**, 305-316, (2014).
81 Zhang, X. *et al.* Tiki1 is required for head formation via Wnt cleavage-oxidation and inactivation. *Cell* **149**, 1565-1577, (2012).
82 Miller, J. R. The Wnts. *Genome Biol* **3**, REVIEWS3001, (2002).
83 Uren, A. *et al.* Secreted frizzled-related protein-1 binds directly to Wingless and is a biphasic modulator of Wnt signaling. *J Biol Chem* **275**, 4374-4382, (2000).
84 Tian, Y. *et al.* Cross-talk of SFRP4, integrin alpha1beta1, and Notch1 inhibits cardiac differentiation of P19CL6 cells. *Cell Signal* **28**, 1806-1815, (2016).
85 Bovolenta, P., Esteve, P., Ruiz, J. M., Cisneros, E. & Lopez-Rios, J. Beyond Wnt inhibition: new functions of secreted Frizzled-related proteins in development and disease. *J Cell Sci* **121**, 737-746, (2008).
86 Scardigli, R. *et al.* Binding of sFRP-3 to EGF in the extra-cellular space affects proliferation, differentiation and morphogenetic events regulated by the two molecules. *PLoS One* **3**, e2471, (2008).
87 Wolf, V. *et al.* DDC-4, an apoptosis-associated gene, is a secreted frizzled relative. *FEBS Lett* **417**, 385-389, (1997).
88 Mahdi, T. *et al.* Secreted frizzled-related protein 4 reduces insulin secretion and is overexpressed in type 2 diabetes. *Cell Metab* **16**, 625-633, (2012).
89 Schiefer, L. *et al.* Epigenetic regulation of the secreted frizzled-related protein family in human glioblastoma multiforme. *Cancer Gene Ther* **21**, 297-303, (2014).
90 Longman, D., Arfuso, F., Viola, H. M., Hool, L. C. & Dharmarajan, A. M. The role of the cysteine-rich domain and netrin-like domain of

secreted frizzled-related protein 4 in angiogenesis inhibition in vitro. *Oncol Res* **20**, 1-6, (2012).
91 Deshmukh, A., Kumar, S., Arfuso, F., Newsholme, P. & Dharmarajan, A. Secreted Frizzled-related protein 4 (sFRP4) chemo-sensitizes cancer stem cells derived from human breast, prostate, and ovary tumor cell lines. *Sci Rep* **7**, 2256, (2017).
92 Warrier, S. *et al.* Cancer stem-like cells from head and neck cancers are chemosensitized by the Wnt antagonist, sFRP4, by inducing apoptosis, decreasing stemness, drug resistance and epithelial to mesenchymal transition. *Cancer Gene Ther* **21**, 381-388, (2014).
93 Bhuvanalakshmi, G., Arfuso, F., Millward, M., Dharmarajan, A. & Warrier, S. Secreted frizzled-related protein 4 inhibits glioma stem-like cells by reversing epithelial to mesenchymal transition, inducing apoptosis and decreasing cancer stem cell properties. *PLoS One* **10**, e0127517, (2015).
94 Xu, J., Prosperi, J. R., Choudhury, N., Olopade, O. I. & Goss, K. H. β-Catenin is required for the tumorigenic behavior of triple-negative breast cancer cells. *PloS one* **10**, e0117097, (2015).
95 Mohammed, M. K. *et al.* Wnt/β-catenin signaling plays an ever-expanding role in stem cell self-renewal, tumorigenesis and cancer chemoresistance. *Genes & Diseases* **3**, 11-40, (2016).
96 Dey, N. *et al.* Wnt signaling in triple negative breast cancer is associated with metastasis. *BMC cancer* **13**, 1, (2013).
97 Khramtsov, A. I. *et al.* Wnt/β-catenin pathway activation is enriched in basal-like breast cancers and predicts poor outcome. *The American journal of pathology* **176**, 2911-2920, (2010).
98 Geyer, F. C. *et al.* beta-Catenin pathway activation in breast cancer is associated with triple-negative phenotype but not with CTNNB1 mutation. *Mod Pathol* **24**, 209-231, (2011).
99 Borg, J.-P. *et al.* Deregulation of the non-canonical pathway in triple-negative breast cancer. *The FASEB Journal* **27**, 610.611-610.611, (2013).
100 Medema, J. P. Cancer stem cells: the challenges ahead. *Nat Cell Biol* **15**, 338-344, (2013).
101 Sicchieri, R. D. *et al.* ABCG2 is a potential marker of tumor-initiating cells in breast cancer. *Tumour Biol* **36**, 9233-9243, (2015).
102 Pogoda, K., Niwinska, A., Murawska, M. & Pienkowski, T. Analysis of pattern, time and risk factors influencing recurrence in triple-negative breast cancer patients. *Med Oncol* **30**, 388, (2013).
103 Cheng, L., Ramesh, A. V., Flesken-Nikitin, A., Choi, J. & Nikitin, A. Y. Mouse models for cancer stem cell research. *Toxicol Pathol* **38**, 62-71, (2010).
104 Atkinson, R. L. *et al.* Cancer stem cell markers are enriched in normal tissue adjacent to triple negative breast cancer and inversely correlated with DNA repair deficiency. *Breast Cancer Res* **15**, R77, (2013).
105 Peiris-Pages, M., Martinez-Outschoorn, U. E., Pestell, R. G., Sotgia, F. & Lisanti, M. P. Cancer stem cell metabolism. *Breast Cancer Res* **18**, 55, (2016).

106 van Amerongen, R., Bowman, A. N. & Nusse, R. Developmental stage and time dictate the fate of Wnt/β-catenin-responsive stem cells in the mammary gland. *Cell stem cell* **11**, 387-400, (2012).
107 Zeng, Y. A. & Nusse, R. Wnt proteins are self-renewal factors for mammary stem cells and promote their long-term expansion in culture. *Cell stem cell* **6**, 568-577, (2010).
108 Howard, B. & Ashworth, A. Signalling pathways implicated in early mammary gland morphogenesis and breast cancer. *PLoS Genet* **2**, e112, (2006).
109 Jang, G. B. *et al.* Blockade of Wnt/beta-catenin signaling suppresses breast cancer metastasis by inhibiting CSC-like phenotype. *Sci Rep* **5**, 12465, (2015).
110 Cleary, A. S., Leonard, T. L., Gestl, S. A. & Gunther, E. J. Tumour cell heterogeneity maintained by cooperating subclones in Wnt-driven mammary cancers. *Nature* **508**, 113-117, (2014).
111 Rangel, M. C. *et al.* Developmental signaling pathways regulating mammary stem cells and contributing to the etiology of triple-negative breast cancer. *Breast cancer research and treatment* **156**, 211-226, (2016).
112 Lefebvre, V., Dumitriu, B., Penzo-Mendez, A., Han, Y. & Pallavi, B. Control of cell fate and differentiation by Sry-related high-mobility-group box (Sox) transcription factors. *Int J Biochem Cell Biol* **39**, 2195-2214, (2007).
113 Kormish, J. D., Sinner, D. & Zorn, A. M. Interactions between SOX factors and Wnt/beta-catenin signaling in development and disease. *Dev Dyn* **239**, 56-68, (2010).
114 Zhang, L. *et al.* CDK1 phosphorylation of TAZ in mitosis inhibits its oncogenic activity. *Oncotarget* **6**, 31399-31412, (2015).
115 Wang, G., Wang, J. & Sadar, M. D. Crosstalk between the androgen receptor and beta-catenin in castrate-resistant prostate cancer. *Cancer Res* **68**, 9918-9927, (2008).
116 Noah, T. K. *et al.* SPDEF functions as a colorectal tumor suppressor by inhibiting beta-catenin activity. *Gastroenterology* **144**, 1012-1023 e1016, (2013).
117 Wang, H., Xi, Q. & Wu, G. Fatty acid synthase regulates invasion and metastasis of colorectal cancer via Wnt signaling pathway. *Cancer Med* **5**, 1599-1606, (2016).
118 Kahlert, U. D. *et al.* Activation of canonical WNT/beta-catenin signaling enhances in vitro motility of glioblastoma cells by activation of ZEB1 and other activators of epithelial-to-mesenchymal transition. *Cancer Lett* **325**, 42-53, (2012).
119 Greenow, K. R., Clarke, A. R., Williams, G. T. & Jones, R. Wnt-driven intestinal tumourigenesis is suppressed by Chk1 deficiency but enhanced by conditional haploinsufficiency. *Oncogene* **33**, 4089-4096, (2014).
120 Huard, C. C., Tremblay, C. S., Magron, A., Levesque, G. & Carreau, M. The Fanconi anemia pathway has a dual function in Dickkopf-1 transcriptional repression. *Proc Natl Acad Sci U S A* **111**, 2152-2157, (2014).

121 Castiglia, D. *et al.* Concomitant activation of Wnt pathway and loss of mismatch repair function in human melanoma. *Genes Chromosomes Cancer* **47**, 614-624, (2008).
122 Xu, H. *et al.* Cohesin Rad21 mediates loss of heterozygosity and is upregulated via Wnt promoting transcriptional dysregulation in gastrointestinal tumors. *Cell Rep* **9**, 1781-1797, (2014).
123 Huang, Y. L., Anvarian, Z., Doderlein, G., Acebron, S. P. & Niehrs, C. Maternal Wnt/STOP signaling promotes cell division during early Xenopus embryogenesis. *Proc Natl Acad Sci U S A* **112**, 5732-5737, (2015).
124 Kikuchi, K., Niikura, Y., Kitagawa, K. & Kikuchi, A. Dishevelled, a Wnt signalling component, is involved in mitotic progression in cooperation with Plk1. *EMBO J* **29**, 3470-3483, (2010).
125 Suzuki, A., Pelikan, R. C. & Iwata, J. WNT/beta-Catenin Signaling Regulates Multiple Steps of Myogenesis by Regulating Step-Specific Targets. *Mol Cell Biol* **35**, 1763-1776, (2015).
126 Chiacchiera, F. *et al.* Polycomb Complex PRC1 Preserves Intestinal Stem Cell Identity by Sustaining Wnt/beta-Catenin Transcriptional Activity. *Cell Stem Cell* **18**, 91-103, (2016).
127 He, T. C. *et al.* Identification of c-MYC as a target of the APC pathway. *Science* **281**, 1509-1512, (1998).
128 Conrad, W. H. *et al.* Regulating the response to targeted MEK inhibition in melanoma: enhancing apoptosis in NRAS- and BRAF-mutant melanoma cells with Wnt/beta-catenin activation. *Cell Cycle* **11**, 3724-3730, (2012).
129 Xu, M. *et al.* Role of MCP-1 in alcohol-induced aggressiveness of colorectal cancer cells. *Mol Carcinog* **55**, 1002-1011, (2016).
130 Yasuhara, R. *et al.* The beta-catenin signaling pathway induces aggressive potential in breast cancer by up-regulating the chemokine CCL5. *Exp Cell Res* **338**, 22-31, (2015).
131 Yu, Q., Xu, M. & Sen, J. M. Beta-catenin expression enhances IL-7 receptor signaling in thymocytes during positive selection. *J Immunol* **179**, 126-131, (2007).
132 Corda, G. *et al.* Functional and prognostic significance of the genomic amplification of frizzled 6 (FZD6) in breast cancer. *J Pathol*, (2016).
133 Yang, L. *et al.* FZD7 has a critical role in cell proliferation in triple negative breast cancer. *Oncogene* **30**, 4437-4446, (2011).
134 Chakrabarti, R. *et al.* ΔNp63 promotes stem cell activity in mammary gland development and basal-like breast cancer by enhancing Fzd7 expression and Wnt signalling. *Nature cell biology* **16**, 1004-1015, (2014).
135 Phesse, T., Flanagan, D. & Vincan, E. Frizzled7: A Promising Achilles' Heel for Targeting the Wnt Receptor Complex to Treat Cancer. *Cancers* **8**, 50, (2016).
136 Yin, S. *et al.* Tumor-initiating cells and FZD8 play a major role in drug resistance in triple-negative breast cancer. *Molecular cancer therapeutics* **12**, 491-498, (2013).
137 Jiang, Q. *et al.* MicroRNA-100 suppresses the migration and invasion of breast cancer cells by targeting FZD-8 and inhibiting Wnt/β-catenin signaling pathway. *Tumor Biology* **37**, 5001-5011, (2016).

138 Yin, S., Cheriyan, V. T., Rishi, A. K. & Reddy, K. B. c-Myc and Frizzled 8 play a major role in the regulation of cancer stem cells and drug resistance in triple-negative breast cancer. *Cancer Research* **75**, 2225-2225, (2015).
139 Badders, N. M. *et al.* The Wnt receptor, Lrp5, is expressed by mouse mammary stem cells and is required to maintain the basal lineage. *PloS one* **4**, e6594, (2009).
140 Lindvall, C. *et al.* The Wnt signaling receptor Lrp5 is required for mammary ductal stem cell activity and Wnt1-induced tumorigenesis. *Journal of Biological Chemistry* **281**, 35081-35087, (2006).
141 Lindvall, C. *et al.* The Wnt co-receptor Lrp6 is required for normal mouse mammary gland development. *PloS one* **4**, e5813, (2009).
142 Liu, C.-C., Prior, J., Piwnica-Worms, D. & Bu, G. LRP6 overexpression defines a class of breast cancer subtype and is a target for therapy. *Proceedings of the National Academy of Sciences* **107**, 5136-5141, (2010).
143 Wang, H. *et al.* SOX9 regulates low density lipoprotein receptor-related protein 6 (LRP6) and T-cell factor 4 (TCF4) expression and Wnt/β-catenin activation in breast cancer. *Journal of Biological Chemistry* **288**, 6478-6487, (2013).
144 Ibrahim, S. A. *et al.* Syndecan-1 (CD138) modulates triple-negative breast cancer stem cell properties via regulation of LRP-6 and IL-6-mediated STAT3 signaling. *PloS one* **8**, e85737, (2013).
145 Nikolova, V. *et al.* Differential roles for membrane-bound and soluble syndecan-1 (CD138) in breast cancer progression. *Carcinogenesis*, bgp001, (2009).
146 Zhang, S. *et al.* ROR1 is expressed in human breast cancer and associated with enhanced tumor-cell growth. *PloS one* **7**, e31127, (2012).
147 Cui, B. *et al.* Targeting ROR1 inhibits epithelial–mesenchymal transition and metastasis. *Cancer research* **73**, 3649-3660, (2013).
148 Henry, C. *et al.* Expression of the novel Wnt receptor ROR2 is increased in breast cancer and may regulate both β-catenin dependent and independent Wnt signalling. *Journal of cancer research and clinical oncology* **141**, 243-254, (2015).
149 Group, E. B. C. T. C. Adjuvant chemotherapy in oestrogen-receptor-poor breast cancer: patient-level meta-analysis of randomised trials. *The Lancet* **371**, 29-40, (2008).
150 Tudoran, O. *et al.* Regulation of stem cells-related signaling pathways in response to doxorubicin treatment in Hs578T triple-negative breast cancer cells. *Molecular and cellular biochemistry* **409**, 163-176, (2015).
151 Sparano, J. A. Defining a role and predicting benefit from platinum-based therapy in breast cancer: An evolving story. *Journal of Clinical Oncology* **33**, 1-3, (2015).
152 Yin, S., Xu, L., Bandyopadhyay, S., Sethi, S. & Reddy, K. B. Cisplatin and TRAIL enhance breast cancer stem cell death. *International journal of oncology* **39**, 891, (2011).

153 Jang, G.-B. *et al.* Wnt/β-catenin small-molecule inhibitor CWP232228 preferentially inhibits the growth of breast cancer stem-like cells. *Cancer research* **75**, 1691-1702, (2015).
154 Takebe, N. *et al.* Targeting Notch, Hedgehog, and Wnt pathways in cancer stem cells: clinical update. *Nature reviews Clinical oncology* **12**, 445-464, (2015).
155 Solzak, J. P., Atale, R., Hancock, B. & Radovich, M. Dual PI3K and Wnt pathway inhibition is a synergistic combination against triple-negative breast cancer. *Cancer Research* **75**, 5340-5340, (2015).
156 Farmer, H. *et al.* Targeting the DNA repair defect in BRCA mutant cells as a therapeutic strategy. *Nature* **434**, 917-921, (2005).
157 Bryant, H. E. *et al.* Specific killing of BRCA2-deficient tumours with inhibitors of poly (ADP-ribose) polymerase. *Nature* **434**, 913-917, (2005).
158 Huang, S. M. *et al.* Tankyrase inhibition stabilizes axin and antagonizes Wnt signalling. *Nature* **461**, 614-620, (2009).
159 Bao, R. *et al.* Inhibition of tankyrases induces Axin stabilization and blocks Wnt signalling in breast cancer cells. *PLoS One* **7**, e48670, (2012).
160 Livraghi, L. & Garber, J. E. PARP inhibitors in the management of breast cancer: current data and future prospects. *BMC medicine* **13**, 1, (2015).
161 Kaufman, B. *et al.* Olaparib monotherapy in patients with advanced cancer and a germline BRCA1/2 mutation. *Journal of Clinical Oncology* **33**, 244-250, (2015).
162 Pahuja, S. *et al.* in *ASCO Annual Meeting Proceedings.* 1015.
163 Tate, C. R. *et al.* Targeting triple-negative breast cancer cells with the histone deacetylase inhibitor panobinostat. *Breast Cancer Res* **14**, R79, (2012).
164 Schech, A., Kazi, A., Yu, S., Shah, P. & Sabnis, G. Histone Deacetylase Inhibitor Entinostat Inhibits Tumor-Initiating Cells in Triple-Negative Breast Cancer Cells. *Molecular cancer therapeutics* **14**, 1848-1857, (2015).
165 Merino, V. F. *et al.* Combined Treatment with Epigenetic, Differentiating, and Chemotherapeutic Agents Cooperatively Targets Tumor-Initiating Cells in Triple-Negative Breast Cancer. *Cancer research* **76**, 2013-2024, (2016).
166 Prasad, C. P. *et al.* Epigenetic alterations of CDH1 and APC genes: relationship with activation of Wnt/beta-catenin pathway in invasive ductal carcinoma of breast. *Life Sci* **83**, 318-325, (2008).
167 Kai, M. *et al.* Targeting breast cancer stem cells in triple-negative breast cancer using a combination of LBH589 and salinomycin. *Breast cancer research and treatment* **151**, 281-294, (2015).
168 Linder, P. Dead-box proteins: a family affair--active and passive players in RNP-remodeling. *Nucleic Acids Res* **34**, 4168-4180, (2006).
169 Linder, P. & Jankowsky, E. From unwinding to clamping - the DEAD box RNA helicase family. *Nat Rev Mol Cell Biol* **12**, 505-516, (2011).
170 Cordin, O., Banroques, J., Tanner, N. K. & Linder, P. The DEAD-box protein family of RNA helicases. *Gene* **367**, 17-37, (2006).

171 Ballut, L. *et al.* The exon junction core complex is locked onto RNA by inhibition of eIF4AIII ATPase activity. *Nat Struct Mol Biol* **12**, 861-869, (2005).
172 Shibuya, T., Tange, T. O., Sonenberg, N. & Moore, M. J. eIF4AIII binds spliced mRNA in the exon junction complex and is essential for nonsense-mediated decay. *Nat Struct Mol Biol* **11**, 346-351, (2004).
173 Collins, R. *et al.* The DEXD/H-box RNA helicase DDX19 is regulated by an {alpha}-helical switch. *J Biol Chem* **284**, 10296-10300, (2009).
174 Perriman, R. J. & Ares, M., Jr. Rearrangement of competing U2 RNA helices within the spliceosome promotes multiple steps in splicing. *Genes & development* **21**, 811-820, (2007).
175 Staley, J. P. & Guthrie, C. Mechanical devices of the spliceosome: motors, clocks, springs, and things. *Cell* **92**, 315-326, (1998).
176 Rocak, S. & Linder, P. DEAD-box proteins: the driving forces behind RNA metabolism. *Nature reviews Molecular cell biology* **5**, 232-241, (2004).
177 Ramalho-Santos, M., Yoon, S., Matsuzaki, Y., Mulligan, R. C. & Melton, D. A. "Stemness": transcriptional profiling of embryonic and adult stem cells. *Science* **298**, 597-600, (2002).
178 Liu, N., Han, H. & Lasko, P. Vasa promotes Drosophila germline stem cell differentiation by activating mei-P26 translation by directly interacting with a (U)-rich motif in its 3' UTR. *Genes & development* **23**, 2742-2752, (2009).
179 Zhang, H. *et al.* Adult human and mouse ovaries lack DDX4-expressing functional oogonial stem cells. *Nat Med* **21**, 1116-1118, (2015).
180 Zarate-Garcia, L., Lane, S. I., Merriman, J. A. & Jones, K. T. FACS-sorted putative oogonial stem cells from the ovary are neither DDX4-positive nor germ cells. *Sci Rep* **6**, 27991, (2016).
181 Hirabayashi, R., Hozumi, S., Higashijima, S. & Kikuchi, Y. Ddx46 is required for multi-lineage differentiation of hematopoietic stem cells in zebrafish. *Stem Cells Dev* **22**, 2532-2542, (2013).
182 Payne, E. M. *et al.* Ddx18 is essential for cell-cycle progression in zebrafish hematopoietic cells and is mutated in human AML. *Blood* **118**, 903-915, (2011).
183 Li, H. *et al.* RNA Helicase DDX5 Inhibits Reprogramming to Pluripotency by miRNA-Based Repression of RYBP and its PRC1-Dependent and -Independent Functions. *Cell Stem Cell* **20**, 462-477 e466, (2017).
184 Taanman, J. W. The mitochondrial genome: structure, transcription, translation and replication. *Biochim Biophys Acta* **1410**, 103-123, (1999).
185 Tu, Y. T. & Barrientos, A. The Human Mitochondrial DEAD-Box Protein DDX28 Resides in RNA Granules and Functions in Mitoribosome Assembly. *Cell Rep*, (2015).
186 Cai, W. *et al.* Wanted DEAD/H or Alive: Helicases Winding Up in Cancers. *J Natl Cancer Inst* **109**, (2017).
187 Wortham, N. C. *et al.* The DEAD-box protein p72 regulates ERalpha-/oestrogen-dependent transcription and cell growth, and is associated

with improved survival in ERalpha-positive breast cancer. *Oncogene* **28**, 4053-4064, (2009).
188 Samaan, S. *et al.* The Ddx5 and Ddx17 RNA helicases are cornerstones in the complex regulatory array of steroid hormone-signaling pathways. *Nucleic Acids Res* **42**, 2197-2207, (2014).
189 He, T. Y. *et al.* DDX3 promotes tumor invasion in colorectal cancer via the CK1epsilon/Dvl2 axis. *Sci Rep* **6**, 21483, (2016).
190 Cruciat, C. M. *et al.* RNA helicase DDX3 is a regulatory subunit of casein kinase 1 in Wnt-beta-catenin signaling. *Science* **339**, 1436-1441, (2013).
191 Sarkar, M., Khare, V., Guturi, K. K., Das, N. & Ghosh, M. K. The DEAD box protein p68: a crucial regulator of AKT/FOXO3a signaling axis in oncogenesis. *Oncogene* **34**, 5843-5856, (2015).
192 Kim, K. H. *et al.* DDX4 (DEAD box polypeptide 4) colocalizes with cancer stem cell marker CD133 in ovarian cancers. *Biochem Biophys Res Commun* **447**, 315-322, (2014).
193 Botlagunta, M. *et al.* Oncogenic role of DDX3 in breast cancer biogenesis. *Oncogene* **27**, 3912-3922, (2008).
194 Xie, M. *et al.* NZ51, a ring-expanded nucleoside analog, inhibits motility and viability of breast cancer cells by targeting the RNA helicase DDX3. *Oncotarget* **6**, 29901-29913, (2015).
195 Guturi, K. K. N., Sarkar, M., Bhowmik, A., Das, N. & Ghosh, M. K. DEAD-box protein p68 is regulated by β-catenin/transcription factor 4 to maintain a positive feedback loop in control of breast cancer progression. *Breast Cancer Research* **16**, 1, (2014).
196 Moore, H. C. *et al.* The RNA helicase p68 modulates expression and function of the Δ133 isoform (s) of p53, and is inversely associated with Δ133p53 expression in breast cancer. *Oncogene* **29**, 6475-6484, (2010).
197 Wang, D., Huang, J. & Hu, Z. RNA helicase DDX5 regulates microRNA expression and contributes to cytoskeletal reorganization in basal breast cancer cells. *Molecular & Cellular Proteomics* **11**, M111. 011932, (2012).
198 Kroiss, M. *et al.* Evolution of an RNP assembly system: a minimal SMN complex facilitates formation of UsnRNPs in Drosophila melanogaster. *Proc Natl Acad Sci U S A* **105**, 10045-10050, (2008).
199 Curmi, F. & Cauchi, R. J. The multiple lives of DEAD-box RNA helicase DP103/DDX20/Gemin3. *Biochem Soc Trans* **46**, 329-341, (2018).
200 Otter, S. *et al.* A comprehensive interaction map of the human survival of motor neuron (SMN) complex. *J Biol Chem* **282**, 5825-5833, (2007).
201 Donker, R. B., Mouillet, J. F., Nelson, D. M. & Sadovsky, Y. The expression of Argonaute2 and related microRNA biogenesis proteins in normal and hypoxic trophoblasts. *Mol Hum Reprod* **13**, 273-279, (2007).
202 Zuckerkandl, E. & Pauling, L. Molecules as documents of evolutionary history. *J Theor Biol* **8**, 357-366, (1965).
203 Lamond, A. I. & Sleeman, J. E. Nuclear substructure and dynamics. *Curr Biol* **13**, R825-828, (2003).

204 Mourelatos, Z. *et al.* miRNPs: a novel class of ribonucleoproteins containing numerous microRNAs. *Genes & development* **16**, 720-728, (2002).
205 Carnegie, G. K. *et al.* Protein phosphatase 4 interacts with the Survival of Motor Neurons complex and enhances the temporal localisation of snRNPs. *J Cell Sci* **116**, 1905-1913, (2003).
206 Cauchi, R. J., Sanchez-Pulido, L. & Liu, J. L. Drosophila SMN complex proteins Gemin2, Gemin3, and Gemin5 are components of U bodies. *Exp Cell Res* **316**, 2354-2364, (2010).
207 Shpargel, K. B. & Matera, A. G. Gemin proteins are required for efficient assembly of Sm-class ribonucleoproteins. *Proc Natl Acad Sci U S A* **102**, 17372-17377, (2005).
208 Neuenkirchen, N. *et al.* Reconstitution of the human U snRNP assembly machinery reveals stepwise Sm protein organization. *EMBO J* **34**, 1925-1941, (2015).
209 Minasaki, R., Puoti, A. & Streit, A. The DEAD-box protein MEL-46 is required in the germ line of the nematode Caenorhabditis elegans. *BMC Dev Biol* **9**, 35, (2009).
210 Mouillet, J. F. *et al.* DEAD-box protein-103 (DP103, Ddx20) is essential for early embryonic development and modulates ovarian morphology and function. *Endocrinology* **149**, 2168-2175, (2008).
211 Climente-Gonzalez, H., Porta-Pardo, E., Godzik, A. & Eyras, E. The Functional Impact of Alternative Splicing in Cancer. *Cell Rep* **20**, 2215-2226, (2017).
212 Meister, G. *et al.* Identification of novel argonaute-associated proteins. *Curr Biol* **15**, 2149-2155, (2005).
213 Yan, X., Mouillet, J. F., Ou, Q. & Sadovsky, Y. A novel domain within the DEAD-box protein DP103 is essential for transcriptional repression and helicase activity. *Mol Cell Biol* **23**, 414-423, (2003).
214 Groenenboom, M. A., Maree, A. F. & Hogeweg, P. The RNA silencing pathway: the bits and pieces that matter. *PLoS Comput Biol* **1**, 155-165, (2005).
215 Takata, A. *et al.* MicroRNA-140 acts as a liver tumor suppressor by controlling NF-kappaB activity by directly targeting DNA methyltransferase 1 (Dnmt1) expression. *Hepatology* **57**, 162-170, (2013).
216 Shin, E. M. *et al.* DEAD-box helicase DP103 defines metastatic potential of human breast cancers. *J Clin Invest* **124**, 3807-3824, (2014).
217 Lee, K. *et al.* Transcriptional factor FOXL2 interacts with DP103 and induces apoptosis. *Biochem Biophys Res Commun* **336**, 876-881, (2005).
218 Gillian, A. L. & Svaren, J. The Ddx20/DP103 dead box protein represses transcriptional activation by Egr2/Krox-20. *J Biol Chem* **279**, 9056-9063, (2004).
219 Lee, M. B. *et al.* The DEAD-box protein DP103 (Ddx20 or Gemin-3) represses orphan nuclear receptor activity via SUMO modification. *Mol Cell Biol* **25**, 1879-1890, (2005).
220 Ou, Q. *et al.* The DEAD box protein DP103 is a regulator of steroidogenic factor-1. *Mol Endocrinol* **15**, 69-79, (2001).

221 Batista, F., Vaiman, D., Dausset, J., Fellous, M. & Veitia, R. A. Potential targets of FOXL2, a transcription factor involved in craniofacial and follicular development, identified by transcriptomics. *Proc Natl Acad Sci U S A* **104**, 3330-3335, (2007).
222 Cai, Q. *et al.* Epstein-Barr virus nuclear antigen 3C stabilizes Gemin3 to block p53-mediated apoptosis. *PLoS Pathog* **7**, e1002418, (2011).
223 Circu, M. L. & Aw, T. Y. Reactive oxygen species, cellular redox systems, and apoptosis. *Free Radic Biol Med* **48**, 749-762, (2010).
224 Halliwell, B. & Cross, C. E. Oxygen-derived species: their relation to human disease and environmental stress. *Environ Health Perspect* **102 Suppl 10**, 5-12, (1994).
225 Szabo, C., Ischiropoulos, H. & Radi, R. Peroxynitrite: biochemistry, pathophysiology and development of therapeutics. *Nat Rev Drug Discov* **6**, 662-680, (2007).
226 Ray, P. D., Huang, B. W. & Tsuji, Y. Reactive oxygen species (ROS) homeostasis and redox regulation in cellular signaling. *Cell Signal* **24**, 981-990, (2012).
227 D'Autreaux, B. & Toledano, M. B. ROS as signalling molecules: mechanisms that generate specificity in ROS homeostasis. *Nat Rev Mol Cell Biol* **8**, 813-824, (2007).
228 Manna, S. K., Zhang, H. J., Yan, T., Oberley, L. W. & Aggarwal, B. B. Overexpression of manganese superoxide dismutase suppresses tumor necrosis factor-induced apoptosis and activation of nuclear transcription factor-kappaB and activated protein-1. *J Biol Chem* **273**, 13245-13254, (1998).
229 Glasauer, A., Sena, L. A., Diebold, L. P., Mazar, A. P. & Chandel, N. S. Targeting SOD1 reduces experimental non-small-cell lung cancer. *J Clin Invest* **124**, 117-128, (2014).
230 Lopez-Otin, C., Blasco, M. A., Partridge, L., Serrano, M. & Kroemer, G. The hallmarks of aging. *Cell* **153**, 1194-1217, (2013).
231 Liou, G. Y. & Storz, P. Reactive oxygen species in cancer. *Free Radic Res* **44**, 479-496, (2010).
232 Markesbery, W. R. Oxidative stress hypothesis in Alzheimer's disease. *Free Radic Biol Med* **23**, 134-147, (1997).
233 Choi, D. H. *et al.* NADPH oxidase 1-mediated oxidative stress leads to dopamine neuron death in Parkinson's disease. *Antioxid Redox Signal* **16**, 1033-1045, (2012).
234 Inoguchi, T. *et al.* Protein kinase C-dependent increase in reactive oxygen species (ROS) production in vascular tissues of diabetes: role of vascular NAD(P)H oxidase. *J Am Soc Nephrol* **14**, S227-232, (2003).
235 Harrison, D., Griendling, K. K., Landmesser, U., Hornig, B. & Drexler, H. Role of oxidative stress in atherosclerosis. *Am J Cardiol* **91**, 7A-11A, (2003).
236 Browning, J. D. & Horton, J. D. Molecular mediators of hepatic steatosis and liver injury. *J Clin Invest* **114**, 147-152, (2004).
237 Dworski, R. Oxidant stress in asthma. *Thorax* **55 Suppl 2**, S51-53, (2000).

238 Chong, S. J., Low, I. C. & Pervaiz, S. Mitochondrial ROS and involvement of Bcl-2 as a mitochondrial ROS regulator. *Mitochondrion* **19 Pt A**, 39-48, (2014).
239 Grivennikova, V. G. & Vinogradov, A. D. Generation of superoxide by the mitochondrial Complex I. *Biochim Biophys Acta* **1757**, 553-561, (2006).
240 Muller, F. L., Liu, Y. & Van Remmen, H. Complex III releases superoxide to both sides of the inner mitochondrial membrane. *J Biol Chem* **279**, 49064-49073, (2004).
241 Murphy, M. P. How mitochondria produce reactive oxygen species. *Biochem J* **417**, 1-13, (2009).
242 Miriyala, S. *et al.* Manganese superoxide dismutase, MnSOD and its mimics. *Biochim Biophys Acta* **1822**, 794-814, (2012).
243 Kowaltowski, A. J., Castilho, R. F. & Vercesi, A. E. Mitochondrial permeability transition and oxidative stress. *FEBS Lett* **495**, 12-15, (2001).
244 Lambeth, J. D. NOX enzymes and the biology of reactive oxygen. *Nat Rev Immunol* **4**, 181-189, (2004).
245 Kuppusamy, P. & Zweier, J. L. Characterization of free radical generation by xanthine oxidase. Evidence for hydroxyl radical generation. *J Biol Chem* **264**, 9880-9884, (1989).
246 Ghosh, R., Alajbegovic, A. & Gomes, A. V. NSAIDs and Cardiovascular Diseases: Role of Reactive Oxygen Species. *Oxid Med Cell Longev* **2015**, 536962, (2015).
247 Bondy, S. C. & Naderi, S. Contribution of hepatic cytochrome P450 systems to the generation of reactive oxygen species. *Biochem Pharmacol* **48**, 155-159, (1994).
248 Catalano, A., Rodilossi, S., Caprari, P., Coppola, V. & Procopio, A. 5-Lipoxygenase regulates senescence-like growth arrest by promoting ROS-dependent p53 activation. *EMBO J* **24**, 170-179, (2005).
249 Caliceti, C., Nigro, P., Rizzo, P. & Ferrari, R. ROS, Notch, and Wnt signaling pathways: crosstalk between three major regulators of cardiovascular biology. *Biomed Res Int* **2014**, 318714, (2014).
250 Zhang, J. *et al.* ROS and ROS-Mediated Cellular Signaling. *Oxid Med Cell Longev* **2016**, 4350965, (2016).
251 Pervaiz, S. & Clement, M. V. Superoxide anion: oncogenic reactive oxygen species? *Int J Biochem Cell Biol* **39**, 1297-1304, (2007).
252 Rhee, S. G. Cell signaling. H2O2, a necessary evil for cell signaling. *Science* **312**, 1882-1883, (2006).
253 Clement, M. V. & Pervaiz, S. Intracellular superoxide and hydrogen peroxide concentrations: a critical balance that determines survival or death. *Redox Rep* **6**, 211-214, (2001).
254 Koh, L. W. *et al.* A distinct reactive oxygen species profile confers chemoresistance in glioma-propagating cells and associates with patient survival outcome. *Antioxid Redox Signal* **19**, 2261-2279, (2013).
255 Pervaiz, S. & Clement, M. V. A permissive apoptotic environment: function of a decrease in intracellular superoxide anion and cytosolic acidification. *Biochem Biophys Res Commun* **290**, 1145-1150, (2002).

256 Funato, Y., Michiue, T., Asashima, M. & Miki, H. The thioredoxin-related redox-regulating protein nucleoredoxin inhibits Wnt-beta-catenin signalling through dishevelled. *Nat Cell Biol* **8**, 501-508, (2006).
257 Kang, D. H. *et al.* Interaction of tankyrase and peroxiredoxin II is indispensable for the survival of colorectal cancer cells. *Nat Commun* **8**, 40, (2017).
258 Son, Y. O. *et al.* Reactive oxygen species mediate Cr(VI)-induced carcinogenesis through PI3K/AKT-dependent activation of GSK-3beta/beta-catenin signaling. *Toxicol Appl Pharmacol* **271**, 239-248, (2013).
259 Padmanabhan, P. K. *et al.* DDX3 DEAD-box RNA helicase plays a central role in mitochondrial protein quality control in Leishmania. *Cell Death Dis* **7**, e2406, (2016).
260 Dewson, G. *et al.* To trigger apoptosis, Bak exposes its BH3 domain and homodimerizes via BH3:groove interactions. *Mol Cell* **30**, 369-380, (2008).
261 Breckenridge, D. G. & Xue, D. Regulation of mitochondrial membrane permeabilization by BCL-2 family proteins and caspases. *Curr Opin Cell Biol* **16**, 647-652, (2004).
262 Kluck, R. M., Bossy-Wetzel, E., Green, D. R. & Newmeyer, D. D. The release of cytochrome c from mitochondria: a primary site for Bcl-2 regulation of apoptosis. *Science* **275**, 1132-1136, (1997).
263 Adrain, C., Creagh, E. M. & Martin, S. J. Apoptosis-associated release of Smac/DIABLO from mitochondria requires active caspases and is blocked by Bcl-2. *EMBO J* **20**, 6627-6636, (2001).
264 Joza, N. *et al.* Essential role of the mitochondrial apoptosis-inducing factor in programmed cell death. *Nature* **410**, 549-554, (2001).
265 Mikhailov, V. *et al.* Bcl-2 prevents Bax oligomerization in the mitochondrial outer membrane. *J Biol Chem* **276**, 18361-18374, (2001).
266 Yi, X., Yin, X. M. & Dong, Z. Inhibition of Bid-induced apoptosis by Bcl-2. tBid insertion, Bax translocation, and Bax/Bak oligomerization suppressed. *J Biol Chem* **278**, 16992-16999, (2003).
267 Oltvai, Z. N., Milliman, C. L. & Korsmeyer, S. J. Bcl-2 heterodimerizes in vivo with a conserved homolog, Bax, that accelerates programmed cell death. *Cell* **74**, 609-619, (1993).
268 Mencalha, A., Victorino, V. J., Cecchini, R. & Panis, C. Mapping oxidative changes in breast cancer: understanding the basic to reach the clinics. *Anticancer Res* **34**, 1127-1140, (2014).
269 Lee, K. M. *et al.* MYC and MCL1 Cooperatively Promote Chemotherapy-Resistant Breast Cancer Stem Cells via Regulation of Mitochondrial Oxidative Phosphorylation. *Cell Metab* **26**, 633-647 e637, (2017).
270 Santidrian, A. F. *et al.* Mitochondrial complex I activity and NAD+/NADH balance regulate breast cancer progression. *J Clin Invest* **123**, 1068-1081, (2013).
271 Kim, D., Koo, J. S. & Lee, S. Overexpression of reactive oxygen species scavenger enzymes is associated with a good prognosis in triple-negative breast cancer. *Oncology* **88**, 9-17, (2015).

272 Loo, S. Y. *et al.* Manganese Superoxide Dismutase Expression Regulates the Switch Between an Epithelial and a Mesenchymal-Like Phenotype in Breast Carcinoma. *Antioxid Redox Signal* **25**, 283-299, (2016).
273 Kinugasa, H. *et al.* Mitochondrial SOD2 regulates epithelial-mesenchymal transition and cell populations defined by differential CD44 expression. *Oncogene* **34**, 5229-5239, (2015).
274 Azimi, I., Petersen, R. M., Thompson, E. W., Roberts-Thomson, S. J. & Monteith, G. R. Hypoxia-induced reactive oxygen species mediate N-cadherin and SERPINE1 expression, EGFR signalling and motility in MDA-MB-468 breast cancer cells. *Sci Rep* **7**, 15140, (2017).
275 Mehta, M. *et al.* HuR silencing elicits oxidative stress and DNA damage and sensitizes human triple-negative breast cancer cells to radiotherapy. *Oncotarget* **7**, 64820-64835, (2016).
276 Angelina, C. *et al.* KIF1Bbeta increases ROS to mediate apoptosis and reinforces its protein expression through O 2(-) in a positive feedback mechanism in neuroblastoma. *Sci Rep* **7**, 16867, (2017).
277 Singh, D. K. *et al.* The strength of receptor signaling is centrally controlled through a cooperative loop between Ca2+ and an oxidant signal. *Cell* **121**, 281-293, (2005).
278 Horak, P. *et al.* Negative feedback control of HIF-1 through REDD1-regulated ROS suppresses tumorigenesis. *Proc Natl Acad Sci U S A* **107**, 4675-4680, (2010).
279 Ming, M. *et al.* Activation of Wnt/beta-catenin protein signaling induces mitochondria-mediated apoptosis in hematopoietic progenitor cells. *J Biol Chem* **287**, 22683-22690, (2012).
280 Hsu, H. C. *et al.* LGR5 regulates survival through mitochondria-mediated apoptosis and by targeting the Wnt/beta-catenin signaling pathway in colorectal cancer cells. *Cell Signal* **26**, 2333-2342, (2014).
281 Lee, J. S. *et al.* A novel sLRP6E1E2 inhibits canonical Wnt signaling, epithelial-to-mesenchymal transition, and induces mitochondria-dependent apoptosis in lung cancer. *PLoS One* **7**, e36520, (2012).
282 Chen, S. *et al.* Wnt-1 signaling inhibits apoptosis by activating beta-catenin/T cell factor-mediated transcription. *J Cell Biol* **152**, 87-96, (2001).
283 Yoon, J. C. *et al.* Wnt signaling regulates mitochondrial physiology and insulin sensitivity. *Genes & development* **24**, 1507-1518, (2010).
284 Brown, K. *et al.* WNT/beta-catenin signaling regulates mitochondrial activity to alter the oncogenic potential of melanoma in a PTEN-dependent manner. *Oncogene* **36**, 3119-3136, (2017).
285 Essers, M. A. *et al.* Functional interaction between beta-catenin and FOXO in oxidative stress signaling. *Science* **308**, 1181-1184, (2005).
286 Essers, M. A. *et al.* FOXO transcription factor activation by oxidative stress mediated by the small GTPase Ral and JNK. *EMBO J* **23**, 4802-4812, (2004).
287 Bolte, S. & Cordelieres, F. P. A guided tour into subcellular colocalization analysis in light microscopy. *J Microsc* **224**, 213-232, (2006).

288 Cerami, E. *et al.* The cBio cancer genomics portal: an open platform for exploring multidimensional cancer genomics data. *Cancer Discov* **2**, 401-404, (2012).
289 Cancer Genome Atlas, N. Comprehensive molecular portraits of human breast tumours. *Nature* **490**, 61-70, (2012).
290 Curtis, C. *et al.* The genomic and transcriptomic architecture of 2,000 breast tumours reveals novel subgroups. *Nature* **486**, 346-352, (2012).
291 Subramanian, A. *et al.* Gene set enrichment analysis: a knowledge-based approach for interpreting genome-wide expression profiles. *Proc Natl Acad Sci U S A* **102**, 15545-15550, (2005).
292 Mootha, V. K. *et al.* PGC-1alpha-responsive genes involved in oxidative phosphorylation are coordinately downregulated in human diabetes. *Nat Genet* **34**, 267-273, (2003).
293 Ashburner, M. *et al.* Gene ontology: tool for the unification of biology. The Gene Ontology Consortium. *Nat Genet* **25**, 25-29, (2000).
294 Brand, A. H. & Perrimon, N. Targeted gene expression as a means of altering cell fates and generating dominant phenotypes. *Development* **118**, 401-415, (1993).
295 Livak, K. J. & Schmittgen, T. D. Analysis of relative gene expression data using real-time quantitative PCR and the 2(-Delta Delta C(T)) Method. *Methods* **25**, 402-408, (2001).
296 Rooney, J. P. *et al.* PCR based determination of mitochondrial DNA copy number in multiple species. *Methods Mol Biol* **1241**, 23-38, (2015).
297 Gordon, L. A. *et al.* Breast cell invasive potential relates to the myoepithelial phenotype. *Int J Cancer* **106**, 8-16, (2003).
298 Chavez, K. J., Garimella, S. V. & Lipkowitz, S. Triple negative breast cancer cell lines: one tool in the search for better treatment of triple negative breast cancer. *Breast Dis* **32**, 35-48, (2010).
299 Carter, M. E. & Brunet, A. FOXO transcription factors. *Curr Biol* **17**, R113-114, (2007).
300 Hoogeboom, D. *et al.* Interaction of FOXO with beta-catenin inhibits beta-catenin/T cell factor activity. *J Biol Chem* **283**, 9224-9230, (2008).
301 Gao, J. *et al.* Integrative analysis of complex cancer genomics and clinical profiles using the cBioPortal. *Sci Signal* **6**, pl1, (2013).
302 Cancer Genome Atlas Research, N. *et al.* The Cancer Genome Atlas Pan-Cancer analysis project. *Nat Genet* **45**, 1113-1120, (2013).
303 Tang, Q. L. *et al.* Glycogen synthase kinase-3beta, NF-kappaB signaling, and tumorigenesis of human osteosarcoma. *J Natl Cancer Inst* **104**, 749-763, (2012).
304 Jamieson, C., Lui, C., Brocardo, M. G., Martino-Echarri, E. & Henderson, B. R. Rac1 augments Wnt signaling by stimulating beta-catenin-lymphoid enhancer factor-1 complex assembly independent of beta-catenin nuclear import. *J Cell Sci* **128**, 3933-3946, (2015).
305 Ogrunc, M. *et al.* Oncogene-induced reactive oxygen species fuel hyperproliferation and DNA damage response activation. *Cell Death Differ* **21**, 998-1012, (2014).

306 Burdon, R. H. & Rice-Evans, C. Free radicals and the regulation of mammalian cell proliferation. *Free Radic Res Commun* **6**, 345-358, (1989).
307 Shin, S. Y. *et al.* Hydrogen peroxide negatively modulates Wnt signaling through downregulation of beta-catenin. *Cancer Lett* **212**, 225-231, (2004).
308 Clerkin, J. S., Naughton, R., Quiney, C. & Cotter, T. G. Mechanisms of ROS modulated cell survival during carcinogenesis. *Cancer Lett* **266**, 30-36, (2008).
309 Cooke, M. S., Evans, M. D., Dizdaroglu, M. & Lunec, J. Oxidative DNA damage: mechanisms, mutation, and disease. *FASEB J* **17**, 1195-1214, (2003).
310 Simon, H. U., Haj-Yehia, A. & Levi-Schaffer, F. Role of reactive oxygen species (ROS) in apoptosis induction. *Apoptosis* **5**, 415-418, (2000).
311 Singer, E. *et al.* Reactive oxygen species-mediated therapeutic response and resistance in glioblastoma. *Cell Death Dis* **6**, e1601, (2015).
312 Galati, G., Chan, T., Wu, B. & O'Brien, P. J. Glutathione-dependent generation of reactive oxygen species by the peroxidase-catalyzed redox cycling of flavonoids. *Chem Res Toxicol* **12**, 521-525, (1999).
313 Harris, I. S. *et al.* Glutathione and thioredoxin antioxidant pathways synergize to drive cancer initiation and progression. *Cancer Cell* **27**, 211-222, (2015).
314 Latunde-Dada, G. O. Ferroptosis: Role of lipid peroxidation, iron and ferritinophagy. *Biochim Biophys Acta* **1861**, 1893-1900, (2017).
315 Ashoori, M. & Saedisomeolia, A. Riboflavin (vitamin B(2)) and oxidative stress: a review. *Br J Nutr* **111**, 1985-1991, (2014).
316 Lento, W. *et al.* Loss of beta-catenin triggers oxidative stress and impairs hematopoietic regeneration. *Genes & development* **28**, 995-1004, (2014).
317 Klotz, L. O. *et al.* Redox regulation of FoxO transcription factors. *Redox Biol* **6**, 51-72, (2015).
318 Almeida, M., Han, L., Martin-Millan, M., O'Brien, C. A. & Manolagas, S. C. Oxidative stress antagonizes Wnt signaling in osteoblast precursors by diverting beta-catenin from T cell factor- to forkhead box O-mediated transcription. *J Biol Chem* **282**, 27298-27305, (2007).
319 Finkel, T. Oxidant signals and oxidative stress. *Curr Opin Cell Biol* **15**, 247-254, (2003).
320 Wang, S. *et al.* Wnt signaling-mediated redox regulation maintains the germ line stem cell differentiation niche. *Elife* **4**, e08174, (2015).
321 Vyas, S., Zaganjor, E. & Haigis, M. C. Mitochondria and Cancer. *Cell* **166**, 555-566, (2016).
322 Guha, M. *et al.* Aggressive triple negative breast cancers have unique molecular signature on the basis of mitochondrial genetic and functional defects. *Biochim Biophys Acta* **1864**, 1060-1071, (2018).
323 Pelicano, H. *et al.* Mitochondrial dysfunction in some triple-negative breast cancer cell lines: role of mTOR pathway and therapeutic potential. *Breast Cancer Res* **16**, 434, (2014).

324 Yadav, N. *et al.* Oxidative phosphorylation-dependent regulation of cancer cell apoptosis in response to anticancer agents. *Cell Death Dis* **6**, e1969, (2015).
325 Chen, N. *et al.* Elevated Mitochondrial DNA Copy Number in Peripheral Blood and Tissue Predict the Opposite Outcome of Cancer: A Meta-Analysis. *Sci Rep* **6**, 37404, (2016).
326 Hollestelle, A., Elstrodt, F., Nagel, J. H., Kallemeijn, W. W. & Schutte, M. Phosphatidylinositol-3-OH kinase or RAS pathway mutations in human breast cancer cell lines. *Mol Cancer Res* **5**, 195-201, (2007).
327 Kim, J. H. *et al.* Involvement of mitophagy in oncogenic K-Ras-induced transformation: overcoming a cellular energy deficit from glucose deficiency. *Autophagy* **7**, 1187-1198, (2011).
328 Serasinghe, M. N. *et al.* Mitochondrial division is requisite to RAS-induced transformation and targeted by oncogenic MAPK pathway inhibitors. *Mol Cell* **57**, 521-536, (2015).
329 Godoy, J. A. *et al.* Wnt-5a ligand modulates mitochondrial fission-fusion in rat hippocampal neurons. *J Biol Chem* **289**, 36179-36193, (2014).
330 Brand, M. D. & Nicholls, D. G. Assessing mitochondrial dysfunction in cells. *Biochem J* **435**, 297-312, (2011).
331 Jastroch, M., Divakaruni, A. S., Mookerjee, S., Treberg, J. R. & Brand, M. D. Mitochondrial proton and electron leaks. *Essays Biochem* **47**, 53-67, (2010).
332 Miyake, N. *et al.* Mitochondrial complex III deficiency caused by a homozygous UQCRC2 mutation presenting with neonatal-onset recurrent metabolic decompensation. *Hum Mutat* **34**, 446-452, (2013).
333 Whitaker-Menezes, D. *et al.* Hyperactivation of oxidative mitochondrial metabolism in epithelial cancer cells in situ: visualizing the therapeutic effects of metformin in tumor tissue. *Cell Cycle* **10**, 4047-4064, (2011).
334 Chan, S. H., Wu, K. L., Chang, A. Y., Tai, M. H. & Chan, J. Y. Oxidative impairment of mitochondrial electron transport chain complexes in rostral ventrolateral medulla contributes to neurogenic hypertension. *Hypertension* **53**, 217-227, (2009).
335 Flynn, J. M. & Melov, S. SOD2 in mitochondrial dysfunction and neurodegeneration. *Free Radic Biol Med* **62**, 4-12, (2013).
336 Ballinger, S. W. *et al.* Hydrogen peroxide- and peroxynitrite-induced mitochondrial DNA damage and dysfunction in vascular endothelial and smooth muscle cells. *Circ Res* **86**, 960-966, (2000).
337 Anderson, E. J., Katunga, L. A. & Willis, M. S. Mitochondria as a source and target of lipid peroxidation products in healthy and diseased heart. *Clin Exp Pharmacol Physiol* **39**, 179-193, (2012).
338 Cortes-Rojo, C. *et al.* Elucidation of the effects of lipoperoxidation on the mitochondrial electron transport chain using yeast mitochondria with manipulated fatty acid content. *J Bioenerg Biomembr* **41**, 15-28, (2009).
339 Konno, N. & Kako, K. J. Effects of hydrogen peroxide and hypochlorite on membrane potential of mitochondria in situ in rat heart cells. *Can J Physiol Pharmacol* **69**, 1705-1712, (1991).
340 Tada-Oikawa, S., Oikawa, S., Kawanishi, M., Yamada, M. & Kawanishi, S. Generation of hydrogen peroxide precedes loss of

mitochondrial membrane potential during DNA alkylation-induced apoptosis. *FEBS Lett* **442**, 65-69, (1999).

341 Kumar, A. P. *et al.* Manganese superoxide dismutase is a promising target for enhancing chemosensitivity of basal-like breast carcinoma. *Antioxid Redox Signal* **20**, 2326-2346, (2014).

342 Gong, J. *et al.* Pigment Epithelium-derived Factor (PEDF) Blocks Wnt3a Protein-induced Autophagy in Pancreatic Intraepithelial Neoplasms. *J Biol Chem* **291**, 22074-22085, (2016).

343 Radyuk, S. N. *et al.* Mitochondrial peroxiredoxins are critical for the maintenance of redox state and the survival of adult Drosophila. *Free Radic Biol Med* **49**, 1892-1902, (2010).

344 Hori, A., Yoshida, M., Shibata, T. & Ling, F. Reactive oxygen species regulate DNA copy number in isolated yeast mitochondria by triggering recombination-mediated replication. *Nucleic Acids Res* **37**, 749-761, (2009).

345 Lee, H. C., Yin, P. H., Lu, C. Y., Chi, C. W. & Wei, Y. H. Increase of mitochondria and mitochondrial DNA in response to oxidative stress in human cells. *Biochem J* **348 Pt 2**, 425-432, (2000).

346 Velasco-Velazquez, M. A., Homsi, N., De La Fuente, M. & Pestell, R. G. Breast cancer stem cells. *Int J Biochem Cell Biol* **44**, 573-577, (2012).

347 Al-Hajj, M., Wicha, M. S., Benito-Hernandez, A., Morrison, S. J. & Clarke, M. F. Prospective identification of tumorigenic breast cancer cells. *Proc Natl Acad Sci U S A* **100**, 3983-3988, (2003).

348 Hadjimichael, C. *et al.* Common stemness regulators of embryonic and cancer stem cells. *World J Stem Cells* **7**, 1150-1184, (2015).

349 Zhang, X., Peterson, K. A., Liu, X. S., McMahon, A. P. & Ohba, S. Gene regulatory networks mediating canonical Wnt signal-directed control of pluripotency and differentiation in embryo stem cells. *Stem Cells* **31**, 2667-2679, (2013).

350 Cailleau, R., Olive, M. & Cruciger, Q. V. Long-term human breast carcinoma cell lines of metastatic origin: preliminary characterization. *In Vitro* **14**, 911-915, (1978).

351 Georgescu, M. M. PTEN Tumor Suppressor Network in PI3K-Akt Pathway Control. *Genes Cancer* **1**, 1170-1177, (2010).

352 Maccario, H., Perera, N. M., Davidson, L., Downes, C. P. & Leslie, N. R. PTEN is destabilized by phosphorylation on Thr366. *Biochem J* **405**, 439-444, (2007).

353 Hermida, M. A., Dinesh Kumar, J. & Leslie, N. R. GSK3 and its interactions with the PI3K/AKT/mTOR signalling network. *Adv Biol Regul* **65**, 5-15, (2017).

354 Patel, R. *et al.* Sprouty2, PTEN, and PP2A interact to regulate prostate cancer progression. *J Clin Invest* **123**, 1157-1175, (2013).

355 Kaveri, D. *et al.* beta-Catenin activation synergizes with Pten loss and Myc overexpression in Notch-independent T-ALL. *Blood* **122**, 694-704, (2013).

356 Schmitt, M., Metzger, M., Gradl, D., Davidson, G. & Orian-Rousseau, V. CD44 functions in Wnt signaling by regulating LRP6 localization and activation. *Cell Death Differ* **22**, 677-689, (2015).

357 Chen, W., Dong, J., Haiech, J., Kilhoffer, M. C. & Zeniou, M. Cancer Stem Cell Quiescence and Plasticity as Major Challenges in Cancer Therapy. *Stem Cells Int* **2016**, 1740936, (2016).
358 Guturi, K. K., Sarkar, M., Bhowmik, A., Das, N. & Ghosh, M. K. DEAD-box protein p68 is regulated by beta-catenin/transcription factor 4 to maintain a positive feedback loop in control of breast cancer progression. *Breast Cancer Res* **16**, 496, (2014).
359 Wu, D. & Pan, W. GSK3: a multifaceted kinase in Wnt signaling. *Trends Biochem Sci* **35**, 161-168, (2010).
360 Ding, V. W., Chen, R. H. & McCormick, F. Differential regulation of glycogen synthase kinase 3beta by insulin and Wnt signaling. *J Biol Chem* **275**, 32475-32481, (2000).
361 Stamos, J. L., Chu, M. L., Enos, M. D., Shah, N. & Weis, W. I. Structural basis of GSK-3 inhibition by N-terminal phosphorylation and by the Wnt receptor LRP6. *Elife* **3**, e01998, (2014).
362 Persad, A. *et al.* Active beta-catenin is regulated by the PTEN/PI3 kinase pathway: a role for protein phosphatase PP2A. *Genes Cancer* **7**, 368-382, (2016).
363 Damsky, W. E. *et al.* beta-catenin signaling controls metastasis in Braf-activated Pten-deficient melanomas. *Cancer Cell* **20**, 741-754, (2011).
364 Ponta, H., Sherman, L. & Herrlich, P. A. CD44: from adhesion molecules to signalling regulators. *Nat Rev Mol Cell Biol* **4**, 33-45, (2003).
365 Liu, S. & Cheng, C. Akt Signaling Is Sustained by a CD44 Splice Isoform-Mediated Positive Feedback Loop. *Cancer Res* **77**, 3791-3801, (2017).
366 Takao, Y., Yokota, T. & Koide, H. Beta-catenin up-regulates Nanog expression through interaction with Oct-3/4 in embryonic stem cells. *Biochem Biophys Res Commun* **353**, 699-705, (2007).
367 Chodelkova, O., Masek, J., Korinek, V., Kozmik, Z. & Machon, O. Tcf7L2 is essential for neurogenesis in the developing mouse neocortex. *Neural Dev* **13**, 8, (2018).
368 Davidson, K. C. *et al.* Wnt/beta-catenin signaling promotes differentiation, not self-renewal, of human embryonic stem cells and is repressed by Oct4. *Proc Natl Acad Sci U S A* **109**, 4485-4490, (2012).
369 Bretones, G., Delgado, M. D. & Leon, J. Myc and cell cycle control. *Biochim Biophys Acta* **1849**, 506-516, (2015).
370 Stacey, D. W. Cyclin D1 serves as a cell cycle regulatory switch in actively proliferating cells. *Curr Opin Cell Biol* **15**, 158-163, (2003).
371 Bechard, M. & Dalton, S. Subcellular localization of glycogen synthase kinase 3beta controls embryonic stem cell self-renewal. *Mol Cell Biol* **29**, 2092-2104, (2009).
372 Ehemann, V., Sykora, J., Vera-Delgado, J., Lange, A. & Otto, H. F. Flow cytometric detection of spontaneous apoptosis in human breast cancer using the TUNEL-technique. *Cancer Lett* **194**, 125-131, (2003).
373 Kuo, Y. H. *et al.* Dual Inhibition of Key Proliferation Signaling Pathways in Triple-Negative Breast Cancer Cells by a Novel Derivative of Taiwanin A. *Mol Cancer Ther* **16**, 480-493, (2017).

374 Shibue, T. & Weinberg, R. A. EMT, CSCs, and drug resistance: the mechanistic link and clinical implications. *Nat Rev Clin Oncol* **14**, 611-629, (2017).
375 Narayanan, B. A. *et al.* Antagonistic effect of small-molecule inhibitors of Wnt/beta-catenin in multiple myeloma. *Anticancer Res* **32**, 4697-4707, (2012).
376 Saran, U., Arfuso, F., Zeps, N. & Dharmarajan, A. Secreted frizzled-related protein 4 expression is positively associated with responsiveness to cisplatin of ovarian cancer cell lines in vitro and with lower tumour grade in mucinous ovarian cancers. *BMC Cell Biol* **13**, 25, (2012).
377 Lamb, R. *et al.* Wnt pathway activity in breast cancer sub-types and stem-like cells. *PLoS One* **8**, e67811, (2013).
378 Galli, L. M. *et al.* Differential inhibition of Wnt-3a by Sfrp-1, Sfrp-2, and Sfrp-3. *Dev Dyn* **235**, 681-690, (2006).
379 Constantinou, T. *et al.* SFRP-4 abrogates Wnt-3a-induced beta-catenin and Akt/PKB signalling and reverses a Wnt-3a-imposed inhibition of in vitro mammary differentiation. *J Mol Signal* **3**, 10, (2008).
380 Ladher, R. K. *et al.* Cloning and expression of the Wnt antagonists Sfrp-2 and Frzb during chick development. *Dev Biol* **218**, 183-198, (2000).
381 Kawano, Y. & Kypta, R. Secreted antagonists of the Wnt signalling pathway. *J Cell Sci* **116**, 2627-2634, (2003).
382 Agostino, M., Pohl, S. O. & Dharmarajan, A. Structure-based prediction of Wnt binding affinities for Frizzled-type cysteine-rich domains. *J Biol Chem* **292**, 11218-11229, (2017).
383 Tada-Oikawa, S., Hiraku, Y., Kawanishi, M. & Kawanishi, S. Mechanism for generation of hydrogen peroxide and change of mitochondrial membrane potential during rotenone-induced apoptosis. *Life Sci* **73**, 3277-3288, (2003).
384 Salvi, M. *et al.* Catalase takes part in rat liver mitochondria oxidative stress defense. *J Biol Chem* **282**, 24407-24415, (2007).
385 Walton, P. A. & Pizzitelli, M. Effects of peroxisomal catalase inhibition on mitochondrial function. *Front Physiol* **3**, 108, (2012).
386 Van Camp, J. K., Beckers, S., Zegers, D. & Van Hul, W. Wnt signaling and the control of human stem cell fate. *Stem Cell Rev* **10**, 207-229, (2014).
387 Nusse, R. Wnt signaling and stem cell control. *Cell Res* **18**, 523-527, (2008).
388 Zhou, D., Shao, L. & Spitz, D. R. Reactive oxygen species in normal and tumor stem cells. *Adv Cancer Res* **122**, 1-67, (2014).
389 Sykiotis, G. P. & Bohmann, D. Keap1/Nrf2 signaling regulates oxidative stress tolerance and lifespan in Drosophila. *Dev Cell* **14**, 76-85, (2008).
390 Morey, M., Serras, F., Baguna, J., Hafen, E. & Corominas, M. Modulation of the Ras/MAPK signalling pathway by the redox function of selenoproteins in Drosophila melanogaster. *Dev Biol* **238**, 145-156, (2001).

391 Deng, C. X. & Brodie, S. G. Knockout mouse models and mammary tumorigenesis. *Semin Cancer Biol* **11**, 387-394, (2001).
392 Kost, G. C. *et al.* A Novel Anti-Cancer Agent, 1-(3,5-Dimethoxyphenyl)-4-[(6-Fluoro-2-Methoxyquinoxalin-3-yl)Aminocarbonyl] Piperazine (RX-5902), Interferes With beta-Catenin Function Through Y593 Phospho-p68 RNA Helicase. *J Cell Biochem* **116**, 1595-1601, (2015).
393 Ranga, A., Gjorevski, N. & Lutolf, M. P. Drug discovery through stem cell-based organoid models. *Adv Drug Deliv Rev* **69-70**, 19-28, (2014).
394 Belousov, V. V. *et al.* Genetically encoded fluorescent indicator for intracellular hydrogen peroxide. *Nat Methods* **3**, 281-286, (2006).
395 Youle, R. J. & van der Bliek, A. M. Mitochondrial fission, fusion, and stress. *Science* **337**, 1062-1065, (2012).

8 APPENDICES

APPENDIX 1 – LIST OF CONFERENCES AND AWARDS

APPENDIX 2 – LIST OF PUBLICATIONS

APPENDIX 3 – PUBLICATIONS AND PERMISSIONS

APPENDIX 1 – LIST OF CONFERENCES AND AWARDS

CONFERENCES

2018 Lorne Conference on Cancer.

"DEAD-Box RNA helicase, DDX20 in redox-dependent regulation of Wnt/β-catenin signaling in triple-negative breast cancer"

2018 Lorne Conference on Cancer.

"Deciphering the combinatorial complexity of Wnt-Frizzled interaction" (co-author)

2018 Lorne - Conference on Cancer

"Structure basis of in integrin antagonism by netrin-like domain-containing proteins" (co-author)

2018 43rd Lorne Conference on Protein Structure and Function.

"DEAD-Box RNA helicase, DDX20 in redox-dependent regulation of Wnt/β-catenin signaling in triple-negative breast cancer"

2018 43rd Lorne Conference on Protein Structure and Function.

"Deciphering the combinatorial complexity of Wnt-Frizzled interaction" (co-author)

2018 43rd Lorne Conference on Structure and Function.

"Structure basis of in integrin antagonism by netrin-like domain-containing proteins" (co-author)

2017 Frontiers in Cancer Science, Singapore

"DEAD-Box RNA helicase, DDX20 in redox-dependent regulation of Wnt/β-catenin signaling in triple-negative breast cancer"

2017 Combined Biological Science Meeting (CBSM)

"The role of Wnt signalling in the regulation of non-tumourigenic and tumourigenic liver progenitor cells" (co-author)

2017 Science on the Swan Conference, Perth

"DEAD-Box Helicase DDX20 influences the redox status of triple-negative breast cancer through Wnt/β-catenin and FOXO signalling"

"Prediction of Wnt-Frizzled binding affinities using structure-based approaches" (Co-author)

2017 Cell Signalling Western Australia, Curtin University (Oral Presentation)

"DEAD-Box Helicase DP103 regulates Wnt/β-catenin Signaling in triple negative breast cancer stem cells"

2016 Science on the Swan Conference, Perth

"DEAD-Box Helicase DP103 regulates Wnt/β-catenin Signaling in triple negative breast cancer stem cells"

2016 EMBO Conference: Wnt Meeting

"DDX20-GSK3β-Wnt Cascade Promotes Wnt/β-catenin Signaling in Parental and Stem Cells from Triple Negative Breast Cancer (co-author)

2016 Mark Liveris Student Seminars, Curtin University (Oral Presentation)

"DEAD-Box Helicase DP103 regulates Wnt/β-catenin Signaling in triple negative breast cancer stem cells"

2016 Combined Biological Science Meeting

DEAD-Box Helicase DP103 regulates Wnt/β-catenin Signaling in triple negative breast cancer stem cells and is downregulated by secreted frizzled related protein 4 (sFRP4)"

AWARDS

2016 Best Poster Award – Science on the Swan Conference

2017 Best Poster Award – Combined Biological Sciences Meeting

2018 Best Poster Award – Lorne Conference on Protein Structure and Function

APPENDIX 2 – LIST OF PUBLICATIONS

SÖG Pohl, M. Agostino, A. Dharmarajan, S Pervaiz. Crosstalk between cellular redox states and the anti-apoptotic protein Bcl-2. *Antioxid Redox Signal.* (2018). Published online Feb 15, doi: 10.1089/ars.2017.7414

J. Olsen*, SÖG Pohl*, A. Deshmukh, M. Visweswaran, N. Ward, F. Arfuso, M. Agostino, A. Dharmarajan. The role of Wnt signalling in angiogenesis. *Clinical Biochem Rev*, (2017) 38(3): 131-142.

M. Agostino, SÖG Pohl, A. Dharmarajan, Structure-based prediction of Wnt binding affinities for Frizzled-type cysteine-rich domains, *J Biol Chem*, (2017) 292: 11218. doi:10.1074/jbc.M117.786269

SÖG Pohl, N. Brook, M. Agostino, F. Arfuso, AP. Kumar, A. Dharmarajan, Wnt signalling in triple-negative breast cancer, *Oncogenesis* 6 (2017), e310.

V. Perumal*, S. Pohl*, K.N. Keane*, F. Arfuso, P. Newsholme, S. Fox, A. Dharmarajan, Therapeutic approach to target mesothelioma cancer cells using the Wnt antagonist, secreted frizzled-related protein 4: Metabolic state of cancer cells, *Exp. Cell Res*. 341 (2016) 218-224.

S. Pohl*, R. Scott*, F. Arfuso, V. Perumal, A. Dharmarajan, Secreted frizzled-related protein 4 and its implications in cancer and apoptosis, *Tumor Biol*. 36 (2015) 143-152.

M. Visweswaran, S. Pohl, F. Arfuso, P. Newsholme, R. Dilley, S. Pervaiz, A. Dharmarajan, Multi-lineage differentiation of mesenchymal stem cells - To Wnt, or not Wnt, *Int J Biochem Cell Biol*. 68 (2015) 139-147.
*denotes equal contribution

APPENDIX 3 – PUBLICATIONS AND PERMISSIONS

ANTIOXIDANTS & REDOX SIGNALING
Volume 00, Number 00, 2018

DOI: 10.1089/ars.2017.7414

FORUM REVIEW ARTICLE

Cross Talk Between Cellular Redox State and the Antiapoptotic Protein Bcl-2

Sebastian Öther-Gee Pohl,[1,2] Mark Agostino,[1–3] Arun Dharmarajan,[1,2] and Shazib Pervaiz[2,4–6]

Abstract

Significance: B cell lymphoma-2 (Bcl-2) was discovered over three decades ago and is the prototype antiapoptotic member of the Bcl-2 family that comprises proteins with contrasting effects on cell fate. First identified as a consequence of chromosomal translocation (t 14:18) in human lymphoma, subsequent studies have revealed mutations and/or gene copy number alterations as well as posttranslational modifications of Bcl-2 in a variety of human cancers. The canonical function of Bcl-2 is linked to its ability to inhibit mitochondrial membrane permeabilization, thereby regulating apoptosome assembly and activation by blocking the cytosolic translocation of death amplification factors. Of note, the identification of specific domains within the Bcl-2 family of proteins (Bcl-2 homology domains; BH domains) has not only provided a mechanistic insight into the various interactions between the member proteins but has also been the impetus behind the design and development of small molecule inhibitors and BH3 mimetics for clinical use.

Recent Advances: Aside from its role in maintaining mitochondrial integrity, recent evidence provides testimony to a novel facet in the biology of Bcl-2 that involves an intricate cross talk with cellular redox state. Bcl-2 overexpression modulates mitochondrial redox metabolism to create a ''pro-oxidant'' milieu, conducive for cell survival. However, under states of oxidative stress, overexpression of Bcl-2 functions as a redox sink to prevent excessive buildup of reactive oxygen species, thereby inhibiting execution signals. Emerging evidence indicates various redox-dependent transcriptional changes and posttranslational modifications with different functional outcomes.

Critical Issues: Understanding the complex interplay between Bcl-2 and the cellular redox milieu from the standpoint of cell fate signaling remains vital for a better understanding of pathological states associated with altered redox metabolism and/or aberrant Bcl-2 expression.

Future Directions: Based on its canonical functions, Bcl-2 has emerged as a potential druggable target. Small molecule inhibitors of Bcl-2 and/or other family members with similar function, as well as BH3 mimetics, are showing promise in the clinic. The emerging evidence for the noncanonical activity linked to cellular redox metabolism provides a novel avenue for the design and development of diagnostic and therapeutic strategies against cancers refractory to conventional chemotherapy by the overexpression of this prosurvival protein. *Antioxid. Redox Signal.* 00, 000–000.

Keywords: B cell lymphoma 2, Bcl2, reactive oxygen species, ROS, oxidative stress, BH domains

[1]Stem Cell and Cancer Biology Laboratory, Curtin Health and Innovation Research Institute, Curtin University, Bentley, Western Australia.
[2]School of Biomedical Sciences and [3]Curtin Institute for Computation, Curtin University, Perth, Western Australia.
[4]Department of Physiology, Yong Loo Lin School of Medicine and [5]NUS Graduate School for Integrative Sciences and Engineering, National University of Singapore, Singapore, Singapore.
[6]National University Cancer Institute, National University Health System, Singapore, Singapore.

Introduction

B cell lymphoma 2: the founding member of a functionally disparate family

BCELL LYMPHOMA 2 (Bcl-2) is the prototypical Bcl-family protein and a major regulator of cell death. Bcl-2 was discovered following the cloning of leukemic cells bearing the t(14;18) (q32;q21) chromosome translocation (175). Subsequent chromosome mapping identified *BCL2* as a putative gene involved in the pathogenesis of B cell and follicular lymphomas (174). McDonnell *et al.* (115) demonstrated that this interchromosomal translocation resulted in the overexpression of Bcl-2 and extended the life span of B cells.

Bcl-2 is primarily localized in the mitochondria (67), however, its localization has also be extended to the nucleus and endoplasmic reticulum (ER). Functionally, Bcl-2 is characterized as an antiapoptotic protein due to its role in inhibiting proapoptotic proteins; these include the Bcl-2 family members Bak and Bax (28). On apoptotic stimulation, death receptor- or drug-induced, a cascade of caspase activation results in the induction of mitochondrial outer membrane permeabilization (MOMP). In the case of death receptor signaling, direct executioner caspase activation is induced in certain cell types where the death initiating signaling complex is efficiently formed (Type 1 or extrinsic pathway); however, in other cell types, the initiator caspase activation is relatively weak to autonomously engage the executioner caspase(s), and therefore, the signal is routed through the mitochondria for efficient death execution (Type 2 or intrinsic signaling). The latter is also the preferred mode of execution triggered on exposure of cells to DNA damaging agents, γ-irradiation, as well as other forms of chemotherapy. Importantly, the recruitment of mitochondria is a function of the proapoptotic members of the Bcl-2 family that, on apoptotic stimulation, translocate to the mitochondria forming oligomeric complexes (40) that compromise the permeability of the outer membrane (15), thereby facilitating the egress of death amplification factors such as cytochrome *c* (83), Smac/direct IAP binding protein with low pI (DIABLO) (1), and apoptosis inducing factor (75). The antiapoptotic members of the Bcl-2 family, in particular Bcl-2 and Bcl-xL, prevent MOMP by competing with and inhibiting the oligomerization of the proapoptotic members, such as Bax and Bak (117, 135, 190). As such, the apoptosis inhibitory function of Bcl-2 is strongly associated with the Type 2 death signaling pathway (Fig. 1).

Bcl-2 expression has also been shown to regulate autophagy, a process of self- consumption induced on starvation or other stress states. Autophagy has emerged as a central player in the removal of damaged organelles as well as a source of nutrients for cells under starvation, hence the association with a prosurvival phenotype. Autophagy has also been linked to cell death signaling in response to certain noxious stimuli. Interestingly, being a survival promoting protein, Bcl-2 has also been shown to have a critical role in regulating autophagy (97). Pattingre *et al.* demonstrated the antiautophagic role of Bcl-2, promoting cell survival, which was dependent on its interaction with Beclin1 (139). This interaction utilized the BH1 and BH2 domains of Bcl-2. Beclin1 expression is low to absent in many cancer cells, leading to loss of autophagy and promotion of cell survival. Cancer cells expressing Beclin1 exhibited higher levels of LC3-induced autophagy, which was inhibited upon overexpression of Bcl-2. The expression of Bcl-2 mutants (G145A/W188A) resulted in the loss of Bcl-2:Beclin1 interaction, as well as the initiation of cellular autophagy. Interestingly, this was only observed when Bcl-2 was localized to the ER, not the mitochondria (139). The interaction was also found to be dependent on JNK1-mediated phosphorylation of Thr69, Ser70, and Ser87. This starvation-dependent phosphorylation resulted in a dissociation of Beclin1 from Bcl-2 and the induction of autophagy (182) (Fig. 2). The inhibitory effect of Bcl-2 on apoptosis and autophagy lends credence to the hypothesis that apoptosis and autophagy work in tandem to regulate processes involved in cellular transformation and its progression.

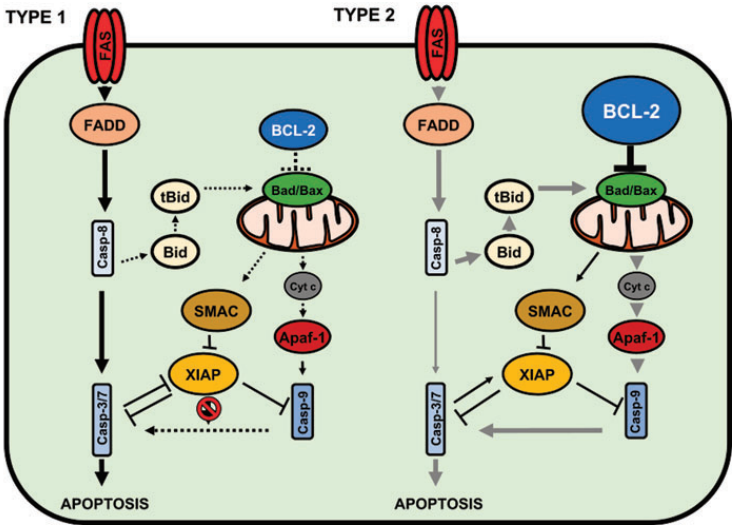

FIG. 1. Schematic of type 1 and type 2 death receptor pathways. Type 1 (*bold black line*) FAS (CD95) death signaling pathway signals independent of the intrinsic pathway. Following FAS ligand binding, signals are transduced through FADD-mediated caspase-8 activation and caspase-3/7 activation for cells to go under apoptosis. Type 2 (*bold gray line*) death signaling through FAS is directed through caspase-8-mediated Bid activation. Bcl-2 is the primary inhibitor of antiapoptosis in type 2 signaling. Bad/Bax can direct apoptosis by the release of cytochrome *c*, and the activation of Apaf-1 and caspase-9. *Dotted lines* indicate no pathway involvement. Bcl-2, B cell lymphoma 2. To see this illustration in color, the reader is referred to the web version of this article at www.liebertpub.com/ars

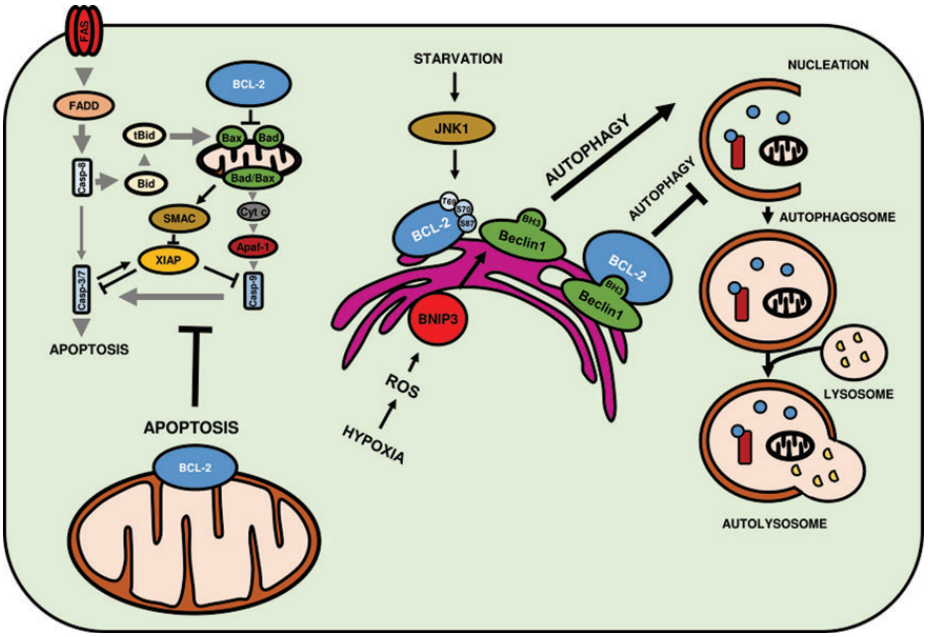

FIG. 2. Schematic of Bcl-2 role in apoptosis and autophagy. Bcl-2 localized to the ER directly interacts with Beclin 1 to inhibit autophagy. Starvation induced JNK1 activation leads to phosphorylation of Thr69, Ser70, and Ser87 of Bcl-2 disrupting the interaction with Beclin1 to induce autophagy. Interaction between the BH3 domains of Beclin1 and Bcl-2 results in the inhibition of autophagy. BNIP3 can interrupt the interaction between Bcl-2 and Beclin1 under conditions of hypoxia-induced ROS inducing autophagy. The autophagy pathway consists of nucleation, autophagosome assembly followed by fusion with the lysosome to result in the formation of an autolysosome. Bad/Bax forms heterodimers with Bcl-2 causing its inactivation and the initiation of apoptosis. BH, Bcl-2 homology domains; BNIP3, Bcl-2/adenovirus E1B 19-kDa protein-interacting protein 3; JNKs, c-Jun N-terminal kinases. To see this illustration in color, the reader is referred to the web version of this article at www.liebertpub.com/ars

Expression in cancer and mutational landscape. Genomic alterations in *BCL2* are common in a variety of cancers. Data sets obtained from The Cancer Genome Atlas (TCGA) accessed by cBioPortal (24, 53) revealed a high percentage of copy number alterations across the majority of cancers surveyed. In this regard, gene amplifications and deletions are the primary alterations (Fig. 3A). Unsurprisingly, amplifications and mutations occurred with higher frequencies in B cell lymphomas. The expression of *BCL2* mRNA was also determined by accessing the same data sets across 21 cancer types. Bcl-2 is not a ubiquitously expressed protein and there seems to be no correlation between organ systems and Bcl-2 expression in cancers, although hematopoietic and lymphoid malignancies were consistently high (Fig. 3B). Although *BCL2* expression was low in carcinomas of the bladder and testicular cancer, it still holds promising predictive power for outcomes in patients (35, 44). Interestingly, the lowest expression was found in hepatocellular carcinoma, where numerous studies have implicated its role as delaying the progression of carcinogenesis by delaying cell cycle progression (148, 177).

The mutational landscape of *BCL2* extends to both hematopoietic and nonhematopoietic tumors. To assist the interpretation of the likely impact of these mutations on Bcl-2 function, we have prepared a putative Bcl-2 homodimer model, based on the crystal structure complex of Bcl-2 with a Bax BH3 peptide (PDB 2XA0) (86), the solution structure of Bcl-xL in its p53-bound conformation (PDB 2ME8) (50), and the crystal structure of the Bcl-xL domain-swapped homodimer (PDB 2B48) (131) (Fig. 3C). Characteristic gain of copy number and expression in diffuse large B cell lymphoma has been associated with R129H missense mutation. In the putative Bcl-2 homodimer, Arg129 appears to facilitate BH2 domain swapping; R129H may facilitate this more efficiently. The G128E mutation was identified in stomach cancer, although was not associated with a variation in copy number. This residue is on the Bcl-2 surface and is not involved in interactions; therefore, the influence of the Gly128 mutation on Bcl-2 function is unclear from the structure.

Numerous G47S mutations have been identified in stomach cancer. Gly47 is located in the large unstructured loop region between the BH4 and BH3 domains and occurs at the dimer interface in the domain-swapped homodimer; G47S would likely enhance homodimer stability. Mutations in melanoma include T96I and A224 V. Thr96 is located at the dimer interface; T96I will likely enhance homodimer stability. Ala224 is located in the TM region of Bcl-2; A224 V will likely embed in the membrane more efficiently. A more comprehensive overview of the mutational landscape is accessible from the TCGA. Further probing of the functional relevance of mutations in *BCL2* is required for the significance in various disease contexts.

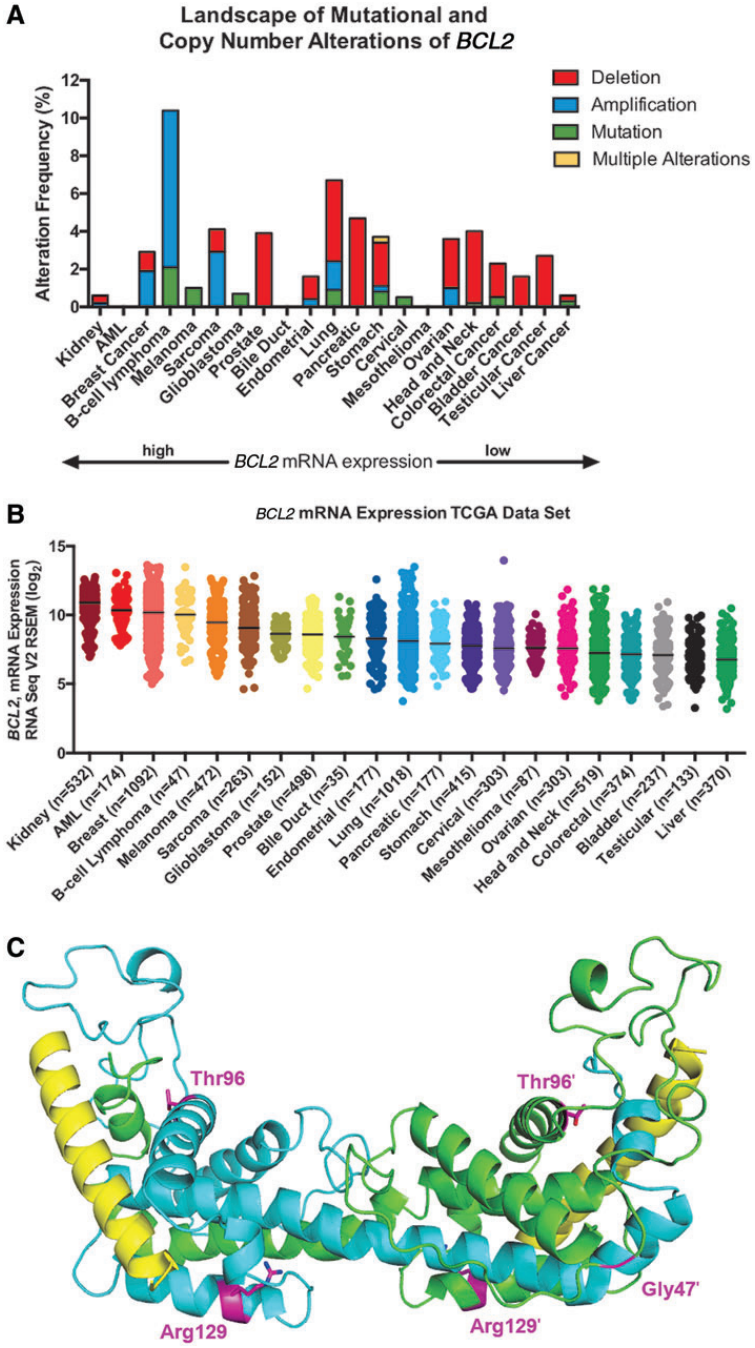

FIG. 3. ***BCL2*** **gene expression, mutational landscape, and copy number variations in cancer. (A)** TCGA data sets retrieved from cBioPortal indicate copy number and mutation alterations across 21 cancer types. Deletions (*red*), amplifications (*blue*), mutations (*green*), and multiple alterations (*yellow*) are shown as their alteration frequency in cancers sorted from high *BCL2* mRNA expression to low *BCL2* mRNA expression. **(B)** *BCL2* mRNA expression across 21 cancer types from TCGA data sets retrieved from cBioPortal. **(C)** Putative homodimer structure of Bcl-2 bound to Bax BH3 peptide with mutations highlighted. Color guide: *blue* - Bcl-2 molecule 1; *green* - Bcl-2 molecule 2; *yellow* - Bax BH3 peptides; *violet* - mutations identified in TCGA (not visible/highlighted: Gly47 in Bcl-2 molecule 1, Gly128 in either Bcl-2 molecule). TCGA, The Cancer Genome Atlas. To see this illustration in color, the reader is referred to the web version of this article at www.liebertpub.com/ars

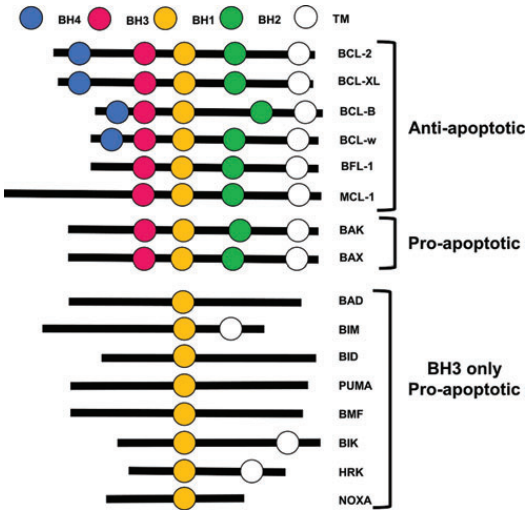

FIG. 4. Schematic view of Bcl-2 family proteins. To see this illustration in color, the reader is referred to the web version of this article at www.liebertpub.com/ars

Structural knowledge of Bcl-2 and its interactions with peptides and small molecule inhibitors. The structure of Bcl-2 family proteins has been extensively characterized by X-ray crystallography and NMR spectroscopy, and in the majority of cases, structural details of interactions with other proteins and prospective inhibitors are known. Bcl-2 family proteins are characterized by the presence of one or more BH domains. The BH3 domain is the most highly conserved, being present in all members of the Bcl-2 antiapoptotic multidomain, proapoptotic multidomain, and BH3-only domain members (Fig. 4). The antiapoptotic members contain all BH1-BH4 domains, except MCL-1 (induced myeloid leukemia cell differentiation protein) and A1, which lack the BH4 motif. Bcl-2 itself features four BH domains (in sequence order, BH4, BH3, BH1, and BH2), which facilitate protein/protein interactions with proteins from and outside of the Bcl-2 family. The majority of the family proteins, excluding some of the BH3-only members (Bad, Bmf, Bid, Puma, and Noxa), possess a TM domain that is critical for homo- and hetero-oligomerization at the mitochondrial membrane (135, 191).

The structure of Bcl-2 was first determined by NMR spectroscopy using a Bcl-2 construct, in which the loop between the BH4 and BH3 motifs was replaced by the equivalently located and shorter loop from the related protein Bcl-xL (146). This construct has been used to provide the majority of Bcl-2 structures (Table 1). The overall structural similarity of Bcl-2 to Bcl-xL, the native (119) and peptide-bound (147, 161) structures of which were already known at the time, was revealed and provided the first indications as to the different peptide binding specificities of the two proteins.

The structure of Bcl-2 has since been resolved with a small range of peptide interactors, including fragments from naturally occurring proteins as well as designed peptides (Table 1). In all cases, binding is achieved *via* an α-helix (13, 74, 86) or α-helix-like (25) structure interacting with a groove formed by the BH3, BH1, and BH2 domains (Fig. 5). Furthermore, peptides are oriented within the groove in the same way in all structures, with the N-terminal oriented

TABLE 1. EXPERIMENTALLY DETERMINED BCL-2 STRUCTURES

PDB ID[a]	*Method*	*Resolution (Å)*	*Resolved portion of structure*[b]	*Bound molecules*[c]	*Reference*
1G5 M	NMR	N/A	3-34, 92-207	None	(146)
1GJH	NMR	N/A	3-34, 92-207	None	(146)
1YSW	NMR	N/A	3-34, 92-207	2-phenethylbenzothiazole analog of Compound **1**	(134)[d]
2O21	NMR	N/A	3-34, 92-207	2-phenethylbenzothiazole analog of Compound **1**	(18)[d]
2O22	NMR	N/A	3-34, 92-207	Compound **1b**	(18)[d]
2O2F	NMR	N/A	3-34, 92-207	Compound **43a**	(18)[d]
2 W3L	X-ray	2.10	9-35, 92–203	Phenylpyrazole **2**	(149)
2XA0	X-ray	2.70	10–31, 92–206	Bax BH3 peptide	(86)
4AQ3	X-ray	2.40	9-31, 92–203	Compound **18**	(141)
4IEH	X-ray	2.10	9-31, 92–204	Compound **6**	(173)
4LVT	X-ray	2.05	9-32, 92–204	Navitoclax (ABT-263)	(167)[d]
4LXD	X-ray	1.90	6-33, 92–204	Compound **2**	(167)[d]
4MAN	X-ray	2.07	8-29, 92–204	Indole analog of compound **2**	(167)[d]
5AGW	X-ray	2.69	8-31, 92–204	***α/β*-1**	(25)
5AGX	X-ray	2.24	8-32, 92–204	***α/β*-1-LIN**	(25)
5FCG	X-ray	2.10	6-34, 92–203	Peptide from HBx protein	(74)
5JSN	X-ray	2.10	7-32, 87–207	αBCL2 peptide	(13)[d]

[a]All structures obtained from Bcl-2:Bcl-x(L) chimera except 2XA0, 5FCG, and 5JSN, which were determined from full-length Bcl-2.
[b]All structures have been determined from the Bcl-2 construct in which the BH4-BH3 loop of Bcl-2 replaced with shorter loop from Bcl-xL, except PDB 5JSN. In the NMR structures, the structure resolved is continuous; the replaced loop is largely not resolved in X-ray.
[c]To avoid long systematic names, compounds are named according to their designation in their original publication; see the original publication cited in the corresponding row of the Reference column for specific compound details.
[d]This study also reports ligand complexes with Bcl-xL; see the respective publication for further details.
Bcl-2, B cell lymphoma 2; BH, Bcl-2 homology domains; N/A, not applicable.

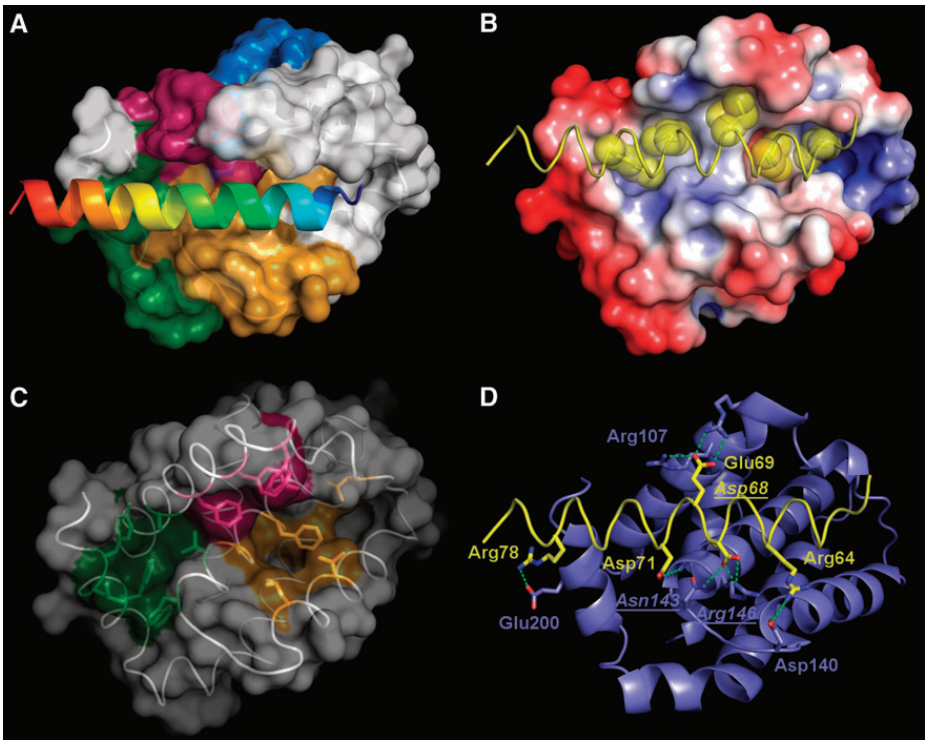

FIG. 5. Overview of the structural basis of Bcl-2 recognition of peptides. (A) Bcl-2 in complex with Bax BH3 peptide (PDB 2XA0). Bcl-2 shown as a surface, with the BH4 (*blue*), BH3 (*magenta*), BH1 (*yellow*), and BH2 (*green*) motifs highlighted. Bax BH3 peptide shown in cartoon view, colored as a *blue* to *red* rainbow from the N to the C terminus. **(B)** Electrostatic potential surface of Bcl-2 in complex with Bax BH3 peptide (*yellow*). Hydrophobic residues of the Bax BH3 peptide interacting with Bcl-2 shown as transparent spheres. Electrostatic potential shown as a *red-white-blue* gradient, from negative (*red*) to neutral (*white*) to positive (*blue*). **(C)** The three major binding sites within the Bcl-2 binding groove. **(D)** Hydrogen bonding interactions observed in the Bax BH3 complex with Bcl-2. Asn143 and Arg146 of Bcl-2, and Asp68 of Bax BH3 labeled in italics and underlined to indicate that these residues are involved in hydrogen bonds replicated in the majority of peptide complexes with Bcl-2. Electrostatic potential calculated using the PDB2PQR/APBS web server; figures generated in PyMOL. To see this illustration in color, the reader is referred to the web version of this article at www.liebertpub.com/ars

toward the BH1 domain and the C-terminal oriented toward the BH2 domain; peptide binding to Bcl-xL also displays the same directionality in all cases (7, 49, 93, 94, 132). Peptide binding to Bcl-2 appears largely mediated by a series of up to five hydrophobic residues (typically branched-chain amino acids) on one face of the peptide helix interacting with hydrophobic pockets along the Bcl-2 binding groove; this feature is present in all peptides cocrystallized with Bcl-2, both naturally derived and designed peptides. Three hydrophobic pockets of Bcl-2 with which peptides interact may be defined: a large pocket formed largely by BH1-derived residues (herein referred to as the ''BH1 pocket''; Leu119, Val133, Leu137, Ala149, and Phe153), a smaller pocket formed from near the end of the BH3 domain (herein referred to as the ''near-BH3 pocket''; Phe104, Tyr108, and Phe112), and a second large pocket formed from residues from the BH3, BH1, and BH2 domains (herein referred to as the ''BH2-incorporating pocket''; Ala100, Phe104, Trp144, Val148, Phe198, Leu201, and Tyr202). Peptides engaging all three pockets generally bind, from N to C terminal, the BH1 pocket with the most N-terminal hydrophobic residues (1–2 residues), the near-BH3 pocket with the middle hydrophobic residue, and then, the BH2-incorporating pocket with the final hydrophobic residues (1–2 residues). The HBx-derived peptide primarily engages the BH1 pocket, while the αBCL2 peptide uses a single leucine to engage the BH1 and near-BH3 pockets. In addition, a range of supporting hydrogen bonds are present in each structure, however, just two are present in all structures (except the HBx complex); these are the interactions of an acidic residue (typically aspartate) between the hydrophobic residues engaging the BH1 and BH2-incorporating pockets with Asn143 and Arg146 of Bcl-2. As the majority of hydrogen bonds in the peptide complexes with Bcl-2 are solvent exposed, these may be transient in typical cellular conditions. These hydrogen bonds are not replicated in any of the small molecules structurally characterized in complex with Bcl-2.

The structure of Bcl-2 has also been extensively characterized in complex with prospective small molecule inhibitors

(Table 1) (18, 134, 141, 149, 167, 173). Due to the similarities between the Bcl-2 and Bcl-xL binding pockets, many of these inhibitors have also been structurally characterized in complex with Bcl-xL; achieving selectivity for Bcl-2 over Bcl-xL is a major challenge in the design of clinically useful Bcl-2 inhibitors (8). Inhibitors structurally characterized in complex with Bcl-2 typically engage Bcl-2 in a remarkably similar way to the peptides, featuring long structures capable of binding to all three of the major pockets of the Bcl-2 binding groove; this also gives the majority of inhibitors molecular weights well over 500 Da, outside the typical range for small molecule drugs (103). Most inhibitors feature a small hydrophobic group, typically a single aromatic ring, bound to the BH1 pocket, a relatively straight structure comprising two rings connected in series, followed by a sulfonamide, lying between the BH1 and BH2-incorporating pockets, and a large flexible hydrophobic group interacting with the BH2-incorporating pocket (Fig. 6); these molecular features are largely carried over from the prototypical Bcl-2 inhibitor, ABT-737 (discussed in further detail in section IV: A Brief Overview of Bcl-2 Inhibitors: Past, Present, and Future). An exception to this is phenylpyrazole **2** (149), which does not engage the BH2-incorporating pocket; despite this, phenylpyrazole **2** exhibits ~10-fold selectivity for Bcl-2 over Bcl-xL, although its overall potency is eclipsed by ABT-737. Further modification of phenylpyrazole **2** yielded compound **18** (141), which does extend to the BH2-incorporating pocket and displays overall greater structural similarity to ABT-737.

Reactive oxygen species and their role in cell signaling

Reactive oxygen species (ROS) collectively refer to oxygen-derived (O_2) free radical and nonradical species (31). Radical ROS include superoxide anion ($O_2^{\cdot-}$), hydroxyl radical (HO•), peroxyl radical (ROO•), and alkoxyl radical (RO•) (61). Nonradical ROS include hydrogen peroxide (H_2O_2) and peroxynitrite ($ONOO^-$) (153, 172). A tight balance between intracellular ROS and ROS regulating systems is critical for maintaining cellular homeostasis (38). Therefore, excessive generation of ROS or deficient antioxidant capacity alters cellular redox state with profound effects on cell growth, proliferation, and survival. Homeostatic levels of ROS are maintained by both enzymatic and nonenzymatic antioxidants. A depletion or overexpression of these antioxidants can alter cell fate. For example, overexpression of antioxidant enzyme SOD2 can protect cells from tumor necrosis factor (TNF)-induced apoptosis (110). This protected the cell from H_2O_2-induced cell death and promoted cell survival. On the contrary, SOD1 has been shown to be a potential therapeutic target in some cancers (56). These contrasting roles for similar antioxidant enzymes demonstrate that the tight balance of ROS levels can determine whether cells will survive or undergo apoptosis. The dogmatic view that any increase in intracellular ROS is linked to cell injury and death has been challenged by substantial experimental evidence attributing a secondary messenger function to a mild increase in ROS or a ''pro-oxidant'' milieu. Alterations in the cellular redox metabolism is linked to aging (105) as well as a host of pathological states, such as cancer (102), Alzheimer's disease (112), Parkinson's disease (29), diabetes (71), atherosclerosis (62), nonalcoholic fatty liver disease (17), and asthma (43).

Intracellular sources of ROS. The mitochondrion serves as an important source of intracellular ROS [elegantly reviewed in (30)], mainly generating $O_2^{\cdot-}$ from Complex I (NADH dehydrogenase) (60) and Complex III (cytochrome *c* reductase) (120), when electrons derived from NADH or $FADH_2$ leak out on to and reduce molecular oxygen (121). The mitochondrial $O_2^{\cdot-}$ levels are regulated by the action of manganese superoxide dismutase (MnSOD) in the inner matrix that generates H_2O_2 in the process (118). H_2O_2 in turn can be scavenged by catalase, glutathione peroxidases, and peroxiredoxins (85). A second important site of $O_2^{\cdot-}$ generation, best exemplified in phagocytic cells, is the NADPH oxidase (NOX) family of enzymes. NOX enzymes are made up of six subunits: a Rho guanosine triphosphatase (GTPase) and five phagocytic oxidase subunits (gp91, p22phox, p40phox, p47phox, and p67phox) (91). Additional sources of ROS include $O_2^{\cdot-}$ from xanthine oxidases (88), cyclooxygenases or prostaglandin-endoperoxide synthase (PTGS) (55), the cytochrome P450 enzyme family (14), and nonheme lipoxygenases (21).

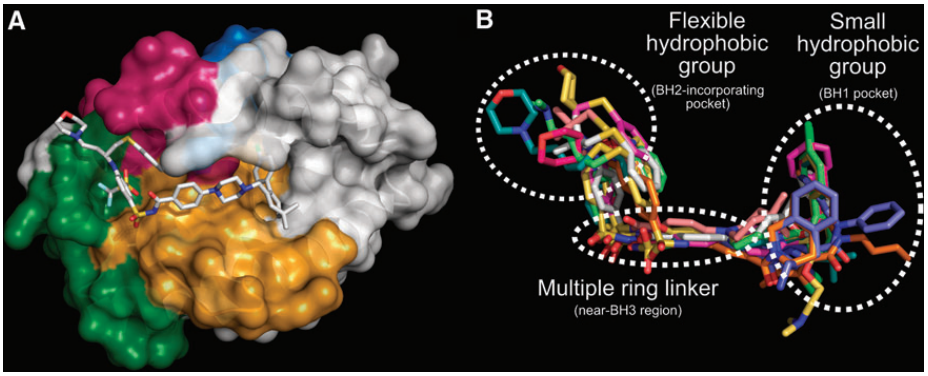

FIG. 6. Structural determinants of small molecule interactions with Bcl-2. (A) Bcl-2 in complex with navitoclax (ABT-263) (PDB 4LVT). **(B)** Overlay of all small molecules structurally characterized in complex with Bcl-2, highlighting key molecular features present in the majority of ligands. To see this illustration in color, the reader is referred to the web version of this article at www.liebertpub.com/ars

ROS as signaling molecules. It is now widely accepted that ROS function as important signaling molecules, implicated in nuclear factor kappa-light-chain-enhancer of activated B cells (NF-κB), mitogen-activated protein kinase (MAPK), Keap1-Nrf2-ARE, PI3K-Akt, Notch, and Wnt signaling pathways (20, 192). The various functional consequences of an altered redox milieu have been associated with a critical balance between the two major ROS molecules, $O_2^{\cdot -}$ and H_2O_2 (34, 145, 156). Whereas an overwhelming increase in either of these species results in cell injury and death, a tilt in the ratio in favor of $O_2^{\cdot -}$ confers a survival advantage, while a significant shift toward H_2O_2 creates a permissive environment for death execution (84, 144). For example, H_2O_2 is known to suppress Wnt/β-catenin signaling, an important survival and growth pathway, through a variety of mechanisms, including targeting the interaction between nucleoredoxin and disheveled (Dvl) (52) and *via* oxidative modification of the zinc-coordinating cysteines of tankyrase resulting in its inactivation (78). Interestingly, ROS-mediated Wnt signaling regulation of *BCL2* involving GSK3β/β-catenin has been reported on chronic exposure to Cr(VI) compounds (166). NF-κB signaling is closely linked to the transcriptional regulation of Bcl-2(22). Furthermore, Nrf2-ARE signaling can also regulate *BCL2* transcription through the antioxidant response elements (ARE) located within the *BCL2* promoter under conditions of oxidative stress (129). Interestingly, there is evidence of considerable cross talk between Nrf2 and NF-κB (181). For a more detailed account of the disparate functional outcomes on changes in intracellular ROS, please refer to these two comprehensive reviews (153, 154).

The cross talk between cellular redox status and Bcl-2

Apart from the role of Bcl-2 as a major regulator of apoptosis and cell fate, there is convincing experimental evidence to indicate a close interplay between cellular redox status and Bcl-2 expression. Of note, there are reported observations supporting both a pro-oxidant activity and an antioxidant activity of Bcl-2 (68, 197). Not only does the expression of Bcl-2 impact intracellular redox milieu but also a reciprocal regulation of Bcl-2 expression and/or function has been associated with intracellular ROS (26). For example, Bcl-2 has been shown to modulate intracellular ROS through increased catalase and glutathione peroxidase/reductase expression (46), as well as increased total levels of NADPH and reduced glutathione (GSH) (47). On the flip side of it, there is emerging and significant evidence that Bcl-2 expression impacts mitochondrial ROS metabolism to stimulate $O_2^{\cdot -}$ production, through increased COX activity, thereby creating a pro-oxidant environment that favors cell survival (26, 145).

The mRNA expression of *BCL2* is also tightly correlated with the expression of genes involved in ROS detoxification and production (Fig. 7). Many peroxidase elimination enzymes, such as peroxiredoxins, and other redox proteins, such as thioredoxins, exhibit a strong negative correlation with *BCL2*. This relationship may be due to an intrinsic mechanism through which cellular redox levels are in a constant pro-oxidant state, facilitating cancer cell survival. This pro-oxidant environment has been established as critical for the stability and antiapoptotic function of Bcl-2 (107). This hypothesis is also supported by a strong positive correlation between $O_2^{\cdot -}$ producing enzymes NADPH oxidases, NOX2 and NOX4. Interesting to note is the strong negative correlation between *BCL2* and *SOD1* across 18 of the 21 cancers surveyed, while SOD2 only exhibits a negative correlation in tumors with higher expression of *BCL2*. *SOD3*, the extracellular superoxide dismutase, was found to be positively correlated with Bcl-2 expression. The negative correlation of *BCL2* with *SOD1* in multiple cancers supports the notion that Bcl-2 may also function to maintain the pro-oxidant intracellular milieu necessary for cell survival (107). These data suggest that the expression of *BCL2* is strongly correlated with the expression of many antioxidant enzymes and the tight interplay between regulating intracellular redox levels plays an important role in cell fate, especially in the context

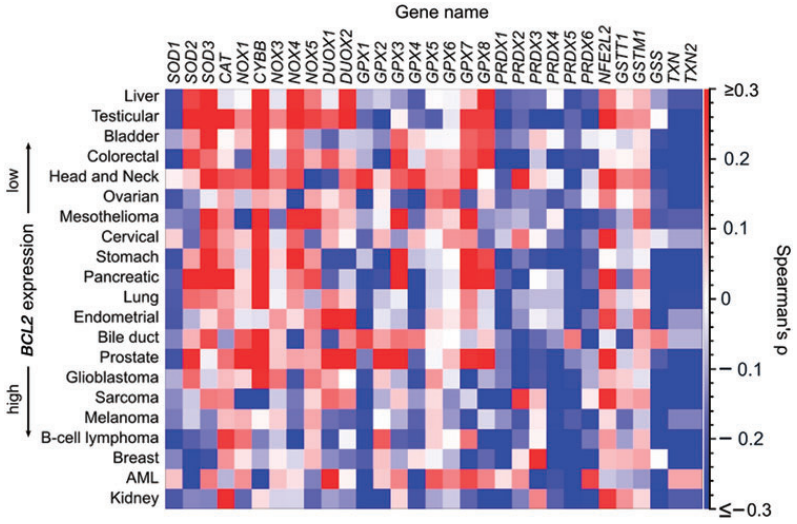

FIG. 7. Correlation between *BCL2* and antioxidant genes. Cancers were sorted from Bcl-2 high to low mean mRNA expression as obtained from TCGA data sets. Correlations (Spearman's ρ) are indicated as *red-white-blue* gradient (positive-none-negative). To see this illustration in color, the reader is referred to the web version of this article at www.liebertpub.com/ars

of carcinogenesis. A list of key publications in terms of Bcl-2 and the regulation of Bcl-2 by ROS have been described in Table 2.

Bcl-2 serves as a protector against oxidative insult. The protective role of Bcl-2 on an overt oxidative stress was originally discovered after Bcl-2-overexpressing cells demonstrated increased resistance to H_2O_2 and menadione-induced cell death (68). Subsequently, contradicting evidence has emerged to suggest that Bcl-2-mediated cellular protection from H_2O_2 was both independent (3) and dependent (73) on NF-κB activation. The latter study indicated that Bcl-2 induces constitutively active NF-κB signaling, resulting in the upregulation of γ-glutamylcysteine ligase, the first enzyme in the biosynthetic pathway of GSH (73). Transcriptional regulation of *BCL2* by NF-κB is now well characterized (22, 63). Bcl-2 is able to provide protection against other oxidizing species, including potassium cyanide, *tert*-butyl hydroperoxide (165), and γ-irradiation (122, 196).

The protective role of Bcl-2 also includes safeguarding against nitric oxide (NO)-induced apoptosis (116). Bcl-2-overexpressing murine macrophages exposed to NO donors, *S*-nitrosoglutathione (GSNO) and spermine-NO, and activators of inducible NO, lipopolysaccharide and interferon-γ, demonstrated apoptotic resistance to that of their *neo* control cells (116). While it has often been hypothesized that the mechanism by which Bcl-2 protects against oxidative insult is an intrinsic antioxidant property (68, 69, 95, 157), current evidence suggests that the antioxidant activity of Bcl-2 is merely a secondary effect (36, 54). Bcl-2 may be thought of as an ''antioxidant-by-proxy'' when in complex with GSH (197); this is discussed in detail in the following section (Mitochondrial-Dependent Regulation of Cellular Redox by Bcl-2). Cox and Hampton (36) demonstrated that Bcl-2 was able to protect cells against apoptotic (<200 μM), but not necrotic (>200 μM), doses of H_2O_2. These cells also showed no difference in the levels of GAPDH and peroxiredoxin 2 oxidation, while exhibiting evidence of increased micronuclei formation and genomic instability. This suggests that the antiapoptotic and pro-oncogenic role of Bcl-2 is through preventing the elimination of cells damaged by oxidation (36). Besides the apparent antioxidant activity of Bcl-2, recent evidence also suggests that Bcl-2 promotes cell survival by providing a pro-oxidant environment capable of supporting tumorigenesis (26, 170, 189).

Mitochondrial-dependent regulation of cellular redox by Bcl-2. Mitochondrial metabolism and its redox environment are highly dependent on Bcl-2 and GSH (111). In this respect, Bcl-2 regulates the mitochondrial pool of GSH and may act as a redox sensor. GSH may be displaced from Bcl-2 *via* competitive binding of BH3-only proteins (*e.g.*, Bim) and BH3 mimetics (*e.g.*, ABT-737) and induces mitochondrial dysfunction, oxidative stress, and cell death (197). Recently, it was demonstrated that Bcl-2 and 2-oxoglutarate carrier (OGC), a glutathione transport molecule, directly interact in the presence of GSH. This suggests that Bcl-2 and OGC participate in the transport of GSH to increase the glutathione

Table 2. List of Milestone Publications for Bcl-2 and Its Interplay with Reactive Oxygen Species

Key publications in the interplay between Bcl-2 and ROS

Authors	*Year*	*Journal*	*Publications*
Tsujimoto *et al.* (175)	1984	*Science*	Cloning of the chromosome breakpoint of neoplastic B cells with the t(14;18) chromosome translocation
Hockenbery *et al.* (67)	1990	*Nature*	Bcl-2 is an inner mitochondrial membrane protein that blocks programmed cell death
Hockenbery *et al.* (68)	1993	*Cell*	Bcl-2 functions in an antioxidant pathway to prevent apoptosis
Oltvai *et al.* (135)	1993	*Cell*	Bcl-2 heterodimerizes *in vivo* with a conserved homolog, Bax, that accelerates programmed cell death
Yin *et al.* (191)	1994	*Nature*	BH1 and BH2 domains of Bcl-2 are required for inhibition of apoptosis and heterodimerization with Bax
Muchmore *et al.* (119)	1996	*Nature*	X-ray and NMR structure of human Bcl-xL, an inhibitor of programmed cell death
Petros *et al.* (146)	2001	*PNAS*	Solution structure of the antiapoptotic protein bcl-2
HIldeman *et al.* (66)	2003	*PNAS*	Control of Bcl-2 expression by reactive oxygen species
Clement *et al.* (33)	2003	*Cell Death and Differentiation*	Decrease in intracellular superoxide sensitizes Bcl-2-overexpressing tumor cells to receptor and drug-induced apoptosis independent of the mitochondria
Oltersdorf *et al.* (134)	2005	*Nature*	An inhibitor of Bcl-2 family proteins induces regression of solid tumours
Cox and Hampton (36)	2007	*Carcinogenesis*	Bcl-2 over-expression promotes genomic instability by inhibiting apoptosis of cells exposed to hydrogen peroxide
Chen and Pervaiz (26)	2007	*Cell Death and Differentiation*	Bcl-2 induces pro-oxidant state by engaging mitochondrial respiration in tumor cells
Chen and Pervaiz (27)	2010	*Cell Death and Differentiation*	Involvement of cytochrome c oxidase subunits Va and Vb in the regulation of cancer cell metabolism by Bcl-2
Velaithan *et al.* (178)	2011	*Blood*	The small GTPase Rac1 is a novel binding partner of Bcl-2 and stabilizes its antiapoptotic activity
Low *et al.* (107)	2014	*Blood*	Ser70 phosphorylation of Bcl-2 by selective tyrosine nitration of PP2A-B56delta stabilizes its antiapoptotic activity

GTPase, guanosine triphosphatase; PP2A, protein phosphatase 2, ROS, reactive oxygen species.

mitochondrial pool, and a mechanism through which the mitochondria are protected from oxidative stress (184). It has been shown that Bcl-2 overexpression relocalized GSH to the nucleus, altering nuclear redox and blocking caspase activation to promote cell survival (179). Glutathione homeostasis regulated by Bcl-2 has been shown in MCF-7 breast cancer cells, where Bcl-2 overexpression increases glutathione content, although this was found to be independent of changes in gene expression related to glutathione synthesis. The inhibition of glutathione synthesis was able to overcome Bcl-2-induced cisplatin resistance (160).

The mechanisms by which Bcl-2 regulates mitochondrial respiration are vital for the understanding and interpretation of the overall cellular redox environment (106). Bcl-2 expression has been linked to the activity of cytochrome *c* oxidase (COX), the rate-limiting enzyme in mitochondrial electron transport chain (ETC), and thus vital in the regulation of mitochondrial respiration (26). Leukemic lymphoblastic cells (CEM cell line) overexpressing Bcl-2 exhibited higher levels of mitochondrial $O_2^{\cdot-}$, oxygen consumption, and higher COX activity, while the opposite was seen after the introduction of siRNA directed at *BCL2* (26, 27). It should be pointed out that the effect of Bcl-2 on mitochondrial COX activity and oxygen consumption is dependent on the redox milieu of the mitochondria. In this regard, under states of normoxia, Bcl-2 upregulates mitochondrial respiration and COX activity through increased import and assembly of COX subunits Va and Vb (27).

Evidence also suggests a possible interaction between Bcl-2 and COX Va, and higher expression of Bcl-2 promoted the mitochondrial translocation of COX Va. On the contrary, during states of overt oxidative stress induced on pharmacologically inhibition of mitochondrial ETC complexes, Bcl-2 overexpression elicited a negative effect on mitochondrial respiration and COX activity. The latter is corroborated by a recent report demonstrating that conditional *BCL2* knockout in murine pancreatic β cells exhibited increased superoxide dismutase (SOD) activity, increased mitochondrial respiration, and ultimately, cell death (2). The regulatory effect of Bcl-2 on mitochondrial respiration has also been reported in neuronal cells (77), in $SOD1^{G93A}$ mouse models of amyotrophic lateral sclerosis (138), rat ascites hepatoma (165), and hepatocytes (176).

Bcl-2-dependent increase in mitochondrial $O_2^{\cdot-}$ levels was also associated with the downstream activation of signal transducer and activator of transcription 3 (STAT3), which was mediated through a function of Rac1 (79). Overexpression of Bcl-2 induced phosphorylation of STAT3 on Tyr705, which was mediated by increased $O_2^{\cdot-}$. Furthermore, constitutively active mutants of STAT3 increased mitochondrial $O_2^{\cdot-}$ production (79). This study demonstrates the numerous signaling pathways that Bcl-2 can influence in regulating mitochondrial redox metabolism.

Bcl-2 family members have also been shown to mediate the switch between mitochondrial fusion and fission, which in turn suggests an influence of the family on mitochondrial metabolism and bioenergetics (183). Mammalian proteins Drp-1 and Fis-1 have been shown to be crucial in mitochondrial fission, while Mfn1/2 and OPA1 have been shown to play a role in fusion events. Bcl-2 family members Bax and Bak are required for mitochondrial fusion, where Bax interacts directly with Mfn2 (80). Bax has also been shown to colocalize with both Drp1 and Mfn2 during apoptosis and promotes mitochondrial fragmentation (164). Mammalian Bcl-2 is yet to be identified in having a role in either profusion or fission events (159), although it has also been described in the *Caenorhabditis elegans* homologue CED-9 (108). The study by Lu *et al.* found that CED-9 interacts with DRP-1 to promote mitochondrial fission. One could then speculate that Bcl-2 may function as a receptor for DRP-1 in a mammalian system to promote changes in mitochondrial dynamics and metabolism, although this is yet to be proven (159).

Taken together, it appears that the regulation of mitochondrial ROS extends into a variety of cellular contexts, and therefore, an alternative therapeutic strategy against refractory cancers could be to target key players involved in the regulation of mitochondrial metabolism to favorably modulate the cellular redox milieu for death execution (142).

Oxidative stress induced transcriptional regulation of *BCL2*. Early studies assessing the relationship between oxidative stress and *BCL2* expression indicated that acute oxidative stress induced by bright light in retinal rod receptor cells and cyclosporin A in human endothelial cells reduced *BCL2* expression (104). Later studies in t(14;18) lymphoma cells revealed that *BCL2* expression is tightly linked to NF-κB activation by the presence of cyclic AMP response element (CRE) and Sp1 binding sites (63). In prostate cancer cells, the overexpression of p50/p65 subunits of NF-κB increased expression of *BCL2*, and likewise, stimulation with TNF-α resulted in an increase in *BCL2* promoter activity (22). In U937 cells, NF-κB has also been implicated in ROS-induced upregulation of *BCL2* (37). *BCL2* transcriptional regulation has also been linked to Sonic hedgehog signaling through gli-1 and Wnt/β-catenin signaling by Wnt3a stimulation in osteoblast progenitor cells (5).

ROS have been shown to regulate *BCL2* gene expression indirectly, through which variations in cellular ROS levels lead to both an increase or decrease in *BCL2* gene expression depending on the cell context. Hildeman *et al.* (66) demonstrated that the addition of antioxidant manganese (III) tetrakis (4-benzoic acid)porphyrin (MnTBAP) to T cells *in vivo* significantly increased *BCL2* gene expression, although did not regulate other Bcl-2 family members, including Bcl-xL, Bad, and BimEL. MnTBAP also decreased intracellular ROS levels and inhibited death execution. ROS production was shown to be upstream of *BCL2* downregulation and to involve a Bim-independent mechanism. These results were mirrored by retroviral expression of catalase, which increased *BCL2* expression and rescued cells from oxidative stress-induced cell death (66). Similarly, H_2O_2 induced downregulation of Bcl-2 protein and gene expression, while concurrently upregulating Bax in cardiac myocytes (113). While the majority of studies have found that *BCL2* was downregulated when exposed to oxidative stress, Kaufmann *et al.* found that aged rats had increased *BCL2* expression in the hippocampus and cerebellum, which was a consequence of oxidative stress (81).

Bcl-2 regulation through oxidative stress was also demonstrated in hippocampal neurons, where the addition of H_2O_2 and glucose oxidase resulted in a decrease in *BCL2* gene and protein expression (150). The downregulation of Bcl-2 and concurrent increase in oxidative stress-induced apoptosis were able to be rescued through the addition of *N*-acetylcysteine (NAC), which subsequently increased Bcl-2 expression (151).

Transcriptional regulation of *BCL2* is partly controlled by cyclic AMP response element binding protein (CREB) (185). Oxidative insult through H_2O_2 or glucose oxidase decreased CREB activity on the *BCL2* promoter, which was reversed in the presence of NAC and manganese (III) tetrakis (1-methyl-4-pyridyl) porphyrin (MnTMPyP) (150). In rat liver, the induction of oxidative stress with triiodothyronine (T3) resulted in increased Bcl-2 expression, which was abrogated with the addition of α-tocopherol (vitamin E) (48). These studies demonstrate that Bcl-2 not only regulates the cellular redox milieu but oxidative stress itself can reciprocally regulate Bcl-2 expression as well.

Posttranslational modifications of Bcl-2 mediated by oxidative stress. The regulation of apoptosis by Bcl-2 has been shown to be mediated through various kinases, ligands, and oxidative stress signals due to changes in the expression and function of antioxidant enzymes. The regulation of Bcl-2 by posttranslational modification induced by oxidative stress is summarized in Figure 8. Bcl-2 suppression of apoptosis is partly facilitated through its direct interaction with extracellular signal-related kinase (ERK) 1/2 (109). This interaction can be regulated through oxidative stress, through which increased H_2O_2 induces Bcl-2 cysteine oxidation and the disruption of the ERK1/2-Bcl-2 complex. Mutagenesis indicated that the key residues regulating this interaction were Cys158 and Cys229. Cys158 is located adjacent to the Bcl-2 BH1 domain and is buried in both the monomeric and putative dimer forms (Fig. 2C) of the protein, although may become exposed during the conformational change that would be required to achieve dimer formation; Cys229 is suggested to be located within the Bcl-2 transmembrane helix. A C158A and C229A double mutant was resistant to oxidation, as well as H_2O_2-induced ubiquitination and subsequent degradation (109). The degradation of Bcl-2 through the ubiquitin-mediated pathway is also regulated by TNF-α-induced oxidative stress. H_2O_2 and TNF-α-induced oxidative stress resulted in degradation of Bcl-2, which was linked to the dephosphorylation of Ser87. The resultant dephosphorylation after TNF-α stimulation was demonstrated to be protein phosphatase 2 (PP2A) and PP2B independent (16). H_2O_2 has also been shown to regulate PKC-mediated Bcl-2 phosphorylation through a phospholipase Cγ1-dependent (PLC-γ1) mechanism. *Plcg1* null cells exhibited reduced viability and reduced Bcl-2 phosphorylation, following an insult with low levels of H_2O_2 (10).

Furthermore, c-Jun N-terminal kinase (JNK) activation can induce apoptosis through phosphorylation and inactivation of Bcl-2 (188). In response to menadione-induced oxidative stress, JNK phosphorylation and degradation of Bcl-2 were increased, but could be blocked on addition of NAC (193). Contrary to this study, Kelkel *et al.* demonstrated

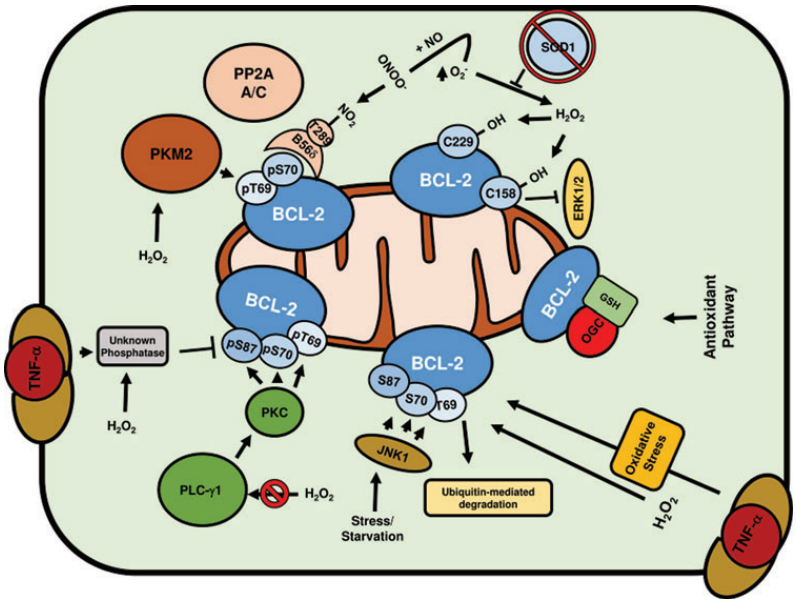

FIG. 8. Schematic of post-translational modifications of Bcl-2 due to oxidative stress. Posttranslational modifications of Bcl-2 occur under an insult of oxidative stress. Depletion or inhibition of SOD1 can initiate nitration of T289 on PP2A's B56δ subunit, preventing binding to the A/C subunits and the generation of the *holo*-enzyme. This prevents dephosphorylation of Ser70 of Bcl-2, stabilizing its antiapoptotic ability. Hydrogen peroxide can stabilize Bcl-2 through PKM2-mediated phosphorylation of T69, as well as causing its degradation through the ubiquitin-mediated pathway. PLC-γ1 mediates hydrogen peroxide resistance allowing phosphorylation of key residues by PKC and stabilization, while the opposite can also occur where hydrogen peroxide can stimulate dephosphorylation of Bcl-2. During cellular stress and starvation, JNK1 has also been shown to phosphorylate Bcl-2 at T69/S70/S87. Bcl-2 interacts with GSH and OGC to regulate the mitochondrial pool of GSH. GSH, glutathione; H_2O_2, hydrogen peroxide; NO, nitric oxide; $ONOO^-$, peroxinitrite; OGC, 2-oxoglutarate carrier; PLC-γ1, phospholipase Cc1-dependent; PPA2, protein phosphatase 2. To see this illustration in color, the reader is referred to the web version of this article at www.liebertpub.com/ars

that JNK activation and phosphorylation of Bcl-2 were independent, *via* the addition of the ROS-inducing agent diallyl tetrasulfide to U937 human histiocytic lymphoma cells (82). These opposing results suggest that redox-dependent post-translational modifications of Bcl-2 are highly dependent on the level of ROS. High levels of H_2O_2 primarily result in oxidation of Bcl-2 and degradation, while low levels initiate phosphorylation and stabilization of Bcl-2.

Functionally, ROS-mediated Bcl-2 phosphorylation has been linked to cell cycle transitions (39). The expression of phosphomimetic, gain-of-function Bcl-2 mutants (S70E and T69E/S70E/S87E) reduced intracellular ROS and inhibited G1/S cell cycle progression. The reduced G1/S phase progression was overridden by the addition of H_2O_2, through the downregulation of p27 and increased activation of Cdk2. Decreased ROS were attributed to increased SOD1 and catalase expression, which resulted in an antioxidant intracellular milieu on expression of the Bcl-2 phosphomimetics (39).

The relationship between the members of the SOD family and Bcl-2 has been explored in a number of cellular contexts. In spinal cord mitochondria, mutant SOD1 (G93A) and wild-type Bcl-2 have been shown to interact in the mitochondria, where they promote structural abnormalities and mitochondrial dysfunction. The mutant SOD1 causes a conformational change in Bcl-2, resulting in the exposure of the BH3 domain, which promotes mitochondrial toxicity (140). Low *et al.* (107) demonstrated that the stability and antiapoptotic function of Bcl-2 were enhanced in a pro-oxidant environment. Specifically, reducing SOD1 activity either by pharmacological means or siRNA directed at *SOD1* increased phosphorylation of Bcl-2 at Ser70 (pSer70). Increased levels of $ONOO^-$, as a result of increased $O_2^{\cdot-}$, induced selective nitration of Tyr289 of the B56δ subunit of PP2A. $ONOO^-$-induced nitration of PP2A at Tyr289 prevented the assembly of the holoenzyme involving the regulatory B subunit and the core A-C subunits. Importantly, SOD1 expression and Bcl-2 pSer70 were found to be negatively correlated *in vivo*; high Bcl-2 p70 could predict a poor patient prognosis. Furthermore, *in vitro* studies showed an association between high levels of Bcl-2 pSer70 and chemoresistance. This suggests the possibility for the use of redox modulators as chemosensitizers in the treatment of lymphomas (107). The study by Low *et al.* provided mechanistic insight to observations published previously by Zhao *et al.*, demonstrating that Bcl-2 pSer70 was required for protection against oxidative stress, which was abolished through the activation of PP2A (194).

Liang *et al.* (100) recently demonstrated that under H_2O_2-induced oxidative stress, Bcl-2 is stabilized through phosphorylation of Thr69 (pThr69) by pyruvate kinase M2 isoform (PKM2), promoting tumorigenesis in glioma cells. Oxidative stress induces mitochondrial translocation and a potential conformational change in PKM2, resulting in the phosphorylation of Bcl-2 at Thr69. This potential conformational change may be facilitated through the ATPase activity of HSP90α1 and permits the binding of PKM2 to Bcl-2. pThr69 prevents ubiquitination by a Cul3-based ubiquitin E3 ligase, thus preventing its degradation. This HSP90α1-PKM2-Bcl-2 axis is crucial in stabilizing the antiapoptotic function of Bcl-2 and driving tumorigenesis (100).

The Bcl-2:Beclin1 interaction has been demonstrated to be potentially redox dependent. Bcl-2/adenovirus E1B 19-kDa protein-interacting protein 3 (BNIP3) is a proapoptotic protein, whose expression is regulated by HIF-1α. It functions as a redox sensor during times of prolonged hypoxia-induced oxidative stress. Dimerization of BNIP3 was shown to be sensitive to H_2O_2-induced oxidative stress (87). Hypoxia-induced BNIP3 expression has been demonstrated to disrupt the interaction between Bcl-2 and Beclin 1 to induce autophagy (12). These studies show that apoptosis and autophagy are clearly linked to specific Bcl-2 binding partners in various cellular components. To that end, *S*-nitrosylation of Bcl-2 negatively regulates autophagy; nitrosylation of Cys158 and Cys229 stabilizes the interaction between Bcl-2 and Beclin1, thereby inhibiting Beclin1 activity and as a result decreasing autophagic flux (187). This effect is reversed on addition of ABT-737, aminoguanidine (NO inhibitor), and a redox-inactive Bcl-2 double-mutant (C158A/C299A). Interestingly, these cysteine residues were previously shown to be prone to H_2O_2-induced oxidation (109).

Furthermore, *S*-nitrosylation of Bcl-2 was previously demonstrated to inhibit its ubiquitin-mediated proteasomal degradation. This NO-mediated effect was independent of Ser87 phosphorylation and decreased cellular apoptosis (9). These studies highlight the importance of NO-driven signaling and Bcl-2 in the regulation of autophagic and apoptotic signaling. NO has also been demonstrated to increase carbonylation of Bcl-2 (19), and IL-1β-induced NO production increased Bcl-2 carbonylation, which preceded its downregulation. The downregulation of Bcl-2 coincided with an increase in NO-mediated DNA fragmentation (19). This is contrary to the previously mentioned studies where NO was associated with resistance to apoptosis, suggesting that the regulation of cell fate by NO is dependent on the precise post-translational modification of Bcl-2.

Bcl-2 and peroxide eliminating enzymes. A study by Gouaze *et al.* (58) demonstrated that glutathione peroxidase-1 (GPx1) overexpressing cells were resistant to CD95-induced apoptosis. T47D cells overexpressing GPx1 exhibited lower levels of ROS and Bcl-2. Similarly, Clement *et al.* (33) showed that Bcl-2 overexpression blocked CD95-induced cell death, which was restored on NOX inhibition or overexpression of dominant-negative Rac1, decreasing overall levels of $O_2^{\cdot-}$. To that end, Rac1 has also been demonstrated to increase $O_2^{\cdot-}$ and inhibit apoptosis in melanoma and bladder carcinoma cells (143). Further studies provided evidence for an interaction between Bcl-2 and Rac1 in leukemic cells that increased intracellular $O_2^{\cdot-}$, thus creating a pro-oxidant environment that favors cell survival and/or inhibits apoptotic execution (178). Synthetic BH3 peptides and BH3 mimetics were able to block the interaction of Rac1 and Bcl-2, decrease $O_2^{\cdot-}$ production, and sensitize human leukemia cells to chemotherapeutics. Previously, it was also demonstrated that Rac1 was needed for the phosphorylation of Bcl-2 by the JNK/stress-activated protein kinase (JNK/SAPKβ) p54-SAPKβ (114).

Peroxiredoxins are functional antioxidant enzymes that control intracellular peroxide levels. *BCL2* mRNA expression has been shown to exhibit a primarily negative correlation with the five peroxiredoxins (*PRDX1*, *PRDX3*, *PRDX4*, *PRDX5*, and *PRDX6*) in a wide range of primary tumor samples. In lung cancer either a weak or negative correlation is observed (Fig. 7). In A549 lung cancer cells with gefitinib resistance (A549/GR), shRNA knockdown of *PRDX2* resulted

in a decrease in Bcl-2 expression and concurrent increase in peroxide levels in the cell, culminating in cell death (89). The change in correlation in gefitinib-resistant cells can be hypothesized to be directly due to JNK/ROS activation, both of which were altered compared to the A549 cells. H_2O_2 also protected cardiomyocytes from oxidative stress-induced apoptosis, which was associated with an increase in Bcl-2. H_2O_2-induced oxidative stress caused a decrease in the level of both Prx2 and Bcl-2, showing a strong correlation between intracellular peroxide levels and Bcl-2 expression (195). Bcl-2 expression has also been shown to be associated with members of the thioredoxin family. The use of antisense *BCL2* therapy in neuroblastoma cells demonstrated that decreasing levels of Bcl-2 were associated with increasing levels of thioredoxin. This seems to be consistent across a range of tumors (Fig. 7) and may involve a cellular compensatory mechanism when cells are undergoing oxidative stress (99).

Redox-dependent regulation of Bcl-2 in viral infection. Intracellular regulation of cellular redox has been shown to be an important factor in viral establishment, replication, and progression (11). A pro-oxidant environment has been demonstrated during infection with influenza (64), human immunodeficiency virus (HIV) (65), and hepatitis C (57). Bcl-2 has been demonstrated to influence cellular redox and alter viral replication in various settings. During influenza A replication, cellular levels of GSH are decreased, resulting in a pro-oxidant environment. Cells overexpressing Bcl-2 exhibited higher levels of GSH and produced less virus (126). Influenza A infection has also been shown to increase ROS in an NOX-4-dependent manner (6). Mechanistically, viral activation in Bcl-2^+ cells induced p38MAPK-mediated phosphorylation of Bcl-2 at Thr56 and Ser87, resulting in cell death. siRNA-mediated knockdown of *BCL2* resulted in increased influenza A replication and viral ribonucleoprotein (vRNP) export (125). In asymptomatic HIV-infected patients, H_2O_2 production was increased in monocytes with parallel downregulation in thioredoxin and Bcl-2. These reductions were suggested to be a result of significantly increased oxidative stress (45). These studies highlight the importance of redox regulation in altering Bcl-2-mediated cell fate in viral infections. The role of Bcl-2 in viral infections and its interaction with viral proteins is comprehensively reviewed by Alibek *et al.* (4) Redox in viral infections have previously been reviewed elsewhere (101, 123, 168).

A brief overview of Bcl-2 inhibitors: past, present, and future

As the discovery and development of Bcl-2 inhibitors have been recently comprehensively reviewed (8, 98), this section focuses primarily on molecules that have been or are currently under investigation through clinical trials (Fig. 9).

Oblimersen is an antisense oligonucleotide targeted to the *BCL2* mRNA, thus preventing Bcl-2 protein expression (41). It was the first molecule against Bcl-2 to be investigated clinically. Oblimersen has been extensively investigated in clinical trials in a wide variety of solid tumors and blood cancers, and in combination with a wide variety of cancer therapeutics, however, its use as a single agent or in combination have not been approved for any clinical indication (51). The related molecule SPC2996 has also been investigated in clinical trials, which failed to demonstrate effective downregulation of Bcl-2 expression (42). Oblimersen was demonstrated in PC3 cells to increase the oxidation of nuclear DNA, measured by 8-hydroxy-2′-deoxyguanosine staining,

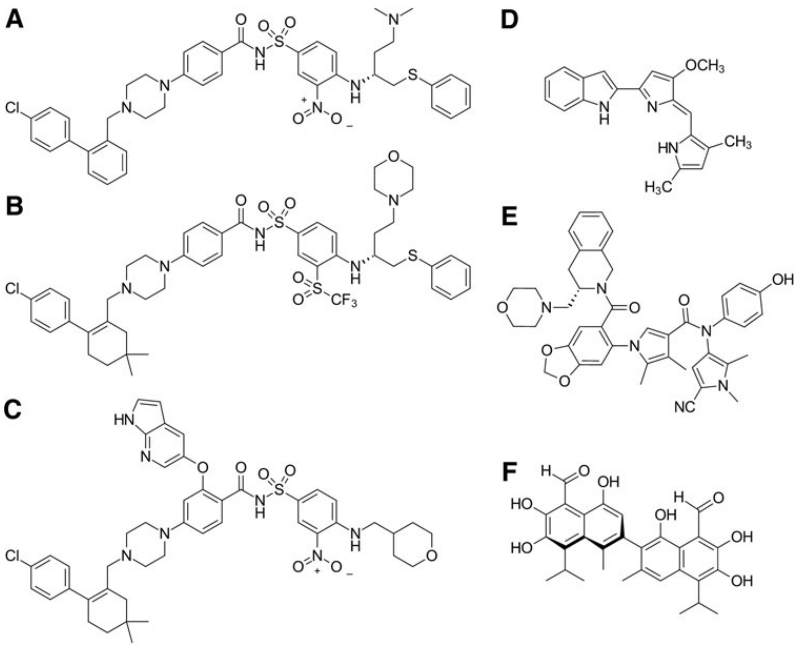

FIG. 9. 2D structures of small molecule Bcl-2 inhibitors. (A) ABT-737. **(B)** Navitoclax (ABT-263). **(C)** Venetoclax (ABT-199). **(D)** Obatoclax. **(E)** Representative molecule from the patent describing the production of S55746-related molecules. **(F)** (-)-Gossypol (AT-101).

suggesting that cell death was due to an ROS-dependent mechanism (90).

ABT-737, which is generally regarded as the prototypical small molecule Bcl-2 family protein inhibitor, was first reported in 2005 (134). ABT-737 was discovered through a SAR by NMR (structure-activity relationship by nuclear magnetic resonance) approach, through which small organic ''fragment'' molecules (<200 Da) were assessed for weak/moderate binding to Bcl-2 *via* NMR approaches (primarily saturation transfer difference spectroscopy and heteronuclear single quantum coherence spectroscopy), and subsequently ''assembled'' to generate molecules capable of tightly binding to Bcl-2. ABT-737 targets the hydrophobic peptide-binding groove of Bcl-family proteins nonselectively. The lack of oral bioavailability of ABT-737 has limited its clinical development, instead prompting the development of alternatives. Hepatocellular carcinoma (HCC) cells with high Bcl-2 expression demonstrated resistance to ABT-737 by suppressing the ROS-JNK pathway. In HCC cells expressing low levels of Bcl-2, apoptosis was induced after treatment with ABT-737 through increased ROS levels and activation of the ROS-JNK pathway (128). This study demonstrates that high levels of Bcl-2 can determine the effectiveness of ABT-737 in a ROS-dependent mechanism.

Navitoclax (ABT-263) is an orally bioavailable analog of ABT-737 that has progressed to Phase II clinical trials. Navitoclax features three modifications relative to ABT-737: (i) replacement of the nitro group with a triflyl group; (ii) replacement of the dimethylamine with a morpholine group; and (iii) replacement of the 4-chlorobiphenyl group with a 1-(4-chlorophenyl)-4,4-dimethyl-cyclohexene group (137). These modifications enhance oral bioavailability relative to ABT-737, while maintaining protein binding and cellular efficacy. Navitoclax elicits thrombocytopenia as a result of Bcl-xL inhibition (32, 158, 186), which limits its tolerated dose and has delayed its clinical development; nonetheless, trials involving navitoclax or combinations thereof are ongoing, largely against blood cancers.

Venetoclax (ABT-199, GDC-0199) is a Bcl-2-selective inhibitor derived from navitoclax, currently approved for the treatment of chronic lymphocytic leukemia. Venetoclax features three modifications relative to navitoclax: (i) replacement of the triflyl group with a nitro group (as in ABT-737); (ii) substitution of the *para*-aminobenzamide motif with a 1*H*-pyrrolo[2,3-*b*]pyridine-5-yloxy group; (iii) replacement of the morpholine and thiophenol arms with a methyl-tetrahydropyran group. Venetoclax retains the oral bioavailability of navitoclax, but is over 100-fold more selective for Bcl-2 over Bcl-xL, thus averting thrombocytopenia induced by navitoclax (167). Current clinical trials involving venetoclax are largely focused on broadening its application to include a wider variety of blood cancers, and involve both therapeutic combinations and venetoclax monotherapy (98).

Obatoclax (GX15-070) is a nonselective Bcl-2 family protein inhibitor, initially identified for its ability to inhibit Mcl-1 (127). Obatoclax features a comparatively simple scaffold compared to ABT-737 and related molecules; combined with its nonselectivity, this suggests that obatoclax may only interact with part of the binding groove present in Bcl-2 family proteins. Obatoclax has been evaluated for childhood cancers (both blood cancers and solid tumors), blood cancers in adults, and lung cancers in adults. Phase I studies indicated that the drug was well tolerated in patients with blood cancers (162), solid tumors (76), and exhibited modest single-agent activity (130). Obatoclax has been demonstrated to induce cell death in oral squamous cell carcinoma cells through a mitochondrial-dependent oxidative stress-induced mechanism (171). However, Phase II studies have generally failed to demonstrate its clinical usefulness (59, 136, 163). Its further development was discontinued in 2013.

S55746 (BCL-201, Servier-1) is an inhibitor developed by Servier selective for Bcl-2, built on the previously reported low-affinity, but highly Bcl-2-selective, phenylpyrazole molecule series (149). Preliminary results from a clinical trial of S55746 in patients with relapsed or refractory non-Hodgkin lymphoma suggest that S55746 monotherapy is safe, tolerable, and efficacious (92). Servier has previously reported S44563, a dual Bcl-2/Bcl-xL inhibitor, an analog of ABT-737 with conformational restriction on the phenylpiperazine region (124). Given this molecule's high similarity to ABT-737, it may also exhibit similarly poor oral bioavailability, which may have prompted the identification of alternative scaffolds and the ultimate development of S55746.

(-)-Gossypol (AT-101), a terpenoid phenol derived from the cotton plant, has been shown to act as a weak inhibitor of Bcl-2 and Bcl-xL (133). In addition to acting as a BH3 mimetic, AT-101 also appears to impair DNA repair mediated by APE1, a redox-active enzyme that is a known binding partner for Bcl-2 (152, 155). Unlike ABT-737 and related molecules, which directly prevent peptide binding to Bcl-2, (-)-gossypol induces a conformational change in Bcl-2 from an antiapoptotic to a proapoptotic state (96). (-)-Gossypol was evaluated in combination with androgen deprivation therapy for the treatment of castration-sensitive metastatic prostate cancer in a Phase II clinical trial (169); the results suggested this combination was not worth further development. (-)-Gossypol has also been evaluated for the treatment of progressive or recurrent glioblastoma multiforme; the majority of patients (62.5%) exhibited disease progression in the trial (72). (-)-Gossypol has been demonstrated to potentiate cell death induced by temozolomide (180); a Phase I clinical trial investigating this combination in the treatment of glioblastoma multiforme has been completed, but results are not currently available (23).

APG-1252 is a dual selective Bcl-2/Bcl-xL inhibitor currently under development by Ascentage Pharma Group. Limited details of this molecule have been made publicly available, however, as of this writing, recruitment is currently underway for a clinical trial of APG-1252 in patients with small-cell lung cancer and other solid tumors (70).

Perspective

It has been more than 30 years since the discovery of Bcl-2 and its association with drug resistance and aggressive hematopoietic malignancies. Over the years, the structural and functional biology of this remarkable protein has been unraveled. These pursuits have resulted in the discovery of a number of related proteins with opposing biological activities and grouped under a broader family, the Bcl-2 family. It is now well established that the balance between the pro- and

antiapoptotic members of the family is critical in cell fate decisions, which is a function of physical interactions between proteins from within and outside of the family. While the canonical antiapoptotic activity of Bcl-2 is associated with its ability to prevent MOMP by sequestering Bax and Bak from oligomerizing at the mitochondria, recent evidence also points to a redox-dependent regulation of cell fate by Bcl-2, which appears to involve its post-translational modification. Furthermore, the altered gene expression and mutational landscape in a host of human cancer, not limited to hematopoietic malignancies, underscore the importance of Bcl-2 as an important ''pro-oncogenic'' protein.

Based on its interacting domains, there has been a continuous focus on developing small molecule inhibitors to overcome chemotherapy resistance induced on Bcl-2 overexpression. Bcl-2 expression has been used as a biomarker for patient response to chemotherapy. Could we now extend this to patient profiles of Bcl-2 expression in terms of ROS high and ROS low, and would this have a stronger predictive power?

There is a large body of evidence that directly links Bcl-2 and cellular redox. Earlier observations suggested an antioxidant role for Bcl-2, however, more recent work indicates a remarkable dichotomy when it comes to Bcl-2 and its effects on cellular redox metabolism. These divergent effects appear to be a function of cellular redox status itself. As such, the effect might differ under states of normoxia, hypoxia, and oxidative stress. To complicate matters further, the same ROS can have seemingly opposite effects on the antiapoptotic activity of Bcl-2. H_2O_2 in one context can cause degradation through oxidation of cysteines and promote cell death, and on the other hand can cause increased stability and promote cell survival. Similarly, the effect of an increase in NO and its reaction product with O_2^{-}, $OONO^{-}$, could be associated with carbonylation or S-NO modification. Interestingly, an altered redox milieu impacts post-translational state of Bcl-2, such as its phosphorylation, which could have different functional consequences depending on whether the phosphorylation is multisite (inhibits its activity) or monosite as with serine 70 (stabilizes its activity). Based on these outcomes, it is imperative to clearly delineate the mechanisms behind the opposing effects of an altered redox state on Bcl-2 biology, particularly from the standpoint of its role in promoting chemotherapy resistance in cancer. This is even more important as many clinically approved drugs induce increases in intracellular ROS, which could fuel the process of carcinogenesis and its progression by promoting Bcl-2 stability.

A number of promising small molecules are being developed and are undergoing clinical evaluation, however, selectivity remains a major issue. The early generation of Bcl-2 inhibitors, based on BH3 domain interaction, did not show the level of stringency in terms of targeting the specific antiapoptotic protein within the family. More recent approaches, such as in the case of venetoclax, appear to have addressed this issue. One possible scenario still needs attention: the reciprocal upregulation of another antiapoptotic member on specific inhibition of one. For example, is it possible that specific inhibition of Bcl-2 might activate the compensatory upregulation of Mcl-1 or *Bcl-xL*? Future strategies could also leverage on the noncanonical function of Bcl-2 in terms of regulating cellular redox status. In this respect, one might envision the potential application of modalities that favorably tailor the cellular redox milieu for death execution as well as overcome the inhibitory effect on putative tumor suppressors, such as the phosphatase PP2A.

Acknowledgments

Sebastian Pohl is supported by funds from the Rotary Club of Belmont, Australian Rotary Health Research Fund, and Curtin University School of Biomedical Sciences. Mark Agostino is a recipient of a Raine Priming Grant (Raine Medical Research Foundation), Operational Research Support from the Curtin Institute for Computation, and a Curtin Research Fellowship. Arun Dharmarajan is supported by strategic research funds from the School of Biomedical Sciences (Curtin University), Commercialisation Advisory Board of Curtin University and Cancer Council of Western Australia. Shazib Pervaiz is supported by research grants from the National Medical Research Council of Singapore.

References

1. Adrain C, Creagh EM, and Martin SJ. Apoptosis-associated release of Smac/DIABLO from mitochondria requires active caspases and is blocked by Bcl-2. *EMBO J* 20: 6627–6636, 2001.
2. Aharoni-Simon M, Shumiatcher R, Yeung A, Shih AZ, Dolinsky VW, Doucette CA, and Luciani DS. Bcl-2 regulates reactive oxygen species signaling and a redox-sensitive mitochondrial proton leak in mouse pancreatic beta-cells. *Endocrinology* 157: 2270–2281, 2016.
3. Albrecht H, Tschopp J, and Jongeneel CV. Bcl-2 protects from oxidative damage and apoptotic cell death without interfering with activation of NF-kappa B by TNF. *FEBS Lett* 351: 45–48, 1994.
4. Alibek K, Irving S, Sautbayeva Z, Kakpenova A, Bekmurzayeva A, Baiken Y, Imangali N, Shaimerdenova M, Mektepbayeva D, Balabiyev A, and Chinybayeva A. Disruption of Bcl-2 and Bcl-xL by viral proteins as a possible cause of cancer. *Infect Agent Cancer* 9: 44, 2014.
5. Almeida M, Han L, Bellido T, Manolagas SC, and Kousteni S. Wnt proteins prevent apoptosis of both uncommitted osteoblast progenitors and differentiated osteoblasts by beta-catenin-dependent and -independent signaling cascades involving Src/ERK and phosphatidylinositol 3-kinase/AKT. *J Biol Chem* 280: 41342–41351, 2005.
6. Amatore D, Sgarbanti R, Aquilano K, Baldelli S, Limongi D, Civitelli L, Nencioni L, Garaci E, Ciriolo MR, and Palamara AT. Influenza virus replication in lung epithelial cells depends on redox-sensitive pathways activated by NOX4-derived ROS. *Cell Microbiol* 17: 131–145, 2015.
7. Ambrosi E, Capaldi S, Bovi M, Saccomani G, Perduca M, and Monaco HL. Structural changes in the BH3 domain of SOUL protein upon interaction with the anti-apoptotic protein Bcl-xL. *Biochem J* 438: 291–301, 2011.
8. Ashkenazi A, Fairbrother WJ, Leverson JD, and Souers AJ. From basic apoptosis discoveries to advanced selective BCL-2 family inhibitors. *Nat Rev Drug Discov* 16: 273–284, 2017.
9. Azad N, Vallyathan V, Wang L, Tantishaiyakul V, Stehlik C, Leonard SS, and Rojanasakul Y. S-nitrosylation of Bcl-2 inhibits its ubiquitin-proteasomal degradation. A novel antiapoptotic mechanism that suppresses apoptosis. *J Biol Chem* 281: 34124–34134, 2006.

10. Bai XC, Deng F, Liu AL, Zou ZP, Wang Y, Ke ZY, Ji QS, and Luo SQ. Phospholipase C-gamma1 is required for cell survival in oxidative stress by protein kinase C. *Biochem J* 363: 395–401, 2002.
11. Beck MA, Handy J, and Levander OA. The role of oxidative stress in viral infections. *Ann N Y Acad Sci* 917: 906–912, 2000.
12. Bellot G, Garcia-Medina R, Gounon P, Chiche J, Roux D, Pouyssegur J, and Mazure NM. Hypoxia-induced autophagy is mediated through hypoxia-inducible factor induction of BNIP3 and BNIP3 L via their BH3 domains. *Mol Cell Biol* 29: 2570–2581, 2009.
13. Berger S, Procko E, Margineantu D, Lee EF, Shen BW, Zelter A, Silva D-A, Chawla K, Herold MJ, Garnier J-M, Johnson R, MacCoss MJ, Lessene G, Davis TN, Stayton PS, Stoddard BL, Fairlie WD, Hockenbery DM, and Baker D. Computationally designed high specificity inhibitors delineate the roles of BCL2 family proteins in cancer. *eLife* 5: e20352, 2016.
14. Bondy SC and Naderi S. Contribution of hepatic cytochrome P450 systems to the generation of reactive oxygen species. *Biochem Pharmacol* 48: 155–159, 1994.
15. Breckenridge DG and Xue D. Regulation of mitochondrial membrane permeabilization by BCL-2 family proteins and caspases. *Curr Opin Cell Biol* 16: 647–652, 2004.
16. Breitschopf K, Haendeler J, Malchow P, Zeiher AM, and Dimmeler S. Posttranslational modification of Bcl-2 facilitates its proteasome-dependent degradation: molecular characterization of the involved signaling pathway. *Mol Cell Biol* 20: 1886–1896, 2000.
17. Browning JD and Horton JD. Molecular mediators of hepatic steatosis and liver injury. *J Clin Invest* 114: 147–152, 2004.
18. Bruncko M, Oost TK, Belli BA, Ding H, Joseph MK, Kunzer A, Martineau D, McClellan WJ, Mitten M, Ng S-C, Nimmer PM, Oltersdorf T, Park C-M, Petros AM, Shoemaker AR, Song X, Wang X, Wendt MD, Zhang H, Fesik SW, Rosenberg SH, and Elmore SW. Studies leading to potent, dual inhibitors of Bcl-2 and Bcl-xL. *J Med Chem* 50: 641–662, 2007.
19. Cahuana GM, Tejedo JR, Jimenez J, Ramirez R, Sobrino F, and Bedoya FJ. Nitric oxide-induced carbonylation of Bcl-2, GAPDH and ANT precedes apoptotic events in insulin-secreting RINm5F cells. *Exp Cell Res* 293: 22–30, 2004.
20. Caliceti C, Nigro P, Rizzo P, and Ferrari R. ROS, Notch, and Wnt signaling pathways: crosstalk between three major regulators of cardiovascular biology. *Biomed Res Int* 2014: 318714, 2014.
21. Catalano A, Rodilossi S, Caprari P, Coppola V, and Procopio A. 5-Lipoxygenase regulates senescence-like growth arrest by promoting ROS-dependent p53 activation. *EMBO J* 24: 170–179, 2005.
22. Catz SD and Johnson JL. Transcriptional regulation of bcl-2 by nuclear factor kappa B and its significance in prostate cancer. *Oncogene* 20: 7342–7351, 2001.
23. Centre SKCC. 2017. Gossypol (AT-101) and Temozolomide With or Without Radiation Therapy in Treating Patients With Newly Diagnosed Glioblastoma Multiforme. https://clinicaltrials.gov/ct2/show/NCT00390403. Access date August 21, 2017.
24. Cerami E, Gao J, Dogrusoz U, Gross BE, Sumer SO, Aksoy BA, Jacobsen A, Byrne CJ, Heuer ML, Larsson E, Antipin Y, Reva B, Goldberg AP, Sander C, and Schultz N. The cBio cancer genomics portal: an open platform for exploring multidimensional cancer genomics data. *Cancer Discov* 2: 401–404, 2012.
25. Checco JW, Lee EF, Evangelista M, Sleebs NJ, Rogers K, Pettikiriarachchi A, Kershaw NJ, Eddinger GA, Belair DG, Wilson JL, Eller CH, Raines RT, Murphy WL, Smith BJ, Gellman SH, and Fairlie WD. a/b-peptide foldamers targeting intracellular protein-protein interactions with activity in living cells. *J Am Chem Soc* 137: 11365–11375, 2015.
26. Chen ZX and Pervaiz S. Bcl-2 induces pro-oxidant state by engaging mitochondrial respiration in tumor cells. *Cell Death Differ* 14: 1617–1627, 2007.
27. Chen ZX and Pervaiz S. Involvement of cytochrome c oxidase subunits Va and Vb in the regulation of cancer cell metabolism by Bcl-2. *Cell Death Differ* 17: 408–420, 2010.
28. Cheng EH, Wei MC, Weiler S, Flavell RA, Mak TW, Lindsten T, and Korsmeyer SJ. BCL-2, BCL-X(L) sequester BH3 domain-only molecules preventing BAX- and BAK-mediated mitochondrial apoptosis. *Mol Cell* 8: 705–711, 2001.
29. Choi DH, Cristovao AC, Guhathakurta S, Lee J, Joh TH, Beal MF, and Kim YS. NADPH oxidase 1-mediated oxidative stress leads to dopamine neuron death in Parkinson's disease. *Antioxid Redox Signal* 16: 1033–1045, 2012.
30. Chong SJ, Low IC, and Pervaiz S. Mitochondrial ROS and involvement of Bcl-2 as a mitochondrial ROS regulator. *Mitochondrion* 19 Pt A: 39–48, 2014.
31. Circu ML and Aw TY. Reactive oxygen species, cellular redox systems, and apoptosis. *Free Radic Biol Med* 48: 749–762, 2010.
32. Clearly JM, Lima CM, Hurwitz HI, Montero AJ, Franklin C, Yang J, Graham A, Busman T, Mabry M, Holen K, Shapiro GI, and Uronis H. A phase I clinical trial of navitoclax, a targeted high-affinity Bcl-2 family inhibitor, in combination with gemcitabine in patients with solid tumors. *Invest New Drugs* 32: 937–945, 2014.
33. Clement MV, Hirpara JL, and Pervaiz S. Decrease in intracellular superoxide sensitizes Bcl-2-overexpressing tumor cells to receptor and drug-induced apoptosis independent of the mitochondria. *Cell Death Differ* 10: 1273–1285, 2003.
34. Clement MV and Pervaiz S. Intracellular superoxide and hydrogen peroxide concentrations: a critical balance that determines survival or death. *Redox Rep* 6: 211–214, 2001.
35. Cooke PW, James ND, Ganesan R, Burton A, Young LS, and Wallace DM. Bcl-2 expression identifies patients with advanced bladder cancer treated by radiotherapy who benefit from neoadjuvant chemotherapy. *BJU Int* 85: 829–835, 2000.
36. Cox AG and Hampton MB. Bcl-2 over-expression promotes genomic instability by inhibiting apoptosis of cells exposed to hydrogen peroxide. *Carcinogenesis* 28: 2166–2171, 2007.
37. Cristofanon S, Morceau F, Scovassi AI, Dicato M, Ghibelli L, and Diederich M. Oxidative, multistep activation of the noncanonical NF-kappaB pathway via disulfide Bcl-3/p50 complex. *FASEB J* 23: 45–57, 2009.
38. D'Autreaux B and Toledano MB. ROS as signalling molecules: mechanisms that generate specificity in ROS homeostasis. *Nat Rev Mol Cell Biol* 8: 813–824, 2007.

39. Deng X, Gao F, and May WS, Jr. Bcl2 retards G1/S cell cycle transition by regulating intracellular ROS. *Blood* 102: 3179–3185, 2003.
40. Dewson G, Kratina T, Sim HW, Puthalakath H, Adams JM, Colman PM, and Kluck RM. To trigger apoptosis, Bak exposes its BH3 domain and homodimerizes via BH3:groove interactions. *Mol Cell* 30: 369–380, 2008.
41. Dias N and Stein CA. Potential role of antisense oligonucleotides in cancer therapy. The example of Bcl-2 antisense oligonucleotides. *Eur J Pharmaceut Biopharmaceut* 54: 263–269, 2002.
42. Dürig H, Dührsen U, Klein-Hitpass L, Worm J, Rode Hansen JB, Ørum H, and Wissenbach M. The novel antisense Bcl-2 inhibitor SPC2996 causes rapid leukemic cell clearance and immune activation in chronic lymphocytic leukemia. *Leukemia* 25: 638–647, 2011.
43. Dworski R. Oxidant stress in asthma. *Thorax* 55 Suppl 2: S51–S53, 2000.
44. Eid H, Gulyas M, Geczi L, Bodrogi I, Institoris E, and Bak M. Expression of bcl-2 in testicular carcinoma: correlation with tumor progression and MDR1/Pgp. *Cancer* 83: 331–336, 1998.
45. Elbim C, Pillet S, Prevost MH, Preira A, Girard PM, Rogine N, Matusani H, Hakim J, Israel N, and Gougerot-Pocidalo MA. Redox and activation status of monocytes from human immunodeficiency virus-infected patients: relationship with viral load. *J Virol* 73: 4561–4566, 1999.
46. Ellerby LM, Ellerby HM, Park SM, Holleran AL, Murphy AN, Fiskum G, Kane DJ, Testa MP, Kayalar C, and Bredesen DE. Shift of the cellular oxidation-reduction potential in neural cells expressing Bcl-2. *J Neurochem* 67: 1259–1267, 1996.
47. Esposti MD, Hatzinisiriou I, McLennan H, and Ralph S. Bcl-2 and mitochondrial oxygen radicals. New approaches with reactive oxygen species-sensitive probes. *J Biol Chem* 274: 29831–29837, 1999.
48. Fernandez V, Tapia G, Varela P, Castillo I, Mora C, Moya F, Orellana M, and Videla LA. Redox up-regulated expression of rat liver manganese superoxide dismutase and Bcl-2 by thyroid hormone is associated with inhibitor of kappaB-alpha phosphorylation and nuclear factor-kappaB activation. *J Endocrinol* 186: 539–547, 2005.
49. Follis AV, Chipuk JE, Fisher JC, Yun MK, Grace CR, Nourse A, Baran K, Ou L, Min L, White SW, Green DR, and Kriwacki RW. PUMA binding induces partial unfolding within BCL-xL to disrupt p53 binding and promote apoptosis. *Nat Chem Biol* 9: 163–168, 2013.
50. Follis AV, Llambi F, Ou L, Baran K, Green DR, and Kriwacki RW. The DNA-binding domain mediates both nuclear and cytosolic functions of p53. *Nat Struct Mol Biol* 21: 535–543, 2014.
51. Frantz S. Lessons learnt from Genasense's failure. *Nat Rev Drug Discov* 3: 542–543, 2004.
52. Funato Y, Michiue T, Asashima M, and Miki H. The thioredoxin-related redox-regulating protein nucleoredoxin inhibits Wnt-beta-catenin signalling through dishevelled. *Nat Cell Biol* 8: 501–508, 2006.
53. Gao J, Aksoy BA, Dogrusoz U, Dresdner G, Gross B, Sumer SO, Sun Y, Jacobsen A, Sinha R, Larsson E, Cerami E, Sander C, and Schultz N. Integrative analysis of complex cancer genomics and clinical profiles using the cBioPortal. *Sci Signal* 6: pl1, 2013.
54. Gardner A, Xu FH, Fady C, Sarafian T, Tu Y, and Lichtenstein A. Evidence against the hypothesis that BCL-2 inhibits apoptosis through an anti-oxidant effect. *Cell Death Differ* 4: 487–496, 1997.
55. Ghosh R, Alajbegovic A, and Gomes AV. NSAIDs and cardiovascular diseases: role of reactive oxygen species. *Oxid Med Cell Longev* 2015: 536962, 2015.
56. Glasauer A, Sena LA, Diebold LP, Mazar AP, and Chandel NS. Targeting SOD1 reduces experimental non-small-cell lung cancer. *J Clin Invest* 124: 117–128, 2014.
57. Gong G, Waris G, Tanveer R, and Siddiqui A. Human hepatitis C virus NS5A protein alters intracellular calcium levels, induces oxidative stress, and activates STAT-3 and NF-kappa B. *Proc Natl Acad Sci U S A* 98: 9599–9604, 2001.
58. Gouaze V, Andrieu-Abadie N, Cuvillier O, Malagarie-Cazenave S, Frisach MF, Mirault ME, and Levade T. Glutathione peroxidase-1 protects from CD95-induced apoptosis. *J Biol Chem* 277: 42867–42874, 2002.
59. Goy A, Hernandez-Ilzaliturri FJ, Kahl B, Ford P, Protomastro E, and Berger M. A phase I/II study of the pan Bcl-2 inhibitor obatoclax mesylate plus bortezomib for relapsed or refractory mantle cell lymphoma. *Leukemia Lymphoma* 55: 2761–2768, 2014.
60. Grivennikova VG and Vinogradov AD. Generation of superoxide by the mitochondrial Complex I. *Biochim Biophys Acta* 1757: 553–561, 2006.
61. Halliwell B and Cross CE. Oxygen-derived species: their relation to human disease and environmental stress. *Environ Health Perspect* 102 Suppl 10: 5–12, 1994.
62. Harrison D, Griendling KK, Landmesser U, Hornig B, and Drexler H. Role of oxidative stress in atherosclerosis. *Am J Cardiol* 91: 7A–11A, 2003.
63. Heckman CA, Mehew JW, and Boxer LM. NF-kappaB activates Bcl-2 expression in t(14;18) lymphoma cells. *Oncogene* 21: 3898–3908, 2002.
64. Hennet T, Peterhans E, and Stocker R. Alterations in antioxidant defences in lung and liver of mice infected with influenza A virus. *J Gen Virol* 73 (Pt 1): 39–46, 1992.
65. Herzenberg LA, De Rosa SC, Dubs JG, Roederer M, Anderson MT, Ela SW, Deresinski SC, and Herzenberg LA. Glutathione deficiency is associated with impaired survival in HIV disease. *Proc Natl Acad Sci U S A* 94: 1967–1972, 1997.
66. Hildeman DA, Mitchell T, Aronow B, Wojciechowski S, Kappler J, and Marrack P. Control of Bcl-2 expression by reactive oxygen species. *Proc Natl Acad Sci U S A* 100: 15035–15040, 2003.
67. Hockenbery D, Nunez G, Milliman C, Schreiber RD, and Korsmeyer SJ. Bcl-2 is an inner mitochondrial membrane protein that blocks programmed cell death. *Nature* 348: 334–336, 1990.
68. Hockenbery DM, Oltvai ZN, Yin XM, Milliman CL, and Korsmeyer SJ. Bcl-2 functions in an antioxidant pathway to prevent apoptosis. *Cell* 75: 241–251, 1993.
69. Ichimiya M, Chang SH, Liu H, Berezesky IK, Trump BF, and Amstad PA. Effect of Bcl-2 on oxidant-induced cell death and intracellular Ca2+ mobilization. *Am J Physiol* 275: C832–C839, 1998.
70. Inc. APG. 2017. A study of APG-1252 in patients with SCLC or other solid tumors. https://clinicaltrials.gov/ct2/show/NCT03080311. Access date August 21, 2017.
71. Inoguchi T, Sonta T, Tsubouchi H, Etoh T, Kakimoto M, Sonoda N, Sato N, Sekiguchi N, Kobayashi K, Sumimoto H, Utsumi H, and Nawata H. Protein kinase C-dependent increase in reactive oxygen species (ROS) production in

vascular tissues of diabetes: role of vascular NAD(P)H oxidase. *J Am Soc Nephrol* 14: S227–S232, 2003.
72. Institute NC. 2017. Gossypol in treating patients with progressive or recurrent glioblastoma multiforme. https://clinicaltrials.gov/ct2/show/NCT00540722. Access date August 21, 2017.
73. Jang JH and Surh YJ. Bcl-2 attenuation of oxidative cell death is associated with up-regulation of gamma-glutamylcysteine ligase via constitutive NF-kappaB activation. *J Biol Chem* 279: 38779–38786, 2004.
74. Jiang TY, Liu MH, J.P. W, and Shi YG. Structural and biochemical analysis of Bcl-2 interaction with the hepatitis B virus protein HBx. *Proc Natl Acad Sci USA* 113: 2074–2079, 2016.
75. Joza N, Susin SA, Daugas E, Stanford WL, Cho SK, Li CY, Sasaki T, Elia AJ, Cheng HY, Ravagnan L, Ferri KF, Zamzami N, Wakeham A, Hakem R, Yoshida H, Kong YY, Mak TW, Zuniga-Pflucker JC, Kroemer G, and Penninger JM. Essential role of the mitochondrial apoptosis-inducing factor in programmed cell death. *Nature* 410: 549–554, 2001.
76. Kaik PK, Rudin CM, Brown A, Rizvi NA, Takebe N, Travis W, James L, Ginsberg MS, Juergens R, Markus S, Tyson L, Subzwari S, Kris MG, and Krug LM. A phase I study of obatoclax mesylate, a Bcl-2 antagonist, plus toptecan in solid tumor malignancies. *Cancer Chemother Pharmacol* 66: 1079–1085, 2010.
77. Kane DJ, Sarafian TA, Anton R, Hahn H, Gralla EB, Valentine JS, Ord T, and Bredesen DE. Bcl-2 inhibition of neural death: decreased generation of reactive oxygen species. *Science* 262: 1274–1277, 1993.
78. Kang DH, Lee DJ, Lee S, Lee SY, Jun Y, Kim Y, Kim Y, Lee JS, Lee DK, Lee S, Jho EH, Yu DY, and Kang SW. Interaction of tankyrase and peroxiredoxin II is indispensable for the survival of colorectal cancer cells. *Nat Commun* 8: 40, 2017.
79. Kang J, Chong SJ, Ooi VZ, Vali S, Kumar A, Kapoor S, Abbasi T, Hirpara JL, Loh T, Goh BC, and Pervaiz S. Overexpression of Bcl-2 induces STAT-3 activation via an increase in mitochondrial superoxide. *Oncotarget* 6: 34191–34205, 2015.
80. Karbowski M, Norris KL, Cleland MM, Jeong SY, and Youle RJ. Role of Bax and Bak in mitochondrial morphogenesis. *Nature* 443: 658–662, 2006.
81. Kaufmann JA, Bickford PC, and Taglialatela G. Oxidative-stress-dependent up-regulation of Bcl-2 expression in the central nervous system of aged Fisher-344 rats. *J Neurochem* 76: 1099–1108, 2001.
82. Kelkel M, Cerella C, Mack F, Schneider T, Jacob C, Schumacher M, Dicato M, and Diederich M. ROS-independent JNK activation and multisite phosphorylation of Bcl-2 link diallyl tetrasulfide-induced mitotic arrest to apoptosis. *Carcinogenesis* 33: 2162–2171, 2012.
83. Kluck RM, Bossy-Wetzel E, Green DR, and Newmeyer DD. The release of cytochrome c from mitochondria: a primary site for Bcl-2 regulation of apoptosis. *Science* 275: 1132–1136, 1997.
84. Koh LW, Koh GR, Ng FS, Toh TB, Sandanaraj E, Chong YK, Phong M, Tucker-Kellogg G, Kon OL, Ng WH, Ng IH, Clement MV, Pervaiz S, Ang BT, and Tang CS. A distinct reactive oxygen species profile confers chemoresistance in glioma-propagating cells and associates with patient survival outcome. *Antioxid Redox Signal* 19: 2261–2279, 2013.
85. Kowaltowski AJ, Castilho RF, and Vercesi AE. Mitochondrial permeability transition and oxidative stress. *FEBS Lett* 495: 12–15, 2001.
86. Ku B, Liang C, Jung JU, and Oh BH. Evidence that inhibition of Bax activation by Bcl-2 involves its tight and preferential interaction with the BH3 domain of Bax. *Cell Res* 21: 627, 2011.
87. Kubli DA, Quinsay MN, Huang C, Lee Y, and Gustafsson AB. Bnip3 functions as a mitochondrial sensor of oxidative stress during myocardial ischemia and reperfusion. *Am J Physiol Heart Circ Physiol* 295: H2025–H2031, 2008.
88. Kuppusamy P and Zweier JL. Characterization of free radical generation by xanthine oxidase. Evidence for hydroxyl radical generation. *J Biol Chem* 264: 9880–9884, 1989.
89. Kwon T, Rho JK, Lee JC, Park YH, Shin HJ, Cho S, Kang YK, Kim BY, Yoon DY, and Yu DY. An important role for peroxiredoxin II in survival of A549 lung cancer cells resistant to gefitinib. *Exp Mol Med* 47: e165, 2015.
90. Lai JC, Benimetskaya L, Santella RM, Wang Q, Miller PS, and Stein CA. G3139 (oblimersen) may inhibit prostate cancer cell growth in a partially bis-CpG-dependent non-antisense manner. *Mol Cancer Ther* 2: 1031–1043, 2003.
91. Lambeth JD. NOX enzymes and the biology of reactive oxygen. *Nat Rev Immunol* 4: 181–189, 2004.
92. Le Gouill S, Wermke M, Morschhauser F, Lim ST, Salles G, Kloos I, de Burgat V, Becquart M, Paux G, Kraus-Berthier L, Pennaforte S, Stilgenbauer S, Walewski J, and Ribrag V. A new Bcl-2 inhibitor (S55746/BCL201) as monotherapy in patients with relapsed or refractory non-Hodgkin lymphoma: preliminary results of the first-in-human study. *Haematol Oncol* 35(S2): 47–48, 2017.
93. Lee EF, Dewson G, Evangelista M, Pettikiriarachchi A, Zhu H, Colman PM, and Fairlie WD. The functional difference of pro-survival and pro-apoptotic B cell lymphoma 2 (Bcl-2) proteins depend on structural differences in their Bcl-2 homology 3 (Bh3) domains. *J Biol Chem* 289: 36001–36017, 2014.
94. Lee EF, Sadowsky JD, Smith BJ, Czabotar PE, Peterson-Kaufman KJ, Colman PM, Gellman SH, and Fairlie WD. High-resolution structural characterization of a helical a/b-peptide foldamer bound to the anti-apoptotic protein Bcl-x(L). *Angew Chem Int Ed* 48: 4318–4322, 2009.
95. Lee M, Hyun DH, Marshall KA, Ellerby LM, Bredesen DE, Jenner P, and Halliwell B. Effect of overexpression of BCL-2 on cellular oxidative damage, nitric oxide production, antioxidant defenses, and the proteasome. *Free Radic Biol Med* 31: 1550–1559, 2001.
96. Lei X, Chen Y, Du G, Yu W, Wang X, Qu H, Xia B, He H, Mao J, Zong W, Liao X, Mehrpour M, Hao X, and Chen Q. Gossypol induces Bax/Bak-independent activation of apoptosis and cytochrome c release via a conformational change in Bcl-2. *FASEB J* 20: E1510–E1519, 2006.
97. Levine B, Sinha S, and Kroemer G. Bcl-2 family members: dual regulators of apoptosis and autophagy. *Autophagy* 4: 600–606, 2008.
98. Levy MA and Claxton DF. Therapeutic inhibition of BCL-2 and related family members. *Expert Opin Investigat Drugs* 26: 293–301, 2017.
99. Li Y, Lu Z, Chen F, Guan J, Hu L, Xu Y, and Chen J. Antisense bcl-2 transfection up-regulates anti-apoptotic

and anti-oxidant thioredoxin in neuroblastoma cells. *J Neurooncol* 72: 17–23, 2005.
100. Liang J, Cao R, Wang X, Zhang Y, Wang P, Gao H, Li C, Yang F, Zeng R, Wei P, Li D, Li W, and Yang W. Mitochondrial PKM2 regulates oxidative stress-induced apoptosis by stabilizing Bcl2. *Cell Res* 27: 329–351, 2017.
101. Limongi D and Baldelli S. Redox Imbalance and Viral Infections in Neurodegenerative Diseases. *Oxid Med Cell Longev* 2016: 6547248, 2016.
102. Liou GY and Storz P. Reactive oxygen species in cancer. *Free Radic Res* 44: 479–496, 2010.
103. Lipinski CA, Lombardo F, Dominy BW, and Feeney PJ. Experimental and computational approaches to estimate solubility and permeability in drug discovery and development settings. *Adv Drug Deliv Rev* 23: 3–25, 1997.
104. Longoni B, Boschi E, Demontis GC, Marchiafava PL, and Mosca F. Regulation of Bcl-2 protein expression during oxidative stress in neuronal and in endothelial cells. *Biochem Biophys Res Commun* 260: 522–526, 1999.
105. Lopez-Otin C, Blasco MA, Partridge L, Serrano M, and Kroemer G. The hallmarks of aging. *Cell* 153: 1194–1217, 2013.
106. Low IC, Kang J, and Pervaiz S. Bcl-2: a prime regulator of mitochondrial redox metabolism in cancer cells. *Antioxid Redox Signal* 15: 2975–2987, 2011.
107. Low IC, Loh T, Huang Y, Virshup DM, and Pervaiz S. Ser70 phosphorylation of Bcl-2 by selective tyrosine nitration of PP2A-B56delta stabilizes its antiapoptotic activity. *Blood* 124: 2223–2234, 2014.
108. Lu Y, Rolland SG, and Conradt B. A molecular switch that governs mitochondrial fusion and fission mediated by the BCL2-like protein CED-9 of *Caenorhabditis elegans*. *Proc Natl Acad Sci U S A* 108: E813–E822, 2011.
109. Luanpitpong S, Chanvorachote P, Stehlik C, Tse W, Callery PS, Wang L, and Rojanasakul Y. Regulation of apoptosis by Bcl-2 cysteine oxidation in human lung epithelial cells. *Mol Biol Cell* 24: 858–869, 2013.
110. Manna SK, Zhang HJ, Yan T, Oberley LW, and Aggarwal BB. Overexpression of manganese superoxide dismutase suppresses tumor necrosis factor-induced apoptosis and activation of nuclear transcription factor-kappaB and activated protein-1. *J Biol Chem* 273: 13245–13254, 1998.
111. Mari M, Morales A, Colell A, Garcia-Ruiz C, and Fernandez-Checa JC. Mitochondrial glutathione, a key survival antioxidant. *Antioxid Redox Signal* 11: 2685–2700, 2009.
112. Markesbery WR. Oxidative stress hypothesis in Alzheimer's disease. *Free Radic Biol Med* 23: 134–147, 1997.
113. Markou T, Dowling AA, Kelly T, and Lazou A. Regulation of Bcl-2 phosphorylation in response to oxidative stress in cardiac myocytes. *Free Radic Res* 43: 809–816, 2009.
114. Maundrell K, Antonsson B, Magnenat E, Camps M, Muda M, Chabert C, Gillieron C, Boschert U, Vial-Knecht E, Martinou JC, and Arkinstall S. Bcl-2 undergoes phosphorylation by c-Jun N-terminal kinase/stress-activated protein kinases in the presence of the constitutively active GTP-binding protein Rac1. *J Biol Chem* 272: 25238–25242, 1997.
115. McDonnell TJ, Deane N, Platt FM, Nunez G, Jaeger U, McKearn JP, and Korsmeyer SJ. bcl-2-immunoglobulin transgenic mice demonstrate extended B cell survival and follicular lymphoproliferation. *Cell* 57: 79–88, 1989.
116. Messmer UK, Reed UK, and Brune B. Bcl-2 protects macrophages from nitric oxide-induced apoptosis. *J Biol Chem* 271: 20192–20197, 1996.
117. Mikhailov V, Mikhailova M, Pulkrabek DJ, Dong Z, Venkatachalam MA, and Saikumar P. Bcl-2 prevents Bax oligomerization in the mitochondrial outer membrane. *J Biol Chem* 276: 18361–18374, 2001.
118. Miriyala S, Spasojevic I, Tovmasyan A, Salvemini D, Vujaskovic Z, St Clair D, and Batinic-Haberle I. Manganese superoxide dismutase, MnSOD and its mimics. *Biochim Biophys Acta* 1822: 794–814, 2012.
119. Muchmore SW, Sattler M, Liang H, Meadows RP, Harlan JE, Yoon HS, Nettesheim D, Chang BS, Thompson CB, Wong SL, Ng SL, and Fesik SW. X-ray and NMR structure of human Bcl-xL, an inhibitor of programmed cell death. *Nature* 381: 335–341, 1996.
120. Muller FL, Liu Y, and Van Remmen H. Complex III releases superoxide to both sides of the inner mitochondrial membrane. *J Biol Chem* 279: 49064–49073, 2004.
121. Murphy MP. How mitochondria produce reactive oxygen species. *Biochem J* 417: 1–13, 2009.
122. Myers KM, Fiskum G, Liu Y, Simmens SJ, Bredesen DE, and Murphy AN. Bcl-2 protects neural cells from cyanide/aglycemia-induced lipid oxidation, mitochondrial injury, and loss of viability. *J Neurochem* 65: 2432–2440, 1995.
123. Nakamura H, Masutani H, and Yodoi J. Redox imbalance and its control in HIV infection. *Antioxid Redox Signal* 4: 455–464, 2002.
124. Némati F, de Montrion C, Lang G, Kraus-Berthier L, Carita G, Sastre-Garau X, Berniard A, Vallerand D, Geneste O, de Plater L, Pierré A, Lockhart B, Desjardins L, Piperno-Neumann S, Depil S, and Decaudin D. Targeting Bcl-2/Bcl-X_L induces antitumor activity in uveal melanoma patient-derived xenografts. *PLoS One* 9: e80836, 2014.
125. Nencioni L, De Chiara G, Sgarbanti R, Amatore D, Aquilano K, Marcocci ME, Serafino A, Torcia M, Cozzolino F, Ciriolo MR, Garaci E, and Palamara AT. Bcl-2 expression and p38MAPK activity in cells infected with influenza A virus: impact on virally induced apoptosis and viral replication. *J Biol Chem* 284: 16004–16015, 2009.
126. Nencioni L, Iuvara A, Aquilano K, Ciriolo MR, Cozzolino F, Rotilio G, Garaci E, and Palamara AT. Influenza A virus replication is dependent on an antioxidant pathway that involves GSH and Bcl-2. *FASEB J* 17: 758–760, 2003.
127. Nguyen M, Marcellus RC, Roulston A, Watson M, Serfass L, Murthy Madiraju SR, Gouley D, Viallet J, Bélec L, Billot X, Acoca S, Purisima E, Wiegmans A, Cluse L, Johnstone RW, Beauparlant P, and Shore GC. Small molecule obatoclax (GX15-070) antagonizes MCL-1 and overcomes MCL-1-mediated resistance to apoptosis. *Proc Natl Acad Sci USA* 104: 19512–19517, 2007.
128. Ni Z, Wang B, Dai X, Ding W, Yang T, Li X, Lewin S, Xu L, Lian J, and He F. HCC cells with high levels of Bcl-2 are resistant to ABT-737 via activation of the ROS-JNK-autophagy pathway. *Free Radic Biol Med* 70: 194–203, 2014.
129. Niture SK and Jaiswal AK. Nrf2 protein up-regulates antiapoptotic protein Bcl-2 and prevents cellular apoptosis. *J Biol Chem* 287: 9873–9886, 2012.
130. O'Brien SM, Claxton DF, Crump M, Faderl S, Kipps T, Keating MJ, Viallet J, and Cheson BD. Phase I study of obatoclax mesylate (GX15-070), a small molecular

pan-Bcl-2 family antagonist, in patients with advanced chronic lympocytic leukemia. *Blood* 113: 299–305, 2009.
131. O'Neill JW, Manion MK, Maguire B, and Hockenbery DM. BCL-XL dimerization by three-dimensional domain swapping. *J Mol Biol* 356: 367–381, 2006.
132. Oberstein A, Jeffrey PD, and Shi Y. Crystal structure of the Bcl-XL-Beclin 1 peptide complex: beclin 1 is a novel BH3-only protein. *J Biol Chem* 282: 13123–13132, 2007.
133. Oliver CL, Miranda MB, Shangary S, Land S, Wang S, and Johnson DE. (-)-Gossypol acts directly on the mitochondria to overcome Bcl-2- and Bcl-X(L)-mediated apoptosis resistance. *Mol Cancer Ther* 4: 23–31, 2005.
134. Oltersdorf T, Elmore SW, Shoemaker AR, Armstrong RC, Augeri DJ, Belli BA, Bruncko M, Deckwerth TL, Dinges J, Hajduk PJ, Joseph MK, Kitada S, Korsmeyer SJ, Kunzer AR, Letai A, Li C, Mitten MJ, Nettesheim DG, Ng S, Nimmer PM, O'Connor JM, Oleksijew A, Petros AM, Reed JC, Shen W, Tahir SK, Thompson CB, Tomaselli KJ, Wang B, Wendt MD, Zhang H, Fesik SW, and Rosenberg SH. An inhibitor of Bcl-2 family proteins induces regression of solid tumours. *Nature* 435: 677–681, 2005.
135. Oltvai ZN, Milliman CL, and Korsmeyer SJ. Bcl-2 heterodimerizes in vivo with a conserved homolog, Bax, that accelerates programmed cell death. *Cell* 74: 609–619, 1993.
136. Paik PK, Rudin CM, Pietanza MC, Brown A, Rizvi NA, Takebe N, Travis W, James L, Ginsberg MS, Juergens R, Markus S, Tyson L, Subzwari S, Kris MG, and Krug LM. A phase II study of obatoclax mesylate, a Bcl-2 antagonist, plus toptecan in relapsed small cell lung cancer. *Lung Cancer* 74: 481–485, 2011.
137. Park C-M, Bruncko M, Adickes J, Bauch J, Ding H, Kunzer A, Marsh KC, Nimmer P, Shoemaker AR, Song X, Tahir SK, Tse C, Wang X, Wendt MD, Yang X, Zhang H, Fesik SW, Rosenberg SH, and Elmore SW. Discovery of an orally bioavailable small molecule inhibitor of prosurvival B-cell lymphoma 2 proteins. *J Med Chem* 51: 6902–6915, 2008.
138. Pasinelli P, Belford ME, Lennon N, Bacskai BJ, Hyman BT, Trotti D, and Brown RH, Jr. Amyotrophic lateral sclerosis-associated SOD1 mutant proteins bind and aggregate with Bcl-2 in spinal cord mitochondria. *Neuron* 43: 19–30, 2004.
139. Pattingre S, Tassa A, Qu X, Garuti R, Liang XH, Mizushima N, Packer M, Schneider MD, and Levine B. Bcl-2 antiapoptotic proteins inhibit Beclin 1-dependent autophagy. *Cell* 122: 927–939, 2005.
140. Pedrini S, Sau D, Guareschi S, Bogush M, Brown RH, Jr., Naniche N, Kia A, Trotti D, and Pasinelli P. ALS-linked mutant SOD1 damages mitochondria by promoting conformational changes in Bcl-2. *Hum Mol Genet* 19: 2974–2986, 2010.
141. Perez HL, Banfi P, Bertrand JA, Cai ZW, Grebinski JW, Kim K, Lippy J, Modugno M, Naglich J, Schmidt RJ, Tebben A, Vianello P, Wei DD, Zhang L, Galvani A, Lombardo LJ, and Borzilleri RM. Identification of a phenylacylsulfonamide series of dual Bcl-2/Bcl-Xl antagonists. *Bioorg Med Chem Lett* 22: 3946, 2012.
142. Pervaiz S. Pro-oxidant milieu blunts scissors: insight into tumor progression, drug resistance, and novel druggable targets. *Curr Pharm Des* 12: 4469–4477, 2006.
143. Pervaiz S, Cao J, Chao OS, Chin YY, and Clement MV. Activation of the RacGTPase inhibits apoptosis in human tumor cells. *Oncogene* 20: 6263–6268, 2001.
144. Pervaiz S and Clement MV. A permissive apoptotic environment: function of a decrease in intracellular superoxide anion and cytosolic acidification. *Biochem Biophys Res Commun* 290: 1145–1150, 2002.
145. Pervaiz S and Clement MV. Superoxide anion: oncogenic reactive oxygen species? *Int J Biochem Cell Biol* 39: 1297–1304, 2007.
146. Petros AM, Medek A, Nettesheim DG, Kim DH, Yoon HS, Swift K, Matayoshi ED, Oltersdorf T, and Fesik SW. Solution structure of the antiapoptotic protein bcl-2. *Proc Natl Acad Sci USA* 98: 3012–3017, 2001.
147. Petros AM, Nettesheim DG, Wang Y, Olejniczak ET, Meadows RP, Mack J, Swift K, Matayoshi ED, Zhang H, Thompson CB, and Fesik SW. Rationale for Bcl-xL/Bad peptide complex formation from structure, mutagenesis, and biophysical studies. *Protein Sci* 9: 2528–2534, 2000.
148. Pierce RH, Vail ME, Ralph L, Campbell JS, and Fausto N. Bcl-2 expression inhibits liver carcinogenesis and delays the development of proliferating foci. *Am J Pathol* 160: 1555–1560, 2002.
149. Porter J, Payne A, de Candole B, Ford D, Hutchinson B, Trevitt G, Turner J, Edwards C, Watkins C, Whitcombe I, Davis J, and Stubberfield C. Tetrahydroisoquinoline amide substituted phenyl pyrazoles as selective Bcl-2 inhibitors. *Bioorg Med Chem Lett* 19: 230–233, 2009.
150. Pugazhenthi S, Nesterova A, Jambal P, Audesirk G, Kern M, Cabell L, Eves E, Rosner MR, Boxer LM, and Reusch JE. Oxidative stress-mediated down-regulation of bcl-2 promoter in hippocampal neurons. *J Neurochem* 84: 982–996, 2003.
151. Pugazhenthi S, Nesterova A, Sable C, Heidenreich KA, Boxer LM, Heasley LE, and Reusch JE. Akt/protein kinase B up-regulates Bcl-2 expression through cAMP-response element-binding protein. *J Biol Chem* 275: 10761–10766, 2000.
152. Qian C, Li M, Sui J, Ren T, Li Z, Zhang L, Zhou L, Cheng Y, and Wang D. Identification of a novel potential antitumor activity of gossypol as an APE1/Ref-1 inhibitor. *Drug Des Devel Ther* 8: 485–496, 2014.
153. Ray PD, Huang BW, and Tsuji Y. Reactive oxygen species (ROS) homeostasis and redox regulation in cellular signaling. *Cell Signal* 24: 981–990, 2012.
154. Reczek CR and Chandel NS. ROS-dependent signal transduction. *Curr Opin Cell Biol* 33: 8–13, 2015.
155. Ren T, Shan J, Li M, Qing Y, Qian C, Wang G, Li Q, Lu G, Li C, Peng Y, Luo H, Zhang S, Yang Y, Cheng Y, Wang D, and Zhou SF. Small-molecule BH3 mimetic and pan-Bcl-2 inhibitor AT-101 enhances the antitumor efficacy of cisplatin through inhibition of APE1 repair and redox activity in non-small-cell lung cancer. *Drug Des Devel Ther* 9: 2887–2910, 2015.
156. Rhee SG. Cell signaling. H2O2, a necessary evil for cell signaling. *Science* 312: 1882–1883, 2006.
157. Rimpler MM, Rauen U, Schmidt T, Moroy T, and de Groot H. Protection against hydrogen peroxide cytotoxicity in rat-1 fibroblasts provided by the oncoprotein Bcl-2: maintenance of calcium homoeostasis is secondary to the effect of Bcl-2 on cellular glutathione. *Biochem J* 340 (Pt 1): 291–297, 1999.
158. Roberts AW, Seymour JF, Brown JR, Wierda WG, Kipps TJ, Khaw SL, Carney DA, He SZ, Huang DC, Xiong

H, Cui Y, Busman TA, McKeegan EM, Krivoshik AP, Enschede SH, and Humerickhouse RA. Substantial susceptibility of chronic lymphocytic leukemia to BCL2 inhibition: results of a phase I study of navitoclax in patients with relapsed or refractory disease. *J Clin Oncol* 10: 488–496, 2012.

159. Rolland SG and Conradt B. New role of the BCL2 family of proteins in the regulation of mitochondrial dynamics. *Curr Opin Cell Biol* 22: 852–858, 2010.
160. Rudin CM, Yang Z, Schumaker LM, VanderWeele DJ, Newkirk K, Egorin MJ, Zuhowski EG, and Cullen KJ. Inhibition of glutathione synthesis reverses Bcl-2-mediated cisplatin resistance. *Cancer Res* 63: 312–318, 2003.
161. Sattler M, Liang H, Nettesheim D, Meadows RP, Harlan JE, Eberstadt M, Yoon HS, Shuker SB, Chang BS, Minn AJ, Thompson CB, and Fesik SW. Structure of Bcl-xL-Bak peptide complex: recognition between regulators of apoptosis. *Science* 275: 983–986, 1997.
162. Schimmer AD, O'Brien S, Kantarijan H, Brandwein J, Cheson BD, Minden MD, Yee K, Ravandi F, Giles F, Schuh A, Gupta V, Adreeff M, Koller C, Chang H, Kamel-Reid S, Berger M, Viallet J, and Borthakur G. A phase I study of the pan bcl-2 family inhibitor obatoclax mesylate in patients with advanced hematologic malignancies. *Clin Cancer Res* 14: 8295–8301, 2008.
163. Schimmer AD, Raza A, Carter TH, Claxton DF, Erba H, DeAngelo DJ, Tallman MS, Goard C, and Borthakur G. A multicenter phase I/II study of obatoclax mesylate administered as a 3- or 24-hour infusion in older patients with previously untreated acute myeloid leukemia. *PLoS One* 9: e108694, 2014.
164. Sheridan C, Delivani P, Cullen SP, and Martin SJ. Bax- or Bak-induced mitochondrial fission can be uncoupled from cytochrome C release. *Mol Cell* 31: 570–585, 2008.
165. Shimizu S, Eguchi Y, Kamiike W, Funahashi Y, Mignon A, Lacronique V, Matsuda H, and Tsujimoto Y. Bcl-2 prevents apoptotic mitochondrial dysfunction by regulating proton flux. *Proc Natl Acad Sci U S A* 95: 1455–1459, 1998.
166. Son YO, Pratheeshkumar P, Wang L, Wang X, Fan J, Kim DH, Lee JY, Zhang Z, Lee JC, and Shi X. Reactive oxygen species mediate Cr(VI)-induced carcinogenesis through PI3K/AKT-dependent activation of GSK-3beta/beta-catenin signaling. *Toxicol Appl Pharmacol* 271: 239–248, 2013.
167. Souers AJ, Leverson JD, Boghaert ER, Ackler SL, Catron ND, Chen J, Dayton BD, Ding H, Enschede SH, Fairbrother WJ, Huang DC, Hymowitz SG, Jin S, Khaw SL, Kovar PJ, Lam LT, Lee J, Maecker HL, Marsh KC, Mason KD, Mitten MJ, Nimmer PM, Oleksijew A, Park CH, Park CM, Phillips DC, Roberts AW, Sampath D, Seymour JF, Smith ML, Sullivan GM, Tahir SK, Tse C, Wendt MD, Xiao Y, Xue JC, Zhang H, Humerickhouse RA, Rosenberg SH, and Elmore SW. ABT-199, a potent and selective BCL-2 inhibitor, achieves antitumor activity while sparing platelets. *Nat Med* 19: 202–208, 2013.
168. Stehbens WE. Oxidative stress in viral hepatitis and AIDS. *Exp Mol Pathol* 77: 121–132, 2004.
169. Stein MN, Hussain M, Stadler WM, Liu G, Tereshchenko IV, Goodin S, Jeyamohan C, Kaufman HL, Mehnert J, and DiPaola R.S. A Phase II study of AT-101 to overcome Bcl-2 mediated resistance to androgen deprivation therapy in patients with newly diagnosed castration sensitive metastatic prostate cancer. *Clin Genitourin Cancer* 14: 22–27, 2016.
170. Steinman HM. The Bcl-2 oncoprotein functions as a prooxidant. *J Biol Chem* 270: 3487–3490, 1995.
171. Sulkshane P and Teni T. BH3 mimetic Obatoclax (GX15-070) mediates mitochondrial stress predominantly via MCL-1 inhibition and induces autophagy-dependent necroptosis in human oral cancer cells. *Oncotarget* 8: 60060–60079, 2017.
172. Szabo C, Ischiropoulos H, and Radi R. Peroxynitrite: biochemistry, pathophysiology and development of therapeutics. *Nat Rev Drug Discov* 6: 662–680, 2007.
173. Touré BB, Miller-Moslin K, Yussuff N, Perez L, Doré M, Joud C, Michael W, DiPietro L, van der Plas S, McEwan M, Lenoir F, Hoe M, Karki R, Springer C, Sullivan J, Levine K, Fiorilla C, Xie X, Kulathila R, Herlihy K, Porter D, and Visser M. The role of the acidity of N-heteroaryl sulfonamides as inhibitors of Bcl-2 family protein-protein interactions. *ACS Med Chem Lett* 4: 186–190, 2013.
174. Tsujimoto Y, Cossman J, Jaffe E, and Croce CM. Involvement of the bcl-2 gene in human follicular lymphoma. *Science* 228: 1440–1443, 1985.
175. Tsujimoto Y, Finger LR, Yunis J, Nowell PC, and Croce CM. Cloning of the chromosome breakpoint of neoplastic B cells with the t(14;18) chromosome translocation. *Science* 226: 1097–1099, 1984.
176. Tzung SP, Kim KM, Basanez G, Giedt CD, Simon J, Zimmerberg J, Zhang KY, and Hockenbery DM. Antimycin A mimics a cell-death-inducing Bcl-2 homology domain 3. *Nat Cell Biol* 3: 183–191, 2001.
177. Vail ME, Chaisson ML, Thompson J, and Fausto N. Bcl-2 expression delays hepatocyte cell cycle progression during liver regeneration. *Oncogene* 21: 1548–1555, 2002.
178. Velaithan R, Kang J, Hirpara JL, Loh T, Goh BC, Le Bras M, Brenner C, Clement MV, and Pervaiz S. The small GTPase Rac1 is a novel binding partner of Bcl-2 and stabilizes its antiapoptotic activity. *Blood* 117: 6214–6226, 2011.
179. Voehringer DW, McConkey DJ, McDonnell TJ, Brisbay S, and Meyn RE. Bcl-2 expression causes redistribution of glutathione to the nucleus. *Proc Natl Acad Sci U S A* 95: 2956–2960, 1998.
180. Voss V, Senft C, Lang V, Ronellenfitsch MW, Steinbach JP, Seifert V, and Kögel D. The pan-Bcl-2 inhibitor (-)-gossypol triggers autophagic cell death in malignant glioma. *Mol Cancer Res* 2010: 1002–1016, 2010.
181. Wardyn JD, Ponsford AH, and Sanderson CM. Dissecting molecular cross-talk between Nrf2 and NF-kappaB response pathways. *Biochem Soc Trans* 43: 621–626, 2015.
182. Wei Y, Pattingre S, Sinha S, Bassik M, and Levine B. JNK1-mediated phosphorylation of Bcl-2 regulates starvation-induced autophagy. *Mol Cell* 30: 678–688, 2008.
183. Westermann B. Bioenergetic role of mitochondrial fusion and fission. *Biochim Biophys Acta* 1817: 1833–1838, 2012.
184. Wilkins HM, Marquardt K, Lash LH, and Linseman DA. Bcl-2 is a novel interacting partner for the 2-oxoglutarate carrier and a key regulator of mitochondrial glutathione. *Free Radic Biol Med* 52: 410–419, 2012.

185. Wilson BE, Mochon E, and Boxer LM. Induction of bcl-2 expression by phosphorylated CREB proteins during B-cell activation and rescue from apoptosis. *Mol Cell Biol* 16: 5546–5556, 1996.
186. Wilson WH, O'Connor OA, Czuczman MS, LaCasce AS, Gerecitano JF, Leonard JP, Tulpule A, Dunleavy K, Xiong H, Chiu YL, Cui Y, Busman T, Elmore SW, Rosenberg SH, Krivoshik AP, Enschede SH, and Humerickhouse RA. Navitoclax, a targeted high-affinity inhibitor of BCL-2, in lymphoid malignancies: a phase 1 dose-escalation study of safety, pharmacokinetics, pharmacodynamics, and antitumour activity. *Lancet Oncol* 11: 1149–1159, 2010.
187. Wright C, Iyer AK, Kulkarni Y, and Azad N. S-Nitrosylation of Bcl-2 negatively affects autophagy in lung epithelial cells. *J Cell Biochem* 117: 521–532, 2016.
188. Yamamoto K, Ichijo H, and Korsmeyer SJ. BCL-2 is phosphorylated and inactivated by an ASK1/Jun N-terminal protein kinase pathway normally activated at G(2)/M. *Mol Cell Biol* 19: 8469–8478, 1999.
189. Yee YH, Chong SJ, and Pervaiz S. The anti-oxidant and pro-oxidant dichotomy of Bcl-2. *Biol Chem* 397: 585–593, 2016.
190. Yi X, Yin XM, and Dong Z. Inhibition of Bid-induced apoptosis by Bcl-2. tBid insertion, Bax translocation, and Bax/Bak oligomerization suppressed. *J Biol Chem* 278: 16992–16999, 2003.
191. Yin XM, Oltvai ZN, and Korsmeyer SJ. BH1 and BH2 domains of Bcl-2 are required for inhibition of apoptosis and heterodimerization with Bax. *Nature* 369: 321–323, 1994.
192. Zhang J, Wang X, Vikash V, Ye Q, Wu D, Liu Y, and Dong W. ROS and ROS-Mediated Cellular Signaling. *Oxid Med Cell Longev* 2016: 4350965, 2016.
193. Zhang L, Blackwell K, Altaeva A, Shi Z, and Habelhah H. TRAF2 phosphorylation promotes NF-kappaB-dependent gene expression and inhibits oxidative stress-induced cell death. *Mol Biol Cell* 22: 128–140, 2011.
194. Zhao M, Eaton JW, and Brunk UT. Bcl-2 phosphorylation is required for inhibition of oxidative stress-induced lysosomal leak and ensuing apoptosis. *FEBS Lett* 509: 405–412, 2001.
195. Zhao W, Fan GC, Zhang ZG, Bandyopadhyay A, Zhou X, and Kranias EG. Protection of peroxiredoxin II on oxidative stress-induced cardiomyocyte death and apoptosis. *Basic Res Cardiol* 104: 377–389, 2009.
196. Zhong LT, Sarafian T, Kane DJ, Charles AC, Mah SP, Edwards RH, and Bredesen DE. bcl-2 inhibits death of central neural cells induced by multiple agents. *Proc Natl Acad Sci U S A* 90: 4533–4537, 1993.
197. Zimmermann AK, Loucks FA, Schroeder EK, Bouchard RJ, Tyler KL, and Linseman DA. Glutathione binding to the Bcl-2 homology-3 domain groove: a molecular basis for Bcl-2 antioxidant function at mitochondria. *J Biol Chem* 282: 29296–29304, 2007.

Address correspondence to:
Prof. Shazib Pervaiz
Department of Physiology
Yong Loo Lin School of Medicine
National University of Singapore
Singapore 117597
Singapore

E-mail: phssp@nus.edu.sg

Date of first submission to ARS Central, October 18, 2017; date of final revised submission, December 5, 2017; date of acceptance, January 5, 2018.

Abbreviations Used

Bcl-2 = B cell lymphoma 2
BH = Bcl-2 homology domains
BNIP3 = Bcl-2/adenovirus E1B 19-kDa protein-interacting protein 3
COX = cytochrome *c* oxidase
CREB = cyclic AMP response binding protein
ER = endoplasmic reticulum
ERK = extracellular signal-regulated kinases
ETC = electron transport chain
GPx1 = glutathione peroxidase-1
GSH = reduced glutathione
GTPase = guanosine trisphosphate
HCC = hepatocellular carcinoma
HIV = human immunodeficiency virus
H_2O_2 = hydrogen peroxide
JNKs = c-Jun N-terminal kinases
MAPK = mitogen-activated protein kinase
MCL-1 = induced myeloid leukemia cell differentiation protein
MnTBAP = manganese (III) tetrakis (4-benzoic acid) porphyrin
MOMP = mitochondrial outer membrane permeabilization
NAC = *N*-acetylcysteine
NF-κB = nuclear factor kappa-light-chain-enhancer of activated B cells
NO = nitric oxide
NOX = NADPH oxidase
$O_2^{\cdot -}$ = superoxide anion
OGC = 2-oxyglutarate carrier
$ONOO^-$ = peroxynitrite
PKM2 = pyruvate kinase M2 isoform
PLC-γ1 = phospholipase Cc1-dependent
PP2A = protein phosphatase 2
ROS = reactive oxygen species
SOD = superoxide dismutase
STAT3 = signal transducer and activator of transcription 3
TCGA = The Cancer Genome Atlas
TNF = tumor necrosis factor

JBC ARTICLE

Structure-based prediction of Wnt binding affinities for Frizzled-type cysteine-rich domains

Received for publication, March 14, 2017, and in revised form, May 9, 2017 Published, Papers in Press, May 22, 2017, DOI 10.1074/jbc.M117.786269

Mark Agostino[‡§1], **Sebastian Öther-Gee Pohl**[‡2], **and Arun Dharmarajan**[‡3]

From the [‡]*Stem Cell and Cancer Biology Laboratory, School of Biomedical Sciences and Curtin Health Innovation Research Institute and* [§]*Curtin Institute of Computation, Curtin University, Kent Street, Bentley, Western Australia 6102, Australia*

Edited by George M. Carman

Wnt signaling pathways are of significant interest in development and oncogenesis. The first step in these pathways typically involves the binding of a Wnt protein to the cysteine-rich domain (CRD) of a Frizzled receptor. Wnt-Frizzled interactions can be antagonized by secreted Frizzled-related proteins (SFRPs), which also contain a Frizzled-like CRD. The large number of Wnts, Frizzleds, and SFRPs, as well as the hydrophobic nature of Wnt, poses challenges to laboratory-based investigations of interactions involving Wnt. Here, utilizing structural knowledge of a representative Wnt-Frizzled CRD interaction, as well as experimentally determined binding affinities for a selection of Wnt-Frizzled CRD interactions, we generated homology models of Wnt-Frizzled CRD interactions and developed a quantitative structure-activity relationship for predicting their binding affinities. The derived model incorporates a small selection of terms derived from scoring functions used in protein-protein docking, as well as an energetic term considering the contribution made by the lipid of Wnt to the Wnt-Frizzled binding affinity. Validation with an external test set suggests that the model can accurately predict binding affinity for 75% of cases and that the error associated with the predictions is comparable with the experimental error. The model was applied to predict the binding affinities of the full range of mouse and human Wnt-Frizzled and Wnt-SFRP interactions, indicating trends in Wnt binding affinity for Frizzled and SFRP CRDs. The comprehensive predictions made in this study provide the basis for laboratory-based studies of previously unexplored Wnt-Frizzled and Wnt-SFRP interactions, which, in turn, may reveal further Wnt signaling pathways.

The Wnt signaling pathway is an evolutionarily conserved pathway found in vertebrates and insects (1). It functions to regulate body axis formation, cell fate, cell proliferation, and morphogenesis in embryonic development (2), whereas aberrant Wnt signaling is a hallmark of many cancers (3). Wnt signaling pathways can be divided into three separate branches: a canonical or β-catenin-dependent pathway and two non-canonical or β-catenin-independent pathways, known as the planar cell polarity (PCP)[4] and Wnt/Ca^{2+} pathways (4, 5) (see Fig. 1). Wnt signaling is generally initiated by the binding of Wnt ligands to a Frizzled (Fzd) receptor (6). In the canonical Wnt signaling pathway (Fig. 1*a*), low-density lipoprotein-related protein 5/6 (LRP5/6) acts as a co-receptor for Wnt binding (7). Signal transduction by the three major Wnt signaling pathways is regulated by the interaction of Fzd with the cytoplasmic protein Dishevelled (Dvl) (8). In the canonical pathway, β-catenin-dependent signaling is mediated through the cytoplasmic "destruction complex" composed of Axin, protein phosphatase 2A, adenomatous polyposis coli protein, glycogen synthase kinase 3 (GSK3), and casein kinase 1α (CK1α) (9). In the presence of Wnt stimulation, Fzd is activated, permitting Dvl binding and resulting in the stabilization of the destruction complex and the accumulation of non-phosphorylated β-catenin, which then translocates to the nucleus and binds to T cell factor/lymphoid enhancer-binding factor transcription factors on the promoter of target genes (4). In the absence of Wnt stimulation, the destruction complex is destabilized, allowing for the phosphorylation of β-catenin by CK1α and GSK3 (10); phosphorylated β-catenin is then proteolytically degraded (11). The Wnt/Ca^{2+} pathway (Fig. 1*b*) is activated through Wnt ligands binding to Fzd receptors, resulting in an increase in intracellular calcium (12). Calcium ions are able to activate both calmodulin-dependent protein kinase II (13) and protein kinase C (PKC) (14), which subsequently activate transcription factors NFκB and cAMP-response element-binding protein. The cytosolic phosphatase calcineurin (Cn) is also activated by calcium ions. Cn-dependent dephosphorylation and activation of

The authors declare that they have no conflicts of interest with the contents of this article.

This article contains supplemental Tables S1 and S5–S14 and Figs. S2–S4, S15, and S16.

[1] Recipient of National Health and Medical Research Council C. J. Martin Early Career Fellowship GNT1054245, a Cancer Council of Western Australia Suzanne Cavanagh Early Career Investigator Grant, a Raine Priming Grant, Operational Research Support from the Curtin Institute for Computation, and a Curtin Research Fellowship. To whom correspondence should be addressed: Stem Cell and Cancer Biology Laboratory, School of Biomedical Sciences, Curtin Health Innovation Research Institute and Curtin Institute of Computation, Curtin University, Kent St., Bentley, Western Australia 6102, Australia. Tel.: 61892669719; E-mail: Mark.Agostino@curtin.edu.au.

[2] Supported by funds from the Rotary Club of Belmont, Australian Rotary Health Research Fund, and Curtin University School of Biomedical Sciences.

[3] Supported by strategic research funds from the School of Biomedical Sciences (Curtin University), Commercialisation Advisory Board of Curtin University, Cancer Council of Western Australia, and Actinogen Ltd., Perth, Western Australia.

[4] The abbreviations used are: PCP, planar cell polarity; CRD, cysteine-rich domain; Fzd, Frizzled; SFRP, secreted Frizzled-related protein; LRP, low-density lipoprotein-related protein; Dvl, Dishevelled; GSK3, glycogen synthase kinase 3; CK1, casein kinase 1; Cn, calcineurin; ROCK, Rho-associated protein kinase; XWnt8, *Xenopus* Wnt8; GPCR, G protein–coupled receptor; BLI, biolayer interferometry; coIP, co-immunoprecipitation; mFzd, mouse Fzd; RMSD, root-mean-squared deviation; mWnt, mouse Wnt; hWnt, human Wnt; hFzd, human Fzd; RMSE, root-mean-squared error; ROR, receptor tyrosine kinase-like orphan receptor.

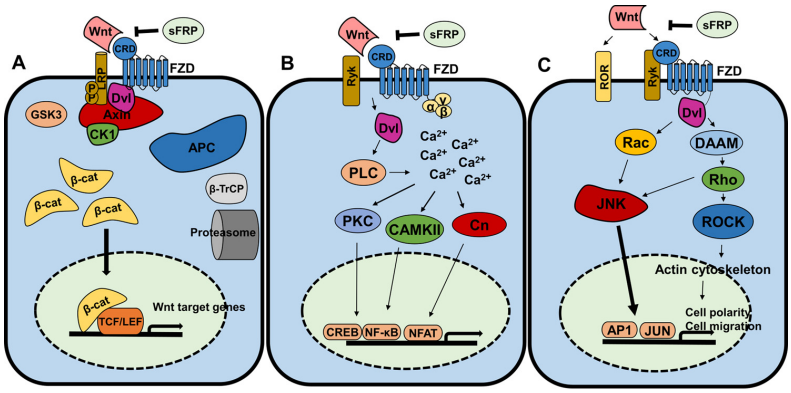

Figure 1. Wnt signaling pathways. *A*, canonical Wnt signaling. Wnt binding to Fzd CRD initiates the destabilization of the cytoplasmic destruction complex (adenomatous polyposis coli protein (APC), Axin, GSK3, CK1, and Dvl). This allows cytosolic β-catenin (β-cat) accumulation and subsequent translocation to the nucleus where it binds to T cell factor/lymphoid enhancer-binding factor (TCF/LEF) transcription factors to transcribe Wnt target genes. SFRPs antagonize this cascade, and β-catenin is polyubiquitinated by β-transducin repeats-containing protein (β-TrCP) and degraded by proteolysis. *B*, the Wnt/Ca^{2+} pathway. Wnt binding to Fzd CRD or Ryk co-receptor activates Dvl, which stimulates calcium release. Downstream effectors PKC, calmodulin-dependent protein kinase II (CaMKII), and Cn activate transcription factors cAMP-response element-binding protein (CREB), NF-κB, and nuclear factor of activated T cells (NFAT). *C*, the PCP pathway. Wnt stimulation is effected initially through Fzd-Dvl interaction and co-receptors ROR/Ryk and passed through multiple effectors (Rac, phospholipase C (PLC), Disheveled-associated activator of morphogenesis (DAAM)) downstream to ROCK and JNK. ROCK regulates the actin cytoskeleton, and JNK activates AP1 and JUN transcription factors to regulate cell polarity and migration.

nuclear factor of activated T cells lead to the transcription of genes in cardiomyocytes, neuronal cells, and skeletal muscle (15). Signal transduction via the PCP pathway (Fig. 1*c*) is initiated through Wnt binding to Fzd and co-receptors ROR and Ryk. Fzd activation leads to Dvl-mediated activation of Rac and Rho. JNK and Rho-associated protein kinase (ROCK) are activated by Rac and Rho, respectively, which mediates actin polymerization and activates transcription factors AP-1 and JUN (16).

Wnts comprise a group of 19 proteins that are subject to numerous post-translational modifications, including the formation of a large number of characteristic disulfide bonds, glycosylation in the endoplasmic reticulum (17), and palmitoylation by Porcupine, which aids in their secretion and facilitates their interaction with Frizzled (18). Structurally, as determined by the co-crystallization of *Xenopus* Wnt8 (XWnt8) with the mouse Fzd8 CRD, Wnts are composed of two domains: an N-terminal domain and a C-terminal domain (19). The N-terminal domain contains 10 cysteine residues forming five disulfide bridges in a cluster of α-helices, whereas the C-terminal domain contains six disulfide bridges and a two-stranded β-sheet (19). Frizzled receptors are a group of 10 membrane-bound receptors comprising the majority of Class F G protein–coupled receptors (GPCRs). Frizzleds, like other GPCRs, consist of seven hydrophobic transmembrane helices but feature an extracellular cysteine-rich domain (CRD) in their N terminus (20). The CRD is characterized by a conserved pattern of 10 cysteines and can bind Wnt and Norrin ligands (21, 22). The five mammalian secreted Frizzled-related proteins (SFRPs) are secreted glycoproteins composed of an N-terminal CRD and a C-terminal netrin-like domain (23). These proteins function to antagonize the Wnt signaling pathway (24) through binding of either the CRD (25) or the netrin-like domain to Wnt ligands (26), thus interfering with Wnt binding to Fzd and preventing β-catenin-mediated gene transcription. The SFRPs have been studied in great detail for their potential roles as tumor suppressors and their implications in carcinogenesis (23).

Because of the large number of possible Wnt-Fzd CRD interactions (which, considering CRDs from both Fzds and SFRPs, totals 285 interactions per species), it is challenging to investigate these experimentally. A recent study utilized biolayer interferometry (BLI) to investigate a small set of mouse Wnt-Fzd CRD interactions in a combinatorial manner (27). Numerous other interactions have been identified via co-immunoprecipitation (coIP) or proposed based on co-expression of particular Wnts with particular Fzds (6). Although coIP and co-expression are valuable methods for suggesting the existence of specific protein-protein interactions, they are unable to provide an indication of the likely strength of an interaction. Computational studies provide the opportunity to complete the knowledge of interactions between Wnts and Fzd CRDs and may reveal previously unexplored high-affinity interactions.

In this study, we have generated homology models of Wnt complexes with both Fzd and SFRP CRDs and predict the likely binding affinity associated with these interactions. For a series of Wnt-Fzd CRD interactions for which dissociation constants have been reported (27), we then evaluated the interaction energy for the protein-protein and lipid-protein components of the interactions; this was achieved through scoring the interactions against the full set of functions contained in CCharPPI (28) (for the protein-protein component) and scoring using Prime MM-GB/SA (for the lipid-protein component). Strike was then used to develop and evaluate binding affinity prediction models using scores obtained from CCharPPI and Prime MM-GB/SA as descriptors for the model building. A model with high predictive performance was identified and subsequently applied to predict the binding affinities of all Wnt-Fzd and Wnt-SFRP CRD interactions in both mouse and human cases.

Table 1
Summary of model quality metrics

	XWnt8-mFzd8 CRD complex	Mouse models[a]	Human models[a]
MolProbity score	1.72	2.13 ± 0.46	2.08 ± 0.42
TM-score[b]	1.00	0.91 ± 0.04	0.91 ± 0.05
Cα RMSD (Å)[b]	0.00	1.39 ± 0.39	1.39 ± 0.45

[a] Mean values ±2 S.D. shown; data for individual complexes shown in supplemental Tables S5–S10.
[b] TM-score and Cα RMSD values calculated with respect to the XWnt8-mFzd8 CRD complex (Protein Data Bank code 4F0A). By definition, the TM-score for an optimally overlaid structure compared with itself is 1; the RMSD for an optimally overlaid structure compared with itself is 0.

Results

Preparation of homology models of Wnt-Fzd CRD complexes

We prepared homology models of all mouse and human Wnts and all mouse and human Fzd and SFRP CRDs; details of UniProt accession numbers, sequence ranges, and sequence alignments used to build the models are provided in supplemental Table S1 and Figs. S2 and S3. The vast majority of proteins modeled did not feature large insertions or deletions relative to either XWnt8 or mFzd8 CRD with the exceptions of mouse and human Wnt6, Wnt10a, and Wnt10b; these Wnts feature insertions relative to XWnt8 larger than that able to be built by Prime (greater than 20 residues). To build these structures, we utilized an alternative procedure incorporating the I-TASSER server (described in detail under "Experimental procedures"), which is capable of building much longer insertions than Prime through its use of an iterative template fragment assembly approach to model building (29).

Following assembly of the complexes and refinement using a procedure automated using KNIME (supplemental Fig. S4), the MolProbity score of all models was calculated. The MolProbity score provides a single value metric of structural quality, summarizing the number of atomic clashes, percentage of backbone conformations in regions outside the Ramachandran favored regions, and the percentage of bad side-chain rotamers (30). The TM-score and the root-mean-squared deviation (RMSD) of the Cα atoms of the models with respect to the XWnt8-mFzd8 CRD complex structure (Protein Data Bank code 4F0A) (19), which was the template for all models, were also calculated. These measures assess differences in the coordinates of two structures (31). The mean value for the MolProbity scores for the mouse and human models was slightly greater than the MolProbity score obtained for the XWnt8-mFzd8 CRD complex structure (Table 1) but nonetheless comparable, indicating the generally high quality of the models. The mean values for the model TM-scores with respect to the template crystal structure were generally high, and the mean values for the model Cα RMSD values very low, further indicating the generally high quality of the models and their limited divergence from the template crystal structure. Selected complexes are shown in Fig. 2. Quality metrics are summarized in Table 1, and full details are provided in supplemental Tables S5–S10.

Development and validation of a Wnt-Fzd CRD binding affinity prediction model

We used a set of mouse Wnt-Fzd CRD binding affinities determined by BLI (27) to develop and validate our binding affinity prediction model. The model building and evaluation procedure is summarized in Fig. 3 and herein described.

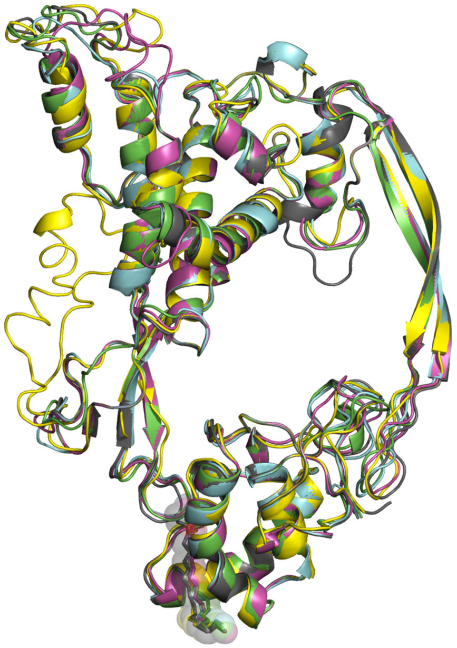

Figure 2. Homology models of selected Wnt-Fzd CRD complexes overlaid to the repaired XWnt8-mFzd8 CRD crystal structure (Protein Data Bank code 4F0A). *Gray*, repaired Protein Data Bank code 4F0A; *pink*, mWnt5-mFzd1 CRD complex; *yellow*, mWnt10a-mFzd6 complex; *green*, hWnt3a-hSFRP4 CRD complex; *cyan*, hWnt2b-hFzd9 CRD complex. Lipid is shown in all structure as *sticks* with *transparent spheres*.

Within the BLI data, we designated a *training* set, used to optimize the model, and a *test* set, used to demonstrate the performance of the model for data against which it had not been trained. Our training set was designated as complexes that were not part of our test set; our test set consisted of complexes involving interactions with either mFzd1 or mWnt4. The definition of the test set in this manner provided a simple means of selecting a test set covering a wide range of affinities. For all of these complexes, we then rescored, with separate procedures, the protein-protein portion and the lipid-protein portion of the interaction. The protein-protein portion was rescored against the majority of functions available within CCharPPI (28) (listed in supplemental Table S11), a server compiling a wide range of scoring functions suitable for use in protein-protein docking. The lipid-protein portion was rescored used Prime MM-GB/SA, which provides a rapid means for evaluating ligand-receptor binding energies with improved accuracy compared with typical docking scoring functions. The Prime MM-GB/SA calculation is also decomposed into its components (Coulomb/electrostatic, covalent binding, van der Waals, lipophilic, polar solvation/desolvation, hydrogen bonding, and π-π components; components used in this study listed in supplemental Table S11). The two strategies function complementarily to one another; the functions in CCharPPI are only capable of considering interactions between standard protein amino

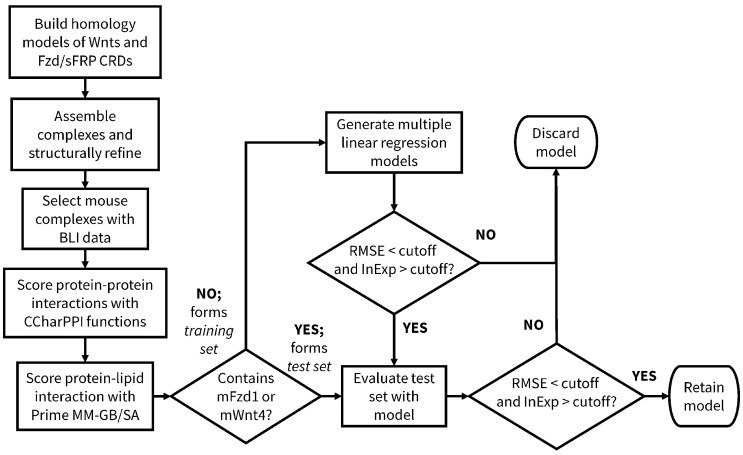

Figure 3. Overview of the model building process. RMSE and InExp cutoffs used to select models at the relevant stages of model building are described in the Experimental Procedures.

Table 2
Best performing four-descriptor models predicting Wnt-Fzd CRD binding energy

Number	Model	$RMSE_{train}$	$RMSE_{test}$	$InExp_{train}$	$InExp_{test}$
		kcal/mol	*kcal/mol*	*%*	*%*
1	$\Delta G = 0.0038165 \times$ AP_calRW $- 0.22506 \times$ MMGBSA dG Bind vdW $-$ $0.24626 \times$ HBOND2 $- 0.049875 \times$ FIREDOCK_AB $- 3.3475$	0.23	0.27	80	75
2	$\Delta G = 0.0021829 \times$ AP_calRWp $- 0.22111 \times$ MMGBSA dG Bind vdW $-$ $0.20861 \times$ HBOND2 $- 0.08699 \times$ ROSETTADOCK $- 7.7974$	0.30	0.23	73	75

acids, whereas Prime MM-GB/SA is capable of studying interactions between small organic molecules with proteins. With this in mind, the Wnt lipid was removed from the CCharPPI calculations, and the Wnt protein was removed from the Prime MM-GB/SA calculations (that is, only the interaction between the Wnt lipid and the Fzd CRD was assessed by Prime MM-GB/SA). Multiple linear regression models combining one Prime MM-GB/SA component with one or more CCharPPI components (all herein referred to as *descriptors*) were then generated, thus allowing the development of a single model considering both the protein-lipid and the protein-protein portions of the interaction.

As it was computationally accessible to consider all possible three-descriptor models incorporating one Prime MM-GB/SA term and two CCharPPI-derived terms, we initially explored these. The performance of all models was evaluated using two principal metrics: 1) the root-mean-squared error (RMSE) between the predicted values and the average experimental values ($RMSE_{train}$ and $RMSE_{test}$); lower values indicate a better fit between the predictions and experimental values; and 2) the percentage of complexes for which the predicted value occurred within the experimental range reported ($InExp_{train}$ and $InExp_{test}$); higher values indicate a better fit between the predictions and experimental values.

High-performing three-descriptor models of Wnt-Fzd CRD binding typically incorporated the van der Waals term of the Prime MM-GB/SA calculation (supplemental Table S12). The lipophilic term of the Prime MM-GB/SA calculation also appears frequently in high-performing models. This is unsurprising considering the physicochemical properties of palmitoleic acid, which would suggest that the binding energy will likely be associated with van der Waals/non-polar interactions. The best performing three-descriptor models generally displayed RMSEs for both the training and test sets in the range of 0.3–0.4 kcal/mol, which is well outside the error range of the experiments of ~0.2–0.3 kcal/mol (27); this indicates that three-descriptor models are insufficiently predictive.

Two models containing four descriptors were identified that were capable of high-prediction performance (Table 2). Both of these displayed RMSEs for the training and test sets less than 0.3 kcal/mol. Both included the van der Waals term of the Prime MM-GB/SA calculation, the PyRosetta hydrogen bonding potential (HBOND2) (32), and either the RW or RWplus statistical potentials (AP_calRW and AP_calRWp) (33). The fourth term in Model 1 is the antibody-antigen energy function of FireDock (FIREDOCK_AB) (34), whereas in Model 2, it is the total RosettaDock weighted energy (ROSETTADOCK). As the performance of Model 1 appeared slightly improved over Model 2, this model was selected for further study. Additionally, Model 1 was preferred over Model 2 for featuring a smaller constant term, suggesting that it may be able to predict affinities over a wider range than Model 2. The RMSE values for Model 1 suggest that the error associated with its use will be slightly larger than, but nonetheless similar to, the error range achieved by experiment.

The maximum difference between any prediction made by the model, either in the training set or the test set, is ~0.6 kcal/mol, which corresponds to a difference in K_d of approximately an order of magnitude (Fig. 4 and Table 3). Because there appears to be no particular Wnts or Fzds for which poor

predictions are made, failure to make accurate predictions most likely occurs randomly and is not associated with a particular Wnt or Fzd structure; this is perhaps expected given the overall high structural quality of the models used. The binding affinities of the vast majority of cases in the training and test sets are predicted within 0.25 kcal/mol of the mean experimental values reported, which is within the experimental error range.

Further elaboration of the selected four-descriptor models into five-descriptor models was performed but did not result in models providing significant improvements in predictions (data not shown); similar RMSEs and a similar number of predictions occurring within the experimental ranges in both the training and test sets were obtained for the best four- and five-descriptor models. Thus, four-descriptor models were deemed sufficient for use in predicting binding affinities.

Prediction of binding affinities of Wnt-CRD interactions

In applying Model 1 to predict Wnt-CRD binding affinities in the mouse proteins, numerous trends are apparent (Fig. 5*A* and supplemental Table S13). Fzd3, Fzd5, SFRP3, and SFRP4 generally display high-affinity, nonspecific binding of Wnts, as evidenced by more than half of the interactions predicted to afford strong binding affinities (*i.e.* <10 nM). Fzd8 also displays nonspecific binding of Wnts; however, the majority of interactions are predicted to be of lower affinity than those with Fzd3, Fzd5, SFRP3, and SFRP4. Fzd1, Fzd4, Fzd7, and Fzd9 generally display moderate affinity for a wide variety of Wnts. Fzd1, Fzd7, and Fzd9 display high affinity for limited Wnts, indicating more selective binding compared with Fzd3, Fzd5, Fzd8, SFRP3, and SFRP4, whereas Fzd4 displays high affinity for several Wnts, indicating less selective binding. Fzd1 displays high affinity for Wnt6, Fzd7 displays high affinity for Wnt10a, and Fzd9 displays high affinity for both Wnt7a and Wnt16. Fzd2, Fzd6, Fzd10, SFRP1, SFRP2, and SFRP5 all display moderate- to high-affinity binding to less than half of the Wnts. However, this does not strictly translate to high selectivity; Fzd6 and Fzd10 bind with moderate affinity to several Wnts. Fzd2 displays high affinity for Wnt3a, Wnt7b, and Wnt10a. SFRP1, SFRP2, and SFRP5 all display high selectivity for specific Wnt ligands but retain moderate affinity for the majority of remaining Wnts. SFRP1 appears highly selective for Wnt7a, whereas SFRP2 is selective for Wnt2b and Wnt3a. SFRP5 displays moderate affinity for Wnt2b, Wnt5b, and Wnt6.

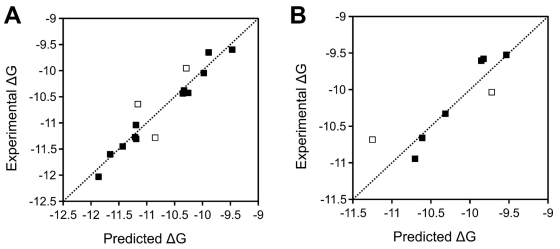

Figure 4. Comparison of binding energy predictions by Model 1 in the training set (*A*) and test set (*B*). Points indicated by *open squares* are those where the predicted binding energy falls outside the model RMSE (0.23 kcal/mol for the training set; 0.27 kcal/mol for the test set).

The human data generally display trends similar to the mouse data (Fig. 5*B* and supplemental Table S14). Fzd3, Fzd5, SFRP3, and SFRP4 still display generally high-affinity, nonspecific binding of Wnts; however, there are some specific points of difference. The interactions of human Fzd3 with Wnt8a and Wnt9a are predicted to be much higher affinity than in the case of the mouse, although the hFzd9-hWnt9a interaction is still predicted to be of only moderate affinity. Conversely, the inter-

Table 3
Comparison of predictions by Model 1 with experimental data for the training and test sets

Interaction	ΔG_{Exp} [a]	ΔG_{Pred} [a]	$\lvert\Delta G_{Exp} - \Delta G_{Pred}\rvert$ [a,b]	Experimental K_d [c]	Predicted K_d [c]	Experimental range (predicted range) [d]	Set
mWnt3a-mFzd2	−10.64	−11.16	0.52	15.7	6.5	+++ (++++)	Training
mWnt3a-mFzd4	−11.27	−11.21	0.06	5.4	6.0	++++ (++++)	Training
mWnt3a-mFzd5	−11.60	−11.65	0.05	3.1	2.9	++++ (++++)	Training
mWnt3a-mFzd7	−11.28	−10.85	0.43	5.3	11.0	++++ (+++)	Training
mWnt3a-mFzd8	−12.03	−11.86	0.17	1.5	2.0	++++ (++++)	Training
mWnt5-mFzd2	−10.38	−10.33	0.05	24.4	26.5	+++ (+++)	Training
mWnt5-mFzd4	−10.38	−10.26	0.12	24.4	29.9	+++ (+++)	Training
mWnt5-mFzd5	−11.31	−11.19	0.12	5.1	6.2	++++ (++++)	Training
mWnt5-mFzd7	−10.05	−9.98	0.07	42.6	47.9	++ (++)	Training
mWnt5-mFzd8	−11.45	−11.43	0.02	4.0	4.1	++++ (++++)	Training
mWnt5b-mFzd2	−9.60	−9.47	0.13	91.0	113.4	++ (+)	Training
mWnt5b-mFzd4	−9.95	−10.29	0.34	50.4	28.4	++ (+++)	Training
mWnt5b-mFzd5	−10.44	−10.35	0.09	22.0	25.7	+++ (+++)	Training
mWnt5b-mFzd7	−9.65	−9.89	0.24	83.7	55.8	++ (++)	Training
mWnt5b-mFzd8	−11.04	−11.19	0.15	8.0	6.2	++++ (++++)	Training
mWnt3a-mFzd1	−10.66	−10.61	0.05	15.2	16.5	++++ (++++)	Test
mWnt4-mFzd2	−9.53	−9.53	0.00	102.5	102.5	+ (+)	Test
mWnt4-mFzd4	−10.04	−9.72	0.32	43.3	74.3	++ (++)	Test
mWnt4-mFzd5	−10.68	−11.25	0.57	14.7	5.6	+++ (++++)	Test
mWnt4-mFzd7	−9.58	−9.83	0.25	94.2	61.7	+ (+)	Test
mWnt4-mFzd8	−10.95	−10.70	0.25	9.3	14.2	++++ (+++)	Test
mWnt5-mFzd1	−10.33	−10.31	0.02	26.5	27.4	+++ (+++)	Test
mWnt5b-mFzd1	−9.60	−9.85	0.25	91.0	59.7	+ (+)	Test

[a] ΔG_{exp} calculated from experimental K_d values as $\Delta G = RT \ln K_d$ where R is the gas constant (1.987×10^{-3} kcal K^{-1} mol^{-1}) and T is the temperature at standard conditions (298 K). Predicted ΔG (ΔG_{pred}) calculated according to Model 1. ΔG values expressed as kcal/mol.
[b] Absolute value of difference between experimental and predicted ΔG values.
[c] K_d values were obtained from Dijksterhuis *et al.* (27) and represent the average values reported. All K_d values expressed in nM.
[d] Guide to affinity range classifications: <10 nM, ++++; 10–40 nM, +++; 40–100 nM, ++; 100–400 nM, +; >400 nM, −. Cases in which the experimental and predicted K_d values occur in different ranges are underlined. Range in which value of experimental K_d occurs shown outside parentheses; range in which predicted K_d value occurs shown inside parentheses.

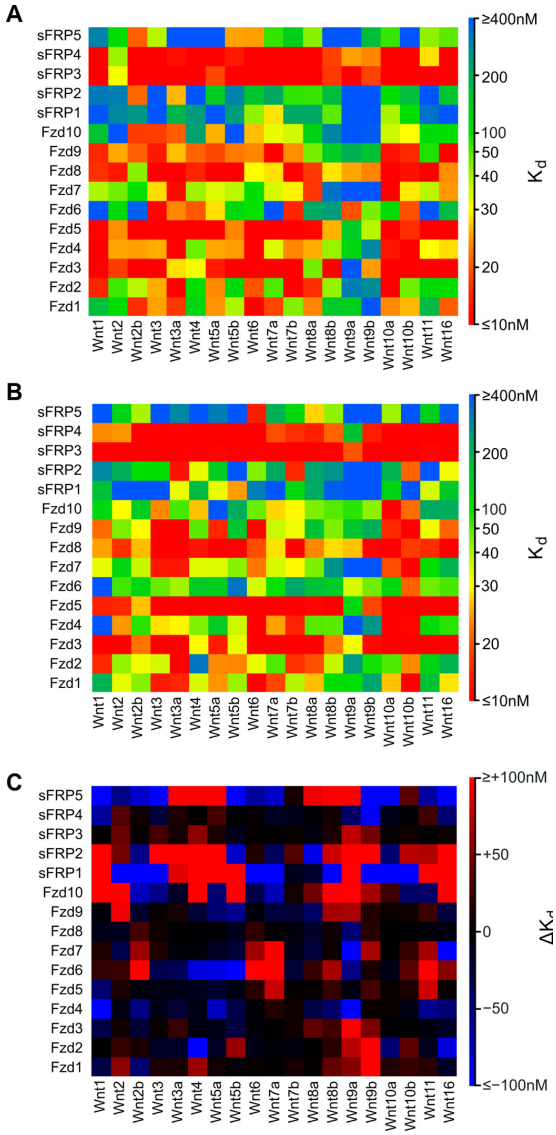

Figure 5. Binding affinity predictions by Model 1 for Wnt-Fzd interactions. *A*, mouse interactions. *B*, human interactions. *C*, binding affinity differences (ΔK_d) between equivalent Wnt-Fzd interactions of mouse and human calculated as ΔK_d = mouse K_d − human K_d. Positive ΔK_d is indicative of a lower affinity interaction in mouse compared with human; negative ΔK_d indicates a higher affinity interaction in mouse compared with human.

action of human Fzd3 with Wnt5b is predicted to be of much lower affinity than the equivalent mouse interaction. The affinity of the mouse Wnt2 for SFRP3 and SFRP4 is predicted to be lower than the equivalent interactions in humans; however, Wnt9a is predicted to have increased affinity for these proteins in mouse compared with human. Significant differences in the predicted affinities of human Fzd4 for Wnt1, Wnt5a, and Wnt11 compared with the mouse interactions are observed; all of these interactions are predicted to be very low in binding affinity in humans, whereas in mice these are all predicted to be very high affinity. Large differences in the predicted affinities occur when comparing the interactions of mouse and human Fzd6, Fzd10, SFRP1, SFRP2, and SFRP5 (Fig. 5*C*); however, these interactions are generally predicted to be of low to moderate affinity and may not be indicative of different roles for Wnt interactions with these proteins in the two species.

Analysis of residues of functional importance to Wnt-Fzd CRD interactions

To propose residues of functional importance to Wnt-Fzd interactions, all 570 Wnt-Fzd CRD models were subject to MM-GB/SA analysis with per-residue decomposition using AMBER14 (35). This calculation allows the identification of specific residues making large contributions to the binding energy, which, in turn, can be used to suggest the most significant intermolecular contacts in the interaction. High-affinity complexes will generally have more residues making large contributions to the binding energy compared with low-affinity complexes; thus, high-affinity complexes will have greater influence on the designation of sequence positions of general importance to Wnt-Fzd CRD interactions.

Analysis of Fzd CRD-binding regions of Wnt indicates two major regions utilized by Wnt in binding Fzd CRDs (Fig. 6*A*). These correspond to the thumb and index finger regions of Wnt, which are already well known as Fzd CRD-binding regions (19, 36). Interestingly, Wnt residues beyond these two regions are rarely implicated in Fzd CRD binding (supplemental Fig. S15), and the majority of Wnt residues in these regions frequently implicated in Fzd CRD binding are highly (often entirely) conserved in human and mouse Wnts.

In contrast to the Fzd CRD-binding regions of Wnt, which appear highly conserved and occupy relatively small sections of the Wnt sequence, the Wnt-binding regions of Fzd CRDs are distributed across several segments of the CRDs and often incorporate poorly conserved residues. Four sequences in the Fzd CRDs can be defined (Fig. 6*A*), two of which interact with the Wnt thumb region and two of which interact with the Wnt index finger region, with several additional residues of importance identified in specific cases (supplemental Fig. S16). Highly conserved Fzd CRD residues frequently implicated in Wnt binding are generally associated with lipid binding: the F*X*P motif, which frequently occurs within a helix forming one side of the lipid-binding site of the Fzd CRD, and the phenylalanine of an F*X*W motif in the latter part of the sequence both interact directly with the Wnt lipid (Fig. 6*B*). Hydrophobic residues adjacent to the final cysteine in the Fzd CRD are frequently implicated in binding the Wnt index finger, as are hydrophobic residues adjacent to the fourth cysteine of the Fzd CRD. However, the involvement of particular Fzd CRD residues in binding is often highly influenced by sequence variation, even for positions frequently implicated in Wnt binding. The greatest deviations in the utilization of Wnt-binding residues with respect to the set of Fzd CRDs occur in Fzd3, Fzd6, SFRP3, and SFRP4. The region corresponding to the F*X*P motif in SFRP4 occurs as YEE; the tyrosine and glutamate residues in this sequence are never implicated as strong contributors to

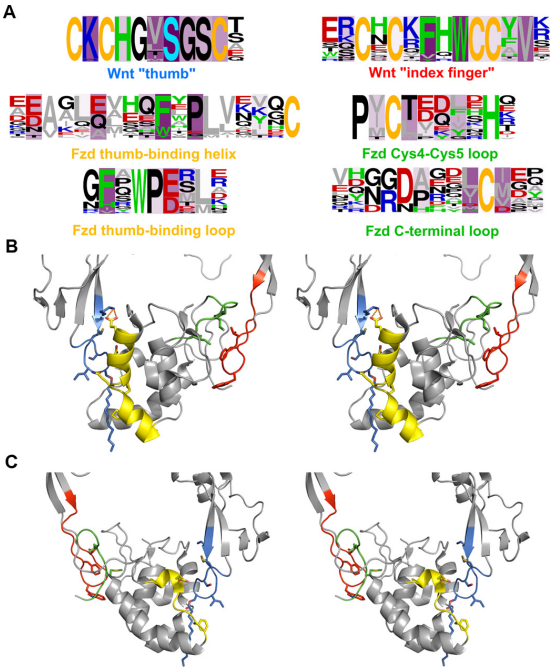

Figure 6. Residues making significant contributions to the binding energy in the majority of Wnt-Fzd CRD complexes. *A*, logo analyses of Wnts (*first row*) and Fzd CRDs (*second two rows*) highlighting the major regions involved in interactions. Fzd sequences interacting with a specific region of Wnt are shown *below* the sequence of Wnt corresponding to that region. *Green*, aromatic residues (Trp, Phe, His, and Tyr); *gray*, aliphatic residues (Val, Leu, Ile, Met, and Ala); *blue*, basic residues (Arg and Lys); *red*, acidic residues (Asp and Glu); *yellow*, cysteine; *light blue*, palmitoleoylserine (*A* only); *black*, all other residues (Gly, Pro, Ser, Thr, Gln, and Asn). Logos are presented as frequency plots. Intensity of *purple shading* indicates the number of complexes in which the residue at that position is a significant contributor to the complex binding energy. *B* and *C*, cross-eyed stereoviews of the "front" (*B*) and "rear" (*C*) of the XWnt8-mFzd8 crystal structure complex (Protein Data Bank code 4F0A) with major interacting regions highlighted. Residues corresponding to positions frequently involved in interactions across the full set of Wnt-Fzd CRD complexes are shown as *sticks*. Regions are colored according to the caption color in *panel A*. The front view displays the regions of the *middle row* of *panel A*; the rear view displays the regions of the *bottom row* of *panel A*.

binding any Wnt. In SFRP3, the phenylalanine of the motif is retained, but the proline is replaced by glycine; the phenylalanine is strongly implicated in binding to all Wnts, whereas this is never the case for glycine. The glutamates of a motif frequently occurring as EAGLE are often implicated in Fzd CRD binding to Wnt. In Fzd3 and Fzd6, the residue corresponding to the first glutamate is never strongly implicated in binding to any Wnt; this is replaced by a threonine in Fzd3 and an isoleucine in Fzd6. Substitution of this residue with aspartate (as occurs in several Fzds and SFRPs) or glutamine (as occurs in SFRP3 and SFRP4) does not appear to greatly influence the frequency with which this residue is involved in Wnt binding. Similarly, replacement of the second glutamate in the motif with alanine, as occurs in Fzd3, SFRP3, and SFRP4, eliminates the importance of this position to Wnt binding, whereas retaining it as a glutamate (as in Fzd6 and other Fzds and SFRPs), aspartate, or even glutamine does not seem to affect the frequency of its importance to binding.

Discussion

In this study, we have developed a model for predicting the binding affinity of Wnt-Fzd interactions. Although the model was developed against a relatively small set of data from a single study, there is nonetheless excellent agreement between affinities predicted in the current study and those experimentally determined in other studies that were not included in model building and testing here. The binding affinity of Wnt3a for the mouse SFRP3 was determined by surface plasmon resonance to be 7.9 nM (37); our model predicts this interaction to be at 0.28 nM, suggesting strong binding affinity. Binding affinities of Wnt3a, Wnt7a, Fzd10, and SFRP4 measured using ELISA (38) confirm our model's prediction that the Fzd5-Wnt3a interaction was stronger than that of Fzd10-Wnt7a and Wnt7a-SFRP4. However, direct comparisons of K_d values predicted by our model and those determined by ELISA are challenging as our model has been optimized against BLI data, where a direct interaction is measured, whereas ELISA is a coupled assay; thus, K_d values obtained from BLI are likely to indicate higher affinity than those obtained from ELISA.

As experimentally determined binding affinities of Wnt-Fzd CRD interactions are largely limited to those included in our training and test sets, it is also pertinent to investigate whether interactions demonstrated experimentally through coIP were predicted by our model to have strong binding affinities. mFzd4-mWnt2b (39), hFzd4-hWnt2 (40), mFzd4-mWnt7b (41), mFzd6-Wnt4 (42), and hWnt3a-hSFRP4 (43), which were shown by coIP to interact, are predicted by our model to bind with an affinity in the intermediate or tighter range (<40 nM). However, the interaction of SFRP1 with Wnt5a, which has been demonstrated by coIP (44), is suggested by our model to bind in the low micromolar range. Although this would be within the range detectable by coIP and is indeed a typical range for other interactions of biological relevance, particularly protein-carbohydrate interactions (45), binding affinities of functionally relevant Wnt-Fzd CRD interactions generally appear to occur in the low-to-mid nanomolar range, as evidenced in the data upon which we have based our prediction model. Therefore, it is likely that the affinity of the SFRP1-Wnt5a interaction is drastically underestimated by the model.

Despite the failure of the model in selected cases to achieve accurate predictions, the model nonetheless performs remarkably well at predicting binding affinities and likely interactors, particularly when considering that the Wnt-Fzd CRD interaction is rather complex due to involvement of both protein-protein and protein-lipid interactions at different sites. This would further suggest its usefulness in predicting the effect of Wnt/Fzd mutations to residues involved in either of the binding sites. The predictive success of the model is likely attributable to two main factors. The first is the use of a test set of cases separated from the training set to validate the model, which is not always performed in developing quantitative structure-activity relationships; even more remarkably, the use of an external data set for model validation appears to be a matter of some debate in the quantitative structure-activity relationship literature (46).

The second is the incorporation of a term in the model specifically considering the contribution to binding made by the lipid. The direct involvement of Wnt lipidation in facilitating the Wnt-Fzd interaction is likely unusual among protein-protein interactions; lipidation typically appears to influence the solubility and localization of proteins, rather than directly facilitate protein-protein interactions (47). However, other post-translational modification of proteins, such as glycosylation, phosphorylation, and methylation, are very common and are often involved in facilitating protein folding and mediating protein-protein interactions (48–50). Because post-translational modifications such as these are generally not accommodated in protein-protein docking and scoring, the strategy demonstrated here is one that could be adapted to facilitate their inclusion in protein-protein docking and scoring.

This study has revealed trends with regard to the selectivity and promiscuity of Wnt ligands for Fzd CRDs. The study particularly highlights the promiscuous nature of SFRP4, a Wnt antagonist of interest to our group (51–56). SFRP3 is predicted to display similarly low selectivity for Wnt ligands, whereas SFRP1, SFRP2, and SFRP5 are predicted to display much higher selectivity. The various levels of selectivity are likely to be due to the evolutionary development of tissue expression patterns of Wnt ligands and Fzd receptors, where SFRPs can partially limit aberrant Wnt signaling for controlled tissue development (57).

This study has focused on the interactions of Wnt proteins with the Frizzled-type cysteine-rich domains of the Fzd receptors and the secreted Frizzled-related proteins. However, a variety of other proteins also contain Frizzled-type CRDs, albeit less closely sequence-related to those of the Fzds and SFRPs. These include Smoothened, atrial natriuretic peptide-converting enzyme (CORIN), the tyrosine protein kinase transmembrane receptors ROR1 and ROR2, the skeletal muscle receptor tyrosine protein kinase (MuSK, for which a structure of the Fzd CRD has been experimentally solved (58)), the collagen XVIII α-1 chain, carboxypeptidase Z, and the membrane Frizzled-related protein. With the exception of the RORs (59–62), it is unknown whether any Wnt binds to these proteins and, if so, whether such an interaction is functionally relevant in the context of Wnt signaling. The approaches utilized in the current study could be applied to investigate the binding of Wnts to the Frizzled-type CRDs of these proteins, which in turn could stimulate further research into alternative Wnt signaling pathways.

It is important to note that a high-affinity interaction between a given Wnt and a given CRD does not necessarily translate into a signal transduction event. Wnt signaling involves several additional proteins both extracellularly and intracellularly. For example, in canonical Wnt signaling, Wnt binds to a Fzd CRD as well as the co-receptor LRP5/6 (63); on the intracellular side, this likely causes a conformational change in Fzd, resulting in movement of the Fzd intracellular loop 3 and C-terminal helix, which in turn permits Dvl binding and subsequent signal transduction (64, 65). Thus, the biological relevance of given Wnt-Fzd CRD interactions will be influenced by the co-expression/co-localization of these other proteins. Recent structural data on LRP6 (66–68) and the Smoothened receptor, a Class F GPCR related to Fzd receptors (69–72), as well as the availability of Dvl domain structures (73–76) and knowledge of key residues in the Fzd-Dvl interaction (64, 77, 78) provide the opportunity to investigate more completely the structural basis of canonical Wnt signaling. Additionally, the structures of several intracellular components in non-canonical Wnt signaling pathways are known or adopt structurally characterized folds, suggesting the potential for structural investigations. The models generated in this study provide a solid basis by which to pursue further structural studies of Wnt signaling and, perhaps of greater importance, given the combinatorial nature of potential Wnt-Fzd interactions, suggest specific interacting partners on which to focus experimental and computational efforts.

Experimental procedures

Template preparation

The template structure for all models was the complex of the XWnt8 with the mouse Fzd8 CRD (Protein Data Bank code 4F0A) (19). This structure was initially processed by the Protein Preparation Wizard, with missing side chains and loops filled in by Prime. Although the identity of the lipid modification to XWnt8 in this structure could not be conclusively determined (19), we have presumed this modification to be palmitoleic acid, as indicated either by direct experimental evidence or comparison with similar sequences for which this modification has been demonstrated (18, 79–83). The lipid in the structure was manually modified using Maestro to be a palmitoleic acid modification, which involved the creation of a double bond between carbons 9 and 10 and the addition of carbons 15 and 16 to the lipid, which were missing from the structure. The lipid was subject to a Monte Carlo multiple minimum conformational search using Macromodel, with the region comprising carbons 9–16, as well as the hydrogen atoms attached to these carbons, defined as a freely moving substructure, residues within 6.0 Å of this defined as a frozen shell, and a torsional constraint to ensure *cis* double bond geometry about carbons 9 and 10. Automatic setup of the substructure was used to define rotatable bonds to be searched; however, all torsion check parameters were removed. Extended torsion sampling was used. A maximum of 10,000 steps was used for the search with a maximum of 2000 steps per rotatable bond. The lowest energy structure obtained from the search provided a template structure for the lipid that was used in all models.

Homology modeling

Sequences of Wnts, Frizzled, and SFRP CRDs from both mouse and human were obtained from the UniProt database (84) (accession numbers are provided in supplemental Table S1). Homology models were prepared using Prime 4.1 (85) (sequence ranges and alignments used are provided in supplemental Figs. S2 and S3). All models were prepared using knowledge-based building; however, because of the presence of large insertions in the human and mouse Wnt6, Wnt10a, and Wnt10b sequences relative to XWnt8, an alternative strategy to building these structures was performed (see below). Disulfide bonds c13–c17 and c16–c24 in Wnt (see Ref. 36 for description of cysteine numbering in Wnts) typically could not be created during the model building process due to being adjacent to insertions/gaps in the sequence alignment; these bonds were

manually inserted, and the residues involved were energy-minimized. The lipid structure generated during template preparation was not included during Wnt model building but manually attached following model building.

To build the structures of the human and mouse Wnt6, Wnt10a, and Wnt10b, an initial model of the complete mouse Wnt10a was generated using the I-TASSER server (86). Structures of the remaining Wnts were then built using knowledge-based building in Prime against both the mouse Wnt10a model generated by I-TASSER (to provide the structure of the insertion) and the XWnt8 structure (to provide a template for modeling the remainder of the structure).

Complex generation and refinement

All combinations of Wnt-CRD complexes were generated by merging the structures of each of the models built in the previous step. The generated complexes were subject to refinement using Prime 4.1. The refinement process was facilitated through the use of a KNIME workflow (supplemental Fig. S4). In each complex, non-template residues and residues within 6.0 Å of the binding interface were subject to Prime Minimization and Prime Side-Chain Prediction, followed by a second Prime Minimization. The Wnt lipidation was excluded from the first minimization to allow CRD residues to relax around it but included in the second minimization. For complexes involving mouse and human Wnt6, Wnt10a, and Wnt10b, the large insertions modeled by I-TASSER were also subject to the refinement procedure. The quality of the refined models was assessed using the MolProbity score as calculated by the MolProbity module within PHENIX (87). The quality of the refined models was also assessed by calculating the RMSD of the Cα atoms and the TM-score with respect to the XWnt8-mFzd8 CRD complex. These measurements were both calculated using MM-align (88), with the option to enforce interface alignment by the default cutoff enabled.

Development and validation of the binding affinity prediction model

Complexes of mouse Wnt3a, Wnt4, Wnt5a, and Wnt5b with mouse Fzd1, Fzd2, Fzd4, Fzd5, Fzd7, and Fzd8 were rescored using all of the scoring functions contained in the CCharPPI server (28). As the scoring functions are generally only capable of considering interactions between protein residues, the lipid modification to Wnt was removed prior to rescoring. To consider contributions to the binding affinity made by the lipid, Prime MM-GB/SA calculations on the interaction between the lipid and the CRDs were performed. For these calculations, the protein component of Wnt was removed.

The scores for each complex by each scoring function in CCharPPI as well as the values of the terms provided by the Prime MM-GB/SA calculations were loaded into Maestro. A property containing the dissociation constants determined by BLI for selected mouse Wnt-Fzd CRD pairs (27) was manually created and used to define the activity property. Complexes involving interactions with either Wnt4 or Fzd1 comprised the test set, whereas all other complexes comprised the training set; the training and test sets are summarized under "Results" (Table 3). Both the training and test sets cover a diverse range of Wnts, Fzds, and binding affinities for Wnt-Fzd interactions.

Strike was used to generate affinity prediction models. Multiple linear regression was used to build models. Functions from CCharPPI and properties from Prime MM-GB/SA provided the descriptors used in model building; the full list of functions and properties considered in model building is provided in supplemental Table S5. The success of the models in predicting binding affinities for complexes in both the training and test sets was evaluated using RMSE and the percentage of complexes for which the predicted value occurred within the experimental range ($RMSE_{train}$, $RMSE_{test}$, $InExp_{train}$, and $InExp_{test}$).

All possible three-descriptor models incorporating one term from Prime MM-GB/SA and the remaining two terms from CCharPPI were investigated. Models with $RMSE_{train}$ less than 0.5 kcal/mol and $InExp_{train}$ greater than 50% were selected for testing. Models performing at least as well for the test set as for the training set (*i.e.* $RMSE_{test} \leq 0.5$ kcal/mol and $InExp_{test} \geq 50\%$) were selected for further elaboration into four-descriptor models, which were generated by adding an additional term from CCharPPI to the best performing three-descriptor models. Four-descriptor models giving $RMSE_{train}$ and $RMSE_{test}$ less than 0.3 kcal/mol and $InExp_{train}$ and $InExp_{test}$ greater than 75% were selected as high-performing models. Elaboration of the four-descriptor models into five-descriptor models was also pursued by adding another term from CCharPPI.

As a final check of model quality, we also checked whether the approximate range of binding affinity predicted by the best models is in that expected. Dijksterhuis *et al.* (27) used a simplified scheme wherein Wnt-Fzd binding affinities were classified as strong (<10 nM; ++++), intermediate (10–40 nM; +++), weak (40–100 nM; ++), very weak (>100 nM; +), and non-binding (−). We have utilized this scheme with some modification; we have considered predictions of 100–400 nM to constitute the very weak (+) category and predictions greater than 400 nM to be effectively non-binding (−); the 400 nM limit was chosen in relation to the intermediate/weak affinity range defined.

Analysis of functional residues in Wnt-Fzd interactions

All 570 Wnt-Fzd CRD models were subject to MM-GB/SA analysis using AMBER14 (35). Wnt-Fzd complexes were parameterized using the ff14SB force field (89). Parameter generation for *O*-palmitoleoylserine was facilitated by Antechamber (90), adapting procedures described in both the AMBER14 reference manual and AMBER tutorials. MMPBSA.py facilitated MM-GB/SA calculations (91). The modified generalized Born model of Onufriev *et al.* (igb = 5) (92) with a salt concentration of 0.1 M was used to calculate the polar desolvation energy. The non-polar desolvation energy was calculated using surface areas derived from the linear combinations of pairwise overlaps (LCPO) method (93) multiplied by surface tension (the default of 0.0072 kcal/(mol Å^2) was used). Energies calculated by MM-GB/SA were decomposed on a per-residue basis with 1–4 terms added to the internal potential terms (idecomp = 1) (94). Residues contributing greater than ±2.0 kcal/mol to the total MM-GB/SA binding energy were selected as being of functional importance to binding. Logo analysis of

regions within the Wnt and Fzd sequences frequently found to contain residues of functional importance to Wnt-Fzd binding was performed using the WebLogo server (95). Sequence logos were generated as frequency plots.

Author contributions—M. A. conceived the idea for the work, conducted the experiments, and analyzed the results. M. A. and S. Ö.-G. P. prepared the manuscript. M. A., S. Ö.-G. P., and A. D. critically reviewed and revised the manuscript. All authors reviewed the results and approved the final version of the manuscript.

Acknowledgment—We gratefully acknowledge Prof. Yvonne Jones (University of Oxford) for critical discussion in the review of the final manuscript.

References

1. Holstein, T. W. (2012) The evolution of the Wnt pathway. *Cold Spring Harb. Perspect. Biol.* **4,** a007922
2. Hikasa, H., and Sokol, S. Y. (2013) Wnt signaling in vertebrate axis specification. *Cold Spring Harb. Perspect. Biol.* **5,** a007955
3. Polakis, P. (2012) Wnt signaling in cancer. *Cold Spring Harb. Perspect. Biol.* **4,** a008052
4. Komiya, Y., and Habas, R. (2008) Wnt signal transduction pathways. *Organogenesis* **4,** 68–75
5. Pohl, S. Ö.-G, Brook, N., Agostino, M., Arfuso, F., Kumar, A. P., and Dharmarajan, A. (2017) Wnt signaling in triple-negative breast cancer. *Oncogenesis* **6,** e310
6. Dijksterhuis, J. P., Petersen, J., and Schulte, G. (2014) WNT/Frizzled signalling: receptor-ligand selectivity with focus on FZD-G protein signalling and its physiological relevance: IUPHAR Review 3. *Br. J. Pharmacol.* **171,** 1195–1209
7. He, X., Semenov, M., Tamai, K., and Zeng, X. (2004) LDL receptor-related proteins 5 and 6 in Wnt/β-catenin signaling: arrows point the way. *Development* **131,** 1663–1677
8. Wallingford, J. B., and Habas, R. (2005) The developmental biology of Dishevelled: an enigmatic protein governing cell fate and cell polarity. *Development* **132,** 4421–4436
9. Clevers, H. (2006) Wnt/β-catenin signaling in development and disease. *Cell* **127,** 469–480
10. Huelsken, J., and Behrens, J. (2002) The Wnt signalling pathway. *J. Cell Sci.* **115,** 3977–3978
11. Stamos, J. L., and Weis, W. I. (2013) The β-catenin destruction complex. *Cold Spring Harb. Perspect. Biol.* **5,** a007898
12. Kohn, A. D., and Moon, R. T. (2005) Wnt and calcium signaling: β-catenin-independent pathways. *Cell Calcium* **38,** 439–446
13. Kühl, M., Sheldahl, L. C., Malbon, C. C., and Moon, R. T. (2000) Ca^{2+}/calmodulin-dependent protein kinase II is stimulated by Wnt and Frizzled homologs and promotes ventral cell fates in *Xenopus*. *J. Biol. Chem.* **275,** 12701–12711
14. Sheldahl, L. C., Park, M., Malbon, C. C., and Moon, R. T. (1999) Protein kinase C is differentially stimulated by Wnt and Frizzled homologs in a G-protein-dependent manner. *Curr. Biol.* **9,** 695–698
15. De, A. (2011) Wnt/Ca^{2+} signaling pathway: a brief overview. *Acta Biochim. Biophys. Sin.* **43,** 745–756
16. Green, J., Nusse, R., and van Amerongen, R. (2014) The role of Ryk and Ror receptor tyrosine kinases in Wnt signal transduction. *Cold Spring Harb. Perspect. Biol.* **6,** a009175
17. Smolich, B. D., McMahon, J. A., McMahon, A. P., and Papkoff, J. (1993) Wnt family proteins are secreted and associated with the cell surface. *Mol. Biol. Cell* **4,** 1267–1275
18. Gao, X., and Hannoush, R. N. (2014) Single-cell imaging of Wnt palmitoylation by the acyltransferase porcupine. *Nat. Chem. Biol.* **10,** 61–68
19. Janda, C. Y., Waghray, D., Levin, A. M., Thomas, C., and Garcia, K. C. (2012) Structural basis of Wnt recognition by Frizzled. *Science* **337,** 59–64
20. Wang, Y., Macke, J. P., Abella, B. S., Andreasson, K., Worley, P., Gilbert, D. J., Copeland, N. G., Jenkins, N. A., and Nathans, J. (1996) A large family of putative transmembrane receptors homologous to the product of the *Drosophila* tissue polarity gene frizzled. *J. Biol. Chem.* **271,** 4468–4476
21. Xu, Q., Wang, Y., Dabdoub, A., Smallwood, P. M., Williams, J., Woods, C., Kelley, M. W., Jiang, L., Tasman, W., Zhang, K., and Nathans, J. (2004) Vascular development in the retina and inner ear: control by Norrin and Frizzled-4, a high-affinity ligand-receptor pair. *Cell* **116,** 883–895
22. Ye, X., Wang, Y., Cahill, H., Yu, M., Badea, T. C., Smallwood, P. M., Peachey, N. S., and Nathans, J. (2009) Norrin, frizzled-4, and Lrp5 signaling in endothelial cells controls a genetic program for retinal vascularization. *Cell* **139,** 285–298
23. Surana, R., Sikka, S., Cai, W., Shin, E. M., Warrier, S. R., Tan, H. J., Arfuso, F., Fox, S. A., Dharmarajan, A. M., and Kumar, A. P. (2014) Secreted frizzled related proteins: implications in cancers. *Biochim. Biophys. Acta* **1845,** 53–65
24. Cruciat, C. M., and Niehrs, C. (2013) Secreted and transmembrane Wnt inhibitors and activators. *Cold Spring Harb. Perspect. Biol.* **5,** a015081
25. Dann, C. E., Hsieh, J. C., Rattner, A., Sharma, D., Nathans, J., and Leahy, D. J. (2001) Insights into Wnt binding and signalling from the structures of two Frizzled cysteine-rich domains. *Nature* **412,** 86–90
26. Lopez-Rios, J., Esteve, P., Ruiz, J. M., and Bovolenta, P. (2008) The Netrin-related domain of Sfrp1 interacts with Wnt ligands and antagonizes their activity in the anterior neural plate. *Neural Dev.* **3,** 19
27. Dijksterhuis, J. P., Baljinnyam, B., Stanger, K., Sercan, H. O., Ji, Y., Andres, O., Rubin, J. S., Hannoush, R. N., and Schulte, G. (2015) Systematic mapping of WNT-FZD protein interactions reveals functional selectivity by distinct WNT-FZD pairs. *J. Biol. Chem.* **290,** 6789–6798
28. Moal, I. H., Jiménez-García, B., and Fernández-Recio, J. (2015) CCharPPI web server: computational characterisation of protein-protein interactions from structure. *Bioinformatics* **31,** 123–125
29. Yang, J., Yan, R., Roy, A., Xu, D., Poisson, J., and Zhang, Y. (2015) The I-TASSER Suite: protein structure and function prediction. *Nat. Methods* **12,** 7–8
30. Chen, V. B., Arendall W. B., 3rd, Headd, J. J., Keedy, D. A., Immormino, R. M., Kapral, G. J., Murray, L. W., Richardson, J. S., and Richardson, D. C. (2010) MolProbity: all-atom structure validation for macromolecular crystallography. *Acta Crystallogr. D Biol. Crystallogr.* **66,** 12–21
31. Zhang, Y., and Skolnick, J. (2004) Scoring function for automated assessment of protein structure template quality. *Proteins* **57,** 702–710
32. Chaudhury, S., Lyskov, S., and Gray, J. J. (2010) PyRosetta: a script-based interface for implementing molecular modeling algorithms using Rosetta. *Bioinformatics* **26,** 689–691
33. Zhang, J., and Zhang, Y. (2010) A novel side-chain orientation dependent potential derived from random-walk reference state for protein fold selection and structure prediction. *PLoS One* **5,** e15386
34. Andrusier, N., Nussinov, R., and Wolfson, H. J. (2007) FireDock: fast interaction refinement in molecular docking. *Proteins* **69,** 139–159
35. Salomon-Ferrer, R., Case, D. A., and Walker, R. C. (2013) An overview of the Amber biomolecular simulation package. *WIREs Comput. Mol. Sci.* **3,** 198–210
36. MacDonald, B. T., Hien, A., Zhang, X., Iranloye, O., Virshup, D. M., Waterman, M. L., and He, X. (2014) Disulfide bond requirements for active Wnt ligands. *J. Biol. Chem.* **289,** 18122–18136
37. Wawrzak, D., Métioui, M., Willems, E., Hendrickx, M., de Genst, E., and Leyns, L. (2007) Wnt3a binds to several sFRPs in the nanomolar range. *Biochem. Biophys. Res. Commun.* **357,** 1119–1123
38. Carmon, K. S., and Loose, D. S. (2010) Development of a bioassay for detection of Wnt-binding affinities for individual frizzled receptors. *Anal. Biochem.* **401,** 288–294
39. Ohta, K., Ito, A., Kuriyama, S., Lupo, G., Kosaka, M., Ohnuma, S., Nakagawa, S., and Tanaka, H. (2011) Tsukushi functions as a Wnt signaling inhibitor by competing with Wnt2b for binding to transmembrane protein Frizzled4. *Proc. Natl. Acad. Sci. U.S.A.* **108,** 14962–14967
40. Klein, D., Demory, A., Peyre, F., Kroll, J., Augustin, H. G., Helfrich, W., Kzhyshkowska, J., Schledzewski, K., Arnold, B., and Goerdt, S. (2008) Wnt2 acts as a cell type-specific, autocrine growth factor in rat hepatic

sinusoidal endothelial cells cross-stimulating the VEGF pathway. *Hepatology* **47,** 1018–1031
41. Wang, Z., Shu, W., Lu, M. M., and Morrisey, E. E. (2005) Wnt7b activates canonical signaling in epithelial and vascular smooth muscle cells through interactions with Fzd1, Fzd10, and LRP5. *Mol. Cell. Biol.* **25,** 5022–5030
42. Lyons, J. P., Mueller, U. W., Ji, H., Everett, C., Fang, X., Hsieh, J. C., Barth, A. M., and McCrea, P. D. (2004) Wnt-4 activates the canonical β-catenin-mediated Wnt pathway and binds Frizzled-6 CRD: functional implications of Wnt/β-catenin activity in kidney epithelial cells. *Exp. Cell Res.* **298,** 369–387
43. Constantinou, T., Baumann, F., Lacher, M. D., Saurer, S., Friis, R., and Dharmarajan, A. (2008) SFRP-4 abrogates Wnt-3a-induced β-catenin and Akt/PKB signalling and reverses a Wnt-3a-imposed inhibition of *in vitro* mammary differentiation. *J. Mol. Signal.* **3,** 10
44. Matsuyama, M., Aizawa, S., and Shimono, A. (2009) Sfrp controls apicobasal polarity and oriented cell division in developing gut epithelium. *PLoS Genet.* **5,** e1000427
45. Agostino, M., Velkov, T., Dingjan, T., Williams, S. J., Yuriev, E., and Ramsland, P. A. (2015) The carbohydrate-binding promiscuity of *Euonymus europaeus* lectin is predicted to involve a single binding site. *Glycobiology* **25,** 101–114
46. Veerasamy, R., Rajak, H., Jain, A., Sivadasan, S., Varghese, C. P., and Agrawal, R. K. (2011) Validation of QSAR models—strategies and importance. *Int. J. Drug Des. Discov.* **2,** 511–519
47. Resh, M. D. (2016) Fatty acylation of proteins: the long and the short of it. *Prog. Lipid Res.* **63,** 120–131
48. Xu, C., and Ng, D. T. (2015) Glycosylation-directed quality control of protein folding. *Nat. Rev. Mol. Cell Biol.* **16,** 742–752
49. Nishi, H., Hashimoto, K., and Panchenko, A. R. (2011) Phosphorylation in protein-protein binding: effect on stability and function. *Structure* **19,** 1807–1815
50. Bedford, M. T., and Clarke, S. G. (2009) Protein arginine methylation in mammals: who, what, and why. *Mol. Cell* **33,** 1–13
51. Perumal, V., Krishnan, K., Gratton, E., Dharmarajan, A. M., and Fox, S. A. (2015) Number and brightness analysis of sFRP4 domains in live cells demonstrates vesicle association signal of the NLD domain and dynamic intracellular responses to Wnt3a. *Int. J. Biochem. Cell Biol.* **64,** 91–96
52. Perumal, V., Pohl, S., Keane, K. N., Arfuso, F., Newsholme, P., Fox, S., and Dharmarajan, A. (2016) Therapeutic approach to target mesothelioma cancer cells using the Wnt antagonist, secreted frizzled-related protein 4: metabolic state of cancer cells. *Exp. Cell Res.* **341,** 218–224
53. Pohl, S., Scott, R., Arfuso, F., Perumal, V., and Dharmarajan, A. (2015) Secreted frizzled-related protein 4 and its implications in cancer and apoptosis. *Tumour Biol.* **36,** 143–152
54. Warrier, S., Balu, S. K., Kumar, A. P., Millward, M., and Dharmarajan, A. (2013) Wnt antagonist, secreted frizzled-related protein 4 (sFRP4), increases chemotherapeutic response of glioma stem-like cells. *Oncol. Res.* **21,** 93–102
55. Wolf, V., Ke, G., Dharmarajan, A. M., Bielke, W., Artuso, L., Saurer, S., and Friis, R. (1997) DDC-4, an apoptosis-associated gene, is a secreted frizzled relative. *FEBS Lett.* **417,** 385–389
56. Muley, A., Majumder, S., Kolluru, G. K., Parkinson, S., Viola, H., Hool, L., Arfuso, F., Ganss, R., Dharmarajan, A., and Chatterjee, S. (2010) Secreted frizzled-related protein 4: an angiogenesis inhibitor. *Am. J. Pathol.* **176,** 1505–1516
57. Bovolenta, P., Esteve, P., Ruiz, J. M., Cisneros, E., and Lopez-Rios, J. (2008) Beyond Wnt inhibition: new functions of secreted Frizzled-related proteins in development and disease. *J. Cell Sci.* **121,** 737–746
58. Stiegler, A. L., Burden, S. J., and Hubbard, S. R. (2009) Crystal structure of the frizzled-like cysteine-rich domain of the receptor tyrosine kinase MuSK. *J. Mol. Biol.* **393,** 1–9
59. Cui, B., Zhang, S., Chen, L., Yu, J., Widhopf, G. F., 2nd, Fecteau, J.-F., Rassenti, L. Z., and Kipps, T. J. (2013) Targeting ROR1 inhibits epithelial-mesenchymal transition and metastasis. *Cancer Res.* **73,** 3649–3660
60. Henry, C., Quadir, A., Hawkins, N. J., Jary, E., Llamosas, E., Kumar, D., Daniels, B., Ward, R. L., and Ford, C. E. (2015) Expression of the novel Wnt receptor ROR2 is increased in breast cancer and may regulate both β-catenin dependent and independent Wnt signalling. *J. Cancer Res. Clin. Oncol.* **141,** 243–254
61. Liu, Y., Rubin, B., Bodine, P. V., and Billiard, J. (2008) Wnt5a induces homodimerization and activation of Ror2 receptor tyrosine kinase. *J. Cell. Biochem.* **105,** 497–502
62. Zhang, S., Chen, L., Cui, B., Chuang, H. Y., Yu, J., Wang-Rodriguez, J., Tang, L., Chen, G., Basak, G. W., and Kipps, T. J. (2012) ROR1 is expressed in human breast cancer and associated with enhanced tumor-cell growth. *PLoS One* **7,** e31127
63. MacDonald, B. T., and He, X. (2012) Frizzled and LRP5/6 receptors for Wnt/β-catenin signaling. *Cold Spring Harb. Perspect. Biol.* **4,** a007880
64. Tauriello, D. V., Jordens, I., Kirchner, K., Slootstra, J. W., Kruitwagen, T., Bouwman, B. A., Noutsou, M., Rüdiger, S. G., Schwamborn, K., Schambony, A., and Maurice, M. M. (2012) Wnt/β-catenin signaling requires interaction of the Dishevelled DEP domain and C terminus with a discontinuous motif in Frizzled. *Proc. Natl. Acad. Sci. U.S.A.* **109,** E812–E820
65. Cong, F., Schweizer, L., and Varmus, H. (2004) Wnt signals across the plasma membrane to activate the β-catenin pathway by forming oligomers containing its receptors, Frizzled and LRP. *Development* **131,** 5103–5115
66. Chang, T. H., Hsieh, F. L., Zebisch, M., Harlos, K., Elegheert, J., and Jones, E. Y. (2015) Structure and functional properties of Norrin mimic Wnt for signalling with Frizzled4, Lrp5/6, and proteoglycan. *eLife* **4,** e06554
67. Cheng, Z., Biechele, T., Wei, Z., Morrone, S., Moon, R. T., Wang, L., and Xu, W. (2011) Crystal structures of the extracellular domain of LRP6 and its complex with DKK1. *Nat. Struct. Mol. Biol.* **18,** 1204–1210
68. Ahn, V. E., Chu, M. L., Choi, H. J., Tran, D., Abo, A., and Weis, W. I. (2011) Structural basis of Wnt signaling inhibition by Dickkopf binding to LRP5/6. *Dev. Cell* **21,** 862–873
69. Wang, C., Wu, H., Evron, T., Vardy, E., Han, G. W., Huang, X. P., Hufeisen, S. J., Mangano, T. J., Urban, D. J., Katritch, V., Cherezov, V., Caron, M. G., Roth, B. L., and Stevens, R. C. (2014) Structural basis for smoothened receptor modulation and chemoresistance to anticancer drugs. *Nat. Commun.* **5,** 4355
70. Wang, C., Wu, H., Katritch, V., Han, G. W., Huang, X. P., Liu, W., Siu, F. Y., Roth, B. L., Cherezov, V., and Stevens, R. C. (2013) Structure of the human smoothened receptor bound to an antitumour agent. *Nature* **497,** 338–343
71. Weierstall, U., James, D., Wang, C., White, T. A., Wang, D., Liu, W., Spence, J. C., Bruce Doak, R., Nelson, G., Fromme, P., Fromme, R., Grotjohann, I., Kupitz, C., Zatsepin, N. A., Liu, H., *et al.* (2014) Lipidic cubic phase injector facilitates membrane protein serial femtosecond crystallography. *Nat. Commun.* **5,** 3309
72. Byrne, E. F., Sircar, R., Miller, P. S., Hedger, G., Luchetti, G., Nachtergaele, S., Tully, M. D., Mydock-McGrane, L., Covey, D. F., Rambo, R. P., Sansom, M. S., Newstead, S., Rohatgi, R., and Siebold, C. (2016) Structural basis of Smoothened regulation by its extracellular domains. *Nature* **535,** 517–522
73. Madrzak, J., Fiedler, M., Johnson, C. M., Ewan, R., Knebel, A., Bienz, M., and Chin, J. W. (2015) Ubiquitination of the Dishevelled DIX domain blocks its head-to-tail polymerization. *Nat. Commun.* **6,** 6718
74. Wong, H. C., Mao, J., Nguyen, J. T., Srinivas, S., Zhang, W., Liu, B., Li, L., Wu, D., and Zheng, J. (2000) Structural basis of the recognition of the dishevelled DEP domain in the Wnt signaling pathway. *Nat. Struct. Biol.* **7,** 1178–1184
75. Zhang, Y., Appleton, B. A., Wiesmann, C., Lau, T., Costa, M., Hannoush, R. N., and Sidhu, S. S. (2009) Inhibition of Wnt signaling by Dishevelled PDZ peptides. *Nat. Chem. Biol.* **5,** 217–219
76. Yu, A., Xing, Y., Harrison, S. C., and Kirchhausen, T. (2010) Structural analysis of the interaction between Dishevelled2 and clathrin AP-2 adaptor, a critical step in noncanonical Wnt signaling. *Structure* **18,** 1311–1320
77. Wong, H. C., Bourdelas, A., Krauss, A., Lee, H. J., Shao, Y., Wu, D., Mlodzik, M., Shi, D. L., and Zheng, J. (2003) Direct binding of the PDZ domain of Dishevelled to a conserved internal sequence in the C-terminal region of Frizzled. *Mol. Cell* **12,** 1251–1260
78. Bertalovitz, A. C., Pau, M. S., Gao, S., Malbon, C. C., and Wang, H.-Y. (2016) Frizzled-4 C-terminus distal to KTXXXW motif is essential for normal dishevelled recruitment and Norrin-stimulated activation of Lef/Tcf-dependent transcriptional activation. *J. Mol. Signal.* **11,** 1

79. Coombs, G. S., Yu, J., Canning, C. A., Veltri, C. A., Covey, T. M., Cheong, J. K., Utomo, V., Banerjee, N., Zhang, Z. H., Jadulco, R. C., Concepcion, G. P., Bugni, T. S., Harper, M. K., Mihalek, I., Jones, C. M., *et al.* (2010) WLS-dependent secretion of WNT3A requires Ser209 acylation and vacuolar acidification. *J. Cell Sci.* **123,** 3357–3367
80. Takada, R., Satomi, Y., Kurata, T., Ueno, N., Norioka, S., Kondoh, H., Takao, T., and Takada, S. (2006) Monounsaturated fatty acid modification of Wnt protein: its role in Wnt secretion. *Dev. Cell* **11,** 791–801
81. Galli, L. M., and Burrus, L. W. (2011) Differential palmit(e)oylation of Wnt1 on C93 and S224 residues has overlapping and distinct consequences. *PLoS One* **6,** e26636
82. Doubravska, L., Krausova, M., Gradl, D., Vojtechova, M., Tumova, L., Lukas, J., Valenta, T., Pospichalova, V., Fafilek, B., Plachy, J., Sebesta, O., and Korinek, V. (2011) Fatty acid modification of Wnt1 and Wnt3a at serine is prerequisite for lipidation at cysteine and is essential for Wnt signalling. *Cell. Signal.* **23,** 837–848
83. Kakugawa, S., Langton, P. F., Zebisch, M., Howell, S. A., Chang, T. H., Liu, Y., Feizi, T., Bineva, G., O'Reilly, N., Snijders, A. P., Jones, E. Y., and Vincent, J. P. (2015) Notum deacylates Wnt proteins to suppress signalling activity. *Nature* **519,** 187–192
84. UniProt Consortium (2015) UniProt: a hub for protein information. *Nucleic Acids Res.* **43,** D204–D212
85. Jacobson, M. P., Friesner, R. A., Xiang, Z., and Honig, B. (2002) On the role of the crystal environment in determining protein side-chain conformations. *J. Mol. Biol.* **320,** 597–608
86. Roy, A., Kucukural, A., and Zhang, Y. (2010) I-TASSER: a unified platform for automated protein structure and function prediction. *Nat. Protoc.* **5,** 725–738
87. Adams, P. D., Afonine, P. V., Bunkóczi, G., Chen, V. B., Davis, I. W., Echols, N., Headd, J. J., Hung, L.-W., Kapral, G. J., Grosse-Kunstleve, R. W., McCoy, A. J., Moriarty, N. W., Oeffner, R., Read, R. J., Richardson, D. C., *et al.* (2010) PHENIX: a comprehensive Python-based system for macromolecular structure solution. *Acta Crystallogr. D Biol. Crystallogr.* **66,** 213–221
88. Mukherjee, S., and Zhang, Y. (2009) MM-align: a quick algorithm for aligning multiple-chain protein complex structures using iterative dynamic programming. *Nucleic Acids Res.* **37,** e83
89. Maier, J. A., Martinez, C., Kasavajhala, K., Wickstrom, L., Hauser, K. E., and Simmerling, C. (2015) ff14SB: improving the accuracy of protein side chain and backbone parameters from ff99SB. *J. Chem. Theory Comput.* **11,** 3696–3713
90. Wang, J., Wang, W., Kollman, P. A., and Case, D. A. (2006) Automatic atom type and bond type perception in molecular mechanical calculations. *J. Mol. Graph. Model.* **25,** 247–260
91. Miller B. R., 3rd, McGee, T. D., Jr., Swails, J. M., Homeyer, N., Gohlke, H., and Roitberg, A. E. (2012) MMPBSA.py: an efficient program for end-state free energy calculations. *J. Chem. Theory Comput.* **8,** 3314–3321
92. Onufriev, A., Bashford, D., and Case, D. A. (2004) Exploring protein native states and large-scale conformational changes with a modified generalized Born model. *Proteins* **55,** 383–394
93. Weiser, J., Shenkin, P. S., and Still, W. C. (1999) Approximate atomic surfaces from linear combinations of pairwise overlaps (LCPO). *J. Comput. Chem.* **20,** 217–230
94. Gohlke, H., Kiel, C., and Case, D. A. (2003) Insights into protein-protein binding by binding free energy calculation and free energy decomposition for the Ras-Raf and Ras-RalGDS complexes. *J. Mol. Biol.* **330,** 891–913
95. Crooks, G. E., Hon, G., Chandonia, J. M., and Brenner, S. E. (2004) WebLogo: a sequence logo generator. *Genome Res.* **14,** 1188–1190

Structure-based prediction of Wnt binding affinities for Frizzled-type cysteine-rich domains

Mark Agostino, Sebastian Öther-Gee Pohl and Arun Dharmarajan

J. Biol. Chem. 2017, 292:11218-11229.
doi: 10.1074/jbc.M117.786269 originally published online May 22, 2017

OPEN

Citation: Oncogenesis (2017) **6**, e310; doi:10.1038/oncsis.2017.14

www.nature.com/oncsis

REVIEW

Wnt signaling in triple-negative breast cancer

SÖ-G Pohl[1,2,3], N Brook[1,2,3], M Agostino[1,2,3,4], F Arfuso[1,2,3], AP Kumar[2,3,5,6,7] and A Dharmarajan[1,2,3]

Wnt signaling regulates a variety of cellular processes, including cell fate, differentiation, proliferation and stem cell pluripotency. Aberrant Wnt signaling is a hallmark of many cancers. An aggressive subtype of breast cancer, known as triple-negative breast cancer (TNBC), demonstrates dysregulation in canonical and non-canonical Wnt signaling. In this review, we summarize regulators of canonical and non-canonical Wnt signaling, as well as Wnt signaling dysfunction that mediates the progression of TNBC. We review the complex molecular nature of TNBC and the emerging therapies that are currently under investigation for the treatment of this disease.

Oncogenesis (2017) **6,** e310; doi:10.1038/oncsis.2017.14; published online 3 April 2017

INTRODUCTION

Breast cancer represents one of the most significant disease burdens of any cancer worldwide. Today, women have a one in eight chance of developing breast cancer over their lifetime, a risk that is significantly increased if they have inherited harmful mutations in *BRCA1* or *BRCA2*.[1] However, breast cancer is a complex, heterogeneous disease characterized by a great multitude of aberrations at the genomic and molecular level, which can manifest in dysregulated signaling pathways. A hallmark of many cancers is aberrant regulation of the Wnt signaling pathway, and breast cancer is no exception.[2]

Triple-negative breast cancer (TNBC), an aggressive subtype of breast cancer with a poor prognosis,[3] is characterized by tumors that do not express estrogen receptors (ERs) or progesterone receptors (PRs), nor display an overexpression of human epidermal growth factor receptor 2 (HER2).[4] Therapies targeted against HER2-positive breast cancers, such as trastuzumab (Herceptin),[5] and those targeted against ER-positive breast cancers, such as tamoxifen,[6] have no therapeutic benefit to individuals with the TNBC subtype. Surgical intervention and chemotherapy have been the major treatment avenues for TNBC; however, recently developed small molecules and immunotherapeutics[7] are showing promise. In this review, we will summarize the involvement of dysregulated Wnt signaling in the progression of TNBC and TNBC stem cells, as well as the emerging therapies that are currently under investigation.

THE WNT SIGNALING PATHWAY

The Wnt/β-catenin pathway (canonical pathway)

There are currently two models of canonical Wnt/β-catenin signaling. In the classical model, the destruction complex remains intact in the absence of Wnt stimulation (Figure 1a). Casein kinase 1 (CK1) primes β-catenin for destruction by phosphorylating Ser45, which then allows activated Glycogen synthase kinase 3 (GSK3) to phosphorylate β-catenin at Ser33, Ser37 and Thr41.[8] The phosphorylated residues of β-catenin interact with the β-propeller domain of the E3 ubiquitin ligase β-TrCP, which then ubiquitinates β-catenin, thus targeting it for proteosomal degradation.[9] Wnt/β-catenin signaling is initiated by Wnt ligands binding to a Frizzled receptor (FZD), as well as the co-receptors low-density lipoproteins 5/6 (LRP5/6). This results in activation of FZD, permitting binding of Dishevelled (Dvl)[10] and phosphorylation of one or more cytoplasmic motifs of LRP5/6. A single phosphorylated motif is sufficient to activate Wnt signaling.[11] Phosphorylated LRP5/6 can then interact with Axin. This interaction destabilizes the β-catenin destruction complex, which requires Axin as a scaffold and contains Dvl, the serine–threonine kinases casein kinase 1α/β (CK1), glycogen synthase kinase 3α/β (GSK3) and adenomatous polyposis coli (APC).[12] Destabilizing the destruction complex prevents phosphorylation of β-catenin, which then accumulates in the cytosol before translocating to the nucleus. Once there, it binds to Transcription factor/lymphoid enhancer-binding factor (TCF/LEF) transcription factors and displaces transcriptional repressor Groucho to initiate the transcription of Wnt target genes (Figure 1b).[13] In the new model,[14–16] the destruction complex is stabilized by Axin in both the presence and absence (Figure 1c) of Wnt activation, and β-catenin is degraded through phosphorylation-mediated recognition by β-TrCP in the intact complex. This allows newly synthesized β-catenin to accumulate in the cytosol before nuclear translocation (Figure 1d). This was demonstrated through co-immunoprecipitation, whereby β-catenin phosphorylated at Ser33/Ser37/Thr41 was shown to interact with the destruction complex upon Wnt activation, which also disrupted the interaction of β-TrCP with the Axin1-β–catenin complex.[15] It has also been proposed that GSK3 inhibition, and thus β-catenin translocation after Wnt activation, is mediated through the sequestration of GSK3 inside multivesicular endosomes.[17] This further demonstrates the complexity of Wnt signaling.

[1]Stem Cell and Cancer Biology Laboratory, Perth, WA, Australia; [2]School of Biomedical Sciences, Curtin University, Perth, WA, Australia; [3]Curtin Health Innovation Research Institute, Curtin University, Perth, WA, Australia; [4]Curtin Institute for Computation, Curtin University, Perth, WA, Australia; [5]Cancer Science Institute of Singapore, National University of Singapore, Singapore, Singapore; [6]Department of Pharmacology, Yong Loo Lin School of Medicine, National University of Singapore, Centre for Translational Medicine, Singapore, Singapore and [7]Department of Biological Sciences, University of North Texas, Denton, TX, USA. Correspondence: Dr AP Kumar, Department of Pharmacology, Yong Loo Lin School of Medicine, National University of Singapore, Centre for Translational Medicine, 14 Medical Drive, #11-01M, Singapore 117599, Singapore.
E-mail: csiapk@nus.edu.sg
or Professor A Dharmarajan, School of Biomedical Sciences, Curtin University, Kent Street, Bentley, Perth, WA 6102, Australia.
E-mail: a.dharmarajan@curtin.edu.au
Received 11 November 2016; revised 9 January 2017; accepted 24 January 2017

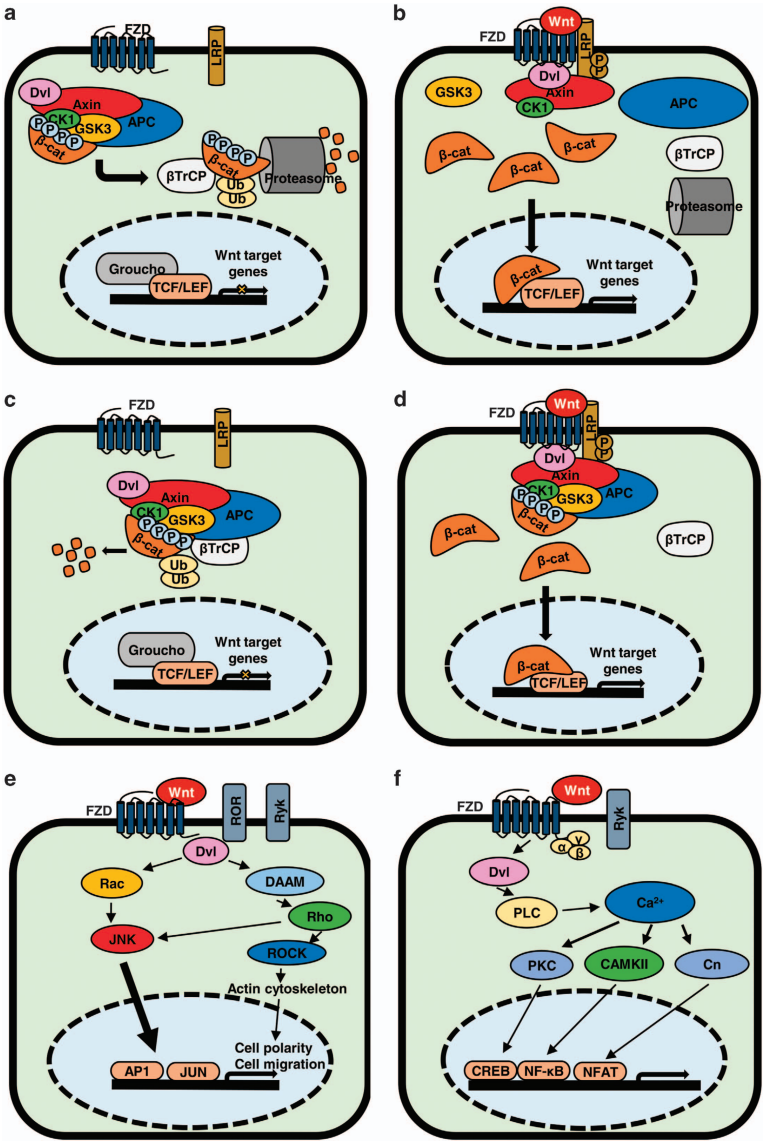

Figure 1. Classical and new Wnt/β-catenin pathway canonical and non-canonical pathways. (**a**) Overview of the 'classical' model of Wnt/β-catenin signaling in OFF state with no ligand bound to FZD receptor. (**b**) Overview of the 'classical' model of Wnt/β-catenin signaling pathway in ON state where Wnt ligand is bound to FZD receptor. (**c**) Overview of 'new' model of Wnt/β-catenin signaling in OFF state with no ligand bound to FZD receptor. (**d**) Overview of the 'new' model of Wnt/β-catenin signaling in ON state with Wnt ligand bound to FZD receptor. (**e**) Overview of Wnt planar cell polarity (PCP) pathway in ON state. Wnt binds multiple receptors including FZD and co-receptors ROR and Ryk. This activates Rho and Rac, which activate ROCK and c-Jun N-terminal kinase (JNK), respectively, leading to actin polymerization and regulates cytoskeletal arrangements. (**f**) Overview of Wnt/Ca^{2+} pathway in ON state. Wnt is able to bind FZD, Ryk to initiate signal transduction, which is effected through Dvl and G proteins (α, β, γ). Gene transcription is induced through proteins PKC, CaMKII and Cn (Calcineurin)-activating transcription factors.

Planar cell polarity pathway

The planar cell polarity pathway (Figure 1e) is a non-canonical, β-catenin-independent pathway that regulates cellular organization and polarity, partly through cytoskeletal organization.[18] Wnt ligands, such as Wnt5a, bind to FZD receptors and co-receptors, including ROR,[19] Ryk[20] and PTK.[21] Dvl interacts with Rac1[22] and Dvl-associated activator of morphogenesis 1 (DAAM1). Rac1 activates c-Jun N-terminal kinase, leading to actin polymerization,[22] while DAAM1 activates Rho, which in turn activates Rho-associated kinase (ROCK) to regulate cellular cytoskeletal arrangements.[23]

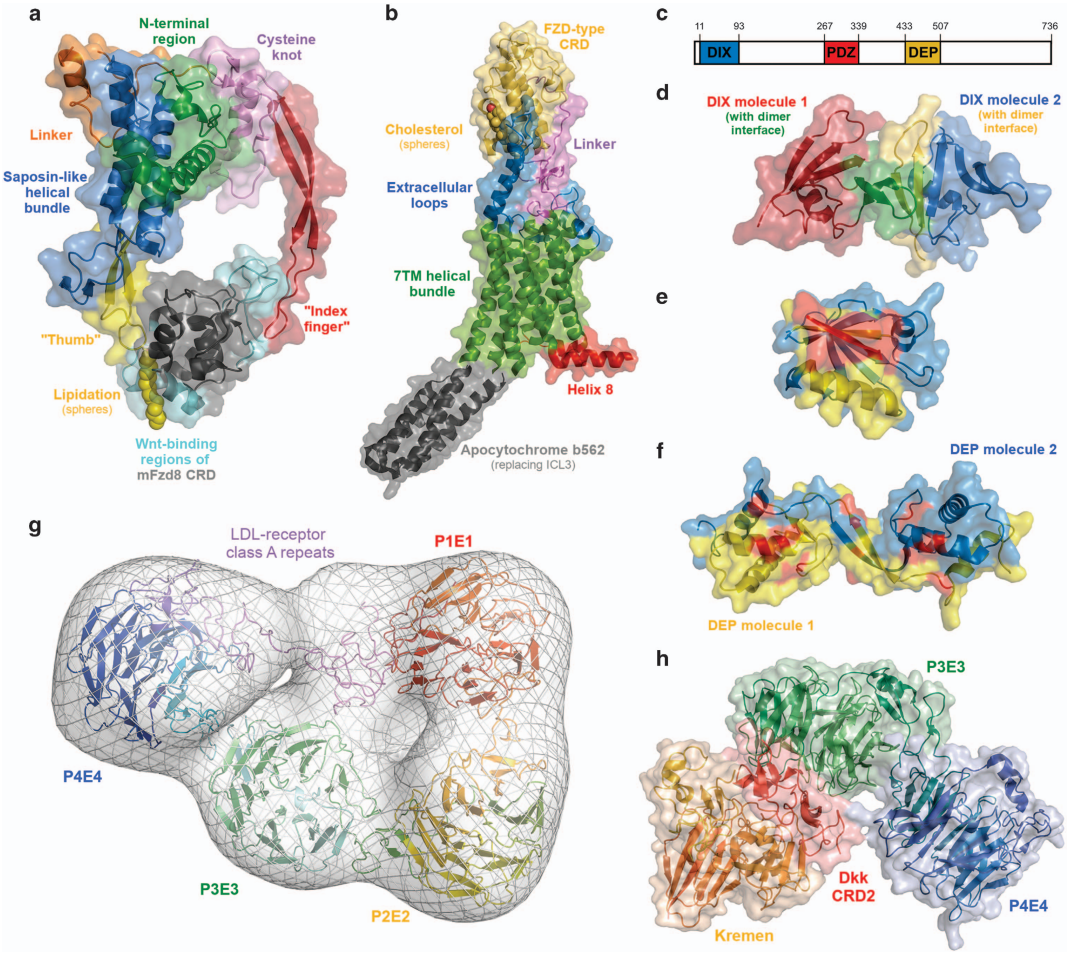

Figure 2. Molecular structures of the key Wnt signaling proteins and interactions. (**a**) X-ray crystal structure of the *Xenopus* Wnt8 complex with the mouse FZD8 cysteine-rich domain (PDB 4F0A). The key structural regions of the Wnt fold are highlighted, as are the major Wnt-interacting regions of the CRD. (**b**) X-ray crystal structure of the Smoothened receptor (PDB 5L7D), a Class F G protein-coupled receptor, related to FZD. The key structural regions of Smo are highlighted, as well as helix 8, which is of relevance for Dishevelled binding by FZD. (**c**) Schematic representation of the location of the DIX, PDZ and DEP domains within Dvl. (**d**) X-ray crystal structure of the DIX homodimer (PDB 4WIP). (**e**) X-ray crystal structure of the PDZ domain bound to a peptide (red; PDB 3CBX). The peptide-binding site is shown in yellow. (**f**) X-ray crystal structure of a DEP homodimer (PDB 5LNP), highlighting residues known to affect Wnt signaling (shown in red). (**g**) Model of the LRP6 ectodomain generated by molecular dynamics flexible fitting of the crystal structures of the P1E1–P2E2 domains (PDB 3S94) and P3E3–P4E4 domains (PDB 4A0P), and a homology model of the LDL-R type A domains (generated in Prime, based on the crystal structure of the LDL receptor ectodomain (PDB 1N7D)) to the electron microscopy structure (EMDatabank accession 1964). Gaps in the crystal structures and between the various components modeled using Prime. (**h**) X-ray crystal structure complex of the cysteine-rich domain 2 of Dickkopf with Kremen and the LRP6 P3E4–P4E4 domains (PDB 5FWW).

The Wnt/Ca^{2+} pathway

The Wnt/Ca^{2+} pathway (Figure 1f) is activated through Wnt binding to FZD, which interacts with G proteins and Dvl.[24] These interactions can activate cGMP-specific phosphodiesterase or phospholipase C, resulting in a release of intracellular calcium. This results in the activation of downstream signaling proteins PKC, calcineurin and CaMKII.[25] CaMKII activates nuclear factor of activated T-cells, which can regulate cell adhesion and migration.[26] Wnt5a induces activation of CaMKII-dependent Wnt/Ca^{2+} signaling. CaMKII phosphorylates transforming growth factor β-activated kinase, which activates Nemo-like kinase.[27] This cascade antagonizes canonical Wnt/β-catenin signaling by Nemo-like kinase phosphorylation of TCF4 and prevents the β-catenin–TCF4 complex from binding to DNA.[28]

Wnt ligands

To date, 19 members of the Wnt family have been identified in mammals, all ranging between 350 and 400 amino acids in length and characterized by a conserved fold containing a conserved motif of 24 cysteine residues (Figure 2a).[29] Wnt ligands are modified by lipidation, specifically, the addition of a palmitoleyl group to a conserved serine by the membrane-bound

O-acyltransferase Porcupine.[30] Wnt lipidation is crucial for secretion from the endoplasmic reticulum[31] and essential for Wnt function. Wnt lipidation was initially suggested to occur at Cys77 of Wnt3a (cysteine 3 of the Wnt fold);[32] however, lipidation at this cysteine has been conclusively disproven by crystallographic,[33] mutational[31] and imaging studies.[30]

FZD receptors

FZD receptors are a group of 10 membrane proteins featuring an extracellular cysteine-rich domain (CRD) and a seven-transmembrane domain.[34] Along with the Smoothened receptor (Smo), the FZDs comprise the family of Class F G protein-coupled receptors. The crystal structure of XWnt8 in complex with the mouse FZD8 CRD[33] revealed an unusual interaction involving the direct binding of the Wnt lipid to a binding site on one side of the CRD (the 'thumb' region), as well as the binding of the region from cysteines 19 to 22 of XWnt8 to the other side of the CRD (the 'index finger' region; Figure 2a).[35] Although no complete structures are available for any FZD, several structures of Smo are known,[36–38] most recently including both the CRD and seven-transmembrane regions (Figure 2b),[39] which are suggestive of the likely structure of FZD.

Disheveled

Three Dvl homologs are known (Dvl1/2/3), sharing high overall sequence similarity.[40] Dvl consists of three structurally defined domains: the DIX, PDZ and DEP domains. These three domains are separated by large insertions of unknown structure (Figure 2c); however, some functional significance has been ascribed to conserved sequences within the unstructured regions.[41]

Dvl polymerizes via the head-to-tail interaction of its DIX domain (Figure 2d). The DIX domain also mediates interaction with Axin.[42] Mutations (V67A, K68A, Y27D) in the polymerization interface of the DIX domain strongly suppress Wnt signaling.[43] The PDZ domain of Dvl (Figure 2e) interacts with a conserved motif in the FZD C-terminal (KTxxxW).[24] The PDZ–FZD interaction is relatively weak, and is likely supplanted by interactions of the DEP domain with FZD. Greater insight in the role of the DEP domain in Wnt signaling was recently revealed, with this domain shown to bind as a monomer to FZD, then undergo subsequent domain swapping to assemble Wnt signalosomes. Furthermore, upon Wnt stimulation, DEP domain swapping initiates DIX-dependent Dvl and Axin polymerization, leading to the inhibition of GSK3 and Wnt signal transduction. Mutants (E499G, D460K, G436P, K438M, D449I and D452I) in the DEP domain strongly diminish Wnt signaling upon Wnt stimulation (Figure 2f).[44,45] Dvl has also been shown to promote ubiquitination-mediated FZD degradation by RNF43.[46] This finding suggests a dual agonist/antagonist role for Dvl in Wnt signaling.

Low-density lipoprotein receptor 5/6

The extracellular domain of LRPs consists of four β-propeller repeats interspersed with epidermal growth factor repeats, followed by three LRP type A repeats (Figure 2g).[10] The majority of Wnts bind to the first β-propeller/epidermal growth factor repeat (P1E1–P2E2), although Wnt3 and Wnt 3a preferentially bind to the second repeat (P3E3–P3E4).[47] Wnt3 and Wnt3a binding to LRPs is competitively inhibited by Dickkopf binding to LRP (Figure 2h).[48–50] The intracellular action of LRP5/6 is less clearly understood, although it is known that Wnt activation initiates phosphorylation of the intracellular PPPSPxP motifs of LRP5/6 by GSK3 and CK1, allowing the recruitment of Axin.[51] Importantly, it has also been shown that without the FZD–Dvl interaction, Wnt is unable to induce phosphorylation of LRP6, reinforcing the complex interplay of proteins involved in Wnt signaling.[24,51]

ROR family receptor tyrosine kinases

The ROR family of receptor tyrosine kinases consists of two evolutionarily conserved members, ROR1 and ROR2.[52] The ROR ectodomains feature a FZD-type CRD most closely related to that of the skeletal muscle receptor tyrosine-protein kinase.[53] ROR2 is involved in Wnt5a-mediated signaling; Wnt5a binding to ROR2 initiates ROR2 homodimerization, stimulating autophosphorylation at Tyr646.[54] It has been demonstrated that Wnt5a and Wnt3a bind to ROR2; however, only Wnt5a is able to initiate the activation of the ROR2 signaling cascade.[55] Recently, high expression of ROR1 has been demonstrated in TNBC cell lines, where it interacts with CK1ε to promote tumor survival and growth after stimulation with Wnt5a to activate phosphoinositide 3-kinase (PI3K)/AKT signaling.[56]

DEAD-box helicases

DEAD-box helicases (DDXs), named for a conserved amino-acid sequence in their ATP-binding domain (Asp-Glu-Ala-Asp), belong to a highly conserved family of ATP-dependent DNA/RNA helicases.[57] They consist of a highly conserved helicase core with two domains, displaying high similarity to the recA bacterial DNA recombination protein (Figure 3).[58] These multifunctional proteins have roles in translation initiation, pre- and post-translational modifications, DNA repair, microRNA (miR) processing, ribosome biogenesis and RNA decay.[59–61] Furthermore, DDXs have been recently implicated in breast tumorigenesis and activation of cancer stem cell (CSC) stemness through various pathways, including Wnt.[62,63] DDXs can be regulated by β-catenin/TCF-driven transcription and have also been shown to regulate upstream Wnt signaling. The role of DDXs is discussed in further detail later in the section titled 'DDXs, Wnt and TNBC'.

BREAST CANCER SUBTYPES

Breast cancer is a diverse and complex disease, broadly characterized by four molecularly distinct subtypes, including luminal A, luminal B, HER2-overexpressed and triple-negative breast cancer (TNBC).[64] The luminal A subtype is characterized as ER/PR-positive and HER2-negative, expressing Bcl-2, cytokeratin 8/18 and low Ki67.[65] Luminal B subtypes are more aggressive ER^+ breast tumors, characterized as $HER2^-$ with high Ki67, or $HER2^+$, PR^- and ER^+,[66] with cyclin B1 overexpression.[67] The HER2 subtype is characterized by amplification of the ERBB2/HER2 gene.[68]

TNBC, including basal-like and claudin-low subtypes, accounts for 10–20% of breast cancers and is characterized by a lack of PR, ER and HER2 overexpression.[69] TNBC patients present with higher

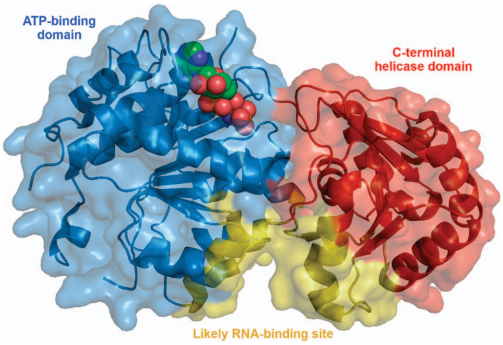

Figure 3. X-ray crystal structure of the ATP-binding and C-terminal helicase domains of the DEAD-box helicase DDX3 (PDB 5E7M). AMP-PNP, a non-hydrolyzable ATP analog, is shown in spheres in the ATP-binding site.

Table 1. Summary of the six molecular subtypes of TNBC characterized by Lehmann *et al.*[73]

TNBC subtype	*Gene ontology pathway (GOP) Genes found in GOPs with Wnt association*	
Luminal androgen receptor (LAR)	Steroid pathway	*FKBP5*[74]
	Androgen metabolism	*SPDEF*[75]
	Fatty-acid synthesis	*FASN*[76]
Mesenchymal (M)/mesenchymal stem-like (MSL)	EMT	*MMP2,*[77] *SNAI2,*[77] *TCF4,*[77] *TWIST1,*[77] *ZEB1*[78]
	Wnt/β-catenin signaling	*CTNNB1,*[73] *DKK2/3,*[73] *TCF4,*[73] *TCF7L2,*[73] *CCND2,*[73] *FZD4,*[73] *CAV1,*[73] *CAV2*[73]
Basal 1 (BL1)/Basal 2 (BL2)	DNA damage	*CHEK1,*[79] *FANCA,*[80] *FANCG,*[80] *MSH2,*[81] *RAD21*[82]
	Proliferation/cell cycle	*AURKB,*[83] *PLK1,*[84] *CENPA,*[84] *BUB1,*[84] *CCNA2,*[85] *PRC1,*[86] *MYC,*[87] *NRAS*[88]
Immunomodulatory (IM)	JAK/STAT cytokine pathway	*CCR2,*[89] *CCR5*[90]
	IL7 pathway	*IL7*[91]

Abbreviations: EMT, epithelial–mesenchymal transition; IL, interleukin; TNBC, triple-negative breast cancer. Various gene ontology pathways were found to be enriched in the LAR, MSL, BL1, BL2 and IM subtypes. Analysis of the genes enriched in these pathways identified genes associated with Wnt signaling.

incidence of distant disease recurrence within 3 years of diagnosis, with a high frequency of visceral metastases.[70] The prognosis for patients diagnosed with TNBC is poor, with patients who respond poorly to adjuvant treatment exhibiting worse outcomes.[4]

TNBC subtypes

TNBC has been categorized into a number of distinct molecular subtypes; however, there remains much intertumoral mutational and transcriptional heterogeneity within these subtypes. The molecular heterogeneity of TNBC confounds the clinical approach to TNBC treatment. TNBCs are characterized by high clonal frequencies of single gene mutations in the key tumorigenesis driver genes, including *TP53*, *PIK3CA* and *PTEN*, indicating that clonal evolution of these mutated genes is an early event in TNBC development.[71] However, mutation frequencies within these genes are not uniform among TNBC cases.[71,72]

Lehmann *et al.*[73] determined gene expression signatures in 587 TNBC cases from 21 breast cancer data sets and identified six molecularly distinct TNBC subtypes. These include basal-like 1, basal-like 2, immunomodulatory, mesenchymal (M), mesenchymal stem-like (MSL), and luminal androgen receptor (LAR). These subtypes, various gene ontology pathways and associated Wnt genes are described in Table 1. Recent RNA profiling performed by Burstein *et al.*[92] showed overlap of LAR and MES subtypes based on Lehmann's gene expression profiling, but was unable to reproduce all observations.[92] The findings of both of these studies indicate the presence of at least four molecularly distinct and stable TNBC subtypes, defined as LAR, mesenchymal (MES), basal-like immune-suppressed (BLIS) and basal-like immune-activated (BLIA).[92] Furthermore, these studies suggest molecular targets for the development of therapeutics specific to the treatment of TNBC.

LAR subtype

The LAR subtype accounts for ~10% of TNBCs, whereby tumor cells exhibit positive staining for androgen receptors (ARs) and are driven by AR signaling.[69,73] The LAR subtype of TNBC displays genomic amplification of *CCND1*, a gene regulated by the Wnt/β-catenin pathway.[92] There is some discordance within the literature in regards to the prognostic utility of AR status, with studies indicating no significant effect on survival rates associated with AR expression,[93] although AR^+ TNBC individuals have been shown to have a positive clinical response to the nonsteroidal antiandrogen, bilcautamide.[94,95] In a study designed to test the benefit of tamoxifen on ER^- and TNBC patients, it was found that expression of AR^+ versus AR^- individuals predicted a decreased recurrence rate and treatment benefit with AR^+ patients;[96] this is a result of tamoxifen exhibiting agonist activity on AR-expressing cells.[97]

MES subtype

The MES subtype, encompassing Lehmann's M, MSL and claudin-low subtypes, is characterized by the overexpression of genes associated with cellular motility, proliferation and growth signaling pathways.[73,92] MES subtypes have high expression of platelet-derived growth factor, insulin-like growth factor 1 and c-kit.[92] MES tumors express mesenchymal stem cell markers, including the breast stem cell marker ALDH1A1, and are enriched in genes associated with epithelial–mesenchymal transition (EMT) and other stem-like properties.[73,98] Within Lehmann's M and MSL subtypes, there are a number of enriched genes associated with EMT that are also modulated by Wnt signaling, including *MMP2, TWIST, SNAI2* and *TCF4.*[77] A gene set involved in Wnt/β-catenin signaling in the M and MSL subtypes, including *CTNNB1* (β-catenin), *DKK2, DKK3, SFRP4, TCF4, TCF7L2* and *FZD4*, was also found to be enriched.[73] MES tumors are associated with a poorer distant metastasis-free survival at 5 years compared to other subtypes, likely associated with increased expression of cellular motility genes leading to increased metastasis.[73]

BLIS subtype

BLIS is characterized as an immune-suppressed TNBC subtype with downregulated immune signaling pathways and reduced expression of immune function genes.[92,99] BLIS tumors exhibit enhanced expression of mitotic and cell cycle pathway genes, with overexpression of proliferative genes, including *CENPF*, *BUB1* and *PRC1,*[99] Sry-related HMG box (SOX) transcription factors, and the immune-regulatory molecule V-domain-containing T-cell activation inhibitor.[92] SOX transcription factors share a closely related consensus binding sequence to TCF/LEF transcription factors[100] and are known modulators of Wnt/β-catenin signaling.[101] Survival analysis shows that patients with the BLIS subtype TNBC experience lower rates of recurrence-free survival compared to other TNBC subtypes.[99]

BLIA subtype

The BLIA subtype is characterized by upregulation of immune activating pathways, with overexpression of STAT transcription factors and cytotoxic T-lymphocyte-associated protein 4.[92] Furthermore, the BLIA subtype demonstrates amplification of *CDK1*, which was recently found to phosphorylate the Wnt regulator TAZ.[92,102] BLIA tumors have increased levels of lymphocytic infiltration and are thus associated with improved disease-free survival rates and patient outcomes compared to other TNBC subtypes, although still associated with a relatively high risk of recurrence (~20%).[92,103]

Wnt dysregulation in TNBC and TNBC stem cells

Aberrant Wnt signaling is a characteristic of TNBC, with both canonical and non-canonical pathways implicated in TNBC tumorigenesis[104,105] and metastasis.[106] Enrichment of Wnt/β-catenin signaling is evident in TNBC and is associated with poor clinical outcomes within this subtype.[107,108] TNBC patients displaying dysregulated Wnt/β-catenin signaling are more likely to develop lung and brain secondary metastases.[106] Studies have shown that nuclear accumulation of β-catenin promotes cell migration, colony formation, stem-like features and chemoresistance of TNBC cells *in vitro* and TNBC tumorigenesis in mouse cancer models, thus suggesting that canonical Wnt signaling is a major driving force of TNBC tumorigenesis.[104] Although the Wnt/β-catenin pathway is associated with the clinicopathological features of TNBC, this is not due to *CTNBB1* mutations.[108] Studies have also implicated dysregulation of non-canonical Wnt signaling pathways in the highly metastatic behavior of TNBC cells and CSCs, specifically through aberrant c-Jun N-terminal kinase activation.[109]

CSCs, or cancer stem-like cells, are a small subset of cells within the heterogeneous tumor bulk that are thought to be responsible for tumor initiation.[110] These cells also have intrinsic mechanisms for chemoresistance, such as upregulation of drug transporters, including the breast cancer resistance protein (also known as ABCG^2).[111] By evading the standard chemotherapeutic treatments, it is thought that the CSCs are also responsible for the relapse experienced in many cancers, especially TNBCs.[112] Studies have also shown that these cells are a main contributor to metastasis, and are able to initiate solid tumor formation when xenotransplanted at low cell densities.[113] TNBC stem cells are isolated from tumors as CD44$^+$ (homing cell adhesion molecule), CD24$^-$ (heat stable antigen), CD49f$^+$ cells.[114] CSCs also differ metabolically to other cancer cells. They are more reliant on mitochondrial respiration, which is supported by their higher mitochondrial reactive oxygen species, enhanced oxygen consumption and higher mitochondrial mass, allowing for features such as resistance to DNA damage.[115]

Wnt signaling is essential for normal breast stem cell function and mammary gland development during embryogenesis, postnatal development and pregnancy,[116] with adult mammary glands containing Wnt-responsive stem cell populations.[117] Studies have shown that aberrant Wnt signaling in breast cancer stem cells (BCSCs) is a key event in breast tumorigenesis.[118] Wnt/β-catenin signaling has been linked to TNBC tumorigenesis by regulating the key tumor-associated characteristics, including migration, stemness, proliferation and chemoresistance in TNBC cells and CSCs.[104] A recent study has also demonstrated that Wnt/β-catenin signaling activity is higher in breast CSCs than the bulk tumor population, based on β-catenin, TCF4 and LEF1 expression in Aldefluor-positive cells versus Aldefluor-negative cells.[119] Treatment with Wnt3a increased the number of ALDH$^+$ breast CSCs, and knockdown of Wnt1 reduced the tumor-forming efficiency of breast CSCs *in vitro*.[119]

Furthermore, studies have shown that Wnt-derived breast tumors are maintained by clones capable of re-activating Wnt overexpression post-Wnt inhibition, indicating that aberrant Wnt activation is a key driver of breast cancer recurrence and progression.[120] A recent review highlighted the potential importance of Wnt/β-catenin signaling, along with other developmental signaling pathways, including Cripto-1 and Notch/CSL, in the regulation of TNBC stem cells and therapy resistance in TNBC.[121] An overview of Wnt signaling dysregulation is given in Figure 4.

FZDs in TNBC

FZD6. FZD6 exhibits increased gene copy number variations and overexpression in breast cancers. This is more frequent in TNBC than ER$^+$ tumors. A study by Corda *et al.*[122] determined that FZD6 was involved in the regulation of cell motility, invasion and three-dimensional (3D) growth, although it did not regulate proliferation in TNBC. This was confirmed by a significant reduction in distant metastases detected in various organs *in vivo* after the injection of MDA-MB-231 cells depleted of FZD6. Short hairpin RNA directed at *FZD6 in vitro* was found to reduce cell invasion through a reduction in active Rho and the subsequent reduction in fibronectin fibres. This indicated that FZD6 regulates cell motility and invasion through non-canonical Wnt signaling. This study also suggests that FZD6 overexpression in TNBC has a high prognostic value in determining the risk of metastasis.[122]

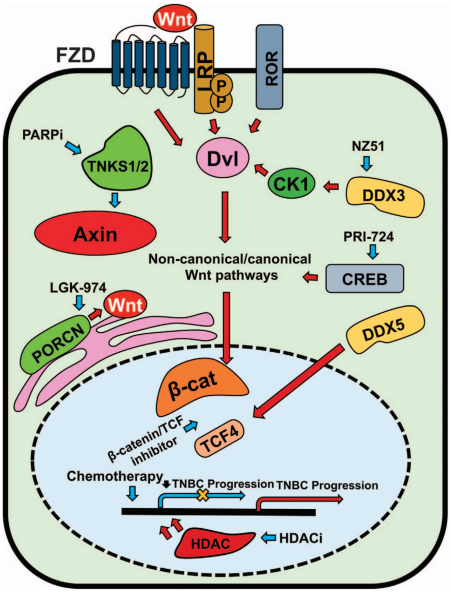

Figure 4. Overview of Wnt signaling regulators contributing to TNBC progression and their targeted therapies. Canonical and non-canonical Wnt pathways are activated through Fzd, LRP and ROR receptors. Blue arrows indicate suppression/inhibition of Wnt regulators and pathways (with a net result of downregulation of Wnt target gene transcription, indicated by yellow cross); red arrows indicate activation of Wnt regulators and pathways.

FZD7. Microarray analysis determined that FZD7 expression is upregulated in TNBC tissue and cell lines, and promotes tumorigenesis via canonical Wnt signaling pathways.[123] Short hairpin RNA-mediated silencing of FZD7 reduced invasiveness and colony formation in TNBC cell lines.[123] A recent study found that ΔNp63, an isoform of Transformation-related protein 63 (p63), enhanced FZD7 expression and increased Wnt signaling in TNBC tumor tissue and cell lines.[124]

Aberrant FZD7 expression is implicated in TNBC stem cell-mediated tumorigenesis. A study recently found that knockdown of ΔNp63 in TNBC cell lines decreased FZD7 expression and tumorsphere formation, indicating that ΔNp63/FZD7 upregulation induced TNBC stem cells and promoted tumor formation in TNBC.[124] The findings of this study highlight the potential clinical importance of ΔNp63/FZD7-Wnt signaling in TNBC stem cells as a key driver of tumorigenesis and progression of TNBC.[124,125]

FZD8. Gene expression studies have recently linked FZD8-driven Wnt signaling to chemoresistance in TNBC cell lines and TNBC stem cells. Treatment with cisplatin and tumor necrosis factor-related apoptosis-inducing ligand (TRAIL) in TNBC cell lines

resulted in increased FZD8 expression in residual tumors of xenograft models.[126] Furthermore, FZD8 silencing led to increased Wnt pathway-driven TNBC cell apoptosis *in vitro* and *in vivo*.[126] The study showed that treatment with TRAIL/cisplatin increased expression of LEF-1 and TCF-7 in residual TNBC stem cells, thus implicating upregulation of Wnt signaling components in the development of chemoresistance.[126] An inverse correlation between FZD8 and miR-100 was shown, where decreased miR-100 expression was linked to increased FZD8 expression and Wnt signaling, resulting in increased loco-regional breast cancer metastasis.[126,127] The role of miRs in Wnt signaling and TNBC is discussed in further detail below. c-Myc overexpression has been linked to FZD8 overexpression in TNBC cell lines, associating c-Myc-driven transcription to chemoresistance and TNBC CSC survival.[128]

LRP5/6 in TNBC

LRP5/6 are essential for normal mammary development by regulating breast stem cell activity and are linked to basal-derived breast tumorigenesis.[129–131] Studies in transgenic mice indicated that LRP5 knockdown led to resistance to Wnt1-induced tumor formation.[130]

Gene expression analyses found that LRP6 is overexpressed in human TNBC.[123,131] *In vivo* studies have shown that LRP6 silencing inhibited tumor growth in TNBC cell line-derived xenograft models.[132] LRP6 and Wnt target gene *SOX9* have been shown to influence regulation of one another in TNBC cell lines. LRP6 overexpression led to *SOX9* upregulation, while knockdown of *SOX9* reduced LRP6 transcription and decreased cell invasion and proliferation.[133]

LRP6 overexpression led to the upregulation of Wnt signaling and was associated with increased stemness in TNBC cells.[134] CD138 (Syndecan-1) is an EMT marker associated with both development and breast tumorigenesis,[135] and has been shown to modulate TNBC stem cell properties by targeting Wnt signaling.[134] Ibrahim *et al.*[134] showed that CD138 modulates Wnt signaling in TNBC stem cells through LRP6, whereby CD138 silencing resulted in downregulated LRP6 expression and Wnt signaling.[134]

RORs in TNBC

Primary breast cancer DNA microarray data set analysis has shown that ROR1 is expressed on breast cancer cells and absent in normal breast cells, with high ROR1 expression associated with poorer survival.[136] Furthermore, the study showed that ROR1 silencing in TNBC cell lines increased apoptosis and reduced cell growth. High ROR1 expression in breast cancer cells is associated with high expression of EMT gene profiles and high incidences of disease recurrence and progression.[137] ROR1 knockdown in TNBC cell lines resulted in reduced EMT-associated protein expression, reduced cell migration and invasion *in vitro*, and inhibited metastasis in xenograft models.[137] ROR2 expression is present in both TNBC and non-TNBC, with $ROR2^{+}$ TNBC patients exhibiting poorer survival outcomes compared to other subtypes.[138] ROR2 knockdown in TNBC cell lines inhibited Wnt signaling and reduced TCF/LEF transcription.[138] These findings indicate the potential prognostic and therapeutic significance of high ROR1/2 expression in TNBC.

DDXs, WNT and TNBC

DDX3. DDX3 is a regulator of Wnt/β-catenin signaling, where it interacts with and increases the kinase activity of casein kinase 1ε and is required for the phosphorylation of Dvl2.[139] It is known to have an oncogenic role in breast cancer, where non-tumorigenic MCF10A cell lines overexpressing DDX3 showed increased EMT, motility and invasiveness.[140] The same study demonstrated that DDX3 expression was positively correlated with a more aggressive phenotype, and was highly expressed in TNBC cell lines. DDX3 overexpression resulted in E-cadherin downregulation and subsequent nuclear β-catenin translocation.[140] Similarly, DDX3 inhibition by NZ51, a ring-expanded nucleoside analog that is predicted to bind to the ATP-binding site of DDX3, led to decreased proliferation, motility and invasiveness in TNBC cell lines and reduced tumor load and metastatic burden in preclinical *in vivo* models.[141]

DDX5 (p68). DDX5 acts as a co-activator of Wnt/β-catenin signaling through regulation of TCF4 expression. In turn, β-catenin/TCF4 regulates DDX5 expression, forming a positive feedback loop associated with increased EMT marker expression in TNBC cells.[142] DDX5 is thought to regulate p53-mediated repair of DNA damage, and DDX5 overexpression contributes to tumorigenesis and progression in breast cancers.[143] DDX5 is highly expressed in basal-like breast cancers compared to luminal-like, and correlates with high EGFR and Ki67 expression in TNBC tissue.[144] Furthermore, the study found that DDX5 regulates the expression of miR-21 and miR-182 in basal breast cancers, and is associated with malignant disease.

THE ROLES OF MIRS IN WNT SIGNALING AND TNBC

miRs are endogenous, short, non-coding RNA molecules that regulate cancer-related genes at the post-transcriptional level.[145] miRs are differentially expressed in BCSCs and cancer cells, indicating that breast cancer-specific miRs are important in maintaining stemness and promoting tumorigenesis in BCSCs.[146] Twenty-seven miRs differentially expressed in locally advanced TNBC have been previously identified, with many of these predicted to be involved in regulation of Wnt signaling pathway genes.[147,148]

miR-374a overexpression led to suppression of Wnt pathway inhibiting components (PTEN and WIF1) and ultimately increased Wnt-mediated EMT and metastasis in multiple TNBC cell lines.[149]

miR-340 is downregulated in TNBC cell lines and has been linked with TNBC tumorigenesis regulation in multiple studies.[150] Induction of miR-340 resulted in downregulation of Wnt pathway target genes (*CTNNB1*, *MYC* and *ROCK1*), decreased proliferation and increased apoptosis in a metastatic TNBC cell line. The study showed that miR-340 overexpression reduced cell motility and invasiveness, indicating that miR-340 has a fundamental role in regulating breast metastases.[151] Another study recently found that induction of miR-340 in TNBC cell lines led to reduced expression of *SOX2*, an oncogene associated with the canonical Wnt signaling pathway.[152]

A study by Isobe *et al.*[153] found that miR-142 upregulation is associated with BCSCs and activates canonical Wnt signaling by promoting APC breakdown in TNBC cell lines. The study found that miR-142 expression activated canonical Wnt signaling, leading to increased miR-150 expression, thereby contributing to breast tissue hyperproliferation, BCSC proliferation and reducing apoptosis in TNBC cell lines.[153]

A recent study has shown that miR-218-5p expression was significantly increased in TNBC, as well as bone metastases, from breast cancer patients.[154] Anti-miR-218-5p led to a reduction in cell proliferation *in vitro* and decreased tumor growth, active osteoclasts and osteolytic lesions *in vivo*, while the opposite was seen with transfection of miR-218-5p. The miR was also shown to directly modulate Wnt/β-catenin signaling by binding to secreted FZD-related protein 1 and SOST. Anti-miR-218-5p suppressed Wnt signaling, which downregulated Parathyroid hormone-related protein expression, reducing breast cancer-induced osteolytic disease.[154]

CURRENT AND EMERGING THERAPIES FOR TNBC AND TNBC STEM CELLS

Systemic cytotoxic chemotherapy is clinically indicated in early TNBC and is associated with a greater treatment benefit than hormone receptor-positive tumors.[155] Numerous early-phase clinical trials are currently underway, investigating various targeted molecules and combination therapies for the treatment of TNBC. In this section, we review current and emerging small molecule therapeutics for the treatment of TNBC (Figure 4); immunotherapeutics are reviewed elsewhere.[7]

Chemotherapy

Anthracycline/taxane-based regimens are currently the standard of care in the treatment of adjuvant and neoadjuvant TNBC. However, a recent *in vitro* study has shown that treatment with docetaxel or doxorubicin had transient and negligible impact on cell growth in two TNBC cell lines, respectively. Furthermore, the study found that docetaxel and doxorubicin treatment resulted in deregulation of genes associated with stemness in TNBC cells.[156] Molecular analysis found that doxorubicin treatment deregulated stem cell signaling pathways associated with cell growth, renewal and differentiation, with altered gene expression demonstrated in components of the Wnt signaling pathway, including FZD2, FZD4, FZD5, FZD6, FZD7, FZD9, Axin1, Wnt11, Wnt10a and Wnt5a. As such, the study concluded that docetaxel and doxorubicin induce stemness in differentiated TNBC cells, which likely accounts for acquired chemoresistance seen in refractory TNBC tumors.[156]

Platinum agents

Platinum-based chemotherapeutics are a class of DNA-damaging agents, including cisplatin, carboplatin and oxaliplatin; these have established efficacy in breast cancer treatment.[157] *In vitro* studies have indicated that combining TRAIL and cisplatin significantly increased BCSC death compared to other standard of care treatments in TNBC cell lines.[158] The study showed that treatment with TRAIL and cisplatin inhibited Wnt1-mediated signaling and expression of cyclin D1, as well as the phosphorylation of β-catenin. Combination treatment with cisplatin and TRAIL also enhanced apoptosis, and inhibited proliferation and tumorsphere formation.[158]

Wnt signaling inhibitors

Treatment with the small molecule β-catenin/TCF inhibitor CWP232228 inhibited β-catenin-mediated transcription, leading to inhibition of stem cell proliferation and reduction in tumor bulk in TNBC cell lines and TNBC patient-derived xenograft models, respectively.[159] PRI-724, a CREB-binding protein inhibitor, and LGK-974, a Porcupine inhibitor, are two small molecules currently undergoing clinical development. Both molecules are currently under investigation for single agent use in ongoing phase I clinical trials in TNBC patients,[160] with interim results yet to be released. Recent *in vitro* studies have shown that LGK-974 in combination with the PI3K/AKT/mTOR inhibitor BKM120 worked synergistically to decrease cell viability and enhance antitumor efficacy in TNBC cell lines.[161]

PARP inhibitors

Poly (ADP-ribose) polymerase (PARP) is an enzyme involved in DNA repair mechanisms necessary for maintaining BRCA-mutated cell viability.[162,163] Included in the PARP enzyme family are tankyrase (TNKS)-1 and TNKS2. TNKS1 and TNKS2 are regulators of Wnt signaling through their interaction with Axin.[164,165] TNBCs share phenotypic characteristics with BRCA-mutated cancers, thus providing support for the use of PARP inhibitors.[166] The small molecule TNKS1/2 inhibitor XAV939 showed effectiveness in the destabilization of Axin and reduction of Wnt activity, although data suggest that a combination approach may be more beneficial.[165] Clinical trials evaluating the oral PARP inhibitor olaparib in BRCA1/2-positive metastatic breast cancer are currently underway, with interim results showing efficacy.[167] Veliparib is another PARP inhibitor currently being evaluated in combination with paclitaxel and carboplatin for metastatic TNBC.[168] Data from Phase I clinical trials of veliparib show acceptable safety, tolerance and good antineoplastic activity.[168]

Histone deacetylase inhibitors

Histone deacetylase (HDAC) inhibitors are emerging as promising anti-TNBC agents because of their multifunctional capacity to regulate gene expression, cell growth and survival, as well as their ability to restore cellular aberrations due to epigenetic effects.[169] Entinostat is an HDAC inhibitor recently shown to have anti-CSC effects in TNBC stem cells. An *in vivo* study found that entinostat treatment reduced TNBC stem cell populations, tumorsphere formation and miR-181a expression in TNBC cell lines.[170] Furthermore, the study found that entinostat treatment in TNBC patient-derived xenografts reduced tumor growth and inhibited the development of lung metastases.[170] Further *in vivo* studies have shown that triple therapy, combining entinostat, all-*trans* retinoic acid and doxorubicin, induced apoptosis of TNBC stem cells in culture and induced differentiation of TNBC CSCs both *in vitro* and *in vivo*.[171] Panobinostat (LBH589) decreased cell survival and cell cycle progression at the G2/M stage in TNBC cell lines and *in vivo*. It also increased acetylation of the histones H3 (Lys3) and H4 (Lys8).[169] Treatment with panobinostat upregulated cadherin-1 (CDH1) and reversed the M phenotype; CDH1 has been identified as a Wnt-signaling component in invasive breast carcinoma.[172] An *in vivo* study found that salinomycin, a compound that selectively inhibits CSCs,[173] in combination with panobinostat, significantly inhibited the growth of TNBC stem cells in TNBC patient-derived xenografts. The study found that salinomycin and panobinostat worked synergistically to inhibit cell cycle progression, enhance apoptosis and regulate EMT in TNBC stem cells.[173]

CONCLUSIONS

The dysregulation of Wnt signaling is synonymous with cancer. TNBC is an aggressive, highly proliferative phenotype, which is characteristic of overactive signaling pathways. The accelerated development of sequencing technologies has allowed us to characterize the highly heterogeneous molecular landscape of TNBC with unprecedented detail. These technologies have allowed the discovery of new potential therapeutic targets, as well as to suggest where existing drugs may be of therapeutic value, for instance, in the use of tamoxifen on AR-positive TNBC patients. Like TNBC, Wnt signaling is highly complex and not yet fully characterized. The discovery of novel regulators in TNBC, such as DDXs, adds to the complexity, but also presents exciting new opportunities for the development of potential therapeutic targets. Structural knowledge of Wnt pathway proteins and interactions has expanded in recent years, providing opportunities for rational/structure-based drug design of novel cancer therapeutics.

CONFLICT OF INTEREST

The authors declare no conflict of interest.

ACKNOWLEDGEMENTS

SP is supported by funds from the Rotary Club of Belmont, Australian Rotary Health Research Fund and Curtin University School of Biomedical Sciences. MA is a recipient

of an NHMRC Early Career Fellowship (GNT1054245), a Cancer Council of Western Australia Suzanne Cavanagh Early Career Investigator Grant and a Raine Priming Grant. AD is supported by strategic research funds from the School of Biomedical Sciences (Curtin University), Commercialization Advisory Board of Curtin University, Cancer Council of Western Australia and Actinogen Ltd, Perth, Western Australia.

REFERENCES

1 Chen S, Parmigiani G. Meta-analysis of BRCA1 and BRCA2 penetrance. *J Clin Oncol* 2007; **25**: 1329–1333.
2 Polakis P. Wnt signaling in cancer. *Cold Spring Harb Perspect Biol* 2012; **4**: a008052.
3 Ovcaricek T, Frkovic SG, Matos E, Mozina B, Borstnar S. Triple negative breast cancer-prognostic factors and survival. *Radiol Oncol* 2011; **45**: 46–52.
4 Foulkes WD, Smith IE, Reis-Filho JS. Triple-negative breast cancer. *N Engl J Med* 2010; **363**: 1938–1948.
5 Hudis CA. Trastuzumab--mechanism of action and use in clinical practice. *N Engl J Med* 2007; **357**: 39–51.
6 Jordan VC. Tamoxifen (ICI46,474) as a targeted therapy to treat and prevent breast cancer. *Br J Pharmacol* 2006; **147**: S269–S276.
7 Pusztai L, Karn T, Safonov A, Abu-Khalaf MM, Bianchini G. New strategies in breast cancer: immunotherapy. *Clin Cancer Res* 2016; **22**: 2105–2110.
8 Wu G, Huang H, Garcia Abreu J, He X. Inhibition of GSK3 phosphorylation of beta-catenin via phosphorylated PPPSPXS motifs of Wnt coreceptor LRP6. *PLoS ONE* 2009; **4**: e4926.
9 Liu C, Kato Y, Zhang Z, Do VM, Yankner BA, He X. beta-Trcp couples beta-catenin phosphorylation-degradation and regulates Xenopus axis formation. *Proc Natl Acad Sci USA* 1999; **96**: 6273–6278.
10 MacDonald BT, He X. Frizzled and LRP5/6 receptors for Wnt/beta-catenin signaling. *Cold Spring Harb Perspect Biol* 2012; **4**: a007880.
11 Tamai K, Zeng X, Liu C, Zhang X, Harada Y, Chang Z *et al.* A mechanism for Wnt coreceptor activation. *Mol Cell* 2004; **13**: 149–156.
12 Clevers H. Wnt/beta-catenin signaling in development and disease. *Cell* 2006; **127**: 469–480.
13 Roose J, Molenaar M, Peterson J, Hurenkamp J, Brantjes H, Moerer P *et al.* The Xenopus Wnt effector XTcf-3 interacts with Groucho-related transcriptional repressors. *Nature* 1998; **395**: 608–612.
14 Azzolin L, Panciera T, Soligo S, Enzo E, Bicciato S, Dupont S *et al.* YAP/TAZ incorporation in the beta-catenin destruction complex orchestrates the Wnt response. *Cell* 2014; **158**: 157–170.
15 Li VS, Ng SS, Boersema PJ, Low TY, Karthaus WR, Gerlach JP *et al.* Wnt signaling through inhibition of beta-catenin degradation in an intact Axin1 complex. *Cell* 2012; **149**: 1245–1256.
16 Azzolin L, Zanconato F, Bresolin S, Forcato M, Basso G, Bicciato S *et al.* Role of TAZ as mediator of Wnt signaling. *Cell* 2012; **151**: 1443–1456.
17 Taelman VF, Dobrowolski R, Plouhinec JL, Fuentealba LC, Vorwald PP, Gumper I *et al.* Wnt signaling requires sequestration of glycogen synthase kinase 3 inside multivesicular endosomes. *Cell* 2010; **143**: 1136–1148.
18 Gomez-Orte E, Saenz-Narciso B, Moreno S, Cabello J. Multiple functions of the noncanonical Wnt pathway. *Trends Genet* 2013; **29**: 545–553.
19 Nishita M, Itsukushima S, Nomachi A, Endo M, Wang Z, Inaba D *et al.* Ror2/Frizzled complex mediates Wnt5a-induced AP-1 activation by regulating Dishevelled polymerization. *Mol Cell Biol* 2010; **30**: 3610–3619.
20 Habu M, Koyama H, Kishida M, Kamino M, Iijima M, Fuchigami T *et al.* Ryk is essential for Wnt-5a-dependent invasiveness in human glioma. *J Biochem* 2014; **156**: 29–38.
21 Golubkov VS, Chekanov AV, Cieplak P, Aleshin AE, Chernov AV, Zhu W *et al.* The Wnt/planar cell polarity protein-tyrosine kinase-7 (PTK7) is a highly efficient proteolytic target of membrane type-1 matrix metalloproteinase: implications in cancer and embryogenesis. *J Biol Chem* 2010; **285**: 35740–35749.
22 Li L, Yuan H, Xie W, Mao J, Caruso AM, McMahon A *et al.* Dishevelled proteins lead to two signaling pathways. Regulation of LEF-1 and c-Jun N-terminal kinase in mammalian cells. *J Biol Chem* 1999; **274**: 129–134.
23 Habas R, Kato Y, He X. Wnt/Frizzled activation of Rho regulates vertebrate gastrulation and requires a novel Formin homology protein Daam1. *Cell* 2001; **107**: 843–854.
24 Wong HC, Bourdelas A, Krauss A, Lee HJ, Shao Y, Wu D *et al.* Direct binding of the PDZ domain of Dishevelled to a conserved internal sequence in the C-terminal region of Frizzled. *Mol Cell* 2003; **12**: 1251–1260.
25 De A. Wnt/Ca2+ signaling pathway: a brief overview. *Acta Biochim Biophys* 2011; **43**: 745–756.
26 Dejmek J, Safholm A, Kamp Nielsen C, Andersson T, Leandersson K. Wnt-5a/Ca2+-induced NFAT activity is counteracted by Wnt-5a/Yes-Cdc42-casein kinase 1alpha signaling in human mammary epithelial cells. *Mol Cell Biol* 2006; **26**: 6024–6036.
27 Ishitani T, Kishida S, Hyodo-Miura J, Ueno N, Yasuda J, Waterman M *et al.* The TAK1-NLK mitogen-activated protein kinase cascade functions in the Wnt-5a/Ca(2+) pathway to antagonize Wnt/beta-catenin signaling. *Mol Cell Biol* 2003; **23**: 131–139.
28 Ishitani T, Ninomiya-Tsuji J, Matsumoto K. Regulation of lymphoid enhancer factor 1/T-cell factor by mitogen-activated protein kinase-related Nemo-like kinase-dependent phosphorylation in Wnt/beta-catenin signaling. *Mol Cell Biol* 2003; **23**: 1379–1389.
29 Cadigan KM, Nusse R. Wnt signaling: a common theme in animal development. *Genes Dev* 1997; **11**: 3286–3305.
30 Gao X, Hannoush RN. Single-cell imaging of Wnt palmitoylation by the acyltransferase porcupine. *Nat Chem Biol* 2014; **10**: 61–68.
31 MacDonald BT, Hien A, Zhang X, Iranloye O, Virshup DM, Waterman ML *et al.* Disulfide bond requirements for active Wnt ligands. *J Biol Chem* 2014; **289**: 18122–18136.
32 Willert K, Brown JD, Danenberg E, Duncan AW, Weissman IL, Reya T *et al.* Wnt proteins are lipid-modified and can act as stem cell growth factors. *Nature* 2003; **423**: 448–452.
33 Janda CY, Waghray D, Levin AM, Thomas C, Garcia KC. Structural basis of Wnt recognition by Frizzled. *Science* 2012; **337**: 59–64.
34 Dijksterhuis JP, Petersen J, Schulte G. WNT/Frizzled signalling: receptor-ligand selectivity with focus on FZD-G protein signalling and its physiological relevance: IUPHAR Review 3. *Br J Pharmacol* 2014; **171**: 1195–1209.
35 Takada R, Satomi Y, Kurata T, Ueno N, Norioka S, Kondoh H *et al.* Monounsaturated fatty acid modification of Wnt protein: its role in Wnt secretion. *Dev Cell* 2006; **11**: 791–801.
36 Wang C, Wu H, Katritch V, Han GW, Huang XP, Liu W *et al.* Structure of the human smoothened receptor bound to an antitumour agent. *Nature* 2013; **497**: 338–343.
37 Wang C, Wu H, Evron T, Vardy E, Han GW, Huang XP *et al.* Structural basis for Smoothened receptor modulation and chemoresistance to anticancer drugs. *Nat Commun* 2014; **5**: 4355.
38 Weierstall U, James D, Wang C, White TA, Wang D, Liu W *et al.* Lipidic cubic phase injector facilitates membrane protein serial femtosecond crystallography. *Nat Commun* 2014; **5**: 3309.
39 Byrne EF, Sircar R, Miller PS, Hedger G, Luchetti G, Nachtergaele S *et al.* Structural basis of Smoothened regulation by its extracellular domains. *Nature* 2016; **535**: 517–522.
40 Sussman DJ, Klingensmith J, Salinas P, Adams PS, Nusse R, Perrimon N. Isolation and characterization of a mouse homolog of the Drosophila segment polarity gene dishevelled. *Dev Biol* 1994; **166**: 73–86.
41 Gao C, Chen YG. Dishevelled: the hub of Wnt signaling. *Cell Signal* 2010; **22**: 717–727.
42 Fiedler M, Mendoza-Topaz C, Rutherford TJ, Mieszczanek J, Bienz M. Dishevelled interacts with the DIX domain polymerization interface of Axin to interfere with its function in down-regulating beta-catenin. *Proc Natl Acad Sci USA* 2011; **108**: 1937–1942.
43 Schwarz-Romond T, Fiedler M, Shibata N, Butler PJ, Kikuchi A, Higuchi Y *et al.* The DIX domain of Dishevelled confers Wnt signaling by dynamic polymerization. *Nat Struct Mol Biol* 2007; **14**: 484–492.
44 Gammons MV, Renko M, Johnson CM, Rutherford TJ, Bienz M. Wnt signalosome assembly by DEP domain swapping of Dishevelled. *Mol Cell* 2016; **64**: 92–104.
45 Tauriello DV, Jordens I, Kirchner K, Slootstra JW, Kruitwagen T, Bouwman BA *et al.* Wnt/beta-catenin signaling requires interaction of the Dishevelled DEP domain and C terminus with a discontinuous motif in Frizzled. *Proc Natl Acad Sci USA* 2012; **109**: E812–E820.
46 Jiang X, Charlat O, Zamponi R, Yang Y, Cong F. Dishevelled promotes Wnt receptor degradation through recruitment of ZNRF3/RNF43 E3 ubiquitin ligases. *Mol Cell* 2015; **58**: 522–533.
47 Gong Y, Bourhis E, Chiu C, Stawicki S, DeAlmeida VI, Liu BY *et al.* Wnt isoform-specific interactions with coreceptor specify inhibition or potentiation of signaling by LRP6 antibodies. *PLoS ONE* 2010; **5**: e12682.
48 Cheng Z, Biechele T, Wei Z, Morrone S, Moon RT, Wang L *et al.* Crystal structures of the extracellular domain of LRP6 and its complex with DKK1. *Nat Struct Mol Biol* 2011; **18**: 1204–1210.
49 Ahn VE, Chu ML, Choi HJ, Tran D, Abo A, Weis WI. Structural basis of Wnt signaling inhibition by Dickkopf binding to LRP5/6. *Dev Cell* 2011; **21**: 862–873.
50 Bourhis E, Wang W, Tam C, Hwang J, Zhang Y, Spittler D *et al.* Wnt antagonists bind through a short peptide to the first beta-propeller domain of LRP5/6. *Structure* 2011; **19**: 1433–1442.
51 Zeng X, Huang H, Tamai K, Zhang X, Harada Y, Yokota C *et al.* Initiation of Wnt signaling: control of Wnt coreceptor Lrp6 phosphorylation/activation via frizzled, dishevelled and axin functions. *Development* 2008; **135**: 367–375.
52 Minami Y, Oishi I, Endo M, Nishita M. Ror-family receptor tyrosine kinases in noncanonical Wnt signaling: their implications in developmental morphogenesis and human diseases. *Dev Dyn* 2010; **239**: 1–15.

53 Stiegler AL, Burden SJ, Hubbard SR. Crystal structure of the frizzled-like cysteine-rich domain of the receptor tyrosine kinase MuSK. *J Mol Biol* 2009; **393**: 1–9.
54 Schlessinger J. Cell signaling by receptor tyrosine kinases. *Cell* 2000; **103**: 211–225.
55 Liu Y, Rubin B, Bodine PV, Billiard J. Wnt5a induces homodimerization and activation of Ror2 receptor tyrosine kinase. *J Cell Biochem* 2008; **105**: 497–502.
56 Zhang S, Chen L, Cui B, Chuang HY, Yu J, Wang-Rodriguez J *et al.* ROR1 is expressed in human breast cancer and associated with enhanced tumor-cell growth. *PLoS ONE* 2012; **7**: e31127.
57 Jarmoskaite I, Russell R. DEAD-box proteins as RNA helicases and chaperones. *Wiley Interdiscip Rev RNA* 2011; **2**: 135–152.
58 Samatanga B, Klostermeier D. DEAD-box RNA helicase domains exhibit a continuum between complete functional independence and high thermodynamic coupling in nucleotide and RNA duplex recognition. *Nucleic Acids Res* 2014; **42**: 10644–10654.
59 Rocak S, Linder P. DEAD-box proteins: the driving forces behind RNA metabolism. *Nat Rev Mol Cell Biol* 2004; **5**: 232–241.
60 Li L, Monckton EA, Godbout R. A role for DEAD box 1 at DNA double-strand breaks. *Mol Cell Biol* 2008; **28**: 6413–6425.
61 Linder P, Jankowsky E. From unwinding to clamping-the DEAD box RNA helicase family. *Nat Rev Mol Cell Biol* 2011; **12**: 505–516.
62 Fuller-Pace FV. DEAD box RNA helicase functions in cancer. *RNA Biol* 2013; **10**: 121–132.
63 Shin EM, Hay HS, Lee MH, Goh JN, Tan TZ, Sen YP *et al.* DEAD-box helicase DP103 defines metastatic potential of human breast cancers. *J Clin Invest* 2014; **124**: 3807–3824.
64 Perou CM, Sørlie T, Eisen MB, van de Rijn M, Jeffrey SS, Rees CA *et al.* Molecular portraits of human breast tumours. *Nature* 2000; **406**: 747–752.
65 Eroles P, Bosch A, Perez-Fidalgo JA, Lluch A. Molecular biology in breast cancer: intrinsic subtypes and signaling pathways. *Cancer Treat Rev* 2012; **38**: 698–707.
66 Creighton CJ. The molecular profile of luminal B breast cancer. *Biologics* 2012; **6**: 289.
67 Eroles P, Bosch A, Pérez-Fidalgo JA, Lluch A. Molecular biology in breast cancer: intrinsic subtypes and signaling pathways. *Cancer Treat Rev* 2012; **38**: 698–707.
68 Prat A, Carey LA, Adamo B, Vidal M, Tabernero J, Cortés J *et al.* Molecular features and survival outcomes of the intrinsic subtypes within HER2-positive breast cancer. *J Natl Cancer Inst* 2014; **106**: dju152.
69 Abramson VG, Lehmann BD, Ballinger TJ, Pietenpol JA. Subtyping of triple-negative breast cancer: implications for therapy. *Cancer* 2015; **121**: 8–16.
70 Kast K, Link T, Friedrich K, Petzold A, Niedostatek A, Schoffer O *et al.* Impact of breast cancer subtypes and patterns of metastasis on outcome. *Breast Cancer Res Treat* 2015; **150**: 621–629.
71 Shah SP, Roth A, Goya R, Oloumi A, Ha G, Zhao Y *et al.* The clonal and mutational evolution spectrum of primary triple-negative breast cancers. *Nature* 2012; **486**: 395–399.
72 Weisman PS, Ng CK, Brogi E, Eisenberg RE, Won HH, Piscuoglio S *et al.* Genetic alterations of triple negative breast cancer by targeted next-generation sequencing and correlation with tumor morphology. *Mod Pathol* 2016; **29**: 476–488.
73 Lehmann BD, Bauer JA, Chen X, Sanders ME, Chakravarthy AB, Shyr Y *et al.* Identification of human triple-negative breast cancer subtypes and preclinical models for selection of targeted therapies. *J Clin Invest* 2011; **121**: 2750–2767.
74 Wang G, Wang J, Sadar MD. Crosstalk between the androgen receptor and beta-catenin in castrate-resistant prostate cancer. *Cancer Res* 2008; **68**: 9918–9927.
75 Noah TK, Lo YH, Price A, Chen G, King E, Washington MK *et al.* SPDEF functions as a colorectal tumor suppressor by inhibiting beta-catenin activity. *Gastroenterology* 2013; **144**: 1012–23 e6.
76 Wang H, Xi Q, Wu G. Fatty acid synthase regulates invasion and metastasis of colorectal cancer via Wnt signaling pathway. *Cancer Med* 2016; **5**: 1599–1606.
77 Laezza C, D'Alessandro A, Paladino S, Maria Malfitano A, Chiara Proto M, Gazzerro P *et al.* Anandamide inhibits the Wnt/beta-catenin signalling pathway in human breast cancer MDA MB 231 cells. *Eur J Cancer* 2012; **48**: 3112–3122.
78 Kahlert UD, Maciaczyk D, Doostkam S, Orr BA, Simons B, Bogiel T *et al.* Activation of canonical WNT/beta-catenin signaling enhances in vitro motility of glioblastoma cells by activation of ZEB1 and other activators of epithelial-to-mesenchymal transition. *Cancer Lett* 2012; **325**: 42–53.
79 Greenow KR, Clarke AR, Williams GT, Jones R. Wnt-driven intestinal tumourigenesis is suppressed by Chk1 deficiency but enhanced by conditional haploinsufficiency. *Oncogene* 2014; **33**: 4089–4096.
80 Huard CC, Tremblay CS, Magron A, Levesque G, Carreau M. The Fanconi anemia pathway has a dual function in Dickkopf-1 transcriptional repression. *Proc Natl Acad Sci USA* 2014; **111**: 2152–2157.
81 Castiglia D, Bernardini S, Alvino E, Pagani E, De Luca N, Falcinelli S *et al.* Concomitant activation of Wnt pathway and loss of mismatch repair function in human melanoma. *Genes Chromosomes Cancer* 2008; **47**: 614–624.
82 Xu H, Yan Y, Deb S, Rangasamy D, Germann M, Malaterre J *et al.* Cohesin Rad21 mediates loss of heterozygosity and is upregulated via Wnt promoting transcriptional dysregulation in gastrointestinal tumors. *Cell Rep* 2014; **9**: 1781–1797.
83 Huang YL, Anvarian Z, Doderlein G, Acebron SP, Niehrs C. Maternal Wnt/STOP signaling promotes cell division during early Xenopus embryogenesis. *Proc Natl Acad Sci USA* 2015; **112**: 5732–5737.
84 Kikuchi K, Niikura Y, Kitagawa K, Kikuchi A. Dishevelled, a Wnt signalling component, is involved in mitotic progression in cooperation with Plk1. *EMBO J* 2010; **29**: 3470–3483.
85 Suzuki A, Pelikan RC, Iwata J. WNT/beta-catenin signaling regulates multiple steps of myogenesis by regulating step-specific targets. *Mol Cell Biol* 2015; **35**: 1763–1776.
86 Chiacchiera F, Rossi A, Jammula S, Piunti A, Scelfo A, Ordonez-Moran P *et al.* Polycomb complex PRC1 preserves intestinal stem cell identity by sustaining Wnt/beta-catenin transcriptional activity. *Cell Stem Cell* 2016; **18**: 91–103.
87 He TC, Sparks AB, Rago C, Hermeking H, Zawel L, da Costa LT *et al.* Identification of c-MYC as a target of the APC pathway. *Science* 1998; **281**: 1509–1512.
88 Conrad WH, Swift RD, Biechele TL, Kulikauskas RM, Moon RT, Chien AJ. Regulating the response to targeted MEK inhibition in melanoma: enhancing apoptosis in NRAS- and BRAF-mutant melanoma cells with Wnt/beta-catenin activation. *Cell Cycle* 2012; **11**: 3724–3730.
89 Xu M, Wang S, Qi Y, Chen L, Frank JA, Yang XH *et al.* Role of MCP-1 in alcohol-induced aggressiveness of colorectal cancer cells. *Mol Carcinog* 2016; **55**: 1002–1011.
90 Yasuhara R, Irie T, Suzuki K, Sawada T, Miwa N, Sasaki A *et al.* The beta-catenin signaling pathway induces aggressive potential in breast cancer by up-regulating the chemokine CCL5. *Exp Cell Res* 2015; **338**: 22–31.
91 Yu Q, Xu M, Sen JM. Beta-catenin expression enhances IL-7 receptor signaling in thymocytes during positive selection. *J Immunol* 2007; **179**: 126–131.
92 Burstein MD, Tsimelzon A, Poage GM, Covington KR, Contreras A, Fuqua SA *et al.* Comprehensive genomic analysis identifies novel subtypes and targets of triple-negative breast cancer. *Clin Cancer Res* 2015; **21**: 1688–1698.
93 Pistelli M, Caramanti M, Biscotti T, Santinelli A, Pagliacci A, De Lisa M *et al.* Androgen receptor expression in early triple-negative breast cancer: clinical significance and prognostic associations. *Cancers* 2014; **6**: 1351–1362.
94 Arce-Salinas C, Riesco-Martinez MC, Hanna W, Bedard P, Warner E. Complete response of metastatic androgen receptor-positive breast cancer to bicalutamide: case report and review of the literature. *J Clin Oncol* 2016; **34**: e21–e24.
95 Gucalp A, Tolaney S, Isakoff SJ, Ingle JN, Liu MC, Carey LA *et al.* Phase II trial of bicalutamide in patients with androgen receptor-positive, estrogen receptor-negative metastatic breast cancer. *Clin Cancer Res* 2013; **19**: 5505–5512.
96 Hilborn E, Gacic J, Fornander T, Nordenskjold B, Stal O, Jansson A. Androgen receptor expression predicts beneficial tamoxifen response in oestrogen receptor-alpha-negative breast cancer. *Br J Cancer* 2016; **114**: 248–255.
97 Ciupek A, Rechoum Y, Gu G, Gelsomino L, Beyer AR, Brusco L *et al.* Androgen receptor promotes tamoxifen agonist activity by activation of EGFR in ERalpha-positive breast cancer. *Breast Cancer Res Treat* 2015; **154**: 225–237.
98 Prat A, Parker JS, Karginova O, Fan C, Livasy C, Herschkowitz JI *et al.* Phenotypic and molecular characterization of the claudin-low intrinsic subtype of breast cancer. *Breast Cancer Res* 2010; **12**: 1.
99 Liu Y-R, Jiang Y-Z, Xu X-E, Yu K-D, Jin X, Hu X *et al.* Comprehensive transcriptome analysis identifies novel molecular subtypes and subtype-specific RNAs of triple-negative breast cancer. *Breast Cancer Res* 2016; **18**: 1.
100 Lefebvre V, Dumitriu B, Penzo-Mendez A, Han Y, Pallavi B. Control of cell fate and differentiation by Sry-related high-mobility-group box (Sox) transcription factors. *Int J Biochem Cell Biol* 2007; **39**: 2195–2214.
101 Kormish JD, Sinner D, Zorn AM. Interactions between SOX factors and Wnt/beta-catenin signaling in development and disease. *Dev Dyn* 2010; **239**: 56–68.
102 Zhang L, Chen X, Stauffer S, Yang S, Chen Y, Dong J. CDK1 phosphorylation of TAZ in mitosis inhibits its oncogenic activity. *Oncotarget* 2015; **6**: 31399–31412.
103 Prat A, Pineda E, Adamo B, Galván P, Fernández A, Gaba L *et al.* Clinical implications of the intrinsic molecular subtypes of breast cancer. *Breast* 2015; **24**: S26–S35.
104 Xu J, Prosperi JR, Choudhury N, Olopade OI, Goss KH. β-Catenin is required for the tumorigenic behavior of triple-negative breast cancer cells. *PLoS ONE* 2015; **10**: e0117097.
105 Mohammed MK, Shao C, Wang J, Wei Q, Wang X, Collier Z *et al.* Wnt/β-catenin signaling plays an ever-expanding role in stem cell self-renewal, tumorigenesis and cancer chemoresistance. *Genes Dis* 2016; **3**: 11–40.
106 Dey N, Barwick BG, Moreno CS, Ordanic-Kodani M, Chen Z, Oprea-Ilies G *et al.* Wnt signaling in triple negative breast cancer is associated with metastasis. *BMC Cancer* 2013; **13**: 1.
107 Khramtsov AI, Khramtsova GF, Tretiakova M, Huo D, Olopade OI, Goss KH. Wnt/β-catenin pathway activation is enriched in basal-like breast cancers and predicts poor outcome. *Am J Pathol* 2010; **176**: 2911–2920.

108 Geyer FC, Lacroix-Triki M, Savage K, Arnedos M, Lambros MB, MacKay A *et al.* beta-Catenin pathway activation in breast cancer is associated with triple-negative phenotype but not with CTNNB1 mutation. *Mod Pathol* 2011; **24**: 209–231.
109 Borg J-P, Belotti E, Daulat A, Lembo F, Bertucci F, Charafe-Jauffret E *et al.* Deregulation of the non-canonical pathway in triple-negative breast cancer. *FASEB J* 2013; **27**: 610.1–.1.
110 Medema JP. Cancer stem cells: the challenges ahead. *Nat Cell Biol* 2013; **15**: 338–344.
111 Sicchieri RD, da Silveira WA, Mandarano LR, de Oliveira TM, Carrara HH, Muglia VF *et al.* ABCG2 is a potential marker of tumor-initiating cells in breast cancer. *Tumour Biol* 2015; **36**: 9233–9243.
112 Pogoda K, Niwinska A, Murawska M, Pienkowski T. Analysis of pattern, time and risk factors influencing recurrence in triple-negative breast cancer patients. *Med Oncol* 2013; **30**: 388.
113 Cheng L, Ramesh AV, Flesken-Nikitin A, Choi J, Nikitin AY. Mouse models for cancer stem cell research. *Toxicol Pathol* 2010; **38**: 62–71.
114 Atkinson RL, Yang WT, Rosen DG, Landis MD, Wong H, Lewis MT *et al.* Cancer stem cell markers are enriched in normal tissue adjacent to triple negative breast cancer and inversely correlated with DNA repair deficiency. *Breast Cancer Res* 2013; **15**: R77.
115 Peiris-Pages M, Martinez-Outschoorn UE, Pestell RG, Sotgia F, Lisanti MP. Cancer stem cell metabolism. *Breast Cancer Res* 2016; **18**: 55.
116 van Amerongen R, Bowman AN, Nusse R. Developmental stage and time dictate the fate of Wnt/β-catenin-responsive stem cells in the mammary gland. *Cell Stem Cell* 2012; **11**: 387–400.
117 Zeng YA, Nusse R. Wnt proteins are self-renewal factors for mammary stem cells and promote their long-term expansion in culture. *Cell Stem Cell* 2010; **6**: 568–577.
118 Howard B, Ashworth A. Signalling pathways implicated in early mammary gland morphogenesis and breast cancer. *PLoS Genet* 2006; **2**: e112.
119 Jang GB, Kim JY, Cho SD, Park KS, Jung JY, Lee HY *et al.* Blockade of Wnt/beta-catenin signaling suppresses breast cancer metastasis by inhibiting CSC-like phenotype. *Sci Rep* 2015; **5**: 12465.
120 Cleary AS, Leonard TL, Gestl SA, Gunther EJ. Tumour cell heterogeneity maintained by cooperating subclones in Wnt-driven mammary cancers. *Nature* 2014; **508**: 113–117.
121 Rangel MC, Bertolette D, Castro NP, Klauzinska M, Cuttitta F, Salomon DS. Developmental signaling pathways regulating mammary stem cells and contributing to the etiology of triple-negative breast cancer. *Breast Cancer Res Treat* 2016; **156**: 211–226.
122 Corda G, Sala G, Lattanzio R, Iezzi M, Sallese M, Fragassi G *et al.* Functional and prognostic significance of the genomic amplification of frizzled 6 (FZD6) in breast cancer. *J Pathol* 2016; **241**: 350–361.
123 Yang L, Wu X, Wang Y, Zhang K, Wu J, Yuan Y *et al.* FZD7 has a critical role in cell proliferation in triple negative breast cancer. *Oncogene* 2011; **30**: 4437–4446.
124 Chakrabarti R, Wei Y, Hwang J, Hang X, Blanco MA, Choudhury A *et al.* ΔNp63 promotes stem cell activity in mammary gland development and basal-like breast cancer by enhancing Fzd7 expression and Wnt signalling. *Nat Cell Biol* 2014; **16**: 1004–1015.
125 Phesse T, Flanagan D, Vincan E. Frizzled7: a promising Achilles' heel for targeting the Wnt receptor complex to treat cancer. *Cancers* 2016; **8**: 50.
126 Yin S, Xu L, Bonfil RD, Banerjee S, Sarkar FH, Sethi S *et al.* Tumor-initiating cells and FZD8 play a major role in drug resistance in triple-negative breast cancer. *Mol Cancer Ther* 2013; **12**: 491–498.
127 Jiang Q, He M, Guan S, Ma M, Wu H, Yu Z *et al.* MicroRNA-100 suppresses the migration and invasion of breast cancer cells by targeting FZD-8 and inhibiting Wnt/β-catenin signaling pathway. *Tumor Biol* 2016; **37**: 5001–5011.
128 Yin S, Cheriyan VT, Rishi AK, Reddy KB. c-Myc and Frizzled 8 play a major role in the regulation of cancer stem cells and drug resistance in triple-negative breast cancer. *Cancer Res* 2015; **75**: 2225.
129 Badders NM, Goel S, Clark RJ, Klos KS, Kim S, Bafico A *et al.* The Wnt receptor, Lrp5, is expressed by mouse mammary stem cells and is required to maintain the basal lineage. *PLoS ONE* 2009; **4**: e6594.
130 Lindvall C, Evans NC, Zylstra CR, Li Y, Alexander CM, Williams BO. The Wnt signaling receptor Lrp5 is required for mammary ductal stem cell activity and Wnt1-induced tumorigenesis. *Journal of Biological Chemistry* 2006; **281**: 35081–35087.
131 Lindvall C, Zylstra CR, Evans N, West RA, Dykema K, Furge KA *et al.* The Wnt co-receptor Lrp6 is required for normal mouse mammary gland development. *PLoS ONE* 2009; **4**: e5813.
132 Liu C-C, Prior J, Piwnica-Worms D, Bu G. LRP6 overexpression defines a class of breast cancer subtype and is a target for therapy. *Proc Natl Acad Sci* 2010; **107**: 5136–5141.
133 Wang H, He L, Ma F, Regan MM, Balk SP, Richardson AL *et al.* SOX9 regulates low density lipoprotein receptor-related protein 6 (LRP6) and T-cell factor 4 (TCF4) expression and Wnt/β-catenin activation in breast cancer. *J Biol Chem* 2013; **288**: 6478–6487.
134 Ibrahim SA, Hassan H, Vilardo L, Kumar SK, Kumar AV, Kelsch R *et al.* Syndecan-1 (CD138) modulates triple-negative breast cancer stem cell properties via regulation of LRP-6 and IL-6-mediated STAT3 signaling. *PLoS ONE* 2013; **8**: e85737.
135 Nikolova V, Koo C-Y, Ibrahim SA, Wang Z, Spillmann D, Dreier R *et al.* Differential roles for membrane-bound and soluble syndecan-1 (CD138) in breast cancer progression. *Carcinogenesis* 2009; **30**: 397–407.
136 Zhang S, Chen L, Cui B, Chuang H-Y, Yu J, Wang-Rodriguez J *et al.* ROR1 is expressed in human breast cancer and associated with enhanced tumor-cell growth. *PLoS ONE* 2012; **7**: e31127.
137 Cui B, Zhang S, Chen L, Yu J, Widhopf GF, Fecteau J-F *et al.* Targeting ROR1 inhibits epithelial–mesenchymal transition and metastasis. *Cancer Res* 2013; **73**: 3649–3660.
138 Henry C, Quadir A, Hawkins N, Jary E, Llamosas E, Kumar D *et al.* Expression of the novel Wnt receptor ROR2 is increased in breast cancer and may regulate both β-catenin dependent and independent Wnt signalling. *J Cancer Res Clin Oncol* 2015; **141**: 243–254.
139 Cruciat C-M, Dolde C, de Groot RE, Ohkawara B, Reinhard C, Korswagen HC *et al.* RNA helicase DDX3 is a regulatory subunit of casein kinase 1 in Wnt–β-catenin signaling. *Science* 2013; **339**: 1436–1441.
140 Botlagunta M, Vesuna F, Mironchik Y, Raman A, Lisok A, Winnard P *et al.* Oncogenic role of DDX3 in breast cancer biogenesis. *Oncogene* 2008; **27**: 3912–3922.
141 Xie M, Vesuna F, Botlagunta M, Bol GM, Irving A, Bergman Y *et al.* NZ51, a ring-expanded nucleoside analog, inhibits motility and viability of breast cancer cells by targeting the RNA helicase DDX3. *Oncotarget* 2015; **6**: 29901–29913.
142 Guturi KKN, Sarkar M, Bhowmik A, Das N, Ghosh MK. DEAD-box protein p68 is regulated by β-catenin/transcription factor 4 to maintain a positive feedback loop in control of breast cancer progression. *Breast Cancer Res* 2014; **16**: 1.
143 Moore HC, Jordan LB, Bray SE, Baker L, Quinlan PR, Purdie CA *et al.* The RNA helicase p68 modulates expression and function of the Δ133 isoform (s) of p53, and is inversely associated with Δ133p53 expression in breast cancer. *Oncogene* 2010; **29**: 6475–6484.
144 Wang D, Huang J, Hu Z. RNA helicase DDX5 regulates microRNA expression and contributes to cytoskeletal reorganization in basal breast cancer cells. *Mol Cell Proteomics* 2012; **11**: M111. 011932.
145 Esquela-Kerscher A, Slack FJ. Oncomirs—microRNAs with a role in cancer. *Nat Rev Cancer* 2006; **6**: 259–269.
146 Shimono Y, Zabala M, Cho RW, Lobo N, Dalerba P, Qian D *et al.* Downregulation of miRNA-200c links breast cancer stem cells with normal stem cells. *Cell* 2009; **138**: 592–603.
147 Avery-Kiejda KA, Braye SG, Mathe A, Forbes JF, Scott RJ. Decreased expression of key tumour suppressor microRNAs is associated with lymph node metastases in triple negative breast cancer. *BMC Cancer* 2014; **14**: 1.
148 Goh JN, Loo SY, Datta A, Siveen KS, Yap WN, Cai W *et al.* microRNAs in breast cancer: regulatory roles governing the hallmarks of cancer. *Biol Rev Camb Philos Soc* 2016; **91**: 409–428.
149 Cai J, Guan H, Fang L, Yang Y, Zhu X, Yuan J *et al.* MicroRNA-374a activates Wnt/β-catenin signaling to promote breast cancer metastasis. *J Clin Invest* 2013; **123**: 566–579.
150 Wu ZS, Wu Q, Wang CQ, Wang XN, Huang J, Zhao JJ *et al.* miR-340 inhibition of breast cancer cell migration and invasion through targeting of oncoprotein c-Met. *Cancer* 2011; **117**: 2842–2852.
151 Mohammadi-Yeganeh S, Paryan M, Arefian E, Vasei M, Ghanbarian H, Mahdian R *et al.* MicroRNA-340 inhibits the migration, invasion, and metastasis of breast cancer cells by targeting Wnt pathway. *Tumor Biol* 2016; **37**: 8993–9000.
152 Mohammadi Yeganeh S, Vasei M, Tavakoli R, Kia V, Paryan M. The effect of miR-340 over-expression on cell-cycle–related genes in triple-negative breast cancer cells. *Eur J Cancer Care* 2016; **7**: 79032–79046.
153 Isobe T, Hisamori S, Hogan DJ, Zabala M, Hendrickson DG, Dalerba P *et al.* miR-142 regulates the tumorigenicity of human breast cancer stem cells through the canonical WNT signaling pathway. *Elife* 2014; **3**: e01977.
154 Taipaleenmaki H, Farina NH, van Wijnen AJ, Stein JL, Hesse E, Stein GS *et al.* Antagonizing miR-218-5p attenuates Wnt signaling and reduces metastatic bone disease of triple negative breast cancer cells. *Oncotarget* 2016; **7**: 79032–79046.
155 Group EBCTC., Adjuvant chemotherapy in oestrogen-receptor-poor breast cancer: patient-level meta-analysis of randomised trials. *Lancet* 2008; **371**: 29–40.
156 Tudoran O, Soritau O, Balacescu L, Visan S, Barbos O, Cojocneanu-Petric R *et al.* Regulation of stem cells-related signaling pathways in response to doxorubicin treatment in Hs578T triple-negative breast cancer cells. *Mol Cell Biochem* 2015; **409**: 163–176.
157 Sparano JA. Defining a role and predicting benefit from platinum-based therapy in breast cancer: an evolving story. *J Clin Oncol* 2015; **33**: 1–3.
158 Yin S, Xu L, Bandyopadhyay S, Sethi S, Reddy KB. Cisplatin and TRAIL enhance breast cancer stem cell death. *Int J Oncol* 2011; **39**: 891.

159 Jang G-B, Hong I-S, Kim R-J, Lee S-Y, Park S-J, Lee E-S *et al.* Wnt/β-catenin small-molecule inhibitor CWP232228 preferentially inhibits the growth of breast cancer stem-like cells. *Cancer Res* 2015; **75**: 1691–1702.
160 Takebe N, Miele L, Harris PJ, Jeong W, Bando H, Kahn M *et al.* Targeting Notch, Hedgehog, and Wnt pathways in cancer stem cells: clinical update. *Nat Rev Clin Oncol* 2015; **12**: 445–464.
161 Solzak JP, Atale R, Hancock B, Radovich M. Dual PI3K and Wnt pathway inhibition is a synergistic combination against triple-negative breast cancer. *Cancer Res* 2015; **75**: 5340.
162 Farmer H, McCabe N, Lord CJ, Tutt AN, Johnson DA, Richardson TB *et al.* Targeting the DNA repair defect in BRCA mutant cells as a therapeutic strategy. *Nature* 2005; **434**: 917–921.
163 Bryant HE, Schultz N, Thomas HD, Parker KM, Flower D, Lopez E *et al.* Specific killing of BRCA2-deficient tumours with inhibitors of poly (ADP-ribose) polymerase. *Nature* 2005; **434**: 913–917.
164 Huang SM, Mishina YM, Liu S, Cheung A, Stegmeier F, Michaud GA *et al.* Tankyrase inhibition stabilizes axin and antagonizes Wnt signalling. *Nature* 2009; **461**: 614–620.
165 Bao R, Christova T, Song S, Angers S, Yan X, Attisano L. Inhibition of tankyrases induces Axin stabilization and blocks Wnt signalling in breast cancer cells. *PLoS ONE* 2012; **7**: e48670.
166 Livraghi L, Garber JE. PARP inhibitors in the management of breast cancer: current data and future prospects. *BMC Med* 2015; **13**: 1.
167 Kaufman B, Shapira-Frommer R, Schmutzler RK, Audeh MW, Friedlander M, Balmaña J *et al.* Olaparib monotherapy in patients with advanced cancer and a germline BRCA1/2 mutation. *J Clin Oncol* 2015; **33**: 244–250.
168 Pahuja S, Beumer JH, Appleman LJ, HA-H Tawbi, Stoller RG, Lee JJ *et al.* (eds). in *ASCO Annual Meeting Proceedings*, Chicago, IL, USA; 29 May-2 June, 2015.
169 Tate CR, Rhodes LV, Segar HC, Driver JL, Pounder FN, Burow ME *et al.* Targeting triple-negative breast cancer cells with the histone deacetylase inhibitor panobinostat. *Breast Cancer Res* 2012; **14**: R79.
170 Schech A, Kazi A, Yu S, Shah P, Sabnis G. Histone deacetylase inhibitor entinostat inhibits tumor-initiating cells in triple-negative breast cancer cells. *Mol Cancer Ther* 2015; **14**: 1848–1857.
171 Merino VF, Nguyen N, Jin K, Sadik H, Cho S, Korangath P *et al.* Combined treatment with epigenetic, differentiating, and chemotherapeutic agents cooperatively targets tumor-initiating cells in triple-negative breast cancer. *Cancer Res* 2016; **76**: 2013–2024.
172 Prasad CP, Mirza S, Sharma G, Prashad R, DattaGupta S, Rath G *et al.* Epigenetic alterations of CDH1 and APC genes: relationship with activation of Wnt/beta-catenin pathway in invasive ductal carcinoma of breast. *Life Sci* 2008; **83**: 318–325.
173 Kai M, Kanaya N, Wu SV, Mendez C, Nguyen D, Luu T *et al.* Targeting breast cancer stem cells in triple-negative breast cancer using a combination of LBH589 and salinomycin. *Breast Cancer Res Treat* 2015; **151**: 281–294.

Experimental Cell Research ■ (■■■■) ■■■–■■■

Contents lists available at ScienceDirect

Experimental Cell Research

journal homepage: www.elsevier.com/locate/yexcr

Research Article

Therapeutic approach to target mesothelioma cancer cells using the Wnt antagonist, secreted frizzled-related protein 4: Metabolic state of cancer cells

Vanathi Perumal [a,1], Sebastian Pohl [b,1], Kevin N. Keane [c,1], Frank Arfuso [b], Philip Newsholme [c], Simon Fox [a], Arun Dharmarajan [b,*]

[a] Molecular Pharmacology Laboratory, School of Pharmacy, Curtin Health Innovation Research Institute, Curtin University, Bentley, WA, Australia
[b] Stem Cell and Cancer Biology Laboratory, School of Biomedical Sciences, Curtin Health Innovation Research Institute, Curtin University, Bentley, WA, Australia
[c] School of Biomedical Sciences, Curtin Health Innovation Research Institute, Curtin University, Bentley, WA, Australia

ARTICLE INFO

Article history:
Received 18 December 2015
Received in revised form
5 February 2016
Accepted 7 February 2016

Keywords:
Mesothelioma
Wnt
Secreted frizzled-related protein 4
Metabolism

ABSTRACT

Malignant mesothelioma (MM) is an aggressive cancer, characterized by rapid progression, along with late metastasis and poor patient prognosis. It is resistant to many forms of standard anti-cancer treatment. In this study, we determined the effect of secreted frizzled-related protein 4 (sFRP4), a Wnt pathway inhibitor, on cancer cell proliferation and metabolism using the JU77 mesothelioma cell line.

Treatment with sFRP4 (250 pg/ml) resulted in a significant reduction of cell proliferation. The addition of the Wnt activator Wnt3a (250 pg/ml) or sFRP4 had no significant effect on ATP production and glucose utilisation in JU77 cells at both the 24 and 48 h time points examined. We also examined their effect on Akt and Glycogen synthase kinase-3 beta (GSK3β) phosphorylation, which are both important components of Wnt signalling and glucose metabolism. We found that protein phosphorylation of Akt and GSK3β varied over the 24 h and 48 h time points, with constitutive phosphorylation of Akt at serine 473 (pAkt) decreasing to its most significant level when treated with Wnt3a+sFRP4 at the 24 h time point. A significant reduction in the level of Cytochrome c oxidase was observed at the 48 h time point, when sFRP4 and Wnt3a were added in combination.

We conclude that sFRP4 may function, in part, to reduce/alter cancer cell metabolism, which may lead to sensitisation of cancer cells to chemotherapeutics, or even cell death.

1. Introduction

Malignant mesothelioma (MM) is a particularly aggressive cancer that is characterised by rapid progression, late metastases, and poor prognosis [1]. Although this tumour is relatively uncommon, the incidence continues to rise in Australia as a consequence of high past asbestos use and the long latency period between exposure to asbestos and subsequent tumour development. MM is highly resistant to conventional forms of anti-cancer therapy, and both radiotherapy and chemotherapy have a limited effect [1]. There is an urgent need for more effective therapies for this cancer based upon identification of molecular targets through improved biological understanding of the disease. The Wnt signalling pathways play a key role in development and homoeostasis. There is convincing evidence in a number of different cancers that chronic activation of Wnt signalling is important in tumorigenesis, and this has fuelled interest in targeting this pathway [2–5]. Aberrations of Wnt signalling have been described in mesothelioma [6], and there is a need to identify the extent to which this pathway drives cell growth and survival in MM. The investigation of biological and immunological therapies for MM in preclinical models has been a major interest. In human and mouse MM cells, we have investigated regulators of the Wnt signalling pathway [7]. In particular, we have shown differential expression of secreted frizzled-related protein 4 (sFRP4) [6], which is a Wnt antagonist, and of longstanding interest to our group for its role in apoptotic signalling in morphogenesis, developmental biology, and neoplasia [8–11].

Cancer cells "rewire" metabolism to maintain continued proliferation. Changes in cellular metabolism occur down-stream of oncogene/tumour suppressors [12]. It has been demonstrated that tumour cells consume large amounts of glucose to yield ATP [13]. It is well established that deregulated pathways in cancer also impact on metabolism. The difference in metabolic properties of cancer cells and normal cells suggests that targeting metabolic dependence could be a selective approach to treat cancer patients.

In 1956, Warburg observed that the rate of glycolysis was

* Corresponding author.
E-mail address: a.dharmarajan@curtin.edu.au (A. Dharmarajan).
[1] These authors contributed equally to this work.

http://dx.doi.org/10.1016/j.yexcr.2016.02.008
0014-4827/

abnormally high in cancer cells. This 'Warburg effect' indicates that cancer cells prefer glycolytic breakdown of glucose for energy, rather than mitochondrial oxidative phosphorylation [14]. Although the molecular mechanisms that define the Warburg effect are not yet fully understood, the increased glycolysis observed in cancer cells is well accepted to be important for the support of malignant phenotypes [15,16].

In this study, we are the first to report the effects of the Wnt-pathway inhibitor, sFRP4, on mesothelioma cancer cell metabolism via assessment of ATP production, glucose utilisation, and bioenergetics, together with downstream signalling molecules such as total and phosphorylated glycogen synthase kinase-3 beta (GSK3β), Protein kinase B (also known as Akt), and cytochrome C oxidase (COX IV).

2. Materials and methods

2.1. Cell culture and treatment

The malignant mesothelioma cell line JU77, originally derived from pleural effusions of different patients presenting with malignant pleural mesothelioma, was used in this study [17]. The cells were cultured in RPMI – 1640 (Hyclone) with 10% FBS (Bovogen), penicillin (100IU/ml), and streptomycin (100 μg/ml) (Life Technologies). JU77 cells were seeded in 6-well plates (Corning) at a density of 30,000/cm^2, and treated with recombinant Wnt3a (250 pg/ml) and sFRP4 (250 pg/ml) (R&D Systems) for 24 and 48 h.

2.2. Morphology

Phase contrast images were obtained following the different treatments using an Olympus bright field microscope.

2.3. MTT assay

Cell proliferation in response to various treatments was quantitated using the MTT ((3-(4,5-dimethylthiazol-2-yl)-2,5-diphenyltetrazolium bromide)) assay. Cells were seeded into 96-well plates at a density of 10,000–20,000 cells/well, depending on the experiment. Following 24 h incubation, treatments were added and cells incubated for a further 24–48 h (depending on experiments). The MTT assay was performed as previously described [18], and absorbance was read at 595 nm with a microplate reader (Enspire, Perkin Elmer). For each treatment, the mean absorbance for the assay replicates (3 wells) was calculated. The data are expressed as mean ± standard deviation for at least 3 independent experiments, and plotted using Prism for Windows v 6.07 (Graphpad Software, CA, USA).

2.4. Viability assay

Trypan blue is a stain used to selectively stain dead cells blue. To minimise operator bias, trypsinised cells were stained with trypan blue, and live and dead cells enumerated using Invitrogen Countess™ Automated Cell Counter chambers [19].

2.5. Measurement of cellular ATP and cellular glycolytic activity

Relative cellular ATP content was measured by the luciferase-based Cell Titer-Glo Luminescent Cell Viability kit (Promega), with modifications from the manufacturer's protocol. Briefly, cells were plated in 96-well plates at 5000 cells per well to allow for attachment overnight. At the desired harvest time, an equal volume of the single-one-step reagent provided by the kit was added to each well and rocked for 15 min at room temperature. Cellular ATP content was measured and quantified using an ATP standard curve and a luminescent plate reader (Enspire, Perkin Elmer).

Glycolytic activity was determined by measuring glucose consumption. Cells were seeded in 96-well cell culture microplates at 5000 cells per well per 100 μl according to their growth rate, and allowed to attach overnight. Fresh medium was replaced the next morning along with treatment conditions and incubated for 24 or 48 h prior to the assay. Cell culture medium with no cells present was used to calculate the initial level of glucose in the medium (11.1 mM). The glucose consumed from the cell culture medium was measured using the Amplex Red Glucose kit (Invitrogen, Molecular Probes). The samples were diluted 150 fold and the assay was performed according to the manufacturer's instructions. The fluorescence emission was measured at 590 nm following excitation at 550 nm using a Perkin Elmer microplate reader. The values were calculated according to the standard curve, and then subtracted from the base line to obtain values of glucose consumption from the growth culture medium by the cells [20]. Data were then presented as a percentage of the initial glucose concentration.

2.6. Seahorse XF^{e}96 measurements and analysis

The Seahorse Bioscience XF^{e}96 Flux analyser and the Mito Stress Test kit (Seahorse Biosciences) were used according to manufacturer's instructions. In brief, cells were seeded into 96 well plates at a density of 5,000 cells/well and allowed to adhere overnight (cell density was previously optimised for oxygen consumption rates (OCR) and proton production rates (PPR)). Prior to Seahorse analysis, the culture medium was changed to serum-free DMEM (pH 7.4) containing 1 mM sodium pyruvate, 2.5 mM Glucose, and without sodium bicarbonate, and plates were then incubated for 60 min at 37 °C in a non-CO_2 incubator. Following instrument calibration, the Mito Stress Test was performed using the following injection strategy: DMEM (2.5 mM glucose) with or without Wnt3a, sFRP4, or Wnt3a and sFRP4 in combination, oligomycin (2 μM), carbonyl cyanide-*p*-trifluoromethoxyphenylhydrazone (FCCP, 0.4 μM), and finally, rotenone/antimycin A in combination (1 μM). OCR and PPR were determined using three 3.5 min assay cycles of mix, and measurement undertaken following each injection. Normalisation of data was performed by determining the cell density using the neutral red uptake assay after the stress test, and measurements were compared to ensure there were no significant changes in relative cell numbers among treatment groups. The concentrations of all inhibitors used were optimised to ensure the lowest concentration was used to produce the maximum effect.

Basal respiration was calculated by subtracting the minimum OCR following addition of rotenone/antimycin A (non-mitochondrial respiration) from the last OCR measurement recorded prior to the addition of oligomycin. Proton leak was calculated by subtracting the minimum OCR following the addition of rotenone/antimycin A (non-mitochondrial respiration) from the minimum OCR measurement recorded after addition of oligomycin. OCR related to ATP production (turnover) was calculated by subtracting the proton leak from the basal respiration. Coupling efficiency percentage was calculated by dividing the ATP turnover-dependent OCR by the basal respiration and multiplying by 100. Max respiration was determined by subtracting the non-mitochondrial respiration from the maximum OCR following the addition of FCCP. The spare respiratory capacity was calculated by subtracting the basal OCR from the maximum OCR after FCCP addition. The glycolytic response of JU77 cells was measured by first correcting the extracellular acidification rate (ECAR) experimental values to PPR by including the buffer capacity of the medium, which was determined by monitoring the pH change of DMEM following 5 additions of a known quantity of protons from 0.1 M

Please cite this article as: V. Perumal, et al., Therapeutic approach to target mesothelioma cancer cells using the Wnt antagonist, secreted frizzled-related protein 4: Metabolic state of cancer cells, Exp Cell Res (2016), http://dx.doi.org/10.1016/j.yexcr.2016.02.008

hydrochloric acid. Basal PPR was indicative of glycolytic response, while glycolytic reserve capacity was determined by subtracting the basal PPR from the maximum PPR following the addition of oligomycin. Each treatment was measured in quadruplicate wells and repeated on 3 independent occasions ($n=3$).

2.7. Western blotting

Whole cell lysates were extracted at 24 and 48 h times points by scraping cells into radio immunoprecipitation assay (RIPA) buffer (Sigma Aldrich) with 200 mM phenylmethylsulphonyl-fluoride (PMSF) and proteinase/phosphatase inhibitor cocktail (100X) (Cell Signalling Technologies). Whole cell lysates were quantified using the Pierce BCA Protein Assay Kit (Thermo Fisher Scientific). The lysates were loaded into a 10% SDS-PAGE gel after being boiled for 5 min at 95 °C. After electrophoresis, the proteins were transferred onto a nitrocellulose membrane using the iBlot Dry Blotting System (Life Technologies). The membranes were blocked with 5% low-fat skim milk powder in phosphate buffered saline with 0.1% Tween-20 (Sigma Aldrich) (PBST) for an hour at room temperature. Antibodies for total GSK3-β, ^{pser9}GSK3-β, total Akt, and Cytochrome c oxidase subunit IV (all Cell Signalling Technologies) were probed at a dilution of 1:1000 using SNAP i.d ® 2.0 (Merck Millipore) for 10 minutes at room temperature, washed with PBST, and incubated in a 1:2000 dilution of HRP-linked anti-rabbit secondary antibody for a further 10 minutes at room temperature. ^{pser473}Akt antibody (1:1000 dilution) (Cell Signalling Technologies) was probed overnight at 4 °C, washed with PBST, and then the HRP-linked anti-rabbit secondary antibody (1:2000) (Cell Signalling Technologies) was added for 1 h at room temperature. All blots were developed using Amersham ECL Prime Western Blotting Detection Reagent (GE Life Sciences).

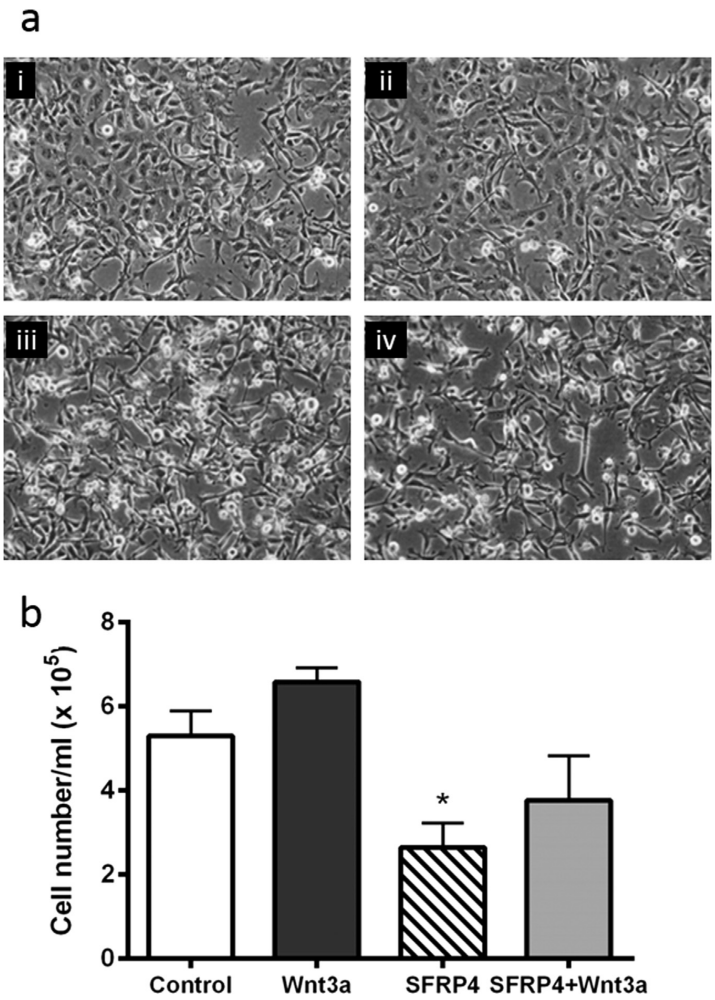

Fig. 1. The Effect of Wnt3a and sFRP4 on cell morphology and viability in JU77 cells. Panel (a) Treatment with sFRP4 had significant morphological effects upon the cultures. Many cells showed a characteristic loss of attachment and a rounded up appearance (Fig. 1a, iii, Nikon inverted microscope-10× magnification). i- Control, ii- Wnt3a (250 pg), iii- sFRP4 (250 pg), iv- Wnt3a+sFRP4 (250 pg). Calculation of viable cell numbers/mL demonstrates the significant reduction in cell viability following the addition of sFRP4 (Fig. 1b).

Please cite this article as: V. Perumal, et al., Therapeutic approach to target mesothelioma cancer cells using the Wnt antagonist, secreted frizzled-related protein 4: Metabolic state of cancer cells, Exp Cell Res (2016), http://dx.doi.org/10.1016/j.yexcr.2016.02.008

2.8. Statistical analysis

Statistical comparison between two groups was performed using an unpaired *t*-test with Instat (Graphpad Software). The difference was determined to be statistically significant if $p < 0.05$.

3. Results

3.1. Wnt signalling molecules modulate mesothelioma cell proliferation

We found that sFRP4 suppressed cell proliferation/viability in JU77 cells at 24 h and 48 h (Figs. 1b and 2). We next determined the effect of the canonical Wnt ligand, Wnt3a, and Wnt3a+sFRP4, on proliferation. Though Wnt3a was able to increase proliferation, it was not statistically significant compared to control. sFRP4 could reduce the Wnt3a-induced proliferation. These results indicate that Wnt signalling molecules can modulate cellular proliferation in mesothelioma cells.

3.2. ATP and glucose utilisation

The addition of Wnt3a (250 pg), sFRP4 (250 pg), or Wnt3a+sFRP4 (250 pg) for 24 and 48 h did not significantly modulate cellular ATP levels or glucose utilisation in JU77 cells (Fig. 2a and b, respectively). ATP levels were slightly decreased following 48 h in comparison with 24 h (panel a). However, ATP levels associated with Wnt3a, sFRP4, or Wnt3a+sFRP4 were not significantly different from the control at 24 and 48 h. As expected, JU77 cells consumed approximately 20% of the glucose present in the medium over 24 h, and a further 20% over an additional 24 h period (48 h in total), and this was independent of the presence of Wnt3a, sFRP4, or Wnt3a+sFRP4 (panel b).

3.3. Acute effect on cellular bioenergetics

Since Wnt3a (250 pg), sFRP4 (250 pg), or Wnt3a+sFRP4 (250 pg) did not significantly alter ATP and glucose utilisation over 24 and 48 h, we investigated the impact of acute exposure of these factors on JU77 cellular bioenergetics using the Seahorse 96^{e} Flux Analyser. Similar to the ATP data above, neither Wnt3a, sFRP4, nor Wnt3a+sFRP acutely modulated ATP turnover, proton leak, nor the coupling efficiency in JU77 cells (Fig. 3a). Furthermore, the basal OCR (respiration) was not significantly altered by acute addition of Wnt3a, sFRP4, or Wnt3a+sFRP4 (Fig. 3b). In addition, no significant change in JU77 max respiration or spare respiratory capacity was observed, indicating that Wnt3a, sFRP4, and Wnt3a+sFRP4 did not impact on oxidative bioenergetics at the chosen concentrations (Fig. 3b). JU77 cells displayed a high level of PPR, suggesting high glycolytic activity indicative of tumour cells. Furthermore, the treatments used did not modulate basal PPR or the reserve glycolytic capacity of these cells (Fig. 3c) (Fig. 4).

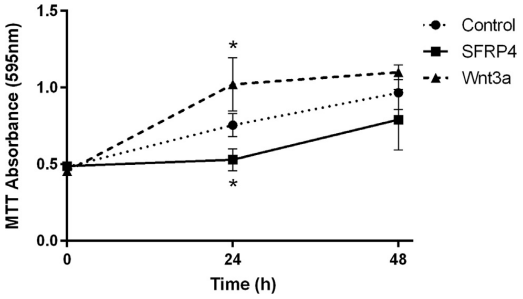

Fig. 2. The effect of sFRP4 on cell proliferation. MTT data demonstrate a significant reduction of cell proliferation following treatment with sFRP4 at 24 h but not at 48 h.

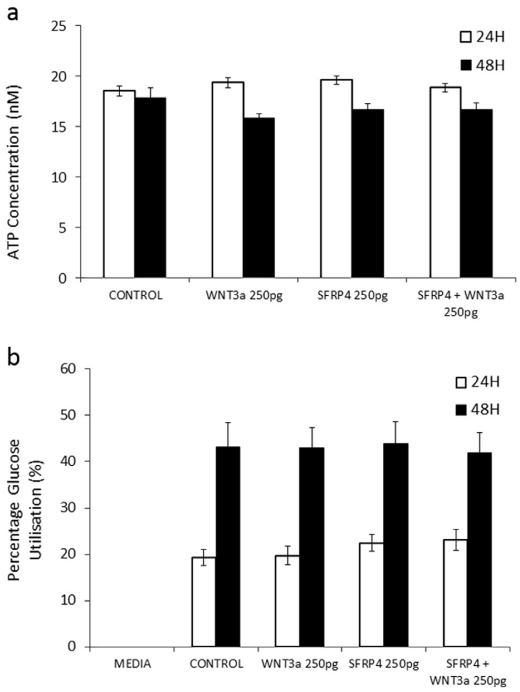

Fig. 3. The Effect of Wnt3a and sFRP4 on ATP and glucose utilisation in JU77 cells. (a) ATP levels in treated cells did not alter significantly among treatment groups, and was only slightly decreased between 24 and 48 h. After 24 h the level of ATP ranged between 19 and 20 nM, while after 48 h it ranged between 16 and 18 nM. (b) Glucose utilisation was also not significantly altered between treatment groups at both time-points. After 24 h JU77 cells utilised approximately 20% of glucose from the initial medium, which doubled to 40% after 48 h, indicating that JU77 cells consumed 20% of glucose per 24 h period.

3.4. Effect on signalling protein phosphorylation and expression

Protein phosphorylation of Akt and GSK3β varied over the 24 h and 48 h time points, with constitutive phosphorylation of Akt at serine 473 (pAkt) decreasing to its most significant level when treated with Wnt3a+sFRP4 at the 24 h time point (Fig. 5d). Although there was a reduction in pAkt at 24 h with the addition of sFRP4 alone, this was not shown to be significant. After 48 h, pAkt was seen to increase with every treatment group relative to the 48 h control (Fig. 5d). Conversely, the most significant reduction in the phosphorylation of GSK3β at serine 9 (pGSK3β) by treatment with sFRP4 occurred at the 48 h time point (Fig. 5b). Interestingly, the reduction of total GSK3β due to the addition of Wnt3a alone and when combined with sFRP4 was significant at the 24 h time period (Fig. 5a), while total Akt was also significantly decreased with Wnt3a treatment at the same time point (Fig. 5c). The only significant reduction in the level of Cytochrome c oxidase (COXIV) was at the 48 h time point, when sFRP4 and Wnt3a were added in combination (Fig. 5e).

4. Discussion

Studies of sFRPs in mesothelioma have mainly investigated

Please cite this article as: V. Perumal, et al., Therapeutic approach to target mesothelioma cancer cells using the Wnt antagonist, secreted frizzled-related protein 4: Metabolic state of cancer cells, Exp Cell Res (2016), http://dx.doi.org/10.1016/j.yexcr.2016.02.008

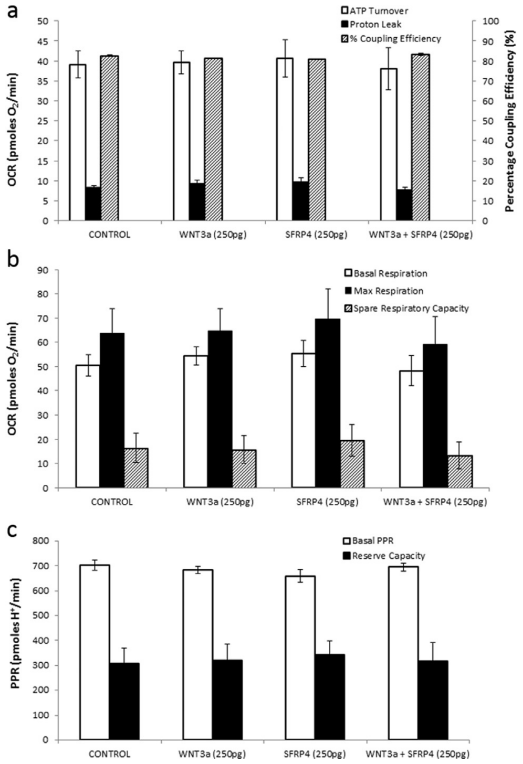

Fig. 4. The acute effect of Wnt3a and sFRP4 on cellular bioenergetics in JU77 cells. JU77 cell bioenergetics was determined using the Seahorse XF^{e}96 and Mito Stress Test kit. (a) No significant change in ATP turnover, proton leak, or coupling efficiency was detected 20 mins after acute addition of Wnt3a, sFRP4, or Wnt3a+sFRP4. (b) Neither factor altered the basal or max respiration of JU77 cells, in addition to the spare respiratory capacity. (c) Interestingly, JU77 cells displayed a high level of PPR, but acute addition of the agents did not modulate basal PPR or the reserve glycolytic capacity.

their role in apoptosis and cancer, and their ability to chemosensitise tumour cells [5]. sFRPs are structurally related to the frizzled receptors [4]. Previously it has been reported that expression of sFRP 1, 3, 4, and 5 were apparently down-regulated in mesothelioma tissue samples and two mesothelioma cell lines [2], and that sFRP4 may suppress growth and induce apoptosis in β-catenin null mesothelioma cells [5]. We have shown that both sFRP4 and Wnt3a may modulate mesothelioma cell growth in more biologically relevant models, since most mesotheliomas express β-catenin [6].

Previous studies have shown that targeting factors that regulate drug-induced apoptosis, cell cycle arrest, or inhibit angiogenesis [9] can influence chemosensitivity [10]. Our previous work was the first to demonstrate that sFRP4 not only plays a key role in the chemo-response of ovarian tumour cells but also, when upregulated in chemoresistant cells, can enable these cells to respond better to Cisplatin treatment [10]. Similar findings have been demonstrated in glioblastoma [21] and other tumours such as breast, prostate, head and neck, and mesothelioma [22]. Another advantage of sFRP4 is that this molecule can suppress tumorigenic growth either in the presence or absence of the canonical Wnt/β-catenin signalling pathway, as demonstrated in mesothelioma cell lines [2,5]. In the present study, we examined the role of sFRP4 role in malignant mesothelioma cell metabolism. The metabolic activities that allow a cell to resist death in a stressful environment are very important for cancer cell survival [23]. In order to continue proliferating, cancer cells have to maintain energy levels when nutrients and oxygen become limited, which can occur due to the disordered vasculature and hypoxic conditions associated with tumours [24].

One of the primary metabolic changes associated with proliferating tumour cells is induction of aerobic glycolysis. Glucose is a critical nutrient for cell division, and in proliferating cancer cells, the majority of the pyruvate generated from glucose (> 90%) is converted to lactate by lactate dehydrogenase, where it is readily secreted into the extracellular environment rather than oxidised to completion [25,26]. Interestingly, we found that while sFRP4, Wnt3a, and Wnt3a+sFRP4 combination treatment altered cell morphology and/or cell proliferation (Figs. 1 and 2), but it did not alter ATP production, intracellular ATP levels, or glucose consumption significantly (Fig. 2a and b). It is possible that MM cells have an inherent capacity to proliferate independent of ATP production or glucose consumption. This could be one reason for their highly chemoresistant nature. Attempts have been made to manipulate metabolic reprogramming by treating highly chemoresistant cells with compounds that inhibit glycolysis [27]. However, it may be possible that the cells are able to use other nutrient sources for energy that does not affect its ability to utilise glucose. In fact, it could well be that glucose utilisation is at its maximum and cannot be increased any further in the controls cells. Since the treatment groups did not significantly alter the ATP and glucose utilisation over the time points examined, we investigated the effect of acute exposure of these factors on JU77 cellular bioenergetics. Interestingly, similar to the ATP data, the treatment groups did not alter ATP turnover, proton leak, the coupling efficiency, basal OCR, max respiration, or spare respiration capacity in JU77 cells (Fig. 3a–c). However, JU77 cells displayed a high level of PPR, suggesting high glycolytic activity indicative of tumour cells. It is surprising that we did not observe any significant changes in metabolic parameters from chronic or acute exposure of sFRP4 at the chosen concentrations. Expression of this factor has been reported to be modulated in metabolic disease, such as type 2 diabetes mellitus (T2DM). It has been demonstrated that sFRP4 was elevated in the serum of T2DM patients, where it impacted on islet Ca^{2+} handling, which is central to insulin release [28,29]. However, the role of sFRPs in metabolism is unclear, as other isoforms, such as sFRP1, have been shown to be initially over-expressed during initial weight gain, but subsequently decreased following progression to obesity, which is a major-risk factor for T2DM [30]. Nonetheless, these reports point to a regulatory function in metabolism, and in fact the pro-apoptotic mechanism of action of sFRP4 is believed to involve higher cellular reactive oxygen species generation, which may possibly stem from enhanced electron transport chain activity. However, the lack of metabolic changes observed in the current study may be due to either cell type- or concentration-dependent effects.

In addition, we observed biphasic modulation of GSK3β phosphorylation by sFRP4 (Fig. 4a–c.). This interesting finding indicates that sFRP4 may be suppressing tumour growth and tumour cell proliferation by not only inhibiting Wnt/β-catenin pathways but also altering GSK3β phosphorylation. The mechanism by which sFRP4 alters GSK3β activity needs to elucidated. Though there was no change in oxygen consumption between treatments or the two time points examined, the COXIV protein level showed a significant reduction at 48 h following combination treatment, suggesting cytochrome c oxidase might be the rate-limiting step of overall respiration in tumour cells and could also serve as the regulatory site for oxidative phosphorylation [31–33]. However, no bioenergetic alterations were observed during the metabolic flux assay, and the COXIV protein expression largely confirm this.

Please cite this article as: V. Perumal, et al., Therapeutic approach to target mesothelioma cancer cells using the Wnt antagonist, secreted frizzled-related protein 4: Metabolic state of cancer cells, Exp Cell Res (2016), http://dx.doi.org/10.1016/j.yexcr.2016.02.008

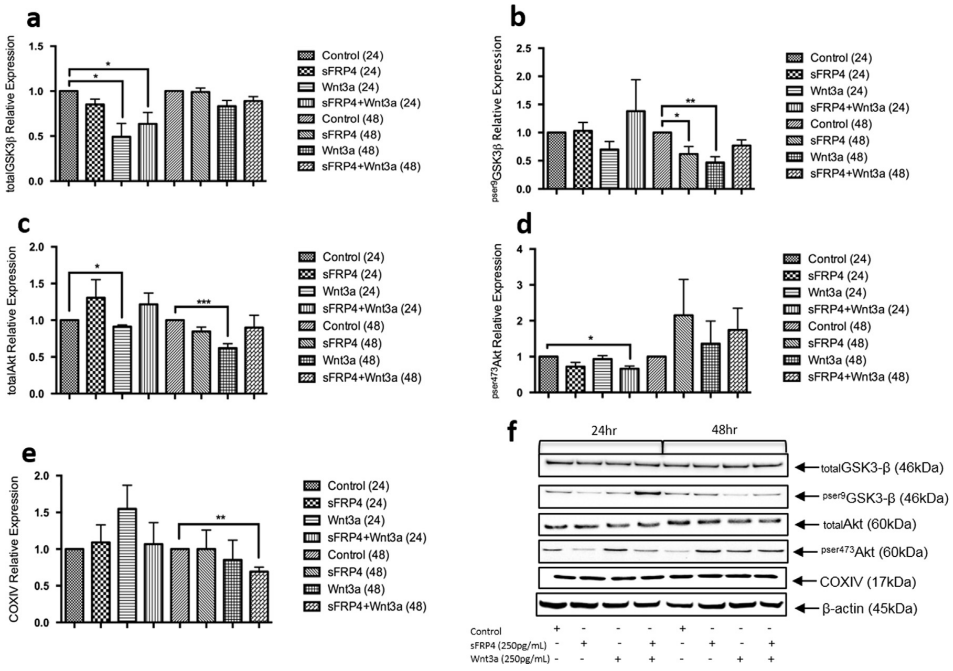

Fig. 5. The effect of Wnt3a and sFRP4 on phosphorylation and expression of GSK3β, Akt, and COXIV. (a) Total GSK3β (totalGSK3β), (b) phosphorylation of GSK3β at serine-9 (p^{ser9}GSK3β), (c) total Akt, (d) phosphorylation of Akt at serine-473 (p^{ser473}Akt) and (e) Cytochrome C oxidase (COXIV) were analysed by Western blot in JU77 cells treated with recombinant sFRP4 (250 pg/mL), Wnt3a (250 pg/mL), Wnt3a+sFRP4, or no treatment (control) at 24 and 48 h time points. These were quantified by densitometric analysis compared to a β-actin loading control. $^{*}p < 0.05$, $^{**}p < 0.01$, $^{***}p < 0.001$. (f) Western blots of total GSK3β, p^{ser9}GSK3β, totalAkt, p^{ser473}Akt, and COXIV from JU77 whole cell lysates after indicated control, sFRP4, or Wnt3a treatments. β-actin was used as a loading control.

Our cell proliferation data using both cell viability and MTT assays indicate that sFRP4 can induce cell death on its own and can also reduce Wnt3a-induced proliferation. The probable mechanism by which sFRP4 causes cell death is by abrogating Akt survival signalling. Interestingly, inactivation of GSK3β through phosphorylation may result in nuclear accumulation of β-catenin and thereby provides a link, at least in one direction, to the classical Wnt/β-catenin pathway. Our data presented here support this view. Being a member of the sFRP family, it is probable that sFRP4 abrogates a Wnt-regulated signal transduction pathway. Since cells treated with sFRP4 showed reduced levels of both Akt kinase activity and reduced GSK3β, we conclude that the observed correlation between sFRP4 expression and increased rate of apoptosis is because of an inactivation of an Akt-dependent survival pathway. Furthermore, caspase-3 activation induced by inhibition of mitochondrial complex I has been shown to be facilitated by GSK3β [34]. Since both Akt as well as Wnt signalling inhibit GSK3β activity, one might speculate that sFRP4-induced inhibition of the Wnt pathway reactivates GSK3β and thereby promotes cell death at the 24 h time point but not at 48 h. It is interesting that the Wnt3a+sFRP4 combination treatment increased total and pAkt, suggesting that sFRP4 was not able to counteract the effect of Wnt3a at the 24 h time point whereas it could at 48 h.

Conflict of interest

The authors declare that they have no competing financial interests.

Acknowledgements

Dr Vanathi Perumal is the recipient of a Curtin International Postgraduate Research Scholarship. Sebastian Pohl is supported by funds from the Rotary Club of Belmont, W.A, Australian Rotary Health Research Fund, and Curtin University. AD is supported by strategic research funds (AD) from the School of Biomedical Sciences (Curtin University), Commercialisation Advisory Board of Curtin University (AD), Cancer Council, WA, and Actinogen Ltd, Perth (AD).

References

[1] P.A. Zucali, G.L. Ceresoli, F. De Vincenzo, M. Simonelli, E. Lorenzi, L. Gianoncelli, A. Santoro, Advances in the biology of malignant pleural mesothelioma, Cancer Treat. Rev. 37 (2011) 543–558.
[2] A.Y. Lee, B. He, L. You, S. Dadfarmay, Z. Xu, J. Mazieres, I. Mikami, F. McCormick, D.M. Jablons, Expression of the secreted frizzled-related protein gene family is downregulated in human mesothelioma, Oncogene 23 (2004) 6672–6676.
[3] A.Y. Lee, B. He, L. You, Z. Xu, J. Mazieres, N. Reguart, I. Mikami, S. Batra, D. M. Jablons, Dickkopf−1 antagonizes Wnt signaling independent of beta-catenin in human mesothelioma, Biochem. Biophys. Res. Commun. 323 (2004) 1246–1250.
[4] H. Kohno, V.J. Amatya, Y. Takeshima, K. Kushitani, N. Hattori, N. Kohno, K. Inai, Aberrant promoter methylation of WIF-1 and SFRP1, 2, 4 genes in mesothelioma, Oncol. Rep. 24 (2010) 423–431.
[5] B. He, A.Y. Lee, S. Dadfarmay, L. You, Z. Xu, N. Reguart, J. Mazieres, I. Mikami, F. McCormick, D.M. Jablons, Secreted frizzled-related protein 4 is silenced by hypermethylation and induces apoptosis in beta-catenin-deficient human mesothelioma cells, Cancer Res. 65 (2005) 743–748.
[6] S.A. Fox, A.K. Richards, I. Kusumah, V. Perumal, E.M. Bolitho, S.E. Mutsaers, A. M. Dharmarajan, Expression profile and function of Wnt signaling mechanisms in malignant mesothelioma cells, Biochem. Biophys. Res. Commun. 440 (2013) 82–87.
[7] S. Fox, A. Dharmarajan, WNT signaling in malignant mesothelioma, Front.

Please cite this article as: V. Perumal, et al., Therapeutic approach to target mesothelioma cancer cells using the Wnt antagonist, secreted frizzled-related protein 4: Metabolic state of cancer cells, Exp Cell Res (2016), http://dx.doi.org/10.1016/j.yexcr.2016.02.008

Biosci. 11 (2006) 2106–2112.
[8] T. Constantinou, F. Baumann, M.D. Lacher, S. Saurer, R. Friis, A. Dharmarajan, SFRP-4 abrogates Wnt – 3a-induced beta-catenin and Akt/PKB signalling and reverses a Wnt – 3a-imposed inhibition of in vitro mammary differentiation, J. Mol. Signal. 3 (2008) 10.
[9] A. Muley, S. Majumder, G.K. Kolluru, S. Parkinson, H. Viola, L. Hool, F. Arfuso, R. Ganss, A. Dharmarajan, S. Chatterjee, Secreted frizzled-related protein 4: an angiogenesis inhibitor, Am. J. Pathol. 176 (2010) 1505–1516.
[10] U. Saran, F. Arfuso, N. Zeps, A. Dharmarajan, Secreted frizzled-related protein 4 expression is positively associated with responsiveness to cisplatin of ovarian cancer cell lines in vitro and with lower tumour grade in mucinous ovarian cancers, BMC Cell Biol. 13 (2012) 25.
[11] D. Longman, F. Arfuso, H.M. Viola, L.C. Hool, A.M. Dharmarajan, The role of the cysteine-rich domain and netrin-like domain of secreted frizzled-related protein 4 in angiogenesis inhibition in vitro, Oncol. Res. 20 (2012) 1–6.
[12] M.G. Vander Heiden, L.C. Cantley, C.B. Thompson, Understanding the Warburg effect: the metabolic requirements of cell proliferation, Science 324 (2009) 1029–1033.
[13] S. Granja, C. Pinheiro, R.M. Reis, O. Martinho, F. Baltazar, Glucose Addiction in Cancer Therapy: Advances and Drawbacks, Curr. Drug Metab. 16 (2015) 221–242.
[14] J.R. Cantor, D.M. Sabatini, Cancer cell metabolism: one hallmark, many faces, Cancer Discov. 2 (2012) 881–898.
[15] J. Lee, M.S. Kim, The role of GSK3 in glucose homeostasis and the development of insulin resistance, Diabetes Res. Clin. Pract. 77 (1) (2007) S49–S57.
[16] C.A. Caneba, L. Yang, J. Baddour, R. Curtis, J. Win, S. Hartig, J. Marini, D. Nagrath, Nitric oxide is a positive regulator of the Warburg effect in ovarian cancer cells, Cell Death Dis. 5 (2014) e1302.
[17] L.S. Manning, D. Whitaker, A.R. Murch, M.J. Garlepp, M.R. Davis, A.W. Musk, B. W. Robinson, Establishment and characterization of five human malignant mesothelioma cell lines derived from pleural effusions, Int. J. cancer 47 (1991) 285–290.
[18] L.R. Whittell, K.T. Batty, R.P. Wong, E.M. Bolitho, S.A. Fox, T.M. Davis, P. E. Murray, Synthesis and antimalarial evaluation of novel isocryptolepine derivatives, Bioorg. Med. Chem. 19 (2011) 7519–7525.
[19] D. Cadena-Herrera, J.E. Esparza-De Lara, N.D. Ramirez-Ibanez, C.A. Lopez-Morales, N.O. Perez, L.F. Flores-Ortiz, E. Medina-Rivero, Validation of threee viable-cell counting methods: Manual, semi-automated, and automated, Biotechnol. Rep. 7 (2015) 9–16.
[20] H. Mao, T. Yang, P.S. Cremer, Design and characterization of immobilized enzymes in microfluidic systems, Anal. Chem. 74 (2002) 379–385.
[21] S. Warrier, S.K. Balu, A.P. Kumar, M. Millward, A. Dharmarajan, Wnt antagonist, secreted frizzled-related protein 4 (sFRP4), increases chemotherapeutic response of glioma stem-like cells, Oncol. Res. 21 (2013) 93–102.
[22] S. Warrier, G. Bhuvanalakshmi, F. Arfuso, G. Rajan, M. Millward, A. Dharmarajan, Cancer stem-like cells from head and neck cancers are chemosensitized by the Wnt antagonist, sFRP4, by inducing apoptosis, decreasing stemness, drug resistance and epithelial to mesenchymal transition, Cancer Gene Ther. 21 (2014) 381–388.
[23] E.G. Armitage, H.L. Kotze, J.W. Allwood, W.B. Dunn, R. Goodacre, K.J. Williams, Metabolic profiling reveals potential metabolic markers associated with Hypoxia Inducible Factor-mediated signalling in hypoxic cancer cells, Sci. Rep. 5 (2015) 15649.
[24] T. Shah, B. Krishnamachary, F. Wildes, Y. Mironchik, S.M. Kakkad, D. Jacob, D. Artemov, Z.M. Bhujwalla, HIF isoforms have divergent effects on invasion, metastasis, metabolism and formation of lipid droplets, Oncotarget 6 (2015) 28104–28119.
[25] P. Chiarugi, P. Cirri, Metabolic exchanges within tumor microenvironment, Cancer Lett. (2015).
[26] P. Esteves, C. Pecqueur, C. Ransy, C. Esnous, V. Lenoir, F. Bouillaud, A.L. Bulteau, A. Lombes, C. Prip-Buus, D. Ricquier, M.C. Alves-Guerra, Mitochondrial retrograde signaling mediated by UCP2 inhibits cancer cell proliferation and tumorigenesis, Cancer Res. 74 (2014) 3971–3982.
[27] U.D. Kahlert, M. Cheng, K. Koch, L. Marchionni, X. Fan, E.H. Raabe, J. Maciaczyk, K. Glunde, C.G. Eberhart, Alterations in cellular metabolome after pharmacological inhibition of Notch in glioblastoma cells, Int. J. Cancer (2015).
[28] T. Mahdi, S. Hanzelmann, A. Salehi, S.J. Muhammed, T.M. Reinbothe, Y. Tang, A. S. Axelsson, Y. Zhou, X. Jing, P. Almgren, U. Krus, J. Taneera, A.M. Blom, V. Lyssenko, J.L. Esguerra, O. Hansson, L. Eliasson, J. Derry, E. Zhang, C. B. Wollheim, L. Groop, E. Renstrom, A.H. Rosengren, Secreted frizzled-related protein 4 reduces insulin secretion and is overexpressed in type 2 diabetes, Cell Metab. 16 (2012) 625–633.
[29] F. Liu, H. Qu, Y. Li, Q. Tang, Z. Yang, H. Wang, H. Deng, Relationship between serum secreted frizzled-related protein 4 levels and the first-phase of glucose-stimulated insulin secretion in individuals with different glucose tolerance, Endocr. J 62 (2015) 733–740.
[30] K.J. Gauger, L.M. Bassa, E.M. Henchey, J. Wyman, B. Bentley, M. Brown, A. Shimono, S.S. Schneider, Mice deficient in Sfrp1 exhibit increased adiposity, dysregulated glucose metabolism, and enhanced macrophage infiltration, PLoS One 8 (2013) e78320.
[31] L.I. Grossman, M.I. Lomax, Nuclear genes for cytochrome c oxidase, Biochim. Biophys. Acta 1352 (1997) 174–192.
[32] B. Kadenbach, M. Huttemann, S. Arnold, I. Lee, E. Bender, Mitochondrial energy metabolism is regulated via nuclear-coded subunits of cytochrome c oxidase, Free Radic. Biol. Med. 29 (2000) 211–221.
[33] C.R. Oliva, T. Markert, G.Y. Gillespie, C.E. Griguer, Nuclear-encoded cytochrome c oxidase subunit 4 regulates BMI1 expression and determines proliferative capacity of high-grade gliomas, Oncotarget 6 (2015) 4330–4344.
[34] T.D. King, G.N. Bijur, R.S. Jope, Caspase-3 activation induced by inhibition of mitochondrial complex I is facilitated by glycogen synthase kinase-3beta and attenuated by lithium, Brain Res. 919 (2001) 106–114.

Please cite this article as: V. Perumal, et al., Therapeutic approach to target mesothelioma cancer cells using the Wnt antagonist, secreted frizzled-related protein 4: Metabolic state of cancer cells, Exp Cell Res (2016), http://dx.doi.org/10.1016/j.yexcr.2016.02.008

The International Journal of Biochemistry & Cell Biology 68 (2015) 139–147

Contents lists available at ScienceDirect

The International Journal of Biochemistry & Cell Biology

journal homepage: www.elsevier.com/locate/biocel

Review article

Multi-lineage differentiation of mesenchymal stem cells – To Wnt, or not Wnt

Malini Visweswaran[a], Sebastian Pohl[a], Frank Arfuso[a], Philip Newsholme[b], Rodney Dilley[c], Shazib Pervaiz[d,e,b], Arun Dharmarajan[a,*]

[a] Stem Cell and Cancer Biology Laboratory, School of Biomedical Sciences, Curtin Health Innovation Research Institute, Curtin University, Perth, Western Australia 6102, Australia
[b] School of Biomedical Sciences, Curtin Health Innovation Research Institute, Curtin University, Perth, Western Australia 6102, Australia
[c] Ear Sciences Centre, University of Western Australia and Ear Science Institute Australia, Perth, Western Australia 6008, Australia
[d] Department of Physiology, Yong Loo Lin School of Medicine, National University of Singapore, Singapore
[e] National University Cancer Institute, National University Health System, Singapore

ARTICLE INFO

Article history:
Received 5 August 2015
Received in revised form
21 September 2015
Accepted 22 September 2015
Available online 26 September 2015

Keywords:
Mesenchymal stem cells
Differentiation
Wnt
Reactive oxygen species
Cellular fate

ABSTRACT

Mesenchymal stem cells (MSCs) are multipotent precursor cells originating from several adult connective tissues. MSCs possess the ability to self-renew and differentiate into several lineages, and are recognized by the expression of unique cell surface markers. Several lines of evidence suggest that various signal transduction pathways and their interplay regulate MSC differentiation. To that end, a critical player in regulating MSC differentiation is a group of proteins encoded by the Wnt gene family, which was previously known for influencing various stages of embryonic development and cell fate determination. As MSCs have gained significant clinical attention for their potential applications in regenerative medicine, it is imperative to unravel the mechanisms by which molecular regulators control differentiation of MSCs for designing cell-based therapeutics. It is rather coincidental that the functional outcome(s) of Wnt-induced signals share similarities with cellular redox-mediated networks from the standpoint of MSC biology. Furthermore, there is evidence for a crosstalk between Wnt and redox signalling, which begs the question whether Wnt-mediated differentiation signals involve the intermediary role of reactive oxygen species. In this review, we summarize the impact of Wnt signalling on multi-lineage differentiation of MSCs, and attempt to unravel the intricate interplay between Wnt and redox signals.

Contents

Abbreviations: ADSCs, adipose tissue-derived MSCs; APC, adenomatous polyposis coli; BIO, 6-bromo-indirubin-3′-oxime; BMP, bone morphogenetic protein; C/EBPα, CCAAT/enhancer binding protein alpha; C/EBPβ, CCAAT/enhancer binding protein beta; CaMKII, calcium/calmodulin-dependent protein kinase II; CK1α, casein kinase 1 alpha; CRD, cysteine-rich domain; CREB, cAMP response element binding protein; Dkk, Dickkopfs; Dvl, Dishevelled; DZNep, 3-deazaneplanocin A; EZH2, Enhancer of Zeste Homology 2; Fz, Frizzled; GPX, glutathione peroxidase; GSK-3β, glycogen synthase kinase-3 beta; H_2O_2, hydrogen peroxide; IGF, insulin-like growth factor; JNK, c-jun N-terminal kinase; KLHL12, Kelch-like 12; LiCl, lithium chloride; LRP5/6, lipoprotein receptor-related protein 5/6; MSCs, mesenchymal stem cells; NAC, N-acetylcysteine; NELL-1, Nel-like protein; NO, nitric oxide; Nox, NADPH oxidase; NRX, nucleoredoxin; PCP, planar cell polarity; PKC, protein kinase C; PPARγ, peroxisome proliferator-activated protein gamma; PRXs, peroxiredoxins; ROS, reactive oxygen species; sFRPs, secreted Frizzled-related proteins; SOD, superoxide dismutase; TCF/LEF, T cell factor/lymphoid-enhancing factor; WIFI, Wnt inhibitory factor 1; YAP1, Yes-associated protein 1.

* Corresponding author.
E-mail address: a.dharmarajan@curtin.edu.au (A. Dharmarajan).

http://dx.doi.org/10.1016/j.biocel.2015.09.008
1357-2725/

1. Introduction

1.1. Clinical significance of mesenchymal stem cells and their differentiation

There has been a recent surge in interest in the clinical use of mesenchymal stem cells (MSCs) in regenerative medicine, tissue repair, and other cell-based therapies (Pittenger et al., 1999). MSCs have been isolated from various sources such as bone marrow (Bianco et al., 2001), adipose tissue (Zuk et al., 2001), umbilical cord tissue (Weiss and Troyer, 2006), periodontal ligament (Seo et al., 2004), synovial membrane (Harvanova, 2011), menstrual fluid (Patel et al., 2008), and dental pulp (Agha-Hosseini et al., 2010). Although bone marrow was the earliest identified source of MSCs (Friedenstein et al., 1970), the utility of marrow-derived MSCs was limited due to several factors such as invasive surgery and subsequent patient discomfort. Hence, sources of MSCs other than the bone marrow, such as described above, have been aggressively explored in recent years.

MSCs are capable of extensive self-renewal in an undifferentiated state, but upon appropriate and specific stimuli are capable of multi-potent differentiation towards various cell lineages. Although the preference is for differentiation to mesenchymal lineages, there is strong experimental evidence for differentiation to all three germ layers – mesoderm, ectoderm, and endoderm (Seo et al., 2004; Choi et al., 2010; Safford et al., 2002; Kuroda et al., 2010; Zuk et al., 2002). As such, a better understanding of the process of MSC differentiation at the molecular level is essential if MSCs are to achieve the potential for their application in regenerative medicine. This demands an understanding of the signal transduction pathways regulating MSC differentiation, amongst which Wnt signalling is one of the key players. Hence, in this review, we highlight how the Wnt signalling network impacts MSCs and influences their fate. Our primary focus will be the interaction between the canonical Wnt signalling pathway and MSC differentiation. Further, we will describe the effect of reactive oxygen species (ROS) on MSC differentiation and the crosstalk between ROS and Wnt to influence MSC differentiation.

1.2. Wnt signalling

Wnt signalling is evolutionarily conserved from nematodes to mammals, regulating various stages of embryonic development as well as tissue homeostasis in adulthood (Cadigan and Nusse, 1997; Wodarz and Nusse, 1998). Wnt signalling affects major cellular events such as proliferation, survival, apoptosis, angiogenesis and cell polarity. It is also involved in regulating self-renewal and differentiation of stem cells in adult tissues, and regulating the regenerative processes in response to disease, trauma, and ageing. The Wnt molecules are secreted glycoproteins composed of 350–400 amino acid residues, of which 23–24 are highly conserved cysteine residues (molecular weight: 39–46 kDa) (Cadigan and Nusse, 1997). The difference in mode of signalling subsequent to the generation of the Wnt signal classifies the Wnt signalling network into two main branches, depending on the intracellular response it triggers. One is the canonical pathway mediated by β-catenin, while another is the non-canonical signalling pathway that involves protein kinase C (PKC) and c-jun N-terminal kinases (JNK).

1.2.1. Canonical Wnt signalling

The canonical Wnt signalling pathway is β-catenin mediated. Here, the Wnt ligand forms a ternary complex with a Frizzled (Fz) receptor and low-density lipoprotein receptor-related protein 5/6 (LRP5/6) co-receptor to activate the intracellular Dishevelled (Dvl) protein. Dvl in turn phosphorylates and inhibits glycogen synthase kinase-3β (GSK-3β) of the destruction complex. The destruction complex is composed of the proteins, axin, adenomatous polyposis coli (APC), casein kinase 1α (CK1α), and GSK-3β, and is responsible for the phosphorylation and subsequent degradation of β-catenin in the absence of Wnt signalling. In the presence of a Wnt stimulus the complex remains inactive, leading to accumulation of the unphosphorylated β-catenin in the cytoplasm and consequent translocation to the nucleus. In the nucleus, β-catenin replaces the co-repressors and binds to the transcriptional factor complex composed of T cell factor/lymphoid-enhancing factor (TCF/LEF), thereby triggering the transcription of the Wnt target genes.

1.2.2. Non-canonical Wnt signalling

Non-canonical Wnt signalling is independent of β-catenin and involves several distinct pathways. One of the non-canonical pathways impacts on cell migration by regulating the activation of calcium/calmodulin-dependent protein kinase II (CaMKII) and protein kinase C (PKC), thereby resulting in the release of intracellular calcium (Huelsken and Behrens, 2002; Komiya and Habas, 2008). This association with cellular Ca^{2+} mobilization has led to the description 'Wnt/Ca^{2+} signalling pathway'. A second, non-canonical pathway controlling cell polarity and cytoskeletal organization is referred to as the Wnt/planar cell polarity (PCP) signalling pathway. It acts by activating Rho-GTPases and Jun N-terminal kinases (JNKs) (Huelsken and Behrens, 2002; Komiya and Habas, 2008). The

molecular events occurring in these non-canonical pathways are generally less well defined than the canonical pathway.

1.2.3. Regulators of the Wnt signalling pathway

Among the various molecules that modulate the Wnt signalling pathway (Nusse, 2005) are extracellular Wnt antagonists such as secreted Frizzled-related proteins (sFRPs), Dickkopfs (Dkks), and Wnt inhibitory factor 1 (WIF1) (Kawano and Kypta, 2003; Gonsalves et al., 2011). Briefly, sFRPs are the first identified secreted antagonists of the canonical and non-canonical Wnt signalling pathways and, in humans, they are five in number (sFRP1-5) (Gonsalves et al., 2011; Wolf et al., 1997; Huang et al., 2009; Jones and Jomary, 2002; Boudin et al., 2013). Among them, the major Wnt antagonist sFRP4 was first isolated by our group by the use of a rat cDNA library (Wolf et al., 1997). By inactivating Wnt, sFRPs prevent the accumulation of active unphosphorylated β-catenin in the cytoplasm, thereby suppressing the activity of Wnt target genes (Kawano and Kypta, 2003; Muley et al., 2010).

The Fz receptors possess an extracellular cysteine-rich domain (CRD) composed of 120 amino acids (Wodarz and Nusse, 1998), which shares structural homology to the CRD in the N-terminal region of sFRPs (Rattner et al., 1997); sFRPs lack the transmembrane domain present in Fz receptors. sFRP anatgonizes Wnt signalling by interfering with the Wnt–Fz interaction through direct binding to the Wnt or to the Fz receptor, thereby forming a non-functional complex. While the latter mechanism (sFRP–Fz binding) is facilitated by the CRD of the sFRPs (Bafico et al., 1999), the former mechanism (sFRP–Wnt binding) can occur either *via* the CRD (Lin et al., 1997) or the domains in the C-terminal region of sFRPs (Uren et al., 2000). In addition, the biphasic regulatory potential of sFRPs has been elucidated by evidence of Wnt binding to the CRD in the N-terminal region of sFRPs and inhibiting β-catenin accumulation; while Wnt binding to the domain in the C-terminal region of sFRP allows the CRD at the N-terminus to interact with Fz, hence facilitating Wnt signalling (Uren et al., 2000).

Other Wnt anatagonists such as the Dickkopf (Dkk) family includes four members (Dkk 1–4), which inhibit only the canonical Wnt signalling by binding to the LRP5/6 co-receptor (Kawano and Kypta, 2003). In addition to these naturally occurring extracellular Wnt antagonists, there are pharmacologically derived antagonists such as XAV939 (Jones and Jomary, 2002) and iCRT3 (Boudin et al., 2013). In this review we focus on how these different Wnt regulators play a role in Wnt signal transduction and influence the cell fate determination of MSCs.

2. Role of Wnt signalling pathways in differentiation of mesenchymal stem cells

2.1. Role of Wnt signalling in adipogenic differentiation

Evidence from the last decade indicates an important role for Wnt signalling in adipogenic differentiation from precursor cells. (Christodoulides et al., 2009). An inhibitory effect on adipogenesis by Wnt-activating molecules such as Wnt 10b, GSK-3β inhibitors such as lithium chloride (LiCl) (Ross et al., 2000), and CHIR 99021 (Bennett et al., 2002) has been demonstrated using 3T3 pre-adipocytes. Wnt4 and Wnt5a, both non-canonical Wnt ligands, have been shown to possess a promoting effect on 3T3 cell adipogenesis through the PKC-CamKII pathway. Additionally, the authors refer to antagonism of the canonical Wnt signalling pathway by Wnt5a (Nishizuka et al., 2008).

In MSCs, the inhibitory effect on adipogenesis has been demonstrated using the GSK-3β inhibitor (Wnt activator) – 6-bromo-indirubin-3′-oxime (BIO) (Zaragosi et al., 2008). Wnt activation (by silencing the Wnt antagonists sFRP4 and Dkk1) was performed in adipose MSCs, which resulted in significant down-regulation of adipogenic differentiation with regard to lipid accumulation as well as adipogenic markers (Park et al., 2008). It has also been reported that a short 48 h treatment with sFRP1 and sFRP4 upregulated adiponectin secretion in human MSCs (Ehrlund et al., 2013).

Additionally, during adipogenic differentiation of MSCs, the levels of the Wnt antagonists sFRP4 and Dkk1 were seen to be higher than in the undifferentiated state (Park et al., 2008). Our laboratory has demonstrated that addition of exogenous sFRP4 promoted adipogenic differentiation of MSCs (Visweswaran et al., 2015). This *in vitro* evidence indicates the presence and significance of the suppressed state of Wnt signalling during adipogenesis. The importance of Wnt antagonist levels has been tested out by a few clinical studies. In one of them, sFRP4 levels were seen to be directly proportional to impaired glucose and triglyceride metabolism (Hoffmann et al., 2014), and in another study sFRP4 was proposed as a biomarker for predicting type II diabetes mellitus (Mahdi et al., 2012). Overall, the activation of the Wnt signalling pathway inhibits adipogenic differentiation in MSCs, while the presence of Wnt antagonists promotes a contrary effect on adipogenesis, which could be considered when developing new strategies to manage obesity and diabetes.

2.2. Wnt signalling regulates osteogenic differentiation

Growing evidence suggests a regulatory role for Wnt signalling in bone development and homeostasis. In MSCs, the *in vitro* potential of Wnt signalling on osteogenic differentiation has been controversial, with both stimulatory and inhibitory effects being reported. It has been shown that the canonical Wnt signalling pathway activates differentiation of MSCs into osteoblasts (Liu et al., 2009). The disruption of Wnt signalling by a functional mutation or targeted destruction of LRP5 in mice has been shown to promote osteoporosis and a low bone mass phenotype (Gong et al., 2001; Kato et al., 2002), while its over-expression leads to a high bone mass syndrome (Boyden et al., 2002). In another study, the supportive role of Wnt proteins towards osteogenesis was shown by preventing apoptosis of osteoblast progenitors and differentiated osteoblasts in the osteoblast cell line OB-6 and pre-osteoblast cell line MC3T3-E1 (Almeida et al., 2005). The Wnt ligand Wnt10b was shown to prevent bone loss occurring due to oestrogen deficiency and ageing in mice (Bennett et al., 2005). It was reported that Wnt signalling favoured osteogenesis at the expense of adipogenesis (Kang et al., 2007; Cawthorn et al., 2012). It was also demonstrated that suppression of PPARγ and C/EBPα, and the simultaneous enhancement of the expression of osteoblastogenic transcription factors such as RunX2, Dlx5, and Osterix occurred in mouse mesenchymal cells (Bennett et al., 2005; Kang et al., 2007).

With regard to the effect of Wnt antagonism on osteogenesis, it has been reported to be mostly inhibitory. In mice over-expressing the Wnt antagonist sFRP4 in osteoblasts, there was a reduction observed in bone formation, leading to a low bone mass (Nakanishi et al., 2008). This inhibitory effect of Wnt antagonists on osteogenesis was also demonstrated by an *in vitro* study where sFRP4 inhibited osteogenic differentiation in MSCs from periodontal tissue (Yamada et al., 2013). Among other Wnt antagonists, sFRP1 over-expression was found to also inhibit *in vivo* bone formation (Yao et al., 2010) and increase the rate of osteoblast and osteocyte cell death (Nakanishi et al., 2008). The lack of sFRP1 reduced apoptosis and accelerated osteoblast proliferation and differentiation in human osteoblasts and MSCs (Bodine et al., 2005), and also enhanced trabecular bone formation and improved fracture healing (Bodine et al., 2005; Gaur et al., 2009; Trevant et al., 2008), indicating the inhibitory effect of Wnt antagonists on osteogenesis.

Many other signalling pathways, such as the Hippo signalling pathway, interact with Wnt. Hippo signalling involves Yes-associated protein 1 (YAP1), which upregulates Dkk1 and, in turn, suppresses canonical Wnt signalling to inhibit the osteogenic potential of MSCs (Seo et al., 2013). The stimulatory effect of Wnt has been shown in human MSCs (Gregory et al., 2005) and also in mouse MSCs (Gaur et al., 2005), where an increased expression of the osteogenic transcription factor RunX2 was observed (Gaur et al., 2005). Overall, these studies indicate that canonical Wnt activation promotes osteogenesis, while Wnt antagonists inhibit osteogenesis from MSCs.

Other studies have reported an inhibition of osteogenesis by the canonical Wnt pathway in human bone marrow MSCs (Boland et al., 2004; de Boer et al., 2004; Baksh et al., 2007). One group reported that sFRP3 promoted osteoblast differentiation (Chung et al., 2004). A recent study explained this phenomenon in further detail by showing that sFRP3 antagonizes the non-canonical Wnt pathway through Wnt5a binding, which in turn blocks Wnt5a's inhibitory effect on the canonical Wnt pathway, and hence promotes osteogenesis (Yamada et al., 2013). This mechanistic approach adds further evidence to the role of canonical Wnt signalling in promoting osteogenic differentiation. All these studies indicate the extensive crosstalk contributed by the Wnt signalling network during osteogenic differentiation, which should be considered when devising possible new therapeutic interventions for bone-related diseases. Moreover, the available evidence reinforces the reciprocal relationship that exists between bone and fat development in response to an activated canonical Wnt pathway.

2.3. Role of Wnt signalling in chondrogenic differentiation

Wnt signalling is one among the main regulators of chondrogenesis. The promoting role of Wnt signalling in chondrogenesis has been demonstrated by a study showing that sFRP1-deficient mice demonstrated enhanced chondrocyte maturation in both *in vivo* and *in vitro* conditions (Gaur et al., 2006). A functional role for Wnt5a, a non-canonical Wnt ligand, in the chondrogenesis of MSCs derived from the chicken wing bud has also been demonstrated (Jin et al., 2006). The level of Wnt5a was up-regulated after treatment with transforming growth factor β (TGFβ), which promoted chondrogenesis. This was further supported by the upregulated pre-cartilage condensation and chondrogenesis in *in vitro* micromass cultures in MSCs transfected with Wnt5a (Jin et al., 2006). The mode of action underlying this could be the blunting of canonical Wnt signalling by the non-canonical Wnt ligand Wnt5a, and hence promoting chondrogenesis. An increased expression of Wnt3a was associated with the chondrogenic differentiation of high density C3H10T1/2 murine mesenchymal cells (Fischer et al., 2002a), and the overexpression of Wnt3a was also demonstrated to promote this process in the same cell line (Fischer et al., 2002b).

On the other hand, it has been reported that continuous treatment with Wnt1 protein for 21 days reduced the expression of chondrogenic-specific markers, while treatment with the Wnt antagonist Dkk1 increased the expression of chondrogenic markers such as collagen II, Sox9, and aggrecan in human adipose-derived MSCs (Luo et al., 2013). These results are corroborated by studies demonstrating that both sFRP1 and Dkk1 enhanced glycosaminoglycan synthesis, Sox9, and type II collagen expression in early chondrogenesis of human MSCs (Im and Quan, 2010), and these Wnt antagonists also exhibited a chondrogenesis-promoting effect in long-term pellet cultures (Im et al., 2011).

2.4. Role of Wnt signalling in cardiogenic differentiation

Previous studies in chick and frog embryos demonstrated that Wnt antagonism induced cardiac development while an activated canonical signalling pathway inhibited the differentiation (Schneider and Mercola, 2001; Marvin et al., 2001). Later, it was found that stimulation of canonical Wnt signalling (by use of LiCl) increased the bioavailability of β-catenin, and hence improved myogenic differentiation in MSCs derived from aged cardiac patients (Brunt et al., 2012). The non-canonical Wnt ligand, Wnt11, promoted cardiomyocyte differentiation in MSCs transduced with Wnt11 by upregulating GATA-4. The authors postulated that the mechanism involved Wnt11-mediated activation of the non-canonical PKC or JNK pathway (He et al., 2011). Contrastingly, MSCs overexpressing sFRP2 have been shown to have reduced apoptosis rates and improved engraftment and cardiac function in mice (Alfaro et al., 2010). Exogenous addition of sFRP2 inhibited type I procollagen maturation, which is important in scar formation post-myocardial infarction (He et al., 2010), and therapeutic concentrations of sFRP2 significantly reduced fibrosis and improved cardiac function in rats (He et al., 2010). However, in another study, a reduced infarct size was observed in sFRP2 null mice, thus the authors referred to the known biphasic effect of sFRP2 to explain their findings (Kobayashi et al., 2009). Overall, an activated Wnt signalling pathway contributes to enhanced cardiogenic differentiation in MSCs and this phenomenon should be considered when devising MSC-based therapies for myocardial infarction.

2.5. Wnt signalling inhibits hepatogenic differentiation

The Wnt pathway has been demonstrated to work synergistically with the MAP/ERK signalling pathway to support hepatic progenitor cell proliferation (Jin et al., 2011). A study on hepatic progenitor cells of the mouse embryo demonstrated that inhibition of Wnt signalling (accomplished using the Wnt antagonist sFRP3) prevented the differentiation of progenitor cells into the hepatic lineage (Bi et al., 2009).

Hepatic differentiation in the mouse has been shown to be tightly regulated, with the distinct expression of Wnt antagonists such as sFRPs and Dkks in embryonic liver tissues (Bi et al., 2009). In humans, hepatic differentiation is differentially regulated by the Wnt signalling pathway, depending on the stem cell source. Wnt signalling was shown to be down-regulated during the hepatic differentiation of adipose tissue-derived MSCs (ADSCs), while it was activated in human embryonic stem cells (hESCs) (Heo et al., 2013). The distinct response seen in hESCs was also observed when Wnt3a pre-treatment facilitated the differentiation of hESCs towards hepatic endoderm (Fletcher et al., 2008).

Similar to the effect seen on ADSCs (Heo et al., 2013), during hepatic differentiation of umbilical cord tissue-derived MSCs, there was a downregulation of canonical Wnt signalling. Hence, suppression of Wnt signalling in turn promoted hepatic differentiation (Yoshida et al., 2007). It has also been demonstrated that application of Frizzled 8 siRNA on MSCs, in which Wnt signalling was reduced, resulting in enhanced hepatic differentiation in human bone marrow-derived MSCs (Ishii et al., 2008). Overall, these studies indicate that enhanced hepatic differentiation is observed in human MSCs following down-regulation of Wnt signalling.

2.6. Wnt signalling promotes myogenic differentiation

The effect of different Wnt molecules on myogenic differentiation has been well documented in embryonic development. In MSCs, the Wnt molecules – Wnt1, Wnt3, Wnt7a, Wnt7b, Wnt4, and Wnt11 had a promoting effect on gene expression of at least one myogenic marker. Among these Wnt proteins, Wnt11 was the most potent activating factor demonstrating gene expression of all myogenic factors-Myf5, MyoD, myogenin, and myogenin regulating factor (Mrf4) (Belema Bedada et al., 2005). The promoting effect of Wnt3a in myogenic differentiation has also been reported

in rat bone marrow MSCs (Shang et al., 2007). The GSK-3β inhibition by LiCl and consequent Wnt activation resulted in an increased bioavailability of β-catenin and enhanced the myogenic differentiation potential in aged MSCs (Brunt et al., 2012). Another study demonstrated that hypoxia-preconditioned MSCs possessed better engraftment potential into ischaemic tissue, and improved skeletal and vascular muscle regeneration when compared to normal MSCs. They found that this enhanced effect was brought about by a Wnt4-dependent pathway, and that hypoxia-preconditioned MSCs had an increased number of Wnt4 transcripts in the ischaemic area compared to the normal MSCs (Leroux et al., 2010). Altogether, it suggests that activated Wnt signalling enhances the myogenic differentiation potential of MSCs.

2.7. Wnt signalling positively influences neurogenic differentiation

It has been demonstrated that Wnt3a protein promotes the differentiation of neural stem cells into neuronal lineages while inhibiting their self-renewal (Muroyama et al., 2004). In cortical mouse neural precursor cells, Wnt7a also enhanced neuronal differentiation (Hirabayashi et al., 2004). Further, in MSCs, the activating role of canonical Wnt signalling has been determined using specific neuronal markers such as neuron-specific enolase and nestin. These markers were up-regulated when Wnt signalling was activated using Wnt3a and down-regulated when Wnt signalling was blocked by siRNA for β-catenin (Yu et al., 2013). It was also found that Wnt7a enhanced neuronal differentiation in human MSCs *via* both canonical and non-canonical signalling pathways (Tsai et al., 2014). Further, the Wnt antagonists Dkk1 and sFRP4 reversed Wnt7a's promoting effect (Tsai et al., 2014). Re-activation of the Wnt signalling pathway reversed the age-related decline in neurogenic differentiation in MSCs derived from dental pulp (Feng et al., 2013). Further investigation into the mechanism of Wnt-induced up-regulation of neurogenic differentiation in MSCs has revealed the role of T-cell leukaemia 3 (Tlx3) in interacting with the TCF3/4 of the canonical Wnt signalling pathway. In this study, it was shown that Wnt1 upregulates Tlx3, and a forced expression of Tlx3 improved neurogenic differentiation (Kondo et al., 2011). Wnt5a promoted neurogenic differentiation in human ADSCs, binding to Fz3 and Fz5, and signalling through the Wnt5a-JNK pathway (Jang et al., 2015). In summary, activation of Wnt signalling plays a key role in promoting the differentiation of MSCs towards a neuronal fate.

The overall impact exerted by the activation of the Wnt signalling pathway on the differentiation of human MSCs has been schematically represented in Fig. 1.

3. Link between Wnt/β-catenin signalling and reactive oxygen species

Recent findings have demonstrated that there is a close association between reactive oxygen species (ROS) and activation of the Wnt/β-catenin pathway. β-Catenin is translocated to the nucleus after the inhibition of the protein complex comprised of Axin, APC, GSK-3β, and CK1α (Korswagen, 2006). This inhibition is assisted by Dishevelled (Dvl), a protein present in the cytoplasm, which inhibits GSK-3β-mediated phosphorylation of β-catenin, allowing its translocation (Li et al., 1999). Dvl and a thioredoxin-like protein, nucleoredoxin (NRX), have been shown to directly interact and inhibit Wnt/β-catenin signalling and this association is attenuated by hydrogen peroxide (H_2O_2), suggesting that Wnt/β-catenin signalling may be modulated by oxidative stress (Funato et al., 2006). Wnt signalling is carefully balanced by the competition between NRX and a Kelch-like 12 (KLHL12) protein, both associated with the PDZ-domain of Dvl. In the absence of a Wnt ligand, the binding of NRX to Dvl promotes the inactive state of Dvl, thereby preventing aberrant activation of the pathway until a sufficient Wnt stimulus occurs. Upon Wnt binding, Dvl frees itself from NRX, activates downstream signalling, and is then ubiquitylated by KLHL12, thus preventing persistent activation of the Wnt signalling pathway (Funato et al., 2010). Recently it was also demonstrated that inhibition of Ca^{2+}-mediated ROS production from the mitochondria attenuated the Dvl/NRX association, which led to a decrease in Wnt/β-catenin activation and inhibited the ability of neuronal cells to differentiate *in vitro* (Rharass et al., 2014). Although a full understanding of ROS activation of the Wnt/β-catenin pathway has yet to be elucidated, it is known that Wnt antagonists also play a role in the modulation of ROS. It has been shown that sFRP4 can increase superoxide and H_2O_2 levels while decreasing catalase activity in endothelial cells, and thus inhibiting angiogenesis (Muley et al., 2010). Further research into the mechanisms of ROS activation of the Wnt/β-catenin pathway has the potential to provide possible treatment options for many Wnt-associated diseases.

3.1. The source and generation of reactive oxygen species

There are many potential sources of ROS within the cell; the primary source of ROS is from the mitochondria where free-radical superoxide anion (O_2^-) is generated *via* the electron transport chain, primarily from complex I (Kushnareva et al., 2002) and III by single electron reduction of molecular oxygen (Chen et al., 2003). Superoxide (O_2^-) is converted to H_2O_2 (which has a much longer half-life) through ROS scavengers such as superoxide dismutase (SOD) in the cytosol (SOD1/CuZn-SOD), mitochondrial matrix (SOD2/MnSOD), and in extracellular compartments (SOD3) (Zelko et al., 2002).

Another important source of ROS is from the nicotinamide adenine dinucleotide phosphate (NADPH) oxidase complexes, which together are known as NOX enzymes (Holmstrom and Finkel, 2014). Oxygen is converted to superoxide through pyridine nucleotide-mediated reduction by NOX enzymes at specific membrane-associated sites (Atashi et al., 2015), thus generating superoxide for release into phagolysosomes (in phagocytic immune cells) and either cytosolic or extracellular release. The superoxide anion can also react with nitric oxide (NO) to form peroxynitrite ($ONOO^-$) (Pacher et al., 2007), which has been shown to induce apoptosis through caspase activation (Zhuang and Simon, 2000).

Hydrogen peroxide is classed as a reactive oxidizing chemical that can be converted to water and oxygen in the peroxisome and cytosol through enzymatic action by catalase. Furthermore, it is reduced to H_2O through the enzymatic action of antioxidant glutathione peroxidases (GPx), which catalyze the reaction $2GSH + H_2O_2 \rightarrow GSSG + 2H_2O$ and by peroxiredoxins (Prxs) in the cytosol, Prxs (reduced) + $H_2O_2 \rightarrow$ Prx (oxidized) + $2H_2O$ (Gough and Cotter, 2011).

Other intracellular sources of ROS include the endoplasmic reticulum as well as other enzyme systems such as xanthine oxidase, lipoxygenase, cyclooxygenase, cytochrome P450, and monooxygenase (Holmstrom and Finkel, 2014). ROS, together with the peroxisomes and mitochondria, serve many functions including cellular proliferation (Gauron et al., 2013), migration (Hurd et al., 2012), differentiation (Atashi et al., 2015), survival (Trachootham et al., 2008; Pervaiz and Clement, 2007; Clement et al., 2003) – and cell signalling (Thannickal and Fanburg, 2000). ROS play a crucial role in cellular homeostasis and a variety of processes within all cell types. Interestingly, the study of ROS within MSCs has gathered pace recently due to its complex nature, the involvement of a variety of cell signalling pathways, including Wnt, a myriad of protein interactions, and its involvement in mesenchymal differentiation.

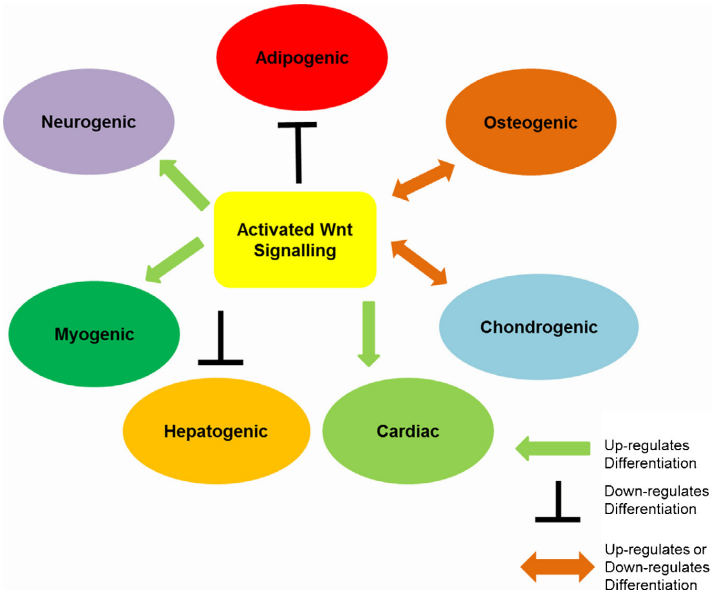

Fig. 1. Schematic illustration of the effect of Wnt signalling on the various MSC differentiation pathways.

3.2. Mesenchymal stem cells and reactive oxygen species

MSCs exhibit relatively low levels of ROS, possibly due to their increased levels of glutathione, SOD1/SOD2, catalase, and GPx (Valle-Prieto and Conget, 2010). It has also been shown that varying levels of ROS control different signalling pathways within MSCs, which are responsible for many cellular functions and cellular differentiation. These pathways include Wnt, Forkhead box (FOXO), Hedgehog (Riss et al., 2006), Nel-like protein 1 (NELL-1), insulin-like growth factor (IGF), and bone morphogenetic protein (BMP). Various, highly defined levels of ROS activate these aforementioned signalling pathways to regulate MSC differentiation into chondrocytes (Kim et al., 2010), adipocytes (Kanda et al., 2011), and osteocytes (Takada et al., 2009). Although the role of redox regulation in MSCs has yet to be fully elucidated, other stem cells such as haematopoietic stem cells and progenitor cells have been described in terms of stem cell development, function, and survival in this regard (Pervaiz et al., 2009). In this review we have aimed to comprehensively summarize the redox regulation of MSC differentiation.

4. Reactive oxygen species-mediated differentiation of mesenchymal stem cells

4.1. Adipogenic differentiation

MSCs differentiate to an adipogenic lineage through the activation of several transcription factors including CCAAT/enhancer binding protein (C/EBP)β, which induces C/EBPα and PPARγ (Rosen et al., 2000). It has now been shown that adipogenic differentiation may be mediated by NADPH oxidase 4 (Nox4) *via* the cAMP response element-binding protein (CREB) (Kanda et al., 2011). It has been shown that CREB over-expression in pre-adipocytes promotes the expression of C/EBPα and RXRα (Reusch et al., 2000); while concurrently, it has been demonstrated that antioxidants such as N-acetylcysteine (NAC) or apocyanin will suppress CREB (Kanda et al., 2011). There is further evidence for ROS-mediated adipogenic differentiation in MSCs by Prx1 over-expression inhibiting lipid accumulation, as well as antioxidant (NAC) inhibition of C/EBPα and PPARγ (Kanda et al., 2011). Superoxide generating complex III has also been implicated in the transcriptional activation of PPARγ (Tormos, 2011), while H_2O_2 increases adipogenesis (Schroder et al., 2009) and diminishes the expression of adipo-cytokines (Atashi et al., 2015). This evidence suggests that increasing intracellular levels of ROS are involved in signalling cascades responsible for the differentiation of MSCs into adipocytes.

4.2. Osteogenic differentiation

There have been numerous signalling pathways implicated in osteogenic differentiation in MSCs including Wnt, FOXO, and Hedgehog; all of which have been shown to be suppressed by high levels of ROS (Atashi et al., 2015). The Wnt signalling pathway is a positive regulator of osteogenesis through the translocation of β-catenin into the nucleus, where it binds TCF/LEF, allowing the activation of Wnt target genes such as *Axin2* as well as increasing the expression of Run2x, Dlx5, and Osterix, which are critical osteogenic transcription factors (Kim et al., 2013). Wnt signalling has been shown to decrease the expression of C/EBPα and PPARγ, and thus favours osteogenesis rather than adipogenesis (Ross et al., 2000); although high levels of ROS, specifically H_2O_2 (which has been shown to inhibit Wnt/β-catenin signalling), would then promote a more favourable adipogenic environment (Shin et al., 2004).

The FOXO signalling pathway is also mediated by ROS, where high levels induce phosphorylation and drive its translocation into the nucleus where it is activated. FOXO has been shown to suppress osteogenic differentiation (Iyer et al., 2013) while concurrently promoting adipocyte differentiation (Nakae et al., 2003). Increased levels of H_2O_2 stimulate FOXO transcription, although it also promotes the association of FOXO with β-catenin, which leads to an inhibition of Wnt target genes essential for osteogenic differentiation (Almeida et al., 2007). Overall, higher levels of oxidative stress antagonize the Wnt/β-catenin pathway, leading to attenuation of osteogenesis while stimulating FOXO-mediated adipogenic

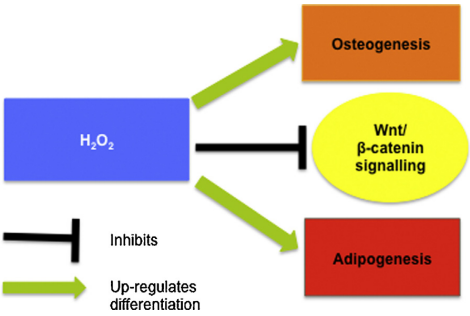

Fig. 2. Schematic demonstrating the effect of ROS (depicted here as H_2O_2) in blocking Wnt/β-catenin signalling and promoting differentiation of MSCs into adipocytes and osteoblasts.

differentiation. It is noteworthy that a shift to adipogenic lineage in MSCs has been reported in patients with osteoporosis. This has been linked to the increased expression of the histone H3 methylating protein Enhancer of Zeste Homology 2 (EZH2) which silences the Wnt genes, and hence pharmacological inhibition of EZH2 with 3-deazaneplanocin A (DZNep) reverted the cells to osteogenic lineage (Jing et al., 2015). These data argue in favour of targeting EZH2 as a potential strategy against osteoporosis. Alternatively, the use of anti-oxidants, such as N-acetyl cysteine (NAC), or SOD mimetics might also serve to tailor the redox environment for osteogenic differentiation.

The interaction between ROS (in the form of H_2O_2) and the Wnt signalling pathway, and the resultant effect on MSC differentiation into adipocytes and osteoblasts is demonstrated in Fig. 2.

4.3. Chondrogenic differentiation

Recent studies have demonstrated that ROS is required for chondrogenic differentiation, primarily through NADPH oxidase 2 and 4 (Nox2 and Nox4) (Kim et al., 2010). This was demonstrated by inhibition of chondrogenic differentiation gene markers Sox9, Col2a1, and Col10a1 by the introduction of the ROS scavenger NAC; and so, provide proof that ROS is necessary for chondrogenic differentiation (Kim et al., 2010). Although less is known in regards to chondrogenic differentiation mediated by ROS in MSCs, this is an attractive area of study and may have wider implications in the field of regenerative medicine.

5. Conclusions

In this review we have exemplified the differential impact that Wnt signalling exerts on MSC differentiation pathways. Summarizing the broad spectrum of the influence of Wnt signalling on MSC differentiation, we have shown that the outcomes of activated Wnt are inhibition of adipogenic and hepatogenic differentiation. On the other hand, a different outcome of activated Wnt signalling favours neurogenic and myogenic differentiation. Wnt signalling exerts mixed effects on osteogenic, chondrogenic, and cardiogenic differentiation, where it can either promote or inhibit the process; and this could be dependent on many factors such as cell type and interaction with other signal transduction pathways, *etc.* The exact mechanism underlying the molecular regulation of differentiation processes remains to be unravelled.

The role of ROS in MSC differentiation has also yet to be completely elucidated, although research has shown that the level of H_2O_2 tends to favour differentiation into adipocytes, chondrocytes, or osteocytes. ROS-mediated differentiation into the other possible MSC lineages such as neuronal cells, hepatocytes, and myocytes has yet to be investigated in detail. MSC differentiation occurs through the interplay of different pathways including the FOXO and Wnt/β-catenin signalling pathways. It has been demonstrated that these pathways can regulate ROS levels, and concomitantly ROS levels can influence the activity of these pathways. ROS signalling has been implicated in osteogenic differentiation, where high levels of H_2O_2 inhibit Wnt/β-catenin signalling and favour osteogenesis, and low levels of H_2O_2 activate Wnt/β-catenin signalling to promote adipogenesis. Further studies into the mechanisms of ROS-mediated differentiation are important for a complete understanding of MSC differentiation.

MSCs have gained a lot of clinical interest, considering their potential for various tissue engineering and reconstructive surgery applications, due to their extensive self-renewal and multipotent differentiation capabilities. Hence the mechanism underlying these differentiation processes, tightly regulated by signal transduction networks such as the Wnt signalling pathway and ROS, needs to be further examined. A profound knowledge about these processes will in turn aid in the development of novel strategies in regenerative medicine. Recent evidence points to a critical role of tissue hypoxia on the proliferation and differentiation of multipotent MSCs (Holzwarth et al., 2010; Valorani et al., 2012). To that end, manipulation of the cellular redox milieu could have potential therapeutic implications, whereby the use of anti-oxidants could serve to switch MSCs from adipogenic to osteogenic differentiation; however, if the desired outcome is to obtain adipogenic differentiation, one could be tempted to employ agonists of the nuclear PPARγ receptor. Furthermore, hypoxia was shown to enhance MSC viability and proliferation as well as differentiation into adipocytes and osteocytes (Valorani et al., 2012), which could have potential implications in regenerative medicine.

Conflict of interests

The authors report no conflict of interests.

Acknowledgements

Malini Visweswaran is supported by scholarship from the Office of Research & Development, Faculty of Health Sciences, Curtin University. Sebastian Pohl is supported by funds from the Rotary Club of Belmont, W.A., Australian Rotary Health Research Fund and Curtin University. The authors additionally thank the School of Biomedical Sciences, Curtin University for research and postgraduate student support.

References

Agha-Hosseini, F., et al., 2010. In vitro isolation of stem cells derived from human dental pulp. Clin. Transplant. 24 (2), E23–E28.
Alfaro, M.P., et al., 2010. sFRP2 suppression of bone morphogenic protein (BMP) and Wnt signaling mediates mesenchymal stem cell (MSC) self-renewal promoting engraftment and myocardial repair. J. Biol. Chem. 285 (46), 35645–35653.
Almeida, M., et al., 2005. Wnt proteins prevent apoptosis of both uncommitted osteoblast progenitors and differentiated osteoblasts by beta-catenin-dependent and -independent signaling cascades involving Src/ERK and phosphatidylinositol 3-kinase/AKT. J. Biol. Chem. 280 (50), 41342–41351.
Almeida, M., et al., 2007. Oxidative stress antagonizes Wnt signaling in osteoblast precursors by diverting beta-catenin from T cell factor- to forkhead box O-mediated transcription. J. Biol. Chem. 282 (37), 27298–27305.
Atashi, F., Modarressi, A., Pepper, M.S., 2015. The role of reactive oxygen species in mesenchymal stem cell adipogenic and osteogenic differentiation: a review. Stem Cells Dev. 24 (10), 1150–1163.
Bafico, A., et al., 1999. Interaction of frizzled related protein (FRP) with Wnt ligands and the frizzled receptor suggests alternative mechanisms for FRP inhibition of Wnt signaling. J. Biol. Chem. 274 (23), 16180–16187.
Baksh, D., Boland, G.M., Tuan, R.S., 2007. Cross-talk between Wnt signaling pathways in human mesenchymal stem cells leads to functional antagonism during osteogenic differentiation. J. Cell. Biochem. 101 (5), 1109–1124.

Belema Bedada, F., et al., 2005. Activation of myogenic differentiation pathways in adult bone marrow-derived stem cells. Mol. Cell. Biol. 25 (21), 9509–9519.
Bennett, C.N., et al., 2002. Regulation of Wnt signaling during adipogenesis. J. Biol. Chem. 277 (34), 30998–31004.
Bennett, C.N., et al., 2005. Regulation of osteoblastogenesis and bone mass by Wnt10b. Proc. Natl. Acad. Sci. U. S. A. 102 (9), 3324–3329.
Bi, Y., et al., 2009. Wnt antagonist SFRP3 inhibits the differentiation of mouse hepatic progenitor cells. J. Cell. Biochem. 108 (1), 295–303.
Bianco, P., et al., 2001. Bone marrow stromal stem cells: nature, biology, and potential applications. Stem Cells 19 (3), 180–192.
Bodine, P.V., et al., 2005. The Wnt antagonist secreted frizzled-related protein-1 controls osteoblast and osteocyte apoptosis. J. Cell. Biochem. 96 (6), 1212–1230.
Boland, G.M., et al., 2004. Wnt 3a promotes proliferation and suppresses osteogenic differentiation of adult human mesenchymal stem cells. J. Cell. Biochem. 93 (6), 1210–1230.
Boudin, E., et al., 2013. The role of extracellular modulators of canonical Wnt signaling in bone metabolism and diseases. Semin. Arthritis Rheum. 43 (2), 220–240.
Boyden, L.M., et al., 2002. High bone density due to a mutation in LDL-receptor-related protein 5. N. Engl. J. Med. 346 (20), 1513–1521.
Brunt, K.R., et al., 2012. Role of WNT/β-catenin signaling in rejuvenating myogenic differentiation of aged mesenchymal stem cells from cardiac patients. Am. J. Pathol. 181 (6), 2067–2078.
Cadigan, K.M., Nusse, R., 1997. Wnt signaling: a common theme in animal development. Genes Dev. 11 (24), 3286–3305.
Cawthorn, W.P., et al., 2012. Wnt6, Wnt10a and Wnt10b inhibit adipogenesis and stimulate osteoblastogenesis through a beta-catenin-dependent mechanism. Bone 50 (2), 477–489.
Chen, Q., et al., 2003. Production of reactive oxygen species by mitochondria: central role of complex III. J. Biol. Chem. 278 (38), 36027–36031.
Choi, Y.S., et al., 2010. Differentiation of human adipose-derived stem cells into beating cardiomyocytes. J. Cell. Mol. Med. 14 (4), 878–889.
Christodoulides, C., et al., 2009. Adipogenesis and WNT signalling. Trends Endocrinol. Metab. 20 (1), 16–24.
Chung, Y.-S., et al., 2004. Effects of secreted frizzled-related protein 3 on osteoblasts in vitro. J. Bone Miner. Res. 19 (9), 1395–1402.
Clement, M.V., Hirpara, J.L., Pervaiz, S., 2003. Decrease in intracellular superoxide sensitizes Bcl-2-overexpressing tumor cells to receptor and drug-induced apoptosis independent of the mitochondria. Cell Death Differ. 10 (11), 1273–1285.
de Boer, J., et al., 2004. Wnt signaling inhibits osteogenic differentiation of human mesenchymal stem cells. Bone 34 (5), 818–826.
Ehrlund, A., et al., 2013. Characterization of the Wnt inhibitors secreted frizzled-related proteins (SFRPs) in human adipose tissue. J. Clin. Endocrinol. Metab. 98 (3), 2012–3416.
Feng, X., et al., 2013. Age-dependent impaired neurogenic differentiation capacity of dental stem cell is associated with Wnt/beta-catenin signaling. Cell. Mol. Neurobiol. 33 (8), 1023–1031.
Fischer, L., Boland, G., Tuan, R.S., 2002a. Wnt signaling during BMP-2 stimulation of mesenchymal chondrogenesis. J. Cell. Biochem. 84 (4), 816–831.
Fischer, L., Boland, G., Tuan, R.S., 2002b. Wnt-3A enhances bone morphogenetic protein-2-mediated chondrogenesis of murine C3H10T1/2 mesenchymal cells. J. Biol. Chem. 277 (34), 30870–30878.
Fletcher, J., et al., 2008. The inhibitory role of stromal cell mesenchyme on human embryonic stem cell hepatocyte differentiation is overcome by Wnt3a treatment. Cloning Stem Cells 10 (3), 331–339.
Friedenstein, A.J., et al., 1970. The development of fibroblast colonies in monolayer cultures of guinea-pig bone marrow and spleen cells. Cell Tissue Kinet. 3 (4), 393–403.
Funato, Y., et al., 2006. The thioredoxin-related redox-regulating protein nucleoredoxin inhibits Wnt-beta-catenin signalling through dishevelled. Nat. Cell Biol. 8 (5), 501–508.
Funato, Y., et al., 2010. Nucleoredoxin sustains Wnt/β-catenin signaling by retaining a pool of inactive dishevelled protein. Curr. Biol. 20 (21), 1945–1952.
Gaur, T., et al., 2005. Canonical WNT signaling promotes osteogenesis by directly stimulating Runx2 gene expression. J. Biol. Chem. 280 (39), 33132–33140.
Gaur, T., et al., 2006. Secreted frizzled related protein 1 regulates Wnt signaling for BMP2 induced chondrocyte differentiation. J. Cell. Physiol. 208 (1), 87–96.
Gaur, T., et al., 2009. Secreted frizzled related protein 1 is a target to improve fracture healing. J. Cell. Physiol. 220 (1), 174–181.
Gauron, C., et al., 2013. Sustained production of ROS triggers compensatory proliferation and is required for regeneration to proceed. Sci. Rep. 3, 2084.
Gong, Y., et al., 2001. LDL receptor-related protein 5 (LRP5) affects bone accrual and eye development. Cell 107 (4), 513–523.
Gonsalves, F.C., et al., 2011. An RNAi-based chemical genetic screen identifies three small-molecule inhibitors of the Wnt/wingless signaling pathway. Proc. Natl. Acad. Sci. U. S. A. 108 (15), 5954–5963.
Gough, D.R., Cotter, T.G., 2011. Hydrogen peroxide: a Jekyll and Hyde signalling molecule. Cell Death Dis. 2, e213.
Gregory, C.A., et al., 2005. How Wnt signaling affects bone repair by mesenchymal stem cells from the bone marrow. Ann. N. Y. Acad. Sci. 1049 (1), 97–106.
Harvanova, D., 2011. Isolation and characterisation of synovial mesenchymal stem cells. Folia Biol. (Praha) 57, 119–124.
He, W., et al., 2010. Exogenously administered secreted frizzled related protein 2 (Sfrp2) reduces fibrosis and improves cardiac function in a rat model of myocardial infarction. Proc. Natl. Acad. Sci. U. S. A. 107 (49), 21110–21115.
He, Z., et al., 2011. Transduction of Wnt11 promotes mesenchymal stem cell transdifferentiation into cardiac phenotypes. Stem Cells Dev. 20 (10), 1771–1778.
Heo, J., et al., 2013. Transcriptional characterization of Wnt pathway during sequential hepatic differentiation of human embryonic stem cells and adipose tissue-derived stem cells. Biochem. Biophys. Res. Commun. 434 (2), 235–240.
Hirabayashi, Y., et al., 2004. The Wnt/beta-catenin pathway directs neuronal differentiation of cortical neural precursor cells. Development 131 (12), 2791–2801.
Hoffmann, M.M., et al., 2014. Association of secreted frizzled-related protein 4 (SFRP4) with type 2 diabetes in patients with stable coronary artery disease. Cardiovasc. Diabetol. 13, 155.
Holmstrom, K.M., Finkel, T., 2014. Cellular mechanisms and physiological consequences of redox-dependent signalling. Nat. Rev. Mol. Cell Biol. 15 (6), 411–421.
Holzwarth, C., et al., 2010. Low physiologic oxygen tensions reduce proliferation and differentiation of human multipotent mesenchymal stromal cells. BMC Cell Biol. 11 (1), 11.
Huang, S.-M.A., et al., 2009. Tankyrase inhibition stabilizes axin and antagonizes Wnt signalling. Nature 461 (7264), 614–620.
Huelsken, J., Behrens, J., 2002. The Wnt signalling pathway. J. Cell Sci. 115 (21), 3977–3978.
Hurd, T.R., DeGennaro, M., Lehmann, R., 2012. Redox regulation of cell migration and adhesion. Trends Cell Biol. 22 (2), 107–115.
Im, G.I., Quan, Z., 2010. The effects of Wnt inhibitors on the chondrogenesis of human mesenchymal stem cells. Tissue Eng. A 16 (7), 2405–2413.
Im, G.I., Lee, J.M., Kim, H.J., 2011. Wnt inhibitors enhance chondrogenesis of human mesenchymal stem cells in a long-term pellet culture. Biotechnol. Lett. 33 (5), 1061–1068.
Ishii, K., et al., 2008. Hepatic differentiation of human bone marrow-derived mesenchymal stem cells by tetracycline-regulated hepatocyte nuclear factor 3beta. Hepatology 48 (2), 597–606.
Iyer, S., et al., 2013. FOXOs attenuate bone formation by suppressing Wnt signaling. J. Clin. Invest. 123 (8), 3409–3419.
Jang, S., Park, J.-S., Jeong, H.-S., 2015. Neural differentiation of human adipose tissue-derived stem cells involves activation of the Wnt5a/JNK signalling. Stem Cells Int. 2015, 7.
Jin, E.J., et al., 2006. Wnt-5a is involved in TGF-beta3-stimulated chondrogenic differentiation of chick wing bud mesenchymal cells. Int. J. Biochem. Cell Biol. 38 (2), 183–195.
Jin, C., et al., 2011. MAPK/ERK and Wnt/beta-catenin pathways are synergistically involved in proliferation of Sca-1 positive hepatic progenitor cells. Biochem. Biophys. Res. Commun. 409 (4), 803–807.
Jing, H., et al., 2015. Suppression of EZH2 prevents the shift of osteoporotic MSC fate to adipocyte and enhances bone formation during osteoporosis. Mol. Ther., http://dx.doi.org/10.1038/mt.2015.152.
Jones, S.E., Jomary, C., 2002. Secreted frizzled-related proteins: searching for relationships and patterns. Bioessays 24 (9), 811–820.
Kanda, Y., et al., 2011. Reactive oxygen species mediate adipocyte differentiation in mesenchymal stem cells. Life Sci. 89 (7–8), 250–258.
Kang, S., et al., 2007. Wnt signaling stimulates osteoblastogenesis of mesenchymal precursors by suppressing CCAAT/enhancer-binding protein alpha and peroxisome proliferator-activated receptor gamma. J. Biol. Chem. 282 (19), 14515–14524.
Kato, M., et al., 2002. Cbfa1-independent decrease in osteoblast proliferation, osteopenia, and persistent embryonic eye vascularization in mice deficient in Lrp5, a Wnt coreceptor. J. Cell Biol. 157 (2), 303–314.
Kawano, Y., Kypta, R., 2003. Secreted antagonists of the Wnt signalling pathway. J. Cell Sci. 116 (13), 2627–2634.
Kim, K.S., et al., 2010. Reactive oxygen species generated by NADPH oxidase 2 and 4 are required for chondrogenic differentiation. J. Biol. Chem. 285 (51), 40294–40302.
Kim, J.H., et al., 2013. Wnt signaling in bone formation and its therapeutic potential for bone diseases. Ther. Adv. Musculoskelet. Dis. 5 (1), 13–31.
Kobayashi, K., et al., 2009. Secreted frizzled-related protein 2 is a procollagen C proteinase enhancer with a role in fibrosis associated with myocardial infarction. Nat. Cell Biol. 11 (1), 46–55.
Komiya, Y., Habas, R., 2008. Wnt signal transduction pathways. Organogenesis 4 (2), 68–75.
Kondo, T., et al., 2011. Wnt signaling promotes neuronal differentiation from mesenchymal stem cells through activation of Tlx3. Stem Cells (Dayt. Ohio) 29 (5), 836–846.
Korswagen, H.C., 2006. Regulation of the Wnt/beta-catenin pathway by redox signaling. Dev. Cell 10 (6), 687–688.
Kuroda, Y., et al., 2010. Unique multipotent cells in adult human mesenchymal cell populations. Proc. Natl. Acad. Sci. U. S. A. 107 (19), 8639–8643.
Kushnareva, Y., Murphy, A.N., Andreyev, A., 2002. Complex I-mediated reactive oxygen species generation: modulation by cytochrome c and NAD(P)+oxidation–reduction state. Biochem. J. 368 (Pt. 2), 545–553.
Leroux, L., et al., 2010. Hypoxia preconditioned mesenchymal stem cells improve vascular and skeletal muscle fiber regeneration after ischemia through a Wnt4-dependent pathway. Mol. Ther. 18 (8), 1545–1552.
Li, L., et al., 1999. Axin and Frat1 interact with dvl and GSK, bridging Dvl to GSK in Wnt-mediated regulation of LEF-1. EMBO J. 18 (15), 4233–4240.

Lin, K., et al., 1997. The cysteine-rich frizzled domain of Frzb-1 is required and sufficient for modulation of Wnt signaling. Proc. Natl. Acad. Sci. U. S. A. 94 (21), 11196–11200.
Liu, G., et al., 2009. Canonical Wnts function as potent regulators of osteogenesis by human mesenchymal stem cells. J. Cell Biol. 185 (1), 67–75.
Luo, S., et al., 2013. Inactivation of Wnt/beta-catenin signaling in human adipose-derived stem cells is necessary for chondrogenic differentiation and maintenance. Biomed. Pharmacother. 67 (8), 819–824.
Mahdi, T., et al., 2012. Secreted frizzled-related protein 4 reduces insulin secretion and is overexpressed in type 2 diabetes. Cell Metab. 16 (5), 625–633.
Marvin, M.J., et al., 2001. Inhibition of Wnt activity induces heart formation from posterior mesoderm. Genes Dev. 15 (3), 316–327.
Muley, A., et al., 2010. Secreted frizzled-related protein 4: an angiogenesis inhibitor. Am. J. Pathol. 176 (3), 1505–1516.
Muroyama, Y., Kondoh, H., Takada, S., 2004. Wnt proteins promote neuronal differentiation in neural stem cell culture. Biochem. Biophys. Res. Commun. 313 (4), 915–921.
Nakae, J., et al., 2003. The forkhead transcription factor Foxo1 regulates adipocyte differentiation. Dev. Cell 4 (1), 119–129.
Nakanishi, R., et al., 2008. Osteoblast-targeted expression of Sfrp4 in mice results in low bone mass. J. Bone Miner. Res. 23 (2), 271–277.
Nishizuka, M., et al., 2008. Wnt4 and Wnt5a promote adipocyte differentiation. FEBS Lett. 582 (21–22), 3201–3205.
Nusse, R., 2005. Wnt signaling in disease and in development. Cell Res. 15 (1), 28–32.
Pacher, P., Beckman, J.S., Liaudet, L., 2007. Nitric oxide and peroxynitrite in health and disease. Physiol. Rev. 87 (1), 315–424.
Park, J.R., Jung, Lee, Y.-S., Kang, K.-S., 2008. The roles of Wnt antagonists Dkk1 and sFRP4 during adipogenesis of human adipose tissue-derived mesenchymal stem cells. Cell Prolif. 41 (6), 859–874.
Patel, A.N., et al., 2008. Multipotent menstrual blood stromal stem cells: isolation, characterization, and differentiation. Cell Transplant. 17 (3), 303–311.
Pervaiz, S., Clement, M.V., 2007. Superoxide anion: oncogenic reactive oxygen species? Int. J. Biochem. Cell Biol. 39 (7–8), 1297–1304.
Pervaiz, S., Taneja, R., Ghaffari, S., 2009. Oxidative stress regulation of stem and progenitor cells. Antioxid. Redox Signal. 11 (11), 2777–2789.
Pittenger, M.F., et al., 1999. Multilineage potential of adult human mesenchymal stem cells. Science 284 (5411), 143–147.
Rattner, A., et al., 1997. A family of secreted proteins contains homology to the cysteine-rich ligand-binding domain of frizzled receptors. Proc. Natl. Acad. Sci. U. S. A. 94 (7), 2859–2863.
Reusch, J.E., Colton, L.A., Klemm, D.J., 2000. CREB activation induces adipogenesis in 3T3-L1 cells. Mol. Cell. Biol. 20 (3), 1008–1020.
Rharass, T., et al., 2014. Ca2+-mediated mitochondrial reactive oxygen species metabolism augments Wnt/beta-catenin pathway activation to facilitate cell differentiation. J. Biol. Chem. 289 (40), 27937–27951.
Riss, J., et al., 2006. Cancers as wounds that do not heal: differences and similarities between renal regeneration/repair and renal cell carcinoma. Cancer Res. 14, 7216–7224.
Rosen, E.D., et al., 2000. Transcriptional regulation of adipogenesis. Genes Dev. 14 (11), 1293–1307.
Ross, S.E., et al., 2000. Inhibition of adipogenesis by Wnt signaling. Science 289 (5481), 950–953.
Safford, K.M., et al., 2002. Neurogenic differentiation of murine and human adipose-derived stromal cells. Biochem. Biophys. Res. Commun. 294 (2), 371–379.
Schneider, V.A., Mercola, M., 2001. Wnt antagonism initiates cardiogenesis in *Xenopus laevis*. Genes Dev. 15 (3), 304–315.
Schroder, K., et al., 2009. Nox4 acts as a switch between differentiation and proliferation in preadipocytes. Arterioscler. Thromb. Vasc. Biol. 29 (2), 239–245.
Seo, B.M., et al., 2004. Investigation of multipotent postnatal stem cells from human periodontal ligament. Lancet 364 (9429), 149–155.
Seo, E., et al., 2013. SOX2 regulates YAP1 to maintain stemness and determine cell fate in the osteo-adipo lineage. Cell Rep. 3 (6), 2075–2087.
Shang, Y.C., et al., 2007. Wnt3a signaling promotes proliferation, myogenic differentiation, and migration of rat bone marrow mesenchymal stem cells. Acta Pharmacol. Sin. 28 (11), 1761–1774.
Shin, S.Y., et al., 2004. Hydrogen peroxide negatively modulates Wnt signaling through downregulation of beta-catenin. Cancer Lett. 212 (2), 225–231.
Takada, I., Kouzmenko, A.P., Kato, S., 2009. Wnt and PPARgamma signaling in osteoblastogenesis and adipogenesis. Nat. Rev. Rheumatol. 5 (8), 442–447.
Thannickal, V.J., Fanburg, B.L., 2000. Reactive oxygen species in cell signaling. Am. J. Physiol. Lung Cell. Mol. Physiol. 279 (6), L1005–L1028.
Tormos, K.V., et al., 2011. Mitochondrial complex III ROS regulate adipocyte differentiation. Cell Metab. 14 (4), 537–544.
Trachootham, D., et al., 2008. Redox regulation of cell survival. Antioxid. Redox Signal. 10 (8), 1343–1374.
Trevant, B., et al., 2008. Expression of secreted frizzled related protein 1, a Wnt antagonist, in brain, kidney, and skeleton is dispensable for normal embryonic development. J. Cell. Physiol. 217 (1), 113–126.
Tsai, H.-L., et al., 2014. Wnts enhance neurotrophin-induced neuronal differentiation in adult bone-marrow-derived mesenchymal stem cells via canonical and noncanonical signaling pathways. PLOS ONE 9 (8), e104937.
Uren, A., et al., 2000. Secreted frizzled-related protein-1 binds directly to Wingless and is a biphasic modulator of Wnt signaling. J. Biol. Chem. 275 (6), 4374–4382.
Valle-Prieto, A., Conget, P.A., 2010. Human mesenchymal stem cells efficiently manage oxidative stress. Stem Cells Dev. 19 (12), 1885–1893.
Valorani, M.G., et al., 2012. Pre-culturing human adipose tissue mesenchymal stem cells under hypoxia increases their adipogenic and osteogenic differentiation potentials. Cell Prolif. 45 (3), 225–238.
Visweswaran, M., et al., 2015. Wnt antagonist secreted frizzled-related protein 4 upregulates adipogenic differentiation in human adipose tissue-derived mesenchymal stem cells. PLOS ONE 10 (2), e0118005.
Weiss, M., Troyer, D., 2006. Stem cells in the umbilical cord. Stem Cell Rev. 2 (2), 155–162.
Wodarz, A., Nusse, R., 1998. Mechanisms of Wnt signaling in development. Ann. Rev. Cell Dev. Biol. 14 (1), 59–88.
Wolf, V., et al., 1997. DDC-4, an apoptosis-associated gene, is a secreted frizzled relative. FEBS Lett. 417 (3), 385–389.
Yamada, A., et al., 2013. Diverse functions of secreted frizzled-related proteins in the osteoblastogenesis of human multipotent mesenchymal stromal cells. Biomaterials 34 (13), 3270–3278.
Yao, W., et al., 2010. Overexpression of secreted frizzled-related protein 1 inhibits bone formation and attenuates parathyroid hormone bone anabolic effects. J. Bone Miner. Res. 25 (2), 190–199.
Yoshida, Y., et al., 2007. A role of Wnt/beta-catenin signals in hepatic fate specification of human umbilical cord blood-derived mesenchymal stem cells. Am. J. Physiol. Gastrointest. Liver Physiol. 293 (5), 20.
Yu, Q., et al., 2013. Wnt/beta-catenin signaling regulates neuronal differentiation of mesenchymal stem cells. Biochem. Biophys. Res. Commun. 439 (2), 297–302.
Zaragosi, L.E., et al., 2008. Effects of GSK3 inhibitors on in vitro expansion and differentiation of human adipose-derived stem cells into adipocytes. BMC Cell Biol. 9 (11), 1471–2121.
Zelko, I.N., Mariani, T.J., Folz, R.J., 2002. Superoxide dismutase multigene family: a comparison of the CuZn-SOD (SOD1), Mn-SOD (SOD2), and EC-SOD (SOD3) gene structures, evolution, and expression. Free Radic. Biol. Med. 33 (3), 337–349.
Zhuang, S., Simon, G., 2000. Peroxynitrite-induced apoptosis involves activation of multiple caspases in HL-60 cells. Am. J. Physiol. Cell Physiol. 279 (2), C341–C351.
Zuk, P.A., et al., 2001. Multilineage cells from human adipose tissue: implications for cell-based therapies. Tissue Eng. 7 (2), 211–228.
Zuk, P.A., et al., 2002. Human adipose tissue is a source of multipotent stem cells. Mol. Biol. Cell 13 (12), 4279–4295.

Tumor Biol. (2015) 36:143–152
DOI 10.1007/s13277-014-2956-z

REVIEW

Secreted frizzled-related protein 4 and its implications in cancer and apoptosis

Sebastian Pohl · Ross Scott · Frank Arfuso · Vanathi Perumal · Arun Dharmarajan

Received: 23 October 2014 / Accepted: 4 December 2014 / Published online: 13 December 2014

Abstract Secreted frizzled-related protein 4 (SFRP4) is a glycoprotein that acts as an antagonist of Wnt ligands, causing inhibition of the canonical Wnt signalling pathway. First noticed due to high expression levels during times of increased apoptosis, SFRP4 has been implicated in cell proliferation and differentiation and plays an important role in carcinogenesis. Many tumours such as endometrial, cervical, ovarian, prostate, bladder, colorectal, mesothelioma, pancreatic, renal, and oesophageal tumours are characterised by aberrant promoter hypermethylation, which causes variations in the expression level of SFRP4 when compared to normal cells. Combined experimental data appear to confirm the suggested role of SFRP4 as a local initiator of apoptosis; however, increased SFRP4 expression may not always correlate with an increase in apoptosis, possibly due to the complex interactions between different signalling pathways. SFRP4 can be explored for its use in novel therapeutic modalities as well as being a potential diagnostic biomarker.

Keywords SFRP4 · Apoptosis · Cancer · Wnt signalling

Sebastian Pohl and Ross Scott are equal contributors.

S. Pohl · R. Scott · F. Arfuso · A. Dharmarajan (✉)
School of Biomedical Science, Faculty of Health Sciences, Curtin University, GPO Box U1987, Perth, Western Australia 6845, Australia
e-mail: a.dharmarajan@curtin.edu.au

S. Pohl
e-mail: sebastian.pohl@postgrad.curtin.edu.au

R. Scott
e-mail: ross.scott@postgrad.curtin.edu.au

F. Arfuso
e-mail: frank.arfuso@curtin.edu.au

F. Arfuso · A. Dharmarajan
School of Anatomy, Physiology and Human Biology, Faculty of Science, The University of Western Australia, 35 Stirling Highway, Crawley, Perth, Western Australia 6009, Australia

V. Perumal
School of Pharmacy, Faculty of Health Sciences, Curtin University, Perth, Western Australia 6845, Australia
e-mail: perumalvanathi@postgrad.curtin.edu.au

Introduction

Secreted frizzled-related proteins (SFRP1–5) are a family of glycoproteins that act as antagonists of the Wnt ligands [1]. Included in this family is secreted frizzled-related protein 4 (SFRP4). This inhibits the canonical Wnt signalling pathway, which normally acts to increase cell proliferation and decrease apoptosis [2]. The Wnt signalling cascade is normally initiated by the binding of the Wnt ligands to the frizzled receptor family [3], which are G-coupled protein receptors located on the cell membrane [4], and binding to the low-density lipoprotein receptor-related proteins (LRP) 5 and 6.

Two classes of Wnt antagonists exist. The first class binds the Wnt ligands and frizzled receptors directly [5], while the second class binds to LRP5/6 [6]. The first class includes SFRPs and Wnt inhibitory factor 1, which is able to inhibit all Wnt signalling pathways. The second class includes Dickkopf and only inhibits the canonical pathway [5]. Various other Wnt antagonists have been recognised, which include Wise/SOST, Cerberus, insulin-like growth factor binding protein 4, adenomatosis polyposis coli down-regulated 1, Shisa, and Tiki1 [7]. Wnt activators such as N-spondin and norrin have also been identified, which are unrelated families of growth factors known to promote Wnt activity [7].

The SFRP4 gene is located on the short arm of chromosome 7 (7p14.1) and is comprised of six coding exons, spanning 10.99 kb [8]. SFRP4 also demonstrates the least structural homology when compared to other members of the SFRP family [9]. This is due in part to the existence of a

region of six conserved cysteine residues that is linked by a disulphide bridge [9]. With a molecular weight of 39.9 kDa [8] and a length of 346 amino acids, SFRP4 is the largest member of the SFRP family [8].

Structurally, SFRPs comprise a C-terminal domain and an N-terminus domain, each operating independently of the other [7]. The N-terminus is comprised of a 120 amino acid long cysteine-rich domain (CRD) made up of a conserved region of ten cysteine residues [8]. It also contains a 20–30 amino acid signal peptide [8]. Studies have shown the CRD is vital in the inhibition of angiogenesis [2]. Within the C-terminal domain is the netrin-like domain (NLD), which precedes a conserved region of six cysteine residues. Recent studies have demonstrated that the NLD can induce apoptosis [2]. The CRD and the NLD have both been shown to increase intracellular calcium levels, leading to the activation of the Wnt/Ca^{2+} signalling pathway [2].

Wnt signalling pathways

Wnt signalling pathways have been implicated in cell fate specification, cell proliferation, body axis patterning, cell migration, embryonic development, and carcinogenesis [10]. Wnt signalling pathways can be grouped into the canonical (Wnt/β-catenin dependent) [11] pathway and the non-canonical (β-catenin independent) pathway, which comprises the Wnt/Ca^{2+}-mediated pathway and the planar cell polarity pathway [12].

Canonical Wnt pathway (Wnt/β-catenin dependent)

The canonical Wnt signalling pathway has two states: an inactive 'off' due to Wnt inhibition by antagonists such as SFRPs, and an active 'on' state where Wnt signalling is initiated by Wnt ligands binding to the frizzled receptors (Fzd) and co-receptor LRP5/6 [8]. This pathway is β-catenin dependent.

The inactive off state (Fig. 1) is characterised by β-catenin being bound by the β-catenin destruction complex (BDC) [13], which is made up of glycogen synthase kinase-3-β (GSK3β), Axin, and adenomatosis polyposis coli (APC) [8]. β-Catenin is phosphorylated by GSK3β, which is then ubiquitylated by β-transducin repeating protein that marks it for proteasome-mediated degradation [8, 13]. Concurrently, Groucho binds to the T cell factor (TCF)/lymphoid enhancing-binding factor (LEF) family, which inhibits transcription in the nucleus [14]. The active on state (Fig. 2) occurs in the presence of β-catenin due to the disruption of the BDC, inhibiting the phosphorylation of β-catenin. This causes an accumulation of β-catenin in the cytoplasm, which then translocates to the nucleus [15]. Inside the nucleus, it binds to transcription factors of the T family such as LEF1, TCF1, and TCF2/3 [16]. This activates the transcription of targeted genes involved in cell proliferation such as *c-myc*, *cyclinD1*, *c-jun*, and *Axin2* [8].

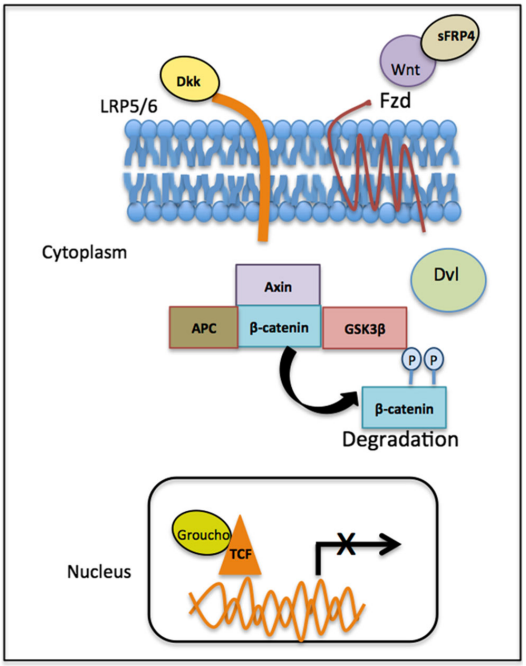

Fig. 1 The inactive Wnt signalling cascade. In the absence of Wnt signalling, due to antagonism by SFRP4, β-catenin is phosphorylated by the Axin/APC/GSK3 β complex, leading to degradation by ubiquitination and leading to the inactive state. *APC* adenomatosis polyposis coli, *Dkk* Dickkopf, *Dvl* Dishevelled, *Fzd* frizzled, *GSK3*β glycogen synthase kinase-3-β, *LRP* low-density lipoprotein receptor-related proteins, *P* phosphorylated, *TCF* T cell factor

Non-canonical Wnt pathways

Planar cell polarity pathway

This pathway operates independently of β-catenin [17] and is believed to be mediated through the frizzled receptor, which also acts independently of LRP5/6 receptors. The Dishevelled protein is a cytoplasmic protein that acts directly downstream of the frizzled receptors and, when activated, stimulates the activation of both GTPases Rho and Rac [18]. The cellular cytoskeleton is then modified [15] due to the activation of Rho-associated kinase [18] and myosin [19]. Rac stimulates c-Jun N-terminal kinase, leading to downstream effects that have not been completely elucidated [15].

Wnt/Ca^{2+} pathway

The Wnt/Ca^{2+} pathway is stimulated by the release of calcium from the endoplasmic reticulum due to the activation of phospholipase Cβ (PLC) [20]. PLC activates protein kinase C [19]

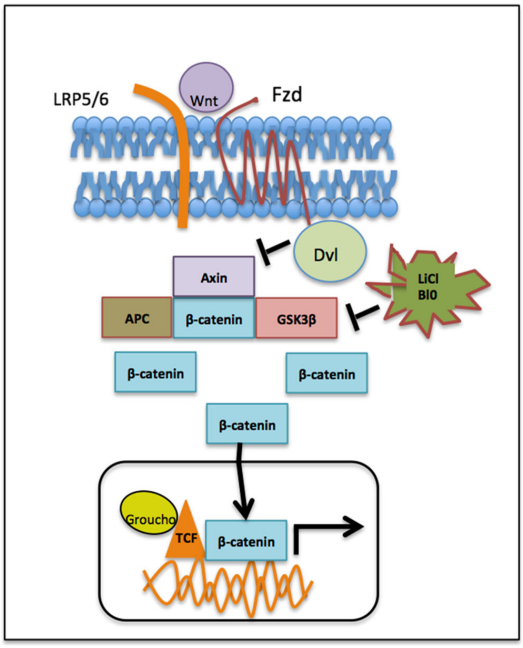

Fig. 2 The active Wnt signalling state. Wnt ligands bind to Fzd receptors and co-receptors LRP5/6. This activates intercellular Dvl, which inhibits GSK3 β. This results in nuclear translocation of β-catenin, activation of the TCF family of transcription factors, and induction of gene translocation. *APC* adenomatosis polyposis coli, *BIO* 6-bromo indirubin 3′-oxime, *Dkk* Dickkopf, *Dvl* Dishevelled, *Fzd* frizzled, *GSK3β* glycogen synthase kinase-3-β, *LiCl* lithium chloride, *LRP* low-density lipoprotein receptor-related proteins, *TCF* T cell factor

and calcium/calmodulin-dependent kinase II (CamK11) [21], which are calcium-sensitive proteins. CamK11 has been shown to activate the transcription factor NEAT in *Xenopus* embryos [22], indicating a role for Camk11 in the Wnt/Ca^{2+} pathway [19].

Aberrant Wnt signalling has been implicated in tumourigenesis, as the downstream targets are involved in cell survival, differentiation, and proliferation; therefore, inhibition of this pathway may be a potential target for cancer therapy. One such way to inhibit the Wnt canonical and non-canonical pathways is through Wnt antagonists, such as SFRPs and more specifically SFRP4.

Research involving SFRP4 and its implications in cancer is beginning to gain momentum due to promising results. SFRP4 is said to be a modulator of cell proliferation and implicated as a tumour suppressor [23], and therefore, recent research has focussed on a correlation between epigenetic modification and gene expression to determine the role of SFRP4 in cancer, which will now be discussed.

SFRP4 and its implications in cancer

Endometrium

SFRP4 is normally expressed in endometrial tissue, although expression levels are higher in the stromal cells during the proliferative phase of the menstrual cycle [24]. It has also been implicated in endometrial cell growth, as it has been found to be expressed at much higher levels in the stromal cells of endometrial carcinomas compared to that of the secretory and menstrual endometrium [25].

Promoter hypermethylation [26] and downregulation of SFRP4 have been independently shown in stromal endometrium sarcomas [27]. The expression of SFRP4 has been shown to be decreased when compared to normal epithelium in both low-grade endometrial sarcoma and the more aggressive, undifferentiated endometrial sarcoma [27]. This was verified by qRT-PCR and in situ hybridization [27]. The expression levels of β-catenin were shown to be inversely related to those of SFRP4, indicating that SFRP4 is a putative modulator of the Wnt signalling pathway, important in endometrial cell proliferation, and may also be implicated as a tumour suppressor [27].

Carmon et al. have shown that Wnt7a activates the canonical Wnt signalling pathway by binding to frizzled receptor 5 (Fzd5) and the non-canonical planar cell polarity pathway by binding to frizzled receptor 10 [26]. Activation of the canonical pathway has been shown to increase the level of cellular proliferation in the endometrium [26]. SFRP4 expression levels were also demonstrated to be decreased in endometrial carcinomas, while stable overexpression of SFRP4 and treatment with recombinant SFRP4 protein could inhibit the growth of endometrial cancer cells in vitro [26]. Furthermore, this study demonstrated that SFRP4 regulates the Wnt7a signalling pathway, which plays an important role in endometrial cell growth.

Cervix

There have been numerous studies on the methylation status of SFRP4 in various cervical cancer cell lines, with the results varying in response to the type of tumour. In two studies of cervical adenocarcinoma (AdCA) samples, promoter methylation was found to occur with an intermediate frequency, with one study giving a range of 33–50 % [28] and the other stating it was 65.2 % [29]. Both of these studies demonstrated a significantly higher methylation frequency in AdCA than in normal cervical tissue [28, 29]. In squamous cell carcinomas (SCC), the promoter was hypermethylated in 67.9 % of samples, while in high-grade squamous intraepithelial lesions (HSIL), it occurred in 36.7 % of samples and only in 4.4 % of low-grade squamous intraepithelial lesions (LSIL) [30]. Both SCC and HSIL showed significantly higher promoter

hypermethylation than that of normal cells [30]. This shows that SFRP4 promoter hypermethylation is associated with cervical carcinogenesis, indicating its use in molecular screening of cervical neoplasias [30]. SFRP4 is absent in cervical carcinoma while present in normal epithelia, leading to the activation of the Wnt canonical pathway and subsequent cell signalling driving cell proliferation [31].

Ovary

Drake et al. have demonstrated, using immunohistochemistry on tissue microarrays, that SFRP4 expression has an inverse correlation with β-catenin expression in 84 % of serous ovarian carcinoma samples [32]. While SFRP4 protein expression was found to decrease in ovarian tumours, it was revealed in a 2008 study that SFRP4 methylation frequencies did not vary significantly between patients with ovarian malignancy, borderline malignancy, and benign tumours [33].

Studies have shown that high levels of SFRP4 expression are present in the tubular epithelium of the ovary, although there is a marked decrease in these levels associated with ovarian malignancy at both the RNA and protein levels [34]. Furthermore, the loss of membranous expression of SFRP4 predicted a poorer outcome and prognosis, while the increased risk of death from this disease was by a factor of 1.8 [34]. These results demonstrated that via inhibition of the Wnt signalling pathway, SFRP4 acts as a tumour suppressor, leading towards its use as a therapeutic agent as well as a predictor for ovarian malignancies [34]. Shortly after publication of these findings, another research group using in vitro experimental models demonstrated that chemosensitive ovarian cancer cell lines expressed significantly higher levels of SFRP4 than chemoresistant ovarian cancer cell lines [35]. Chemoresistant cell lines increased their sensitivity to the chemotherapy drug cisplatin when cells were transfected with SFRP4. Furthermore, following silencing of SFRP4 expression, the chemosensitive cell lines demonstrated an increase in chemoresistance [35]. These results implicate SFRP4 as a predictive biomarker of chemosensitivity in ovarian cancer and suggest a possible therapeutic role for this protein [35].

Prostate

The overexpression of SFRP4 has been functionally associated with a decreased rate in cellular proliferation and invasiveness of the PC-3 prostate cancer cell line [36, 37]. Increased expression of SFRP4 at the membranous level in malignant epithelial cells has also been shown to be a good predictor for a longer biochemical relapse-free period, although this is only relevant for individuals with localised prostate cancer [36]. Concurrently, the loss of SFRP4 expression has been associated with prostate cancer progression.

SFRP4 overexpression has also resulted in morphologic changes in the prostate cancer cell lines, LNCaP and PC-3 [37]. Increased localization of β-catenin and cadherins (E-cadherin in LNCaP and N-cadherin in PC-3) to the cell membrane has also been shown following overexpression of SFRP4 [37]. It has also been demonstrated that SFRP4 is an inhibitor of prostate cell growth and invasion and provides support for the development of new therapeutic strategies using SFRP4 to modulate Wnt signalling [37]. This is significant to both localised androgen-dependent prostate cancer and metastatic disease [37].

Bladder

Promoter methylation of the SFRP4 gene has been demonstrated to be higher in bladder tumour samples than that of samples of adjacent tissues [38]. In one study, bladder tumour tissue samples and the corresponding urine of the patients demonstrated that, in 79.2 % of tissue samples and 54.2 % of urine samples, SFRP4 methylation was evident [38]. The samples were a combination of invasive or superficial bladder tumours and showed that bladder urine levels of SFRP4 may be used as a novel, non-invasive diagnostic biomarker [38]. Furthermore, this study demonstrated the role of hypermethylation of *SFRP4* in bladder tumour pathogenesis [38]. Review articles by Kim et al. [39] and Enokida et al. [40] also give evidence of higher levels of SFRP4 methylation in bladder tumour samples.

Colorectal

SFRP4 has been shown to have less frequent promoter hypermethylation in colorectal carcinomas when compared to other members of the SFRP family [41, 42]. However, there is conflicting evidence for the expression levels of SFRP4 in colorectal carcinomas. It has been shown to be overexpressed in colorectal carcinomas when compared to adjacent normal mucosa in some studies [41, 43] and therefore is a possible candidate marker for colorectal lesions [43]. In other studies, SFRP4 expression was either silenced or significantly reduced in the majority of tumours [44]. Qi et al. demonstrated the silencing or reduction of SFRP4 expression in 61.1 % of colorectal carcinomas and 9.1 % of colorectal adenomas [44]. The reasons for these different observations are unclear. It is also possible that these results indicate that, in colorectal cancer, SFRP4 may not act as a tumour suppressor [41].

However, more recently, a single nucleotide polymorphism (SNP) within the *SFRP4* gene (rs1802073), described as P320T, has been found to have a significant association with an increased risk of rectal cancer and also in the early stages of colorectal carcinoma [45]. It is postulated that this SNP may induce increased Wnt signalling, which can lead to the gradual

loss of apoptotic processes and, therefore, uncontrolled gene expression and tumourigenesis [45].

Mesothelioma

Studies have shown that SFRP4 is downregulated [6, 46, 47] in numerous mesothelioma cell lines, which has been correlated with methylation of the promoter region of *SFRP4* [6, 46, 48]. Lee et al. demonstrated that, in 89 % (17 of 19) of mesothelium tumour tissue samples, SFRP4 methylation had occurred [46]. Furthermore, He et al. have shown that CpG hypermethylation of the promoter region in β-catenin-deficient mesothelioma cell lines correlates with SFRP4 silencing [6]. The same study found that by treating these hypermethylated cell lines with a demethylating agent, 5-aza-2′-deoxycytidine, SFRP4 expression was restored [6]. RNA interference and expression studies have demonstrated that when SFRP4 is silenced, there is promotion of cell growth and inhibition of apoptosis [6, 46], indicating that silencing of SFRP4 enhances the canonical Wnt signalling pathway. These studies suggest a crucial role of SFRP4 in the development of mesothelial tumour cells.

Pancreas

SFRP4 has been associated with pancreatic carcinogenesis in a study by Bu et al. in 2008 [49]. Hypermethylation of SFRP4 occurred in 60 % of pancreatic cancer samples, whereas this only occurred in 10 % of adjacent tissue samples [49]. Furthermore, loss of SFRP4 expression was found to be 55 % in pancreatic cancer samples, compared to 18 % in adjacent tissue samples obtained from patients during surgery. The pancreatic cell lines PC-3, PANC-1, and CFPAC-1 and human tissue sample methylation status were determined by methylation-specific PCR [49]. The hypermethylation and loss of expression of SFRP4 in these samples suggest that SFRP4 may play an important role in pancreatic cancer pathogenesis.

Kidney

SFRP4 expression has a strong trend towards being an independent biomarker in the prediction of renal cell carcinoma (RCC). In a study of 62 patients with RCC, 53.2 % of the individuals showed positive methylation status in their tumour tissue samples, whereas methylation only occurred on the SFRP4 gene in 14.5 % of normal renal tissue samples [50].

Oesophagus

Hypermethylation of *SFRP4* has been implicated as a common early event in the development of oesophageal adenocarcinoma and its precursor, Barrett's oesophagus [51]. Aberrant methylation of the promoter region of *SFRP4* has been found to lower the protein expression of SFRP4 and promote these conditions [51]. Zou et al. used immunohistochemistry to show that protein expression levels of SFRP4 were downregulated in 90 % of cancers [51]. Hypermethylation was detected (using methylation-specific PCR) in 73 % of oesophageal adenocarcinomas and 78 % of Barrett's oesophagus, while no methylation was detected in normal oesophagogastric epithelia [51]. These results demonstrate the potential use of SFRP4 as a biomarker for Barrett's oesophagus.

Glioblastoma multiforme

SFRP4 was examined in relation to its ability to chemosensitise a glioma cell line, U138MG, and glioma stem cells (GSCs) to the chemotherapeutic agents cisplatin and doxorubicin [52]. Cisplatin is an apoptosis-inducing chemotherapeutic agent, while doxorubicin is an inhibitor of replication. U138MG is a grade IV glioblastoma cell line in which the GSCs are U138 enriched. When SFRP4 was added alone, and in combination with the chemotherapeutic agents, it was shown to reduce proliferation and increase cell death through apoptotic pathways in the GSC-enriched population [52].

Western blotting provided evidence of a decrease in β-catenin protein expression, further justifying the role of the Wnt/β-catenin signalling pathway. RT-PCR confirmed an increase in apoptotic markers *Bax* and *p21*, while concurrently demonstrating a decrease in *CycD1*, a pro-proliferative marker, and a decrease in the GSC marker *CD133* [52].

These results provide strong evidence that SFRP4 is able to sensitise glioma cells and glioma stem cells to cisplatin and doxorubicin [52]. Furthermore, this indicates that SFRP4 may be able to destroy GSCs and become an effective treatment of glioblastoma multiforme, one of the most aggressive forms of cancer [52].

Recent research by Schiefer et al. examined four human glioblastoma cell lines, U87, U138, LN18, and A172, to determine the methylation status of their SFRP4 promoter regions and the expression levels of SFRP4 messenger RNA (mRNA) and protein [53]. Methylation-specific PCR demonstrated that SFRP4 was hypermethylated in all four cell lines. All four cell lines were treated with 5-azacytidine to determine the association of promoter demethylation and SFRP4 expression before and after drug treatment. SFRP4 mRNA expression levels showed an increase ranging from 1.6- to 3.5-fold after promoter demethylation. Western blot analysis demonstrated an increase in all cell lines of SFRP4 protein expression after demethylation, with A172 cells exhibiting a 2.3-fold increase. These results show that methylation-induced gene silencing of SFRP4 may be a key feature in human glioblastoma multiforme and validate its potential use as a therapeutic biomarker.

Pituitary adenoma

Pituitary adenomas are usually benign although they can sometimes be aggressive, invading surrounding tissues and becoming difficult to treat. These aggressive pituitary adenomas also have a higher rate of recurrence, requiring extra doses of radiotherapy [54]. A recent study by Wu et al. investigated the levels of SFRP4 mRNA and protein in normal pituitary tissue and compared it to samples from aggressive and non-aggressive pituitary adenomas. RT-qPCR demonstrated that SFRP4 mRNA levels were significantly lower in aggressive pituitary adenomas when compared to normal pituitary tissue and even lower when compared to non-aggressive pituitary adenomas [54]. Western blot analysis of SFRP4 protein levels demonstrated a significant downregulation in aggressive pituitary adenoma when compared to normal and non-aggressive pituitary tissue. These results were further verified by immunohistochemistry, where the percentage of SFRP4-positive cells in aggressive pituitary adenomas was significantly lower than that in both the normal and non-aggressive samples [54]. Methylation status of the promoter region was also determined by MassArray, which showed that the ratio of methylation in aggressive tissues was significantly higher than that in both the normal and non-aggressive sample groups [54].

These results indicate that the downregulation of SFRP4 in pituitary adenomas correlates with methylation of the SFRP4 promoter and that SFRP4 also acts as a tumour suppressor. Furthermore, SFRP4 expression is inversely correlated to the aggressiveness of pituitary adenomas. The progressive loss of SFRP4 observed from normal tissue to aggressive pituitary adenomas validates its potential use as a biomarker with prognostic implications [54].

SFRP4 and its role in apoptosis

First described in 1972 by Kerr et al., apoptosis is the process of controlled elimination of unrequired or damaged cells [55]. This involves the 'killing' of the cell and the removal of debris by phagocytosis and degradation [56]. Apoptosis is activated by either an intracellular or extracellular signal, which leads to the initiation of a proteolytic caspase cascade [57]. Mammalian apoptosis can occur through two pathways termed intrinsic and extrinsic [58]. The intrinsic pathway relies on caspases that cleave specific proteins in the cytoplasm and nucleus, leading to cellular shrinkage, the collapse of the cellular cytoskeleton, disassembly of the nuclear envelope, and fragmentation of the nuclear DNA, following which the cell then undergoes rapid phagocytosis [57]. Caspases exist in the cell as inactive zymogens awaiting activation [59]. Initiator caspases are activated autocatalytically, which in turn activate effector caspases that result in the morphological features associated with apoptosis [58]. The extrinsic pathway is activated by Fas and tumour necrosis factor [60], which recruit procaspase 8 to form a 'death-inducing signalling complex' that transduces a signal cascade resulting in apoptosis [61].

Apoptosis is genetically regulated [62], and disruption in this regulation mechanism can interfere with tissue homeostasis, resulting in developmental disorders, autoimmune disease, and cancers [63]. As previously mentioned, SFRP4 was first noticed owing to its unique expression in mammary gland, ovarian corpus luteum, and ventral prostate, which were tissues that were all undergoing apoptosis [64]. Subsequently, the role it plays in apoptosis has been investigated more thoroughly, as we will now exemplify.

Mammary gland

In the words of Lacher et al., 'the obvious question is whether SFRP4 is causally involved in initiating apoptosis'. They set out to investigate this by conducting a study in which SFRP4 overexpressing, transgenic mice were created and the effects of this overexpression during mammary gland involution were investigated [65]. Lactation insufficiency was observed, coupled with an abnormally high number of apoptotic cells in the alveoli from day 19 of pregnancy to day 4 of lactation, and it was concluded that SFRP4 was involved in reduced levels of cellular survival at the commencement of involution in the mammary gland, especially as it interrupts the Akt/PKB signalling pathway, which is known to block apoptosis [66]. While investigating a novel cancer treatment using hydroxytyrosol, Granados-Principal et al. equated the inhibition of proliferation in rat mammary tumours to an increase in apoptosis that was initiated by an increase in expression levels of SFRP4 [67].

Ovary

It is known that apoptosis is an integral part of the ovulatory process, with levels of expression increasing prior to follicular rupture [68], and studies of ovulation have allowed a greater understanding of the role of SFRP4. Hsieh et al. demonstrated the upregulation of SFRP4 in follicular granulosa cells in response to the administration of human chorionic gonadotropin [69], and Drake et al. conducted an investigation to determine whether levels of SFRP4 expression in the rat ovary increased with levels of apoptosis when ovulation was hormonally induced [70]. TUNEL staining showed higher numbers of apoptotic cells in the ovarian theca, and in situ hybridisation demonstrated a rise in SFRP4 mRNA when ovaries from treated rats were compared with those of healthy controls. These results provided further evidence for a role of SFRP4 in apoptosis. Saran et al. demonstrated differential

expression of SFRP4 between chemosensitive and chemoresistant ovarian cancer cell lines and that higher apoptotic levels in non-cancerous cell lines correlated with higher levels of SFRP4 expression when compared to cancerous cell lines [35].

Corpus luteum

Guo et al., who had previously observed apoptosis-associated upregulation of *SFRP4* in both mammary and prostate tissue [71], carried out a study examining the expression of apoptosis-associated genes in the corpus luteum of the rat [72]. SFRP4 was demonstrated to be specifically expressed in tissues undergoing programmed cell death, and a distinct spike in expression was reported at the commencement of luteal regression, a phenomenon driven by high levels of apoptotic cells. The authors were the first to suggest that SFRP4 functions as an antagonist of Wnt. A further study involving hormonally induced ovulation in mice has also demonstrated that SFRP4 upregulation coincides with an increase in apoptosis in the corpus luteum [69].

Heart

Further evidence of the role of SFRP4 as an initiator of apoptosis has been demonstrated in a study of atrophied cardiac tissue [73]. It is suspected that apoptosis of cardiomyocytes is a contributing factor to the progression of pressure overload-induced heart failure [74], and when healthy cardiac tissue was compared with tissue from failing ventricles, an upregulation in the pro-apoptotic SFRPs 3 and 4 was observed [73].

Mesothelioma

In a study involving β-catenin-deficient mesothelioma cell lines, He et al. demonstrated a relationship between SFRP4 promoter hypermethylation (and therefore gene silencing) and β-catenin deficiency [6]. When SFRP4 expression was restored to these cells, apoptosis was induced; the downregulation of Dishevelled and the apoptosis inhibitor survivin were also observed following SFRP4 re-expression. However, further studies have given inconsistent results when comparing SFRP4 expression levels to cellular β-catenin levels, suggesting that two or more downstream pathways are involved [75]. Numerous other studies have also shown that when upregulation of SFRP4 is induced in cancer cells, the levels of apoptosis increase and a reduction in tumourigenesis is observed [44, 76–79]. Increased silencing of SFRP4 genes is also positively correlated with a reduction in apoptosis and subsequent tumour progression [37, 78, 80].

Skin

Maganga et al. observed an increase in SFRP4 protein levels in conjunction with an increase in apoptosis and differentiation of keratinocytes. They found that the addition of purified SFRP4 protein resulted in a decrease in cell proliferation and an increase in apoptosis [81]. It was also noted, when exposing cells to purified SFRP4, that the onset of apoptosis was delayed in comparison to apoptosis triggered by the addition of the protein kinase-inhibiting antibiotic staurosporine. This suggested that the observed induction of apoptosis was likely to be a biological response to the protein, as opposed to a demonstration of its toxicity. It was also demonstrated that a dose of 500 μg/ml induced greater levels of apoptosis than 250 μg/ml. This study provided strong evidence for the role of SFRP4 as an apoptosis initiator. However, in 2008, in experiments conducted by Cho et al. that involved the treatment of osteoblastic cells with SFRP proteins 1–4, SFRP4 was not observed to affect apoptosis, and only SFRP3 significantly increased apoptotic levels [82]. The reasons for these seemingly anomalous results remain unclear.

SFRP4 as a therapeutic agent

The Wnt signalling pathway is intimately associated with cancer development and spread, as well as the survival of cancer stem cells. Hence, it is not surprising that there have been many attempts to target this pathway in order to eradicate cancer. Several pharmacological Wnt antagonists have been used such as non-steroidal anti-inflammatory drugs, antibodies, RNAis, etc. Their role and effectiveness are beyond the scope of this review, but readers are directed to a comprehensive review of this topic by Takahashi-Yanaga et al. [83].

Our group has shown that recombinant SFRP4 has anti-angiogenic, anti-proliferative, and pro-apoptotic properties when used as a treatment modality for the disruption of cancer growth in a mouse xenograft model of ovarian cancer [23]. Furthermore, we were also able to demonstrate cancer-specific effects of SFRP4, which is an endogenously expressed protein. In addition, we have recently demonstrated that SFRP4 is able to increase chemosensitisation of glioblastoma and head and neck cancer stem cells to the clinically used drugs doxorubicin and cisplatin [52, 84].

Another common occurrence in cancers is the hypermethylation of various genes. We recently demonstrated that in highly aggressive human glioblastomas, the SFRP gene family is hypermethylated [53]. This raises the interesting concept of using pharmacologic modulators to reverse this effect, thus allowing endogenously expressed SFRP4 to exert its normal homeostatic role.

We have recently undertaken further research into the effects of peptides derived from the CRD and NLD of SFRP4, in combination with a variety of clinically used chemotherapeutics, on cancers such as glioma, breast, prostate, and head and neck, and found they are more efficacious in targeting the cancer cells than when using the whole protein (unpublished data). Our preliminary results give us great hope to establish these peptides as clinically applicable therapy in the future.

Conclusions

Since the discovery of SFRP4, this protein has garnered much interest owing to its unique role in apoptosis, as well as a possible therapeutic potential due to its ability to inhibit angiogenesis [2] and chemosensitise some CSCs [52]. The role of SFRP4 and its utilisation for cancer therapy is a relatively new area of study, although results have shown that it may have many uses both therapeutically and as a potential diagnostic biomarker. There are, however, some conflicting reports, particularly in the case of cancerous colon epithelial cells, where increased levels of SFRP4 appear to correlate with increased levels of proliferation and tumour progression [41, 43, 44].

Cancer has often been referred to as a wound that will not heal. Part of the healing process involves the selective removal of defective cells through apoptosis. Hence, aberrations in apoptosis are often associated with cancer development and progression. Combined experimental data confirm the suggested role of SFRP4 as a local initiator of apoptosis [24, 79, 85]. Indeed, our group has demonstrated that SFRP4, when administered as a therapeutic agent, was able to selectively induce apoptosis in tumour endothelium [23]. However, increased SFRP4 expression may not always correlate with an increase in apoptosis [82], which is most likely due to the complex interactions between different signalling pathways.

Acknowledgments AD was supported by a grant from Cancer Council. Raine Medical Foundation. and School of Biomedical Sciences Strategic Research Funds, Curtin University. VP was supported by Curtin University International Postgraduate Research Scholarship.

Conflicts of interest None

References

1. Miller JR. The Wnts. Genome biology 2002;3:REVIEWS3001.
2. Longman D, Arfuso F, Viola HM, Hool LC, Dharmarajan AM. The role of the cysteine-rich domain and netrin-like domain of secreted frizzled-related protein 4 in angiogenesis inhibition in vitro. Oncol Res. 2012;20:1–6.
3. Constantinou T, Baumann F, Lacher MD, Saurer S, Friis R, Dharmarajan A. SFRP-4 abrogates Wnt-3a-induced beta-catenin and Akt/PKB signalling and reverses a Wnt-3a-imposed inhibition of in vitro mammary differentiation. J Mol Signal. 2008;3:10.
4. Malbon CC. Frizzleds: new members of the superfamily of G-protein-coupled receptors. Front Biosci. 2004;9:1048–58.
5. Surana R, Sikka S, Cai W, Shin EM, Warrier SR, Tan HJ, et al. Secreted frizzled related proteins: implications in cancers. Biochim Biophys Acta. 1845;2014:53–65.
6. He B, Lee AY, Dadfarmay S, You L, Xu Z, Reguart N, et al. Secreted frizzled-related protein 4 is silenced by hypermethylation and induces apoptosis in beta-catenin-deficient human mesothelioma cells. Cancer Res. 2005;65:743–8.
7. Cruciat CM, Niehrs C. Secreted and transmembrane WNT inhibitors and activators. Cold Spring Harb Perspect Biol. 2013;5:a015081.
8. Jones SE, Jomary C. Secreted Frizzled-related proteins: searching for relationships and patterns. BioEssays. 2002;24:811–20.
9. Chong JM, Uren A, Rubin JS, Speicher DW. Disulfide bond assignments of secreted Frizzled-related protein-1 provide insights about Frizzled homology and netrin modules. J Biol Chem. 2002;277:5134–44.
10. Yang Y. Wnt signaling in development and disease. Cell Biosci. 2012;2:14.
11. Rao TP, Kuhl M. An updated overview on Wnt signaling pathways: a prelude for more. Circ Res. 2010;106:1798–806.
12. Habas R, Dawid IB. Dishevelled and Wnt signaling: is the nucleus the final frontier? J Biol. 2005;4:2.
13. Gordon MD, Nusse R. Wnt signaling: multiple pathways, multiple receptors, and multiple transcription factors. J Biol Chem. 2006;281:22429–33.
14. Daniels DL, Weis WI. Beta-catenin directly displaces Groucho/TLE repressors from Tcf/Lef in Wnt-mediated transcription activation. Nat Struct Mol Biol. 2005;12:364–71.
15. Komiya Y, Habas R. Wnt signal transduction pathways. Organogenesis. 2008;4:68–75.
16. MacDonald BT, Tamai K, He X. Wnt/beta-catenin signaling: components, mechanisms, and diseases. Dev Cell. 2009;17:9–26.
17. Giles RH, van Es JH, Clevers H. Caught up in a Wnt storm: Wnt signaling in cancer. Biochim Biophys Acta. 2003;1653:1–24.
18. Wallingford JB, Habas R. The developmental biology of Dishevelled: an enigmatic protein governing cell fate and cell polarity. Development. 2005;132:4421–36.
19. Sheldahl LC, Slusarski DC, Pandur P, Miller JR, Kuhl M, Moon RT. Dishevelled activates Ca2+ flux, PKC, and CamKII in vertebrate embryos. J Cell Biol. 2003;161:769–77.
20. Kohn AD, Moon RT. Wnt and calcium signaling: beta-catenin-independent pathways. Cell Calcium. 2005;38:439–46.
21. Kuhl M, Sheldahl LC, Park M, Miller JR, Moon RT. The Wnt/Ca2+ pathway: a new vertebrate Wnt signaling pathway takes shape. Trends Genet. 2000;16:279–83.
22. Winklbauer R, Medina A, Swain RK, Steinbeisser H. Frizzled-7 signalling controls tissue separation during Xenopus gastrulation. Nature. 2001;413:856–60.
23. Muley A, Majumder S, Kolluru GK, Parkinson S, Viola H, Hool L, et al. Secreted frizzled-related protein 4: an angiogenesis inhibitor. Am J Pathol. 2010;176:1505–16.
24. Kawano Y, Kypta R. Secreted antagonists of the Wnt signalling pathway. J Cell Sci. 2003;116:2627–34.
25. Kurihara S, Oda Y, Ohishi Y, Kaneki E, Kobayashi H, Wake N, et al. Coincident expression of beta-catenin and cyclin D1 in endometrial stromal tumors and related high-grade sarcomas. Mod Pathol. 2010;23:225–34.
26. Carmon KS, Loose DS. Secreted frizzled-related protein 4 regulates two Wnt7a signaling pathways and inhibits proliferation in endometrial cancer cells. Mol Cancer Res. 2008;6:1017–28.

27. Hrzenjak A, Tippl M, Kremser ML, Strohmeier B, Guelly C, Neumeister D, et al. Inverse correlation of secreted frizzled-related protein 4 and beta-catenin expression in endometrial stromal sarcomas. J Pathol. 2004;204:19–27.
28. van der Meide WF, Snellenberg S, Meijer CJ, Baalbergen A, Helmerhorst TJ, van der Sluis WB, et al. Promoter methylation analysis of WNT/beta-catenin signaling pathway regulators to detect adenocarcinoma or its precursor lesion of the cervix. Gynecol Oncol. 2011;123:116–22.
29. Lin YW, Chung MT, Lai HC, De Yan M, Shih YL, Chang CC, et al. Methylation analysis of SFRP genes family in cervical adenocarcinoma. J Cancer Res Clin Oncol. 2009;135:1665–74.
30. Chung MT, Sytwu HK, Yan MD, Shih YL, Chang CC, Yu MH, et al. Promoter methylation of SFRPs gene family in cervical cancer. Gynecol Oncol. 2009;112:301–6.
31. Perez-Plasencia C, Duenas-Gonzalez A, Alatorre-Tavera B. Second hit in cervical carcinogenesis process: involvement of Wnt/beta catenin pathway. Int Arch Med. 2008;1:10.
32. Drake J, Shearwood AM, White J, Friis R, Zeps N, Charles A, et al. Expression of secreted frizzled-related protein 4 (SFRP4) in primary serous ovarian tumours. Eur J Gynaecol Oncol. 2009;30:133–41.
33. Su HY, Lai HC, Lin YW, Chou YC, Liu CY, Yu MH. An epigenetic marker panel for screening and prognostic prediction of ovarian cancer. Int J Cancer. 2009;124:387–93.
34. Jacob F, Ukegjini K, Nixdorf S, Ford CE, Olivier J, Caduff R, et al. Loss of secreted frizzled-related protein 4 correlates with an aggressive phenotype and predicts poor outcome in ovarian cancer patients. PLoS One. 2012;7:e31885.
35. Saran U, Arfuso F, Zeps N, Dharmarajan A. Secreted frizzled-related protein 4 expression is positively associated with responsiveness to cisplatin of ovarian cancer cell lines in vitro and with lower tumour grade in mucinous ovarian cancers. BMC Cell Biol. 2012;13:25.
36. Horvath LG, Henshall SM, Kench JG, Saunders DN, Lee CS, Golovsky D, et al. Membranous expression of secreted frizzled-related protein 4 predicts for good prognosis in localized prostate cancer and inhibits PC3 cellular proliferation in vitro. Clin Cancer Res. 2004;10:615–25.
37. Horvath LG, Lelliott JE, Kench JG, Lee CS, Williams ED, Saunders DN, et al. Secreted frizzled-related protein 4 inhibits proliferation and metastatic potential in prostate cancer. Prostate. 2007;67:1081–90.
38. Urakami S, Shiina H, Enokida H, Kawakami T, Kawamoto K, Hirata H, et al. Combination analysis of hypermethylated Wnt-antagonist family genes as a novel epigenetic biomarker panel for bladder cancer detection. Clin Cancer Res. 2006;12:2109–16.
39. Kim WJ, Kim YJ. Epigenetics of bladder cancer. Methods Mol Biol. 2012;863:111–8.
40. Enokida H, Nakagawa M. Epigenetics in bladder cancer. Int J Clin Oncol. 2008;13:298–307.
41. Feng Han Q, Zhao W, Bentel J, Shearwood AM, Zeps N, Joseph D, et al. Expression of sFRP-4 and beta-catenin in human colorectal carcinoma. Cancer Lett. 2006;231:129–37.
42. Suzuki H, Watkins DN, Jair KW, Schuebel KE, Markowitz SD, Chen WD, et al. Epigenetic inactivation of SFRP genes allows constitutive WNT signaling in colorectal cancer. Nat Genet. 2004;36:417–22.
43. Huang D, Yu B, Deng Y, Sheng W, Peng Z, Qin W, et al. SFRP4 was overexpressed in colorectal carcinoma. J Cancer Res Clin Oncol. 2010;136:395–401.
44. Qi J, Zhu YQ, Luo J, Tao WH. Hypermethylation and expression regulation of secreted frizzled-related protein genes in colorectal tumor. World J Gastroenterol. 2006;12:7113–7.
45. Frank B, Hoffmeister M, Klopp N, Illig T, Chang-Claude J, Brenner H. Single nucleotide polymorphisms in Wnt signaling and cell death pathway genes and susceptibility to colorectal cancer. Carcinogenesis. 2010;31:1381–6.
46. Lee AY, He B, You L, Dadfarmay S, Xu Z, Mazieres J, et al. Expression of the secreted frizzled-related protein gene family is downregulated in human mesothelioma. Oncogene. 2004;23:6672–6.
47. Fox S, Dharmarajan A. WNT signaling in malignant mesothelioma. Front Biosci. 2006;11:2106–12.
48. Kohno H, Amatya VJ, Takeshima Y, Kushitani K, Hattori N, Kohno N, et al. Aberrant promoter methylation of WIF-1 and SFRP1, 2, 4 genes in mesothelioma. Oncol Rep. 2010;24:423–31.
49. Bu XM, Zhao CH, Zhang N, Gao F, Lin S, Dai XW. Hypermethylation and aberrant expression of secreted frizzled-related protein genes in pancreatic cancer. World J Gastroenterol. 2008;14:3421–4.
50. Urakami S, Shiina H, Enokida H, Hirata H, Kawamoto K, Kawakami T, et al. Wnt antagonist family genes as biomarkers for diagnosis, staging, and prognosis of renal cell carcinoma using tumor and serum DNA. Clin Cancer Res. 2006;12:6989–97.
51. Zou H, Molina JR, Harrington JJ, Osborn NK, Klatt KK, Romero Y, et al. Aberrant methylation of secreted frizzled-related protein genes in esophageal adenocarcinoma and Barrett's esophagus. Int J Cancer. 2005;116:584–91.
52. Warrier S, Balu SK, Kumar AP, Millward M, Dharmarajan A. Wnt antagonist, secreted frizzled-related protein 4 (sFRP4), increases chemotherapeutic response of glioma stem-like cells. Oncol Res. 2013;21:93–102.
53. Schiefer L, Visweswaran M, Perumal V, Arfuso F, Groth D, Newsholme P, et al. Epigenetic regulation of the secreted frizzled-related protein family in human glioblastoma multiforme. Cancer Gene Ther. 2014;21:297–303.
54. Wu Y, Bai J, Li Z, Wang F, Cao L, Liu C, et al. Low expression of secreted frizzled-related protein 4 in aggressive pituitary adenoma. Pituitary 2014.
55. Denning DP, Hatch V, Horvitz HR. Both the caspase CSP-1 and a caspase-independent pathway promote programmed cell death in parallel to the canonical pathway for apoptosis in Caenorhabditis elegans. PLoS Genet. 2013;9:e1003341.
56. Kerr JF, Wyllie AH, Currie AR. Apoptosis: a basic biological phenomenon with wide-ranging implications in tissue kinetics. Br J Cancer. 1972;26:239–57.
57. Nunez G, Benedict MA, Hu Y, Inohara N. Caspases: the proteases of the apoptotic pathway. Oncogene. 1998;17:3237–45.
58. Watson AJ. Apoptosis and colorectal cancer. Gut. 2004;53:1701–9.
59. Thornberry NA, Lazebnik Y. Caspases: enemies within. Science. 1998;281:1312–6.
60. Danial NN, Korsmeyer SJ. Cell death: critical control points. Cell. 2004;116:205–19.
61. Muzio M, Chinnaiyan AM, Kischkel FC, O'Rourke K, Shevchenko A, Ni J, et al. FLICE, a novel FADD-homologous ICE/CED-3-like protease, is recruited to the CD95 (Fas/APO-1) death-inducing signaling complex. Cell. 1996;85:817–27.
62. Yuan J, Horvitz HR. A first insight into the molecular mechanisms of apoptosis. Cell. 2004;116:S53–6. 1 p following S9.
63. Elliott MR, Ravichandran KS. Clearance of apoptotic cells: implications in health and disease. J Cell Biol. 2010;189:1059–70.
64. Wolf V, Ke G, Dharmarajan AM, Bielke W, Artuso L, Saurer S, et al. DDC-4, an apoptosis-associated gene, is a secreted frizzled relative. FEBS Lett. 1997;417:385–9.
65. Lacher MD, Siegenthaler A, Jager R, Yan X, Hett S, Xuan L, et al. Role of DDC-4/sFRP-4, a secreted frizzled-related protein, at the onset of apoptosis in mammary involution. Cell Death Differ. 2003;10:528–38.
66. Song G, Ouyang G, Bao S. The activation of Akt/PKB signaling pathway and cell survival. J Cell Mol Med. 2005;9:59–71.
67. Granados-Principal S, Quiles JL, Ramirez-Tortosa C, Camacho-Corencia P, Sanchez-Rovira P, Vera-Ramirez L, et al. Hydroxytyrosol inhibits growth and cell proliferation and promotes high expression of sfrp4 in rat mammary tumours. Mol Nutr Food Res. 2011;55 Suppl 1:S117–26.

68. Talbot P, Martin GG, Ashby H. Formation of the rupture site in preovulatory hamster and mouse follicles: loss of the surface epithelium. Gamete Res. 1987;17:287–302.
69. Hsieh M, Mulders SM, Friis RR, Dharmarajan A, Richards JS. Expression and localization of secreted frizzled-related protein-4 in the rodent ovary: evidence for selective up-regulation in luteinized granulosa cells. Endocrinology. 2003;144:4597–606.
70. Drake JM, Friis RR, Dharmarajan AM. The role of sFRP4, a secreted frizzled-related protein, in ovulation. Apoptosis. 2003;8:389–97.
71. Bielke W, Ke G, Feng Z, Buhrer S, Saurer S, Friis RR. Apoptosis in the rat mammary gland and ventral prostate: detection of cell death-associated genes using a coincident-expression cloning approach. Cell Death Differ. 1997;4:114–24.
72. Guo K, Wolf V, Dharmarajan AM, Feng Z, Bielke W, Saurer S, et al. Apoptosis-associated gene expression in the corpus luteum of the rat. Biol Reprod. 1998;58:739–46.
73. Schumann H, Holtz J, Zerkowski HR, Hatzfeld M. Expression of secreted frizzled related proteins 3 and 4 in human ventricular myocardium correlates with apoptosis related gene expression. Cardiovasc Res. 2000;45:720–8.
74. Bing OH. Hypothesis: apoptosis may be a mechanism for the transition to heart failure with chronic pressure overload. J Mol Cell Cardiol. 1994;26:943–8.
75. Wong SC, Lo SF, Lee KC, Yam JW, Chan JK, Wendy Hsiao WL. Expression of frizzled-related protein and Wnt-signalling molecules in invasive human breast tumours. J Pathol. 2002;196:145–53.
76. Bovolenta P, Esteve P, Ruiz JM, Cisneros E, Lopez-Rios J. Beyond Wnt inhibition: new functions of secreted Frizzled-related proteins in development and disease. J Cell Sci. 2008;121:737–46.
77. Nojima M, Suzuki H, Toyota M, Watanabe Y, Maruyama R, Sasaki S, et al. Frequent epigenetic inactivation of SFRP genes and constitutive activation of Wnt signaling in gastric cancer. Oncogene. 2007;26:4699–713.
78. Suzuki H, Gabrielson E, Chen W, Anbazhagan R, van Engeland M, Weijenberg MP, et al. A genomic screen for genes upregulated by demethylation and histone deacetylase inhibition in human colorectal cancer. Nat Genet. 2002;31:141–9.
79. Zhou Z, Wang J, Han X, Zhou J, Linder S. Up-regulation of human secreted frizzled homolog in apoptosis and its down-regulation in breast tumors. Int J Cancer. 1998;78:95–9.
80. Marsit CJ, Karagas MR, Andrew A, Liu M, Danaee H, Schned AR, et al. Epigenetic inactivation of SFRP genes and TP53 alteration act jointly as markers of invasive bladder cancer. Cancer Res. 2005;65:7081–5.
81. Maganga R, Giles N, Adcroft K, Unni A, Keeney D, Wood F, et al. Secreted Frizzled related protein-4 (sFRP4) promotes epidermal differentiation and apoptosis. Biochem Biophys Res Commun. 2008;377:606–11.
82. Cho SW, Her SJ, Sun HJ, Choi OK, Yang JY, Kim SW, et al. Differential effects of secreted frizzled-related proteins (sFRPs) on osteoblastic differentiation of mouse mesenchymal cells and apoptosis of osteoblasts. Biochem Biophys Res Commun. 2008;367:399–405.
83. Takahashi-Yanaga F, Kahn M. Targeting Wnt signaling: can we safely eradicate cancer stem cells? Clin Cancer Res. 2010;16:3153–62.
84. Warrier S, Bhuvanalakshmi G, Arfuso F, Rajan G, Millward M, Dharmarajan A. Cancer stem-like cells from head and neck cancers are chemosensitized by the Wnt antagonist, sFRP4, by inducing apoptosis, decreasing stemness, drug resistance and epithelial to mesenchymal transition. Cancer Gene Ther. 2014;21:381–8.
85. Melkonyan HS, Chang WC, Shapiro JP, Mahadevappa M, Fitzpatrick PA, Kiefer MC, et al. SARPs: a family of secreted apoptosis-related proteins. Proc Natl Acad Sci U S A. 1997;94:13636–41.

Mary Ann Liebert Inc. LICENSE TERMS AND CONDITIONS

Jun 18, 2018

This is a License Agreement between Sebastian OG Pohl ("You") and Mary Ann Liebert Inc. ("Mary Ann Liebert Inc.") provided by Copyright Clearance Center ("CCC"). The license consists of your order details, the terms and conditions provided by Mary Ann Liebert Inc., and the payment terms and conditions.

All payments must be made in full to CCC. For payment instructions, please see information listed at the bottom of this form.

License Number	4359651237759
License date	May 31, 2018
Licensed content publisher	Mary Ann Liebert Inc.
Licensed content title	Antioxidants
Licensed content date	Jan 1, 1999
Type of Use	Thesis/Dissertation
Requestor type	Academic institution
Format	Print, Electronic
Portion	chapter/article
The requesting person/organization is:	Sebastian Pohl
Title or numeric reference of the portion(s)	Entire article
Title of the article or chapter the portion is from	Crosstalk between cellular redox state and the anti-apoptotic protein Bcl-2
Editor of portion(s)	N/A
Author of portion(s)	SOG Pohl, M Agostino, A Dharmarajan, S Pervaiz
Volume of serial or monograph.	N/A
Page range of the portion	
Publication date of portion	15th February 2018
Rights for	Main product
Duration of use	Life of current edition
Creation of copies for the disabled	no
With minor editing privileges	no
For distribution to	Worldwide
In the following language(s)	Original language of publication
With incidental promotional use	no
The lifetime unit quantity of new product	Up to 499
Title	Mediation of Triple-Negative Breast Cancer Cell Fate via Cellular Redox and Wnt Signalling
Instructor name	Arun Dharmarajan
Institution name	Curtin University

Expected presentation date	Jul 2018
Billing Type	Invoice
Billing Address	Sebastian OG Pohl Kent St Bentley, Australia Attn: Sebastian OG Pohl
Total (may include CCC user fee)	0.00 USD

Terms and Conditions

TERMS AND CONDITIONS

The following terms are individual to this publisher:

If you seek a license to use a figure, photograph, table or illustration from a Mary Ann Liebert publication, journal, or article, it is your responsibility to examine each such item as published to determine whether a credit to, or copyright notice of, a third party owner was published adjacent to the item. You may only obtain permission via this Web site to use material owned by Mary Ann Liebert, Inc. publishers. Permission to use any material published in a Mary Ann Liebert, Inc. publisher's publication, journal, or article which is reprinted with permission of a third party must be obtained from the third party owner. Mary Ann Liebert, Inc. publishers disclaims any responsibility for any use you make of items owned by third parties without their permission.

Other Terms and Conditions:

STANDARD TERMS AND CONDITIONS

1. Description of Service; Defined Terms. This Republication License enables the User to obtain licenses for republication of one or more copyrighted works as described in detail on the relevant Order Confirmation (the "Work(s)"). Copyright Clearance Center, Inc. ("CCC") grants licenses through the Service on behalf of the rightsholder identified on the Order Confirmation (the "Rightsholder"). "Republication", as used herein, generally means the inclusion of a Work, in whole or in part, in a new work or works, also as described on the Order Confirmation. "User", as used herein, means the person or entity making such republication.

2. The terms set forth in the relevant Order Confirmation, and any terms set by the Rightsholder with respect to a particular Work, govern the terms of use of Works in connection with the Service. By using the Service, the person transacting for a republication license on behalf of the User represents and warrants that he/she/it (a) has been duly authorized by the User to accept, and hereby does accept, all such terms and conditions on behalf of User, and (b) shall inform User of all such terms and conditions. In the event such person is a "freelancer" or other third party independent of User and CCC, such party shall be deemed jointly a "User" for purposes of these terms and conditions. In any event, User shall be deemed to have accepted and agreed to all such terms and conditions if User republishes the Work in any fashion.

3. Scope of License; Limitations and Obligations.

3.1 All Works and all rights therein, including copyright rights, remain the sole and exclusive property of the Rightsholder. The license created by the exchange of an Order Confirmation (and/or any invoice) and payment by User of the full amount set forth on that document includes only those rights expressly set forth in the Order Confirmation and in these terms and conditions, and conveys no other rights in the Work(s) to User. All rights not expressly granted are hereby reserved.

3.2 General Payment Terms: You may pay by credit card or through an account with us payable at the end of the month. If you and we agree that you may establish a standing account with CCC, then the following terms apply: Remit Payment to: Copyright Clearance Center, 29118 Network Place, Chicago, IL 60673-1291. Payments Due: Invoices are payable upon their delivery to you (or upon our notice to you that they are available to you for downloading). After 30 days, outstanding amounts will be subject to a service charge of 1-1/2% per month or, if less, the maximum rate allowed by applicable law. Unless otherwise specifically set forth in the Order Confirmation or in a separate written agreement signed by

CCC, invoices are due and payable on “net 30” terms. While User may exercise the rights licensed immediately upon issuance of the Order Confirmation, the license is automatically revoked and is null and void, as if it had never been issued, if complete payment for the license is not received on a timely basis either from User directly or through a payment agent, such as a credit card company.

3.3 Unless otherwise provided in the Order Confirmation, any grant of rights to User (i) is “one-time” (including the editions and product family specified in the license), (ii) is non-exclusive and non-transferable and (iii) is subject to any and all limitations and restrictions (such as, but not limited to, limitations on duration of use or circulation) included in the Order Confirmation or invoice and/or in these terms and conditions. Upon completion of the licensed use, User shall either secure a new permission for further use of the Work(s) or immediately cease any new use of the Work(s) and shall render inaccessible (such as by deleting or by removing or severing links or other locators) any further copies of the Work (except for copies printed on paper in accordance with this license and still in User's stock at the end of such period).

3.4 In the event that the material for which a republication license is sought includes third party materials (such as photographs, illustrations, graphs, inserts and similar materials) which are identified in such material as having been used by permission, User is responsible for identifying, and seeking separate licenses (under this Service or otherwise) for, any of such third party materials; without a separate license, such third party materials may not be used.

3.5 Use of proper copyright notice for a Work is required as a condition of any license granted under the Service. Unless otherwise provided in the Order Confirmation, a proper copyright notice will read substantially as follows: “Republished with permission of [Rightsholder’s name], from [Work's title, author, volume, edition number and year of copyright]; permission conveyed through Copyright Clearance Center, Inc. ” Such notice must be provided in a reasonably legible font size and must be placed either immediately adjacent to the Work as used (for example, as part of a by-line or footnote but not as a separate electronic link) or in the place where substantially all other credits or notices for the new work containing the republished Work are located. Failure to include the required notice results in loss to the Rightsholder and CCC, and the User shall be liable to pay liquidated damages for each such failure equal to twice the use fee specified in the Order Confirmation, in addition to the use fee itself and any other fees and charges specified.

3.6 User may only make alterations to the Work if and as expressly set forth in the Order Confirmation. No Work may be used in any way that is defamatory, violates the rights of third parties (including such third parties' rights of copyright, privacy, publicity, or other tangible or intangible property), or is otherwise illegal, sexually explicit or obscene. In addition, User may not conjoin a Work with any other material that may result in damage to the reputation of the Rightsholder. User agrees to inform CCC if it becomes aware of any infringement of any rights in a Work and to cooperate with any reasonable request of CCC or the Rightsholder in connection therewith.

4. Indemnity. User hereby indemnifies and agrees to defend the Rightsholder and CCC, and their respective employees and directors, against all claims, liability, damages, costs and expenses, including legal fees and expenses, arising out of any use of a Work beyond the scope of the rights granted herein, or any use of a Work which has been altered in any unauthorized way by User, including claims of defamation or infringement of rights of copyright, publicity, privacy or other tangible or intangible property.

5. Limitation of Liability. UNDER NO CIRCUMSTANCES WILL CCC OR THE RIGHTSHOLDER BE LIABLE FOR ANY DIRECT, INDIRECT, CONSEQUENTIAL OR INCIDENTAL DAMAGES (INCLUDING WITHOUT LIMITATION DAMAGES FOR LOSS OF BUSINESS PROFITS OR INFORMATION, OR FOR BUSINESS INTERRUPTION) ARISING OUT OF THE USE OR INABILITY TO USE A WORK, EVEN IF ONE OF THEM HAS BEEN ADVISED OF THE POSSIBILITY OF SUCH DAMAGES. In any event, the total liability of the Rightsholder and CCC (including their respective employees and directors) shall not exceed the total amount actually paid by User for this license. User assumes full liability for the actions and omissions of its principals, employees, agents, affiliates, successors and assigns.

6. Limited Warranties. THE WORK(S) AND RIGHT(S) ARE PROVIDED “AS IS”. CCC HAS THE RIGHT TO GRANT TO USER THE RIGHTS GRANTED IN THE ORDER CONFIRMATION DOCUMENT. CCC AND THE RIGHTSHOLDER DISCLAIM ALL OTHER WARRANTIES RELATING TO THE WORK(S) AND RIGHT(S), EITHER EXPRESS OR IMPLIED, INCLUDING WITHOUT LIMITATION IMPLIED WARRANTIES OF MERCHANTABILITY OR FITNESS FOR A PARTICULAR PURPOSE. ADDITIONAL RIGHTS MAY BE REQUIRED TO USE ILLUSTRATIONS, GRAPHS, PHOTOGRAPHS, ABSTRACTS, INSERTS OR OTHER PORTIONS OF THE WORK (AS OPPOSED TO THE ENTIRE WORK) IN A MANNER CONTEMPLATED BY USER; USER UNDERSTANDS AND AGREES THAT NEITHER CCC NOR THE RIGHTSHOLDER MAY HAVE SUCH ADDITIONAL RIGHTS TO GRANT.
7. Effect of Breach. Any failure by User to pay any amount when due, or any use by User of a Work beyond the scope of the license set forth in the Order Confirmation and/or these terms and conditions, shall be a material breach of the license created by the Order Confirmation and these terms and conditions. Any breach not cured within 30 days of written notice thereof shall result in immediate termination of such license without further notice. Any unauthorized (but licensable) use of a Work that is terminated immediately upon notice thereof may be liquidated by payment of the Rightsholder's ordinary license price therefor; any unauthorized (and unlicensable) use that is not terminated immediately for any reason (including, for example, because materials containing the Work cannot reasonably be recalled) will be subject to all remedies available at law or in equity, but in no event to a payment of less than three times the Rightsholder's ordinary license price for the most closely analogous licensable use plus Rightsholder's and/or CCC's costs and expenses incurred in collecting such payment.
8. **Miscellaneous.**
8.1 User acknowledges that CCC may, from time to time, make changes or additions to the Service or to these terms and conditions, and CCC reserves the right to send notice to the User by electronic mail or otherwise for the purposes of notifying User of such changes or additions; provided that any such changes or additions shall not apply to permissions already secured and paid for.
8.2 Use of User-related information collected through the Service is governed by CCC’s privacy policy, available online here:
http://www.copyright.com/content/cc3/en/tools/footer/privacypolicy.html.
8.3 The licensing transaction described in the Order Confirmation is personal to User. Therefore, User may not assign or transfer to any other person (whether a natural person or an organization of any kind) the license created by the Order Confirmation and these terms and conditions or any rights granted hereunder; provided, however, that User may assign such license in its entirety on written notice to CCC in the event of a transfer of all or substantially all of User’s rights in the new material which includes the Work(s) licensed under this Service.
8.4 No amendment or waiver of any terms is binding unless set forth in writing and signed by the parties. The Rightsholder and CCC hereby object to any terms contained in any writing prepared by the User or its principals, employees, agents or affiliates and purporting to govern or otherwise relate to the licensing transaction described in the Order Confirmation, which terms are in any way inconsistent with any terms set forth in the Order Confirmation and/or in these terms and conditions or CCC's standard operating procedures, whether such writing is prepared prior to, simultaneously with or subsequent to the Order Confirmation, and whether such writing appears on a copy of the Order Confirmation or in a separate instrument.
8.5 The licensing transaction described in the Order Confirmation document shall be governed by and construed under the law of the State of New York, USA, without regard to the principles thereof of conflicts of law. Any case, controversy, suit, action, or proceeding arising out of, in connection with, or related to such licensing transaction shall be brought, at CCC's sole discretion, in any federal or state court located in the County of New York, State of New York, USA, or in any federal or state court whose geographical jurisdiction covers the location of the Rightsholder set forth in the Order Confirmation. The parties expressly submit to the personal jurisdiction and venue of each such federal or state court.If you have

any comments or questions about the Service or Copyright Clearance Center, please contact us at 978-750-8400 or send an e-mail to info@copyright.com.
v 1.1

Questions? customercare@copyright.com or +1-855-239-3415 (toll free in the US) or +1-978-646-2777.

American Society for Biochemistry and Molecular Biology LICENSE TERMS AND CONDITIONS

Jun 18, 2018

This is a License Agreement between Sebastian OG Pohl ("You") and American Society for Biochemistry and Molecular Biology ("American Society for Biochemistry and Molecular Biology") provided by Copyright Clearance Center ("CCC"). The license consists of your order details, the terms and conditions provided by American Society for Biochemistry and Molecular Biology, and the payment terms and conditions.

All payments must be made in full to CCC. For payment instructions, please see information listed at the bottom of this form.

License Number	4359660114868
License date	May 31, 2018
Licensed content publisher	American Society for Biochemistry and Molecular Biology
Licensed content title	Journal of biological chemistry
Licensed content date	Jan 1, 1905
Type of Use	Thesis/Dissertation
Requestor type	Academic institution
Format	Print, Electronic
Portion	chapter/article
The requesting person/organization is:	Sebastian Pohl
Title or numeric reference of the portion(s)	Entire article
Title of the article or chapter the portion is from	Structure-based prediction of Wnt binding affinities for Frizzled-type cysteine-rich domains
Editor of portion(s)	George Carman
Author of portion(s)	Mark Agostino, Sebastian Öther-Gee Pohl, Arun Dharmarajan
Volume of serial or monograph.	292
Issue, if republishing an article from a serial	27
Page range of the portion	
Publication date of portion	July 2017
Rights for	Main product
Duration of use	Life of current edition
Creation of copies for the disabled	no
With minor editing privileges	no
For distribution to	Worldwide
In the following language(s)	Original language of publication
With incidental promotional use	no
The lifetime unit quantity of new product	Up to 499
Title	Mediation of Triple-Negative Breast Cancer Cell Fate via Cellular Redox and Wnt Signalling

Instructor name	Arun Dharmarajan
Institution name	Curtin University
Expected presentation date	Jul 2018
Billing Type	Invoice
Billing Address	Sebastian OG Pohl Kent St Bentley, Australia Attn: Sebastian OG Pohl
Total (may include CCC user fee)	0.00 USD

Terms and Conditions

TERMS AND CONDITIONS
The following terms are individual to this publisher:

None

Other Terms and Conditions:
STANDARD TERMS AND CONDITIONS

1. Description of Service; Defined Terms. This Republication License enables the User to obtain licenses for republication of one or more copyrighted works as described in detail on the relevant Order Confirmation (the "Work(s)"). Copyright Clearance Center, Inc. ("CCC") grants licenses through the Service on behalf of the rightsholder identified on the Order Confirmation (the "Rightsholder"). "Republication", as used herein, generally means the inclusion of a Work, in whole or in part, in a new work or works, also as described on the Order Confirmation. "User", as used herein, means the person or entity making such republication.
2. The terms set forth in the relevant Order Confirmation, and any terms set by the Rightsholder with respect to a particular Work, govern the terms of use of Works in connection with the Service. By using the Service, the person transacting for a republication license on behalf of the User represents and warrants that he/she/it (a) has been duly authorized by the User to accept, and hereby does accept, all such terms and conditions on behalf of User, and (b) shall inform User of all such terms and conditions. In the event such person is a "freelancer" or other third party independent of User and CCC, such party shall be deemed jointly a "User" for purposes of these terms and conditions. In any event, User shall be deemed to have accepted and agreed to all such terms and conditions if User republishes the Work in any fashion.
3. Scope of License; Limitations and Obligations.
3.1 All Works and all rights therein, including copyright rights, remain the sole and exclusive property of the Rightsholder. The license created by the exchange of an Order Confirmation (and/or any invoice) and payment by User of the full amount set forth on that document includes only those rights expressly set forth in the Order Confirmation and in these terms and conditions, and conveys no other rights in the Work(s) to User. All rights not expressly granted are hereby reserved.
3.2 General Payment Terms: You may pay by credit card or through an account with us payable at the end of the month. If you and we agree that you may establish a standing account with CCC, then the following terms apply: Remit Payment to: Copyright Clearance Center, 29118 Network Place, Chicago, IL 60673-1291. Payments Due: Invoices are payable upon their delivery to you (or upon our notice to you that they are available to you for downloading). After 30 days, outstanding amounts will be subject to a service charge of 1-1/2% per month or, if less, the maximum rate allowed by applicable law. Unless otherwise specifically set forth in the Order Confirmation or in a separate written agreement signed by CCC, invoices are due and payable on "net 30" terms. While User may exercise the rights licensed immediately upon issuance of the Order Confirmation, the license is automatically revoked and is null and void, as if it had never been issued, if complete payment for the license is not received on a timely basis either from User directly or through a payment agent, such as a credit card company.

3.3 Unless otherwise provided in the Order Confirmation, any grant of rights to User (i) is "one-time" (including the editions and product family specified in the license), (ii) is non-exclusive and non-transferable and (iii) is subject to any and all limitations and restrictions (such as, but not limited to, limitations on duration of use or circulation) included in the Order Confirmation or invoice and/or in these terms and conditions. Upon completion of the licensed use, User shall either secure a new permission for further use of the Work(s) or immediately cease any new use of the Work(s) and shall render inaccessible (such as by deleting or by removing or severing links or other locators) any further copies of the Work (except for copies printed on paper in accordance with this license and still in User's stock at the end of such period).

3.4 In the event that the material for which a republication license is sought includes third party materials (such as photographs, illustrations, graphs, inserts and similar materials) which are identified in such material as having been used by permission, User is responsible for identifying, and seeking separate licenses (under this Service or otherwise) for, any of such third party materials; without a separate license, such third party materials may not be used.

3.5 Use of proper copyright notice for a Work is required as a condition of any license granted under the Service. Unless otherwise provided in the Order Confirmation, a proper copyright notice will read substantially as follows: "Republished with permission of [Rightsholder's name], from [Work's title, author, volume, edition number and year of copyright]; permission conveyed through Copyright Clearance Center, Inc. " Such notice must be provided in a reasonably legible font size and must be placed either immediately adjacent to the Work as used (for example, as part of a by-line or footnote but not as a separate electronic link) or in the place where substantially all other credits or notices for the new work containing the republished Work are located. Failure to include the required notice results in loss to the Rightsholder and CCC, and the User shall be liable to pay liquidated damages for each such failure equal to twice the use fee specified in the Order Confirmation, in addition to the use fee itself and any other fees and charges specified.

3.6 User may only make alterations to the Work if and as expressly set forth in the Order Confirmation. No Work may be used in any way that is defamatory, violates the rights of third parties (including such third parties' rights of copyright, privacy, publicity, or other tangible or intangible property), or is otherwise illegal, sexually explicit or obscene. In addition, User may not conjoin a Work with any other material that may result in damage to the reputation of the Rightsholder. User agrees to inform CCC if it becomes aware of any infringement of any rights in a Work and to cooperate with any reasonable request of CCC or the Rightsholder in connection therewith.

4. Indemnity. User hereby indemnifies and agrees to defend the Rightsholder and CCC, and their respective employees and directors, against all claims, liability, damages, costs and expenses, including legal fees and expenses, arising out of any use of a Work beyond the scope of the rights granted herein, or any use of a Work which has been altered in any unauthorized way by User, including claims of defamation or infringement of rights of copyright, publicity, privacy or other tangible or intangible property.

5. Limitation of Liability. UNDER NO CIRCUMSTANCES WILL CCC OR THE RIGHTSHOLDER BE LIABLE FOR ANY DIRECT, INDIRECT, CONSEQUENTIAL OR INCIDENTAL DAMAGES (INCLUDING WITHOUT LIMITATION DAMAGES FOR LOSS OF BUSINESS PROFITS OR INFORMATION, OR FOR BUSINESS INTERRUPTION) ARISING OUT OF THE USE OR INABILITY TO USE A WORK, EVEN IF ONE OF THEM HAS BEEN ADVISED OF THE POSSIBILITY OF SUCH DAMAGES. In any event, the total liability of the Rightsholder and CCC (including their respective employees and directors) shall not exceed the total amount actually paid by User for this license. User assumes full liability for the actions and omissions of its principals, employees, agents, affiliates, successors and assigns.

6. Limited Warranties. THE WORK(S) AND RIGHT(S) ARE PROVIDED "AS IS". CCC HAS THE RIGHT TO GRANT TO USER THE RIGHTS GRANTED IN THE ORDER CONFIRMATION DOCUMENT. CCC AND THE RIGHTSHOLDER DISCLAIM ALL OTHER WARRANTIES RELATING TO THE WORK(S) AND RIGHT(S), EITHER EXPRESS OR IMPLIED, INCLUDING WITHOUT LIMITATION IMPLIED WARRANTIES OF MERCHANTABILITY OR FITNESS FOR A PARTICULAR

PURPOSE. ADDITIONAL RIGHTS MAY BE REQUIRED TO USE ILLUSTRATIONS, GRAPHS, PHOTOGRAPHS, ABSTRACTS, INSERTS OR OTHER PORTIONS OF THE WORK (AS OPPOSED TO THE ENTIRE WORK) IN A MANNER CONTEMPLATED BY USER; USER UNDERSTANDS AND AGREES THAT NEITHER CCC NOR THE RIGHTSHOLDER MAY HAVE SUCH ADDITIONAL RIGHTS TO GRANT.

7. Effect of Breach. Any failure by User to pay any amount when due, or any use by User of a Work beyond the scope of the license set forth in the Order Confirmation and/or these terms and conditions, shall be a material breach of the license created by the Order Confirmation and these terms and conditions. Any breach not cured within 30 days of written notice thereof shall result in immediate termination of such license without further notice. Any unauthorized (but licensable) use of a Work that is terminated immediately upon notice thereof may be liquidated by payment of the Rightsholder's ordinary license price therefor; any unauthorized (and unlicensable) use that is not terminated immediately for any reason (including, for example, because materials containing the Work cannot reasonably be recalled) will be subject to all remedies available at law or in equity, but in no event to a payment of less than three times the Rightsholder's ordinary license price for the most closely analogous licensable use plus Rightsholder's and/or CCC's costs and expenses incurred in collecting such payment.

8. **Miscellaneous.**

8.1 User acknowledges that CCC may, from time to time, make changes or additions to the Service or to these terms and conditions, and CCC reserves the right to send notice to the User by electronic mail or otherwise for the purposes of notifying User of such changes or additions; provided that any such changes or additions shall not apply to permissions already secured and paid for.

8.2 Use of User-related information collected through the Service is governed by CCC's privacy policy, available online here: http://www.copyright.com/content/cc3/en/tools/footer/privacypolicy.html.

8.3 The licensing transaction described in the Order Confirmation is personal to User. Therefore, User may not assign or transfer to any other person (whether a natural person or an organization of any kind) the license created by the Order Confirmation and these terms and conditions or any rights granted hereunder; provided, however, that User may assign such license in its entirety on written notice to CCC in the event of a transfer of all or substantially all of User's rights in the new material which includes the Work(s) licensed under this Service.

8.4 No amendment or waiver of any terms is binding unless set forth in writing and signed by the parties. The Rightsholder and CCC hereby object to any terms contained in any writing prepared by the User or its principals, employees, agents or affiliates and purporting to govern or otherwise relate to the licensing transaction described in the Order Confirmation, which terms are in any way inconsistent with any terms set forth in the Order Confirmation and/or in these terms and conditions or CCC's standard operating procedures, whether such writing is prepared prior to, simultaneously with or subsequent to the Order Confirmation, and whether such writing appears on a copy of the Order Confirmation or in a separate instrument.

8.5 The licensing transaction described in the Order Confirmation document shall be governed by and construed under the law of the State of New York, USA, without regard to the principles thereof of conflicts of law. Any case, controversy, suit, action, or proceeding arising out of, in connection with, or related to such licensing transaction shall be brought, at CCC's sole discretion, in any federal or state court located in the County of New York, State of New York, USA, or in any federal or state court whose geographical jurisdiction covers the location of the Rightsholder set forth in the Order Confirmation. The parties expressly submit to the personal jurisdiction and venue of each such federal or state court.If you have any comments or questions about the Service or Copyright Clearance Center, please contact us at 978-750-8400 or send an e-mail to info@copyright.com.

v 1.1

Questions? customercare@copyright.com or +1-855-239-3415 (toll free in the US) or +1-978-646-2777.

Nature Publishing Group LICENSE TERMS AND CONDITIONS

Jun 18, 2018

This is a License Agreement between Sebastian OG Pohl ("You") and Nature Publishing Group ("Nature Publishing Group") provided by Copyright Clearance Center ("CCC"). The license consists of your order details, the terms and conditions provided by Nature Publishing Group, and the payment terms and conditions.

All payments must be made in full to CCC. For payment instructions, please see information listed at the bottom of this form.

License Number	4359650882224
License date	May 31, 2018
Licensed content publisher	Nature Publishing Group
Licensed content title	Oncogenesis
Licensed content date	Jan 1, 2011
Type of Use	Thesis/Dissertation
Requestor type	Academic institution
Format	Print, Electronic
Portion	chapter/article
The requesting person/organization is:	Sebastian Pohl
Title or numeric reference of the portion(s)	Entire article
Title of the article or chapter the portion is from	Wnt signaling in triple-negative breast cancer
Editor of portion(s)	N/A
Author of portion(s)	SÖG Pohl, N Brook, M Agostino, F Arfuso, AP Kumar, A Dharmarajan
Volume of serial or monograph.	6
Issue, if republishing an article from a serial	e310
Page range of the portion	
Publication date of portion	April 2017
Rights for	Main product
Duration of use	Life of current edition
Creation of copies for the disabled	no
With minor editing privileges	no
For distribution to	Worldwide
In the following language(s)	Original language of publication
With incidental promotional use	no
The lifetime unit quantity of new product	Up to 499
Title	Mediation of Triple-Negative Breast Cancer Cell Fate via Cellular Redox and Wnt Signalling
Instructor name	Arun Dharmarajan

Institution name	Curtin University
Expected presentation date	Jul 2018
Billing Type	Invoice
Billing Address	Sebastian OG Pohl Kent St Bentley, Australia Attn: Sebastian Pohl
Total (may include CCC user fee)	0.00 USD

Terms and Conditions

TERMS AND CONDITIONS

The following terms are individual to this publisher:

Nature Publishing Group hereby grants you a non-exclusive license to reproduce this material for this purpose, and for no other use, subject to the conditions below:

1. NPG warrants that it has, to the best of its knowledge, the rights to license reuse of this material. However, you should ensure that the material you are requesting is original to Nature Publishing Group and does not carry the copyright of another entity (as credited in the published version). If the credit line on any part of the material you have requested indicates that it was reprinted or adapted by NPG with permission from another source, then you should also seek permission from that source to reuse the material.
2. Permission granted free of charge for material in print is also usually granted for any electronic version of that work, provided that the material is incidental to the work as a whole and that the electronic version is essentially equivalent to, or substitutes for, the print version. Where print permission has been granted for a fee, separate permission must be obtained for any additional, electronic re-use (unless, as in the case of a full paper, this has already been accounted for during your initial request in the calculation of a print run).
3. Permission granted for a first edition does not apply to second and subsequent editions and for editions in other languages (except for signatories to the STM Permissions Guidelines, or where the first edition permission was granted for free).
4. Nature Publishing Group's permission must be acknowledged next to the figure, table or abstract in print. In electronic form, this acknowledgement must be visible at the same time as the figure/table/abstract, and must be hyperlinked to the journal's homepage.
5. The credit line should read:Reprinted by permission from Macmillan Publishers Ltd: [JOURNAL NAME] (reference citation), copyright (year of publication)For AOP papers, the credit line should read:Reprinted by permission from Macmillan Publishers Ltd: [JOURNAL NAME], advance online publication, day month year (doi: 10.1038/sj.[JOURNAL ACRONYM].XXXXX) Note: For republication from the British Journal of Cancer, the following credit lines apply.Reprinted by permission from Macmillan Publishers Ltd on behalf of Cancer Research UK: [JOURNAL NAME] (reference citation), copyright (year of publication) For AOP papers, the credit line should read:Reprinted by permission from Macmillan Publishers Ltd on behalf of Cancer Research UK: [JOURNAL NAME], advance online publication, day month year (doi: 10.1038/sj.[JOURNAL ACRONYM].XXXXX)
6. Adaptations of single figures do not require NPG approval. However, the adaptation should be credited as follows:Adapted by permission from Macmillan Publishers Ltd: [JOURNAL NAME] (reference citation), copyright (year of publication)Note: For adaptation from the British Journal of Cancer, the following credit line applies.Adapted by permission from Macmillan Publishers Ltd on behalf of Cancer Research UK: [JOURNAL NAME] (reference citation), copyright (year of publication)
7. Translations of 401 words up to a whole article require NPG approval. Please visit http://www.macmillanmedicalcommunications.com for more information. Translations of up to a 400 words do not require NPG approval. The translation should be credited as follows:Translated by permission from Macmillan Publishers Ltd: [JOURNAL NAME] (reference citation), copyright (year of publication).Note: For translation from the British

Journal of Cancer, the following credit line applies.Translated by permission from Macmillan Publishers Ltd on behalf of Cancer Research UK: [JOURNAL NAME] (reference citation), copyright (year of publication)

We are certain that all parties will benefit from this agreement and wish you the best in the use of this material. Thank you.

Other Terms and Conditions:

STANDARD TERMS AND CONDITIONS

1. Description of Service; Defined Terms. This Republication License enables the User to obtain licenses for republication of one or more copyrighted works as described in detail on the relevant Order Confirmation (the "Work(s)"). Copyright Clearance Center, Inc. ("CCC") grants licenses through the Service on behalf of the rightsholder identified on the Order Confirmation (the "Rightsholder"). "Republication", as used herein, generally means the inclusion of a Work, in whole or in part, in a new work or works, also as described on the Order Confirmation. "User", as used herein, means the person or entity making such republication.

2. The terms set forth in the relevant Order Confirmation, and any terms set by the Rightsholder with respect to a particular Work, govern the terms of use of Works in connection with the Service. By using the Service, the person transacting for a republication license on behalf of the User represents and warrants that he/she/it (a) has been duly authorized by the User to accept, and hereby does accept, all such terms and conditions on behalf of User, and (b) shall inform User of all such terms and conditions. In the event such person is a "freelancer" or other third party independent of User and CCC, such party shall be deemed jointly a "User" for purposes of these terms and conditions. In any event, User shall be deemed to have accepted and agreed to all such terms and conditions if User republishes the Work in any fashion.

3. Scope of License; Limitations and Obligations.

3.1 All Works and all rights therein, including copyright rights, remain the sole and exclusive property of the Rightsholder. The license created by the exchange of an Order Confirmation (and/or any invoice) and payment by User of the full amount set forth on that document includes only those rights expressly set forth in the Order Confirmation and in these terms and conditions, and conveys no other rights in the Work(s) to User. All rights not expressly granted are hereby reserved.

3.2 General Payment Terms: You may pay by credit card or through an account with us payable at the end of the month. If you and we agree that you may establish a standing account with CCC, then the following terms apply: Remit Payment to: Copyright Clearance Center, 29118 Network Place, Chicago, IL 60673-1291. Payments Due: Invoices are payable upon their delivery to you (or upon our notice to you that they are available to you for downloading). After 30 days, outstanding amounts will be subject to a service charge of 1-1/2% per month or, if less, the maximum rate allowed by applicable law. Unless otherwise specifically set forth in the Order Confirmation or in a separate written agreement signed by CCC, invoices are due and payable on "net 30" terms. While User may exercise the rights licensed immediately upon issuance of the Order Confirmation, the license is automatically revoked and is null and void, as if it had never been issued, if complete payment for the license is not received on a timely basis either from User directly or through a payment agent, such as a credit card company.

3.3 Unless otherwise provided in the Order Confirmation, any grant of rights to User (i) is "one-time" (including the editions and product family specified in the license), (ii) is non-exclusive and non-transferable and (iii) is subject to any and all limitations and restrictions (such as, but not limited to, limitations on duration of use or circulation) included in the Order Confirmation or invoice and/or in these terms and conditions. Upon completion of the licensed use, User shall either secure a new permission for further use of the Work(s) or immediately cease any new use of the Work(s) and shall render inaccessible (such as by deleting or by removing or severing links or other locators) any further copies of the Work (except for copies printed on paper in accordance with this license and still in User's stock at the end of such period).

3.4 In the event that the material for which a republication license is sought includes third party materials (such as photographs, illustrations, graphs, inserts and similar materials) which are identified in such material as having been used by permission, User is responsible

for identifying, and seeking separate licenses (under this Service or otherwise) for, any of such third party materials; without a separate license, such third party materials may not be used.

3.5 Use of proper copyright notice for a Work is required as a condition of any license granted under the Service. Unless otherwise provided in the Order Confirmation, a proper copyright notice will read substantially as follows: “Republished with permission of [Rightsholder’s name], from [Work's title, author, volume, edition number and year of copyright]; permission conveyed through Copyright Clearance Center, Inc. ” Such notice must be provided in a reasonably legible font size and must be placed either immediately adjacent to the Work as used (for example, as part of a by-line or footnote but not as a separate electronic link) or in the place where substantially all other credits or notices for the new work containing the republished Work are located. Failure to include the required notice results in loss to the Rightsholder and CCC, and the User shall be liable to pay liquidated damages for each such failure equal to twice the use fee specified in the Order Confirmation, in addition to the use fee itself and any other fees and charges specified.

3.6 User may only make alterations to the Work if and as expressly set forth in the Order Confirmation. No Work may be used in any way that is defamatory, violates the rights of third parties (including such third parties' rights of copyright, privacy, publicity, or other tangible or intangible property), or is otherwise illegal, sexually explicit or obscene. In addition, User may not conjoin a Work with any other material that may result in damage to the reputation of the Rightsholder. User agrees to inform CCC if it becomes aware of any infringement of any rights in a Work and to cooperate with any reasonable request of CCC or the Rightsholder in connection therewith.

4. Indemnity. User hereby indemnifies and agrees to defend the Rightsholder and CCC, and their respective employees and directors, against all claims, liability, damages, costs and expenses, including legal fees and expenses, arising out of any use of a Work beyond the scope of the rights granted herein, or any use of a Work which has been altered in any unauthorized way by User, including claims of defamation or infringement of rights of copyright, publicity, privacy or other tangible or intangible property.

5. Limitation of Liability. UNDER NO CIRCUMSTANCES WILL CCC OR THE RIGHTSHOLDER BE LIABLE FOR ANY DIRECT, INDIRECT, CONSEQUENTIAL OR INCIDENTAL DAMAGES (INCLUDING WITHOUT LIMITATION DAMAGES FOR LOSS OF BUSINESS PROFITS OR INFORMATION, OR FOR BUSINESS INTERRUPTION) ARISING OUT OF THE USE OR INABILITY TO USE A WORK, EVEN IF ONE OF THEM HAS BEEN ADVISED OF THE POSSIBILITY OF SUCH DAMAGES. In any event, the total liability of the Rightsholder and CCC (including their respective employees and directors) shall not exceed the total amount actually paid by User for this license. User assumes full liability for the actions and omissions of its principals, employees, agents, affiliates, successors and assigns.

6. Limited Warranties. THE WORK(S) AND RIGHT(S) ARE PROVIDED “AS IS”. CCC HAS THE RIGHT TO GRANT TO USER THE RIGHTS GRANTED IN THE ORDER CONFIRMATION DOCUMENT. CCC AND THE RIGHTSHOLDER DISCLAIM ALL OTHER WARRANTIES RELATING TO THE WORK(S) AND RIGHT(S), EITHER EXPRESS OR IMPLIED, INCLUDING WITHOUT LIMITATION IMPLIED WARRANTIES OF MERCHANTABILITY OR FITNESS FOR A PARTICULAR PURPOSE. ADDITIONAL RIGHTS MAY BE REQUIRED TO USE ILLUSTRATIONS, GRAPHS, PHOTOGRAPHS, ABSTRACTS, INSERTS OR OTHER PORTIONS OF THE WORK (AS OPPOSED TO THE ENTIRE WORK) IN A MANNER CONTEMPLATED BY USER; USER UNDERSTANDS AND AGREES THAT NEITHER CCC NOR THE RIGHTSHOLDER MAY HAVE SUCH ADDITIONAL RIGHTS TO GRANT.

7. Effect of Breach. Any failure by User to pay any amount when due, or any use by User of a Work beyond the scope of the license set forth in the Order Confirmation and/or these terms and conditions, shall be a material breach of the license created by the Order Confirmation and these terms and conditions. Any breach not cured within 30 days of written notice thereof shall result in immediate termination of such license without further notice. Any unauthorized (but licensable) use of a Work that is terminated immediately upon notice thereof may be liquidated by payment of the Rightsholder's ordinary license price therefor; any unauthorized (and unlicensable) use that is not terminated immediately for any

reason (including, for example, because materials containing the Work cannot reasonably be recalled) will be subject to all remedies available at law or in equity, but in no event to a payment of less than three times the Rightsholder's ordinary license price for the most closely analogous licensable use plus Rightsholder's and/or CCC's costs and expenses incurred in collecting such payment.

8. **Miscellaneous.**

8.1 User acknowledges that CCC may, from time to time, make changes or additions to the Service or to these terms and conditions, and CCC reserves the right to send notice to the User by electronic mail or otherwise for the purposes of notifying User of such changes or additions; provided that any such changes or additions shall not apply to permissions already secured and paid for.

8.2 Use of User-related information collected through the Service is governed by CCC's privacy policy, available online here:
http://www.copyright.com/content/cc3/en/tools/footer/privacypolicy.html.

8.3 The licensing transaction described in the Order Confirmation is personal to User. Therefore, User may not assign or transfer to any other person (whether a natural person or an organization of any kind) the license created by the Order Confirmation and these terms and conditions or any rights granted hereunder; provided, however, that User may assign such license in its entirety on written notice to CCC in the event of a transfer of all or substantially all of User's rights in the new material which includes the Work(s) licensed under this Service.

8.4 No amendment or waiver of any terms is binding unless set forth in writing and signed by the parties. The Rightsholder and CCC hereby object to any terms contained in any writing prepared by the User or its principals, employees, agents or affiliates and purporting to govern or otherwise relate to the licensing transaction described in the Order Confirmation, which terms are in any way inconsistent with any terms set forth in the Order Confirmation and/or in these terms and conditions or CCC's standard operating procedures, whether such writing is prepared prior to, simultaneously with or subsequent to the Order Confirmation, and whether such writing appears on a copy of the Order Confirmation or in a separate instrument.

8.5 The licensing transaction described in the Order Confirmation document shall be governed by and construed under the law of the State of New York, USA, without regard to the principles thereof of conflicts of law. Any case, controversy, suit, action, or proceeding arising out of, in connection with, or related to such licensing transaction shall be brought, at CCC's sole discretion, in any federal or state court located in the County of New York, State of New York, USA, or in any federal or state court whose geographical jurisdiction covers the location of the Rightsholder set forth in the Order Confirmation. The parties expressly submit to the personal jurisdiction and venue of each such federal or state court.If you have any comments or questions about the Service or Copyright Clearance Center, please contact us at 978-750-8400 or send an e-mail to info@copyright.com.

v 1.1

Questions? customercare@copyright.com or +1-855-239-3415 (toll free in the US) or +1-978-646-2777.

Elsevier Science and Technology Journals LICENSE TERMS AND CONDITIONS

Jun 18, 2018

This is a License Agreement between Sebastian OG Pohl ("You") and Elsevier Science and Technology Journals ("Elsevier Science and Technology Journals") provided by Copyright Clearance Center ("CCC"). The license consists of your order details, the terms and conditions provided by Elsevier Science and Technology Journals, and the payment terms and conditions.

All payments must be made in full to CCC. For payment instructions, please see information listed at the bottom of this form.

License Number	4372240854647
License date	Jun 18, 2018
Licensed content publisher	Elsevier Science and Technology Journals
Licensed content title	Experimental cell research
Licensed content date	Jan 1, 1950
Type of Use	Thesis/Dissertation
Requestor type	Academic institution
Format	Electronic
Portion	chapter/article
Number of pages in chapter/article	7
The requesting person/organization is:	Sebastian Pohl
Title or numeric reference of the portion(s)	All
Title of the article or chapter the portion is from	Therapeutic approach to target mesothelioma cancer cells using the Wnt antagonist, secreted frizzled-related protein 4: Metabolic state of cancer cells
Editor of portion(s)	N/A
Author of portion(s)	Vanathi Perumal, Sebastian Pohl, Kevin N. Keane, Frank Arfuso, Philip Newsholme, Simon Fox, Arun Dharmarajan
Volume of serial or monograph.	341
Issue, if republishing an article from a serial	2
Page range of the portion	218-224
Publication date of portion	February 2016
Rights for	Main product
Duration of use	Life of current edition
Creation of copies for the disabled	no
With minor editing privileges	no
For distribution to	Worldwide
In the following language(s)	Original language of publication
With incidental promotional use	no

The lifetime unit quantity of new product	Up to 499
Title	Mediation of Triple-Negative Breast Cancer Cell Fate via Cellular Redox and Wnt Signalling
Instructor name	Arun Dharmarajan
Institution name	Curtin University
Expected presentation date	Jul 2018
Billing Type	Invoice
Billing Address	Sebastian OG Pohl Kent St Bentley, Australia Attn: Sebastian OG Pohl
Total (may include CCC user fee)	0.00 USD
Terms and Conditions	

TERMS AND CONDITIONS
The following terms are individual to this publisher:

None

Other Terms and Conditions:
STANDARD TERMS AND CONDITIONS

1. Description of Service; Defined Terms. This Republication License enables the User to obtain licenses for republication of one or more copyrighted works as described in detail on the relevant Order Confirmation (the "Work(s)"). Copyright Clearance Center, Inc. ("CCC") grants licenses through the Service on behalf of the rightsholder identified on the Order Confirmation (the "Rightsholder"). "Republication", as used herein, generally means the inclusion of a Work, in whole or in part, in a new work or works, also as described on the Order Confirmation. "User", as used herein, means the person or entity making such republication.
2. The terms set forth in the relevant Order Confirmation, and any terms set by the Rightsholder with respect to a particular Work, govern the terms of use of Works in connection with the Service. By using the Service, the person transacting for a republication license on behalf of the User represents and warrants that he/she/it (a) has been duly authorized by the User to accept, and hereby does accept, all such terms and conditions on behalf of User, and (b) shall inform User of all such terms and conditions. In the event such person is a "freelancer" or other third party independent of User and CCC, such party shall be deemed jointly a "User" for purposes of these terms and conditions. In any event, User shall be deemed to have accepted and agreed to all such terms and conditions if User republishes the Work in any fashion.
3. Scope of License; Limitations and Obligations.
3.1 All Works and all rights therein, including copyright rights, remain the sole and exclusive property of the Rightsholder. The license created by the exchange of an Order Confirmation (and/or any invoice) and payment by User of the full amount set forth on that document includes only those rights expressly set forth in the Order Confirmation and in these terms and conditions, and conveys no other rights in the Work(s) to User. All rights not expressly granted are hereby reserved.
3.2 General Payment Terms: You may pay by credit card or through an account with us payable at the end of the month. If you and we agree that you may establish a standing account with CCC, then the following terms apply: Remit Payment to: Copyright Clearance Center, 29118 Network Place, Chicago, IL 60673-1291. Payments Due: Invoices are payable upon their delivery to you (or upon our notice to you that they are available to you for downloading). After 30 days, outstanding amounts will be subject to a service charge of 1-1/2% per month or, if less, the maximum rate allowed by applicable law. Unless otherwise specifically set forth in the Order Confirmation or in a separate written agreement signed by CCC, invoices are due and payable on "net 30" terms. While User may exercise the rights

licensed immediately upon issuance of the Order Confirmation, the license is automatically revoked and is null and void, as if it had never been issued, if complete payment for the license is not received on a timely basis either from User directly or through a payment agent, such as a credit card company.

3.3 Unless otherwise provided in the Order Confirmation, any grant of rights to User (i) is "one-time" (including the editions and product family specified in the license), (ii) is non-exclusive and non-transferable and (iii) is subject to any and all limitations and restrictions (such as, but not limited to, limitations on duration of use or circulation) included in the Order Confirmation or invoice and/or in these terms and conditions. Upon completion of the licensed use, User shall either secure a new permission for further use of the Work(s) or immediately cease any new use of the Work(s) and shall render inaccessible (such as by deleting or by removing or severing links or other locators) any further copies of the Work (except for copies printed on paper in accordance with this license and still in User's stock at the end of such period).

3.4 In the event that the material for which a republication license is sought includes third party materials (such as photographs, illustrations, graphs, inserts and similar materials) which are identified in such material as having been used by permission, User is responsible for identifying, and seeking separate licenses (under this Service or otherwise) for, any of such third party materials; without a separate license, such third party materials may not be used.

3.5 Use of proper copyright notice for a Work is required as a condition of any license granted under the Service. Unless otherwise provided in the Order Confirmation, a proper copyright notice will read substantially as follows: "Republished with permission of [Rightsholder's name], from [Work's title, author, volume, edition number and year of copyright]; permission conveyed through Copyright Clearance Center, Inc. " Such notice must be provided in a reasonably legible font size and must be placed either immediately adjacent to the Work as used (for example, as part of a by-line or footnote but not as a separate electronic link) or in the place where substantially all other credits or notices for the new work containing the republished Work are located. Failure to include the required notice results in loss to the Rightsholder and CCC, and the User shall be liable to pay liquidated damages for each such failure equal to twice the use fee specified in the Order Confirmation, in addition to the use fee itself and any other fees and charges specified.

3.6 User may only make alterations to the Work if and as expressly set forth in the Order Confirmation. No Work may be used in any way that is defamatory, violates the rights of third parties (including such third parties' rights of copyright, privacy, publicity, or other tangible or intangible property), or is otherwise illegal, sexually explicit or obscene. In addition, User may not conjoin a Work with any other material that may result in damage to the reputation of the Rightsholder. User agrees to inform CCC if it becomes aware of any infringement of any rights in a Work and to cooperate with any reasonable request of CCC or the Rightsholder in connection therewith.

4. Indemnity. User hereby indemnifies and agrees to defend the Rightsholder and CCC, and their respective employees and directors, against all claims, liability, damages, costs and expenses, including legal fees and expenses, arising out of any use of a Work beyond the scope of the rights granted herein, or any use of a Work which has been altered in any unauthorized way by User, including claims of defamation or infringement of rights of copyright, publicity, privacy or other tangible or intangible property.

5. Limitation of Liability. UNDER NO CIRCUMSTANCES WILL CCC OR THE RIGHTSHOLDER BE LIABLE FOR ANY DIRECT, INDIRECT, CONSEQUENTIAL OR INCIDENTAL DAMAGES (INCLUDING WITHOUT LIMITATION DAMAGES FOR LOSS OF BUSINESS PROFITS OR INFORMATION, OR FOR BUSINESS INTERRUPTION) ARISING OUT OF THE USE OR INABILITY TO USE A WORK, EVEN IF ONE OF THEM HAS BEEN ADVISED OF THE POSSIBILITY OF SUCH DAMAGES. In any event, the total liability of the Rightsholder and CCC (including their respective employees and directors) shall not exceed the total amount actually paid by User for this license. User assumes full liability for the actions and omissions of its principals, employees, agents, affiliates, successors and assigns.

6. Limited Warranties. THE WORK(S) AND RIGHT(S) ARE PROVIDED "AS IS". CCC HAS THE RIGHT TO GRANT TO USER THE RIGHTS GRANTED IN THE ORDER

CONFIRMATION DOCUMENT. CCC AND THE RIGHTSHOLDER DISCLAIM ALL OTHER WARRANTIES RELATING TO THE WORK(S) AND RIGHT(S), EITHER EXPRESS OR IMPLIED, INCLUDING WITHOUT LIMITATION IMPLIED WARRANTIES OF MERCHANTABILITY OR FITNESS FOR A PARTICULAR PURPOSE. ADDITIONAL RIGHTS MAY BE REQUIRED TO USE ILLUSTRATIONS, GRAPHS, PHOTOGRAPHS, ABSTRACTS, INSERTS OR OTHER PORTIONS OF THE WORK (AS OPPOSED TO THE ENTIRE WORK) IN A MANNER CONTEMPLATED BY USER; USER UNDERSTANDS AND AGREES THAT NEITHER CCC NOR THE RIGHTSHOLDER MAY HAVE SUCH ADDITIONAL RIGHTS TO GRANT.

7. Effect of Breach. Any failure by User to pay any amount when due, or any use by User of a Work beyond the scope of the license set forth in the Order Confirmation and/or these terms and conditions, shall be a material breach of the license created by the Order Confirmation and these terms and conditions. Any breach not cured within 30 days of written notice thereof shall result in immediate termination of such license without further notice. Any unauthorized (but licensable) use of a Work that is terminated immediately upon notice thereof may be liquidated by payment of the Rightsholder's ordinary license price therefor; any unauthorized (and unlicensable) use that is not terminated immediately for any reason (including, for example, because materials containing the Work cannot reasonably be recalled) will be subject to all remedies available at law or in equity, but in no event to a payment of less than three times the Rightsholder's ordinary license price for the most closely analogous licensable use plus Rightsholder's and/or CCC's costs and expenses incurred in collecting such payment.

8. **Miscellaneous.**

8.1 User acknowledges that CCC may, from time to time, make changes or additions to the Service or to these terms and conditions, and CCC reserves the right to send notice to the User by electronic mail or otherwise for the purposes of notifying User of such changes or additions; provided that any such changes or additions shall not apply to permissions already secured and paid for.

8.2 Use of User-related information collected through the Service is governed by CCC’s privacy policy, available online here:
http://www.copyright.com/content/cc3/en/tools/footer/privacypolicy.html.

8.3 The licensing transaction described in the Order Confirmation is personal to User. Therefore, User may not assign or transfer to any other person (whether a natural person or an organization of any kind) the license created by the Order Confirmation and these terms and conditions or any rights granted hereunder; provided, however, that User may assign such license in its entirety on written notice to CCC in the event of a transfer of all or substantially all of User’s rights in the new material which includes the Work(s) licensed under this Service.

8.4 No amendment or waiver of any terms is binding unless set forth in writing and signed by the parties. The Rightsholder and CCC hereby object to any terms contained in any writing prepared by the User or its principals, employees, agents or affiliates and purporting to govern or otherwise relate to the licensing transaction described in the Order Confirmation, which terms are in any way inconsistent with any terms set forth in the Order Confirmation and/or in these terms and conditions or CCC's standard operating procedures, whether such writing is prepared prior to, simultaneously with or subsequent to the Order Confirmation, and whether such writing appears on a copy of the Order Confirmation or in a separate instrument.

8.5 The licensing transaction described in the Order Confirmation document shall be governed by and construed under the law of the State of New York, USA, without regard to the principles thereof of conflicts of law. Any case, controversy, suit, action, or proceeding arising out of, in connection with, or related to such licensing transaction shall be brought, at CCC's sole discretion, in any federal or state court located in the County of New York, State of New York, USA, or in any federal or state court whose geographical jurisdiction covers the location of the Rightsholder set forth in the Order Confirmation. The parties expressly submit to the personal jurisdiction and venue of each such federal or state court.If you have any comments or questions about the Service or Copyright Clearance Center, please contact us at 978-750-8400 or send an e-mail to info@copyright.com.

v 1.1

Elsevier Science and Technology Journals LICENSE TERMS AND CONDITIONS

Jun 18, 2018

This is a License Agreement between Sebastian OG Pohl ("You") and Elsevier Science and Technology Journals ("Elsevier Science and Technology Journals") provided by Copyright Clearance Center ("CCC"). The license consists of your order details, the terms and conditions provided by Elsevier Science and Technology Journals, and the payment terms and conditions.

All payments must be made in full to CCC. For payment instructions, please see information listed at the bottom of this form.

License Number	4372241285385
License date	Jun 18, 2018
Licensed content publisher	Elsevier Science and Technology Journals
Licensed content title	The international journal of biochemistry
Licensed content date	Jan 1, 1995
Type of Use	Thesis/Dissertation
Requestor type	Academic institution
Format	Electronic
Portion	chapter/article
Number of pages in chapter/article	9
The requesting person/organization is:	Sebastian Pohl
Title or numeric reference of the portion(s)	All
Title of the article or chapter the portion is from	Multi-lineage differentiation of mesenchymal stem cells – To Wnt, or not Wnt
Editor of portion(s)	N/A
Author of portion(s)	Malini Visweswaran, Sebastian Pohl, Frank Arfuso, Philip Newsholme, Rodney Dilley, Shazib Pervaiz, Arun Dharmarajan
Volume of serial or monograph.	68
Issue, if republishing an article from a serial	1
Page range of the portion	139-147
Publication date of portion	November 2015
Rights for	Main product
Duration of use	Life of current edition
Creation of copies for the disabled	no
With minor editing privileges	no
For distribution to	Worldwide
In the following language(s)	Original language of publication
With incidental promotional use	no
The lifetime unit quantity of	Up to 499

new product	
Title	Mediation of Triple-Negative Breast Cancer Cell Fate via Cellular Redox and Wnt Signalling
Instructor name	Arun Dharmarajan
Institution name	Curtin University
Expected presentation date	Jul 2018
Billing Type	Invoice
Billing Address	Sebastian OG Pohl Kent St Bentley, Australia Attn: Sebastian OG Pohl
Total (may include CCC user fee)	0.00 USD
Terms and Conditions	

TERMS AND CONDITIONS
The following terms are individual to this publisher:

None

Other Terms and Conditions:
STANDARD TERMS AND CONDITIONS

1. Description of Service; Defined Terms. This Republication License enables the User to obtain licenses for republication of one or more copyrighted works as described in detail on the relevant Order Confirmation (the "Work(s)"). Copyright Clearance Center, Inc. ("CCC") grants licenses through the Service on behalf of the rightsholder identified on the Order Confirmation (the "Rightsholder"). "Republication", as used herein, generally means the inclusion of a Work, in whole or in part, in a new work or works, also as described on the Order Confirmation. "User", as used herein, means the person or entity making such republication.
2. The terms set forth in the relevant Order Confirmation, and any terms set by the Rightsholder with respect to a particular Work, govern the terms of use of Works in connection with the Service. By using the Service, the person transacting for a republication license on behalf of the User represents and warrants that he/she/it (a) has been duly authorized by the User to accept, and hereby does accept, all such terms and conditions on behalf of User, and (b) shall inform User of all such terms and conditions. In the event such person is a "freelancer" or other third party independent of User and CCC, such party shall be deemed jointly a "User" for purposes of these terms and conditions. In any event, User shall be deemed to have accepted and agreed to all such terms and conditions if User republishes the Work in any fashion.
3. Scope of License; Limitations and Obligations.
3.1 All Works and all rights therein, including copyright rights, remain the sole and exclusive property of the Rightsholder. The license created by the exchange of an Order Confirmation (and/or any invoice) and payment by User of the full amount set forth on that document includes only those rights expressly set forth in the Order Confirmation and in these terms and conditions, and conveys no other rights in the Work(s) to User. All rights not expressly granted are hereby reserved.
3.2 General Payment Terms: You may pay by credit card or through an account with us payable at the end of the month. If you and we agree that you may establish a standing account with CCC, then the following terms apply: Remit Payment to: Copyright Clearance Center, 29118 Network Place, Chicago, IL 60673-1291. Payments Due: Invoices are payable upon their delivery to you (or upon our notice to you that they are available to you for downloading). After 30 days, outstanding amounts will be subject to a service charge of 1-1/2% per month or, if less, the maximum rate allowed by applicable law. Unless otherwise specifically set forth in the Order Confirmation or in a separate written agreement signed by CCC, invoices are due and payable on "net 30" terms. While User may exercise the rights licensed immediately upon issuance of the Order Confirmation, the license is automatically

revoked and is null and void, as if it had never been issued, if complete payment for the license is not received on a timely basis either from User directly or through a payment agent, such as a credit card company.

3.3 Unless otherwise provided in the Order Confirmation, any grant of rights to User (i) is "one-time" (including the editions and product family specified in the license), (ii) is non-exclusive and non-transferable and (iii) is subject to any and all limitations and restrictions (such as, but not limited to, limitations on duration of use or circulation) included in the Order Confirmation or invoice and/or in these terms and conditions. Upon completion of the licensed use, User shall either secure a new permission for further use of the Work(s) or immediately cease any new use of the Work(s) and shall render inaccessible (such as by deleting or by removing or severing links or other locators) any further copies of the Work (except for copies printed on paper in accordance with this license and still in User's stock at the end of such period).

3.4 In the event that the material for which a republication license is sought includes third party materials (such as photographs, illustrations, graphs, inserts and similar materials) which are identified in such material as having been used by permission, User is responsible for identifying, and seeking separate licenses (under this Service or otherwise) for, any of such third party materials; without a separate license, such third party materials may not be used.

3.5 Use of proper copyright notice for a Work is required as a condition of any license granted under the Service. Unless otherwise provided in the Order Confirmation, a proper copyright notice will read substantially as follows: "Republished with permission of [Rightsholder's name], from [Work's title, author, volume, edition number and year of copyright]; permission conveyed through Copyright Clearance Center, Inc. " Such notice must be provided in a reasonably legible font size and must be placed either immediately adjacent to the Work as used (for example, as part of a by-line or footnote but not as a separate electronic link) or in the place where substantially all other credits or notices for the new work containing the republished Work are located. Failure to include the required notice results in loss to the Rightsholder and CCC, and the User shall be liable to pay liquidated damages for each such failure equal to twice the use fee specified in the Order Confirmation, in addition to the use fee itself and any other fees and charges specified.

3.6 User may only make alterations to the Work if and as expressly set forth in the Order Confirmation. No Work may be used in any way that is defamatory, violates the rights of third parties (including such third parties' rights of copyright, privacy, publicity, or other tangible or intangible property), or is otherwise illegal, sexually explicit or obscene. In addition, User may not conjoin a Work with any other material that may result in damage to the reputation of the Rightsholder. User agrees to inform CCC if it becomes aware of any infringement of any rights in a Work and to cooperate with any reasonable request of CCC or the Rightsholder in connection therewith.

4. Indemnity. User hereby indemnifies and agrees to defend the Rightsholder and CCC, and their respective employees and directors, against all claims, liability, damages, costs and expenses, including legal fees and expenses, arising out of any use of a Work beyond the scope of the rights granted herein, or any use of a Work which has been altered in any unauthorized way by User, including claims of defamation or infringement of rights of copyright, publicity, privacy or other tangible or intangible property.

5. Limitation of Liability. UNDER NO CIRCUMSTANCES WILL CCC OR THE RIGHTSHOLDER BE LIABLE FOR ANY DIRECT, INDIRECT, CONSEQUENTIAL OR INCIDENTAL DAMAGES (INCLUDING WITHOUT LIMITATION DAMAGES FOR LOSS OF BUSINESS PROFITS OR INFORMATION, OR FOR BUSINESS INTERRUPTION) ARISING OUT OF THE USE OR INABILITY TO USE A WORK, EVEN IF ONE OF THEM HAS BEEN ADVISED OF THE POSSIBILITY OF SUCH DAMAGES. In any event, the total liability of the Rightsholder and CCC (including their respective employees and directors) shall not exceed the total amount actually paid by User for this license. User assumes full liability for the actions and omissions of its principals, employees, agents, affiliates, successors and assigns.

6. Limited Warranties. THE WORK(S) AND RIGHT(S) ARE PROVIDED "AS IS". CCC HAS THE RIGHT TO GRANT TO USER THE RIGHTS GRANTED IN THE ORDER CONFIRMATION DOCUMENT. CCC AND THE RIGHTSHOLDER DISCLAIM ALL

OTHER WARRANTIES RELATING TO THE WORK(S) AND RIGHT(S), EITHER EXPRESS OR IMPLIED, INCLUDING WITHOUT LIMITATION IMPLIED WARRANTIES OF MERCHANTABILITY OR FITNESS FOR A PARTICULAR PURPOSE. ADDITIONAL RIGHTS MAY BE REQUIRED TO USE ILLUSTRATIONS, GRAPHS, PHOTOGRAPHS, ABSTRACTS, INSERTS OR OTHER PORTIONS OF THE WORK (AS OPPOSED TO THE ENTIRE WORK) IN A MANNER CONTEMPLATED BY USER; USER UNDERSTANDS AND AGREES THAT NEITHER CCC NOR THE RIGHTSHOLDER MAY HAVE SUCH ADDITIONAL RIGHTS TO GRANT.

7. Effect of Breach. Any failure by User to pay any amount when due, or any use by User of a Work beyond the scope of the license set forth in the Order Confirmation and/or these terms and conditions, shall be a material breach of the license created by the Order Confirmation and these terms and conditions. Any breach not cured within 30 days of written notice thereof shall result in immediate termination of such license without further notice. Any unauthorized (but licensable) use of a Work that is terminated immediately upon notice thereof may be liquidated by payment of the Rightsholder's ordinary license price therefor; any unauthorized (and unlicensable) use that is not terminated immediately for any reason (including, for example, because materials containing the Work cannot reasonably be recalled) will be subject to all remedies available at law or in equity, but in no event to a payment of less than three times the Rightsholder's ordinary license price for the most closely analogous licensable use plus Rightsholder's and/or CCC's costs and expenses incurred in collecting such payment.

8. **Miscellaneous.**

8.1 User acknowledges that CCC may, from time to time, make changes or additions to the Service or to these terms and conditions, and CCC reserves the right to send notice to the User by electronic mail or otherwise for the purposes of notifying User of such changes or additions; provided that any such changes or additions shall not apply to permissions already secured and paid for.

8.2 Use of User-related information collected through the Service is governed by CCC's privacy policy, available online here:
http://www.copyright.com/content/cc3/en/tools/footer/privacypolicy.html.

8.3 The licensing transaction described in the Order Confirmation is personal to User. Therefore, User may not assign or transfer to any other person (whether a natural person or an organization of any kind) the license created by the Order Confirmation and these terms and conditions or any rights granted hereunder; provided, however, that User may assign such license in its entirety on written notice to CCC in the event of a transfer of all or substantially all of User's rights in the new material which includes the Work(s) licensed under this Service.

8.4 No amendment or waiver of any terms is binding unless set forth in writing and signed by the parties. The Rightsholder and CCC hereby object to any terms contained in any writing prepared by the User or its principals, employees, agents or affiliates and purporting to govern or otherwise relate to the licensing transaction described in the Order Confirmation, which terms are in any way inconsistent with any terms set forth in the Order Confirmation and/or in these terms and conditions or CCC's standard operating procedures, whether such writing is prepared prior to, simultaneously with or subsequent to the Order Confirmation, and whether such writing appears on a copy of the Order Confirmation or in a separate instrument.

8.5 The licensing transaction described in the Order Confirmation document shall be governed by and construed under the law of the State of New York, USA, without regard to the principles thereof of conflicts of law. Any case, controversy, suit, action, or proceeding arising out of, in connection with, or related to such licensing transaction shall be brought, at CCC's sole discretion, in any federal or state court located in the County of New York, State of New York, USA, or in any federal or state court whose geographical jurisdiction covers the location of the Rightsholder set forth in the Order Confirmation. The parties expressly submit to the personal jurisdiction and venue of each such federal or state court.If you have any comments or questions about the Service or Copyright Clearance Center, please contact us at 978-750-8400 or send an e-mail to info@copyright.com.

v 1.1

Springer Science and Bus Media B V LICENSE TERMS AND CONDITIONS

Jun 18, 2018

This is a License Agreement between Sebastian OG Pohl ("You") and Springer Science and Bus Media B V ("Springer Science and Bus Media B V") provided by Copyright Clearance Center ("CCC"). The license consists of your order details, the terms and conditions provided by Springer Science and Bus Media B V, and the payment terms and conditions.

All payments must be made in full to CCC. For payment instructions, please see information listed at the bottom of this form.

License Number	4359660849709
License date	May 31, 2018
Licensed content publisher	Springer Science and Bus Media B V
Licensed content title	Tumor biology
Licensed content date	Jan 1, 1987
Type of Use	Thesis/Dissertation
Requestor type	Academic institution
Format	Print, Electronic
Portion	chapter/article
The requesting person/organization is:	Sebastian Pohl
Title or numeric reference of the portion(s)	Entire article
Title of the article or chapter the portion is from	Secreted frizzled-related protein 4 and its implications in cancer and apoptosis
Editor of portion(s)	N/A
Author of portion(s)	Sebastian Pohl, Ross Scott, Frank Arfuso, Vanathi Perumal, Arun Dharmarajan
Volume of serial or monograph.	36
Issue, if republishing an article from a serial	1
Page range of the portion	
Publication date of portion	January 2015
Rights for	Main product
Duration of use	Life of current edition
Creation of copies for the disabled	no
With minor editing privileges	no
For distribution to	Worldwide
In the following language(s)	Original language of publication
With incidental promotional use	no
The lifetime unit quantity of new product	Up to 499
Title	Mediation of Triple-Negative Breast Cancer Cell Fate via Cellular Redox and Wnt Signalling

Instructor name	Arun Dharmarajan
Institution name	Curtin University
Expected presentation date	Jul 2018
Billing Type	Invoice
Billing Address	Sebastian OG Pohl Kent St Bentley, Australia Attn: Sebastian OG Pohl
Total (may include CCC user fee)	0.00 USD

Terms and Conditions

TERMS AND CONDITIONS

The following terms are individual to this publisher:

A maximum of 10% of the content may be licensed for republication.
The user is responsible for identifying and seeking separate licenses for any third party materials that are identified anywhere in the work. Without a separate license, such third party materials may not be reused.

Other Terms and Conditions:

STANDARD TERMS AND CONDITIONS

1. Description of Service; Defined Terms. This Republication License enables the User to obtain licenses for republication of one or more copyrighted works as described in detail on the relevant Order Confirmation (the "Work(s)"). Copyright Clearance Center, Inc. ("CCC") grants licenses through the Service on behalf of the rightsholder identified on the Order Confirmation (the "Rightsholder"). "Republication", as used herein, generally means the inclusion of a Work, in whole or in part, in a new work or works, also as described on the Order Confirmation. "User", as used herein, means the person or entity making such republication.
2. The terms set forth in the relevant Order Confirmation, and any terms set by the Rightsholder with respect to a particular Work, govern the terms of use of Works in connection with the Service. By using the Service, the person transacting for a republication license on behalf of the User represents and warrants that he/she/it (a) has been duly authorized by the User to accept, and hereby does accept, all such terms and conditions on behalf of User, and (b) shall inform User of all such terms and conditions. In the event such person is a "freelancer" or other third party independent of User and CCC, such party shall be deemed jointly a "User" for purposes of these terms and conditions. In any event, User shall be deemed to have accepted and agreed to all such terms and conditions if User republishes the Work in any fashion.

3. Scope of License; Limitations and Obligations.

3.1 All Works and all rights therein, including copyright rights, remain the sole and exclusive property of the Rightsholder. The license created by the exchange of an Order Confirmation (and/or any invoice) and payment by User of the full amount set forth on that document includes only those rights expressly set forth in the Order Confirmation and in these terms and conditions, and conveys no other rights in the Work(s) to User. All rights not expressly granted are hereby reserved.
3.2 General Payment Terms: You may pay by credit card or through an account with us payable at the end of the month. If you and we agree that you may establish a standing account with CCC, then the following terms apply: Remit Payment to: Copyright Clearance Center, 29118 Network Place, Chicago, IL 60673-1291. Payments Due: Invoices are payable upon their delivery to you (or upon our notice to you that they are available to you for downloading). After 30 days, outstanding amounts will be subject to a service charge of 1-1/2% per month or, if less, the maximum rate allowed by applicable law. Unless otherwise specifically set forth in the Order Confirmation or in a separate written agreement signed by CCC, invoices are due and payable on "net 30" terms. While User may exercise the rights licensed immediately upon issuance of the Order Confirmation, the license is automatically

revoked and is null and void, as if it had never been issued, if complete payment for the license is not received on a timely basis either from User directly or through a payment agent, such as a credit card company.

3.3 Unless otherwise provided in the Order Confirmation, any grant of rights to User (i) is "one-time" (including the editions and product family specified in the license), (ii) is non-exclusive and non-transferable and (iii) is subject to any and all limitations and restrictions (such as, but not limited to, limitations on duration of use or circulation) included in the Order Confirmation or invoice and/or in these terms and conditions. Upon completion of the licensed use, User shall either secure a new permission for further use of the Work(s) or immediately cease any new use of the Work(s) and shall render inaccessible (such as by deleting or by removing or severing links or other locators) any further copies of the Work (except for copies printed on paper in accordance with this license and still in User's stock at the end of such period).

3.4 In the event that the material for which a republication license is sought includes third party materials (such as photographs, illustrations, graphs, inserts and similar materials) which are identified in such material as having been used by permission, User is responsible for identifying, and seeking separate licenses (under this Service or otherwise) for, any of such third party materials; without a separate license, such third party materials may not be used.

3.5 Use of proper copyright notice for a Work is required as a condition of any license granted under the Service. Unless otherwise provided in the Order Confirmation, a proper copyright notice will read substantially as follows: "Republished with permission of [Rightsholder's name], from [Work's title, author, volume, edition number and year of copyright]; permission conveyed through Copyright Clearance Center, Inc. " Such notice must be provided in a reasonably legible font size and must be placed either immediately adjacent to the Work as used (for example, as part of a by-line or footnote but not as a separate electronic link) or in the place where substantially all other credits or notices for the new work containing the republished Work are located. Failure to include the required notice results in loss to the Rightsholder and CCC, and the User shall be liable to pay liquidated damages for each such failure equal to twice the use fee specified in the Order Confirmation, in addition to the use fee itself and any other fees and charges specified.

3.6 User may only make alterations to the Work if and as expressly set forth in the Order Confirmation. No Work may be used in any way that is defamatory, violates the rights of third parties (including such third parties' rights of copyright, privacy, publicity, or other tangible or intangible property), or is otherwise illegal, sexually explicit or obscene. In addition, User may not conjoin a Work with any other material that may result in damage to the reputation of the Rightsholder. User agrees to inform CCC if it becomes aware of any infringement of any rights in a Work and to cooperate with any reasonable request of CCC or the Rightsholder in connection therewith.

4. Indemnity. User hereby indemnifies and agrees to defend the Rightsholder and CCC, and their respective employees and directors, against all claims, liability, damages, costs and expenses, including legal fees and expenses, arising out of any use of a Work beyond the scope of the rights granted herein, or any use of a Work which has been altered in any unauthorized way by User, including claims of defamation or infringement of rights of copyright, publicity, privacy or other tangible or intangible property.

5. Limitation of Liability. UNDER NO CIRCUMSTANCES WILL CCC OR THE RIGHTSHOLDER BE LIABLE FOR ANY DIRECT, INDIRECT, CONSEQUENTIAL OR INCIDENTAL DAMAGES (INCLUDING WITHOUT LIMITATION DAMAGES FOR LOSS OF BUSINESS PROFITS OR INFORMATION, OR FOR BUSINESS INTERRUPTION) ARISING OUT OF THE USE OR INABILITY TO USE A WORK, EVEN IF ONE OF THEM HAS BEEN ADVISED OF THE POSSIBILITY OF SUCH DAMAGES. In any event, the total liability of the Rightsholder and CCC (including their respective employees and directors) shall not exceed the total amount actually paid by User for this license. User assumes full liability for the actions and omissions of its principals, employees, agents, affiliates, successors and assigns.

6. Limited Warranties. THE WORK(S) AND RIGHT(S) ARE PROVIDED "AS IS". CCC HAS THE RIGHT TO GRANT TO USER THE RIGHTS GRANTED IN THE ORDER CONFIRMATION DOCUMENT. CCC AND THE RIGHTSHOLDER DISCLAIM ALL

OTHER WARRANTIES RELATING TO THE WORK(S) AND RIGHT(S), EITHER EXPRESS OR IMPLIED, INCLUDING WITHOUT LIMITATION IMPLIED WARRANTIES OF MERCHANTABILITY OR FITNESS FOR A PARTICULAR PURPOSE. ADDITIONAL RIGHTS MAY BE REQUIRED TO USE ILLUSTRATIONS, GRAPHS, PHOTOGRAPHS, ABSTRACTS, INSERTS OR OTHER PORTIONS OF THE WORK (AS OPPOSED TO THE ENTIRE WORK) IN A MANNER CONTEMPLATED BY USER; USER UNDERSTANDS AND AGREES THAT NEITHER CCC NOR THE RIGHTSHOLDER MAY HAVE SUCH ADDITIONAL RIGHTS TO GRANT.

7. Effect of Breach. Any failure by User to pay any amount when due, or any use by User of a Work beyond the scope of the license set forth in the Order Confirmation and/or these terms and conditions, shall be a material breach of the license created by the Order Confirmation and these terms and conditions. Any breach not cured within 30 days of written notice thereof shall result in immediate termination of such license without further notice. Any unauthorized (but licensable) use of a Work that is terminated immediately upon notice thereof may be liquidated by payment of the Rightsholder's ordinary license price therefor; any unauthorized (and unlicensable) use that is not terminated immediately for any reason (including, for example, because materials containing the Work cannot reasonably be recalled) will be subject to all remedies available at law or in equity, but in no event to a payment of less than three times the Rightsholder's ordinary license price for the most closely analogous licensable use plus Rightsholder's and/or CCC's costs and expenses incurred in collecting such payment.

8. **Miscellaneous.**

8.1 User acknowledges that CCC may, from time to time, make changes or additions to the Service or to these terms and conditions, and CCC reserves the right to send notice to the User by electronic mail or otherwise for the purposes of notifying User of such changes or additions; provided that any such changes or additions shall not apply to permissions already secured and paid for.

8.2 Use of User-related information collected through the Service is governed by CCC's privacy policy, available online here:
http://www.copyright.com/content/cc3/en/tools/footer/privacypolicy.html.

8.3 The licensing transaction described in the Order Confirmation is personal to User. Therefore, User may not assign or transfer to any other person (whether a natural person or an organization of any kind) the license created by the Order Confirmation and these terms and conditions or any rights granted hereunder; provided, however, that User may assign such license in its entirety on written notice to CCC in the event of a transfer of all or substantially all of User's rights in the new material which includes the Work(s) licensed under this Service.

8.4 No amendment or waiver of any terms is binding unless set forth in writing and signed by the parties. The Rightsholder and CCC hereby object to any terms contained in any writing prepared by the User or its principals, employees, agents or affiliates and purporting to govern or otherwise relate to the licensing transaction described in the Order Confirmation, which terms are in any way inconsistent with any terms set forth in the Order Confirmation and/or in these terms and conditions or CCC's standard operating procedures, whether such writing is prepared prior to, simultaneously with or subsequent to the Order Confirmation, and whether such writing appears on a copy of the Order Confirmation or in a separate instrument.

8.5 The licensing transaction described in the Order Confirmation document shall be governed by and construed under the law of the State of New York, USA, without regard to the principles thereof of conflicts of law. Any case, controversy, suit, action, or proceeding arising out of, in connection with, or related to such licensing transaction shall be brought, at CCC's sole discretion, in any federal or state court located in the County of New York, State of New York, USA, or in any federal or state court whose geographical jurisdiction covers the location of the Rightsholder set forth in the Order Confirmation. The parties expressly submit to the personal jurisdiction and venue of each such federal or state court.If you have any comments or questions about the Service or Copyright Clearance Center, please contact us at 978-750-8400 or send an e-mail to info@copyright.com.

v 1.1

Questions? customercare@copyright.com or +1-855-239-3415 (toll free in the US) or +1-978-646-2777.